FINAL REPORT

Risk Quantification for Sustaining Coastal Military Installation Assets and Mission Capabilities

SERDP Project RC-1701

JUNE 2014

Kelly A. Burks-Copes, Ph.D.
Edmond J. Russo, Jr., Ph.D., P.E., D.CE, D.NE, D.WRE
Scott Bourne
Mike Case, Ph.D.
Austin Davis
Craig Fischenich, Ph.D.
Mike Follum
Honghai Li, Ph.D.
Lihwa Lin, Ph.D.
Steve Lofton
Kyle McKay, Ph.D.
Paul Mlakar, Ph.D.
Andrew Morang, Ph.D.
Steve Pranger
Ryan Pickett
Jay Ratcliff, Ph.D.
José Rullán-Rodríguez
Martin Schultz, Ph.D.
Janet Sims, Ph.D.
Eric Smith
Jane Smith, Ph.D.
Cary Talbot, Ph.D.
Kevin Winters
U.S. Army Engineer Research and Development Center (ERDC)

SERDP
DOD ▪ EPA ▪ DOE

Page Intentionally Left Blank

Page Intentionally Left Blank

REPORT DOCUMENTATION PAGE

Form Approved
OMB No. 0704-0188

1. REPORT DATE *(DD-MM-YYYY)*	**2. REPORT TYPE**	**3. DATES COVERED** *(From - To)*
14-04-2014	Final Technical Report	1 Jan 2009 – 14 Apr 2014

4. TITLE AND SUBTITLE

Mission Capabilities: Final Technical Report

5a. CONTRACT NUMBER

5b. GRANT NUMBER

6. AUTHOR(S)
Burks-Copes, K., E. Russo, S. Bourne, M. Case, A. Davis, C. Fischenich, M. Follum, H. Li, L. Lin, S. Lofton, K. McKay, P. Mlakar, A. Morang, S. Pranger, R. Pickett, J. Ratcliff, J. Rullán-Rodríguez, M. Schultz, J. Simms, E. Smith, J. Smith, C. Talbot, and K. Winters.

5c. PROGRAM ELEMENT NUMBER

5d. PROJECT NUMBER

5e. TASK NUMBER

5f. WORK UNIT NUMBER
RC-1701

7. PERFORMING ORGANIZATION NAME(S) AND ADDRESS(ES) AND ADDRESS(ES)
U.S. Army Engineer Research and Development Center
3909 Halls Ferry Road
Vicksburg, MS 39180

8. PERFORMING ORGANIZATION REPORT

9. SPONSORING / MONITORING AGENCY E(S) AND ADDRESS(ES)

10. SPONSOR/MONITOR'S ACRONYM(S)

11. SPONSOR/MONITOR'S REPORT NUMBER(S)

12. DISTRIBUTION / AVAILABILITY STATEMENT
Approved for public release; distribution is unlimited

13. SUPPLEMENTARY NOTES

14. ABSTRACT

The best available evidence indicates that sea level rise is occurring at unprecedented rates, and while military commanders may be situationally aware of their installation's vulnerabilities, demonstrable risk-based assessments are needed to proactively adapt military systems, processes, and protocols in the face of this pervasive threat multiplier. This report describes the development and testing of a risk assessment framework – a coastal hazard risk assessment approach that incorporates sea level rise threats and communicates the risk of mission impairment to the military in a meaningful manner that supports mission adaptation and sustainability into the future. The approach is tested on a North Atlantic naval base (Naval Station Norfolk, VA) using a variety of prescribed sea level rise scenarios (0-2m) in combination with simulated coastal storms ranging in intensities of 1-yr to 100-yr return intervals. Forcings (waves, winds, sediment, flooding, etc.) are generated using a group of high fidelity numerical storm models. Installation assets and missions are decomposed (i.e., broken down into critical assets and capabilities that contribute to mission performance), and storm damage to the infrastructure network are assessed using probabilistic Bayesian analyses. The risk-based approach and step-by-step procedures presented here can be used to assess risks to mission on other military installations facing similar threats from coastal hazards and rising sea levels. Moreover, the approach can be used to assess vulnerability and risks at the regional scale to encourage preparedness and enhance coastal resiliency both on and off military installations. In effect, this study offers a robust, scientifically defensible approach that transparently communicates potential risks, improves military readiness, and promotes sustainability in the face of climate change and sea level rise.

15. SUBJECT TERMS
Climate Change, Sea Level Rise, Land Use Conversion, Hurricanes, Coastal Storms, Flooding, Asset Capability Network, Structural Damage, Mission Performance Impairment, Risk Assessment

16. SECURITY CLASSIFICATION OF:			**17. LIMITATION OF ABSTRACT**	**18. NUMBER OF PAGES**	**19a. NAME OF RESPONSIBLE PERSON**
Unclassified					Kelly A. Burks-Copes
a. REPORT	**b. ABSTRACT**	**c. THIS PAGE**		366	**19b. TELEPHONE NUMBER** 601-634-2290

Standard Form 298 (Rev. 8-98)
Prescribed by ANSI Std. Z39.18

Page Intentionally Left Blank

Table of Contents

List of Figures

List of Tables

List of Acronyms

2D	Two-Dimensional
3D	Three-Dimensional
ACN	Asset Capability Network
ADCIRC	ADvanced CIRCulation model
AdH	Adaptive Hydrology model
ASL	Absolute Sea Level
BFE	Base Flood Elevation
CAD	Computer-Aided-Design
CDR	Commander
CERL	Construction Engineering Research Laboratory
CHL	Coastal and Hydraulics Laboratory
CIP	Critical Infrastructure Protection
CIRP	Coastal Inlets Research Program
CMB	Computational Model Builder
CMS	Coastal Modeling System
CORS	National Geodetic Survey's Continuously Operating Reference Station Network
CPT	Conditional Probability Table
CRREL	Cold Regions Research and Engineering Laboratory
CVN	Aircraft carriers carrying fixed wing aircraft and nuclear powered
DAG	Directed Acyclic Graph
DCIP	Defense Critical Infrastructure Program
DEM	Digital Elevation Model
DFIRMs	Digital Flood Insurance Rate Maps
DoD	Department of Defense
DSN	Damage State Node
DVP	Dominion Virginia Power
EL	Environmental Laboratory
EM	Electromagnetic
EM-X	Electromagnetic Induction System (Number X)
ERDC	U.S. Army Engineer Research and Development Center
Term	Definition
ESC	Engineering Services Center, Naval Facilities Engineering Command
ESRI	Environmental System Research Institute, Inc.
ESTCP	Environmental Security Technology Certification Program
FACEDAP	Facility and Component Explosive Damage Assessment Program
FEMA	Federal Emergency Management Agency
FN	Function Node
FOUO	For Official Use Only
GCM	Global Circulation Models
GIS	Geographic Information System
GMS	DoD Groundwater Modeling System
GMSLR	Global Mean Sea Level Rise

GPS	Global Positioning System
GSL	Geotechnical and Structures Laboratory
GSSHA	Gridded Surface-Subsurface Hydrologic Analysis
GUI	Graphic User Interface
GWCE	Generalized Wave Continuity Equation
HAZUS-MH MR	Hazards U.S. Multi-Hazards Software
HPC	High Performance Computing system
IOKA	Interactive Objective Kinematic Analysis system
IPCC	Intergovernmental Panel on Climate Change
JPM-OS	Joint Probability Method of Optimal Sampling
LACPR	Louisiana Coastal Protection and Restoration Project
LSML	Local Mean Sea Level
LiDAR	Light Detection and Ranging
LULC	Land Use and Land Cover
MHHW	Mean Higher High Water
MHW	Mean High Water
MLLW	Mean Lower Low Water
MLW	Mean Low Water
MPI	Mission performance Index
MPT	Marginal Probability Table
Term	Definition
MSL	Mean Sea Level
MTL	Mean Tide Level
NAD83	North American Datum of 1983
NASA	National Aeronautics and Space Administration
NAVD88	North American Vertical Datum of 1988
NAVFAC	Naval Facilities Engineering Command
NCDC	National Climatic Data Center
NGDC	National Geophysical Data Center
NIC	National Intelligence Council
NLCD	National Land Cover Database
NSN	Naval Station Norfolk
NOAA	National Oceanic and Atmospheric Administration
NOS	National Ocean Service
NRC	National Research Council
NTDE	National Tidal Datum Epoch
NRCS	Natural Resources Conservation Service
NWF	National Wildlife Federation
NWI	National Wetlands Inventory
NWLON	NOAA's National Water Level Observation Network
ODASN IS&A CIP	Office of the Deputy Assistant Secretary of the Navy, Infrastructure Strategy and Analysis, Critical Infrastructure Protection
PBL	Planetary Boundary Layer
POL	Petroleum, Oils, & Lubricants
QDR	Quadrennial Defense Review

RC	Resource Conservation and Climate Change Program Area
RSL	Relative Sea Level
SDSFIE	Spatial Data Standard for Facilities, Infrastructure and Environment
SERDP	Strategic Environmental Research and Development Program
SEV	Coastal Storm Severity Categories in the NSN Risk Model
SISON-09-05	2009-05 SERDP Statement of Need
SLAMM	Sea Level Affecting Marshes Model
SLR	Sea Level Rise
Term	Definition
SSURGO	Soil Survey Geographic Database
SUA	Structural Units of Analysis
SWAN	Simulating WAves Nearshore model
SWL	Still Water Level (aka surge)
TC96	TC96 Planetary Boundary Layer (PBL) wind model
TDC	Technical Discipline Coordinator
TDS	Total Dissolved Solids
TFCC	Task Force Climate Change
TNC	The Nature Conservancy
USACE	U.S. Army Corps of Engineers
USCG	U.S. Coast Guard
USGS	U.S. Geological Survey
WASH123D	Watershed model
WMS	Watershed Modeling System
WSE	Water Surface Elevation

Keywords

Climate Change, Sea Level Rise, Land Use Conversion, Hurricanes, Coastal Storms, Flooding, Asset Capability Network, Structural Damage, Mission Performance Impairment, Risk Assessment

Acknowledgements

The RC-1701 Project was one of four research initiatives funded under the Resource Conservation and Climate Change Program Area of the Strategic Environmental Research and Development Program (SERDP) 2009 - 2012. The work described herein was funded by SERDP under the direction of Dr. Jeffrey Marqusee, Executive Director, SERDP and Dr. John Hall, Resource Conservation and Climate Change Program Manager, SERDP/ESTCP. The authors wish to acknowledge the following U.S. Navy personnel and thank them for their assistance in this endeavor:

- CAPT Mark R. Libonate, Commanding Officer Naval Facilities Engineering Command (NAVFAC) Mid-Atlantic, Civil Engineer Corps, United States Navy
- CDR Frederick A. Hintermister, Office of the Deputy Assistant Secretary of the Navy, Infrastructure Strategy and Analysis, Critical Infrastructure Protection (ODASN IS&A CIP)
- Mr. Anthony L. Farmer, Structural Engineering Technical Discipline Coordinator (TDC), Capital Improvements Business Line, NAVFAC Mid-Atlantic
- Mr. Robert Baldwin, Regional Community Plans and Liaison Officer, Asset Management Branch, NAVFAC Mid Atlantic
- Dr. Shun Ling, Environmental Office Head, Engineering Services Center (ESC), NAVFAC
- Dr. Richard A. Gardner, Environmental Department Head, ESC, NAVFAC
- Mr. Timothy J. McHale, ESC, NAVFAC
- Ms. Jennie Dummer ESC, NAVFAC
- Mr. Robert L. Butters, P.E., Facilities Planner, NAVFAC
- Mr. John H. Salley, R.A., Deputy Public Works Officer, NAVFAC

Final Technical Report

Risk Quantification for Sustaining Coastal Military Installation Assets and Mission Capabilities (SERDP RC-1701)

Abstract

Objectives. The objective of this study was to develop (and test) a risk-based methodology to evaluate threats to critical installation assets and quantify the potential loss of mission performance when installation capabilities were impacted by a combination of rising sea levels and coastal storm hazards.

Technical Approach. Our step-wise risk assessment approach used predictive inferences to quantify vulnerabilities of critical assets based on their exposure, sensitivity, and adaptive capacity to withstand storm forcings (tidal fluctuations, waves, winds, surge, sedimentation, saltwater intrusion, flooding, etc.) exacerbated by sea level rise. Hierarchical aggregations of assets were then arrayed in a relational network to capture interdependencies, and service interruptions were monitored from a systems perspective to capture the overall risk to mission performance.

Our approach began with an environmental and geomorphological characterization of the baseline conditions of a region. We then mapped the potential changes likely to occur to the coastline under a variety of SLR scenarios in a Geographic Information System (GIS) to better visualize the system's response to the combination of inundation and vegetative switching. We then used high fidelity numerical models to simulate coastal storms and assess regional, nearshore, surface, and subsurface conditions under a range of SLR scenarios. These models generated a series of resultant forcings (winds, waves, surge, etc.) that impacted both the installation and its surrounding environs. An installation-specific Asset Capability Network (ACN) model was created and then used to capture the unique position, condition, and interdependencies of the installation's critical infrastructure in supporting the mission. An assessment of possible damages to the installation network was undertaken, and risks of mission impairment were then quantified using probabilistic Bayesian analyses under the various storm and SLR scenarios.

We selected the Naval Station Norfolk (NSN) in Hampton Roads, Virginia (located at the mouth of the Chesapeake Bay, North Atlantic coast of the United States) to test the efficacy of our approach. All modeling efforts for the case study focused on a series of 25 scenarios comprised of five prescribed sea level rise conditions ranging from 0.0 m to 2.0 m (by 2100) in combination with five simulated coastal storms ranging in intensity from 1-yr to 100-yr return intervals. In addition, three historical nor'easters were incorporated into the storm analysis (at the request of NSN managers) to capture the localized impacts of these unique storms, but were omitted from the risk-based analysis due to time and budgetary constraints.

Results. The project has had several significant outcomes. We have produced a robust, scientifically informed risk-based approach that is applicable to coastal military installations threatened by coastal hazards and rising sea levels. As part of this effort, we have established a series of stepwise procedures to couple multiple high fidelity coastal storms models with installation-specific asset models and regional ecosystem response models to systematically assess risks to mission in a probabilistic manner using Bayesian networking.

A successful test of the framework on Naval Station Norfolk clearly illustrated the efficacy of our procedures and the benefits of deploying a risk-based approach. Numerous products were generated for the test case. For example, each model application generated a series of 25 forcings datasets and accompanying high resolution maps that captured the existing conditions and quantified the storm forcings (winds, waves, surge, etc.) impacting the area under the various SLR scenarios. Accompanying these analyses, several associated GIS-based products (model meshes, digital elevation models, land use cover classifications) have been produced for the study area. Although not a primary objective of this study, it is important to note that our test case has also generated a series of GIS-based maps of forcings (winds, waves, surge, flooding, etc.) for the entire Hampton Roads area (for each of the SLR-storm scenarios studied) that can now be used to assess vulnerability of assets both inside and outside the installation, supporting community efforts to address the threats of SLR and coastal storm hazards from a regional perspective. The asset network model developed for the site offered a unique highly detailed systems perspective of the installation's service production (i.e., electric supply, water supply, waste removal, etc.), and has now been stored in the GIS database for use in future management and operations activities by the installation's personnel. The Bayesian model developed for the test site now holds more than 13,000 conditional probabilities characterizing the fragility of the assets with regards to their location, condition, and structural composition The relational Bayesian network quantifies impacts to capabilities and the risks to mission performance due to exposure to storm hazards and SLR.

Based on our analysis of NSN's site-specific vulnerabilities, we found sea level rise to be a significant and pervasive threat multiplier to mission sustainability, significantly increasing loadings on built infrastructure, and dramatically increasing risks to system capabilities and service provisioning. Using our framework, we were able to identify several critical systems on the study site that were particularly vulnerable and likely to be incapacitated once sea levels rise above 1.0 meter on the site. Our results show that the probabilities of damage to infrastructure and losses in mission performance increased dramatically once 0.5 meters of SLR was experienced, indicating a "tipping point" or threshold that should be considered when undertaking future planning or operational activities on the installation.

Benefits. The analytical framework described herein can be used to evaluate relative performance of existing conditions, future no-action conditions, as well as structural and non-structural risk mitigating alternatives to sustain critical assets and mission capabilities at an actionable scale under a wide range of SLR and storm scenarios. Deploying our approach, installations can identify critical thresholds where minor mission impairment annoyances (on the order of ~1-2 hour delays in performance) evolve into catastrophic events (i.e., on the order of weeks or months). Once communicated to the planners and managers both on and offsite in an actionable construct through maps and network diagrams, installations can consider altering the

status quo to incorporate proactive management strategies to prevent or anticipate impairments based on the risks (i.e., regret management). Moreover, military leadership can use these experiences to develop new guidance and policy to proactively address systemic, commonly occurring failures across the range of the military's holdings. In effect, this study offers a robust, scientifically defensible approach that transparently communicates potential risks to installations, while helping policymakers develop guidance to promote military readiness and sustainability in the face of climate change and sea level rise.

1. Objectives

1.1. Strategic Environmental Research and Development Program (SERDP) Statement of Need (SON)

This project was undertaken in response to the SERDP Statement of Need SISON-09-05, *Assessment of the Impact of Sea-Level Rise on Military Infrastructure*.[1] The SISON requirements included the following:

- Develop analysis methods to assess the impacts of local mean sea-level rise of 0.5 m, 1.0 m, 1.5 m, and 2.0 m, and utilize these methods to assess the impacts to a coastal military installation.
- Include an assessment of the potential impacts caused by an increase in the frequency and intensity of storms.
- Include an analysis of the impacts due to: (1) inundation of land; (2) increased storm and flood damage; (3) loss of wetlands; (4) changes in erosion patterns and rates; (5) salt water intrusion in surface and ground waters; (6) rising water tables; and (7) changes in tidal flows and currents.
- For the specific military installation selected, examine:
  - loss of or damage to mission essential infrastructure;
  - loss or degradation of mission capabilities;
  - loss of training and testing lands;
  - loss of transportation means, facilities and/or corridors;
  - increased risk of storm damage; and
  - increased potential for loss of life (not including disease or other indirect health impacts).
- Utilize routinely available data and existing models.
- Develop methodologies capable of implementation at any DoD installation worldwide that may be affected by a rise in sea level.

1.2. Problem Statement for the Study

The military needs a robust, scientifically defensible approach to quantify sea level risks and transparently communicate these to the end user, providing leadership with relevant information to develop guidance that promotes sustainable mission performance, and empowering on-the-ground military planners with actionable information to make risk-informed decisions regarding threats to existing and future infrastructure development, considering the potential for climate change and SLR. Although commanders may be situationally aware of their installation's vulnerabilities, demonstrable risk-based assessments have yet to be developed that can assist them in proactively adapting military systems, processes, and protocols to meet these pervasive threats (Figure 1).

[1] http://www.serdp.org/Program-Areas/Resource-Conservation-and-Climate-Change (Accessed December 2010).

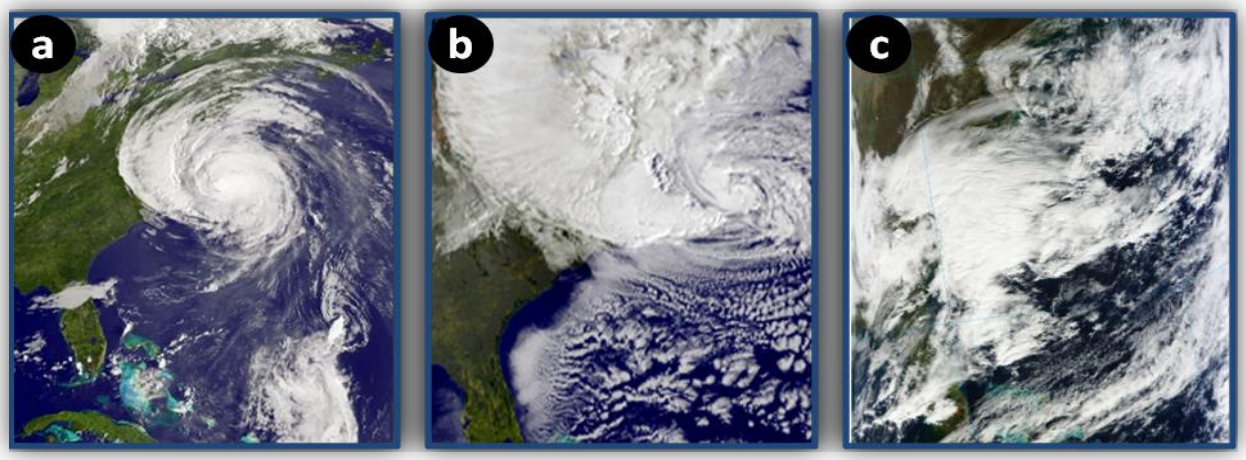

Figure 1. Natural hazards such as (a) the 2010 Hurricane Earl, (b) the 2012 Hurricane Sandy, and (c) the 2012 Post Election Day Nor'easter can impair installation performance. Climate change and SLR can act as threat multipliers impacting mission performance and national security.

1.3. Goals and Objectives of the Study

Risk-informed decision making implemented within the traditional military planning paradigm, requires information produced with decision-relevant risk analysis. Several guiding research questions have been used to fashion the study's technical approach:

1) What are the key pieces of information necessary to operationalize the risk assessment?
2) What is the risk of mission impairment or even failure if future SLR were to happen at some level and a tropical (or extra-tropical) storm were to impact the study site?
3) Are there critical points of failure (i.e., specific assets that were most vulnerable) under any or all of the five prescribed SLR scenarios? These then could be provided to the managers to consider upgrades in advance of the potential threat.
4) What are the thresholds or tipping points?

With these motivations in mind, we have developed a series of goals and objectives to guide us in the development of a risk assessment framework. Our goals have been to:

- **Characterize** the **scope** and **magnitude of sea level change effects** in existing and future no-action coastal installation conditions;
- **Identify thresholds** of significant onset of installation losses due to coastal hazard impacts; and
- Advance the military's knowledge and capabilities for **risk assessment** as a **strategic enabler** to risk management.

To meet these overall goals, we have defined a series of project specific goals to measure success, including:

- Developing an **integrated** coastal hazard risk assessment framework that manages SLR scenario uncertainty;

- Testing the approach on a site and show that the approach is both **robust** and **scientifically defensible,** supporting decisions to **manage** installations and **ensure** mission sustainability when threatened by coastal hazards and SLR;
- Ensuring that the approach and tools are **general** and **agile** enough to support potential **"plug-and-play"** assessments regionally and at other coastal settings worldwide[2]; and
- **Transferring the knowledge** (and capabilities) developed under this study to the military community of practice.

The primary objective of this study has been to develop (and test) a risk-based methodology to evaluate threats to critical installation assets (i.e., both built and natural infrastructure) and quantify the potential loss of mission performance when installation capabilities were impacted by a combination of rising sea levels and coastal storms. The stepwise procedure requires:

1) Coastal storm modeling to quantify the magnitude of storm forcings (winds, waves, surge, etc.) under a variety of storm and SLR scenarios;
2) Asset decomposition (i.e., identifying the critical assets, and noting their position and relational condition within a system) to determine vulnerability (i.e., exposure, fragility and adaptive capacity);
3) Risk analysis to probabilistically quantify the operational risk[3] to mission; and the
4) Visualization of the scenario outcomes (Figure 2).

[2] Note that the development of a portable framework does not imply that a transfer of the approach will be simple or uncomplicated, but rather that our approach must be somewhat generic and agile. The technological transfer and implementation of our approach will always require the additional acquisition of site-specific data, a revision of the coastal storm modeling for the new region, and the development of a site-specific infrastructure asset and capability network whose details will be determined on a case-by-case basis.

[3] We define operational risk here as the probability a hazard would act on an operation resulting in mission impairment and a reduction in operational performance. The degree to which a system is subjected to losses when hazards are imposed is defined as its vulnerability.

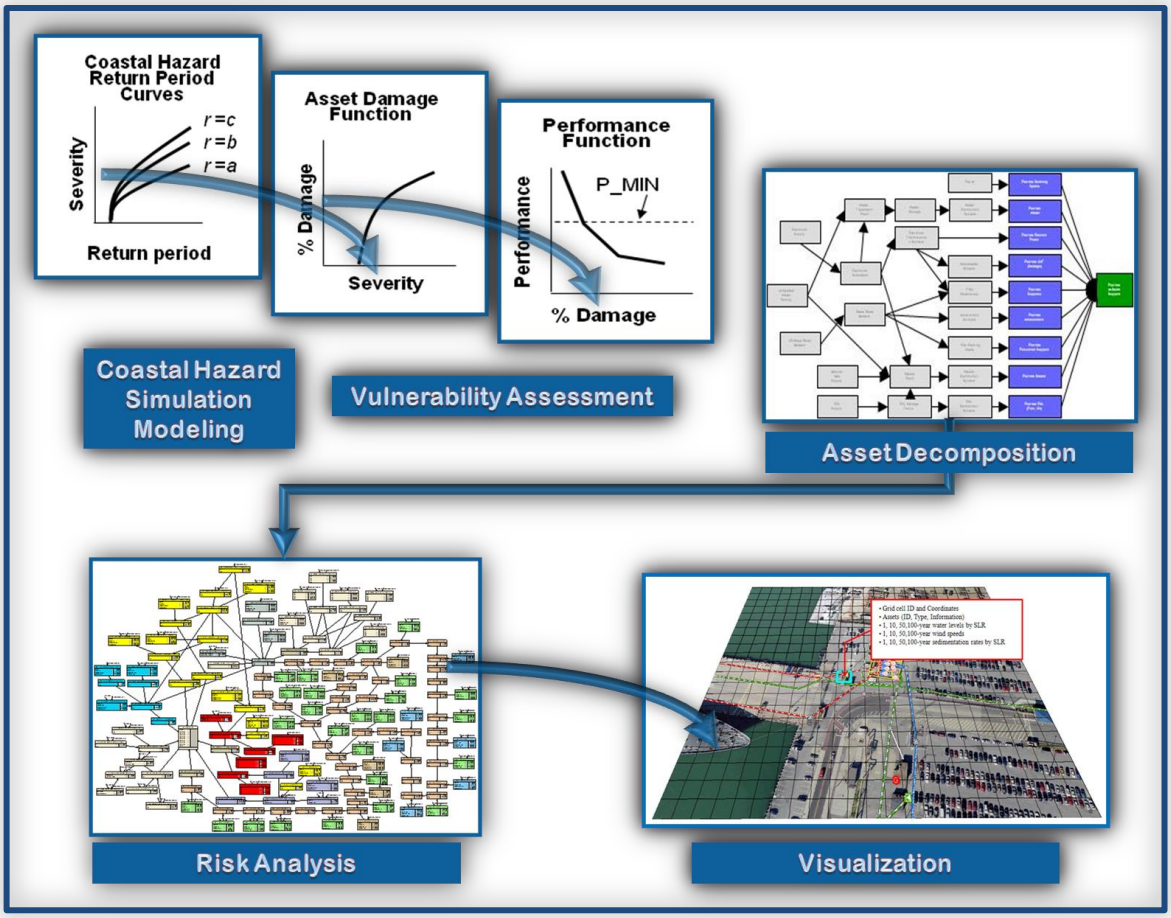

Figure 2. Conceptual model demonstrating the approach to quantify the potential risks of mission impairment due to coastal hazards simulated under a range of SLR and coastal storm scenarios.

As the figure illustrates, our strategy requires that we develop a series of risk communication tools for installation planners and managers in visually engaging mediums (i.e., tables, graphics, and risk maps) to transparently convey the potential individual and collective asset impairments. Deploying our approach, installations will be able to discern thresholds where minor annoying systems performance losses (on the order of ~1-2 hour delays in performance) turn into catastrophic systems failures (i.e., resulting in weeks of mission impairment). These thresholds, or "tipping points," are central to our study efforts – the intent is to communicate the potential risks to the military in an actionable analytical construct so that installations and their military leaders can consider altering the status quo to incorporate proactive management strategies in anticipation of SLR possibilities to prevent impairments to critical infrastructure based on the potential risks.

1.4. Case Study: Naval Station Norfolk

Many installations in the Hampton Roads area are exposed to threats of SLR and coastal hazards due to their proximity to the Atlantic Ocean, and their relatively low elevations above mean sea level. For purposes of testing the efficacy of our approach, we have selected Naval Station

Norfolk (NSN), Virginia (located at the mouth of the Chesapeake Bay, North Atlantic coast of the United States) (Figure 3) for our case study.

Figure 3. Naval Station Norfolk (NSN) serves as a test case for our study's risk-based impact assessment approach.

NSN is the largest naval installation in the United States (1,740 ha/4,300 ac) and provides fleet support and facilities to ensure readiness for the entire U.S. Atlantic Fleet. Extensive port infrastructure on NSN was constructed to support, deploy, and sustain surface and submarine vessels of a variety of classes. The installation also supports and maintains important airfield operations for fixed-wing and rotary-wing aircraft within its boundaries. Bounded on the north by Willoughby Bay, on the west by the confluence of the Elizabeth and James Rivers, the installation is located within a major metropolitan area (Norfolk, VA) and is dependent on the region for its utilities and many support services. NSN consists of approximately 4,000 buildings, 20 piers, and an airfield. The 20 piers range from 6 to 60+ years old, with 11 piers at least 50 years old. Ships reach the piers from the ocean via channels that are maintained at a minimum depth of ~14 m (45 ft).

Given the installation's low elevation (less than 5.6 m above MSL), and its proximity to the Atlantic Ocean, the base's built infrastructure is regularly exposed to coastal storm hazards (winds, waves, surge). Although the docks, piers, and other coastal protections at this site present a hardened defense against geomorphologic change, sea level rise coupled with significant storm surge could flood the periphery if not completely submerge the installation in its entirety. As such, NSN offers a good testing ground to illustrate the utility of our approach to reveal critical asset vulnerabilities and quantifying risks to mission performance.

2. Background

2.1. Sea Level Rise (SLR) and Its Implications

The best available scientific evidence based on observations from the long-term monitoring networks indicates that increasing atmospheric concentrations of greenhouse gases (potentially amplified by anthropogenic contributions) is warming the atmosphere and the oceans at an accelerated rate (IPCC 2007, IPCC 2014, Parris et al. 2012, and references therein). The world's oceans have an enormous capacity to store this heat, but the result is ocean warming and all the cascading changes in processes tied to increasing ocean temperature (e.g., glacial and icecap melting, upper ocean thermal expansion, etc.) that when combined, result in an increase in ocean volume. At the same time, many coastal shorelines are eroding and/or subsiding, and terrestrial extractions of groundwater and changes in storm water runoff have led to aquifer seepage. The overall net effect is a measureable change in sea level (Figure 4).

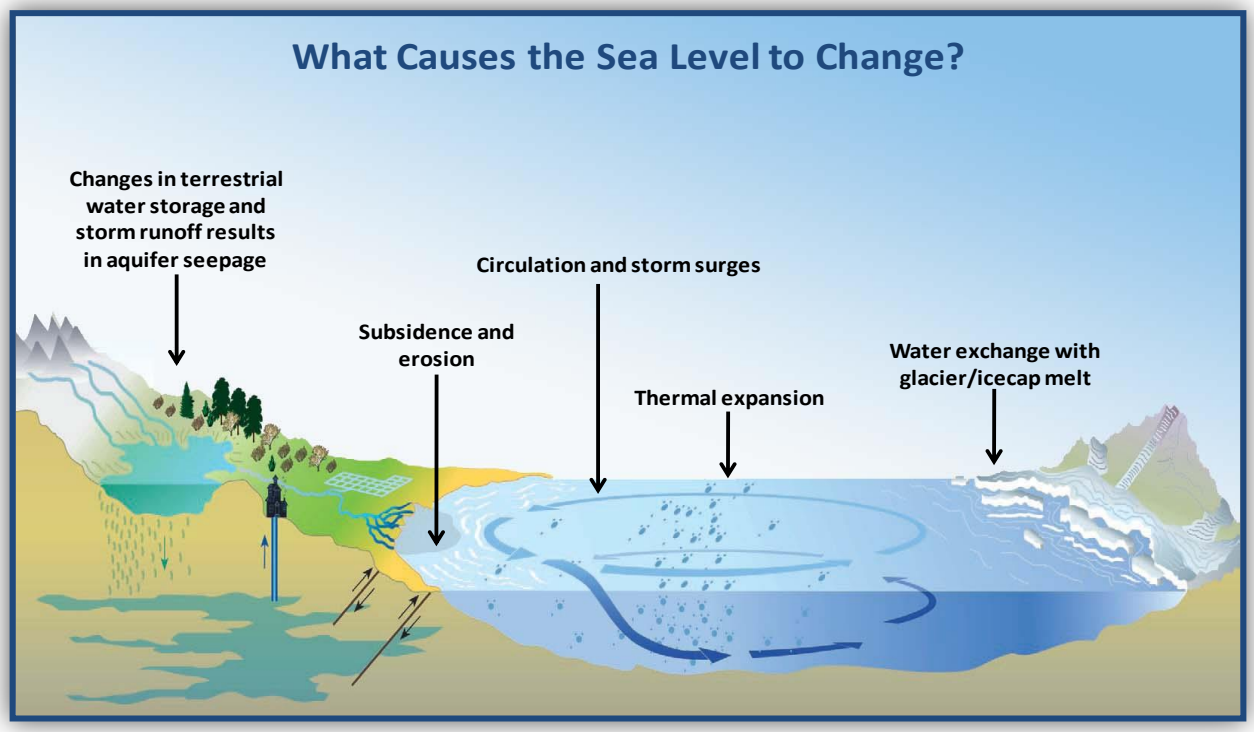

Figure 4. Processes that contribute to sea level change (adapted from http://maps.grida.no/go/graphic/causes-of-sea level-rise-from-climate-change, accessed December 2010).

Unfortunately for many coastal areas, the levels are rising at an unprecedented rate (IPCC 2007, IPCC 2014, Anderson 2009, Parris et al. 2012, and references therein) (Figure 5).

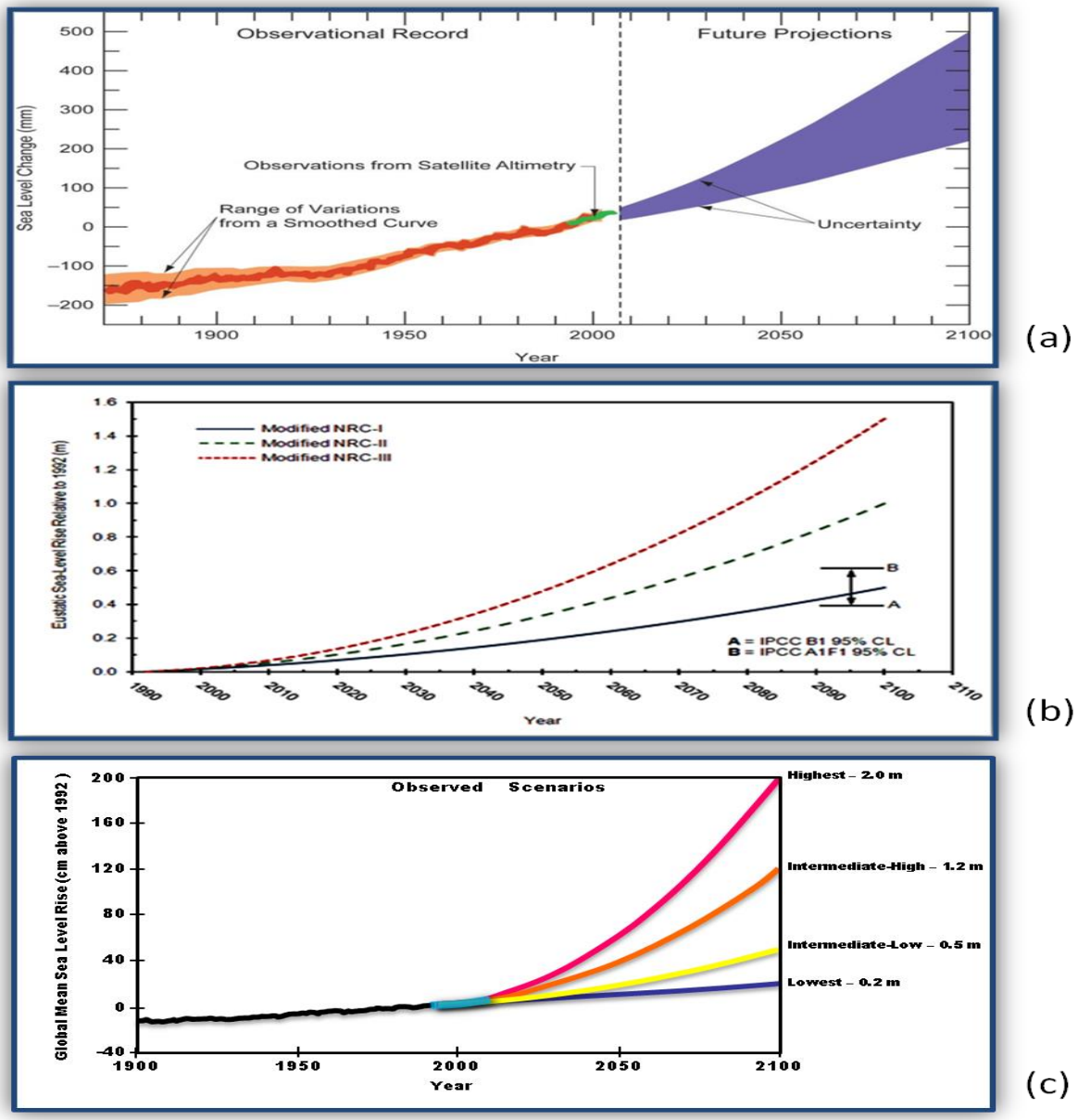

Figure 5. (a) Observed global mean sea level rise (GMSLR) (shown in orange) projections from tide gauges and satellites are compared with the Intergovernmental Panel on Climate Change (IPCC 2007) projections (shown in the blue wedge). (b) Modified National Research Council (NRC 1987) GMSLR rise scenarios and the IPCC (2007) scenario estimates are prescribed by EC-1165-2-211 [U.S. Army Corps of Engineers (USACE) 2011] – guidance for incorporating sea level change considerations in civil works programs.[1] (c) GSLR scenarios have been adopted by the 2013 National Climate Assessment to "help assessment experts and their stakeholders analyze the vulnerabilities and impacts associated with uncertain possible futures" (adapted from Parris et al. 2012).

[1] Note that EC-1165-2-211 has since been superseded by ER 1100-2-8162 (USACE 2013), and will soon be supported by TL 1100-2-xx (USACE 2014).

Global mean sea level rise (GMSLR) can be estimated from physical evidence such as observations of sea level and land ice variability (Pfeffer et al. 2008), expert judgment (NRC, 1987, 2011, 2012), general circulation models (GCMs) (IPCC 2007), and from semi-empirical methods that utilize both observations and general circulation models (Grinsted et al. 2010; Horton et al. 2008; Jevrejeva et al. 2010; Vermeer and Rahmstorf 2009). Based on these figures, we can confidently surmise (Parris et al. 2012):

1) GMSLR rose at a rate of 1.7 millimeters per year (mm/yr),[2]
2) The GMSLR rate has increased to over 3 mm/yr over the last 20 years, and
3) Projections indicate a high confidence (greater than 9 in 10 chances) that GMSLR will rise 0.2 – 2.0 m by the end of this century.

More importantly, climate change does not force SLR at the same rate everywhere – there are spatial variations of SLR superimposed on this global average rise (Sallenger et al. 2012). In fact, some regions along the North Atlantic Coast are today experiencing greater relative sea level rise (RSLR) than the global rates due to regional factors including land subsidence, gravitational redistribution of ice-sheet meltwater, ocean circulation changes, and regional ocean thermostatic effects (Burkett and Davidson 2012). For example, water level measurements in the Hampton Roads area (Chesapeake Bay, Virginia, USA), obtained from tide gauge data, show that over the past few decades the relative sea level has been rising in the area faster than the globally mean absolute sea level trend [Sallenger et al. 2012, National Oceanic and Atmospheric Administration (NOAA) 2012, and others]. Several projections suggest these levels could exceed 0.6 m in the next 50-100 years (Boon 2012, Ezer and Corlett 2012a,b, Wu et al. 2009, and others) (Figure 6), and one study even links the acceleration to climate-related shift and weakening of the Gulf Stream (Ezer et al. 2013).

[2] Note that the IPCC (2007) concluded that global mean sea levels rose at an average rate of about 1.7 ± 0.5 mm/year during the twentieth century. Note that the projections of future projections of SLR in the report disregarded ice sheet dynamics and observed emissions have been higher than predicted by the IPCC in 2007.

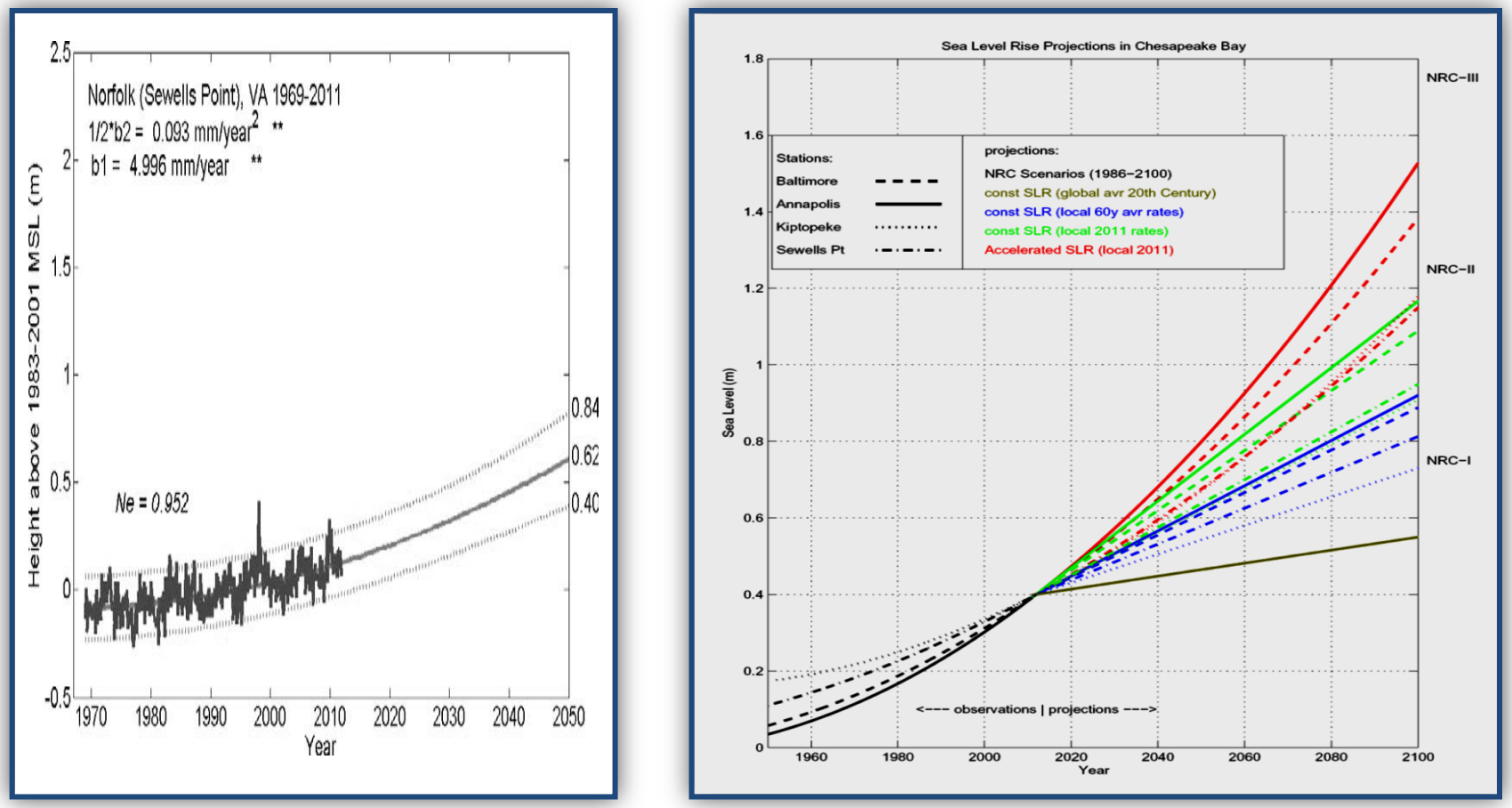

(a) **(b)**

Figure 6. (a) Projected RSL trends developed by Boon (2012) using data from the Sewells Point tidal gauge (Norfolk, VA). RSL is projected to rise 0.62 ± 0.22 m above 1983–2001 MSL by 2050 in a quadratic rather than linear fashion. (b) Relative sea level projections developed by Ezer and Corlett (2012a,b) for Baltimore (dashed line), Annapolis (solid line), Kiptopeke (dotted line) and Sewells point (dash-dot line). Black lines are the trends for 1950-2011 calculated from the last Hilbert-Huang Transform mode of each station; colored lines are various SLR scenarios. Also shown on the right are the three NRC (1987) scenarios based on 0.5 m, 1.0 m, and 1.5 m SLR between 1986 and 2100.

Therefore, it is important to recognize and incorporate these spatial variations into any assessment of impacts because future SLR projections may affect each coastal location differently.

Although the uncertainty surrounding the rate of rise cannot be resolved, scientists agree that its effects will be far reaching (Titus et al. 2009 and references therein). Accelerated GSLR will exacerbate the episodic effects of coastal storms causing increased damage to coastal infrastructure, more rapid coastal erosion and shoreline change, saltwater intrusion into aquifers and surface waters, rising water tables, and changes in tidal prism (IPCC 2007, Titus et al. 2009, Karl, et al. 2009, Church et al. 2010, and references within all).[3] Impacts of RSLR are already in evidence, and will likely increase significantly during this century and beyond (IPCC 2007, Titus et al. 2009, Karl, et al. 2009, Church et al. 2010, and references within all). Low elevation coastal plains, particularly those that are densely populated (e.g., the Mid-Atlantic), will experience the compounding effects of subsidence, making them particularly vulnerable (McGranahan et al. 2007, Williams et al. 2009, Boon et al. 2010).

With over 30 percent of the total United States population residing in coastal counties, changes in sea level represent a significant threat to coastal residents, infrastructure, and their way of life (Gill et al. 2009). As a major U.S. land management agency, the Department of Defense (DoD) owns and operates numerous coastal facilities that are threatened. These Mid-Atlantic facilities carry out diverse tasks ranging from outdoor training activities (e.g., Camp Lejeune, North Carolina) to port and harbor facilities (e.g., NSN in Virginia) to air combat training (e.g., Langley Air Force Base, Virginia). In 2008, 30 of these installations were already experiencing increased risk due to SLR [National Intelligence Council (NIC) 2008].

The Mid-Atlantic coast (including these installations) supports a diverse ecological community and provides significant economic benefit to the region (e.g., migratory waterfowl hunting and blue crab shellfishery). Under SLR, both built and natural systems will undergo changes in structure and function which could drastically alter the system's capacity to provide these benefits and services. Although inundation is a primary concern, other effects of SLR such as increased storm susceptibility, barrier island migration, coastal erosion, wetland drowning, and saltwater intrusion should be accounted for to adequately understand the impacts of SLR on coastal installations (Gesch et al. 2009). Of particular concern, conversion, migration, or loss of beach, marsh, or swamp features could result in loss of critical habitat and change storm surge attenuation.

Taken together, the findings suggest that DoD assets positioned on coasts and islands will be threatened by increased coastal hazards, which will ultimately threaten the Department's ability

[3] Coastal storms approaching the shore experience decay in making landfall. SLR has the potential to alter the horizontal and vertical expanses of the nearshore. This phenomenon generally affords landfalling storm energy, and thus attendant surge/waves, to propagate relatively further inland, with respect to current sea levels. Note that climate change itself has the potential to alter the physical parameters that propagate coastal storms, potentially resulting in changes in storm intensity/frequency trends. Although these climate change-induced intensification effects are not considered part of this study, we consider these effects an active area of ongoing research.

to sustain those resources needed for training, day-to-day operations, and assigned missions, in the face of climate change and sea level rise.

2.2. Military Readiness in the Face of Climate Change

Although the Department of Defense (DoD) recognizes climate change as an emerging issue with national security implications [OSD 2011, Strategic Environmental Research and Development Program (SERDP) 2011, Russo and Hall 2012], the current U.S. military standard operating procedures are based on the premise that sea levels are stable, shorelines are static, and that storms occur on a regular or predictable basis.[4] Often cognizant dissonance (i.e., "anchoring" to pre-existing ideas, even when evidence indicates that one's assumptions are in error) dominates the military decision making paradigm. For this reason, short-term planning horizons grounded in the assumption of climate stationarity[5] tend to prevail (DoD 2010a, Russo et al. 2010, SERDP 2013). At the tactical level, investments in military readiness in advance of potential SLR are not easily justified. Instead, military operations tend to view climate change as a strategic issue – SLR impacts might not be realized for several decades, uncertainties surrounding climate change predictions cloud the issue, and appropriately-scaled tools to support risk-based decision making at the installation level are virtually nonexistent (DoD 2010a, Russo et al. 2010, SERDP 2013).

The prospect of accelerated SLR now underscores an immediate need to overcome institutional inertia and acknowledge potential risks exposed by SLR. While commanders may be situationally aware of their installation's vulnerabilities, there are no known comprehensively-integrated scientific and technological means readily available to quantify the operational risk[6] from a systems perspective[7] to effectively and transparently support decision makers on an actionable scale. Unique and regionally significant assets and mission capabilities that support national and international military missions must be sustained against potential losses, considering that the threat of SLR poses a serious non-stationary potential risk to our nation's security. Consequently, the United States has a strong national security interest in both assessing the vulnerabilities and understanding the potential risks posed by coastal hazards and SLR on coastal military installation assets and mission capabilities.

---

[4] An Engineering Circular (EC) for the US Army Corps of Engineers (USACE) provides guidance in incorporating sea level change considerations in civil works programs (EC-1165-2-211) (USACE 2011). Just recently, the USACE has implemented an Engineering Regulation (ER-1100-2-8162) (USACE 2013), and will soon publish a Technical Letter (TL 1100-2-1) to provide procedures to the civil works program to direct evaluation of SLR impacts, responses and adaptations (USACE 2014).

[5] The concept that while climate may exhibit variability - the underlying statistics that describe the climate (such as its mean and variance) do not change over time. Rather, these characteristics are stationary. This leads to an assumption that the past represents a reasonable proxy for the future (Brekke et al. 2009).

[6] We define operational risk here as the probability a hazard would act on an operation resulting in mission impairment and a reduction in operational performance. The degree to which a system is subjected to losses when hazards are imposed is defined as its vulnerability.

[7] Operating from a systems perspective requires the risk assessor to consider the system in holistic terms, identifying and exploring relationships amongst the system components (i.e., assets), rather than addressing each component individually and in isolation.

How the U.S. military responds to these threats will have far-reaching economic and environmental ramifications. To assure mission sustainability into the long term, the military should consider strategically implementing a risk-informed decision making paradigm to quantify the potential impacts of coastal hazards on critical infrastructure under a variety of SLR scenarios.[8]

[8] Throughout this document, we refer to "scenarios" which we define as "prescribed future sequences of possible events, or future circumstances." Note that this definition mirror's Burkett and Davidson's (2013) position that these prescribed scenarios do not predict future changes. Instead, we use our prescribed scenarios to describe future potential conditions in a manner that supports decision-making under conditions of uncertainty – developing models and testing decisions under a range of plausible futures. This approach strengthens our ability to recognize and adaptively manage risks over time.

3. Materials and Methods

3.1. Technical Approach

For this study, we have devised a step-by-step strategy to characterize baseline conditions, and assess future impacts using predictive inferences to quantify vulnerabilities of critical assets based on their exposure, sensitivity, and adaptive capacity to withstand storm forcings (tidal fluctuations, waves, winds, surge, sedimentation, saltwater intrusion, flooding, etc.) exacerbated by sea level rise. Hierarchical aggregations of assets have then been arrayed in a relational network to capture interdependencies, and service interruptions are monitored from a systems perspective to capture the overall risk to mission performance. Our approach has been guided by several leading questions:

1) What are the conditions of the shoreline, and how might they change under the various alternative futures?
2) How will the land coverages change in response to these scenarios?
3) What types of storms are anticipated, and how might their resultant forcings (wind, floodwater levels, and sedimentation) affect the installation?
4) How are the nearshore processes affected as these storms approach? What sediment loads can be anticipated? How might the bathymetry and land coverages affect the waves and surge as they overtopped the shoreline?
5) What magnitudes of flooding are expected, and where on the installation can we expect to see the greatest magnitude of flooding?
6) What does the installation's asset capability network look like? What are the key components necessary to characterize mission performance? Are there dependencies amongst assets? How might the assets be aggregated to simplify the model, yet maintain the unique character of the station's infrastructure?
7) Given the anticipated storm forcings, and the structure of the network (including interdependencies), what types of damage can we expect under a given storm assuming one of the five prescribed SLR scenarios is experienced?
8) What are the tolerances (fragilities) of the various structural units of the infrastructure network? What is the probability of failure? What tipping points can be identified across the five SLR scenarios?
9) And finally, how might one convey these risks to end-users and policymakers in a meaningful, actionable manner?

To meet the study objectives and answer these questions, we have developed a multi-scaled technical approach that involves six specific tasks:

1) Define a range of coastal storm and SLR scenarios to evaluate in the assessment;
2) Characterize the baseline environmental and geomorphological conditions in the region, and use GIS-based models and mapping procedures to visualize potential changes (inundation and vegetative switching) likely to occur with SLR;
3) Simulate hurricanes and nor'easters moving across the region and then quantify the resultant forcings (winds, floodwater levels, and sedimentation) using high fidelity

numerical modeling of regional, nearshore, surface, and subsurface processes under the various SLR scenarios;

4) Develop a functional asset-based network model of the installation to capture the unique position and condition of the base's built (and natural) infrastructure;
5) Assess damage to both structures and capabilities given the storm forcings at the local scale; and
6) Quantify the potentials risks to mission performance attributed to storm forcings simulated by the multiple storm and SLR scenarios (Figure 7).

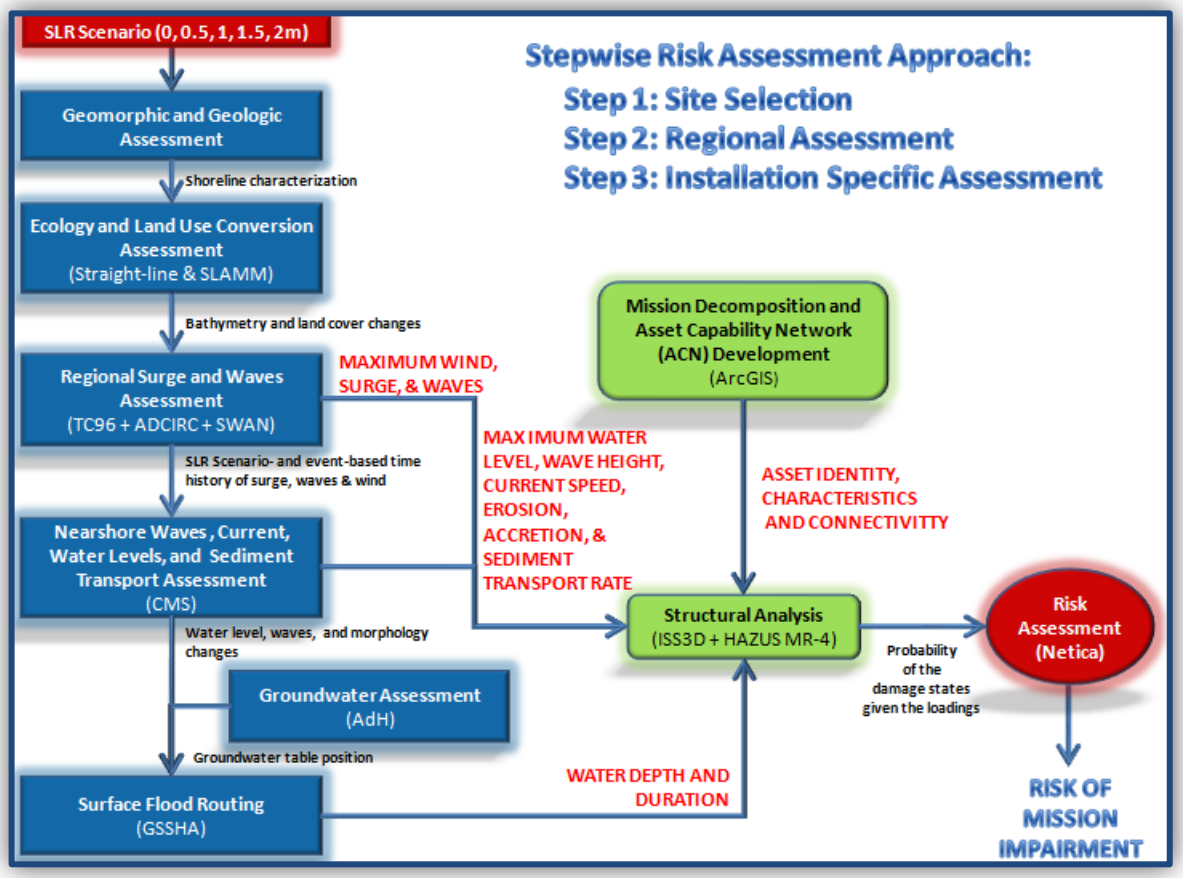

Figure 7. Simple rendering of the steps involved in our probabilistic risk framework.

As the figure indicates, we have selected a suite of models (shown in **blue**) to characterize the forcings generated by the coastal storms. These models and simulation techniques are well developed, tested, and have been widely applied on high priority national studies by numerous proponents.[1,2,3,4] The strengths and weaknesses of these models have been reviewed extensively in the literature (for examples see Kerr et al. 2013, Lin et al. 2010).

[1] Interagency Performance Evaluation Task Force (IPET) (2005 Hurricane Katrina), http://www.nytimes.com/packages/pdf/national/20060601_ARMYCORPS_SUMM.pdf (Accessed April 2014).

We have devised a probabilistic network model approach to estimate the probabilities of damage to infrastructure and loss of function (shown in **green**). Information about the state of networked infrastructure is now related to mission performance through multi-attribute value functions to estimate the extent of mission impairment on the installation and the probability of realizing potential levels of mission impairment. We have used a Bayesian network to provide a flexible framework for characterizing the uncertainty of the systems and conducting both diagnostic and predictive inference of the infrastructure damage resulting from storm forcings from the same modeling platform using *Netica* (shown in **red**). In essence, the approach has allowed us to consider multiple failure states for each component of the system. The capabilities and missions on an installation are then supported by a network of infrastructure capturing a complex set of asset dependencies. The Bayesian network has allowed us to represent these dependencies efficiently within its structural hierarchy.

Note that varying scales and modeling boundaries have been employed in the assessment of the case study site (Figure 8).

---

[2] Louisiana Coastal Protection and Restoration (LaCPR) study (2005 Hurricane Katrina and 2005 Hurricane Rita), http://www.mvn.usace.army.mil/Missions/Environmental/LaCPR.aspx (Accessed April 2014).

[3] FEMA Region III Storm Surge Study, http://www.r3coastal.com/home/storm-surge-study (Accessed April 2014).

[4] North Atlantic Coastal Comprehensive Study (NACCS) (2012 Superstorm Sandy) http://www.nad.usace.army.mil/CompStudy.aspx (Accessed April 2014).

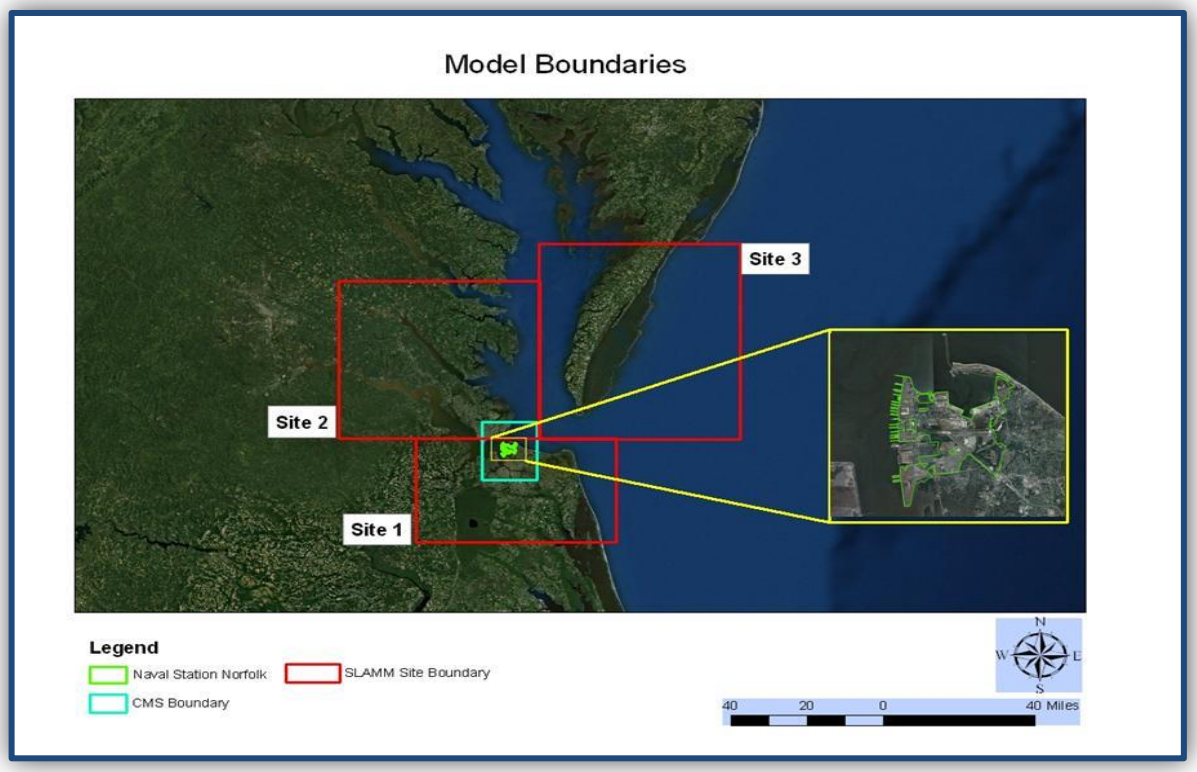

Figure 8. Modeling boundaries for the proof of concept.

As the figure indicates, regional wave and surge modeling have been conducted across the entire region (well beyond the boxes displayed in **red**). Regional assessments of land use/land cover and the geomorphologic condition of the shoreline have focused on *Sites 1*, *2*, and *3* (**red** boxes). Local nearshore process modeling has only been deployed inside the *Site 1* and *2* boundaries (**turquoise** box). Flood routing, infrastructure network modeling, structural damage projections and risk assessments have been restricted to the installation's boundary (**green** boundary inside the pull-out box on the right-hand side of the figure). Solid **green** shading highlights the boundaries of the groundwater modeling domain.

3.1.1 Constraints

The study has been undertaken with the intent of "testing" these techniques rather than performing a comprehensive risk assessment and management application. As such, we have selectively addressed only a handful of critical missions, hazards, and prescribed SLR scenarios to assess. To fully investigate the risks of SLR on a military installation in the region, both a comprehensive review of all drivers and stressors on the system and the identification of all inputs and outputs of the system would be needed to establish the entire range of quantifiable risks associated with future potential SLR thereon. It is important to recognize that we did not predict SLR in this investigation, and the results of the risk-based assessment have not been devised to establish military policy or guidance, but rather have been conceived with the intent of informing decision makers with regard to the potential risks to mission performance under a fixed set of coastal storm and SLR scenarios.

3.1.2 Sea Level Rise Scenarios

Definitions of key terms have been developed and utilized throughout the study to describe critical processes and conditions assessed involved in the analyses. For purposes of this study, the term "sea level" (i.e., mean sea level) refers to the average level of tidal waters, generally measured by tide gauges over a 19-year period (Figure 9).

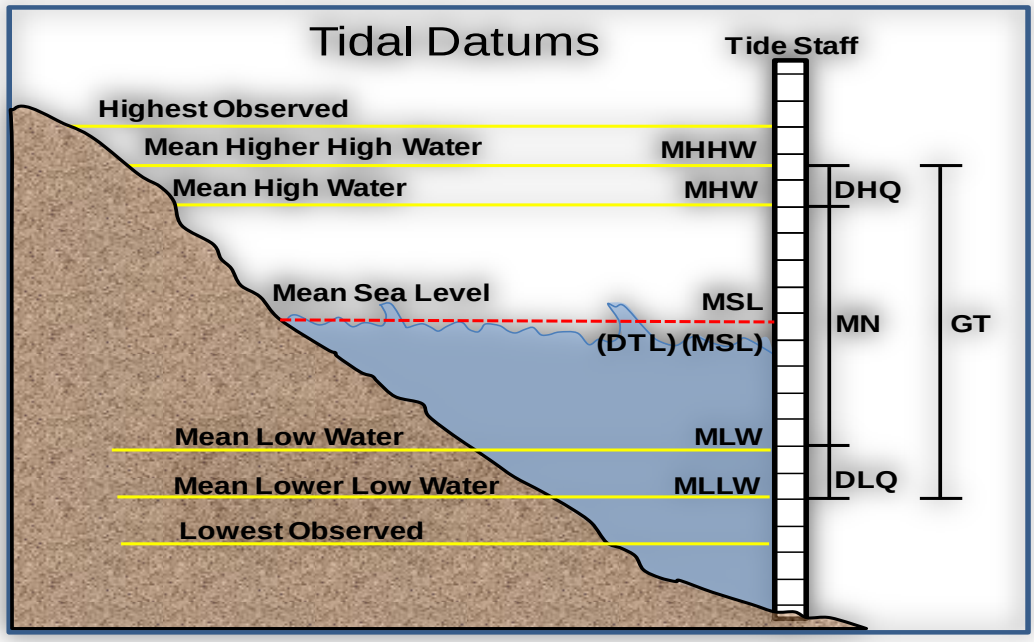

Figure 9. Illustration depicting the relationship between mean SLR (in **red**) and other tidal datums used to establish sea level according to NOAA (adapted from http://tidesandcurrents.noaa.gov/datum_options.html, accessed December 2010).[5]

In general, a datum is defined as a base elevation used as a reference from which to calculate heights or depths. A tidal datum is assumed to be a standard elevation defined by a certain phase of the tide. In order that they could be recovered when needed, such datums are referenced to fixed points known as bench marks. Tidal datums serve as the basis for establishing privately owned land, state owned land, territorial sea, exclusive economic zone, and high seas boundaries.

These measurements indicate the water level relative to the land, and thus incorporate changes in the elevation of the land (i.e., subsidence or uplift) as well as absolute changes in sea level (i.e., rise in sea level caused by increasing the ocean's volume due to expansion or adding water). But the concept of "mean sea level" is considered somewhat artificial because the sea is in constant motion driven by winds and affected by lunar cycles. In order to characterize sea level change, the best we can do is to select a geographic location, calculate the mean sea level at that point, and use this point as a benchmark or datum. Because mean sea level varies around the world (due to local gravity effects), researchers often choose the mean sea level at one specific point

[5] Refer to Table 1 for definitions of these terms.

and use it as the standard "sea level" for all mapping and surveying. For purposes of measuring sea level changes over the course of this study, the North American Vertical Datum of 1988 (i.e., NAVD88) has been adopted.[6] SLR has been projected in relation to this vertical datum for this study. But SLR itself varies on a decadal time scale and is comprised of both a global component and a local component. Thus mean sea level at any given site (e.g., on the study site) can be higher or lower than the NAVD88 datum indicated. Table 1 shows the various tidal datums for the relevant NOAA tide station near the study site (Sewell's Point). Conversions between local mean sea level and NAVD88 datums have been performed using tabulated conversion factors at the relevant NOAA tide station.[7]

Table 1. The project's sea levels have been mapped using the Sewell's Point tide gauge data presented here, which has been correlated to the NAVD88 datum. The NAVD88 datum is approximately 0.077 m higher than this gauge's mean sea level readings.

Datum	Value (m)	Description
MHHW	2.176	Mean High-High Water
MHW	2.114	Mean High Water
DTL	1.756	Mean Diurnal Tide Level
MTL	1.744	Mean Tide Level
MSL	1.748	Mean Sea Level
MLW	1.374	Mean Low Water
MLLW	1.336	Mean Lower-Low Water
GT	0.841	Great Diurnal Range
MN	0.74	Mean Range of Tide
DHQ	0.062	Mean Diurnal High Water Inequality
DLQ	0.038	Mean Diurnal Low Water Inequality
HWI	1.55	Greenwich High Water Interval
LWI	7.83	Greenwich Low Water Interval
NAVD	1.827	North American Vertical Datum
Maximum	3.78	Highest Water Level on Station Datum
Max Date	19330823	Date of Highest Water Level
Max Time	9:18	Times of Highest Water Level
Minimum	0.244	Lowest Water Level on Station Datum
Min Date	19660131	Date of Lowest Water Level
Min Time	10:00	Time of Lowest Water Level

[6] NAVD88 is a geodetic datum that is the official US (and USACE) reference datum for all land based elevations. Horizontal datums are used to describe a point on the earth's surface, in latitude and longitude. The four studies funded by SERDP in response to the SISON agreed to adopt the North American Datum of 1983 (i.e., NAD83) for their assessments. NAD83 is the official datum used for the primary geodetic network in North America.

[7] The project's sea levels have been mapped using the Sewell's Point tide gauge data, which in turn has been correlated to the NAVD88 datum. The NAVD88 datum is approximately 0.077 m (0.25 ft) higher than this gauge's mean sea level readings.

Furthermore, there are several definitions of SLR to consider for the application. For example:

Global mean sea level rise (GMSLR) is defined as the average increase in the level of the world's oceans that has occurred due to a variety of factors, the most significant being thermal expansion of the oceans and the addition of water by melting of continental ice sheets, ice caps, and glaciers.

Local sea level rise refers to the change in sea level relative to the elevation of the adjacent land, which can also subside or rise due to natural and human-induced factors.

Relative sea level rise (RSLR) refers to the combination of worldwide average increases in sea level (*global sea level rise*), and the changes in vertical elevation of land surface (*local sea level rise*).

Sea level rise (SLR) utilized throughout this report, referred to the scenarios mandated for the study by the SISON-09-05[8] (SERDP's "Statement of Need" under which the current work has been funded).

To reiterate, this study has not produced a forecast of future SLR rates. Rather, it has evaluated the implications of five relative SLR scenarios dictated by the SISON. These scenarios have been assumed to be cumulative rises of 0.0, 0.5, 1.0, 1.5, and 2.0 meters (m) in mean sea level. The period of analysis was prescribed by SERDP – namely 100 years starting at 2000 and ending in 2100. These rates of rise coincided with the work of the U.S. Army Corps of Engineers (2011), which itself was based upon the formulation laid out by the National Research Council (NRC) (1987) that led to a set of rate-of-rise curves (Figure 10) and underlying formulas for the five scenarios represented by the quadratic relationship:

$$S - S_0 = a\,(Y - Y_0) + b\,(Y - Y_0)^2 \qquad \textbf{(1)}$$

where S and S_0 represent the sea level at years Y and Y_0, a is the linear rate of SLR, and b is the rate of increase in the rate of rise (acceleration). The unit for a is L/T while the unit for b is L/T^2 where L represents length and T is time in whatever units of measure are being used.

[8] http://www.serdp.org/content/download/7654/96571/file/SISON-09-05%20Sea%20Level%20Rise%, Accessed November 2012.

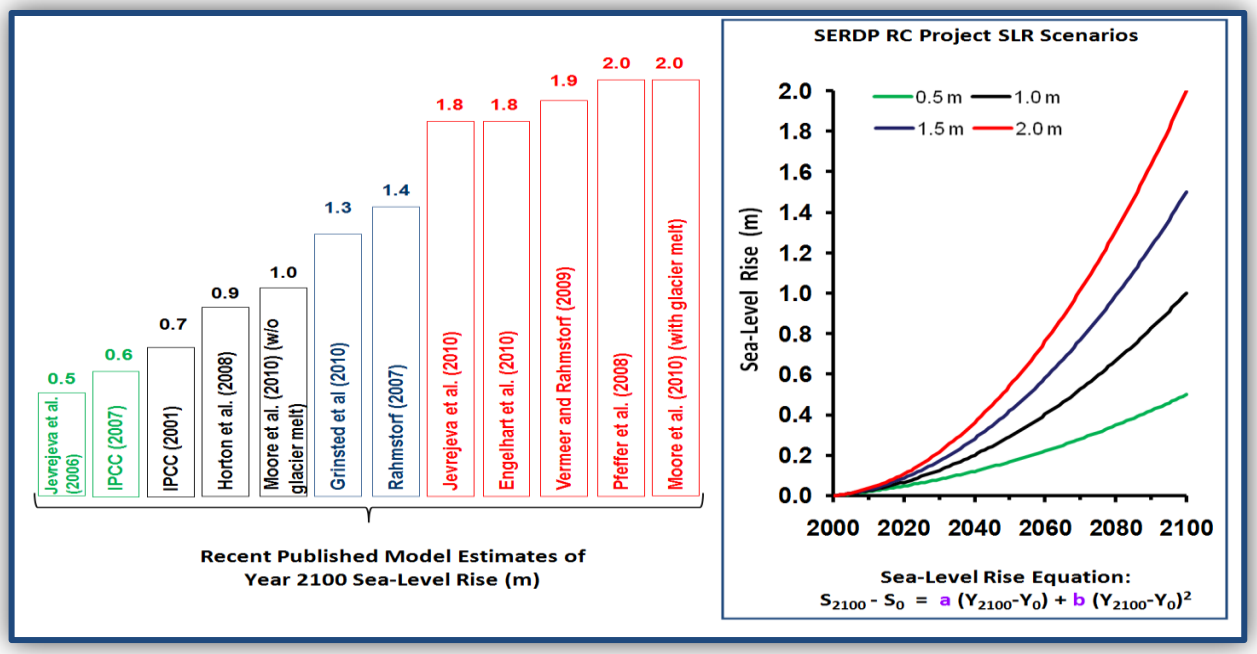

Figure 10. On the right, the SERDP-prescribed SLR scenarios used in this study to evaluate risks, and on the left, a series of recently published maximum SLR projections suggesting that the SERDP prescribed scenarios are reasonably supported in the peer reviewed literature.[9]

Taking $Y_0 = 2000$ as the initial reference year and considering SLR relative to it, then $S_0 = 0$. In this way we have simplified *Equation 1* to the straightforward form:

$$S = a\,Y + b\,Y^2 \qquad \textbf{(2)}$$

where the year Y is now years after 2000 (i.e. 2000 = 0, 2005 = 5, etc.) and S is the sea level relative to zero at year 2000. Table 2 below gives the coefficients a and b as a function of the specified year-2100 end point values of SLR. In practice, the S_0 term has been adjusted to account for the local mean sea level condition at time Y_0.

Table 2. Coefficients in the quadratic SLR formula used in the study.

Scenario Designation	2100 Sea Level Rise (m)	a	b
NRC I	0.5	1.700×10^{-3}	3.300×10^{-5}
NRC II	1.0	2.030×10^{-3}	7.970×10^{-5}
NRC III	1.5	2.570×10^{-3}	1.243×10^{-4}
SERDP	2.0	2.570×10^{-3}	1.743×10^{-4}

More importantly, the drivers underlying SLR do not need to be identified to be able to quantify the risks in our study. Subsidence, global climate change, ocean expansion, glacial melt, or even

[9] Graphics adapted from Donoghue et al. 2010 presentation at the SERDP/ESTCP Partner's Conference - http://symposium.serdp-estcp.org/content/download/9024/108368/version/1/file/2A_Donoghue.pdf (Accessed December 2010).

a combination of these various factors could lead to sea level changes. It is more important for this study to determine the rate of rise rather than focus on the causation.

3.1.3 Assumptions

The following assumptions govern the application of our approach on the case study site.

1) **Sea levels will rise within the range of uncertainty as described by the SERDP SISON.**[10]

2) **No storm severity amplifications have been assumed.** The current effort has not been funded to undertake a sensitivity analysis nor predict changes in storm parameter arising from global climate change. We therefore have assumed that all storm parameters will remain constant, and only the resulting water levels, inundation, wave heights, and sediment transport will be affected by the five prescribed SLR scenarios.

3) **Storm frequency has been held constant.** This study has only been scoped and funded to consider potential increases in floodwater levels, maximum wave heights, sediment loadings, and winds – not to predict potential changes in frequency or intensity of storms

4) **No changes in wind patterns and intensities altered by climate change have been assumed.** In that same vein, it was further assumed that changes in winds will be due solely to alterations in land cover (increases in open water surfaces) and associated changes in surface drag. No additional climate change drivers and stressors (i.e., changes in sea surface temperatures, ocean currents, salinity, etc.) have been used to amplify the winds in the storm simulations.

5) **No feedbacks have been assumed between the flood routing and nearshore assessments.** There currently exists no hard-coded feedback loop between the nearshore process models and surface flood routing models used in this study. Thus, inland flooding has not been included in the nearshore process results because the nearshore process models are run prior to the flood routing models. For the purpose of this study, we have assumed there will be no increase in water levels, wave heights, current velocities, or the sediment rates due to feedbacks from inland flooding changes in routing. The rationale being that nearshore processes serving as inputs to flood routing on land will be expected to be orders of magnitude larger, thus overwhelming any potential feedbacks within predictive model uncertainty.

6) **Historical precipitation patterns and surface temperatures have not been amplified by global climate change in surface floodwater route modeling.** The

[10] http://www.serdp.org/content/download/7654/96571/file/SISON-09-05%20Sea%20Level%20Rise%, accessed January 2011.

current study assumes statistical stationarity in precipitation patterns and surface temperatures. Study efforts have been based on rainfall runoff simulations using precipitation intensities that corresponded to the simulated tropical and extra-tropical (nor'easter) storms (water levels at the 50- and 100-year (yr) return intervals).[11] We have used historical records to generate rainfall runoff simulations for lower storm intensities (water levels at the 1- and 10-yr return periods).

7) **Retreat/fortification issues remain unresolved in the analysis.** Although a variety of public/private landowner responses exist with regards to issues of fortification vs. retreat of shorefront properties in the study area, no assumption(s) have been made in the analyses with regards to this issue, and the area has been assessed as if its current state is perpetuated into the future.[12]

8) **A status quo condition has been assumed with regards to climate change mitigation in the region.** For this study, we have assumed that there will be no change in current operations and management on the study site and or in the surrounding area. We have not assumed nor have we incorporated into the analysis potential mitigation responses to SLR by the military or the surrounding civilian community.

[11] Statistical techniques, through a process called frequency analysis, have been used to estimate the probability of the occurrence of a given coastal storm event. The recurrence interval has been based on the probability that the given event will be equaled or exceeded in any given year as follows:

Recurrence interval	Probability of occurrence in any given year	Percent chance of occurrence in any given year
100-yr	1 in 100	1%
50-yr	1 in 50	2%
10-yr	1 in 10	10%
1-yr	1 in 1	100%

[12] In the face of rising sea levels, land owners would likely either retreat inland, or fortify in place. We have not incorporated either of these scenarios into our analysis, and instead have assumed that no change would take place. Future potential applications could certainly incorporate these alternative scenarios into the risk assessment.

3.2. Geomorphic and Geologic Assessment Methodology

In response to SLR, loss of land from erosion or wetlands converting to open water could increase open water fetch, which would allow larger waves to form during storms. This could contribute to hazardous conditions at docks, reduce berthing times, damage infrastructure, and contribute to more flooding of low areas. As a first step in our approach, a geomorphic assessment must be undertaken to characterize the geologic conditions in the study area, with the intent of predicting the extent of coastal and landform alteration that might occur under the various SLR scenarios (Figure 11).

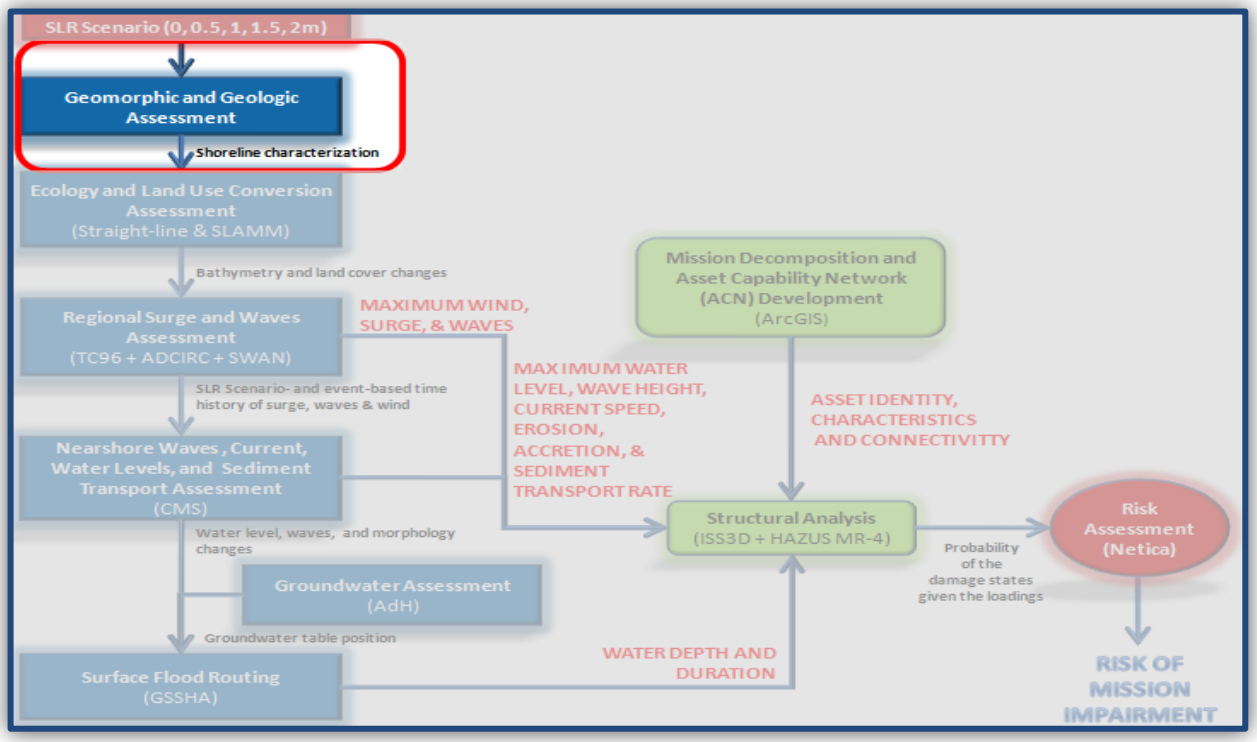

Figure 11. Project analysis and tasks: *Geomorphic and Geologic Characterization*.

To complete the assessment, a review of current geological literature is undertaken to assess the degree to which the study area is experiencing land subsidence (a contributing factor to SLR in the region). As the figure indicates, outputs (*i.e.*, shoreline characterizations in the form of GIS shapefiles) from the assessment are then used in the next step to inform the land use conversion analysis.

3.2.1 Classification Strategy for the Case Study Area

Given the potential effects of the James River and Delmarva Peninsula on storm surge, it was necessary to map the degree of shore armoring to provide input for the land use conversion models. A simplified 5-category shoreline classification scheme/procedures was developed to map the shore characteristics.

This analysis consisted of interpreting shoreline type for the James River estuary and surrounding region using various sources, preparing ESRI shapefiles, and spot-checking the interpretations during site visits. Interpretation of the shore type was based on visual inspection of aerial and ground-level photographs from Google™ Earth Pro, with most imagery from 2006-2009, and elevation data from U.S. Geological Survey topographic maps. A simple five-category shoreline classification was developed to represent overall geomorphic conditions in the area. Using ArcGIS™ software version 9.3, we imported a NOAA vector shoreline from 1993 and topographic maps in the form of georeferenced raster graphics. We then converted the 1993 shoreline into the appropriate classification types throughout the region. For example, if a 3 kilometer (km) stretch of shore was high banks, the appropriate part of the shoreline was truncated, copied, and labeled as bluffs/bank within the database. Site visits on August 23-26, 2010, provided additional details and refinement of the interpretations.

Prior experiences throughout the United States indicate that once property has been developed for commercial use or as residential lots, the area was vigorously protected against real and perceived erosion threats. Homeowners often build seawalls, dikes, or revetments to mark the seaward line of their property to hold the line against any encroachment of the sea. Municipalities invariably support homeowners in their armoring efforts because towns and counties derive significant tax revenues from valuable coastal property. Even sheltered coasts consisting of lightly developed sand/silt/clay banks have been extensively armored (Committee on Mitigating Shore Erosion along Sheltered Coasts 2007).

Inputs for the geomorphic and shoreline characterization included aerial photography, contemporary shoreline position vector data, elevation data (from topographic maps), and observations from site visits. Discussions with USACE employees at Norfolk District provided additional information. The study area encompassed the lower portion of Chesapeake Bay and the lower James River (Figure 12).

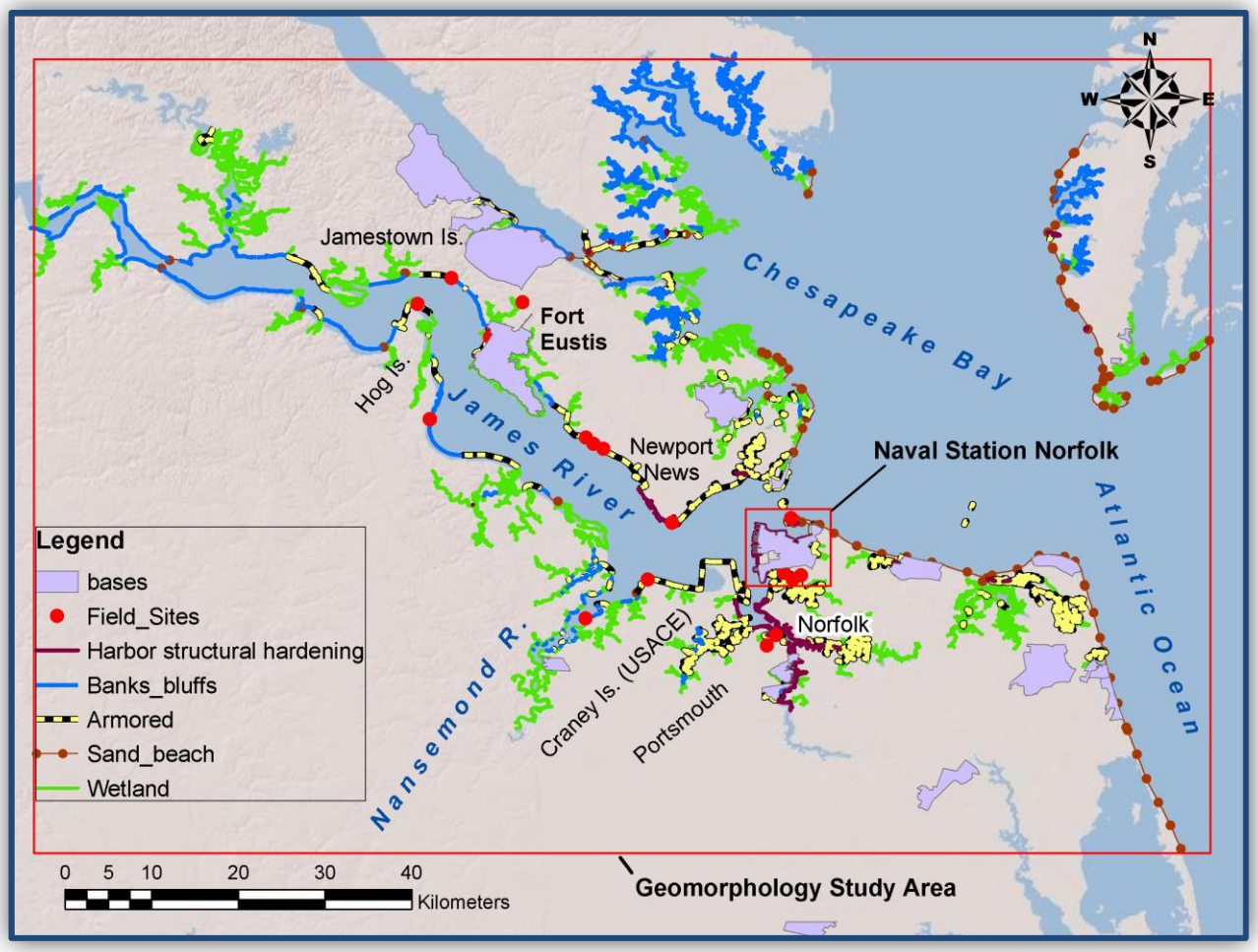

Figure 12. Study area for the geomorphological assessment.

NSN and the Norfolk-Portsmouth port complex were within the smaller red box in the figure. Mapping of the shore morphology extended 90 km up the James River and to a lesser distance up the Chesapeake Bay, Delmarva Peninsula, and along the Atlantic Ocean coast. Shoreline position was downloaded from NOAA.

3.3. Ecology and Land Use Conversion Assessment Methodology

In the next century, military assets, capabilities, and operations will be directly affected by a combination of inundation from SLR and coastal storm hazard impacts. Indirect effects of geomorphic evolution and resultant changes in the ecological communities closely associated with these military assets could further magnify these impacts. The next step in our approach requires an assessment of land use conversion to capture geomorphological and ecological response to SLR (Figure 13).

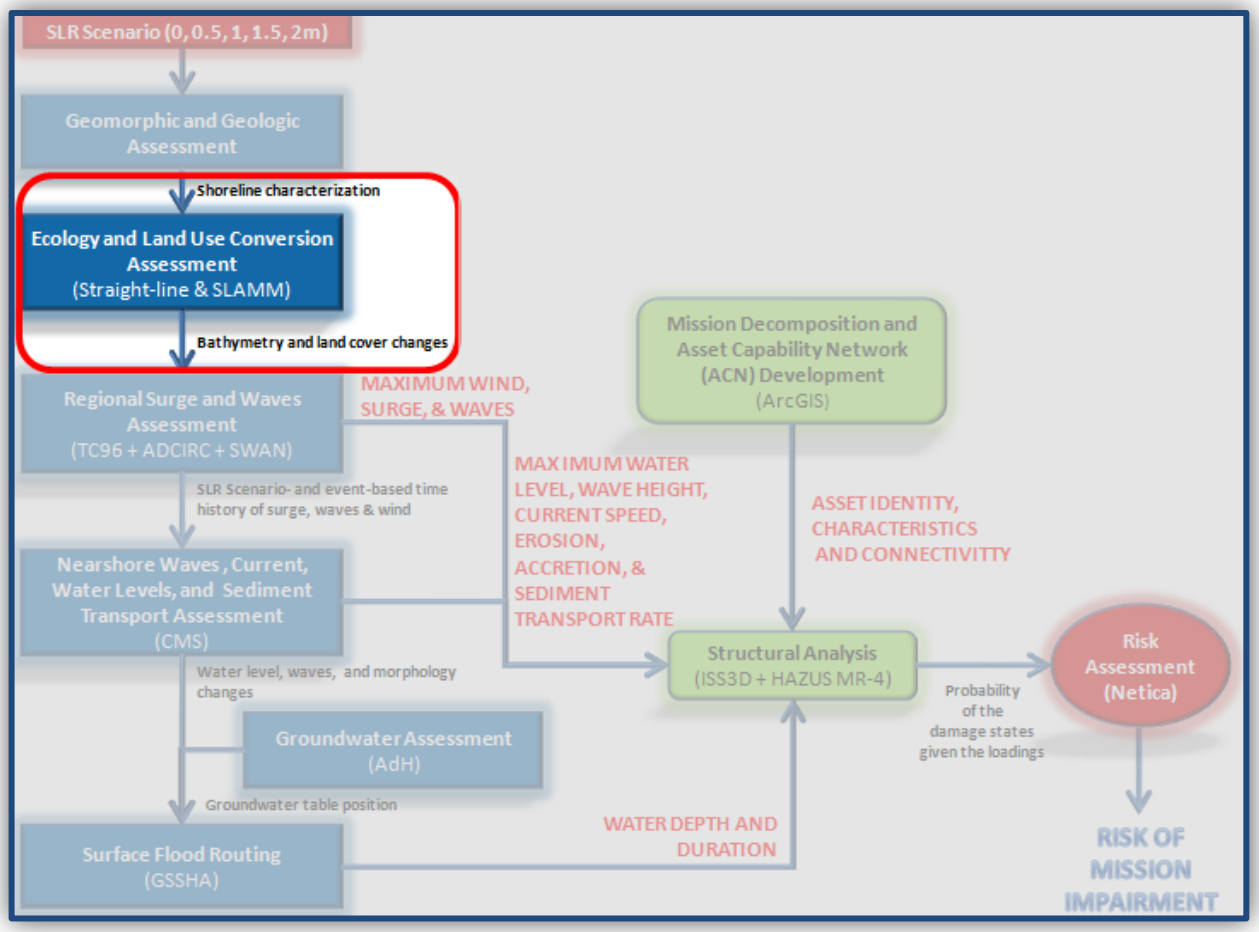

Figure 13. Project analysis and tasks: *Ecology and Land Use Conversion Assessment*.

The goal is to model dominant processes and simulate successive ecosystem conversions and shoreline evolutions under various SLR scenarios at the regional scale. The idea is to map land use and land cover changes, predict biome shifts, and characterize the ecological consequences of ecosystem alterations. In other words, the assessment is used to predict the ecosystem response to SLR scenarios. As the figure illustrates, shoreline characterizations derived in the previous step (i.e., the geomorphological assessment described in *Section 3.2 above*) are incorporated into these simulations to better characterize critical geomorphological conditions (i.e., drivers of ecological change). Outputs generated in this modeling effort (*i.e.*, GIS shapefiles characterizing shifts in geomorphology and vegetative coverage) are then used in the next step to inform the regional storm simulations.

3.3.1 Model and Approach

In the past, the majority of SLR analyses have focused solely on the effects of SLR-driven inundation, disregarding changes to overall storm susceptibility triggered by barrier island migration, coastal erosion, wetland drowning, and saltwater intrusion (Gesch et al. 2009). At the time of this study, comprehensive, mechanistic accounting of these various processes, namely

the ability to forecast geomorphic evolution, was not only challenging, but intractable (Pilkey and Cooper 2004, Stolper et al. 2005, Cowell et al. 2006, Gutierrez et al. 2009, Titus and Craghan 2009). In an attempt to move beyond "inundation-only" analyses, Park et al. (1986) created the Sea Level Affecting Marsh Model (SLAMM), a model designed specifically to "simulate the dominant processes involved in wetland conversions and shoreline modifications" in response to SLR scenarios (Clough et al. 2010).[13]

In effect, SLAMM is a spatially-explicit, raster-driven model designed to apply a set of theoretical, empirical, and/or qualitative "rules" to capture the effects of SLR as they pertain to six key processes: inundation, salinity, saturation, accretion, erosion, and barrier island overwash (Clough and Larson 2010, Clough et al. 2010). Three of these processes (i.e., inundation, salinity, saturation) incorporated in SLAMM are used to examine thresholds for switching to an alternative habitat type. The remaining processes (i.e., accretion, erosion, overwash) are used to characterize internal and external processes acting to maintain or degrade the current habitat type. Table 3 briefly reviews SLAMM's handling of the six processes for the project.

Table 3. Description of processes influencing geomorphic change in the SLAMM modeling of our case study area. For more background, refer to Clough and Larson 2010 and Clough et al. 2010.

Process	Description
Inundation	We have specified elevation thresholds for each habitat type relative to the five water surface elevations (garnered from local tidal observations): 1. Mean lower low water (MLLW): daily mean of lower low water 2. Mean tide level (MTL) 3. Mean higher high water (MHHW): daily mean of higher high water 4. Salt boundary: the elevation expected to flood at least once per month
Salinity	An optional salinity module is applied to examine habitat switching. This module assumed salinity was distributed throughout the estuary based on a linear salt wedge with user-specified slope and annually-averaged freshwater inflow.
Saturation	Rises in the water table and resultant habitat switching are accounted for using a simple model approximating these changes as a function of distance to open water.
Accretion	Rate of sediment accumulation (organic and inorganic) was specified based on land cover type or by a model as a function of elevation, salinity, and proximity to channels.
Erosion	Coastal erosion was specified in the model as a function of the maximum fetch length a particular cell was exposed to. Based on Knutson et al. (1981), erosion was triggered when fetch exceeded 9 km with the rate of lateral erosion specified by the user.
Overwash	Within the study area, barrier islands of less than 500 m were assumed to be overwashed during large storm events at a user-specified interval (SLAMM defaults to a 25 year overwash recurrence). SLAMM then applied a series of assumptions regarding the effects of overwash events on beach and marsh morphology near any barrier islands.

Three of the primary components of SLAMM center on the specification of thresholds that induced habitat switching. When switching occurred, SLAMM 6 applies a decision tree

[13] Since its initial deployment in 1986, SLAMM has undergone multiple revisions (six in total) and has been applied broadly for predicting the long-term effects of SLR on wetlands and shorelines. Refer to Park 1991; Park et al. 1989a, 1989b; Titus et al. 1991 for nationwide applications; Glick et al. 2008 for a Chesapeake Bay application; Galbraith et al. 2002, 2005 for applications in Delaware Bay; Mickler 2008, Mickler and Welch 2009 for applications in North Carolina; Ehman 2008 for an application in South Carolina; Lee et al. 1992, Craft et al. 2009a for applications in Georgia; Park et al. 2003 for an application in San Francisco Bay; and Park et al. 1993, Glick et al. 2007 for applications in Puget Sound.

specifying the habitat type resulting from the switch (Table 4). For instance, when a scrub-shrub marsh has been inundated, SLAMM 6 assumes that it is converted to a salt marsh community. On the other hand, when the same scrub-shrub marsh switches due to coastal erosion, it is assumed to convert to tidal flats.

Table 4. SLAMM 6 decision tree for habitat switching (from Clough et al. 2010).

Converted From:	Inundation: Non-adjacent to Open Water on Fetch < 9 km (non tropical systems) Converts To:	Erosion: Adjacent to Open Water and Fetch > 9 km (erosion) Converts To:
Dry Land	Transitional salt marsh, ocean beach, or estuarine beach, depending on context (see below)	Erosion of dry land was ignored.
Swamp	Transitional salt marsh	Erosion to Tidal Flat
Cypress Swamp	Open Water	Erosion to Tidal Flat
Inland Fresh Marsh	Transitional Salt Marsh	Erosion to Tidal Flat
Tidal Swamp	Tidal Fresh Marsh	Erosion to Tidal Flat
Tidal Fresh Marsh	Irregularly Flooded Marsh	Erosion to Tidal Flat
Scrub-Shrub, Irregularly Flooded Marsh	To Salt Marsh	Erosion to Tidal Flat
Regularly Flooded Marsh	To Tidal Flat	Erosion to Tidal Flat
Mangrove	To Estuarine Waters	Erosion & Inundation to Estuarine Water
Ocean Flat	To Open Ocean	Erosion to Open Ocean
Tidal Flat	Erosion, Inundation to Estuarine Water	Erosion to Estuarine Water
Estuarine Beach, Ocean Beach	Open Water	Erosion to Open Water

In addition to the physical and biological processes described above, SLAMM 6 provides an algorithm that examines the relatively "social" aspects of fortification decisions (refer again to *Section 3.2 above* for the origination of these determinations). The model allows us to specify areas in a Boolean format as either "protected" or "unprotected." Protected lands are not allowed to undergo geomorphic change during the simulations. In other words, by identifying lands as "protected," the assumption is made that an infinite amount of resources have been expended to maintain flood protection through engineered measures such as levees and floodwalls.

3.3.2 Modeling Inputs

3.3.2.1 Model Domain and SLR Definition

For the case study analysis, we deployed the SLAMM model on a regional scale at three sites (refer to *Sites 1-3* in Figure 14) using the five prescribed SLR scenarios (i.e., 0.0, 0.5, 1.0, 1.5, and 2.0 m) and a 100 year period of analysis (2000-2100).

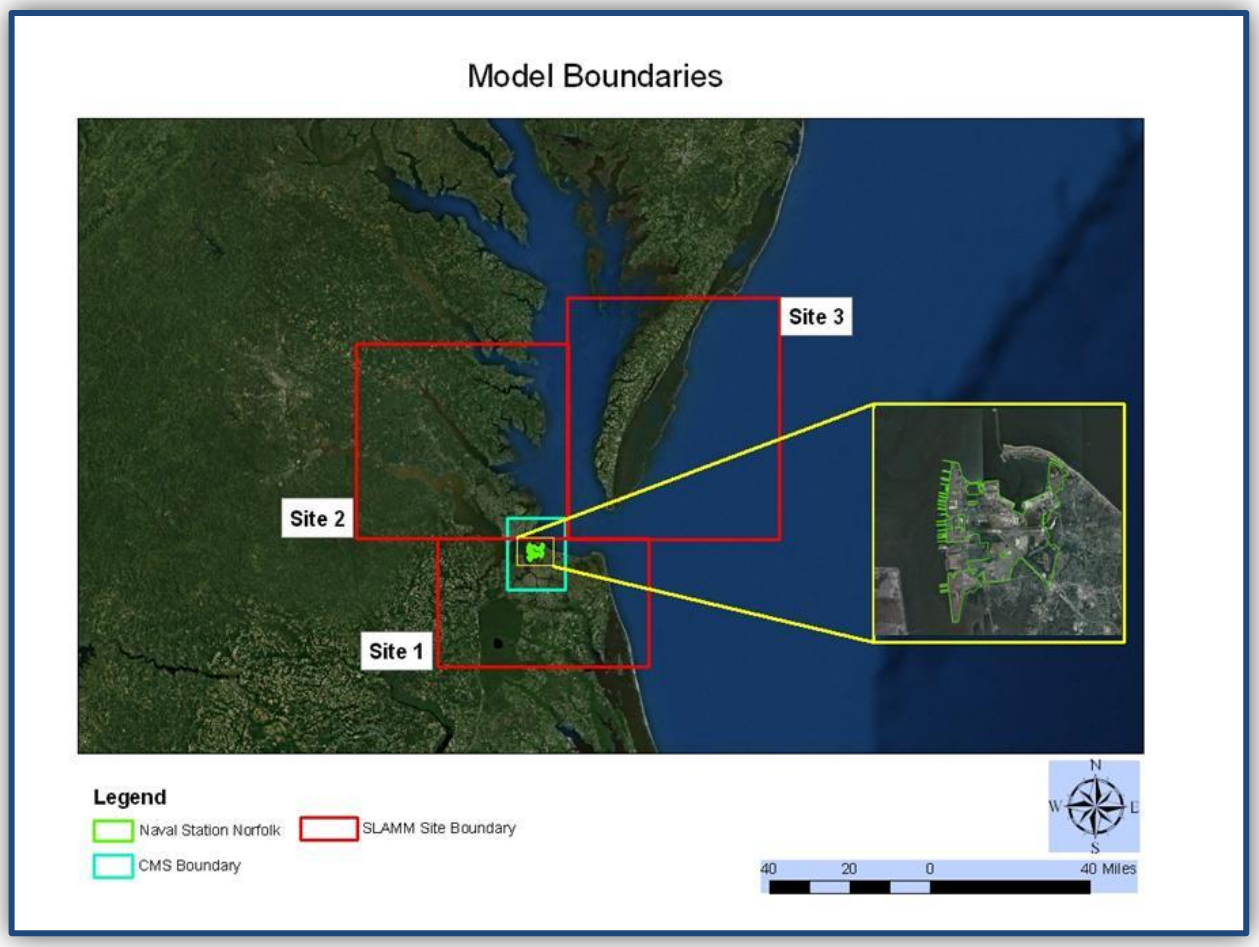

Figure 14. Regional assessments of land use/land cover and the geomorphologic condition of the shoreline were conducted in Sites 1, 2, and 3 (red boxes) using SLAMM 6.0.

We varied the rates of sea level rise non-linearly for each scenario with the intent of reaching the desired sea level elevation at the end of the 100 year period. Modeling started at time zero or the year 2000. We executed SLAMM by entering the desired level (e.g., 2.0 m for the worse-case scenario) which was attained by the year 2100. SLAMM computed the rate of rise within this interval by scaling the IPCC 2007 A1B Mean sea level rise curve up to reach 2.0 m after 100 years. Note that this rate of rise followed closely to the USACE modified National Research Council (NRC) 1987 Curve III. SLAMM did not allow specific rates of rise to be hard-coded into the simulation. However, due to the small differences between the two curves, model results were not appreciably different.[14]

[14] Although beyond the scope of this analysis, sensitivity analysis could be used to investigate these differences further.

3.3.2.2 Elevation, Accretion and Erosion Parameterization

In 2008, the National Wildlife Federation (NWF) applied SLAMM (version 5) to examine the effects of SLR on Chesapeake Bay (Glick et al. 2008). For that effort, twenty representative sites were chosen from across the region, and trends in habitat change and loss were examined. Although their analyses included the Norfolk, VA area, newly available data sources, a new model version (SLAMM 6), and additional computation capabilities, warranted the re-application of SLAMM for our case study. Our new analysis has now taken into consideration site-specific factors such as land subsidence and marsh accretion which have significantly altered land elevations since 2008. For our simulations, we emulated NWF's approach (Glick et al. 2008, page 115-116) and used a simplifying assumption of localized linear rates of subsidence and accretion (i.e., they will not change) over time (3.75 mm/yr) to capture these unique governing processes.[15]

In past studies, assessments of coastal change with SLR were found to be highly dependent upon the accuracy of elevation data used in the analysis (Gesch et al. 2009). Following the NWF assessment, and to address these concerns, we obtained additional high resolution elevation data through Light Detection and Ranging (LiDAR) elevation data collection as well as recent bathymetric surveys. These data were compiled by an interagency team to develop a Digital Elevation Model (DEM) (accurate at a 10-meter resolution) containing both topographic and bathymetric elevations of the region (Forte et al. 2011). For the model domains shown in Figure 14 above, the elevation map was used to create a modeling grid. A 20 m^2 cell size was selected as a compromise between computational speed and data resolution. Given SLAMM's significant dependence on elevation thresholds, these data alone were deemed critical enough to characterize geomorphic evolution.

Elevation, accretion, and erosion rates were adopted from the NWF analysis (Glick et al. 2008, Table 5). Overwash frequency was taken as the model default value (1 event per 25 years).

[15] Note that this assumption could be inaccurate. Over time, both accretion and subsidence rates could change for a number of reasons, including shifts in biomes, changes in sedimentation and erosion rates, and withdrawals of groundwater. Ongoing monitoring will be necessary to hone these values. Nevertheless, this demonstration provided a useful snapshot of the potential impacts, which will help inform critical on-the-ground installation management decisions in the near and long term.

Table 5. Model parameterization for the three regional sites specified in Figure 14 above.

Parameter	Site 1: Norfolk	Site 2: James Peninsula	Site 3: Delmarva Peninsula
Elevation Inputs (m)			
Tidal Range	0.68	0.51	0.66
Mean tide level (MTL)	-0.10	-0.09	-0.10
Salt Boundary	0.45	0.34	0.44
Accretion rate (mm/yr)			
Salt marsh	3.9	5.0	3.9
Brackish marsh	4.7	6.0	4.7
Tidal fresh marsh	5.9	7.5	5.9
Beach	0.5	0.5	0.5
Erosion rate (m/yr)			
Marsh	1.8	1.8	1.8
Swamp	1.0	1.0	1.0
Flat	6.0	6.0	6.0

3.3.2.3 Shoreline Protection Parameterization

Kirwan and Murray (2008) demonstrated the importance of adequately representing dikes and shoreline hardening when forecasting coastal evolution, and input based on the updated shoreline classification was expected to produce more realistic predictions of coastal transformation under various SLR scenarios. In the study area, armored or artificial shorelines were commonly found in most urban/suburban areas and in rural areas where private property was vulnerable to erosion. Protected shorelines were incorporated into the model to represent areas that would not experience geomorphic changes or habitat switching. Using aerial photography validated by ground-truthing, a shoreline protection classification was developed for the region (Figure 15) and parameterized in the model.

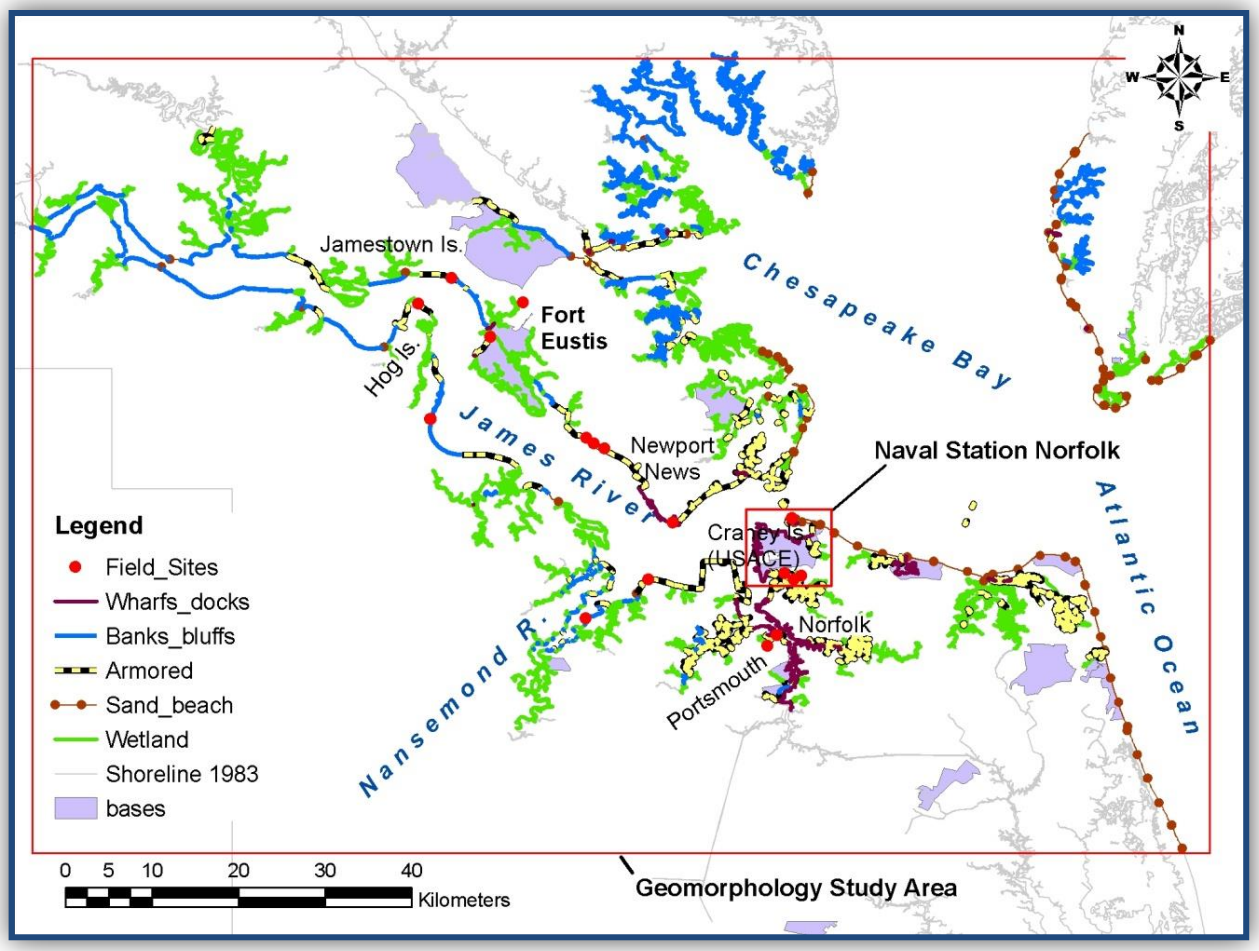

Figure 15. Shoreline protection (i.e., armoring shown here as a dotted yellow line) serves as a critical input into the SLAMM 6.0 analysis.

3.3.2.4 Land Use Land Cover Parameterization

The primary input to the SLAMM model was the classification of Land Use and Land Cover (LULC). In the previous NWF analysis of Chesapeake Bay, wetland classes were determined based on the 1996 National Wetland Inventory (NWI) maps (Glick et al. 2008). These wetland classes and coverage areas were updated with 2001 NWI maps and merged with 2001/2002 National Land Cover Database (NLCD) maps (http://www.mrlc.gov) to provide more current land cover classifications. SLAMM assumed that wetland types occurred within a range of elevations based on the user-specified elevation values (Figure 16).

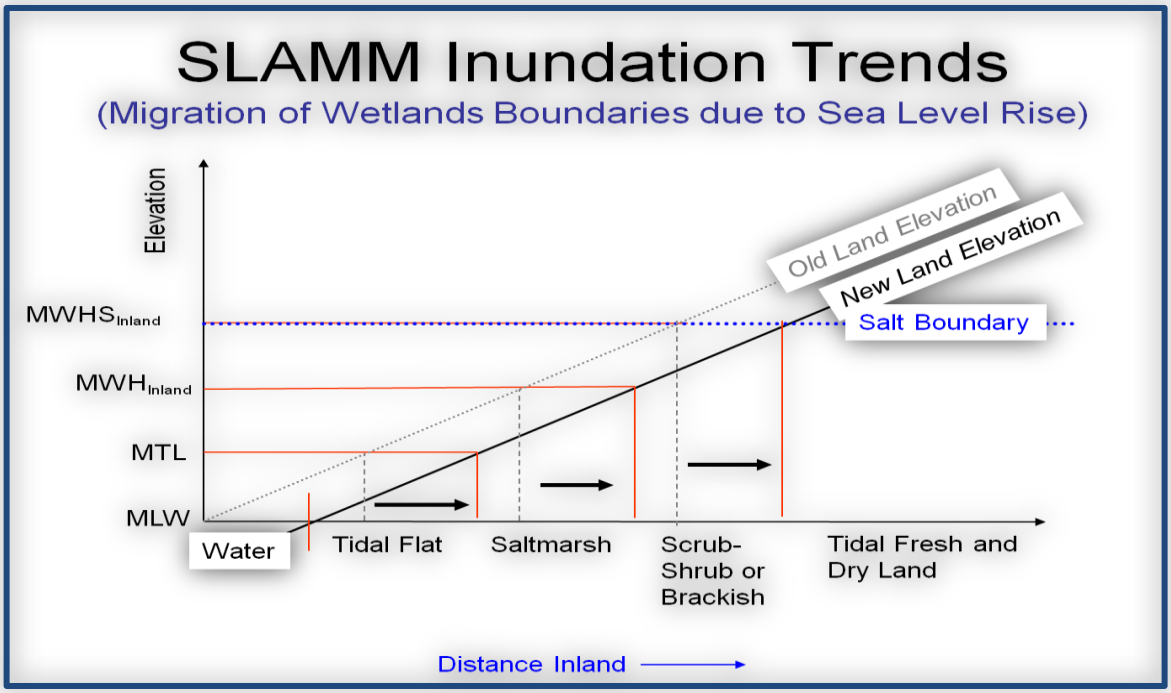

Figure 16. Heuristics driving LULC classifications in SLAMM 6.0 (available online at http://warrenpinnacle.com/prof/SLAMM/SLAMM_Presentation.ppt, accessed November 2012).

For instance, salt marshes reside in areas between MTL and MHHW elevations. SLAMM 6 provides the capability to validate these input elevation thresholds by cross-referencing the elevation thresholds with the observed NWI data files (Clough et al. 2010).

Although the model was executed using SLAMM's 22 land classification types, analyses was aggregated based on categories of similar physiography for clarity of presentation here (Table 6).

Table 6. Simplification of SLAMM land classification. Classifications were carried through the analysis as SLAMM types and simplified only for presentation of results.

SLAMM Classification	Simplified Classification
Developed Dry Land	Dry Land
Undeveloped Dry Land	Dry Land
Non Tidal Swamp	Swamp
Cypress Swamp	Swamp
Inland Fresh Marsh	Marsh
Tidal Fresh Marsh	Marsh
Transitional Marsh/Scrub Shrub	Marsh
Regularly Flooded Marsh	Marsh
Mangrove	Marsh
Estuarine Beach	Beach-Shore
Tidal Flat	Flat
Ocean Beach	Beach-Shore
Inland Open Water	Water
Riverine Tidal Open Water	Water
Estuarine Open Water	Water
Open Ocean	Water
Irregularly Flooded Marsh	Marsh
Inland Shore	Beach-Shore
Tidal Swamp	Swamp

The model reproduced NWI classifications (Figure 17) of sufficient quality for the elevation thresholds specified in Table 5 above.

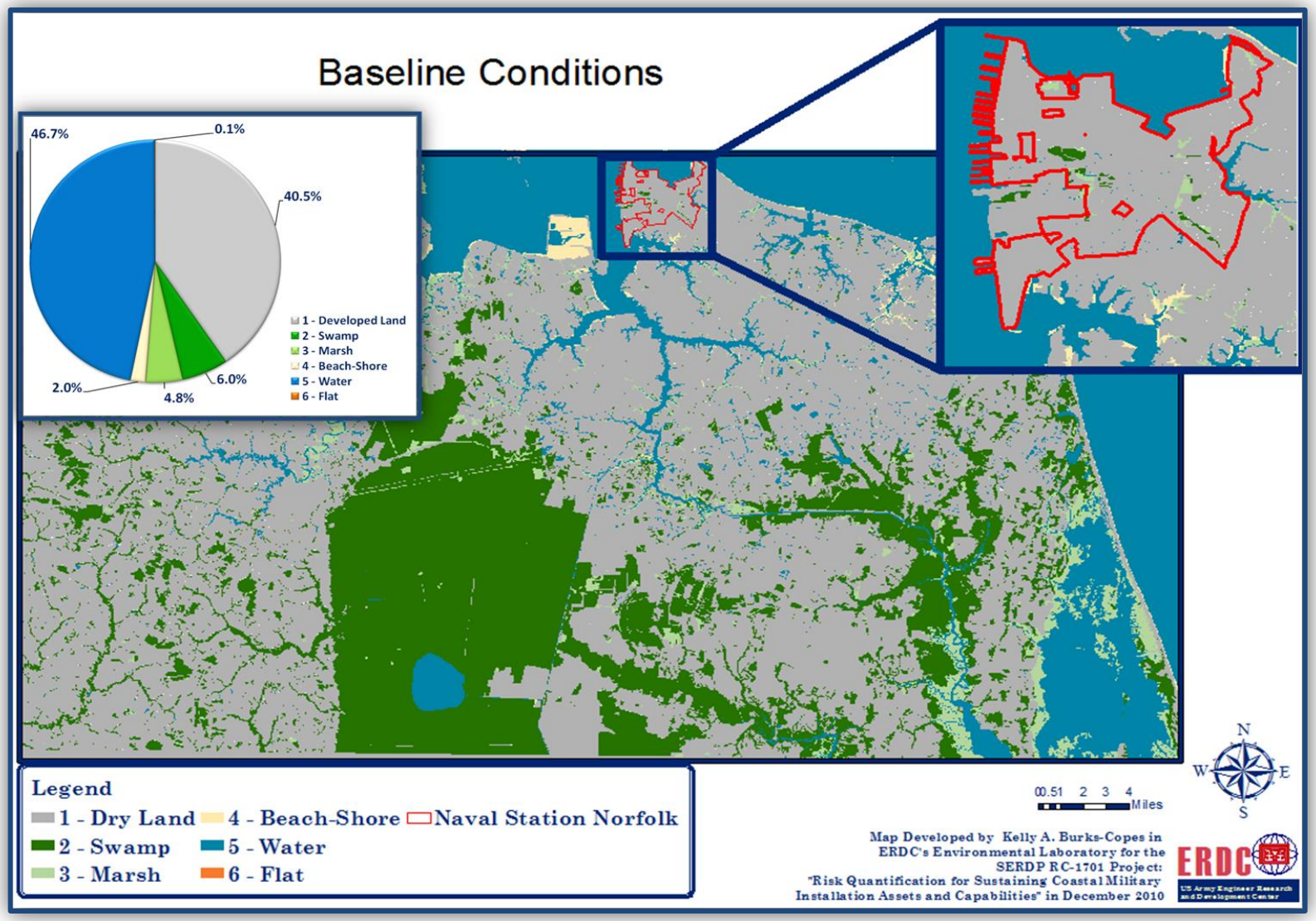

Figure 17. Initial land classification representing year 2000.

As the figure indicates, the majority of the LULC coverage in 2000 was dedicated to developed/undeveloped dry areas (40.5 percent) and water (46.7 percent) (Table 7). The remaining 12.8 percent was distributed across more natural habitats (i.e., marshes, beaches, flats, and swamps).

Table 7. Existing (2000) land coverage at each SLAMM domain site within the study area.

Land Cover	Site 1 (ha)	Percent (%)	Site 2 (ha)	Percent (%)	Site 3 (ha)	Percent (%)
Dry Land	216,676	56.1%	613,642	66.0	79,557	8.5
Swamp	80,256	20.8%	41,254	4.4	13,488	1.4
Marsh	12,030	3.1%	51,155	5.5	43,769	4.7
Beach / Shore	2,386	0.6%	2,173	0.2	39,363	4.2
Flat	0	0.0%	0	0.0	1,661	0.2
Water	75,029	19.4%	221,778	23.8	754,405	80.9
Total	**386,376**	**100.0%**	**930,003**	**100.0**	**932,243**	**100.0**

3.3.2.5 Model Sensitivity

Uncertainty associated with long-term modeling of open systems such as coasts has been shown to be significant (Cowell and Zeng 2003). Given the SLAMM model's complexity and simulation configurations, computational times ranged from approximately 8 to 22 hours per 100-yr simulation on a 64-bit workstation. As such, a complete uncertainty analysis exploring ranges of all parameters was infeasible under the scope of this study. However, six scenarios were identified to "bound" the uncertainties associated with the analysis (Table 8).

Table 8. Scenarios applied to examine SLAMM sensitivity.

Scenario	Description
S1	Baseline scenario where developed dry lands were protected based on existing shoreline protection
S2	Modified S1 such that all dry lands were protected.
S4	Modified S1 such that no developed lands were protected and shoreline erosion was allowed to freely occur.
S5	Modified S1 such that storm frequency was increased from 1 in 25 years to 1 in 10 years.
S6	Modified S1 by assuming 20% lower accretion rates and 20% higher erosion rates.
S7	Modified S1 by assuming 20% higher accretion rates and 20% lower erosion rates.

Scenario 1 (*S1*) represents the baseline condition with inputs specified in Table 5 above. SLAMM treated shoreline protection as a binary input where cells were either protected or not. As such, *S2* and *S4* presented alternative shoreline protection scenarios intended to represent the range of potential decisions regarding "defense" versus "retreat" of coastal communities. *Scenarios 5-7* presented alternative model parameterizations. *S5* represented a condition where overwash of barrier islands occurred more frequently. In their analysis of the Georgia coast, Craft et al. (2009b) observed that relative to SLR, SLAMM was somewhat insensitive to accretion and erosion rates. We therefore sought to replicate (or refute) these findings with our own test of SLAMM's sensitivity. *S6* and *S7* alter accretion and erosion rates by 20% of their expected values based on Hamby's (1995) recommendations for simplistic sensitivity testing of model input parameters. In addition to the six input scenarios described, our three diverse test sites provide an opportunity to examine sensitivity to existing land cover (refer again to Table 8

above). In total, the model was executed 90 times for the study region (five levels of SLR, six sensitivity scenarios, and three regional sites).

3.4. Regional Surge and Waves Assessment Methodology

Although storms occur intermittently, they can have long-term impacts on the military's infrastructure and mission performance. Coupled with a rise in sea level, these impacts can be more extensive in the future due to changes in storm intensity, frequency and track. In addition to higher sea levels, surge from hurricanes can become higher and more intense rainfall can raise the potential for flooding from land runoff. A rise in mean sea level will nonlinearly shift the maximum water levels and wave heights produced by storms. The next step in our approach focuses on characterizing the expected variations in water level and wave hazards under the prescribed SLR scenarios using regional surge and wave models (Figure 18).

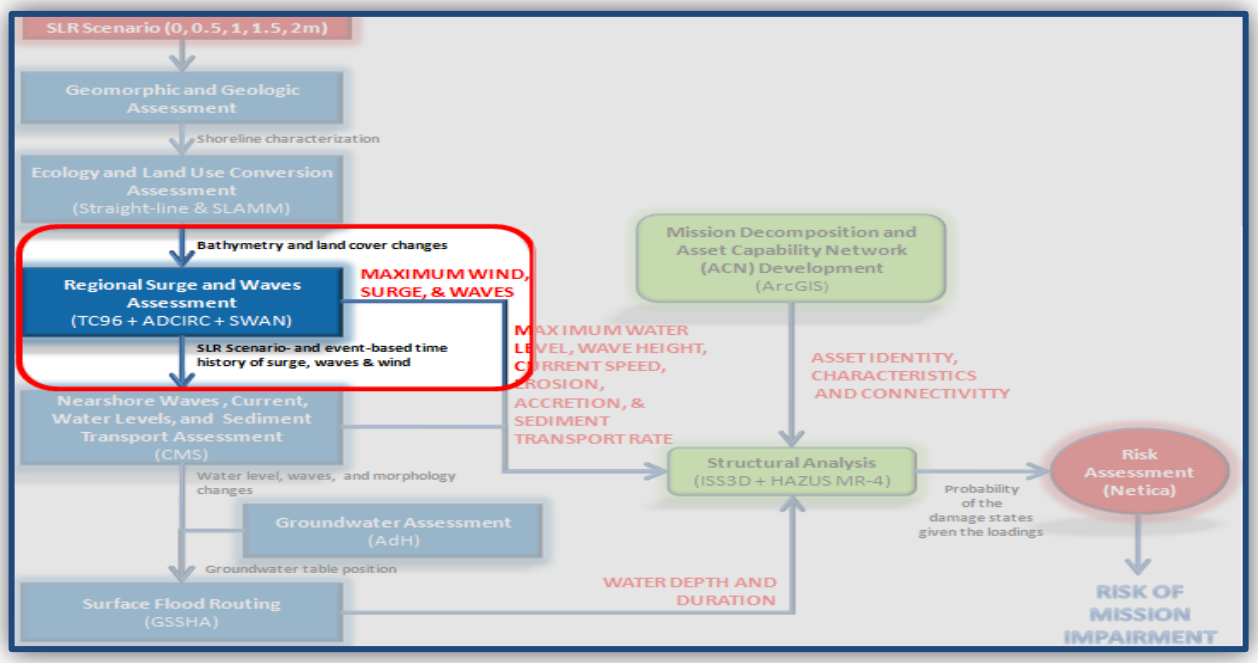

Figure 18. Project analysis and tasks: *Regional Surge and Waves Assessment*.

As the figure illustrates, results from the previous steps (i.e., shoreline characterization, land cover changes, and bathymetry) are incorporated into a series of high fidelity storm simulations to generate resultant forcings (winds, water levels, and waves) that threaten critical assets and mission performance. The idea is to generate a series of maps (and videos) that visualize the extent of the threat for each storm under each SLR scenario. The outputs are then used to both inform the nearshore wave modeling in the next step, and characterize threats to critical assets in the follow-on steps of our risk-based framework.

3.4.1 Models and Approach

We used three high fidelity numerical models to simulate tropical and extra-tropical storms for our case study, capturing regional surge and wave processes and generating forcings that impact critical assets system wide:

1) **Hurricane winds** have been generated using the Planetary Boundary Layer (PBL) wind model TC96 (Thompson and Cardone 1996),
2) **Surge** has been simulated using the ADvanced CIRCulation model ADCIRC (Westerink et al. 2008, Luettrich and Westerink 2004), and
3) **Waves** have been simulated using the Simulating WAves Nearshore model SWAN (Booij et al. 1999, Ris et al. 1999, Zijlema 2010).

The PBL and ADCIRC models are standard USACE models that have been well validated for storm surge modeling for a number of hurricanes. The SWAN wave model is also a well-validated community model used in several USACE applications to capture storm surge (refer back to *Footnotes 1-4* in *Section 3.1* for a list of recent applications). The PBL-ADCIRC-SWAN model suite has been selected for this study to take advantage of the extensive modeling already executed under the USACE-led FEMA Region III study (grid generation, model validation, storm selection, and model runs).[16] In addition, we direct the reader to two studies, one by Kerr et al. (2013) and the other by Lin et al. (2010), who compare and contrast the application of these models with other options [namely the U.S. Geological Survey's Sea, Lake, and Overland Surge from Hurricane (SLOSH) model].

Below, we offer extensive background describing each of these models in greater detail.

3.4.1.1 Planetary Boundary Layer (PBL) Winds

The TC96 wind model computes surface stress and average wind speed and direction in the PBL of a tropical cyclone. The model inputs are meteorological storm parameters. The model is based on the numerical primitive equation model of the PBL in a translating tropical cyclone. The surface drag formulation is based on a similarity model and is coupled with a roughness parameter specification for the water surface. The model relies on the concept that a tropical cyclone changes structure relatively slowly (period of hours), so the cyclone can be represented by a small number of snapshots representing distinct phases of the storm evolution. Although the structure of the storm changes relatively slowly, the storm position could change quickly. Wind velocity components are linearly interpolated in space and time between the snapshots.

The TC96 PBL model is based on the Reynolds-averaged primitive equations of motion. Wind averaging intervals are typically 30-60 min and a 10-m height reference is used in most instances. The model incorporates a moving vortex and is based on the equation of horizontal momentum, vertically averaged through the depth of the PBL. Acceleration, horizontal diffusion of momentum, and vertical advection of momentum are neglected. The tropical cyclone is

[16] FEMA Region III Storm Surge Study, http://www.r3coastal.com/home/storm-surge-study (Accessed April 2014).

translated with a moving Cartesian coordinate system with the origin at the low pressure center of the cyclone:

$$f\vec{K}\times(\vec{V}-\vec{V}_g)=-\frac{1}{\rho}\nabla p_c-\frac{C_D}{h}\left|\vec{V}+\vec{V}_c\right|(\vec{V}+\vec{V}_c) \quad \textbf{(3)}$$

where V is the average horizontal velocity vector, V_g is the geostrophic velocity vector at the low center, V_c is the velocity vector of the moving reference system, K is a unit vector in the vertical direction, ρ is mean air density, p_c is pressure representing the tropical cyclone, C_D is the drag coefficient, and h is the depth of the PBL (Thompson and Cardone 1996). The cyclone pressure is defined by an axisymmetrical exponential pressure or by defining a Holland B parameter that represents the asymmetry of the pressure field. Wind fields for hurricanes are generated with the model by inputting the central pressure deficient, radius of maximum winds, Holland B parameter, storm forward speed and storm track.

3.4.1.2 ADvanced CIRCulation Model (ADCIRC)

ADCIRC is a continuous-Galerkin, finite-element, two-dimensional (2D), horizontal shallow-water model that solved for water levels and currents at a range of scales. Galerkin indicates the method uses to convert differential equations to discrete problems (similar to the method of variation of parameters). Water levels are obtained through solution of the Generalized Wave Continuity Equation (GWCE):

$$\frac{\partial^2\zeta}{\partial t^2}+\tau_0\frac{\partial\zeta}{\partial t}+\frac{\partial\tilde{J}_x}{\partial x}+\frac{\partial\tilde{J}_y}{\partial y}-UH\frac{\partial\tau_0}{\partial x}-VH\frac{\partial\tau_0}{\partial y}=0 \quad \textbf{(4)}$$

where:

$$\tilde{J}_x=-Q_x\frac{\partial U}{\partial x}-Q_y\frac{\partial U}{\partial y}+fQ_y-\frac{g}{2}\frac{\partial\zeta^2}{\partial x}-gH\frac{\partial}{\partial x}\left[\frac{P_s}{g\rho_0}-\alpha\eta\right]+\frac{\tau_{sx,wind}+\tau_{sx,waves}-\tau_{bx}}{\rho_0}$$

$$+\left(M_x-D_x\right)+U\frac{\partial\zeta}{\partial t}+\tau_0Q_x-gH\frac{\partial\zeta}{\partial x} \quad \textbf{(5)}$$

$$\tilde{J}_y=-Q_x\frac{\partial V}{\partial x}-Q_y\frac{\partial V}{\partial y}-fQ_x-\frac{g}{2}\frac{\partial\zeta^2}{\partial y}-gH\frac{\partial}{\partial y}\left[\frac{P_s}{g\rho_0}-\alpha\eta\right]+\frac{\tau_{sy,wind}+\tau_{sy,waves}-\tau_{by}}{\rho_0}$$

$$+\left(M_y-D_y\right)+V\frac{\partial\zeta}{\partial t}+\tau_0Q_y-gH\frac{\partial\zeta}{\partial y} \quad \textbf{(6)}$$

and the currents are obtained from the vertically-integrated momentum equations:

$$\frac{\partial U}{\partial t}+U\frac{\partial U}{\partial x}+V\frac{\partial U}{\partial y}-fV=-g\frac{\partial}{\partial x}\left[\zeta+\frac{P_s}{g\rho_0}-\alpha\eta\right]+\frac{\tau_{sx,winds}+\tau_{sx,waves}-\tau_{bx}}{\rho_0 H}+\frac{M_x-D_x}{H} \quad \textbf{(7)}$$

and:

$$\frac{\partial V}{\partial t}+U\frac{\partial V}{\partial x}+V\frac{\partial V}{\partial y}+fU=-g\frac{\partial}{\partial y}\left[\zeta+\frac{P_s}{g\rho_0}-\alpha\eta\right]+\frac{\tau_{sy,winds}+\tau_{sy,waves}-\tau_{by}}{\rho_0 H}+\frac{M_y-D_y}{H} \quad \textbf{(8)}$$

where $H = \zeta + h$ is total water depth; ζ is the deviation of the water surface from the mean; h is bathymetric depth; U and V are depth-integrated currents in the x- and y-directions, respectively; $Q_x = UH$ and $Q_y = VH$ are fluxes per unit width; f is the Coriolis parameter; g is gravitational acceleration; P_s is atmospheric pressure at the surface; ρ_0 is the reference density of water; η is the Newtonian equilibrium tidal potential and α is the effective earth elasticity factor; $\tau_{s,winds}$ and $\tau_{s,waves}$ are surface stresses due to winds and waves, respectively; τ_b is bottom stress; M are lateral stress gradients; D are momentum dispersion terms; and τ_0 is a numerical parameter that optimizes the phase propagation properties. ADCIRC computes water levels ζ and currents U and V on an unstructured, triangular mesh by applying a linear Lagrange interpolation and solving for three degrees of freedom at every mesh vertex (node).[17]

3.4.1.3 Simulating WAves Nearshore Model (SWAN)

SWAN is a 2D spectral wave generation and transformation model. SWAN predicts the evolution in geographical space $\vec{x}$ and time t of the wave action density spectrum $N(\vec{x},t,\sigma,\theta)$, with σ the relative frequency and θ the wave direction, as governed by the action balance equation:

$$\frac{\partial N}{\partial t}+\nabla_{\vec{x}}\cdot\left[\left(\vec{c}_g+\vec{U}\right)N\right]+\frac{\partial c_\theta N}{\partial\theta}+\frac{\partial c_\sigma N}{\partial\sigma}=\frac{S_{tot}}{\sigma} \quad \textbf{(9)}$$

The terms on the left-hand side represent, respectively, the change of wave action in time, the propagation of wave action in $\vec{x}$-space (with $\nabla_{\vec{x}}$ the gradient operator in geographic space, $\vec{c}_g$ the wave group velocity, and $\vec{U}$ the ambient current vector), depth- and current-induced refraction and approximate diffraction (with propagation velocity or turning rate c_θ), and the shifting of σ due to variations in mean current and depth (with propagation velocity or shifting rate c_σ). The source term, S_{tot}, represent wave growth by wind; action lost due to whitecapping,

[17] User note - Mesh instabilities are normal occurrences encountered during the process of creating large domains required for storm surge modeling. The primary causes are due to sharp or steep slopes between triangular elements which occur when interpolating high resolution digital elevation models onto the mesh. In this study, the FEMA team resolved most of these initial instabilities with only two to three modifications needed to complete the current study effort. Additional simulations can readily be performed using the final study's mesh without encountering significant mesh instabilities. However, instabilities cannot be ruled out all together because other storms which vary in track and intensity may produce forces outside of the project study region in other locations of the mesh.

surf breaking, and bottom friction; and action exchanged between spectral components in deep and shallow water due to nonlinear effects. The associated SWAN parameterizations are given by Booij *et al.* (1999). The unstructured-mesh version of SWAN implements an analog to the four-direction Gauss-Seidel iteration technique employs in the structured version, and it maintains SWAN's unconditional stability (Zijlema 2010). SWAN computes the wave action density spectrum $N(\vec{x}, t, \sigma, \text{and } \theta)$ at the vertices of an unstructured triangular mesh, and orders the mesh vertices so it can sweep through and update the action density using information from neighboring vertices. It then sweeps through the mesh in opposite directions until the wave energy is propagated sufficiently through geographical space in all directions

SWAN is driven by winds, water levels and currents computed at the vertices by ADCIRC. Marine winds are input to ADCIRC in a variety of formats, and these winds are adjusted directionally to account for surface roughness (Bunya et al. 2010). ADCIRC interpolates spatially and temporally to project these winds to the computational vertices, and then it passes them to SWAN. The water levels and ambient currents are computed in ADCIRC before being passed to SWAN, where they are used to calculate all related wave processes (wave propagation, depth-induced breaking, etc.). The ADCIRC model is driven partly by radiation stress gradients that are computed using information from SWAN. These gradients, $\tau_{s,waves}$, are computed by:

$$\tau_{sx,waves} = -\frac{\partial S_{xx}}{\partial x} - \frac{\partial S_{xy}}{\partial y} \tag{10}$$

and:

$$\tau_{sy,waves} = -\frac{\partial S_{xy}}{\partial x} - \frac{\partial S_{yy}}{\partial y} \tag{11}$$

where S_{xx}, S_{xy} and S_{yy} are the wave radiation stresses:

$$S_{xx} = \rho_0 g \iint \left(\left(n\cos^2\theta + n - \frac{1}{2} \right) \sigma N \right) d\sigma d\theta \tag{12}$$

$$S_{xy} = \rho_0 g \iint \left(n \sin\theta \cos\theta \sigma N \right) d\sigma d\theta \tag{13}$$

and:

$$S_{yy} = \rho_0 g \iint \left(\left(n\sin^2\theta + n - \frac{1}{2} \right) \sigma N \right) d\sigma d\theta \tag{14}$$

where n is the ratio of group velocity to phase velocity. The radiation stresses are computed at the mesh vertices using *Equations (12)-(14)*.

ADCIRC and SWAN are run in series on the same local mesh and core. The two models "leap frog" through time, each being forced with information from the other model. Because of the sweeping method used by SWAN to update the wave information at the computational vertices, it can take much larger time steps than ADCIRC, which is diffusion- and Courant-time-step limited due to its semi-explicit formulation and its wetting-and-drying algorithm. Because wave properties in the nearshore and the coastal floodplain are generally more dependent on circulation (water level) and changed more slowly, the ADCIRC model is run first.

3.4.2 Modeling Inputs

The wind, wave, and circulation models all required inputs for the case study application. The wind model required input of hurricane parameters to generate representative wind fields for events with 50- and 100-yr return periods. The wind fields were then used to drive the circulation/surge and wave models. The circulation and wave models also required bathymetry/topography and land cover to define the environment. The circulation and wave models also interacted with each other, exchanging water level and radiation stress information (Figure 19).

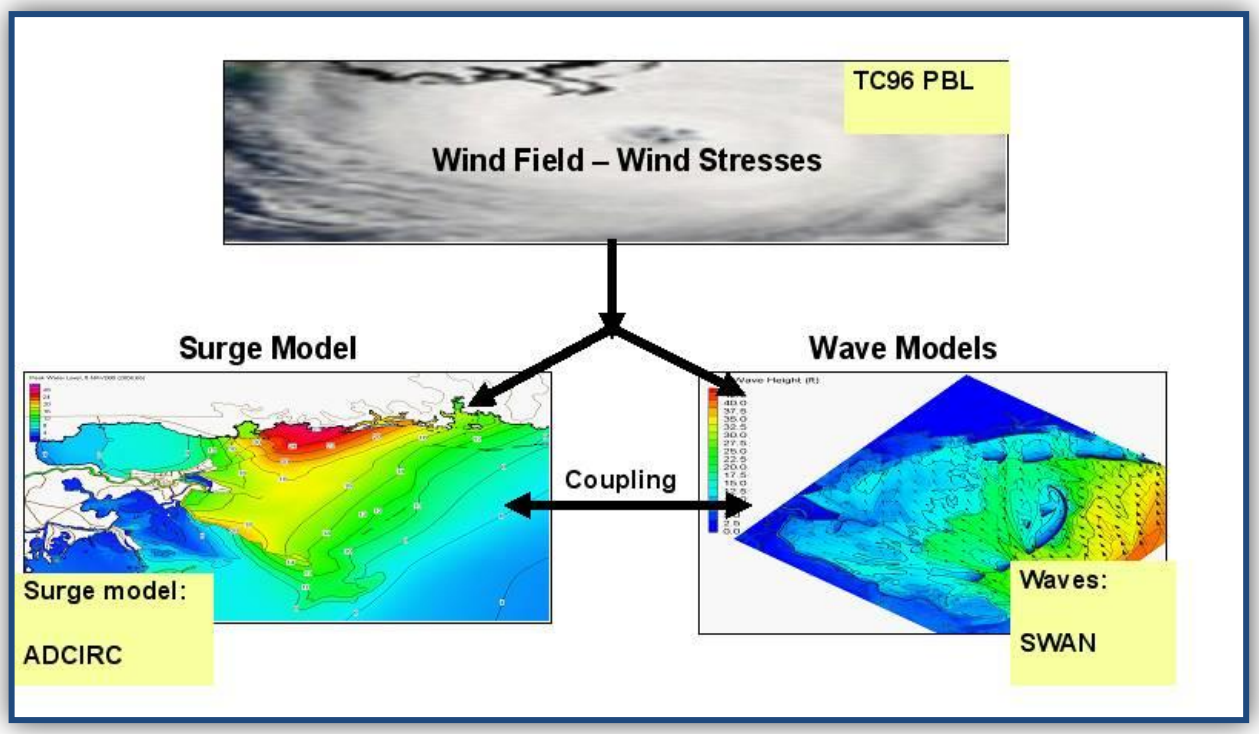

Figure 19. Inputs and outputs of the regional surge and wave assessment.

3.4.2.1 Atlantic Storm Parameterization

Under a FEMA study to develop flood maps for the Virginia coast, analyses were performed to characterize the storm climate and design 460 synthetic hurricanes for simulation.[18] The FEMA study implemented the Joint Probability Method with Optimal Sampling (JPM-OS) for storm parameterization following the methodology used by the USACE in the 2007 Louisiana Coastal Protection and Restoration (LACPR) Project and in the coastal Mississippi Flood Insurance Study (Blanton et al. 2011). The 460 hurricanes included three headings (-55, -10, and 5 deg relative to North), three central pressure deficits [34, 51, and 65 millibar (mbar)], two forward speeds [5.5 and 13 meters per second (m/s)], three radius of maximum winds (mean value +/- 1.22 standard deviations), and three Holland B parameters (mean value +/- 1.22 standard deviations, defining the asymmetry of the wind fields) together with a range of land-fall locations (refer to Figure 20 to review storm tracks).

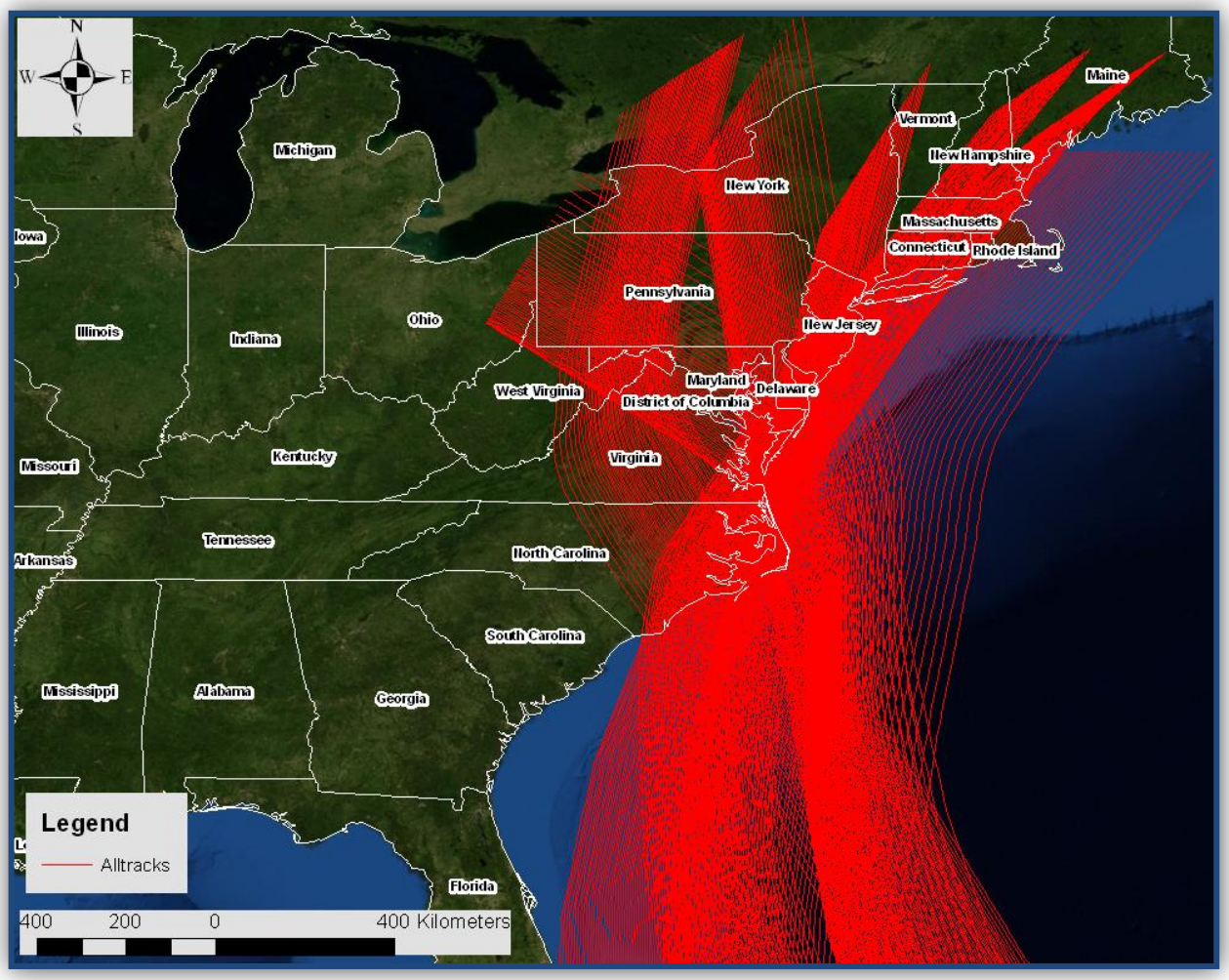

Figure 20. FEMA Region III Study storm tracks.

[18] FEMA Region III Storm Surge Study, http://www.r3coastal.com/home/storm-surge-study (Accessed April 2014).

3.4.2.2 Selection of Representative Tropical Storms (Hurricanes) for the Study

Limited resources for the analysis made it impractical to assess all 460 simulated hurricanes generated by the FEMA study. Therefore, we devised a systematic approach that strategically culled down the potential storms to a reasonable sample size. Ultimately, we selected 17 tropical storms for this application (Figure 21).

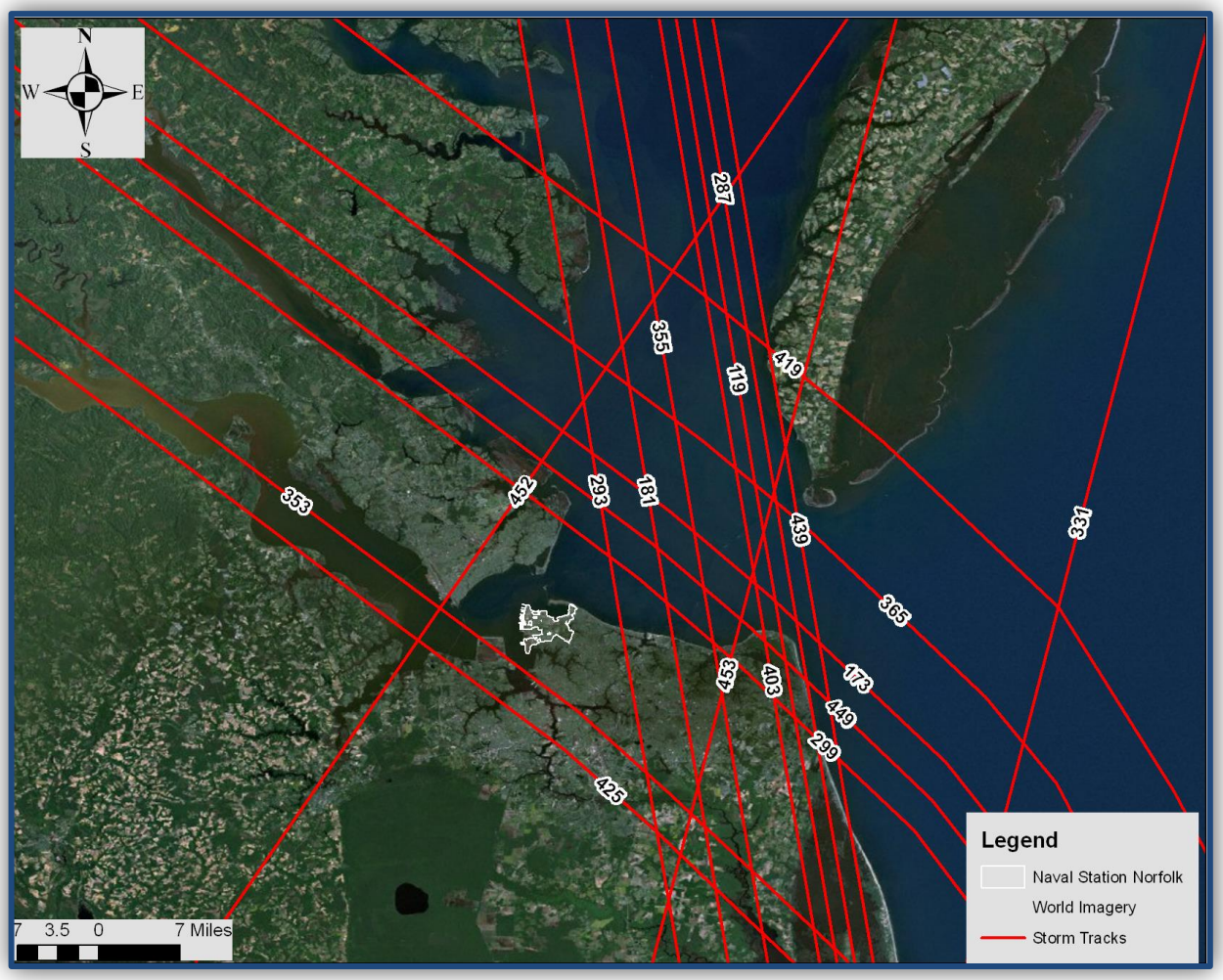

Figure 21. The 17 simulated hurricane tracks selected for the regional surge and wave assessment.

It was important to note that the probability assigned to the individual storms based on their unique physical characteristics did not necessarily correspond to the probability of occurrence of the water levels and waves with 50- or 100-yr return periods. Instead, the selected storms provided us with storms producing a range of water levels and waves within the 50 to 100-yr return period. As a result, storm selection was based primarily on the water levels produced in the area of interest (i.e., NSN). Wind fields for the hurricanes were generated with the TC96 PBL model (refer to Table 9 to review selected hurricanes).

Table 9. Characteristics of the 17 simulated hurricanes selected for this study.

Storm Number	C_p[1] (mbar)	R_{max}[2] (km)	C_p diff[3] (mbar)
119	973.4	32.0	39.6
173	975.6	58.8	37.4
181	973.4	48.4	39.6
287	954.7	50.4	58.3
293	954.7	44.4	58.3
299	956.9	54.1	56.1
331	954.7	85.7	58.3
353	941.5	28.7	71.5
355	939.3	26.8	73.7
365	941.5	29.1	71.5
403	939.3	45.8	73.7
419	941.5	45.5	71.5
425	941.5	84.3	71.5
439	939.3	84.7	71.5
449	941.5	84.7	71.5
452	926.6	67.5	86.35
453	939.3	77.3	73.7

[1]Cp = central pressure
[2]Rmax = radius of maximum winds
[3]Cp diff = central pressure deficit.

3.4.2.3 Selection of Representative Extra-tropical Storms (Nor'easters) for the Study

Thirty historical extra-tropical storms (nor'easters) that impacted the region between 1975 and 2008 were reviewed as potential candidates for the project. Three of the most severe storms were selected for modeling. The selection process was based on the maximum measured water levels at Sewells Point and Chesapeake Bay Bridge Tunnel National Ocean Service (NOS) tide gauges in lower Chesapeake Bay (Table 10). These storms produced water levels with return periods in the range of 5-10 years. In general, nor'easters produced lower peak water levels than hurricanes in this region, but the nor'easter elevated water levels for days (instead of hours for hurricanes), and these elevated water levels (and waves) produced greater shoreline damages. The wind fields for the storms listed in Table 10 were generated by Oceanweather, Inc., using the Interactive Objective Kinematic Analysis (IOKA) system (Cox et al.1995). This technique used wind and atmospheric pressure data from a number of sources i.e., (National Centers for Environmental Prediction/National Center for Atmospheric Research, National Data Buoy Center and Coastal Manned Stations, National Weather Service and National Ocean Service, ship reports, and scatterometer wind estimates).

Table 10. Extra-tropical storms simulated for this study.

Storm Number	Date	Sewells Point Measured Water Level, NOS station 8638610 (m, MTL)	Chesapeake Bay Bridge Tunnel Measured Water Level, NOS station 8638863 (m, MTL)
801	28 JAN 1998	1.40	1.37
803	05 FEB 1998	1.52	1.37
805	25 OCT 1982	1.31	1.16

Extra-tropical storm #805 was selected for nearshore modeling of extra-tropical events.

3.4.2.4 Bathymetry and Land Cover

A 10-meter resolution DEM for the Chesapeake Bay region was completed through the FEMA floodplain re-mapping project.[19,20] A large domain hydrodynamic model grid was constructed using the resultant DEM. The mesh was unstructured with triangular elements varying in size from kilometers to a very high horizontal resolution of up to 20 m. A view of mesh bathymetry truncated to the area of interest is shown in Figure 22 (depths truncated to 20 m).

[19] FEMA Region III Storm Surge Study, http://www.r3coastal.com/home/storm-surge-study (Accessed April 2014).

[20] Lidar error for the FEMA Region III Storm Surge Study was 15 cm root mean square error (RMSE). Note that an RMSE of 15 cm is common, and that these errors are often non- uniform, such that the reported error could be higher or lower at various locations. Although conducting a sensitivity analysis to test the impacts of RMSE on these analyses was outside the study's scope, we acknowledge that the RSME could impact the results of the modeling exercise.

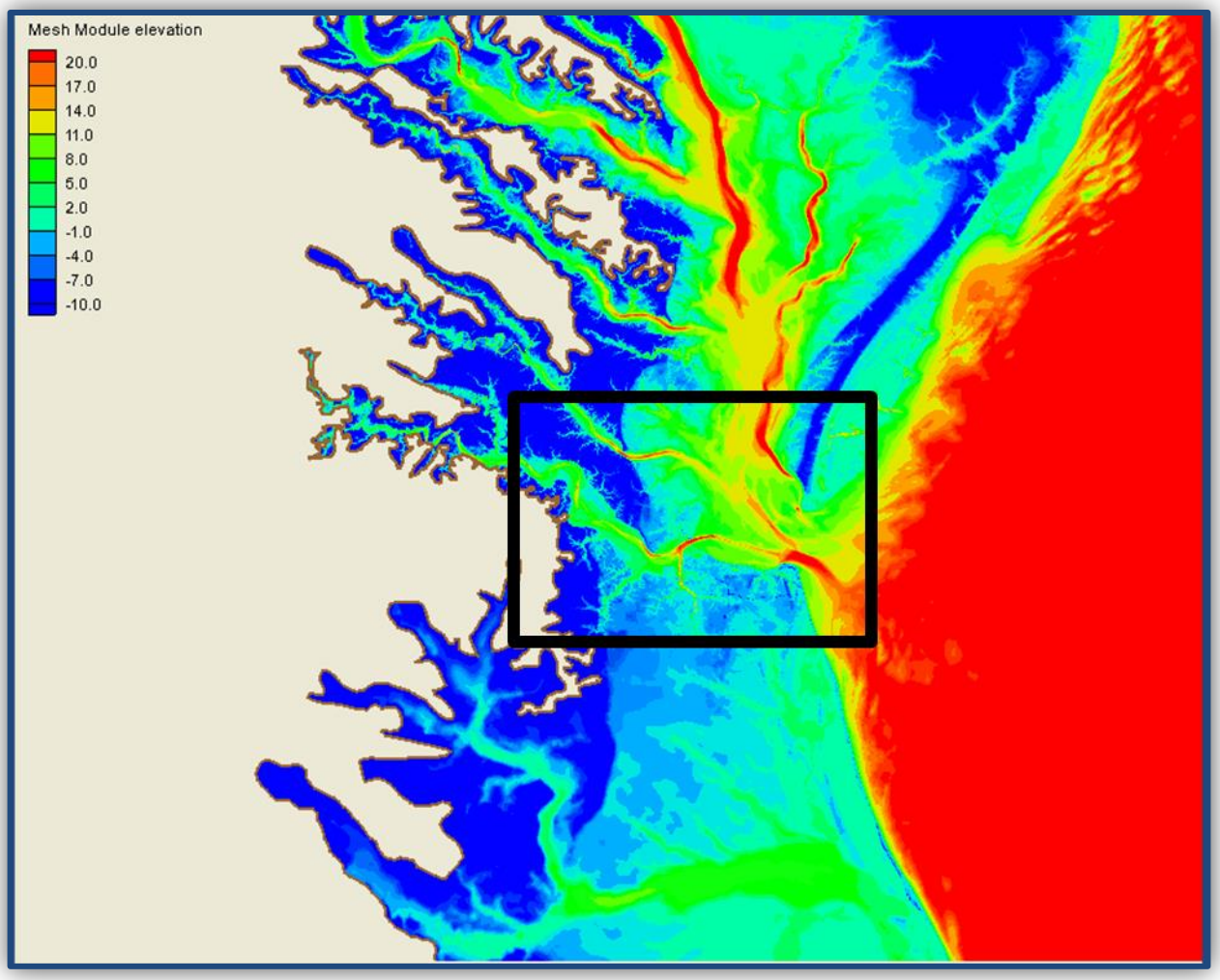

Figure 22. Bathymetry for the ADCIRC/SWAN model mesh.

Elevation in the figure is relative to Mean Tide Level (MTL). The black box in Figure 22 above shows the Norfolk area and the mesh within the black box is shown in Figure 23. The final mesh included 3,689,518 elements (triangles) and 1,855,105 nodes (vertices) (Figure 23).

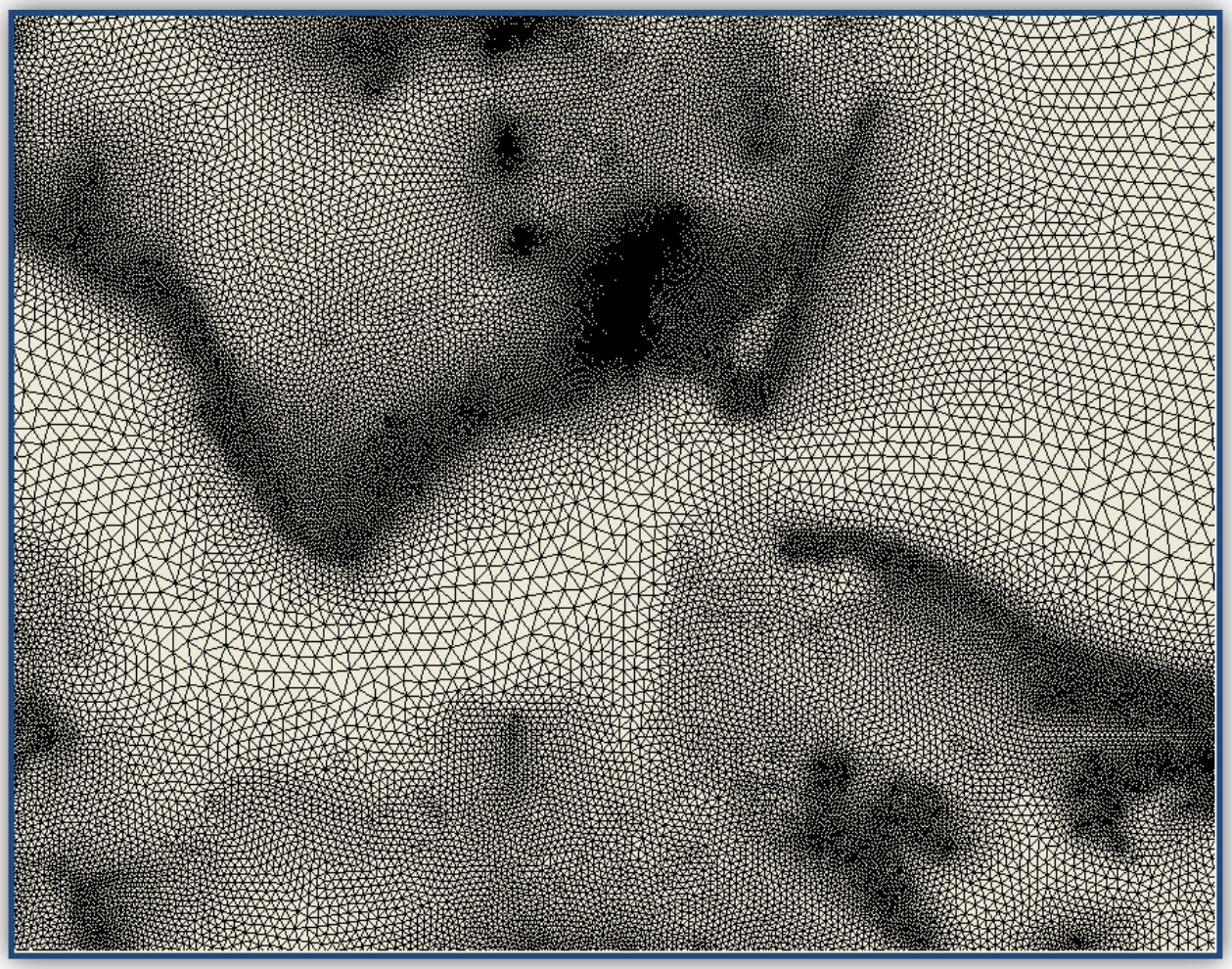

Figure 23. Model mesh for the Norfolk, VA, area (black box in Figure 22).

Land cover was also used as an input to the circulation and wave models, which in turn allowed us to specify the bottom roughness through Manning's-n coefficients. Frictional surface roughness was modeled using Manning's-n coefficients based upon land cover types. The 2000/2001 NLCD (http://www.mrlc.gov/, accessed 23 February 2012) land cover types were represented with Manning's-n values following FEMA HAZUS model implementations.

3.5. Nearshore Assessment Methodology

Barrier islands and dunes, bluffs and cliffs, mainland beaches, deltas, estuaries and bays, and wetlands along the North Atlantic coast are products of dynamic interactions between: 1) physical processes that act on the coastline (i.e., storms, waves, currents, sand sources and sinks, and RSLR); 2) human activity such as dredging, dams, and coastal engineering; and 3) the geological character of the coastline and nearshore settings (Burkett and Davidson 2012). The complex interactions between these elements make the relationship between SLR and shoreline change difficult to model and predict. While SLR will have a profound effect on nearshore conditions (increasing flooding frequency and inundating low-lying coastal areas), other driving

processes such as erosion and sediment accretion will compound the effects on coastal nearshore and shoreline evolution. Whereas the large scale, regional storm surge and wave models (refer to *Section 3.4 above*) provide information on storm development and progression at the regional scale, a high-resolution integrated surge, wave, and sediment transport model that assesses escalating surge, accretion and erosion associated with coastline evolution in the nearshore setting is required to resolve nearshore coastal and land coverage features at the local scale. Coupling with the regional model, the local model is then able to calculate the changes in water surface elevation, storm surge, and storm waves, as well as sediment transport and morphological changes in the nearshore and low-lying coastal settings surrounding the study site. The next step in our approach focuses on modeling the nearshore effects of coastal storms (i.e., changes in water levels, waves, currents, sediment transport rates, etc.) under the prescribed SLR scenarios using nearshore coastal models (Figure 24).

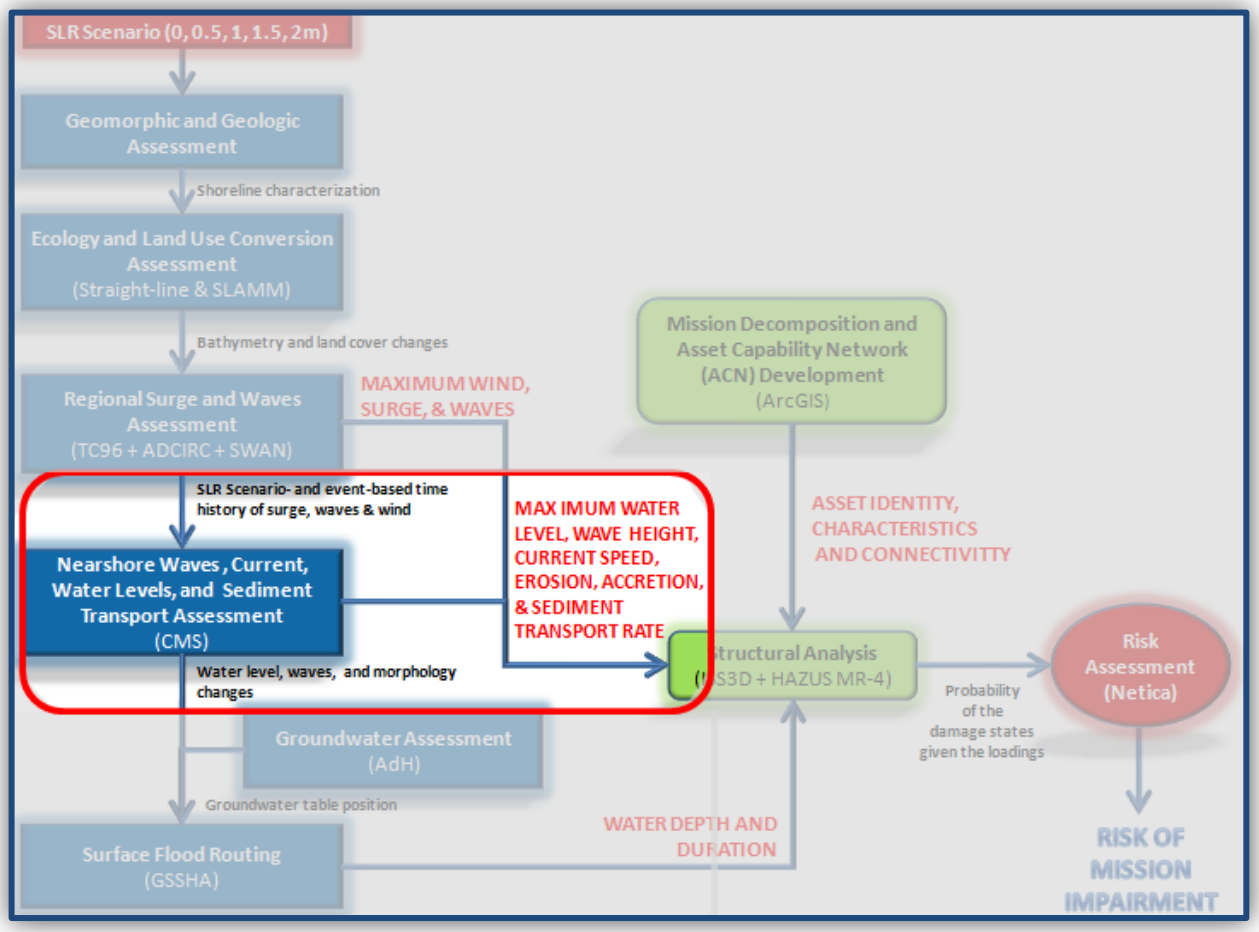

Figure 24. Project analysis and tasks: *Nearshore Assessment*.

As the figure illustrates, results from the previous steps (i.e., regional surge and wave levels) are incorporated into a series of nearshore storm simulations to generate resultant forcings (maximum water levels, wave heights, current speeds, erosion/accretion rates) that threaten critical assets and mission performance. The idea is to generate a second series of maps (and

videos) that visualize the extent of the threat that can be attributed to nearshore effects for each storm under each SLR scenario. The outputs are then used to both inform the surface (and subsurface) flood routing models in the next step, and capture threats to critical assets in the follow-on steps of our risk-based framework.

3.5.1 Models and Approach

We selected the Coastal Modeling System (CMS)[21] to capture nearshore effects of coastal storms for our case study. The CMS is an integrated suite of numerical models for simulating water surface elevation, current, waves, sediment transport, and morphology change for coastal and inlet applications, and is capable of identifying water bottom and land surface erosion and accretion areas in extreme storms. The CMS consists of a hydrodynamic model, CMS-Flow, and a spectral wave model, CMS-Wave. CMS-Flow and CMS-Wave is coupled and operates through a Steering Module developed within the Surface-water Modeling System (SMS) (Zundel 2006). The CMS (CMS-Flow and CMS-Wave) is specifically designed for applications in inlets, harbors, bays and estuaries. As a practical engineering tool, it is PC-based and has a desktop user-friendly interface. With the capability to perform sediment transport calculations, the flow-wave coupled CMS offers a unique, robust, and accurate methodology to address relevant coastal processes.

CMS-Flow is a three-dimensional (3D) finite-volume model that solves the mass conservation and shallow-water momentum equations of water motion on a non-uniform Cartesian grid. Three sediment transport formulations are available: 1) a sediment mass balance, 2) an equilibrium advection-diffusion method, and 3) a non-equilibrium advection-diffusion transport. The model can run in a 2D mode based on the depth-integrated continuity equation. The wave radiation stress and wave field information calculated by CMS Wave is supplied to CMS Flow for the flow and sediment transport calculations. Currents, water level, and morphology changes are inputs into CMS-Wave that increase the accuracy of the wave transformation predictions (Buttolph et al. 2006) (Figure 25).

[21] Developed by the ERDC Coastal and Hydraulics Laboratory (http://cirp.usace.army.mil, accessed 21 March 2012)

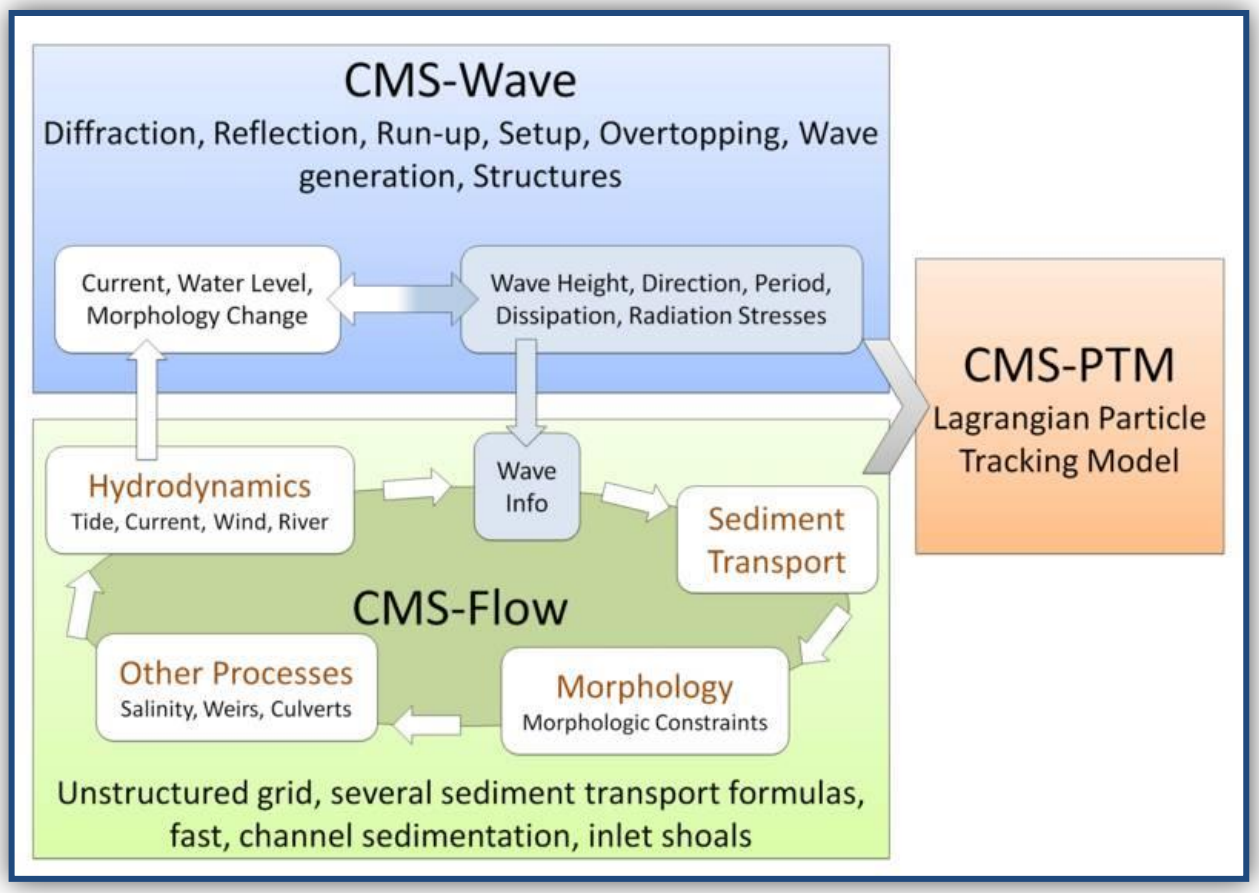

Figure 25. The CMS operational flow chart.

CMS-Wave is a 2D spectral wave transformation model that solves the steady-state wave-action balance and diffraction equation on a non-uniform Cartesian grid (Lin et al. 2008). The model simulates important wave processes at coastal inlets including diffraction, refraction, reflection, wave breaking and dissipation mechanisms, wave-wave and wave-current interactions, and wave generation and growth. It is a full-plane model with primary waves propagating from open boundaries toward inside domain. If the reflection option is selected from one open boundary, CMS-Wave performs a backward marching computation that establishes the boundary reflection after the forwarding-marching calculation is completed. The fundamental wave diffraction process is theoretically developed and calculated in the wave-action balance equation (Mase 2001). CMS-Flow is forced by offshore water surface elevation (typically from tide and storm surge), wind, waves, and river discharge. CMS-Wave is driven by wave spectra and wind, which are often obtained from offshore ocean buoys. In the dynamic coupling, CMS-Wave passes wave radiation stress to CMS-Flow and receives information of current, water surface elevation, and morphology change from CMS-Flow. Additional model features include grid nesting capabilities, variable rectangle cells, wave run-ups on beach faces, wave transmissions through structures, wave over-toppings, and storm wave generation (Figure 25 above). CMS-Wave includes strong wave-current-structure interactions. It is robust in the wind-wave generation, and is computationally more efficient than SWAN in the PCs. The state-of-the-art model interface,

Surface-Water Modeling System, is well-developed for the CMS. The CMS has been widely applied to U.S. coasts, bays, estuaries, and Great Lakes. Some recent applications include Grays Harbor, WA, San Francisco Bay and Bar, CA, Noyo Bay, CA, Galveston Bay, TX, Matagorda Bay, TX, Chesapeake Bay, Shark River Inlet, NJ, the Big Island of Hawaii, HI, Cleveland Harbor in Lake Erie, and Rhode Island coast and lagoons (http://cirpwiki.info/wiki/CMS, accessed May 2014).

3.5.2 Modeling Inputs

. Water surface elevations along the CMS open boundaries were retrieved from the large scale ADCIRC model outputs (refer to *Section 3.4* above). The local wind speeds and directions as input to CMS were provided by the storm analysis and wave spectra from SWAN (refer again to *Section 3.4* above). Each simulation was designed to run over a four-day duration to cover a 12-hour ramping of transition from normal to storm condition, and the passage of a storm. Surge information was retrieved from the large scale regional model output and tide data were obtained from the NOAA gage at Sewells Point, VA. The combination of the two datasets provided the water surface elevation forcing along the CMS open boundaries (see below). The bottom friction of the CMS was based on the bottom roughness information provided by the regional model for the different SLR scenarios. For sediment transport analyses, the grain size distributions of bottom sediment, and land erodibility were derived from the detail land coverage features.

3.5.2.1 Coastal Modeling System (CMS) Model Domain

To begin, a CMS domain was established surrounding the NSN (Figure 26).

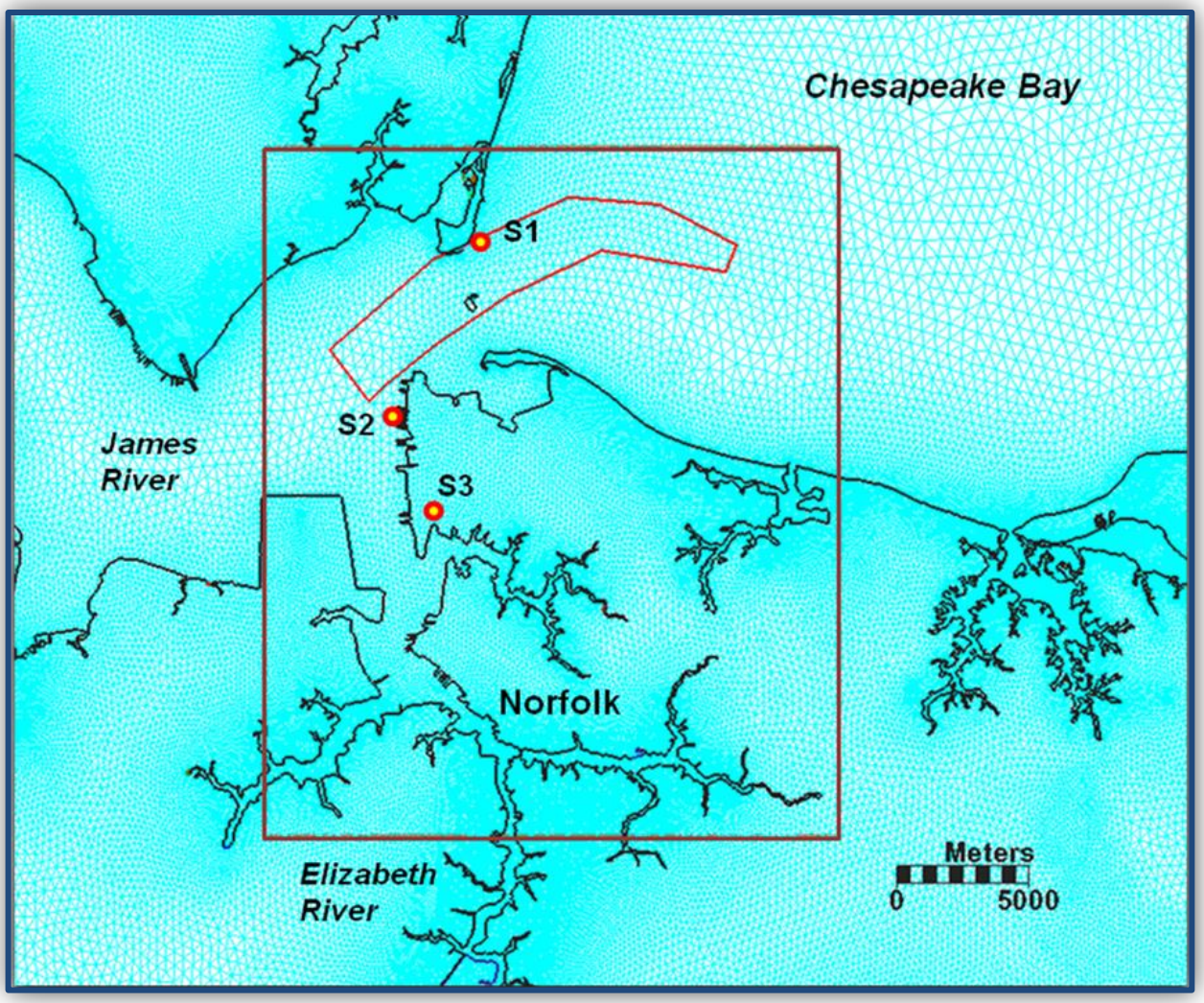

Figure 26. The CMS domain. White dots are time series stations in the Hampton Roads navigation channel (*S1*), near Naval Piers (*S2*), and on land (*S3*). Bed volume change was examined within the red polygon area. Time series of water surface elevations were analyzed at three locations: *Sites S1*, *S2*, and *S3*.

As the figure illustrates, the model domain covered the mouths of the James River and the Elizabeth River, a portion of the lower Chesapeake Bay (Hampton Roads area), and extended approximately 20 km from east to west and 24 km from north to south. The western open boundary was located over the mouths of the rivers and the northern and eastern open boundary in the Chesapeake Bay. In this application, a non-uniform rectangular grid system with more than half million grid cells was created to discretize the entire installation and the nearshore region. The grid system permitted much finer resolution (10 m) in areas of high interest such as the NSN. The mesh of the regional model, also shown in Figure 26 above, was coupled with the CMS through data mapping.

3.5.2.2 Coastline Characterization

Detailed coastline information, accurate topographic data, and land surface features in the Hampton Roads area were used to create a small-scale, high-resolution storm surge and sediment transport model for the NSN case study. Coastline information around the NSN and the Hampton Roads area was extracted for this study from the shoreline database of the National Geophysical Data Center (NGDC) of NOAA (http://www.ngdc.noaa.gov/mgg/shorelines/ , accessed 21 March 2012). The aerial photographs were downloaded from Google Earth Pro 5.1 (http://earth.google.com, accessed 21 March 2012).

LiDAR data provided the land topography in the NSN. The data (at 1-m resolution) allowed the CMS to describe local land features, such as buildings, roads, airport, and other infrastructures in the area. Topographic information of other land areas and bathymetry for the water domain were provided by a 10-m resolution coastal DEM of Virginia Beach (Taylor et al. 2008). Figure 27 shows water depth and land surface topography contours (relative to MSL) from the two datasets.

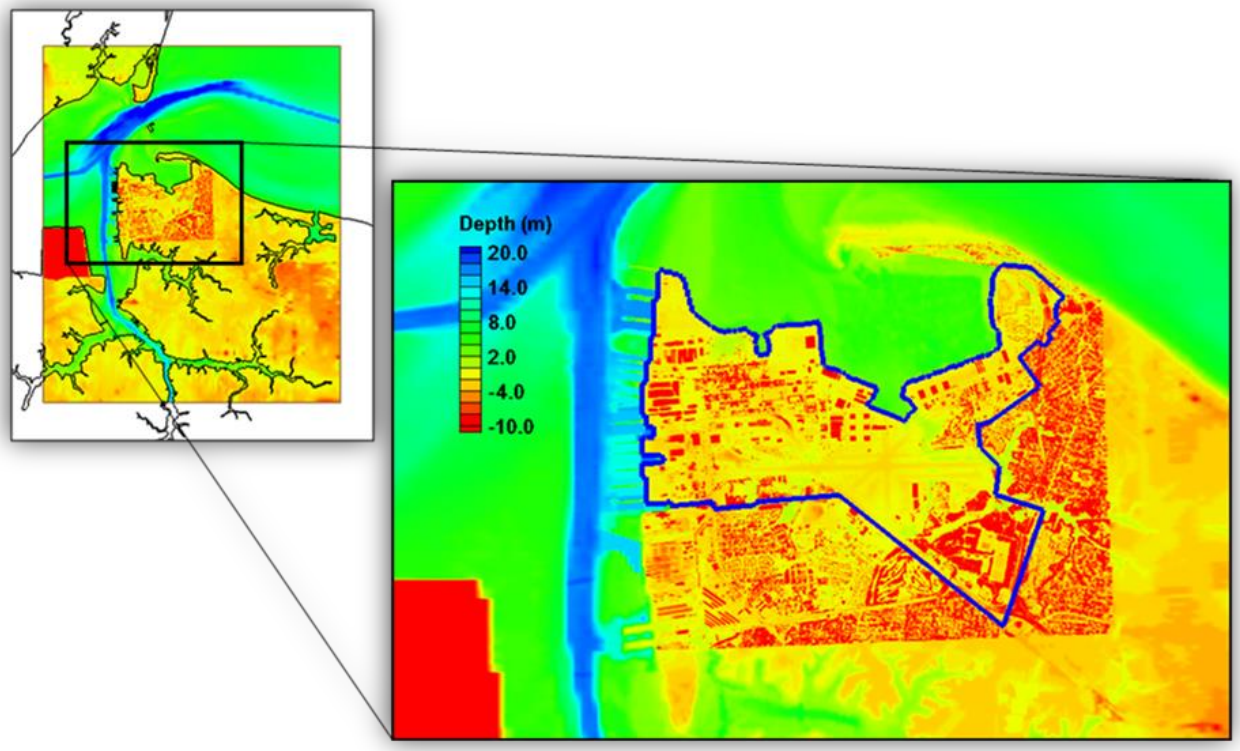

Figure 27. Topographic map of the study area.

The blue line in the right panel of Figure 27 outlines the NSN. Note the deep-draft Hampton Roads navigation channel running to the north of the domain (shown in blue), the Norfolk Harbor entrance channel, and a few small channels to the military piers on the Naval Station water front. The data ranged from the highest elevation of more than 10 m on land (negative values) to more than 30 m in the navigation channel (positive values). The red coloration in the

lower left corner of Figure 27 pinpoints the Craney Island Dredged Material Management Area. The dikes built surrounding the area have a height of about 12 m above MSL.

Upland coverage characterization was used to assess erodibility in the analysis. Figure 28 shows different upland land classes identified (i.e., grass, forest, concrete, roads, etc.) on NSN.

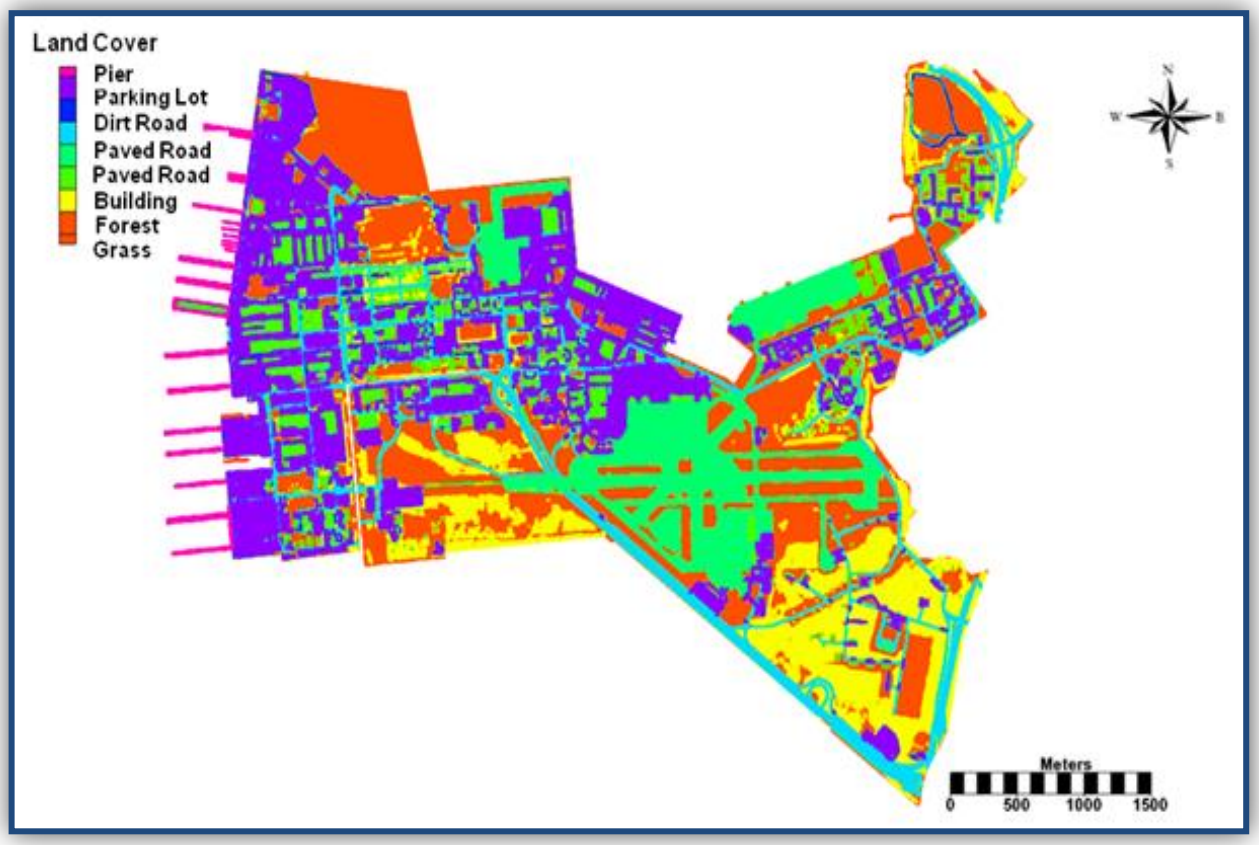

Figure 28. Land coverage (5 x 5 m) at NSN.

Based on these data, sediment grain size, erodibility, and bottom friction were specified in the CMS (Table 11).

Table 11. Specifications of land erodibility and sediment grain size in the CMS based on land coverage data.

Land Coverage	Erodibility	Grain Size (mm)
Grass	None	N/A
Forest	Limited	0.3
Building	None	N/A
Paved Road	None	N/A
Dirt Road	Limited	0.5
Parking Lot	None	N/A
Pier	N/A	N/A

Because the NSN and its surrounding area are largely covered by concrete surface and buildings, a large part of land surface was specified as non-erodible. A median grain size of 0.2 millimeter (mm) was specified for the remaining study domain, and a non-erodible bottom was assigned for the land area surrounding Norfolk (Figure 28 above).

3.5.2.3 Forcing Parameterization (Tides, Surge, Winds and Waves)

Tide, surge, wind, and waves served as physical forcing inputs to the nearshore modeling exercise. The regional surge and wave modeling efforts provided synthesized storms with 50-yr and 100-yr return interval periods and a winter extra-tropical storm (i.e., the 1982 nor'easter) (refer to *Section 3.4* above). For the 1-yr and 10-yr return interval storms, extremal statistics were computed for water surface elevations at NOAA gauge 8638610 (Sewells Point, VA), waves at NDBC buoy 44099 (Cape Henry, VA), and wind at NOAA gauge CBBV2 (Chesapeake Bay Bridge Tunnel) (refer to definitions of these forcings in Table 12). Based on the statistical results and the driving forcings for the 50-yr return interval storm, time series of water surface elevation, wind, and wave parameters for the 1- and 10-yr return interval storms were constructed and applied directly in the CMS analysis.

Table 12. Water surface elevation, waves, and wind for 1-yr and 10-yr return interval storms.

Return Interval Storm	Water Surface Elevation (m)	Wave Height (m)	Wave Period (sec)	Wind Speed (m/sec)
1-yr	1.200	2.100	10.000	21.00
10-yr	1.700	2.600	12.000	28.40

Figure 29 and Figure 30 highlight wind and wave conditions associated with the 100-yr return interval storm, respectively. The wind plots indicate that the tropical storm passing over the study area had a peak speed of 33 m/s (74 mph). Storm waves propagated from the Chesapeake Bay side with a wave period of 16 seconds and a peak wave height greater than four meters. Tidal data at Sewells Point, VA, were available on the NOAA website, http://tidesandcurrents.noaa.gov (accessed 21 March 2012). Four-day water surface elevation was downloaded during a spring tidal period and incorporated into the surge of the 2.0 m SLR scenario for the CMS. The combination of the surge and the spring tide increased the maximum water surface elevation by more than half a meter (Figure 31).

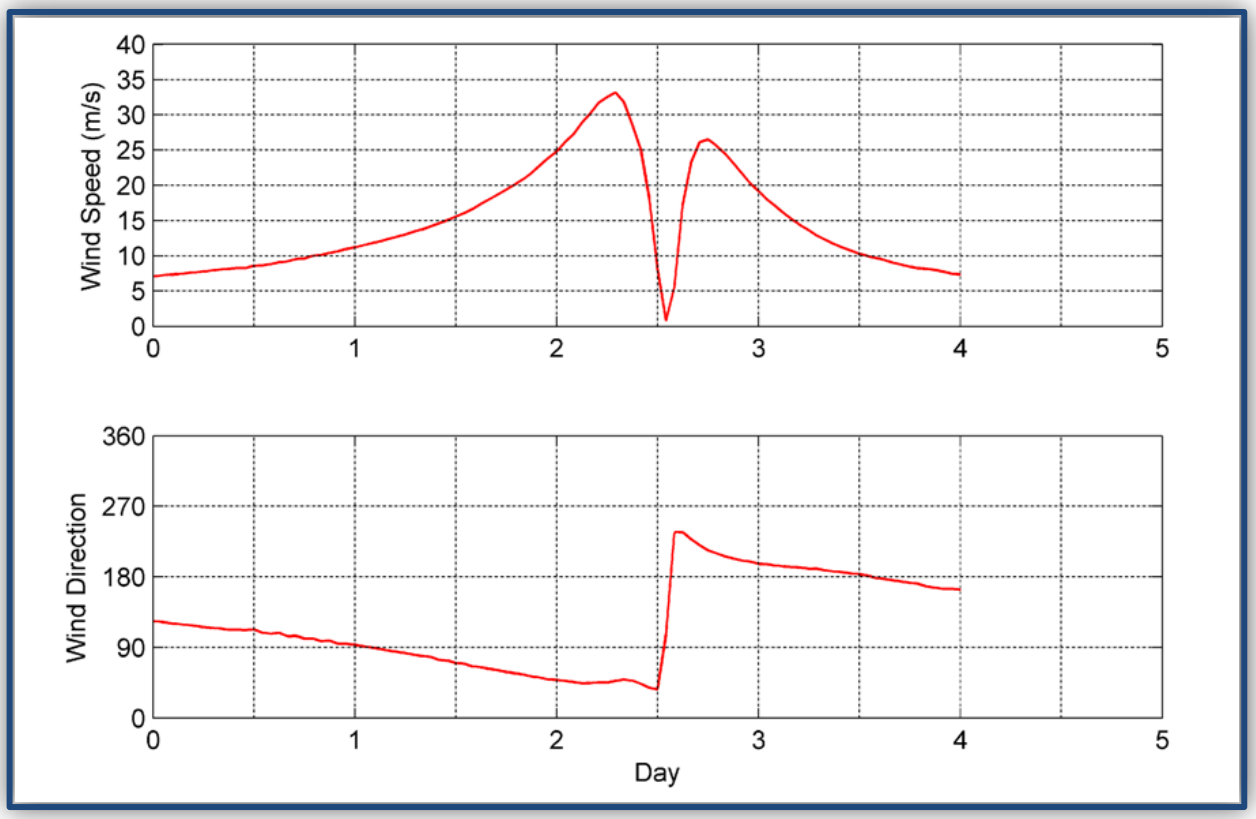

Figure 29. Wind speed and direction attributed to the 100-yr return interval storm.

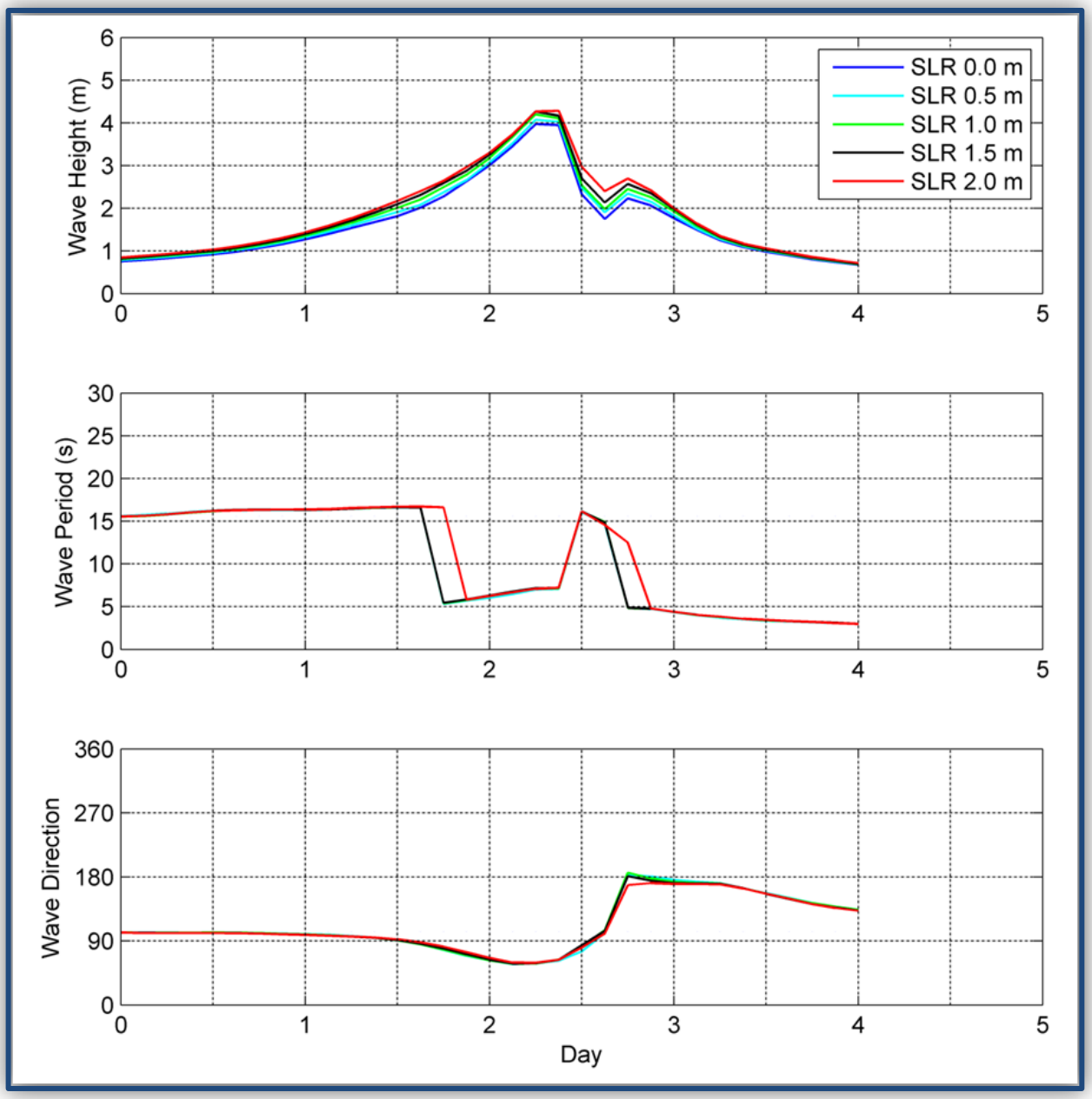

Figure 30. Wave parameters attributed to the 100-yr return interval storm under the five SLR scenarios.

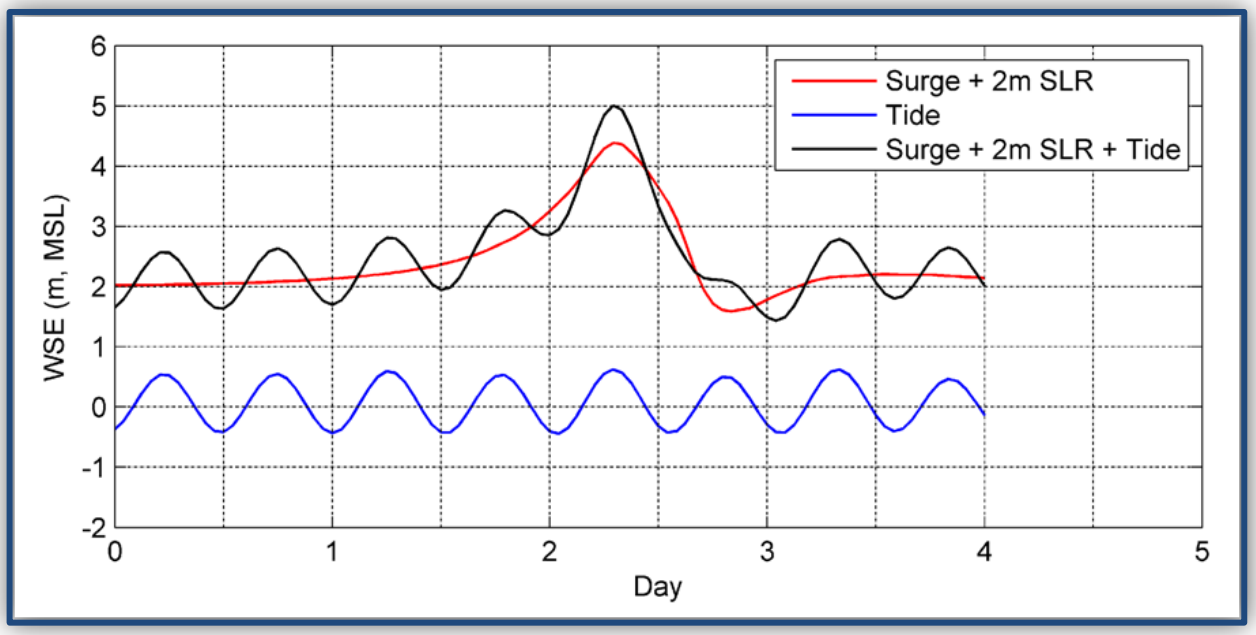

Figure 31. Maximum water surface elevation (WSE) at the NOAA Gage 8638610 (Sewells Point, VA) under the 2.0 m SLR scenario with the spring high tide.

Sustained SLR inundated land and created new wetland areas along coastal regions. To accurately calculate nearshore hydrodynamics, storm surge models characterized the SLR by capturing changes in vegetation types using corresponding adjustments to bottom frictional roughness. Consistent with the regional surge and wave model, the CMS employs five sets of bottom roughness (Manning's-n values) for the five SLR scenarios. For example, in the 2.0 m SLR scenario (Figure 32), a small Manning's-n of 0.02 was specified for water covered areas and increased to as large as 0.15 on concrete covered land areas.

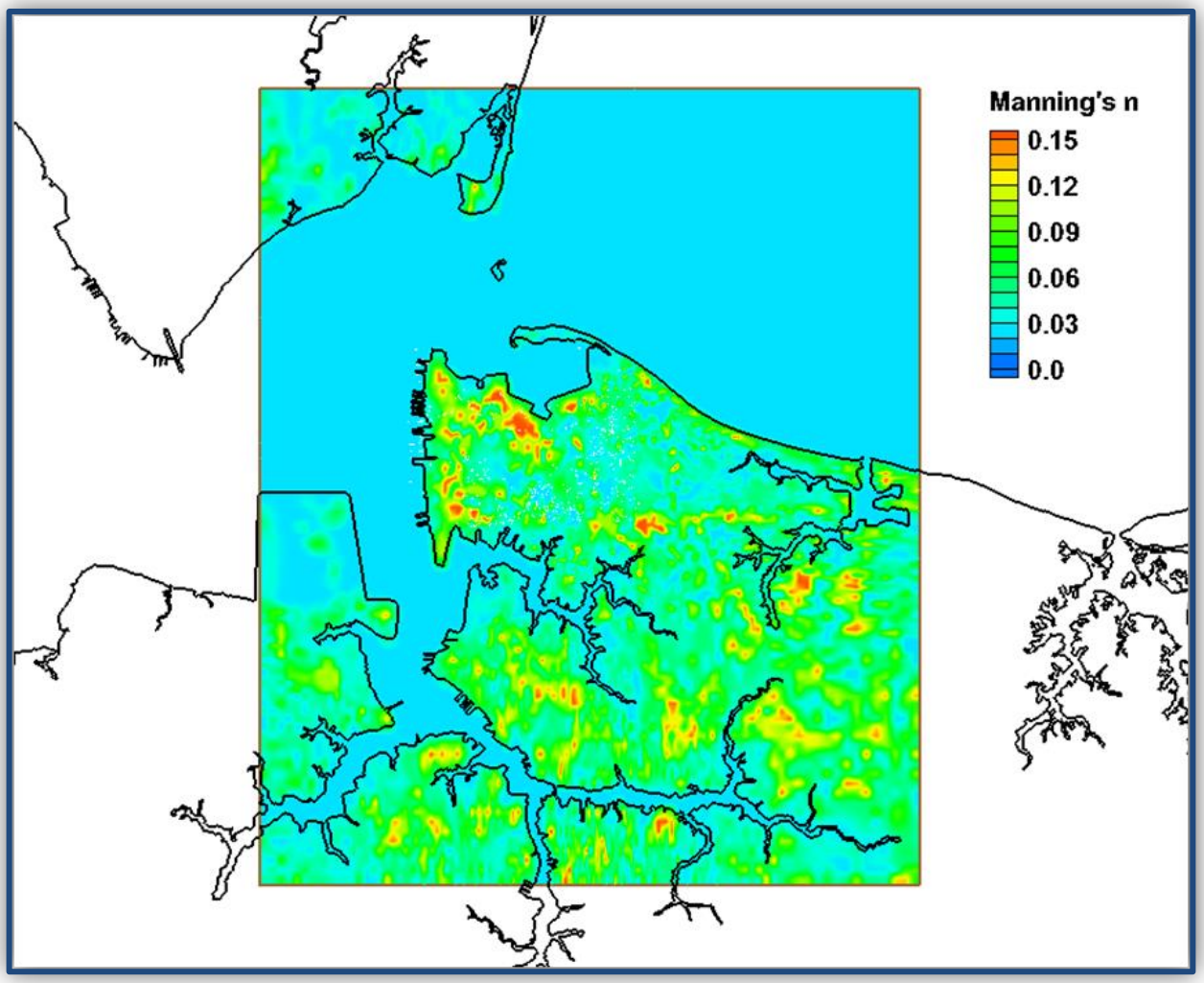

Figure 32. Spatially varying Manning's-n under the 2.0 m SLR scenario.

3.6. Surface Flood Routing Assessment Methodology

Rising sea levels increase the potential for coastal flooding by providing a higher base for storm surges to build upon, and diminishing the rates at which low-lying areas can drain, thereby increasing the risk of flooding from storm events. The next step in our approach focuses on modeling the onshore effects of coastal storms (i.e., maximum water depths and duration) under the prescribed SLR scenarios Figure 33.

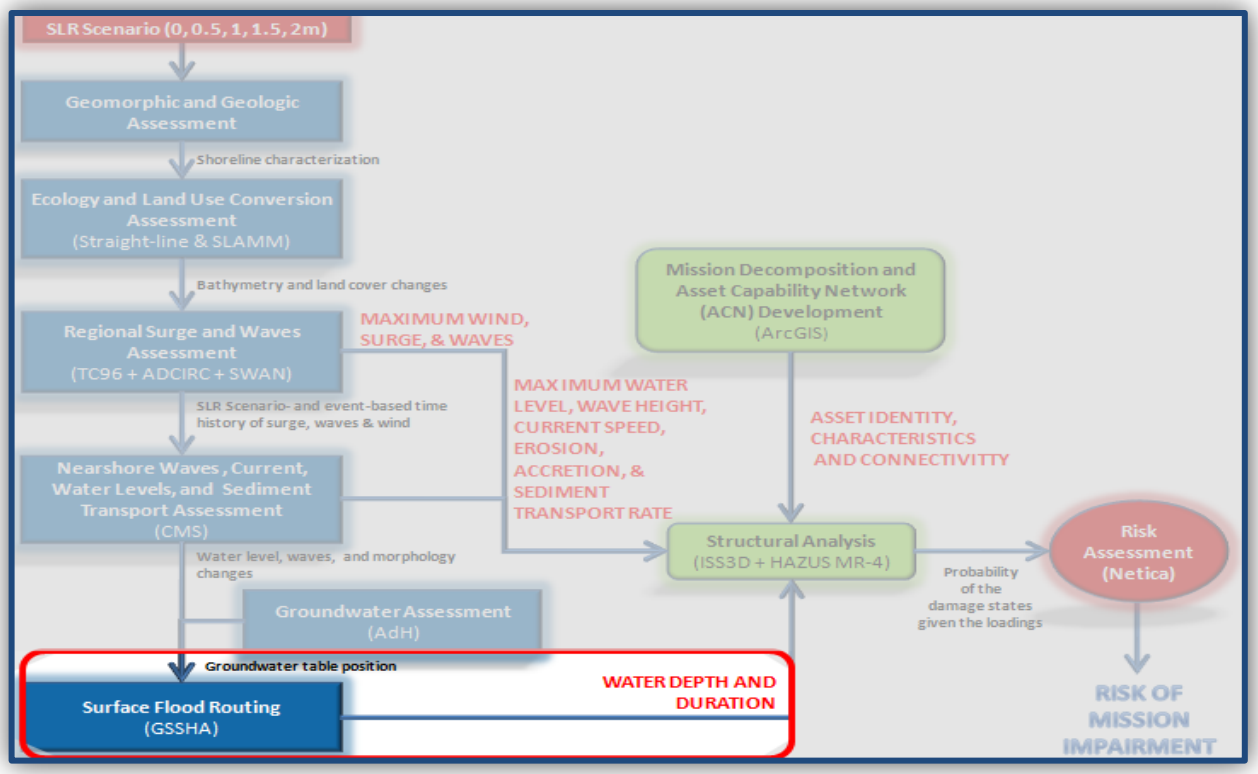

Figure 33. Project analysis and tasks: *Surface Flood Routing Assessment*.

As the figure illustrates, storm surge and wave overtopping data from the previous steps (i.e., regional and nearshore modeling) combined with hydrologic and installation-specific data are used to simulate onsite inland flooding in response to the prescribed scenarios. The intent is to generate a third series of maps (and videos) that visualize the extent of the compounding threat for each storm under each SLR scenario attributed to onshore effects. The outputs (i.e., maximum flood depths and durations per $10m^2$ grid cell) are then used to assess threats to the structural integrity of critical assets in the next steps of our risk-based framework.

3.6.1 Models and Approach

Flood analysis for all key installation assets were computed by means of the Gridded Surface-Subsurface Hydrologic Analysis (GSSHA) numerical simulation tool, a spatially distributed, physically-based hydrologic simulator (Downer and Ogden 2004, 2006). GSSHA is a complete watershed analysis model that was developed and is now maintained by ERDC. The model simulated processes in GSSHA related to the generation of runoff, stream routing, overland and stream sediment processes, constituent transport, as well as interactions with storm drainage networks in urban settings (Figure 34). GSSHA was designed to identify and realistically simulate hydrologic processes in watersheds. At the time of the study, GSSHA had been used in numerous studies by the USACE, other federal agencies, private engineering firms, and academia in a variety of hydrologic investigation and engineering projects (unpublished data available at http://gsshawiki.com, accessed December 2010).

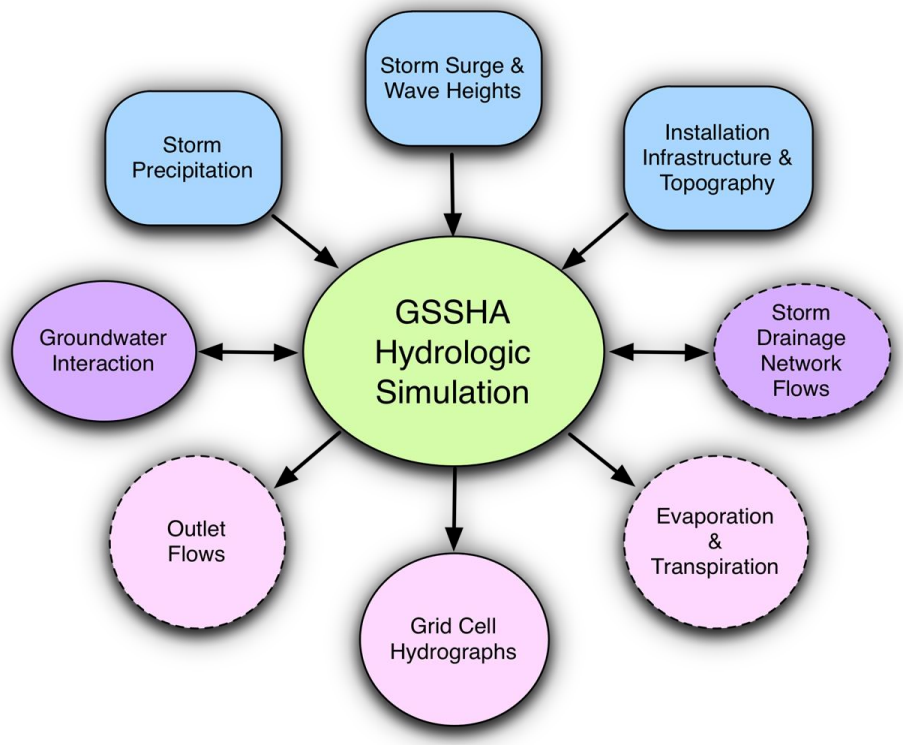

Figure 34. Inputs and outputs of the GSSHA model's flood routing assessment. Items outlined in dashes were considered, but ultimately dropped from the case study application.

There are three main reasons why GSSHA has been selected to assess surface flood routing in our framework. First, the physically-based nature of GSSHA provides the ability to simulate hydrologic process response as opposed to a lumped watershed response where various physical processes are grouped together in an overall runoff response parameter such as a "curve number" or other empirical values that are commonly used in non-distributed hydrologic models. This is important for simulations of future SLR scenarios for which there are no recorded data to calibrate an empirical parameter. Second, the spatially distributed nature of the GSSHA computational grid allows for flood hydrographs of depth to be computed on a grid cell-by-grid cell basis, a critical requirement of the next steps (asset damage function computations) in our risk assessment framework. Third, the capability of GSSHA to simulate the interaction of storm drain networks with hydrologic runoff processes is essential in the highly urbanized setting. In other words, GSSHA is the best tool available with which to conduct the surface flood routing assessment for the study.

3.6.2 Modeling Inputs

To begin, a 10 m computation grid was constructed from available detailed topographic, land use, and soil type data on the NSN study site along with GIS-based data of the existing installation road and storm drainage networks.[22] Rainfall runoff was simulated using

[22] Note - this grid served as the spatially-explicit risk assessment platform for case study. In other words, structural analyses were conducted within these same $10m^2$ grid cells, and risks were assessed as this scale as well.

precipitation intensities that corresponded to the return intervals of the prescribed storm intervals. Storm surge water levels and wave heights were provided for the GSSHA analyses from previous analyses (refer to *Sections 3.4 and 3.5*) and served as the primary source of inland flooding to the surface flood routing computations.

3.6.2.1 Gridded Surface-Subsurface Hydrologic Analysis (GSSHA)

A site-specific GSSHA model was developed for the case study that captured infiltration, overland flow, and coastal wave propagation within the NSN boundary (Figure 35).

Figure 35. GSSHA modeled area for NSN.

The parameters for these physical processes were selected based on accepted values for the soil, vegetation, land use, and hydrologic runoff characteristics of the installation. Precipitation data was available from monitoring stations near the study area from monitoring stations near the study area, but unfortunately, no other surface data such as soil moisture or streamflow were available. *Sections 3.6.2.4 and 3.6.2.5 below* describe the affects this data limitation had on the analysis and the procedures used to extrapolate representative values for these missing data.

It is important to note that the NSN installation is highly urbanized with an extensive drainage network both above and below ground. However, this drainage network is beyond its design life and is in varying states of dysfunctionality (i.e., some sections are plugged, collapsed and/or leaking). According to installation personnel, water in the drainage network flows in both directions with the rise and fall of the tides, indicating its relatively low elevation and its lack of backflow prevention. As a result, the drainage network configuration could provide a secondary source of interior flooding under elevated sea levels and/or a storm surges. To be conservative, we made the assumption that the drainage network was effectively inoperative, and our results depict a "blocked network" scenario.[23] It should be noted that this assumption could lead to a slight overestimation of the surface water depths if the system functions as previously designed.

With the exception of a drainage ditch running along the south east side of the airfield, surface runoff features (e.g., streams) on NSN are essentially non-existent. The majority of surface runoff migrates and pools in paved areas, eventually moving to storm drains and open areas, where it infiltrates down into the groundwater aquifer. Infiltration in opens areas occurs rapidly because the predominant underlying soil type is sand. The lack of surface drainage features (i.e., streams) makes it impossible to quantify overland flow values across the study site. As such, the overland flow model results could not be calibrated against observed data.[24]

3.6.2.2 Model Domain, Digital Elevation Model (DEM), and Structured Grid

The digital elevation dataset used in this study was sampled from LiDAR dataset with a one-meter resolution. Stream networks were excluded from the analysis (their absence of the landscape precluded their incorporation). The coastal boundaries were set approximately 20 m offshore from the coast and/or piers. The inland boundaries followed the higher-elevation ground running the perimeter of the study site. The total area modeled was approximately 15.87 km^2 with a minimum elevation of 0.0 m and a maximum terrestrial elevation of approximately 5.6 m. The physical characteristics of the area (namely elevation, land use, and soils) were projected onto a 10-meter resolution grid as seen in Figure 36. This resolution captured the streets and structures as well as the diversity of the topography while still allowing for computational efficiency.

[23] Furthermore, no effects were taken into consideration of any non-water fluids that potentially reside in the subsurface that could possibly influence the analysis.

[24] We believe this lack of validation is of little consequence to the overall findings based on the magnitude of the results.

Figure 36. GSSHA model domain with 10-m structured grid overlay.

3.6.2.3 Land Surface Data

The land use dataset for the Norfolk model was derived using the FEMA Hazards U.S. Multi-Hazards Software (HAZUS-MH MR) database and the 2000/2001 NLCD (http://www.mrlc.gov/, accessed January 2011). The HAZUS-MH MR database was used to obtain Manning's-n values, which were used as a measure of surface roughness. These values were then transposed into land cover types based on the 2000/2001 NLCD. The overland flow processes within GSSHA relied on the roughness coefficient associated with each land use classification to accurately model how flow moved over the land surface. Land use classifications were also derived for the Norfolk area under different SLR scenarios, assuming that when the sea levels rose, the land use characteristics would also change. For each of the five prescribed SLR scenarios, Table 13 lists the land use classification, Manning's-n roughness coefficient, and the percent area of each land use within the model domain. Figure 37 depicts the current land use classifications within the model domain.

Table 13. Manning's-n roughness coefficients under prescribed SLR scenarios.

NLCD Class Number	Land Use Description	Manning's-n	Percent Area Based on SLR (m)				
			0.0	0.5	1.0	1.5	2.0
21	Developed - Open Space	0.020	38.73	32.30	31.56	28.65	24.13
22	Developed - Low Intensity	0.050	9.04	10.45	12.20	14.42	16.91
23	Developed - Med Intensity	0.100	21.23	22.28	20.96	20.62	19.10
24	Developed - High Intensity	0.150	20.48	17.70	17.50	15.32	13.76
31	Barren Land (Rock/Sand/Clay)	0.090	1.85	2.82	2.50	1.94	3.00
42	Evergreen Forest	0.110	3.23	4.05	4.23	3.24	3.00
51	Dwarf Scrub	0.040	0.00	3.06	4.22	6.42	9.80
72	Sedge/Herbaceous	0.030	0.00	2.12	2.12	4.58	5.87
74	Moss	0.025	0.00	0.32	0.02	0.69	1.25
81	Pasture/Hay	0.033	1.80	1.67	1.67	1.36	1.04
82	Cultivated Crops	0.037	3.18	2.75	2.54	2.50	1.67
95	Emergent Herbaceous Wetlands	0.045	0.49	0.47	0.48	0.26	0.46

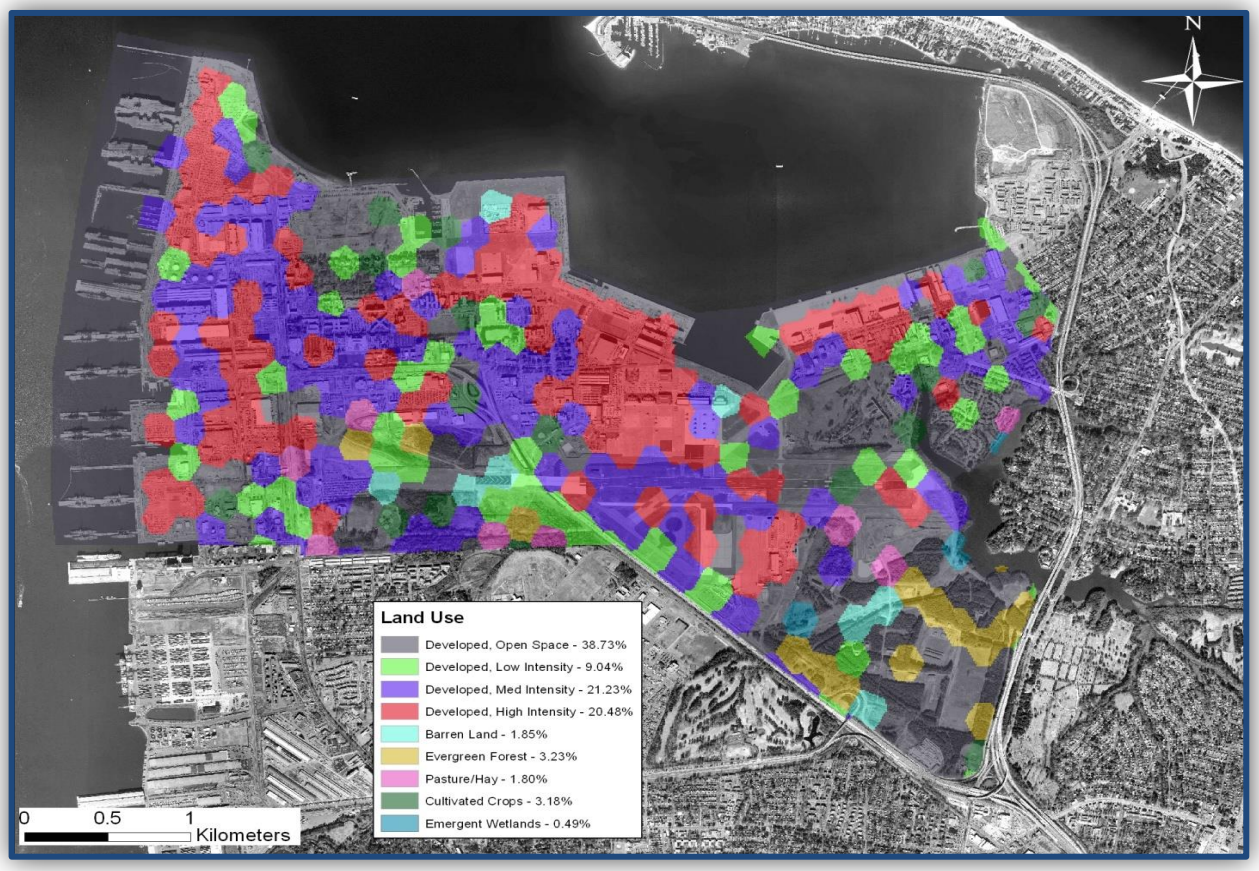

Figure 37. Current land use classification (based on HAZUS-MH MR).

3.6.2.4 Soils Data

Soils data for the Norfolk model were obtained using the SSURGO soils dataset from the Natural Resources Conservation Service (NRCS) (NRCS 2010), and software within the DoD's

Watershed Modeling System (WMS) (Nelson 2001) was used to classify the different soil types. The infiltration processes within GSSHA relied on physical parameters (e.g., hydraulic conductivity, capillary head, porosity, pore index, residual saturation, field capacity, and wilting point) based on these soil classifications. The soil parameters were based on both SSURGO estimates and literature (Rawls et al. 1982; Rawls 1983; Ralwls et al. 1983; Rawls and Brakensiek 1985; Ogden and Saghafian 1997) (Table 14 and refer to Figure 38 for classifications displayed across the model domain). Because infiltration was also dependent on land use, if an area was covered by high-intensity development (NLCD class number 24), the hydraulic conductivity of the area was set to 0.0001 to prevent infiltration.

Table 14. Soil parameter estimates used in the study.

SSURGO Soil Classification	Sandy Loam	Fine Sandy Loam	Loam	Silty Clay	Clay
Percent by Area (%)	3.25	60.86	0.25	0.46	35.17
Hydraulic Conductivity (cm/hr)[a]	1.09	0.15	0.66	0.05	0.03
Capillary Head (cm) [a]	11.01	21.85	8.89	29.22	31.63
Effective Porosity (m^3/m^3)[a]	0.412	0.33	0.434	0.423	0.385
Pore Index (cm/cm)[b]	0.378	0.319	0.252	0.15	0.165
Residual Saturation (m^3/m^3) [a]	0.041	0.068	0.027	0.056	0.09
Field Capacity (m^3/m^3)[c]	0.145	0.118	0.118	0.352	0.271
Wilting Point (m^3/m^3) [a]	0.095	0.148	0.117	0.25	0.272

[a] Values based on Rawls and Brakensiek (1983) and (1985), and Rawls et al. (1982) and (1983)
[b] Values based on Ogden and Saghafian (1997)
[c] Values based on SSURGO estimates

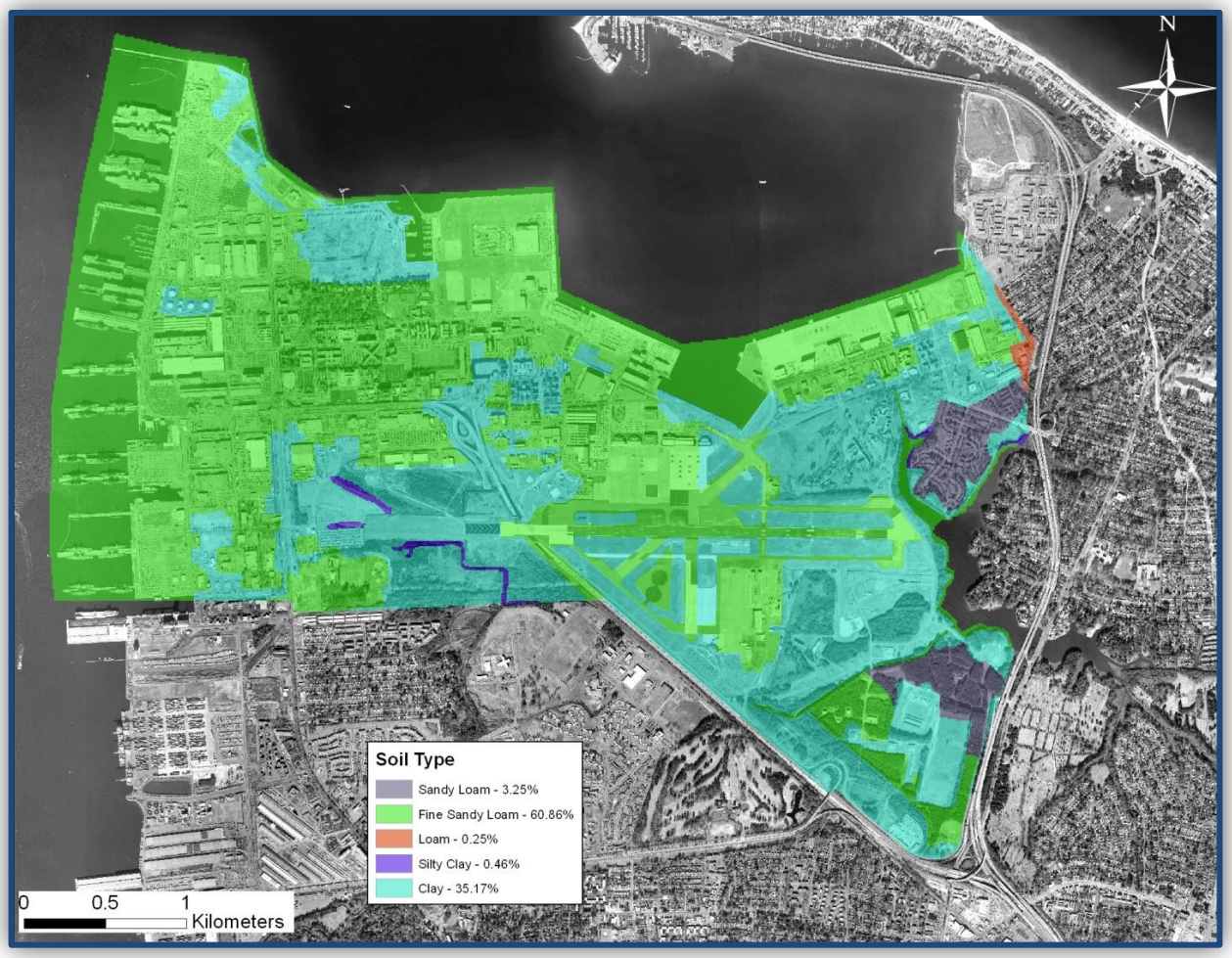

Figure 38. Soil classification based on SSURGO soil data.

3.6.2.5 Hydrometeorological Forcing Data

Hydrometeorological forcing data was used as input into the model to simulate the physical processes within a watershed, such as rainfall runoff, evapotranspiration, infiltration, etc. Precipitation was an important hydrometeorological input for this project because it drove both the soil moisture and inland flooding. Given that the storm simulations for this study were short-term events and that the majority of the study area was intensively developed (see Figure 37 above), it was assumed that evapotranspiration was not a significant physical process for this study and was therefore not included in the model. For this reason no temperature, pressure, humidity, or radiation data were required for the study. Recurrence event precipitation data was obtained to determine the precipitation amounts that could affect NSN under various storm severities. Recorded precipitation for the 1982 nor'easter was also obtained in order to demonstrate a historical precipitation event.

3.6.2.5.1 Recurrence Event Storm Precipitation

Recurrence event precipitation data (24-hour intensity and total precipitation) were obtained for the 1-, 10-, 50-, and 100-yr storm events using the NOAA ATLAS 14 dataset (Bonnin et al. 2006) (Table 15).

Table 15. Recurrence interval precipitation estimates based on NOAA ATLAS 14.

Average Recurrence Interval (years)	Precipitation Intensity Estimates over 24 hrs (cm/hr)[a]	Precipitation Estimates over 24 hr period (in)[a]
1	0.30	7.32
10	0.58	14.02
50	0.83	2.01
100	0.97	23.16
[a] Precipitation frequency estimates based on NOAA Atlas 14		

This dataset was chosen to obtain the various precipitation events primarily because it was a more recent dataset and it was the approved dataset used in hydraulic design by the Virginia Department of Transportation (Hydraulic Design Advisory 05-03; http://www.virginiadot.org/business/resources/HDA_05-03rev.pdf). These recurrence precipitation rates and totals were based on data from the Norfolk WSO Airport, Virginia. As recommended by the NOAA ATLAS 14 dataset, a 24-hr SCS Type III storm distribution was used to develop a 24-hour storm event for each SLR scenario (Figure 39). The timing of the peak precipitation intensity was chosen to correspond to the timing of the peak storm surge (see *Section 3.6.2.6* below) in order to simulate the worst-case scenario of inland flooding across the installation. While it was unlikely that the peak precipitation would occur simultaneously with the arrival of the peak storm surge, the assumption of coincident peak conditions provided a conservative estimate of the maximum flooding conditions.

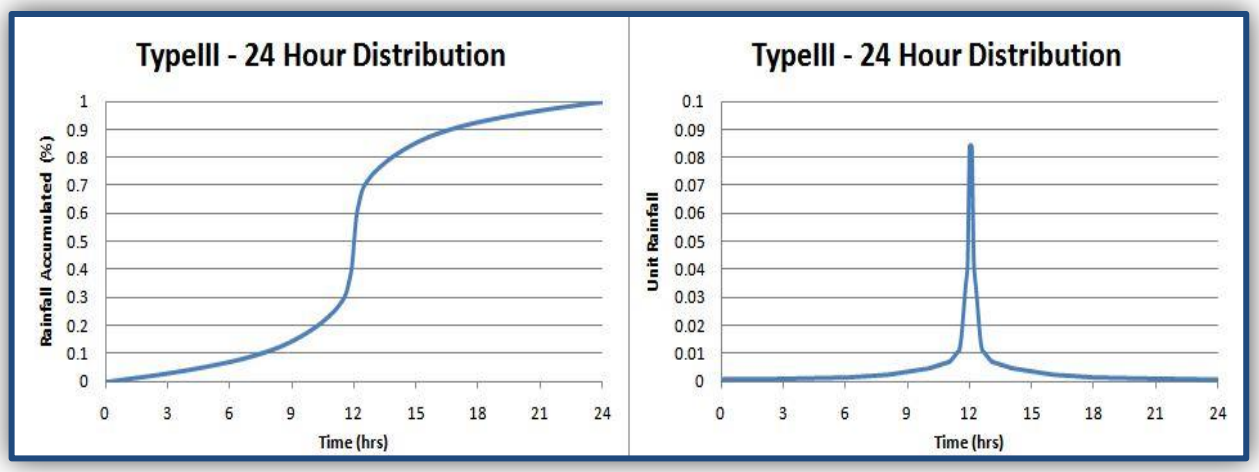

Figure 39. Unit hydrograph for Type III – 24 hour distribution.

3.6.2.5.2 1982 Nor'easter Storm Precipitation

Precipitation data was also collected from a recorded Nor'easter that affected the Norfolk area in October 1982. Precipitation data from October 23-27, 1982 (Figure 40) was collected from the Norfolk International Airport (KORF) via the Air Force 14th Weather Squadron. The peak rainfall rate was 1.09 inches per hour (in/hr) with a maximum 24-hour accumulation of 6.15 in. Based on the recurrence precipitation shown in Table 15 above, the precipitation associated with the October, 1982 Nor'easter had approximately a 1-yr average recurrence interval.

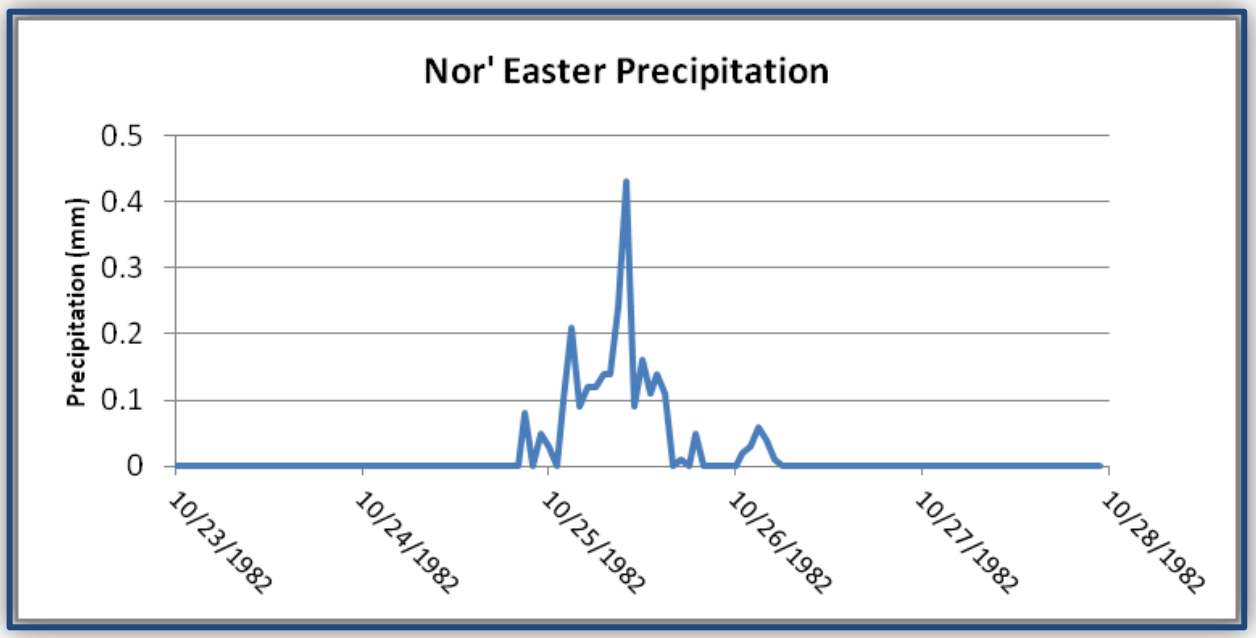

Figure 40. October 23-27, 1982 Nor'easter precipitation.

3.6.2.6 Coastal Surge Input

The amount of inland flooding caused by coastal storm surge across the installation was simulated by GSSHA using spatially- and temporally-varied hydraulic heads as boundary conditions on the coastal perimeter of the model (Figure 41).

Figure 41. Coastal hydraulic head boundary locations.

These hydraulic heads were supplied by the output from the nearshore modeling task (refer to Figure 33 above in *Section* 3.6). As indicated in *Section 3.6.2.5.1*, the peak surge and peak precipitation were chosen to occur simultaneously in order to simulate the maximum potential flooding under the surge and precipitation scenarios. *Equation 20* was used to determine the hydraulic head at each cell along the coastal boundary of the model.

$$H = MSL + SLR + Surge + WH/2 \quad \textbf{(20)}$$

where *H* was the head applied to the boundary, *MSL* was the current mean sea level, *SLR* was the prescribed SLR scenario (i.e., 0.0 m – 2.0 m), *Surge* was the coastal surge, and *WH* was the wave height (m).

Figure 41 above shows the locations to which the hydraulic head boundary was applied, while Figure 42 depicts the average storm surge applied to this boundary over the length of the simulation for the five SLR scenarios under the 100-yr return interval storm event, referenced to

the mean sea level datum for the project. Note that the peak average storm surge value for the 2.0 m SLR 100-yr return interval storm event was nearly 8.0 m.

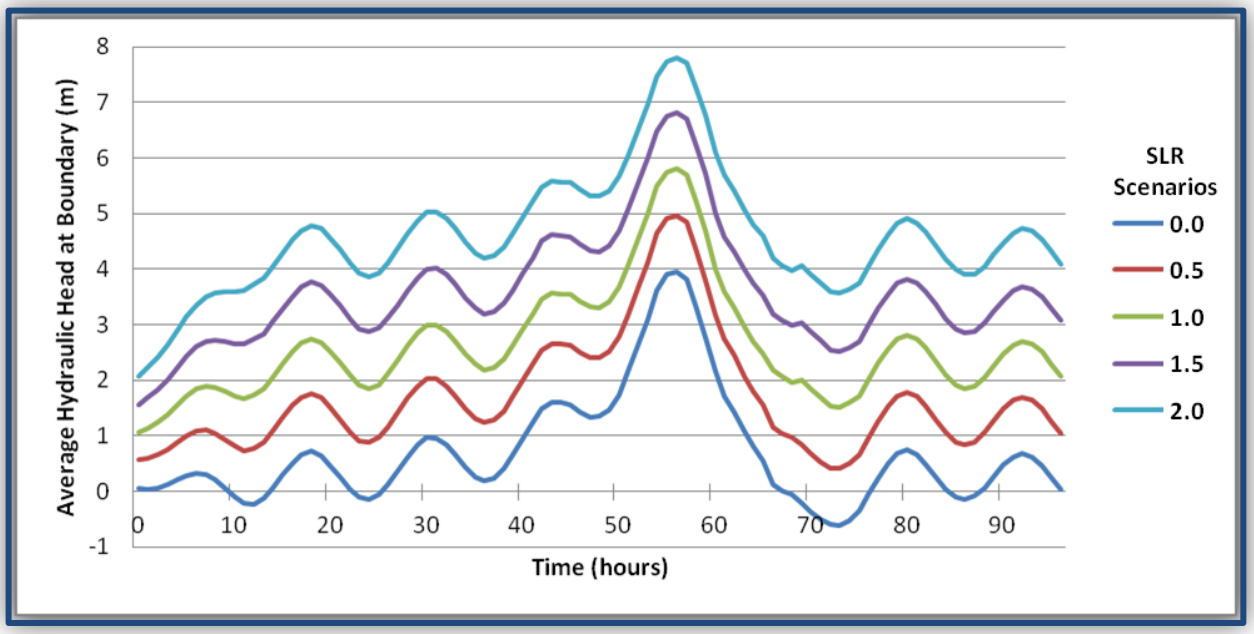

Figure 42. Average hydraulic head applied as boundary conditions for 100-yr return interval storm under the five SLR scenarios.

For the purposes of this study, it was assumed that the feedback between the surface runoff due to precipitation and the storm surge values computed by the nearshore model (*Section 3.6*) were negligible. However, a complete assessment of inland flooding across the installation would necessarily include coupled interaction between the storm surge computations and the inland flooding computations, to capture the combined effects of flooding from precipitation and the storm surge. The storm surge computations in this study did not include the accumulation of runoff from precipitation, therefore the storm surge estimates at the boundary as indicated in Figure 41 above were likely to be somewhat lower than what they should otherwise have been if the nearshore modeling was able to consider the surface precipitation runoff. However, since GSSHA computed the surface runoff, but was also dependent on the storm surge computation as input, an iterative feedback process would be necessary to bring these two model computations into agreement with one another as to the proper storm surge value at the boundary. Such an iterative feedback process was deemed beyond the scope of the project because it was likely to generate only a minor increase in storm surge value given the large storm surge values that were considered in the prescribed SLR scenarios. The magnitudes of the simplifying assumptions described above are small compared to the amounts of storm surge, particularly when coupled with SLR. The cumulative effect of the assumptions is also assumed to be insignificant in its impact on the water level results.

3.7. Mission Decomposition and Asset Capability Network (ACN) Development Methodology

Beyond capturing the system's exposure (i.e., the magnitude of storm loadings exacerbated by rising sea levels), the question of impact to military missions remains. Answering this question requires the identification of each installation's critical missions and the development of a methodology to quantify the relationship between those missions and the infrastructure that assures their performance. The Critical Infrastructure Protection (CIP) community typically models these relationships as system networks, where the physical components of the infrastructure and the more abstract idea of mission are represented in a box-arrow diagram (Lewis 2006, Rinaldi et al. 2001, Dudenhoeffer 2006). Although these seminal studies offer useful context with regards to systems analyses, they have failed thus far to explicitly address risk of system failure in consideration of environmental change – specifically failures driven by coastal hazards and rising sea levels. As a next step in our process, we use these foundational interdependency modeling principles to govern the strategic architecture of the damage and risk assessment framework Figure 43.

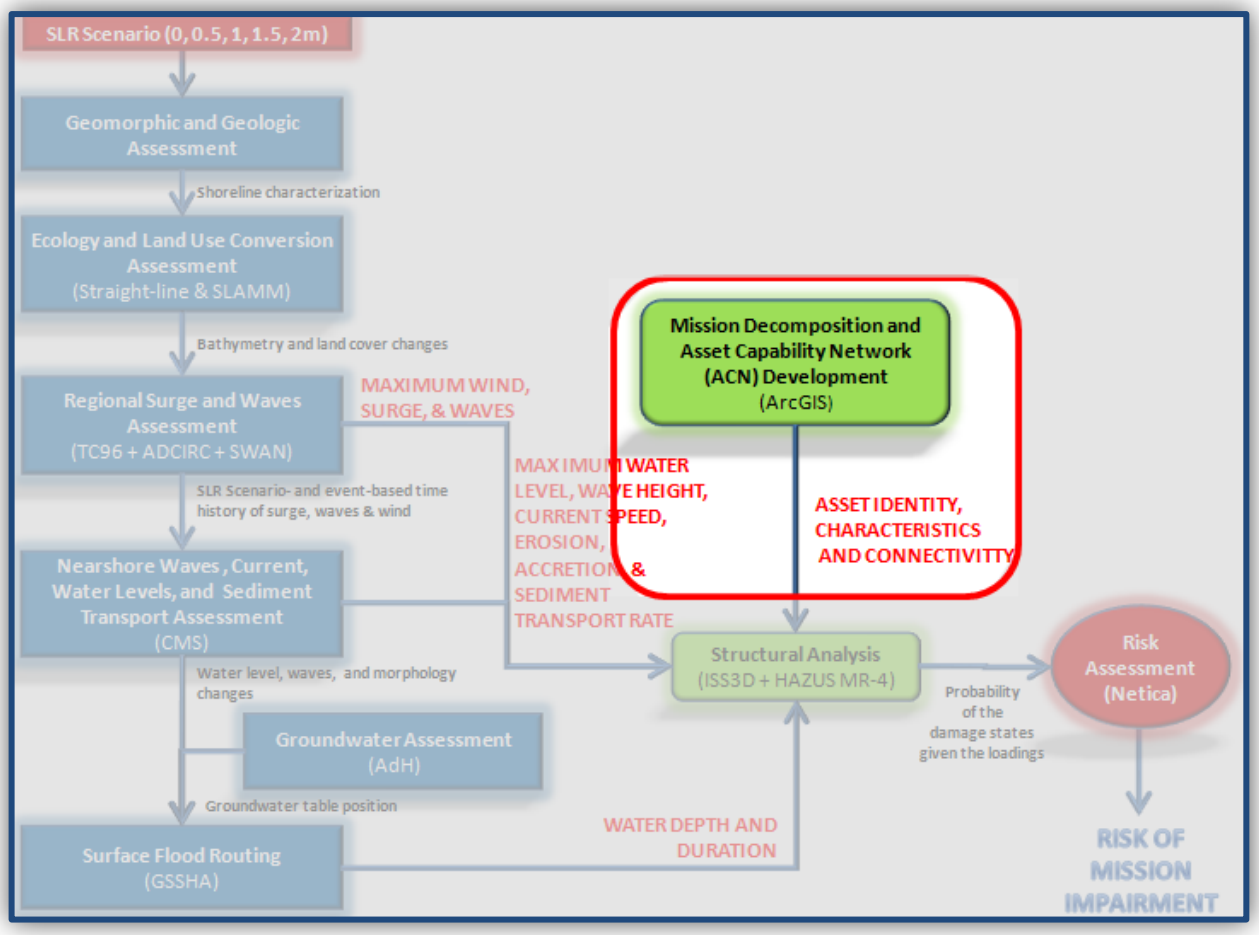

Figure 43. Project analysis and tasks: *Mission Decomposition and ACN Development*.

We call our novel approach an *Asset Capability Network (ACN)* which captures the intricate, highly interdependent relationships between infrastructure assets, capabilities, and mission performance. To assess risks, two tasks must be undertaken: 1) the decomposition or breaking down of the mission into key assets (i.e., built and natural infrastructure) that provide critical services or capabilities in support of the mission, and 2) the construction of a Bayesian network (i.e., a probabilistic model presented in graphical format to represent a set of random variables and their conditional dependencies). This section describes our decomposition of the NSN mission for the case study application. *Section 3.9* then describes the construction and application of the Bayesian network.

3.7.1 Models and Approach

At the time of the project, readily available data regarding critical infrastructure was typically stored in enterprise-based GIS databases [i.e., TRITON (Unclassified), HD-MAP (SIPRNET), or SMADS (SIPRNET)], or stored onsite as GIS data, Computer-Aided-Design (CAD) data, paper, or microfiche files. To begin, the enterprise-wide databases at the study site (i.e., NSN) were searched for content as a prelude to contacting the installation and arranging for an onsite visit. Working through the chain of command, we contacted Commander (CDR) Fred Hintermister (ODASN IS&A CIP), the Service Liaison to the Defense Critical Infrastructure Program. CDR Hintermister put us in contact with CDR Eric Abby, the Public Works Officer at NSN, who in turn referred us to Mr. Bob Butters, Waterfront Planner. A series of telephone interviews were conducted in the October-November 2009 timeframe, followed by on-site visits in December of 2009, and again in August of 2010. The purpose of these interviews and visits was to elicit information about missions at NSN and to gather quantitative data about the infrastructure that supported those missions. The December 2009 visit was a preliminary visit intended to familiarize us with the study site. The August 2010 visit focused on gathering more detailed data, tracing connectivity, and initiating assessment of damage modes for the built infrastructure.

As a result of these visits, we decided to focus on collecting ACN data for two missions: *At-Berth Support* and *Support Ship Harbor Movement*, as installation personnel considered these "critical," and we believed they were vulnerable to SLR and coastal storm impacts. Notional or alpha version ACN networks were constructed based on initial data. Figure 44 shows the initial *At-Berth Support* network and Figure 45 shows the *Support Ship Harbor Movement* network. The explicit ACN characteristics and their descriptions are also defined in Table 16)

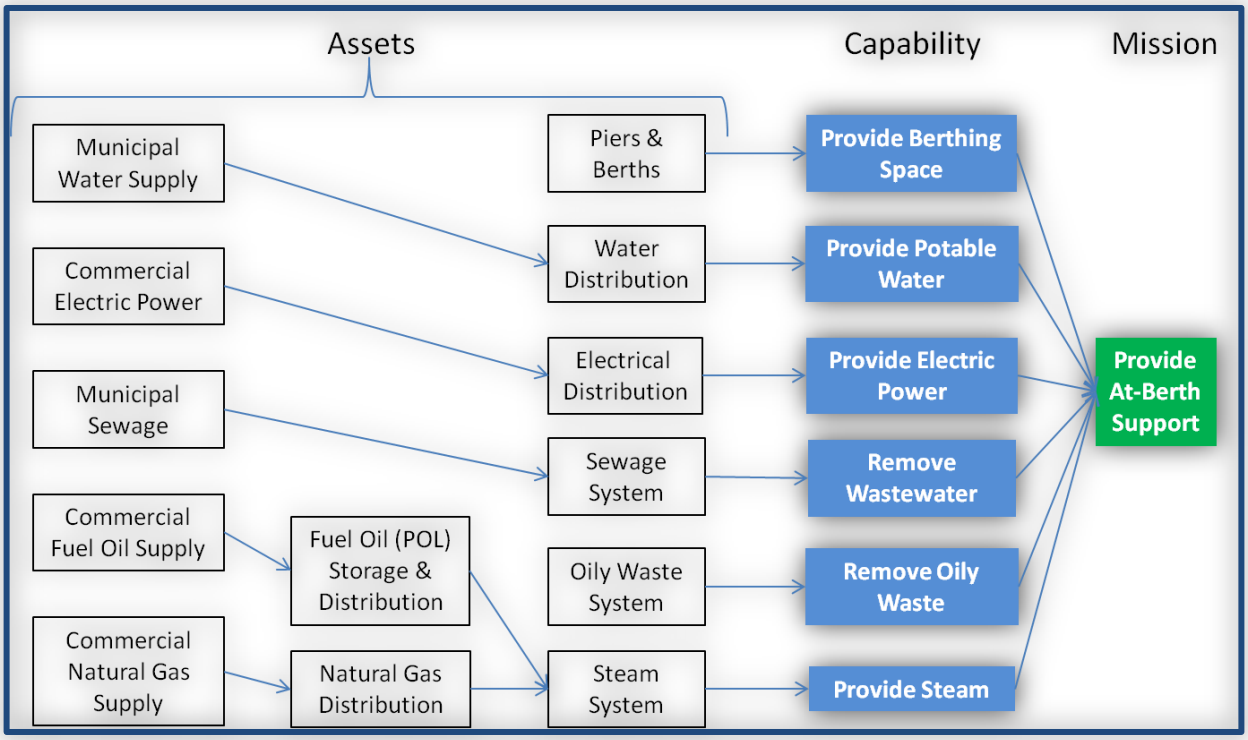

Figure 44. The ACN diagram detailing the capabilities and assets supporting the *Provide At-Berth Support* mission.

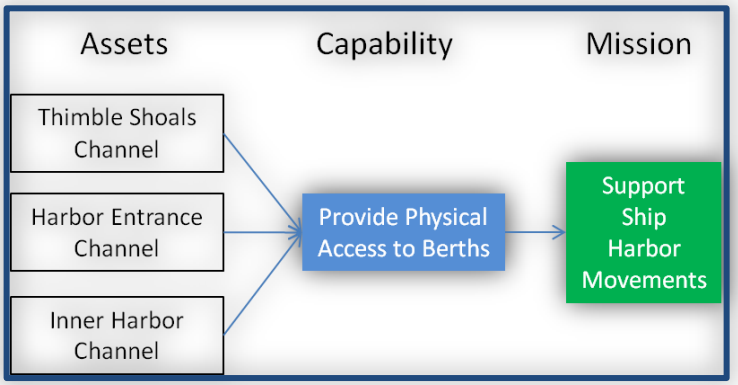

Figure 45. The ACN diagram detailing the capabilities and assets supporting the *Support Ship Harbor Movements* mission.

Table 16. ACN characteristics and descriptions.

ACN Characteristic	Description
Explicit representation of mission, capabilities and assets	This project sought to assess risk to mission. Thus, there was a requirement to explicitly enumerate missions of interest. These missions were supported by capabilities – a deliberate statement of function at a higher level of abstraction than the physical infrastructure that supported them. Assets represented tangible entities, infrastructure, or organizations that supported capabilities. All of these components were considered "nodes" in the ACN.
Connectivity	The nodes of the ACN were connected by "edges" (sometimes called links) that represented dependencies, or paths for the propagation of effects through the network. Although physical systems often exhibited cyclical dependencies, so the risk assessment approach required the ability to represent networks as Directed Acyclic Graphs (DAGs). The ACN allowed cycles as long as there was an ability to transform them to DAGs as needed.
Decomposability	Infrastructure and organizational systems were decomposed into hierarchical subsystems. Ideally, segments of the network were represented by a smaller set of single nodes with inputs and outputs that accurately reflected the behavior of their component pieces (e.g., electrical, steam, water, etc.).
Interdependency	Infrastructure subsystems were analyzed using specialized subject matter experts (e.g., electrical, mechanical, civil engineers). These systems were often coupled. For example, a pump for the water system was dependent upon power from the electrical system. Interdependency was a specialized function of connectivity between explicitly enumerated subsystems.
Geospatial representation	In assessing the effects of SLR and coastal flooding, it was necessary to consider the geospatial location of assets. For purposes of the study, assets were located by single points, lines, or polygons. Storm- and SLR-related loadings were represented within a raster (grid), which allowed for multiple loadings to be applied to different parts of the same asset at any given time.
Impact analysis	Given a set of spatially-distributed loadings, it was necessary to calculate risk of damage to a group of assets, rather than a single asset. Damage functions were developed for each asset group in the network to asses loading potential.
Temporal representation	One of the more pressing questions in infrastructure failures was often not "what failed," but "how long would it take to repair." For purposes of this study, failure of an asset was only considered important to the mission analysis if the damage required excessive time to remediate. Nodes in the ACN captured anticipated remediation times as well as (in some cases), dependency on assets required to repair another asset.

3.7.2 Modeling Inputs

The case study's ACN attribution (i.e., network connections and logic) is presented in Table 17.

Table 17. The logical components together represent the ACN. Note that these descriptions are generic inclusions that may or may not be directly represented in this study.

Logical Components		**Example**
Mission	Operational Task	The fulfillment of a mission required the realization of one or more capabilities which were uniquely aligned to the site's activities and purpose(s).
Capability	Abstract function that supports a Mission	Provided support for one or more of the missions. Examples included *Provide Electric Power* and *Provide Steam*.
Asset	Physical Resource that Supports Capabilities	Provided support for one or more capabilities. Examples included: personnel, warehouses, data and communication centers, transportation networks (*e.g.*, bridges, roads, railroads), land, loading docks, cranes, navigation channels, fuel depot, housing (*e.g.*, barracks, mess), utilities, water and wastewater treatment facilities, etc.
Relationships	A link that represents dependency between nodes	Dependencies generally flowed from the mission to the supporting assets. For instance, the *Provide At-Berth Support* mission (A) was dependent on the *Provide Steam* capability (B), so there was an edge from A to B in the study. In turn, B depended on the 150 pounds per square inch (psi) steam line coming onto the pier (C), so there was an edge from B to C.

Our alpha data schema for the original ACN was determined to be overly complex for the quantification of risks due to SLR and coastal hazards at the installation-level resolution, so we streamlined the approach to capture only the essential missions, capabilities, and assets on the site. Table 18 shows the data fields required to populate the missions, capabilities, and assets, while Table 19 shows the data fields required to populate the edges.

Table 18. Mission, capability, and asset data fields for the ACN.

Field name	**Description**
Name	Name of the asset
Description	Description of the node
Type	Mission, Capability, or Asset
Label	Unique label for each node

Table 19. Edge data fields for the ACN.

Field name	**Description**
Parent	ACNID of the node that was dependent on another node (e.g., a pump was dependent on upon electric power).
Child	ACNID of the node that was depended upon

3.8. Structural Analysis Methodology

In order to support base managers in making risk-informed decisions with regards to threats of SLR and storm intensification, structural analyses must be performed at an "actionable scale" (i.e., at the asset level). The next step in our process is to describe each asset's damage state (in terms of conditional probabilities) based on structural loadings at each level of storm severity under the various SLR scenarios Figure 46.

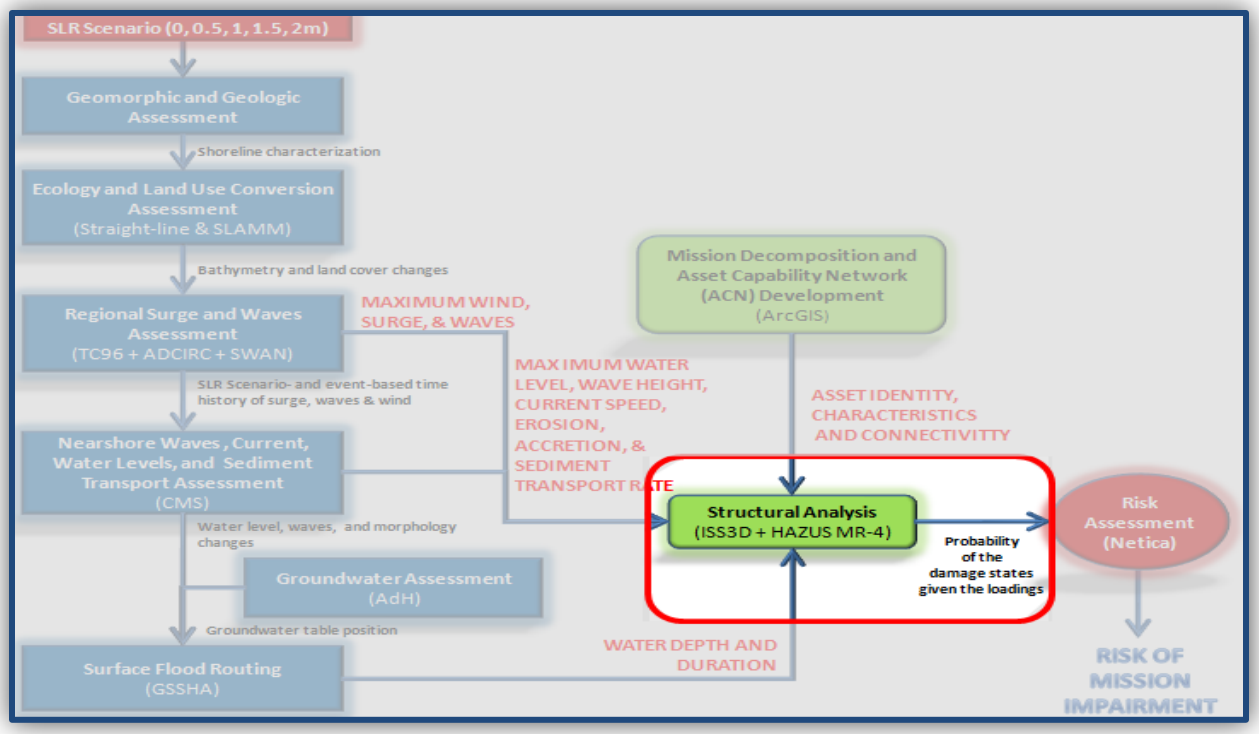

Figure 46. Project analysis and tasks: *Structural Analysis*.

The overall objective is to generate a series of fragility curves for each critical asset that describes the probability that they will fail as a function of the loads on the system. Note that Schultz et al. 2010 discuss four approaches to develop fragility curves for assets (e.g., judgmental, empirical, analytical, and hybrid). Judgmental approaches tend to be limited by subjectivity of expert assessments, whereas empirical approaches tend to be limited by the availability of observational data. Analytical approaches tend to be limited by modeling deficiencies, restrictive assumptions, and/or computational burdens (Schultz et al. 2010). For purposes of this study, we deployed a hybrid approach using all three techniques (judgmental, empirical and analytical) depending on data availability and analytical model capabilities.

3.8.1 Analysis Approach

We define assets as physical resources that support one or more capability required to support a mission. Thus a boiler, a steam line, an electrical substation, or even a building is considered an asset under our risk assessment paradigm. Note that each asset must be defined by their unique physical characteristics, including their location on the study site, and the characterization of their vulnerabilities in order to assess the risk to mission performance if they fail. As such, the structural composition of the assets dictates the types of analyses required to operationalize any ACN.

In essence, the structural assessment can be conducted in 5-steps:[25]

1) Determine which loadings (i.e., winds, waves, flooding depths, etc.) were threats to the various assets;
2) Identify the most likely load of failure (i.e., bending, shearing, tensile failure, etc.);
3) Calculate the capacity of the asset to resist that failure;
4) Calculate the load acting (the demand) that produced that mode of failure; and
5) Generate the probability of damage (i.e., fragility curve) based on the capacity and demand.

The following sections walk through the five steps of the process as they were applied to the case study.

3.8.1.1 Steps 1 & 2: Identification of Loadings and Failure Modes

Table 20 summarizes the modes of failure for each asset and the hazard(s) associated with these entities. The majority of the assets on NSN are vulnerable to electromechanical damage caused by flooding. For purposes of the case study, we assumed that the piers and common storage tanks would avoid permanent damage given the loadings generated by the worse-case scenario (i.e., 100-yr return period storm and 2.0 m SLR).

[25] The majority of the details surrounding the operationalization of the NSN ACN were considered For Official Use Only (FOUO) in content. Specific results of this structural assessment have been relegated to a series of FOUO supplemental materials. However a high-level description of the strategy used to conduct the structural assessment has been provided here.

Table 20. Summary of systems, damages and modes of failure.

System & Component	Loadings	Mode of Failure
Steam System		
Pylon Support	Wind and Hydrodynamic Loads	Bending of pylon
Short Pylon Support	Wind and Hydrodynamic Loads	Bending of pipe
Building support (3,5, and 8 story)	Winds	Loss of support
Steam plant building	Winds	Structural damage
Pipelines at Piers	Waves	Bending of pipes and connection failure
Water Supply System		
Water Treatment Plants	Depths of Flooding	Electromechanical
Pumps	Depths of Flooding	Electromechanical
Metal building housing the pumps	Winds	Structural damage
Water Tank	Water Velocities	External stability and buckling of walls
Pipelines at Piers	Waves	Bending of pipes and connection failure
Electric System		
Electrical Substations	Depths of Flooding	Electromechanical
Power generators	Depths of Flooding	Electromechanical
Wastewater System		
Lift Stations	Depths of Flooding	Electromechanical
Oily Waste System		
Oily Waste Tank	Water Velocities	External stability and buckling of walls
Pumps	Depths of Flooding	Electromechanical
Masonry Building housing the pumps	Winds	Structural damage
Piers		
Pier 11	Storm Surge and Wave Elevations	Bending and axial failure of piles
Piers 12 and 14	Storm Surge and Wave Elevations	Bending and axial failure of piles
Petroleum, Oil, & Lubricants (POL) System		
Diesel fuel tanks	Depths of Flooding	External stability

3.8.1.2 Steps 3 & 4: Calculate the Capacity and the Demand

The capacity of each asset to resist failure, and the measure of loads acting on these assets that generate these modes of failure, is captured in damage state tables. In general, these damage states correspond to those described in HAZUS, although Facility and Component Explosive Damage Assessment Program (FACEDAP) (USACE 1994) damage criteria can be used to define damage states to assets other than buildings. The FACEDAP computer program calculates the response of individual structural components. FACEDAP compares the properties that determine dynamic response characteristics of structural components (i.e., mass, stiffness and strength of the components) to calculated load conditions. Two to four damage states are then defined for the assessment (Table 21).

Table 21. Directives used to define and describe asset damage states.

Damage State (D_i)	Explanation
None	Asset fully functional.
Minor	Describe in sufficient / reasonable detail what constituted *minor* damage to this asset such that it was non-functional.

Moderate	Describe in sufficient / reasonable detail what constituted *moderate* damage to this asset such that it was non-functional.
Severe	Describe in sufficient / reasonable detail what constituted *severe* damage to this asset such that it was non-functional.

In a *None* damage state, we assume that no appreciable damage is experienced, and the component is assumed to be reusable without repair. In a *Minor* damage state, we assume a moderate level of damage is experienced, and that the component is repairable. In a *Moderate* damage state, we assumed that severe damage is experience, and that the component is not worth repairing (although it could be repaired). In a *Severe* damage state, we assume that the component is beyond repair, although it has not necessarily collapsed. Note that these breakpoints must be refined or honed on a case-by-case basis to reflect the different structural components of the site's critical capabilities (refer back to *Section 3.7*).

3.8.1.3 Step 5: Fragility Curve Development

Ultimately, the results of the parameter analysis are used to inform the development of damage functions in fragility curves (i.e., curves that describe the probability that a system will fail as a function of the load on that system) (Figure 47).

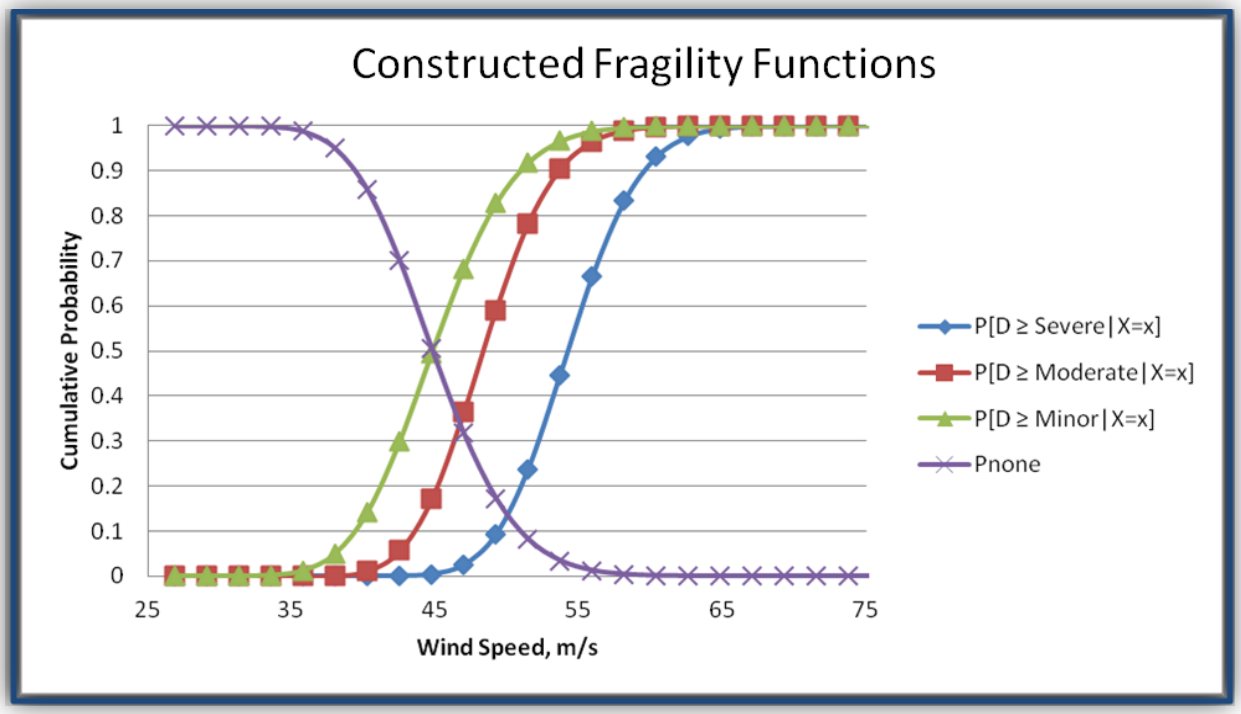

Figure 47. An example of multiple fragility curves generated for the case study. Here, the mathematical functions estimate the cumulative probability of four damage states (*None*, *Minor*, *Moderate*, *and Severe*), defined in terms of damage to an asset. In this example, cumulative probabilities are expressed as a function of one loading (i.e., wind speeds).

3.8.1.4 Software Deployed

For purposes of the case study, the internal curves included in the HAZUS-MH MR-4 software (http://www.fema.gov/library/viewRecord.do?id=3726, accessed November 2012) were used to evaluate damage to buildings subjected to hazard loadings under the combination of the prescribed SLR scenarios and storms moving over the region. It was necessary for us to manually enter NSN's building identifiers and specifications into the HAZUS program for the case study because information regarding military bases is considered *classified* data,. Predicted wind speeds, water depths and wave velocities generated by the storm analyses (described in the previous sections) were fed into the HAZUS curves, and damages were generated for the varying water heights under the five prescribed SLR scenarios. Predictions of the extent of structural damages to buildings were then estimated. Figure 48 illustrates the differences between assessing structures versus flood heights in a typical risk assessment.

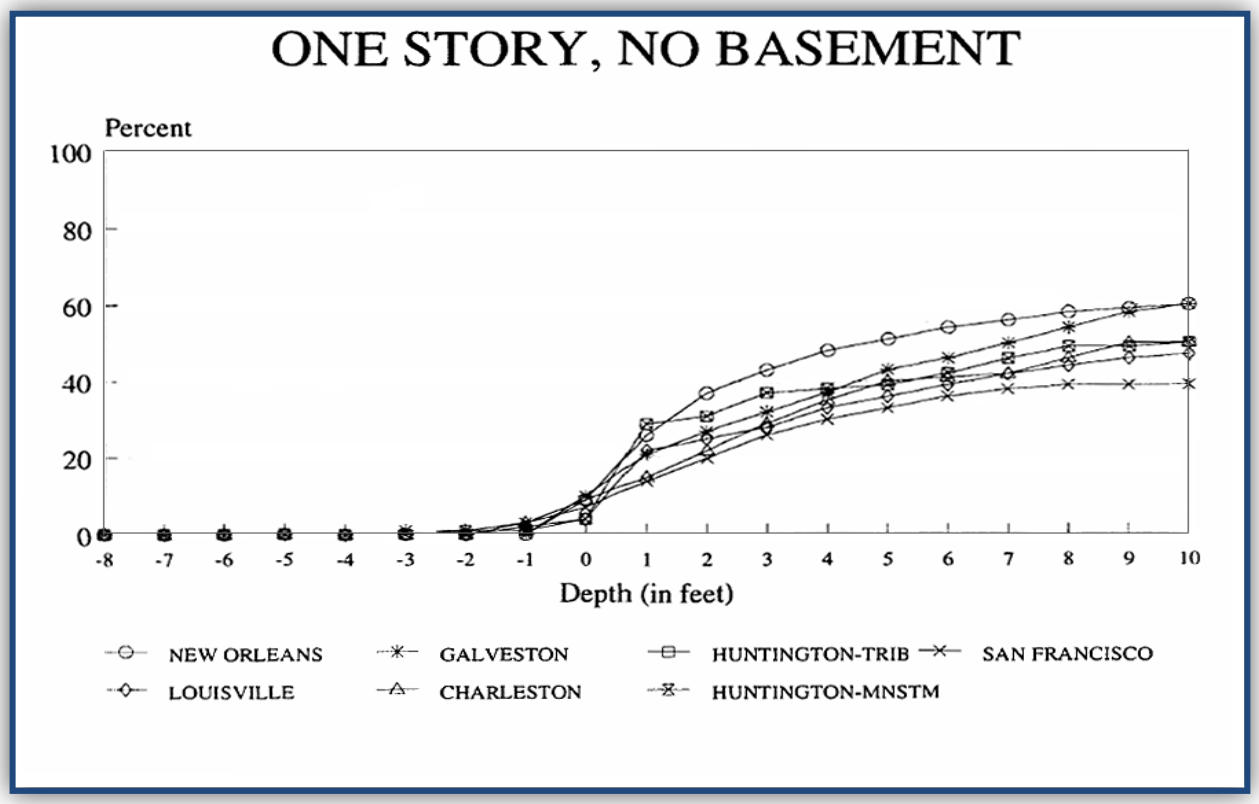

Figure 48. Example damage versus flood depth relationship for a specific type of residential structure in various USACE regions.

SAP2000 (http://www.sap2000.org/, accessed November 2012) was used to estimate the response of the piers under a combination of the various SLR scenarios. SAP2000 is an integrated software commonly used in structural analysis and design. SAP2000 provides linear and nonlinear, static and dynamic analysis and design of three-dimensional structures. This tool had been validated extensively and was deemed suitable to perform the structural analysis of the piers for the study.

For structure types other than buildings, a new approach was required. We devised structural models sensitive to the hazards of concern for this study, namely wind, current and flood surge. The resolution of the models was consistent with that of the available structural descriptions and the loadings. We included frame models for low resolution structures where little information was available and developed detailed finite element models for structures when the information was available. Parameter studies were performed with the models to develop damage envelopes such as those in Figure 48 above. Then the actual predicted wind and flood scenarios were used to develop damage estimates. Depending on the number of structures and level of effort in this project, it was necessary to aggregate structural assets and delineate a representative sample to be modeled rather than develop a model of every asset in the ACN individually. In addition, detailed cross-sections of Piers 11, 12, and 14 were obtained for this assessment.

3.8.2 Inputs

The required inputs needed to perform the structural analysis for the study included:

- Material properties cross-sections, elevations, and connection details for each asset;
- Soil properties at the base of poles and columns; and
- Loading environments as functions of the elevations of storm wind and surge forcings.

FACEDAP was then used to generate the damage states for each asset.

3.9. Risk Assessment Methodology

Coastal storms can interfere with the performance of missions at coastal military installations by causing damage to physical assets that support the mission. Figure 49 (a) illustrates how mission performance at a hypothetical military installation might respond to a coastal storm over time.

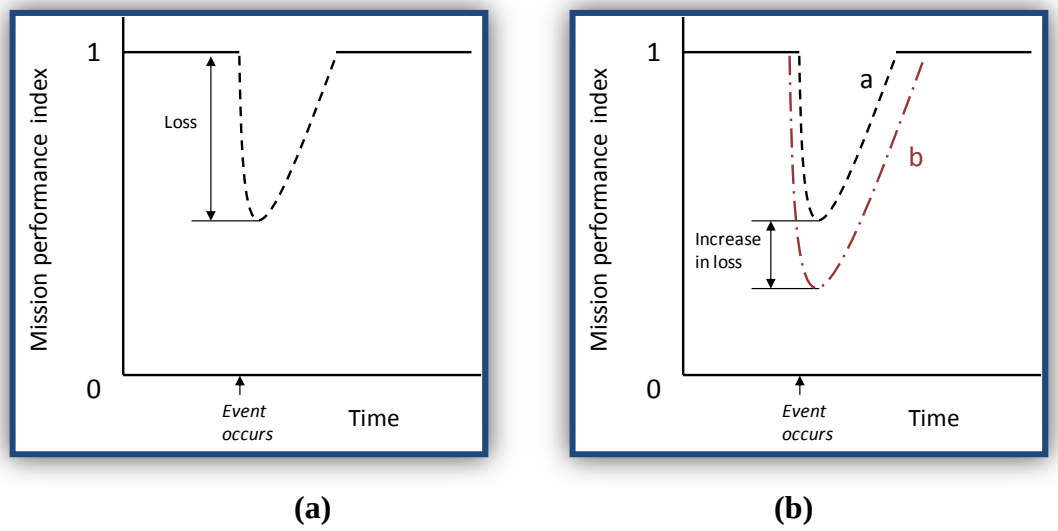

Figure 49. (a) The effect of a coastal storm on mission performance, and (b) the effect of an increase in either storm intensity or SLR on mission performance.

We can assume that the quality of performance on a military installation is influenced by coastal storms and can be described in terms of a response index. Mission performance is then evaluated on the ordinate axis (i.e., y-axis) in terms of an index bounded by 0 and 1, with higher values of the index representing higher levels of mission performance. Prior to the event, we assume that the installation is operating at full performance, thus the nominal value of the index is 1. If the quality of performance is dependent on the availability of infrastructure that is vulnerable to damage from coastal storms, then coastal storms will tend to have a negative impact on operations, causing the mission performance index to fall below 1. This impairment in mission performance represents a loss on the installation, as illustrated in Figure 49 (a).

Storms of greater intensity are associated with more severe loads, thus they are expected to cause greater damages to physical assets and greater levels of mission impairment than storms of lesser intensity. As sea level rises, the severity of loads on physical infrastructure caused by storms of a given intensity may also increase. Thus, it is expected that if sea level were to rise, the frequency, level, and duration of mission impairments will tend to increase. This effect of an increase in storm intensity and/or an increase in SLR on the loss in mission performance is illustrated in Figure 49 (b). Increasing storm intensity (or sea level rise) from curve *a* to *b* causes an earlier onset of mission impairment, greater losses in mission performance, and a longer duration of recovery period.

The loss in mission performance can be defined as a function of random variables that determine storm severity:

$$L = g\left(h\left(r, \mathbf{x}\right)\right) \qquad \textbf{(21)}$$

Where L is the loss in mission performance and the function $h\left(r, \mathbf{x}\right)$ characterizes storm severity as a function of a change in sea level (r) and a vector of random variables ($\mathbf{x}$) that are determinants of storm severity. Examples of random variables that determine storm severity were introduced in an earlier section of this report (refer to *Section 3.4*), and include parameters such as storm track or heading, central pressure, forward speed, and radius to maximum winds. The function g describes the response of the response index to storm severity.

The objective of the risk assessment approach is to assess the probability of potential losses in mission performance and determine the effect of prescribed SLR on those probabilities. If the mission performance function is known or can somehow be estimated, then losses that are associated with a storm event of any given severity can be obtained directly from *Equation 21*. Uncertainty in potential losses can be obtained by propagating the uncertainty from the random variables to the mission performance impairment. The probability of exceeding any potential level of loss in mission performance can then be calculated for each SLR scenario and the effect of SLR on the probability of a potential loss is the difference in the probability of exceeding a given level of loss under two SLR scenarios. This approach, in which the mission performance function is known, might be termed a "top-down" approach. The challenge for risk assessment under the study was to develop an approach to estimate mission performance losses as a function of storm severity and SLR without having an explicit representation of the mission performance function.

In comparison to the "top-down" approach, our approach might be characterized as a "bottom-up" approach because it requires the development of information about the relationship between physical assets and mission performance on the installation. In summary, we have devised an procedure that focuses on the identification of specific missions of interest, the decomposition of the missions into a set of capabilities that are needed to perform the mission(s), and the description of the functional dependence between the capabilities and physical assets on the installation. This process of mission decomposition has already been described in *Section 3.7 above*. Once the physical assets that support the mission are identified, fragility curves are developed for each asset to calculate the probability of damage given modeled storm loads. Development of these fragility curves has been described in *Section 3.8 above*. This information is then used to construct a Bayesian network, the purpose of which is to estimate the probability of damages to physical assets, as well as the probability of potential losses in capabilities and mission performance that arise from damages to physical assets from coastal storms under the prescribed SLR scenarios. Figure 50 shows that calculation of risks to mission impairment is the final step in our overall risk assessment framework.

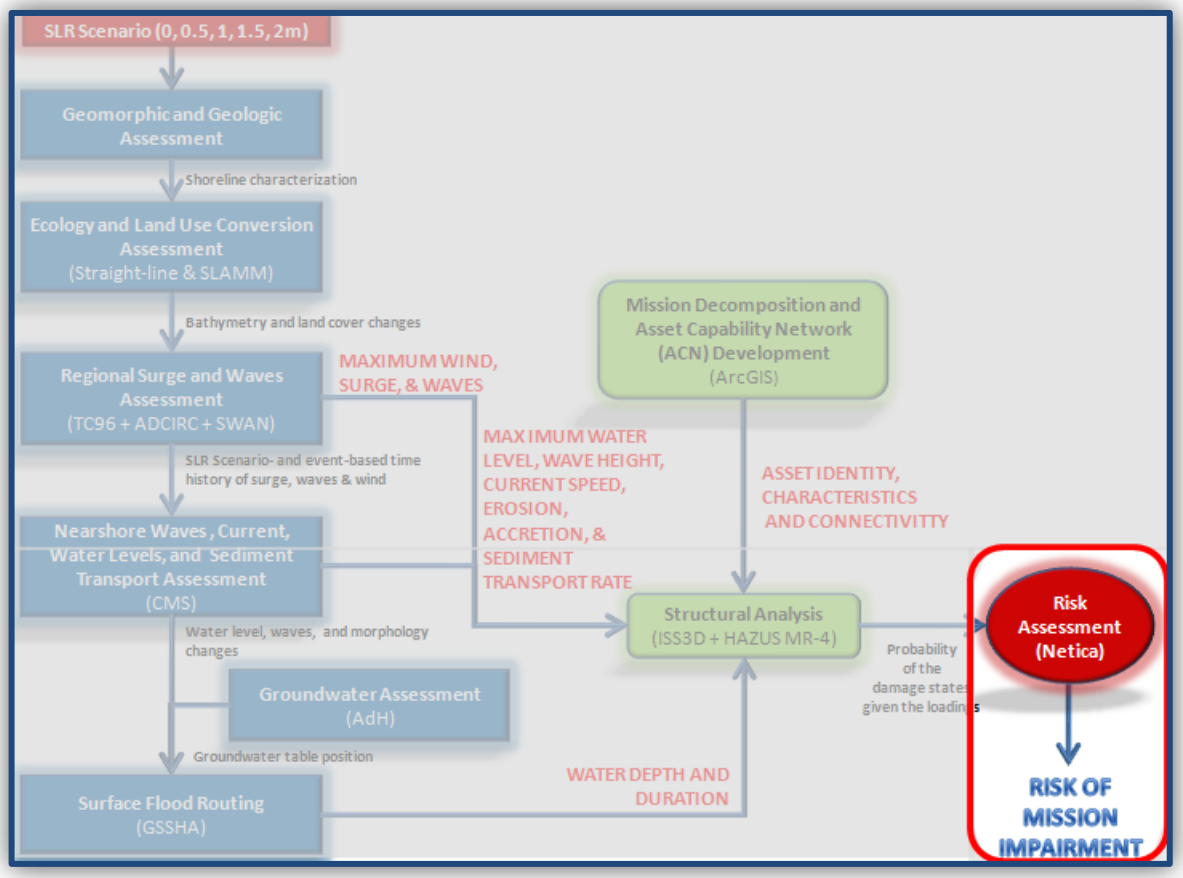

Figure 50. Project analysis and tasks: *Risk Assessment*.

3.9.1 Models and Approach

Bayesian networks are an elegant and popular framework for modeling uncertainty. They provide a principled approach to dealing with uncertainty through the use of probability theory, and an effective approach to coping with complexity through the use of graph theory (Koller et al. 2007). A Bayesian network is a factorization of a joint probability distribution over random variables (Pearl 1988). Any joint probability distribution can be represented using a Bayesian network (Pourret 2008). A Bayesian network consists of two parts, a Directed Acyclic Graph (DAG) that depicts dependence and conditional independence among nodes representing elements of a system and a set of conditional probability tables that quantify the relationships among elements of that system. In general, a graph is a data structure consisting of a set of nodes, $\{X_i, \ldots X_j, \ldots, X_n\}$ and a set of directed edges that link nodes. Given a pair of nodes $X_i \rightarrow X_j$, X_i is defined as the parent node and X_j is termed the child node. A graph is considered a DAG if all edges are directed and no path exists within the graph from any parent node leading back to that parent node in the direction of the edges (Koller and Freidman 2009). The nodes of a DAG represent well-defined elements in a system of interest about which we may have knowledge (information). The presence of a directed edge between two nodes signifies dependence. For example, Figure 51 shows a graphical model that illustrates the dependence and conditional independence relationships among five elements of a system (X_1, X_2, X_3, X_4, and X_5).

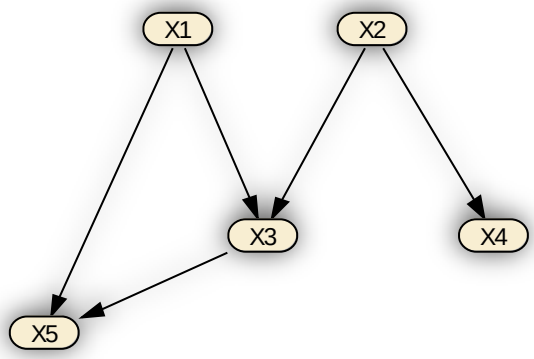

Figure 51. A DAG consisting of five nodes and five directed edges.

The dependence and independence relationships in Figure 51 above are as follows. Nodes X_3 and X_5 are directly dependent upon X_1. Nodes X_3 and X_4 are directly dependent upon X_2. The absence of a directed edge between two nodes indicates conditional independence. For example, nodes X_1 and X_2, and nodes X_2 and X_5, are conditionally independent.

A Bayesian network is a DAG in which the nodes represent discrete or discretized random variables, the edges signify the existence of direct causal influences between linked variables, and the strengths of these influences are expressed by forward conditional probabilities (Pearl 1988, p. 117). The Bayesian network describes a factorization of the joint probability distribution over the random variables, where the factorization is given by the structure of the network. In general, the factorization of the joint probability distribution can be written:

$$P(X_1, X_2, ..., X_n) = \prod_{i=1}^{n} P(X_i \mid X_{pa(i)}) \quad \textbf{(22)}$$

Where the notation *pa*(*i*) means *X* is a parent of node *i* and the notation $P(X_i \mid X_{pa(i)})$ means the probability that *X* is in state, *i*, given the state of parent nodes (Pearl 1988).

Nodes with parents are defined by conditional probability tables that give, for every possible state of the variable, a probability of being in that state given the state of all parent node variables. Nodes without any parents are called *roots* and are defined by marginal probability distributions.

A set of two or more potential states must be defined for each random variable. These states may be quantitative or qualitative. While there is a great deal of flexibility in defining the states for each random variable, it is a requirement of the method that the set of potential states for each must be mutually exclusive and collectively exhaustive. The term *mutually exclusive* means that, if the state of a random variable is observed in nature, it can be associated with exactly one of the potential states in the model. The term *collectively exhaustive* means that the set of potential states for a random variable represents the universe of potential states for that random variable. For example, consider a random variable that represents the state of a traffic light. One might identify three potential states for the random variable: green, yellow, and red. This is a mutually exclusive set of potential states because the traffic light can show only one color at a time. If the light is green, it cannot also be yellow or red. However, this is not a collectively exhaustive set of possibilities. For example, the traffic light may also be broken, in which case it could not be assigned to any one of these potential states. Therefore, a mutually exclusive and collectively exhaustive set of potential states is: green, yellow, red, and broken. Alternatively, one might identify a different set of potential states: green and not green. This is also a mutually exclusive and collectively exhaustive set of potential states because the state "not green" captures all other possibilities. Although this set of states provides less information than the former, it may be sufficient for making whatever inferences are desired from the model. In general, a fewer number of states is desirable for computational purposes. However, statistical inferences from a Bayesian network can be sensitive to the discretization of random variables.

Statistical inference using Bayesian networks is accomplished by entering evidence in the network. Hard evidence is entered by specifying knowledge about the state of one or more variables. Soft evidence is entered in the form a probability distribution describing imperfect knowledge about the state of one or more variables. Once a finding is entered in a network, all probabilities in the network are updated using Bayes' theorem (Bayes 1763). When hard or soft evidence is entered into a node to reflect observations about a variable in the system, the objective is to compute the *posterior probabilities* for all the nodes in the network. The posterior probability of *Y* given the state of one or more random variables, *X*, is simply the probability that *Y* is in a particular state given the observations or evidence about other nodes, *X*. This process of updating the probabilities in the network is accomplished using Bayes' theorem:

$$P(Y_{j=i} \mid X) = \frac{P(X \mid Y_{j=i})P(Y_{j=i})}{P(X)} \quad . \qquad \textbf{(23)}$$

The term on the left hand side of the equation is the posterior probability, the probability that variable *Y*, with *j*={1, 2, …,*i*,…*n* } possible states, is in state *i* given evidence about the distribution of parent nodes, *X*. $P(Y_{j=i})$ is called the *prior probability*, the probability that *Y* is in the i^{th} state before the evidence became available. $P(X \mid Y_{j=i})$ is the likelihood, which is the conditional probability of observing the evidence (*X*) given that *Y is* in the j^{th} state. By the theorem of total probability, the denominator is:

$$P(X) = \sum_{j=1}^{n} P(X \mid Y_j)P(Y_j) \qquad \textbf{(24)}$$

This computation of posterior probabilities can be burdensome and it is only with the advent of algorithms capable of performing these calculations efficiently that practical applications became possible.

Bayesian networks were introduced in the field of artificial intelligence and have proven to be a powerful and broadly applicable technique for reasoning under uncertainty. Since they were first introduced, applications of Bayesian networks have been developed for predictive and diagnostic reasoning in many fields, including for example genetics (Rodin and Boerwinkle 2005), medicine (Onisko 2008, Nicholson et al. 2008), insurance, air traffic control (Fenton and Neil 2001), ecological risk assessment (Pollino et al. 2007a, Pollino et al. 2007b), environmental management (Marcot 2006), and fisheries management (Kuikka et al 1999).

Over the past decade, Bayesian networks have increasingly been applied to infrastructure risk and reliability assessments (Langseth and Portinale 2005, Langseth 2008). These include applications to assess component risks to nuclear power systems (Almond 1992), to assess infrastructure risks from seismic events (Bensi et al. 2009), to assess the reliability of networked infrastructure such as electric power systems (Lynn et al. 1998, Yu et al. 2005, Attoh-Okine et al. 2009), and to assess the reliability of missile defense systems (Wilson et al. 2007). The goal of systems level reliability assessments is generally to assess the probabilities of system states. This is typically accomplished through the use of fault trees and reliability block diagrams (Modarres, Kaminskiy, and Krivtsov 2010). One of the reasons that reliability engineers have become attracted to Bayesian networks is that the method generalizes fault trees and reliability block diagrams by allowing components and subsystems to be related by conditional probabilities instead of deterministic Boolean relationships (Wilson and Huzurbazar 2007). The approach offers greater flexibility and the opportunity to apply statistical inference to diagnose the reasons that risks of failure might be high as well as to predict the probabilities of system states.

Although the inability to represent feedbacks within a system is a limitation of the method, in general, there are numerous advantages associated with using Bayesian networks for infrastructure reliability assessment. They provide a flexible framework for reasoning about uncertainty and conducting both diagnostic and predictive inference on the same modeling

platform. They can handle both qualitative and quantitative variables and permit the integration of objective and subjective information. Because of the graphic representation of dependencies within the system, they are particularly useful for communicating with domain experts (Langseth and Portinale (2007). Bayesian networks can also be augmented with decision and utility nodes to create influence diagrams that model decisions, such as infrastructure investment decisions. With respect to conventional reliability analysis methods specifically, the advantages of Bayesian networks include the ability to model multiple failure states simultaneously (fault trees cannot) (Langseth and Portinale 2007) and the ability to update information about component reliability.

It is just as important to understand the limitations of Bayesian networks as it is to understand their advantages. Bayesian network graphs are directed acyclic graphs. As such, they cannot contain feedback loops, making it impossible to represent feedback systems (Uusitalo et al. 2007, Barton et al. 2008). It is also very difficult to represent time dependent process, such as time dependent failure modes, although some progress seems to have been made in this regard (Langseth 2008). Generally, Bayesian networks are constructed with discrete variables because of limitations of the solution algorithms, although again, some progress has been made at incorporating continuous variables (Langseth 2008). It is frequently observed that conditional probability tables are difficult to construct, particularly if they are large. Conditional probability tables can be constructed using data, model outputs, or engineering judgment.

The capabilities and missions on the installation are supported by a network of infrastructure in which there are a complex set of functional dependencies. The Bayesian network enables us to represent those functional dependencies within its structure efficiently. This is the primary motivation for using a Bayesian network approach on this project. The alternative to a Bayesian network approach is relatively inefficient. For example, in a paper discussing the resilience of networked infrastructure to coastal storms, Reed et al. (2009) described the use of an interoperability matrix in which each element of the matrix describes the probability of a networked component failure given the failure of every other networked component. This approach requires data on the reliability of each networked component given the state of all other networked components independent of causal effects. The causal structure of the Bayesian network eliminates the burden of computing conditional probabilities of failure between components where cause and effect relationships are absent. In addition, the approach enables us to consider multiple failure states for each component of the system.

3.9.1.1 Graphical Structure of the NSN Risk Model

The graphical structure of the case study's risk model (hereafter referred to as the *NSN Risk Model*) arose from the asset capability network introduced in the preceding section on mission and infrastructure decomposition (refer to *Section 3.7*). As described earlier, the ACN captures functional dependence among the infrastructure assets and capabilities needed to carry out the mission (i.e., *Provide At-Berth Support* for CVNs on NSN in the case study). Figure 52 illustrates this network and identifies the assets and capabilities explicitly considered in the NSN Risk Model for the case study.

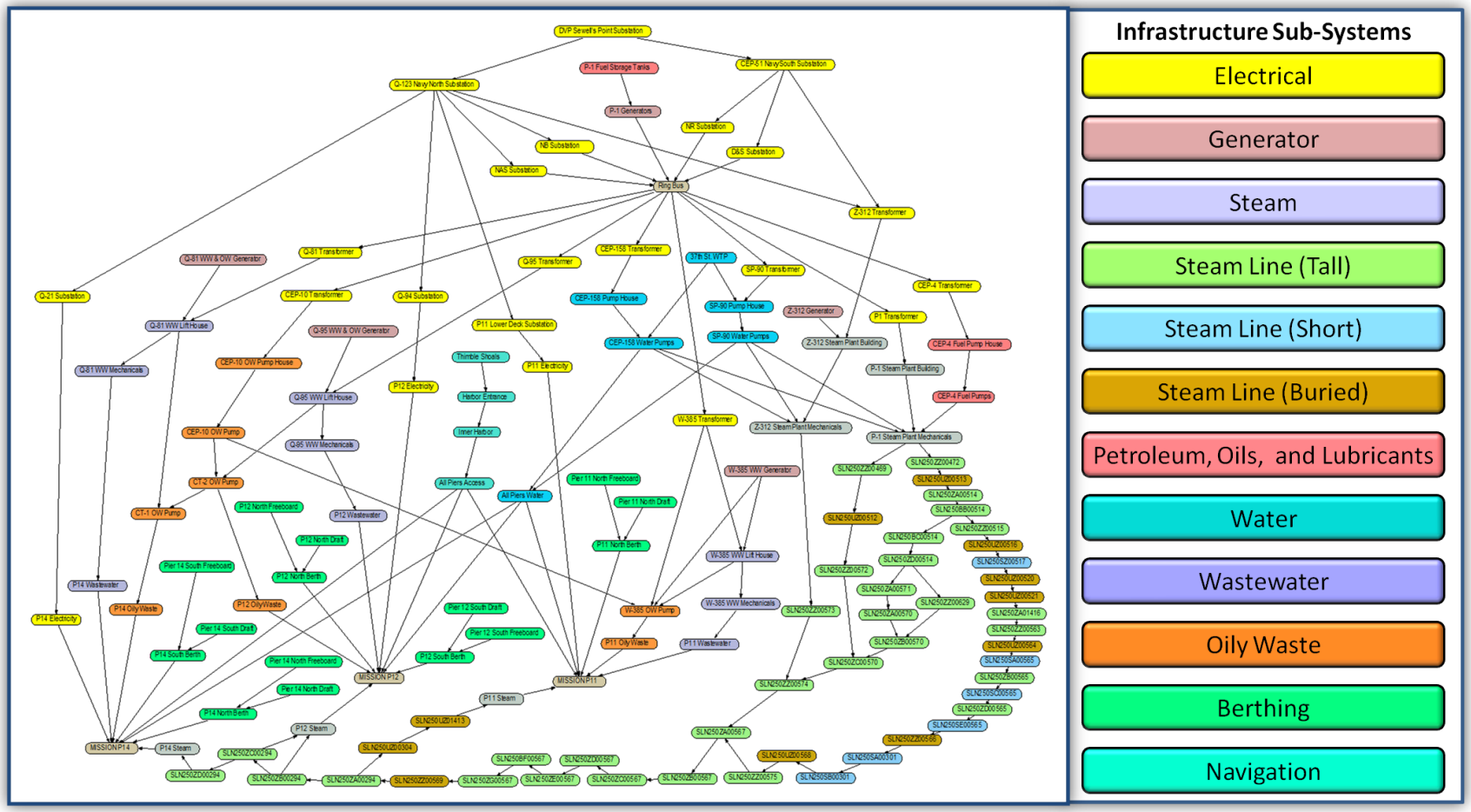

Figure 52. Dependence among assets, capabilities, and missions is represented as a graphical model for the case study.

As the figure illustrates, the network included one node for each physical asset, capability, or mission as described in *Section 3.7*, except for a few instances where adjustments were needed as described elsewhere in this section. To facilitate navigation of the network, each asset has been color-coded in the diagram to indicate its membership in an infrastructure sub-system. Edges that link one node to another indicate functional dependence among assets in the direction of the edge. The capabilities needed to *Provide At-Berth Support* were directly dependent upon one or more physical assets in the network. As with asset nodes, capability nodes have been color-coded in the diagram to indicate infrastructure sub-system membership. However, these have also been distinguished from asset nodes by their titles, which begin with a pier reference (*P11, P12, or P14*). The graph terminates in three mission support nodes (*Mission P11, Mission P12, and Mission P14*), which were directly dependent upon the capabilities. These nodes represent the mission to *Provide At-Berth Support* at each of the three piers on the installation that were capable of docking CVNs at the study site.

The full graphical structure of the NSN Risk Model is illustrated in Figure 53.

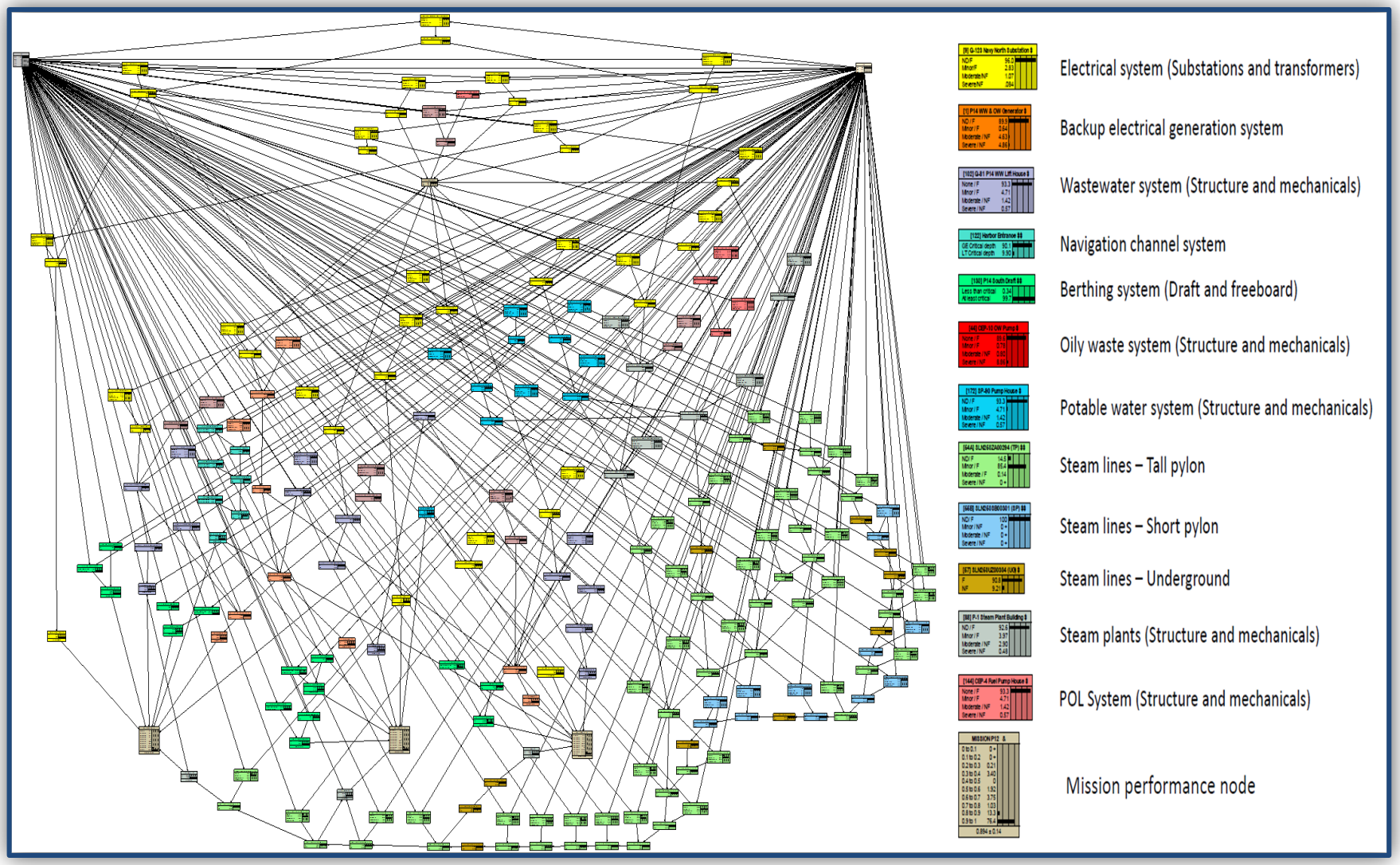

Figure 53. The graphical NSN Risk Model.

The NSN Risk Model is an expanded version of the asset capability network that defines two random variables for each asset and nodes for risk drivers on the installation. A generic schematic of the NSN Risk Model is provided in Figure 54 for the purpose of illustrating what types of random variables were included in the network, the relationships among these variables, and their potential states.

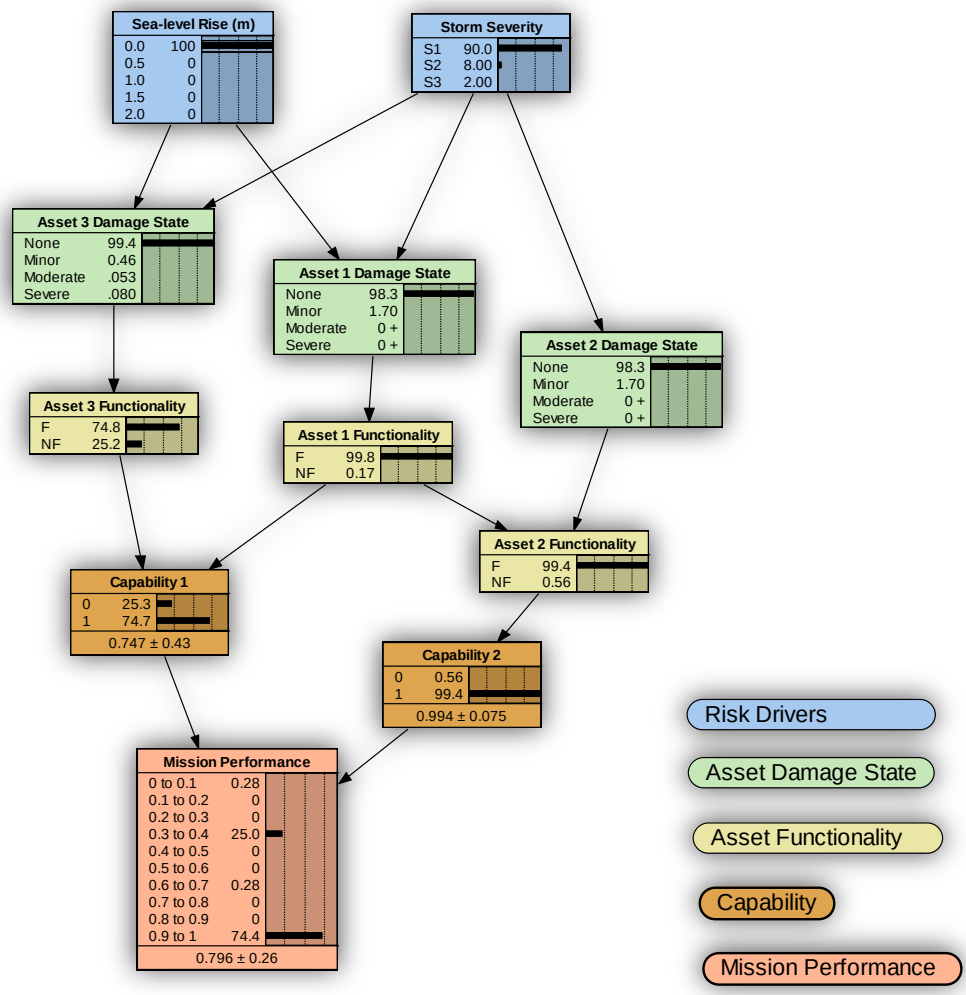

Figure 54. Illustrative graphical model showing relationships among five different types of random variables (i.e., risk drivers, asset damage states, asset functionalities, capabilities, and mission performance).

In this example, the mission of interest is supported by two capabilities (*Capability 1 and Capability 2*). Each capability is dependent on the functional state of three assets (*Asset 1, Asset 2, and Asset 3*). *Capability 1* is directly dependent upon *Asset 1 Functionality* and *Asset 3 Functionality*. *Capability 2* is directly dependent upon *Asset 2 Functionality*. The relationship between *Asset 1 Functionality* and *Capability 1* is one of conditional independence. This means that, if the functionality of *Asset 2* is known (i.e., *Asset 2* was functional or non-functional), then knowing something about the probability of *Asset 1* being functional or non-functional provided

no information that enabled us to predict the ability to perform *Capability 2*. The ability to represent these relationships of conditional independence is an important feature of the approach.

As illustrated in Figure 54 above, the NSN Risk Model includes five types of random variables with the following states and relationships:

1) **Risk Driver Nodes**: In the context of this study, a risk driver is a natural force on the installation that has the potential to cause damage to physical infrastructure. The risk drivers considered in this study were coastal storm severity (*SEV*) and *SLR*. *SEV* was a random variable with three potential states [*S1*, *S2*, and *S3*] representing increasing levels of storm severity. *S1* represented a level of storm severity between the modeled 1- and 10-yr return interval storm, *S2* represented a level of storm severity between the modeled 10- and 50-yr return interval storm, and *S3* represented a level of storm severity between the modeled 50- and 100-yr return interval storm. For the purposes of the NSN Risk Model, this set of three storms represented the full range of potential storms that might have affected the installation, with at least an *S1* storm assumed to occur in any given year. The second risk driver considered in this analysis was SLR, defined as a random variable with five possible states (0.0, 0.5, 1.0, 1.5, or 2.0), where 0.0 represented the baseline condition (i.e., present-day sea level) and 2.0 represented the condition of a 2.0 m SLR relative to baseline conditions.

2) **Asset Damage Nodes:** An asset is defined as a physical resource that supports one or more capabilities that are required to *Provide At-Berth Support*. For example, an asset could be an electrical substation, an electrical transformer, an electrical generator, or a structure. Each asset is associated with a set of defining characteristics including a physical location on the installation, a set of potential damage states, a damage function that describes the potential damage state as a function of storm loads, and a fragility curve that describes the probability that asset is in a damage state given any particular storm load. In the NSN Risk Model, assets were associated with two or four damage states. In general, these damage states corresponded to those described in HAZUS, as outlined in *Section 3.8*. In some cases, the physical assets on the installation were collocated and shared all of their defining characteristics. In such cases, these physical assets were lumped into a single node. Moveable assets (vehicles, portable transformers, cranes, etc.) and personnel were not considered assets for purposes of this study because they lacked a fixed location. We assumed that moveable assets and personnel were adequately protected before a storm occurred.

3) **Asset Function Nodes**: A function is defined as the ability of an asset to perform a specific task within the network. Asset function nodes are random variables defined over two potential damage states [*Functional (F), Non-functional (NF)*]. An asset function node is jointly dependent on its own damage state and the damage state of all other assets that support its function. For example, an electrical transformer might itself be undamaged, but is functional only if the electrical substation from which it draws power is also functional.

4) **Capability Nodes**: A capability is defined as the ability to perform a task that directly supports the mission, such as *Provide Electric Power to CVNs* at a specific pier. In contrast to asset function nodes, capability nodes describe the functionality of the network of relevant infrastructure assets on the installation. Capability is a random variable with two potential states that are directly dependent on one or more function nodes. In contrast to asset function nodes, which have two nominal states, the capability node is real-valued. If the asset function node has a value of *F*, the dependent capability node assumes a value of 1. Likewise, if the asset function node has a value of *NF*, the dependent capability node assumes a value of 0. The expected value of a capability node is a capability score. The capability score is defined as the probability that a pier-side service is not disrupted by a coastal storm (nor'easter's excluded) at least once a year. In Figure 54 above, the mean and standard deviation of the capability scores are reported at the bottom of the capability nodes. In most cases, the capability nodes are directly dependent on the asset function nodes of a single asset. In such cases, it provides no new information to the model, but serves the purpose of transforming the information about asset damage states and function states to a real-valued capability score that is used in evaluating mission performance.

5) **Mission Performance Nodes**: A mission is defined as an operational task (i.e., the focus of the case study's risk assessment). The performance of a mission requires the integration of a set of well-defined capabilities. The mission performance node is a continuous random variable that is defined as a multi-attribute value function of capability scores that serves as a Mission Performance Index (MPI) at each pier. The value function is parameterized using weights representing command-level priorities. The MPI is at a maximum when all capability scores are equal to one, indicating that there is no chance that a coastal storm can interrupt any capability. MPI is at a minimum when all of the capabilities needed to perform the mission (i.e., *Provide At-Berth Support* for the case study) are interrupted at least once during the year because of damages caused by coastal storms. For purposes of the study, the NSN Risk Model included three mission performance nodes, one for each pier.

3.9.1.2 Parameterization of Network Nodes

Each node in the network is parameterized by calculating a Marginal Probability Table (MPT) or a Conditional Probability Table (CPT). For nodes that lack parents, an MPT gives the unconditional probability of each potential node state. For nodes with at least one parent, a CPT gives the probability of each node state conditional on the state(s) of the parent node(s). Figure 55 illustrates the parameterization of random variable nodes in the illustrative network.

SLR	SEV	Asset 3 Damage State			
		None	Minor	Moderate	Severe
0.0	S1	9.98E-01	9.27E-04	2.13E-04	6.60E-04
0.0	S2	9.71E-01	2.46E-02	2.53E-03	1.82E-03
0.0	S3	9.01E-01	8.89E-02	6.99E-03	3.22E-03
0.5	S1	9.75E-01	2.09E-02	2.24E-03	1.71E-03
0.5	S2	7.76E-02	7.55E-01	1.39E-01	2.79E-02
0.5	S3	2.77E-04	4.80E-01	4.24E-01	9.62E-02
1.0	S1	9.04E-01	8.63E-02	6.81E-03	3.17E-03
1.0	S2	9.46E-05	4.25E-01	4.64E-01	1.11E-01
1.0	S3	7.15E-12	4.46E-02	5.79E-01	3.77E-01
1.5	S1	6.75E-01	2.96E-01	2.19E-02	6.66E-03
1.5	S2	1.02E-11	4.71E-02	5.82E-01	3.71E-01
1.5	S3	0.00E+00	6.70E-05	1.69E-01	8.31E-01
2.0	S1	2.09E-01	6.89E-01	8.38E-02	1.80E-02
2.0	S2	0.00E+00	5.11E-05	1.59E-01	8.41E-01
2.0	S3	0.00E+00	1.49E-12	2.16E-03	9.98E-01

SLR: Sea-level Rise (m)				
0.0	0.5	1.0	1.5	2.0
0.20	0.20	0.20	0.20	0.20

SEV: Storm Severity Index		
S1	S2	S3
0.9	0.08	0.02

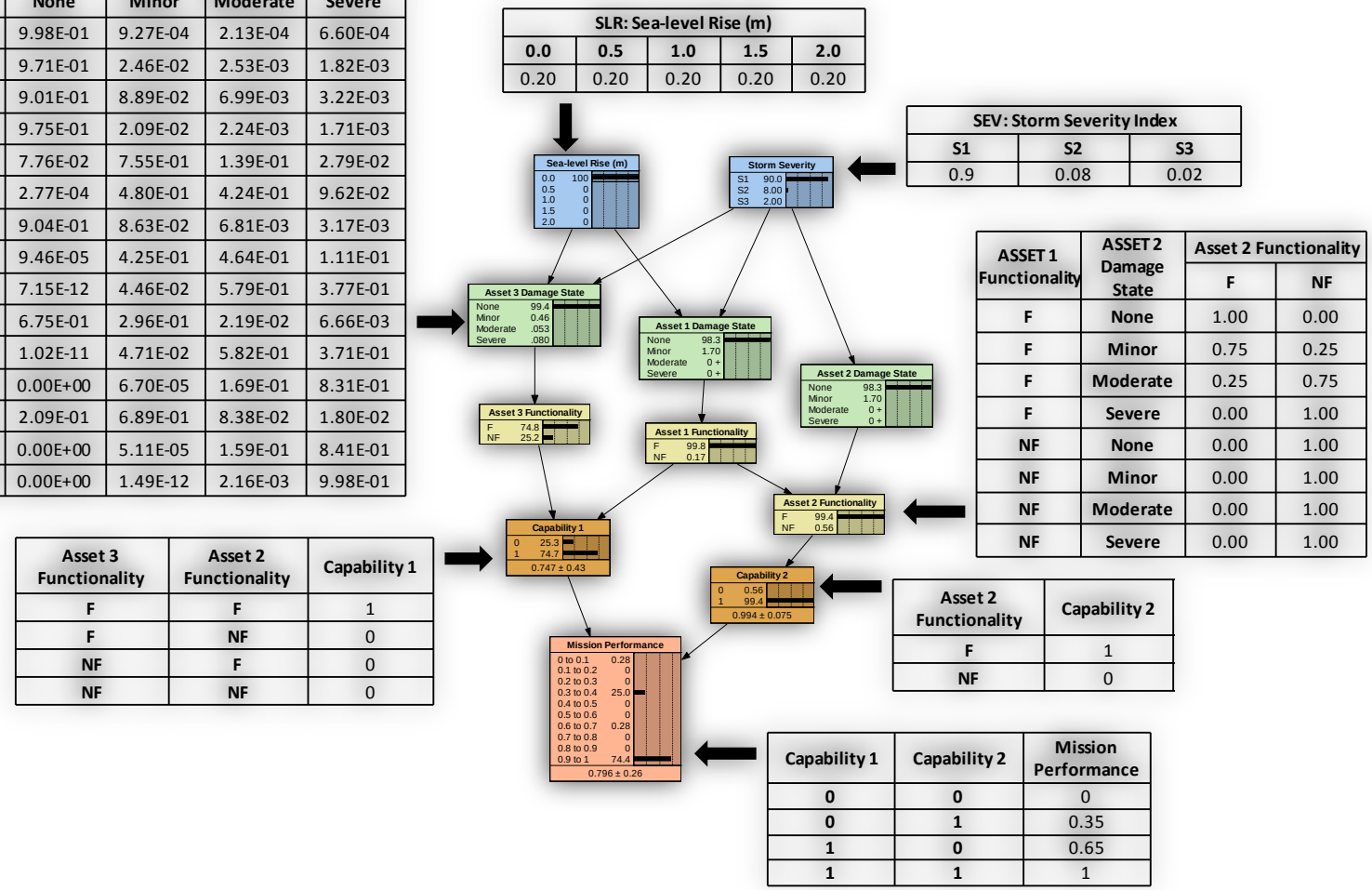

ASSET 1 Functionality	ASSET 2 Damage State	Asset 2 Functionality	
		F	NF
F	None	1.00	0.00
F	Minor	0.75	0.25
F	Moderate	0.25	0.75
F	Severe	0.00	1.00
NF	None	0.00	1.00
NF	Minor	0.00	1.00
NF	Moderate	0.00	1.00
NF	Severe	0.00	1.00

Asset 3 Functionality	Asset 2 Functionality	Capability 1
F	F	1
F	NF	0
NF	F	0
NF	NF	0

Asset 2 Functionality	Capability 2
F	1
NF	0

Capability 1	Capability 2	Mission Performance
0	0	0
0	1	0.35
1	0	0.65
1	1	1

Figure 55. Marginal and conditional probability tables of the illustrative graphical model.

The *SLR* and *SEV* nodes are parameterized using MPTs. In the case study, the MPT for *SLR* showed a uniform distribution over the five potential SLR states. The MPT for *SEV* showed that an *S1* storm had an annual probability of occurrence equal to 0.9, and an *S2* storm had an annual probability of occurrence equal to 0.08, and an *S3* storm had an annual probability of occurrence equal to 0.02. These probabilities were derived from the modeled storm return periods.

Damage state nodes give the probability that an asset is in any one of several damage states given information about storm severity and sea level rise. For example, in Figure 54 above, the *Asset 3 Damage State* node has four potential damage states, each with probabilities conditioned on *SEV* and *SLR*. These probabilities are calculated using information about storm loads in grid cells where the asset is located and fragility curves previously developed for each type of asset. For those assets that are distributed across multiple grid cells, algorithms are developed to aggregate the probabilities of damage states to arrive at a single probability for the asset as a whole. Asset damage states for each type of asset were defined earlier in Table 21 of *Section 3.8 above*.

Asset Function nodes describe whether the asset is functional or not given information about its damage state and the functionality of other assets upon which its functionality is dependent. For example, in Figure 55 above, *Asset 2* functionality is dependent on the functionality of *Asset 1*. If *Asset 1* is non-functional, then *Asset 2* is non-functional with a probability of 1. If *Asset 1* is functional, then the state of the *Asset 2's* asset function node is dependent entirely upon the damage state of *Asset 2*. If the damage state is *None*, then *Asset 2* is functional with a probability of 1. However, if *Asset 1* is functional, and the damage state of *Asset 2* is *Minor*, then *Asset 2* is functional with a probability of 0.75. If the damage state of *Asset 2* is *Moderate*, then *Asset 2* is functional with a probability of 0.25. If the damage state of *Asset 2* is *Severe*, then *Asset 2* is non-functional with a probability of 1. These probabilities describe uncertainty in the consequences of damage to physical assets that comprise the infrastructure network.

Capability nodes are parameterized using deterministic tables. These nodes provide no new information to the model. The purpose of a capability node is to transform information about the state of one or more parent asset function nodes into a real-valued capability score. The capability score is an estimate of the probability that a capability is *not* disrupted at least once during the course of a year because of damages to physical assets caused by coastal storms. For example, in Figure 55 above, *Capability 2* has a value of 1 if *Asset 2* is functional and a value of 0 if *Asset 2* is non-functional. The mean score for *Capability 2*, which is directly dependent upon the state of the *Asset 2* function node, is 0.994. The standard deviation of the capability score is 0.075. These values are reported at the base of the capability node.

The **Mission Performance** node describes uncertainty in an index of mission performance. The index is a multi-attribute value function (Keeney and Raiffa 1993). This value function describes mission performance at each pier as a function of capability scores weighted by command-level priorities for supplying services to CVNs at berth in the study. The MPI ranges from between 0 and 1, with 0 representing the lowest possible level of performance and 1 representing the highest possible level of performance. In Figure 55 above, a mean and standard deviation of the MPI are reported for the network at the bottom of the node. For this study network, the expected mission performance was 0.796 and the standard deviation of the index was 0.26. The low

resolution in the mission performance table for this study network can be attributed to the small number of capabilities in the network. Resolution increased as more capabilities were considered.

The NSN Risk Model included 217 nodes, including two risk drivers, 95 asset damage nodes, 97 asset function nodes, nineteen capability nodes, and three mission performance nodes (Table 22).

Table 22. Inventory of network nodes by infrastructure subsystem and node type.

Infrastructure Subsystem	Asset Damage Nodes	Asset Function Nodes	Capability Nodes
Steam distribution system	-	-	3
Tall pylon-supported steam lines	31	31	-
Short pylon-supported steam lines	6	6	-
Underground steam lines	-	11	-
Steam plants, pumps, and mechanicals	4	4	-
Electrical distribution system	-	-	3
Substations	10	10	-
Transformers	9	9	-
Ring bus	0	1	-
Potable water storage and distribution	5	5	1
Oily wastewater management	2	5	3
Wastewater management	7	6	3
Navigation channels	3	3	1
Berthing area draft and freeboard	10	-	5
Petroleum, oil, and lubricants (POL)	3	2	-
Backup electrical generators	5	5	-
Total	**95**	**97**	**19**

The remainder of this section describes the methods that were used to parameterize each network node.

3.9.1.2.1 Risk Drivers

Risk driver nodes are the root nodes of the Bayesian network and are parameterized using MPTs.

Sea level Rise (SLR): For study purposes, no assumptions about the probability of SLR scenarios were made in this study. A uniform distribution over the potential SLR states was used to indicate lack of knowledge about future rates of sea level change. The application of the NSN Risk Model could not be meaningfully interpreted with this uniform distribution because it did not portray a legitimate belief about the probabilities of SLR scenarios. Thus, the risk model was implemented in this study by instantiating (i.e., setting the instance of) the SLR node to one of its possible states (i.e., 0 – 2.0 m) to perform a "what-if" analysis of risks to mission performance.

Storm Severity (*SEV*): For study purposes, the *SEV* node took one of three possible states [*S1*, *S2*, or *S3*] representing levels of severity at the midpoint of each return period interval. *S1* represented a level of storm severity between the modeled 1- and 10-yr return interval storm, *S2* represented a level of storm severity between the modeled 10- and 50-yr return interval storm, and *S3* represented a level of storm severity between the modeled 50- and 100-yr return interval storm. This transformation was necessary so that probabilities could be assigned to a discrete set

of storm events. Probabilities were calculated for each of the potential *SEV* states from their lower and upper bound storm return periods, r_L and r_U, respectively:

$$P(SEV) = r_L^{-1} - r_U^{-1} \quad \textbf{(25)}$$

For the maximum *SEV*, r_U^{-1} was assumed to be infinitesimally small to force the probabilities to sum to one.

As described in preceding sections of this report, several hydrodynamic models (ADCIRC, SWAN, CMS, and GSSHA) were implemented to simulate loadings (***X***) for each modeled storm. Storm loads included wind speeds, flood depths, wave heights, wave velocities, and sediment loads. These loads varied from grid cell to grid cell, dependent upon the resolution of the meshes in the coastal storm models used to estimate their values. A vector of storm loads was calculated for each SEV index level by calculating the midpoint of loadings for each return period increment in each 10 m^2 grid cell:

$$X_{SEV} = X_L + 0.5(X_U - X_L) \quad \textbf{(26)}$$

S1 loads were at the midpoint between those predicted for the 1-yr and 10-yr return interval storms, *S2* loads were at the midpoint between those predicted for the 10-yr to 50-yr return interval storms and *S3* loads were at the midpoint of those predicted for the 50-yr and 100-yr return interval storms. This resulted in P(*SEV*) being the same in each grid cell, while the loadings for each *SEV* level varied across grid cells. As noted in *Section 3.4*, the return periods of storm events did not necessarily correspond to the return periods for storm loads such as storm surge elevations, wind speeds, and wave heights. Return periods for storm loads were usually estimated by simulating many storms. However, because it was only possible to model a very limited number of storms for application purposes, storm return periods were used as a proxy for the return periods of storm loads.

3.9.1.2.2 Asset Damage Nodes

The conditional probability of an asset being in any one of its potential damage states given the severity of a potential storm is calculated using fragility curves (refer to *Section 3.8*). Fragility curves are defined as cumulative probability distribution functions that estimate the probability that an asset is in a damage state of at least severity *i* as a function of one or more coastal storm loads in the grid cell where the asset is located. The fragility curve for damage state *i*, $F_X(x)_i$, describes the uncertainty in the load, *X*, that causes an asset to be in a damage state of at least severity *i*. In general, the conditional probability of realizing a damage state given the loadings for a storm of severity *SEV* and an *SLR* scenario is the difference between the cumulative probability of realizing the damage states *i* and *i*+1:

$$P(D_i \mid SEV,\ SIR) = F_X(x)_i - F_X(x)_{i+1}. \quad \textbf{(27)}$$

With the exception of wind loads, coastal storm loads in the case study tended to become more severe as sea levels rose; therefore, asset damage state probabilities were conditioned on both SEV and SLR. An exception to this rule existed in the case of structures, which were potentially damaged by wind loads. Since wind loads were not influenced by changes in sea level, asset damage nodes for building structures were not dependent on SLR (refer to the FOUO supplemental materials for more details). Details regarding the navigation channels and berthing areas have been provided below.

3.9.1.2.2.1 Berthing Areas

In this study, five berthing areas were identified in the network (i.e., *Pier 11 North*, *Pier 12 South*, *Pier 12 North*, *Pier 14 South*, and *Pier 14 North*). SLR and coastal storms have the potential to impact berthing areas in one of two ways: 1) the loss of freeboard,[26] and 2) the loss of draft. If sea levels rise beyond a critical point, it is possible that insufficient freeboard would be available to accommodate CVNs. Therefore, we made the freeboard nodes directly dependent upon the SLR node. Freeboard nodes were not directly dependent upon the *SEV* node because we assumed that ships would move out to sea in advance of a storm and would return after any storm surge had abated. Therefore, we assumed the ability to tie-up to a pier would not be affected by storm surge. As the analysis in Table 23 shows, none of the pier decks were overtopped under the 2.0 m SLR scenario. Since interviews with personnel at NSN indicated that ships would be capable of docking at piers even if very little freeboard was available, the network assumed that no damage or loss of function would occur as a result of sea level rise in this study.

Table 23. Steam line and deck elevations at each pier relative to MLLW (m).

Pier Feature	Pier 11 (m)	Pier 12 (m)	Pier 14 (m)
Top of Second Deck	6.85	-	-
Top of First Deck	2.39	3.09	3.09
Steam Line Elevation	5.26	1.59	1.59
Steam Isolation level (Tide above MLLW)	-	1.37	1.37

Under SLR scenarios of two meters or more, it was possible that pier decks could be regularly over-topped by wave action during non-storm periods, and this over-topping could interfere with activity on the pier itself. At mean high water, the difference between sea level and the top of the pier is 0.31 meter (approximately one foot). While wave heights greater than 0.3 meter could wash over the top of the pier decks and interfere with normal operations on the piers, the application of the NSN Risk Model considered only risks to missions arising from coastal storm events and did not consider the risks of overtopping during non-storm periods.

Sufficient freeboard is also needed at each pier to enable the delivery of steam. NAVFAC has determined the tide level at which delivery of steam should be interrupted to each pier. At Piers 12 and 14, steam lines are mounted beneath the pier decks at approximately 1.59 meter above MLLW. The NAVFAC steam isolation level for these piers is 1.37 meter (4.5 ft) above MLLW

[26] Freeboard is the distance between the water surface and the top of the pier deck.

(NAVFAC n.d.), thus SLR between 1.0 and 1.5 m would interfere with steam delivery. At Pier 11, steam lines are mounted beneath the second deck at approximately 5.26 m, thus SLR up to two meters would not interfere with steam delivery at Pier 11. The steam isolation issue has been addressed below in the definition of steam capability nodes.

Sufficient draft is also needed in each berthing area to accommodate ships at berth. CVNs have a draft of 12.8 m (42 ft), but require 15.09 m (49.5 ft) of draft at MLLW (NAVFAC 1998). The ability to berth CVNs was determined by assessing the fraction of grid cells located within berthing area boundaries that had controlling depths following each storm simulation that satisfied berthing requirements. The mean and standard deviation of final controlling depths was calculated for grid cells located within the boundaries of each berthing area and these parameters were used to fit a normal probability distribution function to final controlling depths. The fraction of grid cells satisfying the controlling depth criteria were calculated from the normal distribution function.

3.9.1.2.2.2 Navigation Channels

Ships entering Chesapeake Bay in transit to NSN travel through four navigation channels. These include the Atlantic Channel, the Thimble Shoals Channel, the Harbor Entrance Channel, and the Inner Harbor Channel. CVNs require a minimum 15.24 m (50 ft) of draft in these navigation channels (NAVFAC 1998). The Atlantic Channel is located beyond the limits of the CMS grid and, therefore, was not included in the Bayesian network for purposes of this case study. The remaining channels were represented by asset damage nodes that had two possible states [*Sufficient depth, Insufficient depth*]. These nodes were parameterized as follows. The mean and standard deviation of final controlling depths was calculated for grid cells located within the boundaries of each navigation channel for each SLR and storm severity scenario. These parameters were then used to fit a normal probability distribution function to the final controlling depth of the channel, which was the limiting depth of the channel after the storm had occurred. The fraction of grid cells in the navigation channel with depths satisfying CVN draft requirements were calculated from the normal distribution function.

For purposes of this study, it was assumed that the probability that a channel was navigable was correlated with the fraction of grid cells with depths greater than the required draft for CVNs. Although the results based on this assumption could be inaccurate due to the presence/absence of shoaling, informal conversations with personnel at NSN and USACE Norfolk District have revealed that it has not been necessary to dredge navigation channels following named storms to restore navigability in the past.

3.9.1.2.3 Asset Function Nodes

In the NSN Risk Model, each asset was represented by an asset function node that was dependent on the damage state for that asset and the function state of other assets that supported its function. In the NSN Risk Model, non-probabilistic conclusions about the functionality of assets were woven into the definitions of the damage states presented in the preceding section on structural analysis (refer to *Section 3.8*). While only in extreme cases would it be possible to predict the functionality of an asset with certainty given only information about its damage state,

no information was available to characterize this uncertainty for the NSN Risk Model at the time of this study. Therefore, these nodes were parameterized with deterministic functions that described the functionality of an asset as outlined in damage state definitions. Future developments of this model could, if appropriate, incorporate information about uncertainty into the functionality of an asset given information about its damage state. While asset function nodes introduced no new uncertainties into the NSN Risk Model, they served to integrate information about the damage states of multiple supporting assets.

3.9.1.2.4 Capability Nodes

The purpose of capability nodes is to transform information about the functionality of terminal assets supporting a capability into a real-valued capability score. As described above, the capability score is an estimate of the probability that a capability will not be interrupted at least once during the course of a year because of damages to physical assets caused by coastal storms. Capability scores are used to calculate mission performance indices.

3.9.1.2.5 Mission Performance Nodes

For purposes of this study, the NSN Risk Model included three mission performance nodes, one for each pier. Each mission performance node was parameterized using a multi-attribute value function that was transformed to a CPT when the network was compiled. The value functions described mission performance at each pier as a weighted sum of the capability scores:

$$Z_k = \sum_j w_{jk} C_{jk} \quad . \qquad \textbf{(29)}$$

Where Z_k is an index of mission performance at pier k. The weights, w, are defined for j = (1, 2, 3, …, J) capabilities, C, to reflect command level priorities for supplying capabilities to ships at berth.

The weights used in the NSN Risk Model were obtained from U.S. Navy personnel on the installation using a method of swing weighting (von Winterfeldt and Edwards 1986). The mission performance index ranged from between 0 and 1, with 0 representing the lowest possible level of performance and 1 representing the highest possible level of performance. This transformation of information about infrastructure network reliability to a mission performance index was value-laden. In other words, one command on the installation might assess a different level of mission performance than another because of differing priorities in terms of what capabilities, or utilities, were provided to ships at berth.

The method of swing weighting was used to elicit weights for the multi-attribute value function at each pier. Weight elicitation was accomplished with the cooperation of individuals representing the NAVFAC MIDLANT Ship Support Office. The goal of the weight elicitation was to determine the relative importance of the various capabilities needed to *Provide At-Berth Support* for CVNs. This assessment was inherently subjective and even personnel within the same command provided very different perspectives regarding which capabilities made the greatest contribution to performance of the mission. The swing weight method (von Winterfeldt

and Edwards 1986) was implemented by first reviewing the minimum and maximum capability scores over the five prescribed SLR scenarios. Assuming that all scores were at their lowest possible level, participants then ranked the potential improvements in each capability score based on the relative importance of that potential improvement to overall mission performance. When assessing relative importance, participants were instructed to consider the relative inconvenience to operations on board the ship and on the installation as well as the relative cost of implementing the contingency plans for each capability. Participants were asked not to consider information that was not conveyed by the capability score (i.e., they were asked to ignore the severity and duration of the interruption of a capability, as well as the cost to restore a capability). After the participants ranked the capabilities, the first-ranked capability was given an arbitrary rating of 100. Each lower ranked capability was then given a rating between 0 and 100 to indicate its importance relative to the top-ranked capability. Lower-ranked capabilities received ratings that were less than or equal to the next-highest ranked capability. If two capabilities had the same rating, this indicated they were equally important. Swing weights were obtained for each pier by dividing each individual rating by the sum of the ratings for that pier.

3.10. Groundwater Assessment Methodology

Climate change impacts such as rising sea levels and changes in historic precipitation patterns could potentially change the delicate balance that currently exists between salt and fresh water bodies in coastal aquifers (McLean et al. 2001). These changes could have negative impacts on the availability of potable water supply, coastal vegetation, and the surface hydrology of coastal military installations. Understanding the nature and potential magnitude of these impacts allows us to take appropriate preventative measures, including policy and guidance changes.

Late in the summer of 2011, SERDP directed us to expand our framework to include groundwater modeling to capture potential changes in aquifer storage capacity arising from salt water intrusion driven by SLR. In response, we inserted a step in our framework (after the nearshore modeling assessment, but before the surface flood routing assessment) to capture decreases in potential infiltration rates due to these reductions in aquifer storage capacity (Figure 56).

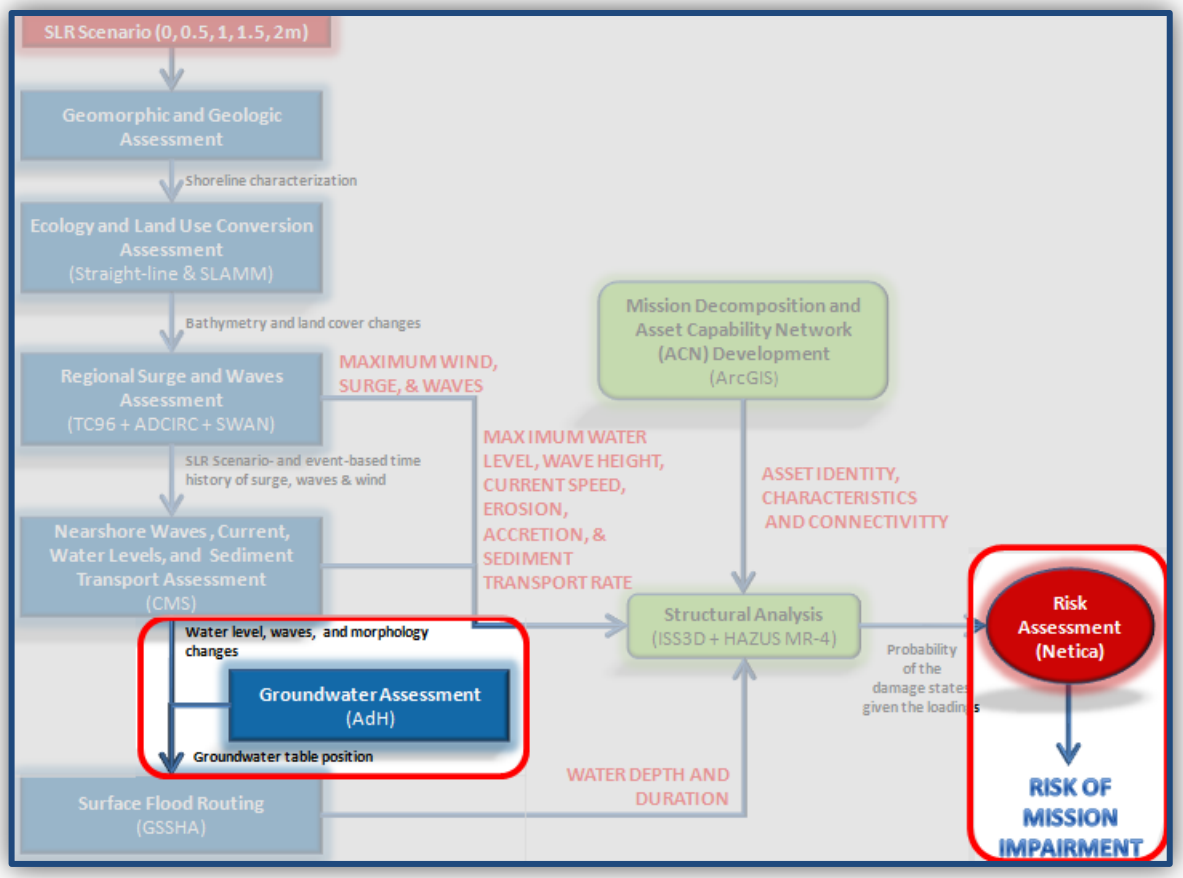

Figure 56. Project analysis and tasks: G*roundwater Assessment and Re-Assessment of Risks to Mission Impairment.*

As the figure illustrates, changes in the groundwater aquifer's isohaline boundary can be modeled and incorporated into the GSSHA analyses to generate new estimates of maximum flooding depths – this time taking account of the loss of storage capacity and subsequent reductions in infiltration. The intent of this new modeling step is to generate a fourth series of maps that visualize the difference between ignoring groundwater storage capacity and including groundwater storage capacity in the overall assessment of exposure. As before, the outputs (maximum flood depths and durations per $10m^2$ grid cell) offer new information characterizing the threats to critical infrastructure under the prescribed scenarios for the overall risk assessment.

3.10.1 Models and Approach

Researchers studying the projections of relative SLR in the in the case study area, have predicted an average MSL rise in excess of 60 cm by 2100 (Boon 2012, Ezer and Corlett 2012a,b, Wu et al. 2009, and others). Moreover, projections in precipitation rates in the same area indicate declining trends in precipitation amounts when compared with historical averages and more frequent occurrences of high precipitation intensity storms (Scheraga 2008). Both of these anticipated changes would have significant impacts on the surface and subsurface hydrology of installations in mid-Atlantic coastal zone.

From the perspective of surface hydrology, a SLR would increase surface runoff from coastal watersheds (Masterson and Garabedian 2007, Nuttle and Portnoy 1992). The rising water levels of the sea would bring about a corresponding rise in inland water table elevation, thus reducing the amount of available storage in the soil for infiltrated water from precipitation events. Additionally, a rise in groundwater table elevation would induce more discharge from the aquifer to the surface streams in inland coastal areas (Masterson and Garabedian 2007). Nuttle and Portnoy (1992) found this effect to occur in areas where a large portion of the watershed was above the level of high tide but not too far above the water table. The definition of "too far" was dependent on the particular soil characteristics of the watershed in question. In their study, Nuttle and Portnoy calculated that surface runoff could increase by as much as 70% from a 21 cm rise in sea level. The projected precipitation pattern changes would also add to the increase in surface runoff as less frequent but higher intensity storms would likely cause less infiltration and more peak flow discharge to occur.

An increase in surface runoff would most likely bring about a corresponding decrease in groundwater flow from the aquifer to the sea. The rise in water table associated with SLR would cause the head gradient between land and shore to decrease thus producing less groundwater discharge of fresh water to the coastal system. This would likely induce changes in the salt-water concentrations of nearshore water bodies, particularly in the bays and inlets near fresh water discharges. Indeed, a rise in Chesapeake Bay salinity associated with SLR had already been noted (Hilton et al. 2008). Additionally, groundwater discharge would further be reduced if evapotranspiration increased in response to wetter soil conditions (Nuttle and Portnoy 1992).

The reduction in groundwater discharge coupled with the increased surface water discharge would impact nearshore ecosystems in a number of ways. Sub-marine groundwater discharge controls the gradient in sediment salinity between surface and marine ecosystems (Johannes 1980). This shift in isohaline balance would induce changes in coastal vegetation given the sensitivity of these species to salt concentrations (Cahoon et al. 2006; Scheraga 2008). An increase in surface runoff, derived from groundwater discharge within a coastal watershed at the expense of submarine groundwater discharge, would deliver more nitrates directly to the receiving water body, which promotes conditions for algal blooms (Nuttle and Portnoy 1992).

Potable water systems could also be put at risk by SLR, including systems that derive their supplies from surface water and groundwater. In the case of surface water, only systems where water was stored in estuarine, low-lying water bodies not protected by structures such as dams were those likely to potentially be impacted by rising sea levels (Scheraga 2008). Nearshore groundwater systems could potentially be at risk from impact by rising sea levels as well. Figure 57 depicts the intrusion of salt water into a coastal aquifer system where pumps withdrew water from a fresh water source.

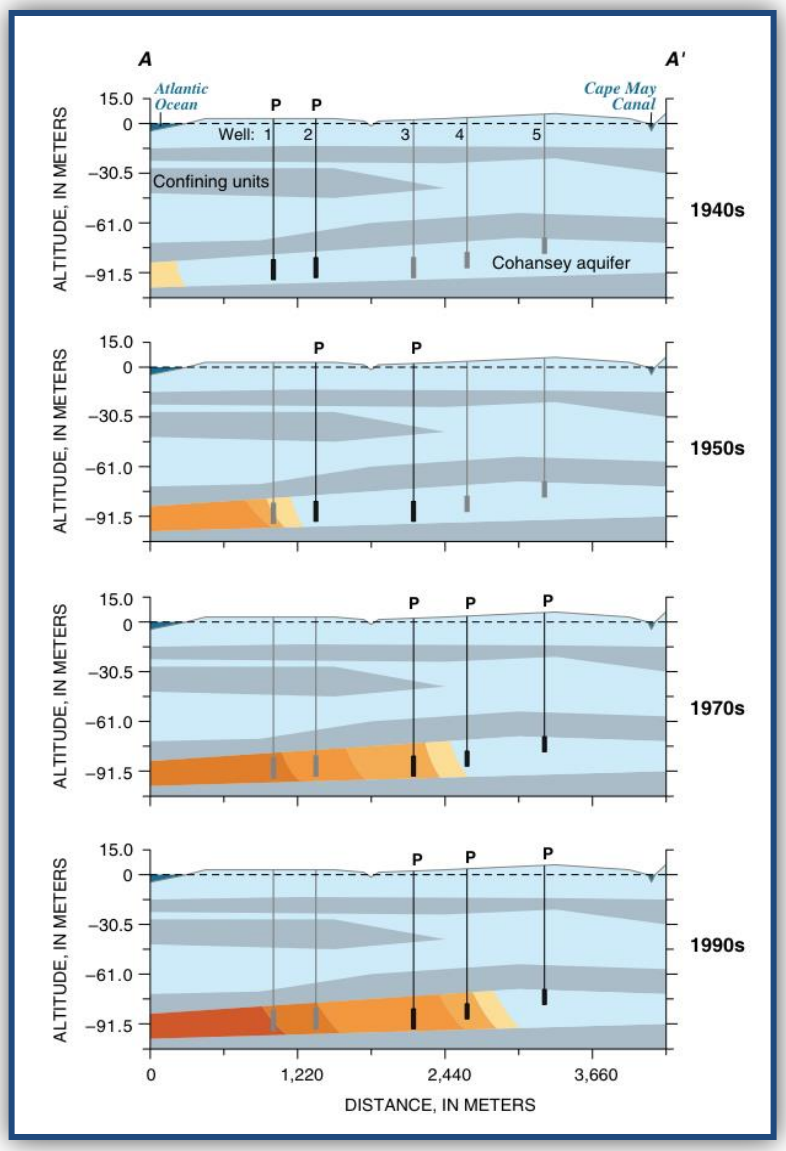

Figure 57. Hydrogeologic sections showing lateral encroachment of saltwater and contamination of supply wells in the Cohansey aquifer at the Cape May City (New Jersey) well field, 1940s to 1990s. (Barlow and Reichard 2010).

When rising sea levels move the isohaline lines further inland, scenarios such as that depicted in Figure 57 above become increasingly possible. Once tainted with salt water, formerly fresh water aquifers would become unusable for potable water supplies without expensive treatment processes. In the coastal southern Virginia area, most municipal water systems were considered surface water-based with some supplement from groundwater resources. However structures such as dams protected those surface water bodies from potential SLR impacts. Groundwater resources were mainly used in reserve capacity situations when surface water levels were low. They withdraw water from aquifers in areas adjacent to surface water reservoirs that were set back some distance from the coast (Figure 58).

Figure 58. Location of water supply reservoirs and groundwater wells in the Norfolk, Virginia area. (Source: www.norfolk.gov).

To address these concerns, we employed a four-step approach that included:

1) a geophysical survey of the installation to locate the isohaline boundary,
2) the construction and deployment of a coupled 2D distributed surface water hydrologic model and a 3D subsurface groundwater hydrologic model to simulate SLR and saltwater intrusion into the aquifer,
3) a re-assessment of surface-subsurface hydrologic conditions (i.e., flood routing) given new infiltration capacities derived from the groundwater modeling, and
4) a re-assessment of risks to mission impairment given these new flooding results.

3.10.2 Modeling Inputs

Inputs to the re-analysis of flood routing and risks included the derivation of the isohaline boundary and the construction/deployment of the new groundwater model. Below we provide the details of these efforts in more detail.

3.10.2.1 Geophysical Survey to Detect the Isohaline Boundary

A geophysical study was conducted on NSN to determine the depth of the groundwater table and identify the freshwater/saltwater interface. From this data, initial groundwater table elevation and isohaline boundary locations were determined to generate initial conditions for the groundwater model. The geophysical effort included electrical resistivity and electromagnetic surveys at multiple locations on the installation and along the perimeter of the study area boundary. An earthen electrical resistivity survey measured how well an electrical current flowed through the subsurface. This allowed us to detect differences between unsaturated and saturated sediments, as well as fresh and saline water. Conductance and groundwater depth data were taken from onsite monitoring wells to calibrate the electrical resistivity data. The location of the nine resistivity surveys and eight monitoring wells measured are shown on Figure 59.

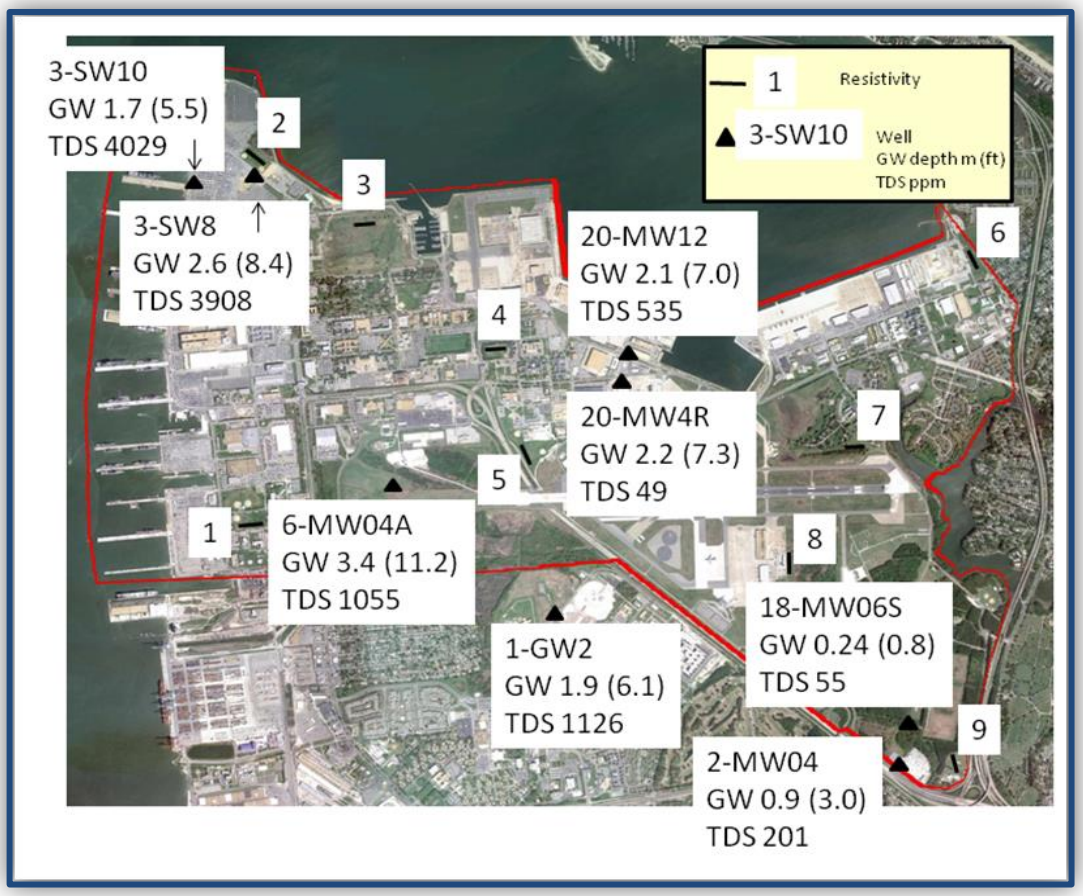

Figure 59. Location of the study area on NSN, and the location of the electrical resistivity survey lines and monitoring wells we measured. "GW" is ground water; depth below ground surface in meters (ft). Total dissolved solids (TDS) is presented in parts per million (ppm) and represents the average value measured.

Much of the area is industrialized and covered with concrete or asphalt, and aboveground steam distribution lines are common. Unfortunately, we were not given access to the largest areas containing open grass fields (i.e., inside the airfield boundary). Instead, we conducted the resistivity surveys on the installation's ball fields, recreational areas, golf courses, and open areas proximal to buildings (although some underground utilities were present at these locations which interfered with our ability to survey). The resistivity survey site numbers, their corresponding site name, and the monitoring wells measured are listed in Table 24.

Table 24. List of resistivity survey sites and monitoring wells measured.

Resistivity Surveys	
Site Number	**Site/Well Name**
1	Ball Field-M
2	Ball Field
3	Golf Course
4	Historical Parade Ground
5	Recreational Area
6	Northeast Area
7	Airfield
8	Control Tower
9	Turtle Park
Wells	
Site Number	**Site/Well Name**
1	GW2
2	MW04
3	SW8
3	SW10
6	MW04A
18	MS06S
20	MW4R
20	MW12

The soils in this geophysical study belong to the Columbia Group, which is comprised of unconsolidated fine sands and silts, and impermeable silt, clay, and sandy clay. The soils in the Columbia Group can extend to a depth of 18 m (60 ft). The fine sands and silts comprise the upper 6 - 12 m (20 - 40 ft), whereas the impermeable silt and clay are found in the lower 6 - 12 m (20 - 40 ft). The clay layer is often discontinuous and absent in some areas. The water-table aquifer is present in the sandy soils in the upper 6 - 12 m (20 - 40 ft) of the Columbia Group. The depth to the water table is usually less than 2.5 m (eight feet). The general range of resistivity (conductivity) values for wet to moist silty and sandy soils can vary from 10s to 100s ohm-m (Ω-m) [10's to 100's milliSiemens per meter (mS/m)], whereas for wet to moist clayey soil the resistivity (conductivity) can vary from 1s to 10s Ω-m (100's to 1000's mS/m). The intrusion of saltwater will decrease (increase) these resistivity (conductivity) values. Note that there is an overlap in resistivity values amongst the different soil types and moisture conditions, and that the presence of saline water in saturated sands can be misinterpreted as wet clay.

3.10.2.1.1 Electrical Resistivity

We used a Schlumberger sounding array electrical resistivity survey method to characterize the Earth resistivity structure with depth. To begin, we inserted a series of metal stakes (electrodes) 10 to 20 cm (four to eight inches) into the ground along a transect line. Four electrodes were used to make a single measurement, with the two outer electrodes acting as the current electrodes (C_1, C_2) and the two inner electrodes as potential electrodes (P_1, P_2). A current I was injected into the ground through the current electrodes, and the potential difference ΔV was measured between the potential electrodes. The potential difference was related to the apparent resistivity ρ_a of the subsurface material through the geometry k of the electrode configuration:

$$\rho a = 2\pi k(\Delta V/I) \quad \textbf{(30)}$$

$$k = 1 / \{(1/\mathrm{r1} - 1/\mathrm{r2}) - (1/\mathrm{r3} - 1/\mathrm{r4})\} \quad \textbf{(31)}$$

where r_1, r_2, r_3, and r_4 represent the linear distance between electrodes C_1P_1, P_1C_2, C_1P_2, and P_2C_2, respectively (Figure 60a).

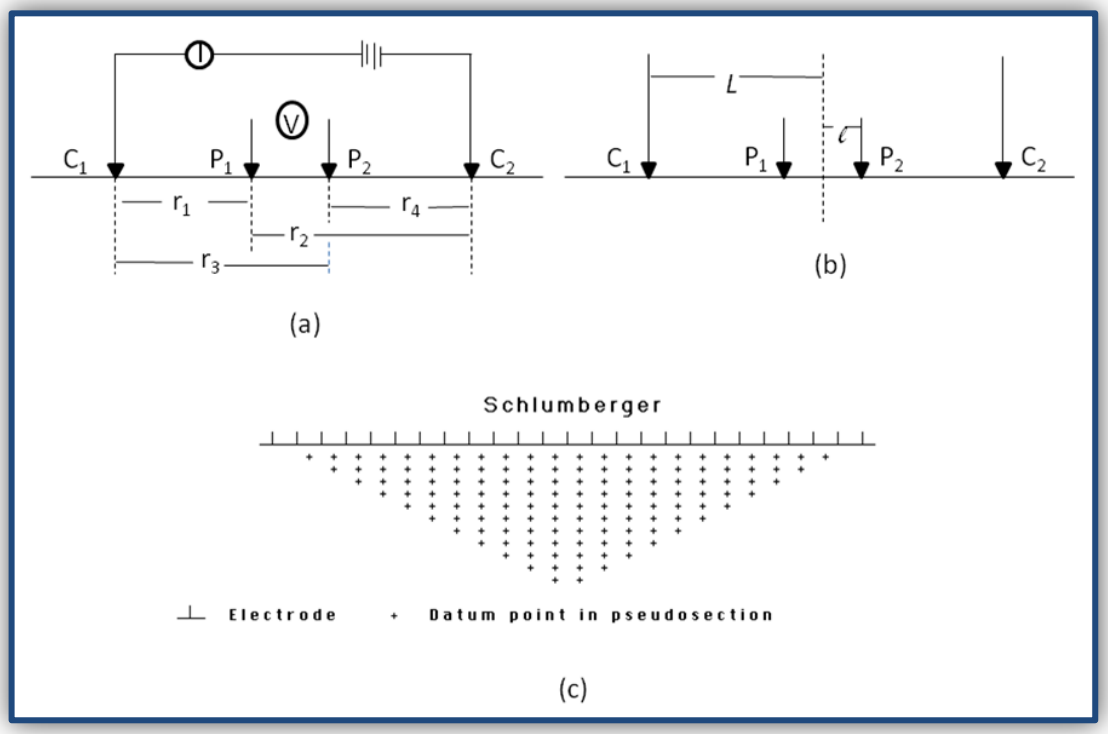

Figure 60. (a) General electrode configuration for a linear resistivity array. (b) Electrode configuration for a Schlumberger array, L>l. (c) Arrangement of measurement plotting locations for 2D Schlumberger resistivity pseudo-section.

For the Schlumberger array (Figure 60b above), the current electrode spacing was much greater than the potential electrode spacing, therefore *Equation 31* reduces to:

$$\rho a = (\pi L2/2l)(\Delta V/I) \quad \textbf{(32)}$$

The distance between the electrodes was increased to achieve a greater depth of investigation. A total of 112 electrodes were used, each spaced 1-m apart. A combination of the maximum current and potential electrode spacing allowed a maximum depth of investigation of 15.8 m. An AGI SuperSting R8 resistivity system was used (Figure 61a).

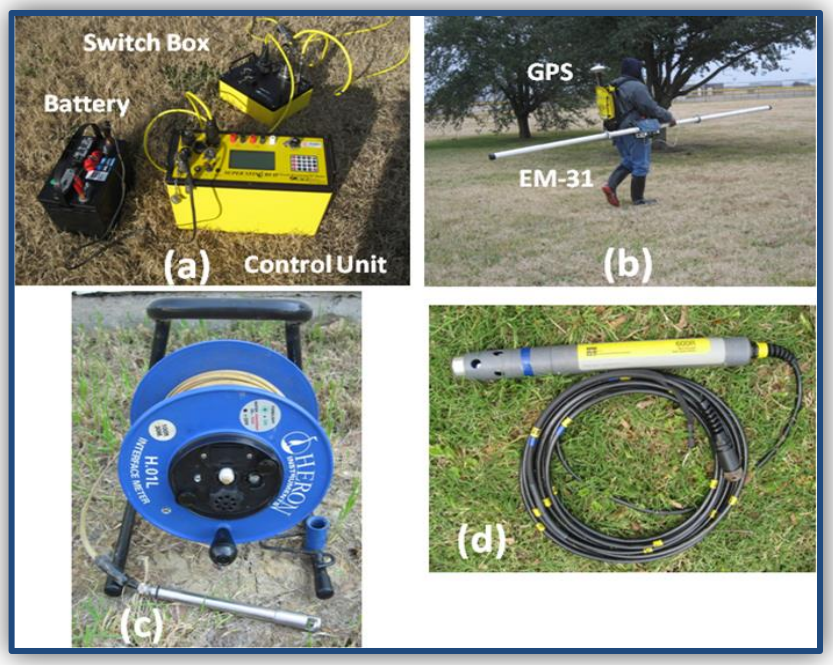

Figure 61. (a) AGI SuperSting R8 resistivity system with control unit, electrode switch box, and battery. (b) Geonics EM-31 terrain conductivity meter. (c) Heron Instruments H.01L Interface Meter for measuring depth to the water table in a well. (d) YSI 600R sonde was used to determining specific conductance.

This instrument allows automatic switching of electrodes, so once the electrodes and cables are in place, the system can run unattended with only periodic monitoring. A single survey was completed in approximately six hours (two hours setup/breakdown and four hours data acquisition). The data were then plotted as 2D pseudo-sections, with the data value plotted below the midpoint of the four-electrode array at the median depth of investigation of the array (Figure 61c above). Data collected in this manner must be inverted to obtain the true resistivities and depths. The resistivity unit of measure is Ω-m.

3.10.2.1.2 Electromagnetic Inductance

A terrain conductivity survey was conducted along each resistivity line to: 1) determine the trend of the shallow subsurface conductivity, and 2) to identify the presence of buried utilities or anomalous features. The Geonics EM-31 is a man-portable instrument 4-m in length with a depth of investigation of about six meters (Figure 61b above). It has a frequency domain electromagnetic (EM) induction system that operates at 9.8 kilohertz (kHz). For purposes of this study, the data were acquired at five samples per second and a Trimble DS232 differential Global Positioning System (GPS) system was used for positioning. The EM-31 measures two components, quadrature phase and inphase. The quadrature component is related to the ground conductivity, whereas the inphase component is useful for detecting metallic objects. Conductivity (quadrature component) is a positive valued parameter, although the instrument can give negative values when a highly conductive object (such as metal) is present. The unit of measure is mS/m; conductivity is the inverse of resistivity. The inphase measurement is a relative measurement with units of parts per thousand (ppt); the values can be positive or

negative. The EM-31 data were collected along the resistivity survey lines and were presented as profile lines.

3.10.2.1.3 Water Depth and Specific Conductance

The water depth in the monitoring wells was determined using a Heron Instruments H.01L Interface Meter (Figure 61c above). The sensor, which was attached to an incremented tape, was lowered down the well and emitted a tone when it contacted water. The water depth was measured at a point on the well (generally top of casing) where the elevation was known.

A YSI 600R sonde equipped with temperature and conductivity sensors (Figure 61d above) was used to acquire specific conductance readings at various depths in the monitoring wells. The specific conductance (25° Celsius) was obtained by applying a temperature compensation factor to the measured conductivity values. The specific conductance is related to the Total Dissolved Solids (TDS) in the water. The electrical conductivity of the water is caused by the presence of dissolved ionic species, including dissolved salts. To accurately determine the TDS conversion factor, it was necessary to collect water samples from the well, and both dry and weigh the solids. However, a default value of 0.67 can be used to convert specific conductance to TDS to obtain a gross estimate of TDS. An estimated TDS value was used in this study and was sufficient for determining the presence of saltwater intrusion. Levels (in ppm) of TDS for fresh/potable water were less than 1,000 ppm; palatable water less than 500 ppm. The U.S. Geological Survey (USGS) classifies saline water in three categories: slightly saline 1,000 to 3,000 ppm; moderately saline 3,000 to 10,000 ppm; and highly saline 10,000 to 35,000 ppm. Seawater has a salinity of about 35,000 ppm; brine is greater than 35,000 ppm TDS.

3.10.2.2 Construction and Deployment of the Groundwater Model

3.10.2.2.1 Modeling Approach

An AdH-WASH model was used to compute coupled density-dependent flow and solute transport fields and a combination of GMS v8.2 and CMB v2.0 was used as a pre- and post-processing tool to develop and evaluate the AdH-WASH module simulation results.

The AdH includes the following physical models:

1) saturated and unsaturated groundwater flow,
2) overland flow,
3) three-dimensional Navier-Stokes flow, and
4) two- or three-dimensional shallow water problems.

Although AdH includes both density-dependent flow and transport equations, we opted to deploy an external WASH module to perform these calculations. It is important to note that this module's capabilities are being incorporated into AdH and its results are based on the WASH123D (Yeh et al. 1998) model's capabilities. WASH123D is a physically-based finite element numerical model that can be used to compute coupled density-dependent flow and solute transport in the groundwater system. The 3D subsurface density-dependent flow and solute

transport equations were solved using the AdH-WASH model for this study. The Galerkin finite element method was used to solve the flow equation, while the Lagragian-Eulerian finite element method was used to solve the transport equation.

3.10.2.2.1.1 Groundwater Modeling System (GMS, v. 8.2)

The GMS (v.8.2) program (developed by ERDC and Aquaveo, LLC) is considered the most sophisticated groundwater modeling environment available. GMS provides an integrated and comprehensive computational environment to develop models used to simulate subsurface flow, contaminant fate/transport, and the efficacy and design of remediation systems. GMS integrates and simplifies the process of groundwater flow and transport modeling by bringing together all of the tools needed to complete a successful study. GMS provides a comprehensive graphical environment for numerical modeling, tools for site characterization, model conceptualization, mesh and grid generation, geostatistics, and sophisticated tools for graphical visualization. The WASH123D Graphic User Interface (GUI) is used to generate input files for flow simulation. For the transport simulations, the FEMWATER GUI is used to generate the transport input file that is subsequently translated to the AdH-WASH format.

3.10.2.2.1.2 Computational Model Builder (CMB)

The CMB (developed by ERDC and Kitware Inc.) is a suite of general, multi-dimensional GUIs for pre- and post-processing of numerical simulations. The CMB is built on a client/server framework that can be adapted to different user needs. The CMB design delays full mesh generation as long as possible to keep problem sizes manageable, working with 2D edges or 3D shells when tagging for boundary conditions. From a complete conceptual model, simple meshes can be generated locally or the model can be exported for mesh generation by HPC-based meshing tools.

3.10.2.2.2 Modeling Inputs

The three-dimensional finite element mesh for the AdH-WASH simulations encapsulated the existing GSSHA computational grid and extended to the south beyond NSN. Refer to Figure 62 for the model domains of AdH-WASH and GSSHA. The groundwater model was created using available topographic, geologic, and climate data. Littoral boundary conditions were input corresponding to the five prescribed SLR scenarios. The formation of the domain and input parameters are described below.

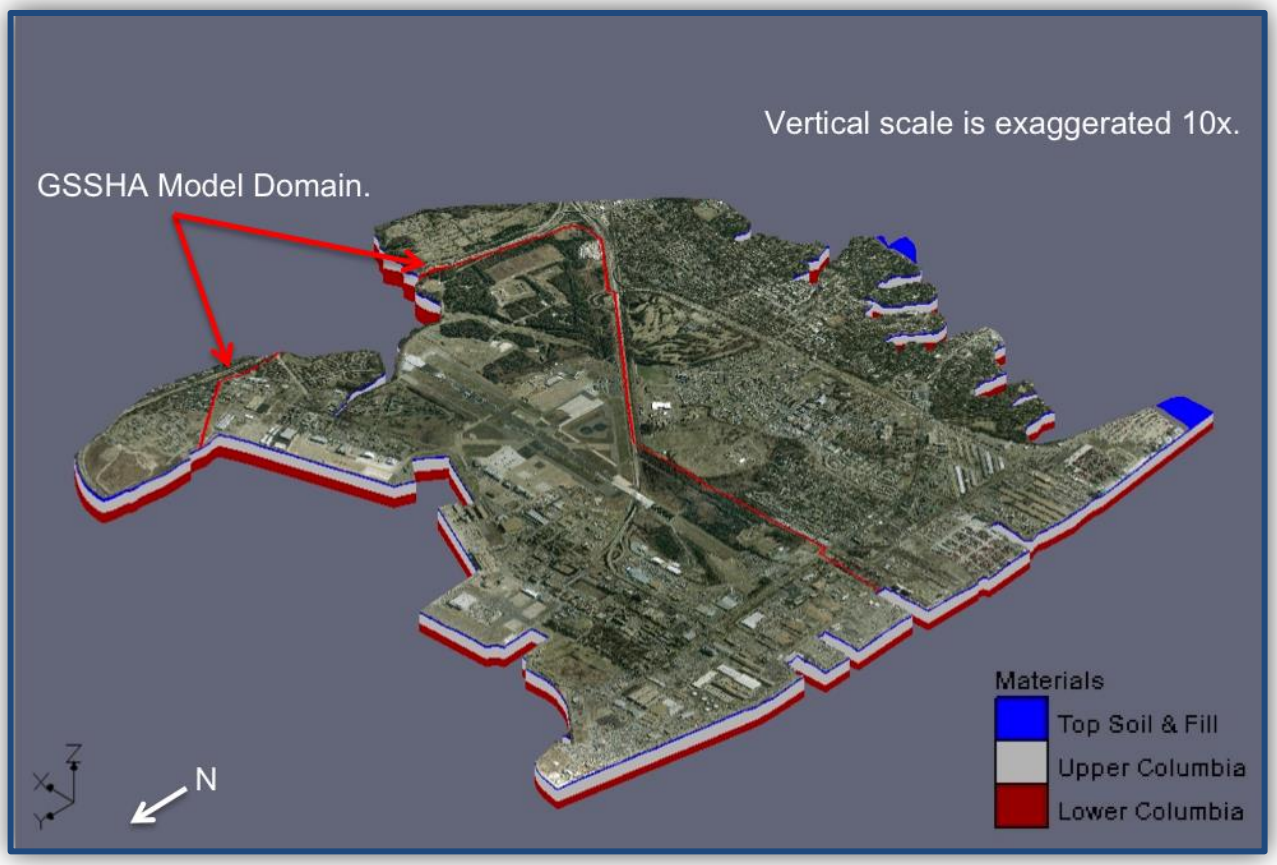

Figure 62. The Norfolk AdH-WASH groundwater model domain and hydrogeologic units. The GSSHA model domain is shown with a red line within the AdH-WASH model

3.10.2.2.2.1 AdH-WASH Model for NSN

An AdH-WASH model of the unconfined surficial aquifer underneath the site was developed to both simulate the water table with saltwater intrusion and compute soil moisture. Note that the installation is positioned near the mouth of the Chesapeake Bay and is surrounded by the brackish water of the Lafayette River to the south, Elizabeth River on the west and Willoughby Bay on the north; and the freshwater Mason Creek on the east. The creek, whose outlet into Willoughby Bay has been channelized and covered, is tidally influenced, has limited mixing, and is therefore considered freshwater for purposes of this study. Underlying the installation, the shallow surficial Columbia aquifer is unconfined, open to the atmosphere, and subject to recharge from infiltrating rainfall. This aquifer is also hydraulically connected to the surrounding surface-water bodies. We assume that the salinity of the coastal water causes the water to be denser than freshwater, and creates a concentration gradient that, with tidal fluctuations, allows salinity to intrude into the coastal aquifer. The hydraulic gradient created by recharge counteracts this intrusion by creating a flow field towards the coastal water that pushes the saltwater out of the aquifer. Although each process is variable, a relatively stable boundary between the two water bodies is assumed to have form as a wedge with freshwater floating on top.

The stabilization of the modeled salinity boundary to stressors was a long-term event compared to the storm scenarios of the risk assessment, therefore the groundwater model was designed to simulate decades of slow change. Accordingly, constant average inputs replaced the highly variable tidal fluctuations and periodic rainstorms. Only the five prescribed SLR scenarios and the general groundwater flow field influenced the location of the salinity boundary. The AdH-WASH model developed for this study included density-dependent flow in saturated and unsaturated zones where salinity was treated as a transport constituent.

3.10.2.2.2.2 Geology and Hydrogeologic Conceptual Model

The geology in the area of NSN is comprised of two main formations: (1) the Columbia Group, and (2) the Yorktown Formation (CH2MHill 2000, 2011). These two formations are overlain by topsoil and fill materials that were placed during construction of the NSN and subsequent base development. The upper most geologic formation of the Columbia Group is the Sand Bridge Formation (approximately 6 to 14 m) consisting of unconsolidated fine sands and silts of low to moderate permeability. The Norfolk Formation (approximately 6 to 14 m) makes up the lower Columbia Group and consists of relatively impermeable silt, clay, and sandy clay (CH2MHill 2000, 2011). Underlying the Columbia Group is the Yorktown Formation which is comprised of moderately consolidated coarse sand and gravel.

The hydrogeology of the NSN area consists of two hydraulically significant aquifer systems: (1) the water table aquifer, and (2) the Yorktown aquifer (CH2MHill 2000, 2011). The water table aquifer comprises the upper part of the Columbia Group coinciding with the more permeable Sand Bridge Formation. The Yorktown Aquifer is a semi-confined aquifer separated from the water table aquifer by the discontinuous aquitards of the Norfolk and the upper Yorktown Formations.

The water table aquifer was the only aquifer modeled in the effort. Since the Yorktown Aquifer is essentially confined, it was assumed to be hydraulically disconnected from the Columbia and would therefore not affect the groundwater table or salt-water intrusion due to SLR. The geologic conceptual model used to characterize the water table aquifer was idealized and consisted of three material types (Figure 62 above).

The uppermost material type is a top soil/fill combination that we initially classified as two materials, but to one material to avoid convergence issues due to aspect ratio. The middle material called the Upper Columbia is a fine sand and silt layer indicative of the Sand Bridge Formation of the Columbia. This material represents the section of the water table aquifer that is the most transmissive. The third material type represents the Norfolk Formation of the lower Columbia Group (referred to as the Lower Columbia) composed of relatively impermeable silt, clay, and sandy clay.

The material layers were defined using boring logs from several environmental reports of NSN. There were numerous boring logs but most were highly concentrated at the remediation sites on the installation. Due to the high numbers of borings at project sites, the available borings were reviewed and then limited to a few representative borings for each site. The geologic solid was constructed from these borings and representative borings. The hydrogeologic parameters were

then applied by material layer and were varied across the domain as discussed earlier in this section.

3.10.2.2.2.3 Model Domain and Mesh

The groundwater domain boundary was delineated from high-resolution imagery to follow the shoreline, cutting across the base of NSN piers and the commercial port, proceeding up tributaries of both Willoughby Bay and Lafayette River to the narrowest overland transects to the Mason Creek shoreline. The pier structures were not incorporated into the domain because they were man-made and inconsequential to the characterization of the aquifer. This boundary was utilized to clip a processed LiDAR elevation dataset, triangulate a mesh, and assign boundary conditions. The domain encapsulated a surface area of 26.5 km^2.

The same one-meter resolution LiDAR elevation dataset previously utilized by the GSSHA domain was processed by CMB's PointsBuilder tool to create a bare-earth DEM. Large buildings and trees were manually truncated prior to executing an automatic terrain extraction algorithm to remove remaining artifacts (e.g. walls and vegetation), to fill the resulting data holes, and to resample the DEM to a 10-meter resolution.

The domain boundary was filled with a 2D finite element mesh consisting of triangles with an average edge length of 25 m. This mesh was used as a template to build a 3D mesh from the geology model with the DEM representing the top surface. The final 3D mesh consisted of roughly one million triangular prism elements in ten layers with three soil material regions - the Top Soil/Fill material was limited to the top two element layers while the Upper and Lower Columbia material regions were each four element layers thick. The surface elevations varied from zero to eight meters. For purposes of this study, the resolution was chosen to reduce the element size of the mesh and hence the computational footprint, while still providing a satisfactory depiction of the groundwater system. GMS and CMB's MeshViewer tools were utilized to generate and verify the mesh, respectively.

3.10.2.2.2.4 Soil Material Properties

The saturated/unsaturated flow and transport processes within AdH-WASH were physics-based processes dependent on material properties, such as hydraulic conductivity, porosity, etc. The standard input type for soil material properties for AdH-WASH was zonal classification, which applied a set of properties to an entire material region. The properties specified for the site's materials, listed in Table 25, were based on literature and informed by site characterization reports when available. To more closely match the natural heterogeneity of the site's geology, the hydraulic conductivity was allowed to spatially vary in the horizontal plane.

Table 25. Soil material properties on the study site.

Soil Material	Top Soil/Fill	Upper Columbia	Lower Columbia
Zonal Horizontal Hydraulic Conductivity, K_h (m/s)	10.0	6.0	0.1
Kriged K_h (m/s)	2.0 – 42.59	1.3 – 30.0	0.02 - 0.5
Vertical Hydraulic Conductivity Anisotropy Factor	0.1	0.1	0.1
Effective Porosity (m^3/m^3)	0.33	0.3	0.25
Modified Compressibility (1/m)	0.0	0.0	0.0
van Genuchten Alpha (1/m)	3.0	2.6	1.6
van Genuchten Exponent	1.5	1.5	1.2
Bulk Density (kg/m^3)	2100	2000	1900
Longitudinal Dispersivity (m)	20	20	20
Transverse Dispersivity Anisotropy Factor	0.1	0.1	0.1
Tortuosity	1.0	1.0	1.0

A “kriged” hydraulic conductivity value was interpolated at each mesh element’s centroid using ordinary kriging informed by a uniformly distributed set of points with values constrained within an order of magnitude, centered on the original “zonal” hydraulic conductivity. This probable realization created preferential pathways of higher permeability between the upper two materials since their hydraulic conductivity ranges overlapped. Images of each material’s kriged values can be found in (Figure 63) below.

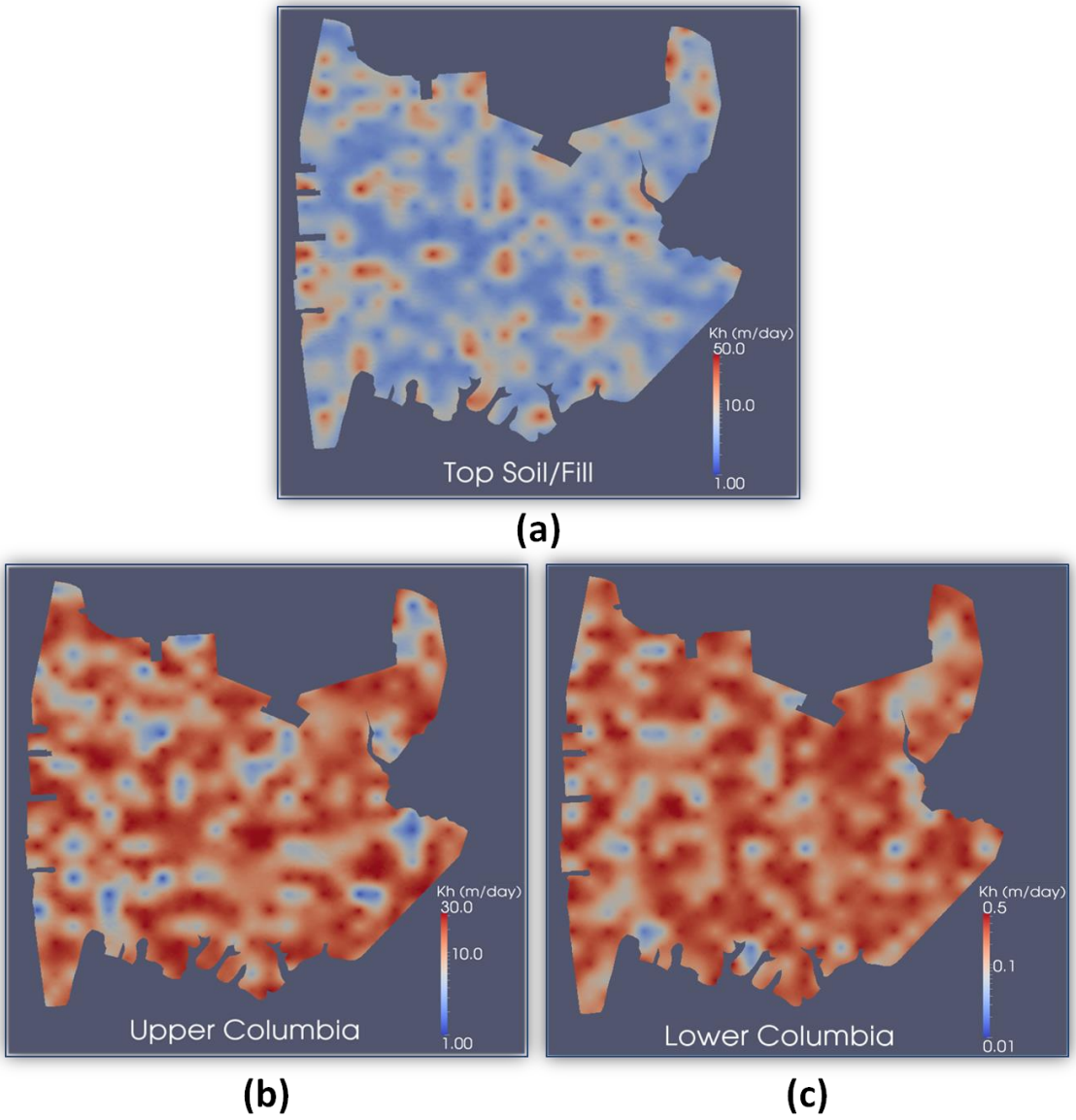

Figure 63. Kriged horizontal hydraulic conductivity for the (a) Top Soil/Fill, (b) Upper Columbia, and (c) Lower Columbia materials.

3.10.2.2.2.5 Boundary Conditions

The AdH-WASH model was used to reproduce the general aquifer conditions below the study site ignorant of varying conditions (e.g. storm surge and precipitation) but converged to the various SLR scenarios. For each scenario, the littoral boundaries (Elizabeth and Lafayette Rivers, Willoughby Bay, and Mason Creek) were assigned a specified head type condition with heads of 0, 0.5, 1.0, 1.5, and 2.0 m, respectively. It was assumed that Mason Creek, an inland water body, would rise to the same height as the Chesapeake Bay water bodies. This boundary type was applied to the vertical and submerged top surface nodes of the mesh. Submerged top

surface nodes did not exist in the 0.0 m SLR scenario mesh, however, for each additional rise, the number of nodes declared "inundated" (i.e., elevation below sea level) increased.

The vertical model faces following the overland transects between the Mason Creek and the Chesapeake Bay water bodies were assigned a "no flow" boundary type, implying a zero flux across these faces. These assignments were in locations where groundwater was assumed to flow parallel to the boundary, from high head to the low head of the surface-water bodies. The bottom faces of the mesh were also specified as "no flow".

For the aquifer to reach a state of equilibrium, a hydrometeorological forcing, specified as 6.4 x 10^{-5} meters per day (m/day) [approximately two percent of NSN's average annual rainfall obtained from NOAA's National Climatic Data Center (NCDC) http://www.ncdc.noaa.gov/oa/ncdc.html, accessed November 2012] was required to recharge the aquifer. This forcing was applied as a specified flux boundary type to all non-submerged top surface faces of the mesh. The value was derived to drive long-term groundwater flow while accounting for processes limiting infiltration such as storm water management and evapotranspiration.

A specified concentration boundary type was assigned to all mesh boundary nodes with values representing salinity. Although the salinity of the brackish Chesapeake Bay varies seasonally and diminishes with distance from the mouth of the bay (Chesapeake Bay Program Water Quality Database, https://explore.data.gov/Geography-and-Environment/Chesapeake-Bay-Program-Water-Quality-Database/fw52-5emx, accessed November 2012) , a conservative maximum constant value of 26 ppt was specified for the three Chesapeake Bay water body boundaries, including the corresponding submerged top surface nodes. All other boundaries were assigned a salinity of zero parts per thousand. Again, it was assumed that Mason Creek was a freshwater body with salinity of zero parts per thousand. The fresh water boundary on Mason Creek made the model conservative with respect to salt-water infiltration, which meant that this was a minimum salt-water infiltration scenario. This was considered appropriate since no data was available for salt concentration in Mason Creek. Even with direct connection between Chesapeake Bay and Mason Creek, it was believed the concentration of Mason Creek was toward the lower end of the possible range of 0 to 26 ppt.

3.10.2.2.2.6 Initial Conditions

Each SLR scenario used an initial head dataset that ensured the mesh was fully saturated at the simulation start. This method allowed the groundwater system to drain and reach an equilibrium flow state where the water table stabilized. Similarly, an initial transport dataset depicting salinity deceasing from 26 ppt at the Chesapeake Bay boundaries to a value of zero parts per thousand over a distance of 300 m, moving perpendicularly inland was utilized. The freshwater and "no flow" boundaries, and the mesh interior were initialized as zero parts per thousand. The initial wall of saltwater seeded the density dependent flow field, setting up the computational formation of a saltwater wedge.

3.10.2.2.3 Model Evaluation

The AdH-WASH model was evaluated with two simulation types. The first simulation was a "flow only" simulation, conducted with no saltwater, allowing the model setup to be evaluated before introducing increased complexity. The second simulation was a density-dependent flow and transport simulation, which included five different initial water level boundary conditions based on the five prescribed SLR scenarios.

3.10.2.2.3.1 Flow Only without Salinity

The "flow only" run was a steady state simulation with no density dependence due to salinity. The model setup was evaluated after this run to uncover any inconsistencies with the conceptual model of the study site and the numerical model setup. The results showed mounding of the water table in the center of the model domain. The elevation of the water table ranged from the existing sea level (0.0 m) along the littoral boundaries to a maximum 1.13 m at the center of the model domain. The flow model was found to be acceptable and the simulation was ready for the simulation of transport and density dependence.

3.10.2.2.3.2 Density Dependent Flow and Salinity Transport Models

The density dependent transport model simulations were set up with the aforementioned head boundary conditions for the five prescribed SLR scenarios, as well as the addition of concentration boundary conditions. The results were analyzed by observing the change in water table, the change in potential infiltration capacity, and the behavior of the salt water compared to the geophysical findings.

Water Table: The base scenario (0.0 m SLR) model simulation predicted the same mounding of water in the center of the domain as the flow only simulation, with the same water table elevation ranges (0 to 1.13m, Figure 64).

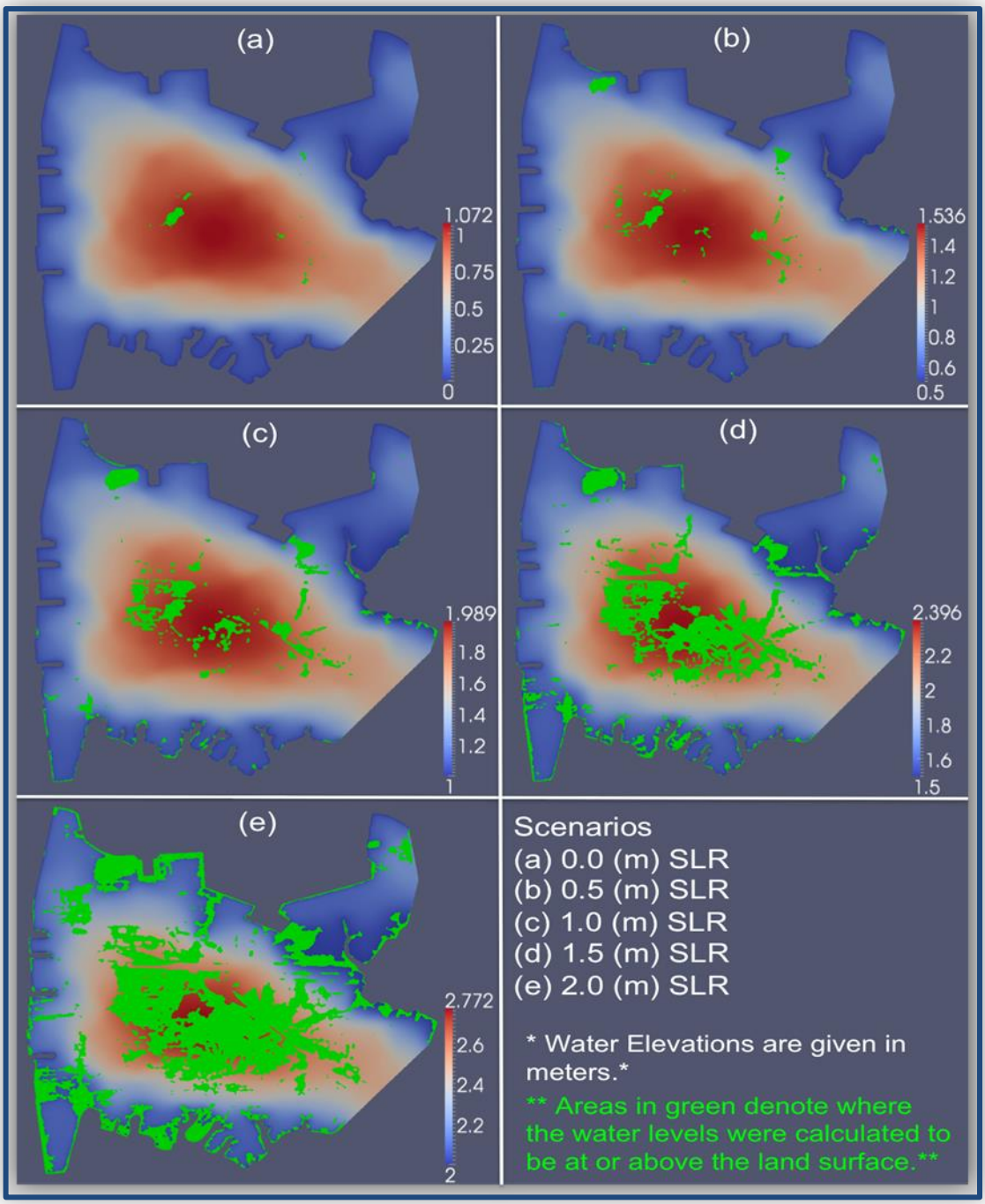

Figure 64. Water table elevations for each prescribed SLR scenario: (a) 0.0 m, (b) 0.5 m, (c) 1.0 m, (d) 1.5 m, and (e) 2.0 m. Areas in green denote water levels at or above the land surface.

The water table was high enough in a few locations to cause water to collect on the surface if unimpeded. These locations, shown in green in Figure 65, were low-lying areas and included known wetlands.

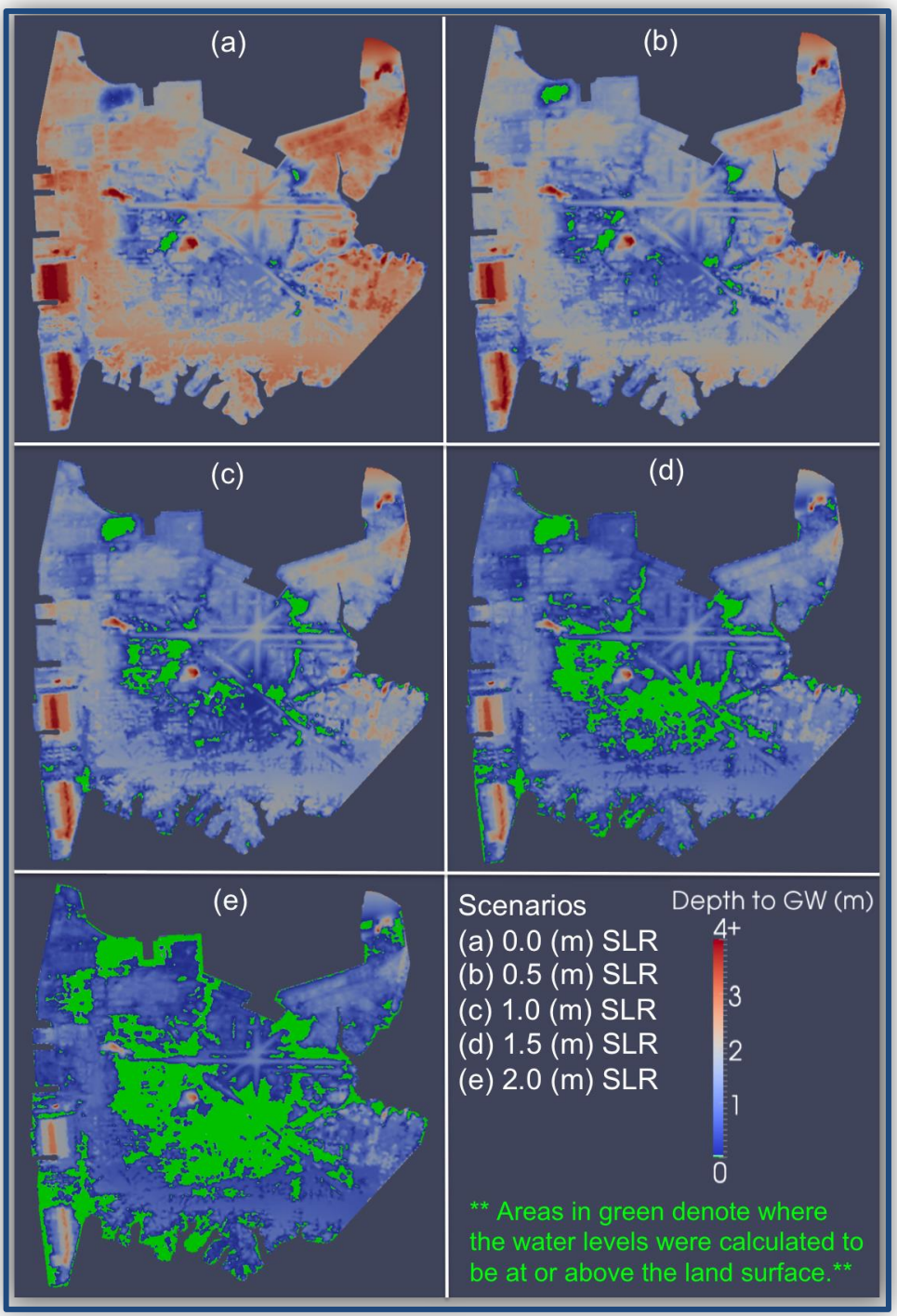

Figure 65. Depth to groundwater for each prescribed SLR scenario: (a) 0.0 m, (b) 0.5 m, (c) 1.0 m, (d) 1.5 m, and (e) 2.0 m. Areas in green denote water levels calculated to be at or above the land surface.

The depth to the water table varied between zero meters and over four meters in areas of higher land surface elevations. The change in water table due to the addition of salinity and density

dependence for the 0.0 m SLR scenario was subtle. The average difference of the pressure head data sets was 0.09 m, but the general shape and location of the water table were consistent.

As expected, increasing sea levels generated an increase in the water table elevation and a decrease in the depth to water as the area became completely saturated (Figure 65 (a-e) above). The mounding effect of the water in the center of the domain increased slightly from 1.07 to 1.08 m for the 0.5 m SLR scenario and then decreased as the SLR increased for the remainder of the scenarios. The mounding levels were 1.03, 0.94, and 0.87 m for the 1.0 m, 1.5 m, and 2.0 m SLR scenarios respectively. The decrease in mounding corresponded with an increase in surface inundation, which allowed the aquifer to drain.

Potential Infiltration Capacity: The decreasing depth to water table due to increasing sea levels caused a reduction in the available pore space to accommodate the infiltration of water. The amount of pore space available, and the decrease in pore space was calculated for each prescribed SLR scenario (Table 26). Infiltration capacity decreases ranged from 23 to 80 percent for the five prescribed SLR scenarios (0.5 m – 2.0 m). This large loss in capacity did not include the soil moisture in the partially saturated sediments above the water table, which would have decreased the infiltration capacity further.

Table 26. Decreases in potential infiltration capacities under the prescribed SLR scenarios.

SLR Scenario (m)	Decrease from Base Scenario	Decrease from Previous Scenario
0.5	23%	-
1.0	45%	29%
1.5	64%	34%
2.0	80%	45%

The available area for infiltration was affected by not only the total pore space but the amount of moisture taking up the pore space. Figure 66 shows the near surface soil moisture results that were passed to the watershed-modeling group.

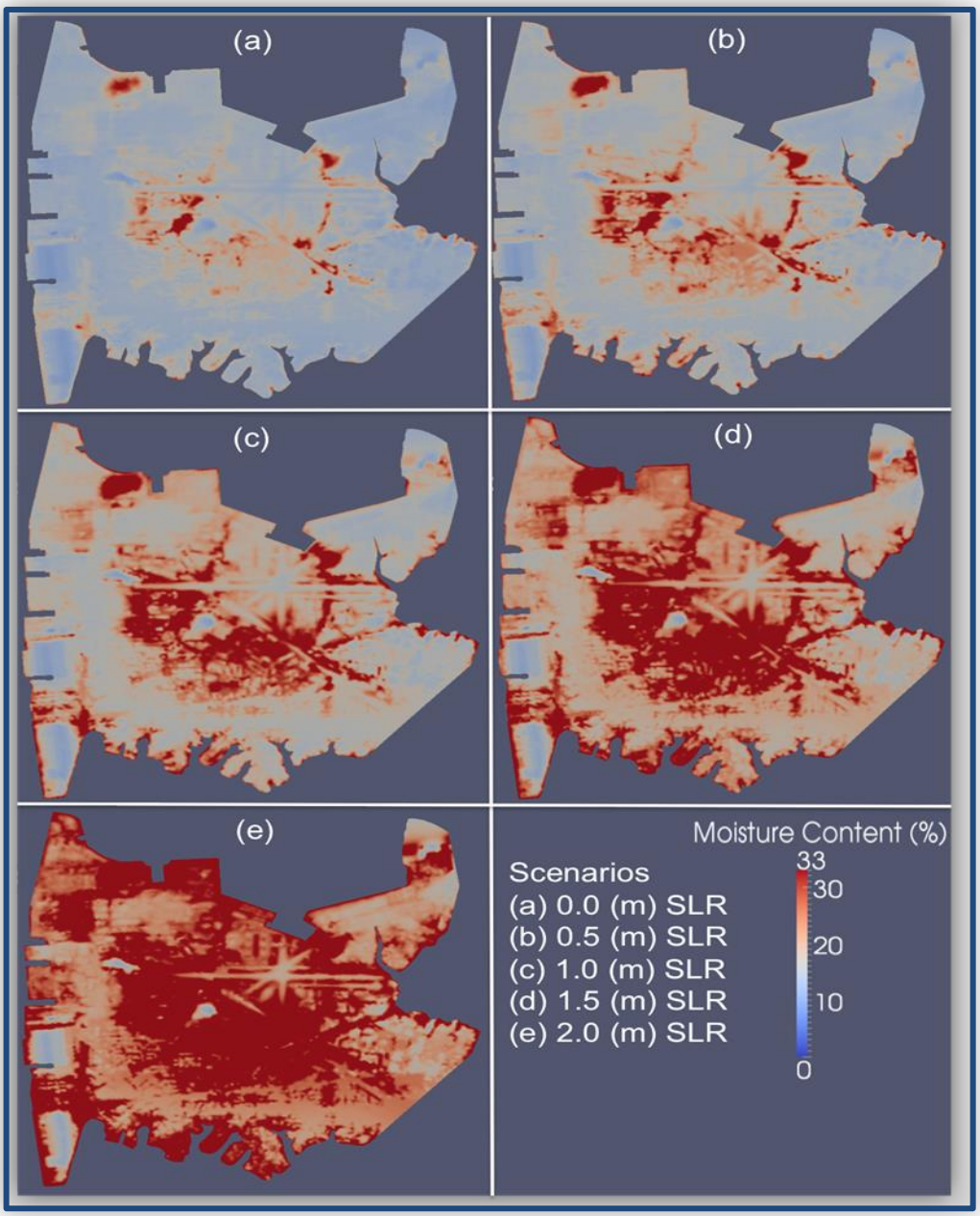

Figure 66. Moisture Content at the near surface for each prescribed SLR scenario: (a) 0.0 m, (b) 0.5 m, (c) 1.0 m, (d) 1.5 m, and (e) 2.0 m. Areas in green denote water levels calculated to be at or above the land surface.

The near surface was defined as the top of the Upper Columbia group since the top soil/fill layer was thin and the watershed model defines they soil properties of the top soil by a land usage map. The moisture content results from each model scenario served as inputs into the GSSHA re-assessment of flood routing discussed later in this section.

Salinity Intrusion: The saltwater intrusion results from each scenario generated similar results. There was little intrusion into the domain after the model reaches equilibrium as the aquifer flow

field pushed the saltwater towards the Chesapeake Bay surface bodies. For the purposes of this study, saltwater was defined as water having a salt concentration equal to the maximum of the Chesapeake Bay (26 ppt) and saline water as any concentration over the secondary drinking water standard of 250 milligrams per liter (mg/L) (0.25 ppt t or approximately one percent of saltwater). For the base condition (0.0 m SLR), the salinity wedge that formed extended approximately 300 m into the domain at the bottom and tapered to approximately 125 m near the top of the mesh, in most locations. Figure 67 shows the salinity concentration results for the 0.0 m SLR scenario.

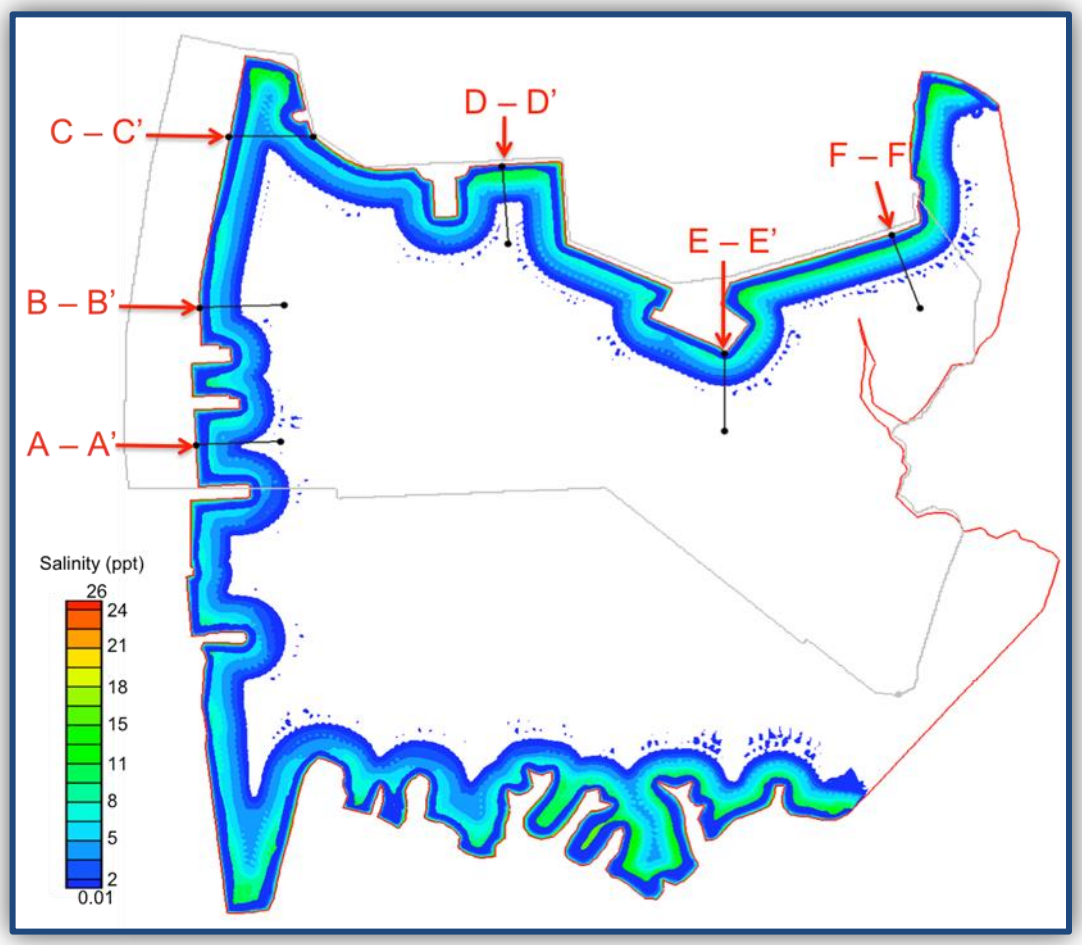

Figure 67. Plan view of concentration results from 0.0 m SLR scenario with model domains and cross section locations.

These findings agreed with the results of the geophysical survey, which found possible salinity intrusion at *Sites 2* and *3*. Figure 67 above also shows no salinity above 0.01 ppt in the center of the model domain. This could be a byproduct of the assumption that the Mason Creek (western) boundary was comprised entirely of fresh water. Any slight salinity seen in the middle of the domain by the geophysical report reflected elevated salinity levels in Mason Creek.

The only places within the domain under the 0.0 m SLR scenario where salinity extended more than the average were at locations that were surrounded by the Chesapeake Bay on multiple sides. For example, cross section C-C' transects from the Elizabeth River to Willoughby Bay across the northwest tip of the domain (Figure 67 above) exhibited a continuous strip of salinity (where the two wedges joined) (Figure 68).

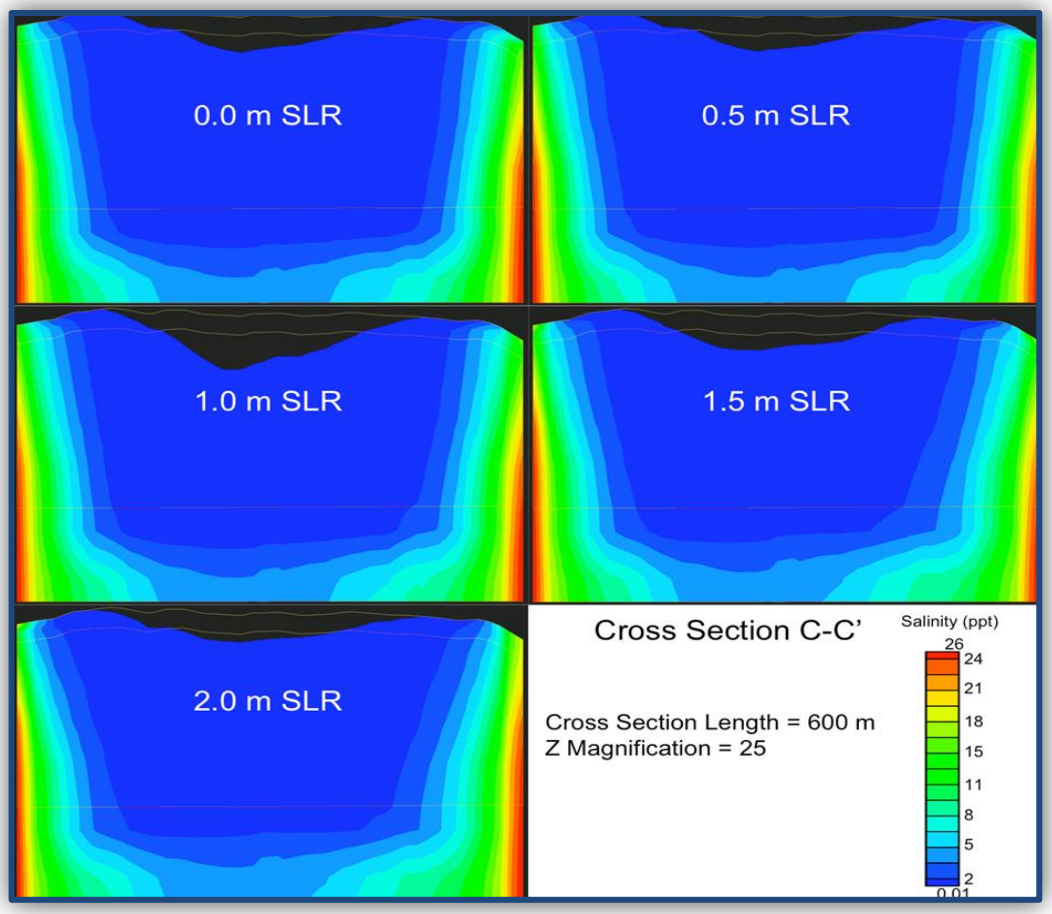

Figure 68. Cross Section C-C' for all five prescribed SLR scenarios.

The five prescribed SLR scenarios had a minimal effect on the salinity levels at the study site (refer to Figure 68 above). The rise in sea level did not increase the extent of the salinity intrusion, but did increase the salinity levels of the upper material layers. For each scenario, the highest concentrations remained near the boundaries, while the inland portions exhibited lower concentrations ranging from 0.01 to 5 ppt.

The largest changes in the overall salinity extents occurred where rising sea levels caused saltwater to inundate low-lying littoral areas (Figure 69).

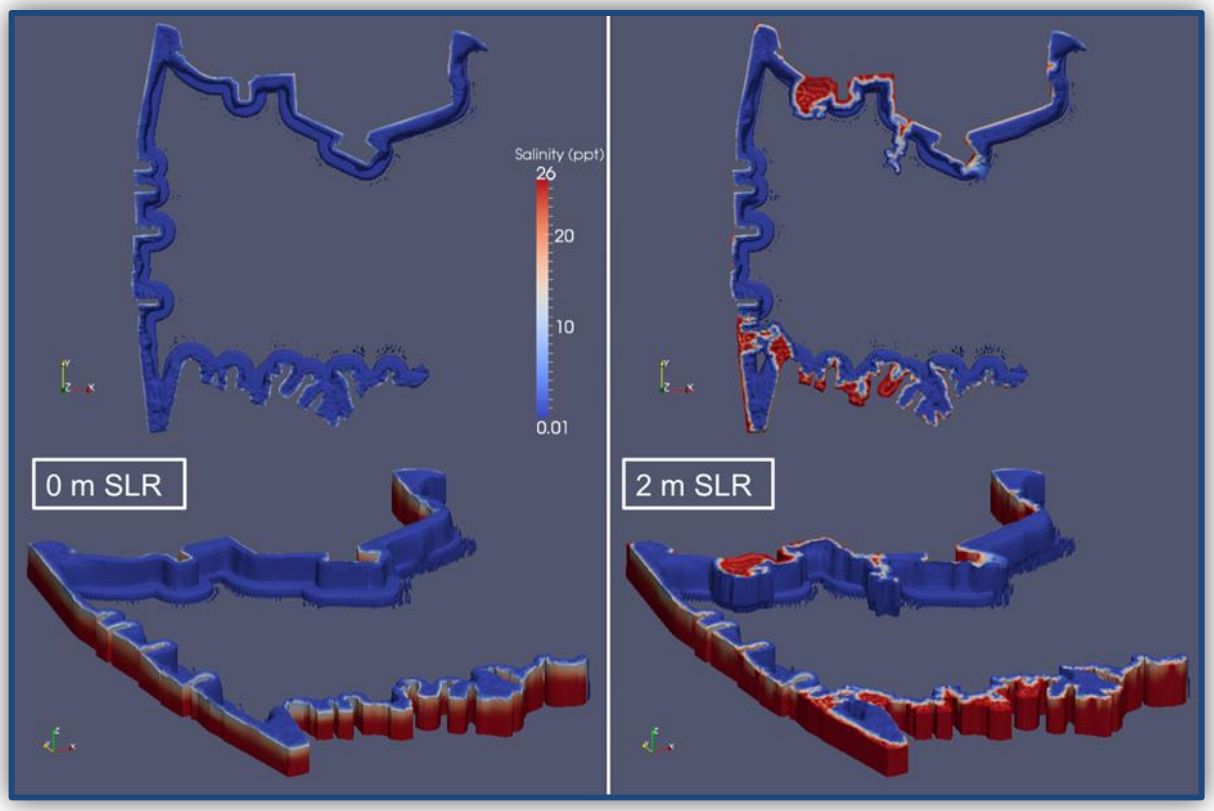

Figure 69. Comparison of salinity intrusion extents for the 0.0 m and 2.0 m SLR scenarios.

The additional specified head and concentration boundaries successively added by each SLR scenario generated increased flooding and increased saltwater flux into the domain. The salinity added to the system from the surface was transported more quickly through the upper material layers than the less permeable Lower Columbia, such that the salinity intrusion appeared to bulge from the side boundaries.

The groundwater modeling indicated that there was mounding of the water table near the center of the domain. Although this mounding decreased under successive SLR scenarios, SLR caused additional low-lying areas to become completely saturated, which resulted in less infiltration capacity. The saltwater did not intrude very far into the domain and therefore, did not cause a significant additional rise in the water table. It was important to note that the Mason Creek boundary condition assumption was conservative toward a minimum salinity intrusion modeling result.

3.10.2.3 Additional Data Requirements

The detailed topographic, land use, and soil data used as input for the GSSHA model was the same as that described in *Section 3.6*. Since the analysis utilized the same surge and precipitation events as the initial assessment, the forcing data were unchanged from those described in *Section 3.6*. For GSSHA to simulate subsurface groundwater flow, the following additional data were required:

1) aquifer bottom elevation,
2) water table elevation,
3) aquifer porosity, and
4) aquifer hydraulic conductivity data.

An additional benefit of simulating groundwater flow in GSSHA was the ability to specify spatially varied soil moisture profiles. These data sets are discussed in detail in the following sections.

3.10.2.3.1 Aquifer Data

Aquifer bottom elevation, water table elevation, aquifer porosity, and aquifer hydraulic conductivity data were specified spatially, grid cell-by-grid cell, on the 10-m^2 GSSHA grid which was coincident with the project's risk assessment grid. Water table elevation, aquifer porosity and aquifer hydraulic conductivity values were interpolated from the AdH-WASH model mesh to the cells of the GSSHA grid. The aquifer bottom elevation over the entire domain was specified as a constant 20 m below MSL. Over the relatively short timeframes of the simulated storms, lateral groundwater motion was negligible in this aquifer given the low hydraulic gradients and hydraulic conductivities. Therefore, the GSSHA groundwater simulation only needed to compute the varying groundwater head across the domain of the study area. GSSHA groundwater heads in these simulations were influenced by each cell's initial starting head, which was specified as an input value from the AdH-WASH simulation, and the amount of water that reached the water table through vertical infiltration in that cell. Variations in the aquifer bottom elevation were irrelevant to these calculations in short-term storm simulations such as those where lateral groundwater movement was essentially non-existent.

3.10.2.3.2 Soil Moisture Data

In the initial GSSHA simulations presented in *Section 3.6*, infiltration was simulated and represented as a loss of water to the surface water system. Soil moisture, an important parameter for determining infiltration rates, was assigned as a constant across the installation since no groundwater effects were simulated, but there was no means to compute varying soil moisture values. The AdH-WASH simulations, however, computed soil moisture across the domain of the model and these were used to parameterize the GSSHA grid with initial soil moisture estimates in a spatially varying fashion, providing a more accurate computation of infiltration rates across the study area.

4. Results and Discussion

4.1. Geomorphic and Geologic Assessment

Two key outputs were derived from these efforts: 1) shoreline classification shapefiles, and 2) estimates of subsidence rates for use in follow-on physical and ecological modeling efforts within the framework. Below we describe these results in greater detail.

4.1.1 Shoreline Classifications

This final classification of the region's shorelines included five categories:

1) ***Harbor structural hardening or commercial seawall*.** This category included hardened, permanent, massive structures such as seawalls at Newport News, Norfolk, and Portsmouth. Many of these areas also include other major structures such as piers (Figure 70) and wharfs, which may be open or may function as both dock facility and seawall. This infrastructure could be damaged by SLR or its functionality could be impaired, but because of extensive paving and other alterations, no geological changes are expected to occur.

Figure 70. Pier 11 at NSN - an example of a shore-perpendicular structure in a heavily- altered coastal terrain with shore armoring, seawalls, and pavement (photo taken 23 August 2010).

2) ***Armored shore.*** This category included shorelines protected with stone riprap, seawalls, bulkheads, concrete rubble, or closely-spaced detached or T-shaped breakwaters. The main geological issue in these areas was little sediment interchange occurred between water and land. The shoreline was assumed to be fixed except under unusually extreme events like hurricanes. Two main classes of armoring were observed. In the cities, low shores along rivers, creeks, and bays have been extensively bulk-headed to protect private or public property and to define property limits [Figure 71 (a)]. The second class consisted of stone revetments or concrete rubble placed along the base of banks and bluffs to prevent bluff erosion [Figure 71 (b) and (c)]. Along these armored shores, limited geological changes were likely to occur for years unless a greater frequency of hurricanes and nor'easter affects the area.

(a)

(b)

(c)

Figure 71. (a) Example of bulkheads along creek draining into Lafayette River, Norfolk. Tide was unusually high and yards were only about 0.3 m above the water surface. (b) Revetment installed by property developer along north shore of James River at Wareham's Pond Road, near Williamsburg, VA. (c) Professionally-installed bluff armoring, north shore of James River near Newport News. Photographs 24-25 August 2010.

3) ***Wetland.*** These areas would be most vulnerable to drowning and conversion to open water as sea level rises. Originally, the Hampton Roads area featured extensive marsh and wetlands (Figure 72). In low-lying terrain near the Atlantic and in and around Norfolk, Portsmouth, and Newport News, most creeks and inlets were at one time filled with marsh. However, as private property was developed, many homeowners built bulkheads to define the limits of their property and prevent marsh encroachment onto their land. In the James estuary, wetlands border higher clay and sand banks, particularly along shores of small creeks and rivers. For this classification, if a river or bay was largely filled with wetland, it was classified as wetland, but if shoreline was fringed by only a few meters width of wetland, it was classified as an alternative category (i.e., armored or bank/bluff).

Figure 72. Creek at James River Country Club, Newport News, VA. Photograph 24 August 2010. Areas like this were classified as wetland.

4) ***Banks and bluffs.*** Much of the topography along the James and York Rivers consisted of sand and clay banks or bluffs, sometimes exceeding 10 m in height (Figure 71(b) and (c) above, and Figure 73). The flat-lying country along the rivers and creeks was underlain by Pleistocene sediments deposited by ancient rivers during higher stands of sea level. In some areas, banks were fringed with narrow sand beaches or marshes, but the classification was based on banks being the dominant geomorphic form. Banks/bluffs could experience erosion when subject to rising sea level, but the retreat rate would be in the range of centimeters (cm) per year, much less than wetland retreat. Bluffs were popular for residential development because of sightlines, and as a result, many

kilometers along the James River were armored with stone revetment. These sections of shoreline were classified as armored with the assumption that limited changes would occur with SLR.

Figure 73. High bluffs (greater than 10 m) along south side of James River at Holly Point Way, near Rushmere, VA. Vegetation in foreground is kudzu. The bluffs experienced severe erosion during Hurricane Isabel. Photograph 26 August 2010.

5) ***Sand beaches*.** These were concentrated east of the mouth of the James River, facing Chesapeake Bay and the Atlantic Ocean. Some minor stretches of sand beach were also found in the lower James River. Along Willoughby Spit, north of NSN, beaches were artificially nourished and partly protected with detached breakwaters (Figure 74). Because of the spit's value for recreation and flood damage protection and the presence of private property, the spit probably would be re-nourished in the future. A lifeguard informed this author that the city brought in sand by truck following severe erosion caused by the November 2009 Mid-Atlantic northeaster (NOAA 2010).

Figure 74. Willoughby Beach from Sarah Constant Beach Park, view to northwest. The beach was renourished with sand delivered by truck after damage caused by the November 2009 nor'easter. Photograph 23 August 2010.

One of the main findings of the classification analysis and site visits was that a much of the shoreline along the James River was armored (Figure 75). This was a highly developed coast with valuable commercial, military, and private property, and most of the shore is challenged to be considered "natural" any longer.

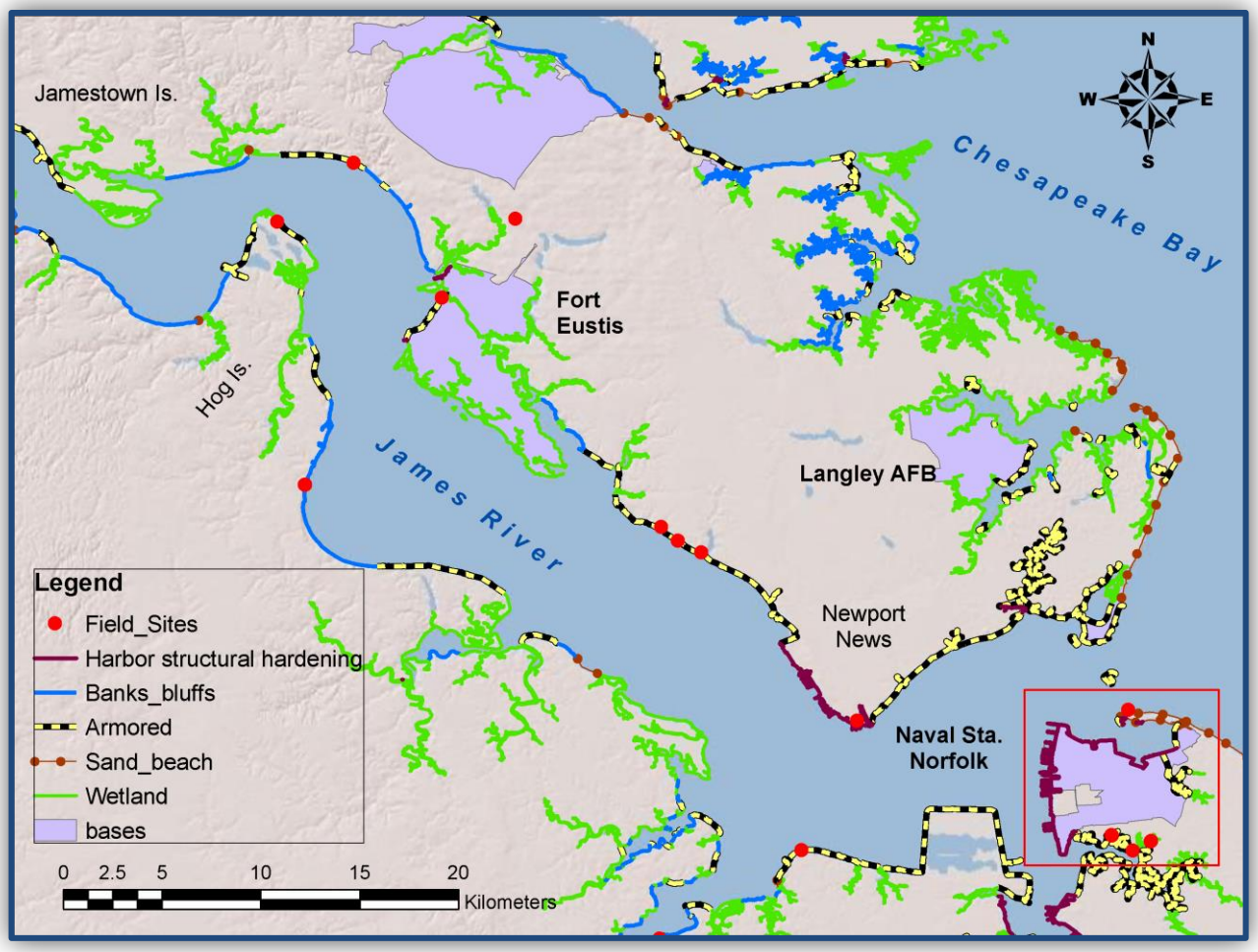

Figure 75. Armored and natural shoreline along the lower James estuary.

Most of the bluffs along the river were now occupied by private residences, institutions, and commercial entities. Erosion must have been a serious concern over the previous decades because most bluffs were lined with stone revetment or bulkheads of timber or steel sheet pile [Figure 71 (a) and (b)]. What would be the response if more storms coupled with SLR produced accelerated erosion along the remaining unprotected sections of bluff or along areas with deficient protection? In some communities, wealthy residents could opt for engineered shore protection. We observed this response along the western shore of the Nansemond River, which was battered by the November 2009 nor'easter. Near Cedar Point Country Club, residents had contracted engineering firms to import soil and line the bluffs with geocloth and three layers of stone (Figure 76). In contrast, near the town of Rushmere, a resident stated that professional shore protection was beyond her means and the house, built in 1929, was vulnerable if more storms like Hurricane Isabel (September 2003) or the November 2009 nor'easter were to strike the area in the future. She stated that she and other long-term residents had seen more erosion since Isabel than in many decades before. Isabel was the costliest tropical cyclone in Virginia history, with a storm surge of 2.7 m at Richmond [USACE and Federal Emergency Management Agency (FEMA) 2005].

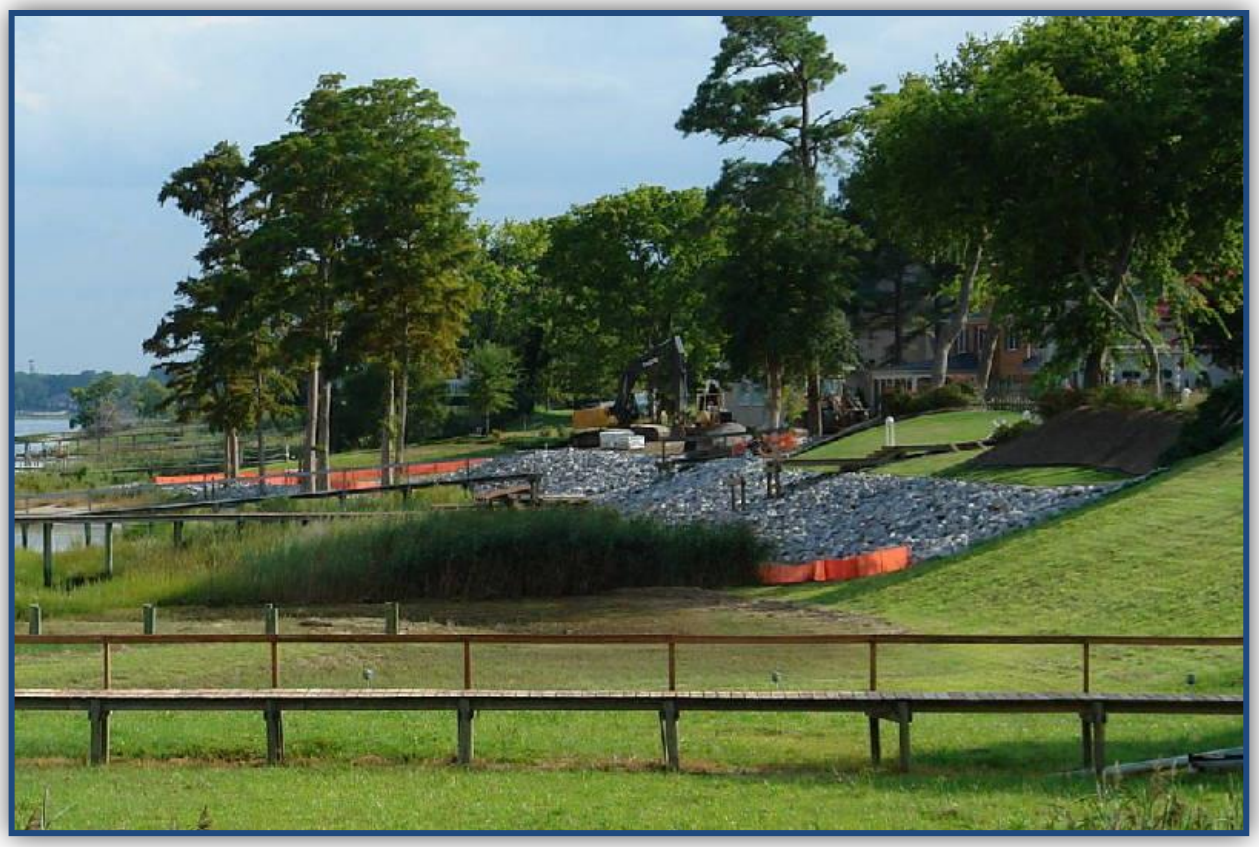

Figure 76. Bluff protection being installed along the shore of the Nansemond River near Cedar Point Country Club. This area was battered by the November 2009 nor'easter. Photograph 25 August 2010.

A few areas along the James estuary were still natural and could partially convert to open water, depending on SLR and regional subsidence. In the lower estuary, East Island, Hog Island (beyond the Surrey Nuclear Power Station), Fort Eustis (Mulberry Island), and Jamestown Island had low elevations and were unarmored. In the urban areas of Newport News, Norfolk, and Portsmouth, much of the shoreline was either armored or consisted of industrial wharves and dock. Despite the vulnerability of the remaining marshy areas, over time, the percentage of open water along the James and Elizabeth Rivers was not likely to substantially change under most SLR scenarios.

The rivers and creeks near the cities were almost totally armored because residents have built bulkheads to mark the boundaries of their properties (Figure 77). Residents in Norfolk currently experience flooding during unusually high tides or storms. How would this terrain change over decades as sea level rises? Two scenarios were thought possible. The first was resisting change via construction. When faced with rising sea level and increasing frequency of flooding in their yards, we hypothesized some owners would attempt to protect their property by raising their bulkheads and bringing in fill. This would be feasible if undertaken gradually, over years. Under this scenario, the fringing wetlands in the region would slowly disappear as they were squeezed out. Depending on storm severity, the fringing wetlands would be damaged rapidly in discrete events. The second scenario we hypothesized included the acceptance of some inundation. If

relative sea levels were to rise quickly, coupled with more intense storms at more frequent intervals, homeowners would be overwhelmed and would not be able to bring in sediment rapidly enough to prevent flooding of portions of their lands. In this case, wetlands would be able to migrate landward in some areas, especially in some of the inner creeks which had not been fully bulk-headed.

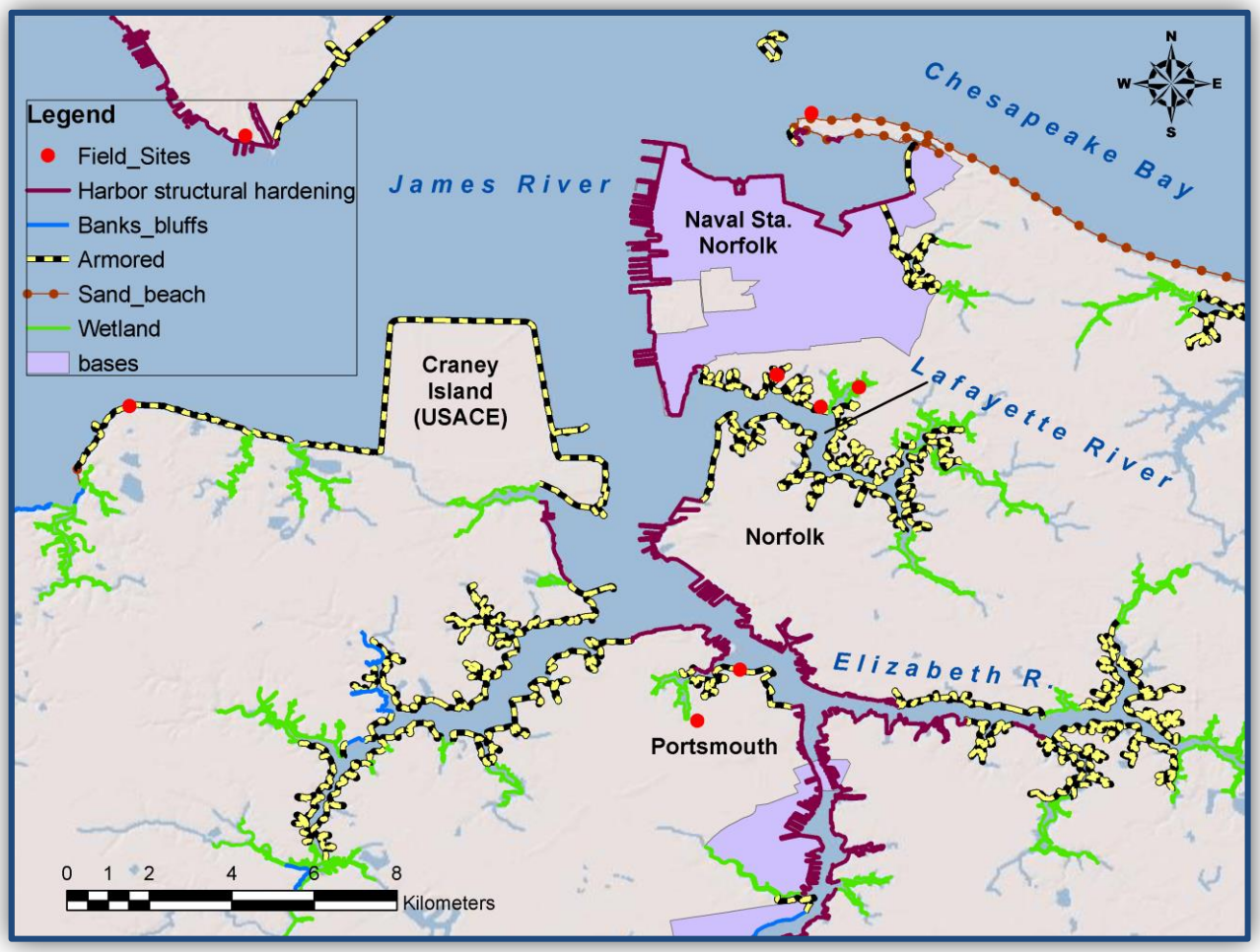

Figure 77. Shoreline classification in Norfolk and Portsmouth. Craney Island was developed as a USACE dredge material disposal site and designed with 13 m [42 feet (ft)] dikes along its shoreline. Much of the shoreline was armored or consisted of docks and industrial waterfront.

The fate of Willoughby spit that protected the north shore of the NSN from Chesapeake Bay wave action was hard to predict. The spit was nourished and partially protected with detached breakwaters. For valuable beach-front property in the United States, the trend during most of the 20th century was to initiate engineering projects to protect beaches. Despite occasional debates revolving around strategic retreat from vulnerable areas, all evidence suggested that most towns or municipalities will continue to protect beaches. However, land subsidence in the Norfolk area may make future shore protection very costly (Koch 2010).

4.1.2 Local Subsidence Rates

Although the SERDP SISON mandate was to assume SLR regardless of causality (i.e., ocean expansion, subsidence, glacial melt, etc), one of the follow-on ecological models in particular (refer to *Section 3.3*), could be calibrated to accept rates of accretion or subsidence. Thus, a limited initiative was undertaken to review subsidence in the Hampton Roads area and proffer inputs to parameterize the model. Luckily, Boon et al. (2010) discussed the phenomena in depth (including causality – isostatic rebound, groundwater withdrawals, and effects of large comet/meteor impact, i.e., the Chesapeake Bay Impact Crater), and offered rates of -1.11 to -4.00 mm/yr for 10 of NOAA's National Water Level Observation Network (NWLON) stations located around the Chesapeake Bay (Table 27 and Figure 78).

Table 27. Chesapeake Bay subsidence rate estimates taken from Boon et al. (2010).

Station	Code	RSLR (1976-2007[1])	Subsidence[2] (mm/yr)	Relative Change[3] (%)
Baltimore, MD	BALT	3.09 ± 0.55	-1.29	42%
Annapolis, MD	ANNA	3.68 ± 0.58	-1.88	51%
Washington, DC	WASH	2.91 ± 0.82	-1.11	38%
Cambridge, MD	CAMB	3.44 ± 0.49	-1.64	48%
Solomons Island, MD	SOLI	3.61 ± 0.54	-1.81	50%
Lewisetta, VA	LEWI	5.15 ± 0.55	-3.35	65%
Gloucester Point, VA	GLPT	4.30 ± 0.62	-2.50	58%
Kiptopeke, VA	KIPT	3.51 ± 0.58	-1.71	49%
Chesapeake Bay Bridge Tunnel	CBBT	5.80 ± 0.62	-4.00	69%
Sewells Point, VA	SWPT	4.52 ± 0.66	-2.72	60%

[1] uncertainty expressed by 95% confidence interval about RSLR

[2] subsidence = GSLR – RSLR ≈ 1.8 mm/yr – RSLR

[3] average subsidence was 53 % of average RSLR 1976-2007

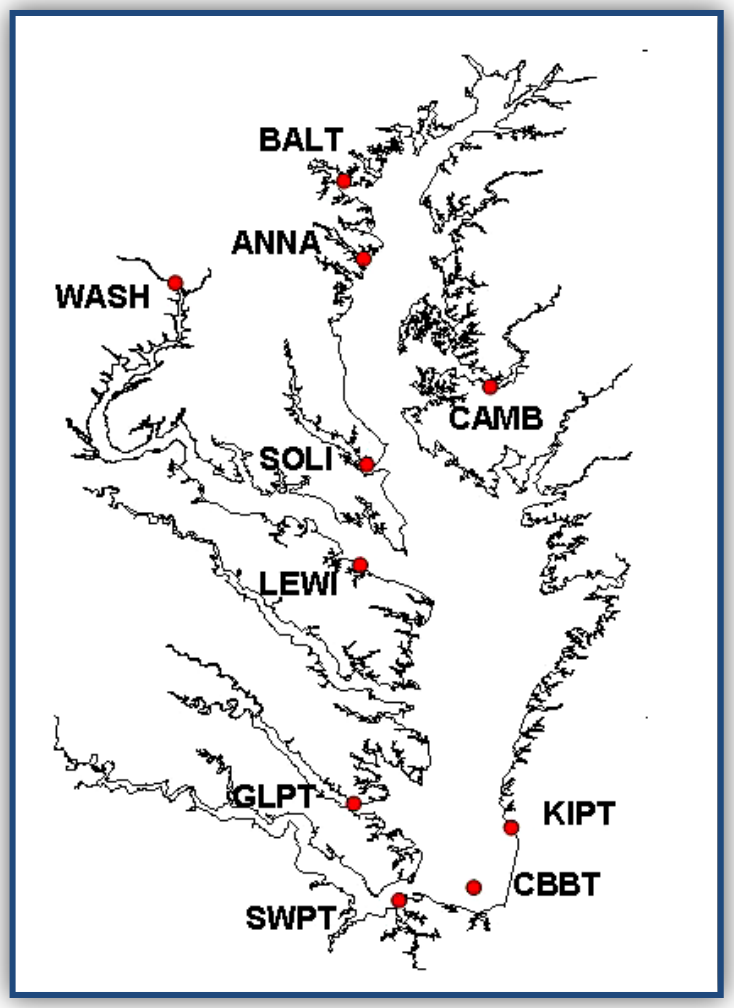

Figure 78. Tide stations used in analysis by Boon et al. (2010, Figure 3 on page 6). SWPT = Sewells Point, closest station to NSN.

These numbers, along with the assessment of shoreline stability and protection were carried forward into the analysis of ecological response to SLR conducted in the next step of the study's analytical framework.

4.2. Ecology and Land Use Conversion Assessment

4.2.1 Outputs and Technical Results

SLAMM results have been organized and tabulated below based on scenario, SLR, and SLAMM output scheme. For each of the 90 model executions, land cover was exported out of the system at 25-year intervals (i.e., 2000, 2025, 2050, 2075, and 2100). The quantity of output data precludes its complete presentation in this report. However, it was constructive to examine representative outputs. Figure 79 presents coastal evolution of the NSN site through time for 2.0 m SLR. Furthermore, for clarity of presentation in this report, *Site 2* and *Site 3* were presented as a combined quantity (*Sites 2* and *3*). Table 28 presents SLAMM output for each scenario and

each site for 2.0 m SLR. Note that *Site 2* and *3* comprises an area nearly five times larger than *Site 1*.

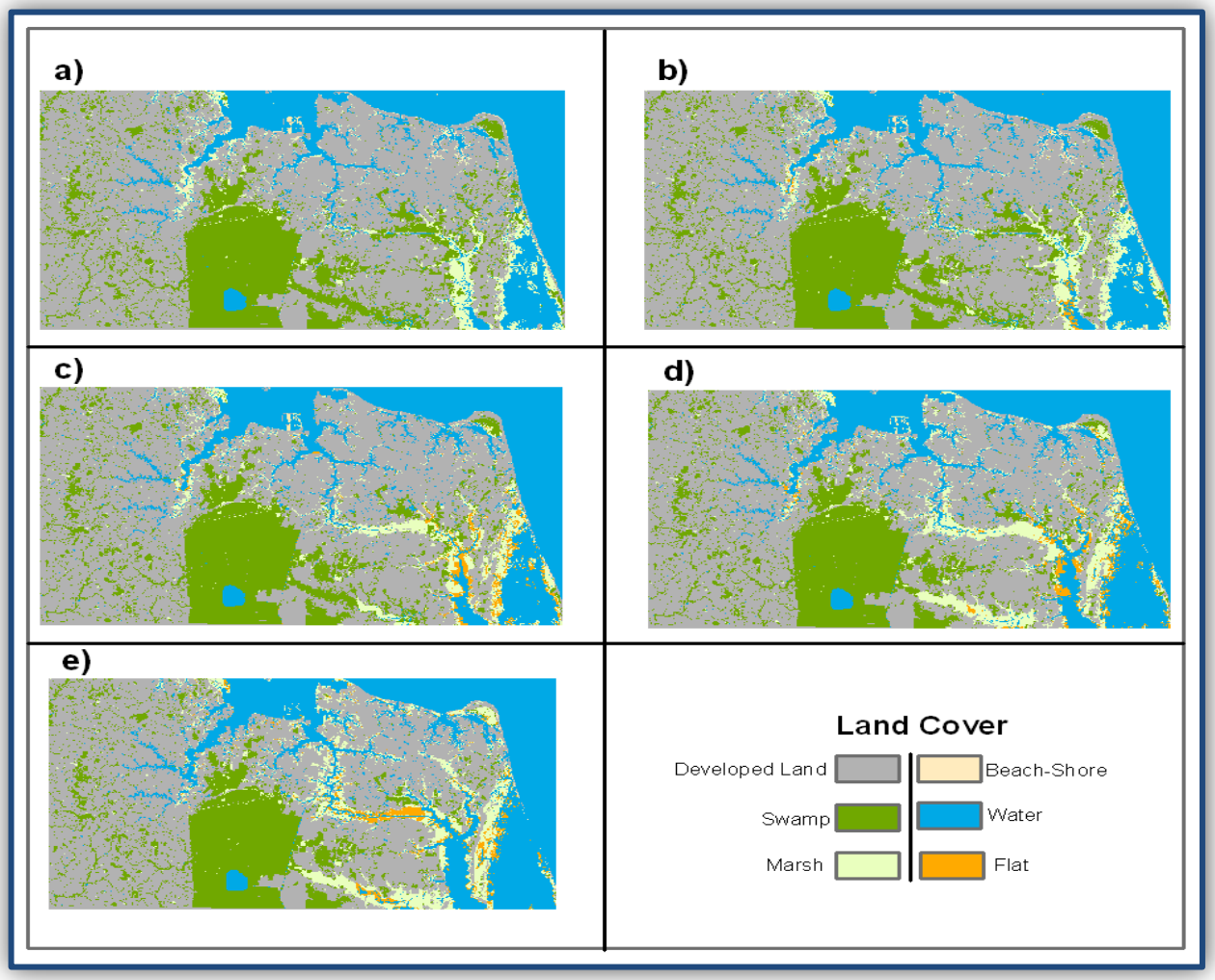

Figure 79. Coastal evolution for the site (Site 1) for the S1 analysis under the prescribed 2.0 m SLR scenario in (a) year-2000, (b) year-2025, (c) year-2050, (d) year-2075, and (e) year-2100.

Table 28. LULC predictions for the year 2100 under seven sensitivity scenarios S1 – S7 assuming the prescribed 2.0 m SLR scenario.

A) Site 1

Habitat Types	Initial	S1	S2	S4	S5	S6	S7
Dry Land	216,676	190,924	216,676	190,579	190,924	190,924	190,924
Swamp	80,256	63,012	63,009	63,009	63,012	63,012	63,012
Marsh	12,030	29,687	10,615	29,754	29,687	29,590	29,796
Beach-Shore	2,386	310	115	311	310	309	310
Flat	0	7,609	4,639	7,621	7,609	7,420	7,757
Water	75,029	94,836	91,323	95,102	94,836	95,122	94,577
Total (ha)	**386,376**	**386,376**	**386,376**	**386,376**	**386,376**	**386,376**	**386,376**

B) Sites 2 and 3

Habitat Types	Initial	S1	S2	S4	S5	S6	S7
Dry Land	692,164	647,392	692,164	647,056	647,392	647,392	647,392
Swamp	54,742	40,965	40,773	40,773	40,965	40,963	40,968
Marsh	94,924	78,241	52,536	78,246	78,241	76,618	79,864
Beach-Shore	41,537	769	238	774	769	768	771
Flat	1,661	31,993	25,345	32,106	31,993	31,490	32,847
Water	975,182	1,060,849	1,049,153	1,061,253	1,060,849	1,062,978	1,058,368
Total (ha)	**1,860,209**	**1,860,209**	**1,860,209**	**1,860,209**	**1,860,209**	**1,860,209**	**1,860,209**

The percent difference in area between scenario outputs in 2100 and 2000 (the initial condition) was herein applied as a consistent metric to compare between scenarios and sites. Figure 80 presents this metric for all scenarios at 2.0 m SLR. The minimal presence of tidal flats in the region induced a large relative difference (i.e., often greater than 1,000 percent) and these results were excluded from the figure. SLAMM was also found to be extremely sensitive to local conditions (e.g., habitat distribution and extent). For instance, marsh areas increased at the highly developed site (*Site 1*) whereas marsh decreased at the less developed James and Delmarva sites (*Sites 2* and *3*). This was likely due to the large initial extent of marsh at *Sites 2* and *3*. While regionally marsh extent was likely to decrease, there could be isolated regions of expansion. Also note that for all sites, water and flat area increased, while dry land, swamp, and beach/shore decreased.

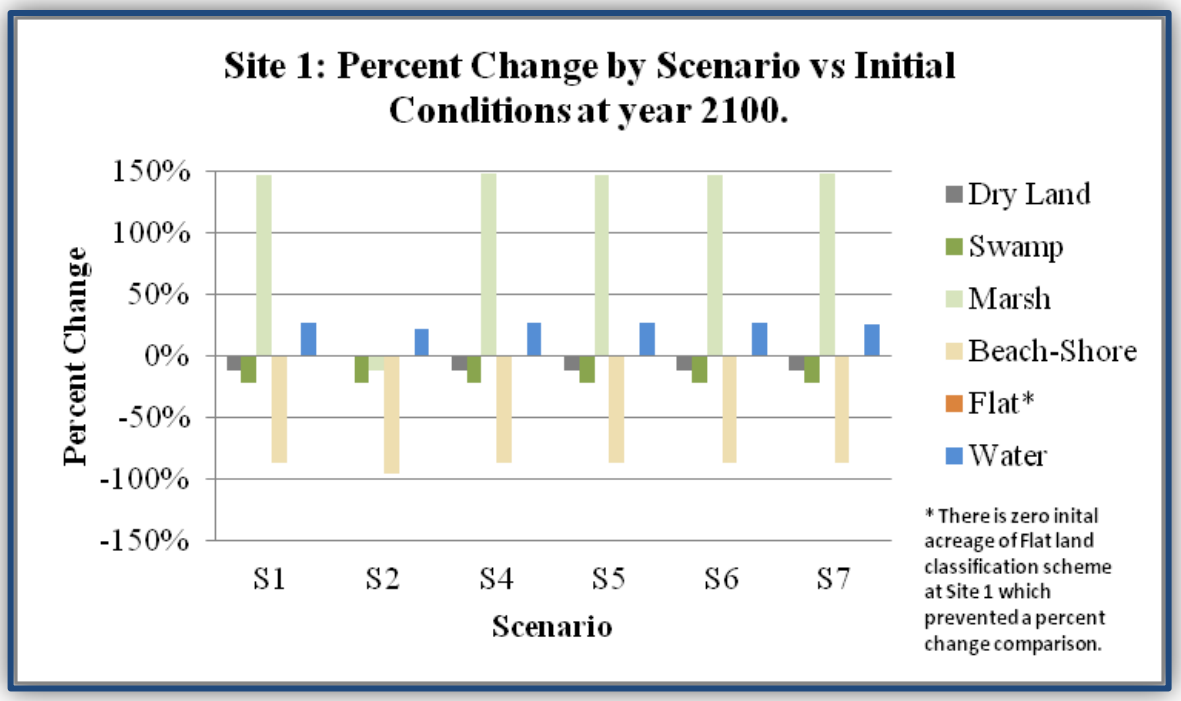

(a)

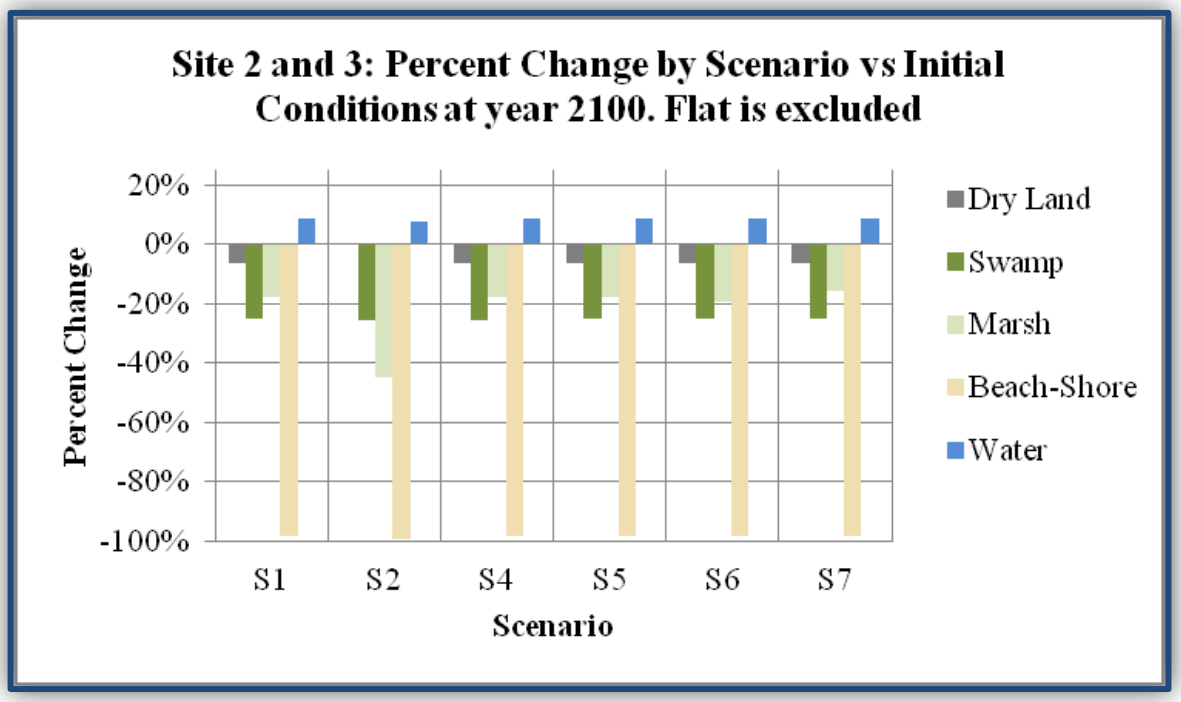

(b)

Figure 80. Percent change in area from initial conditions for 2.0 m SLR. (a) Site 1 and (b) Site 2.

Scenario output results were also compared to the baseline scenario (*S1*) to examine the relative model sensitivity. The changes were measured as the percent change of a given scenario relative to *S1*. Figure 81 present these results for the 2.0 m SLR scenario.

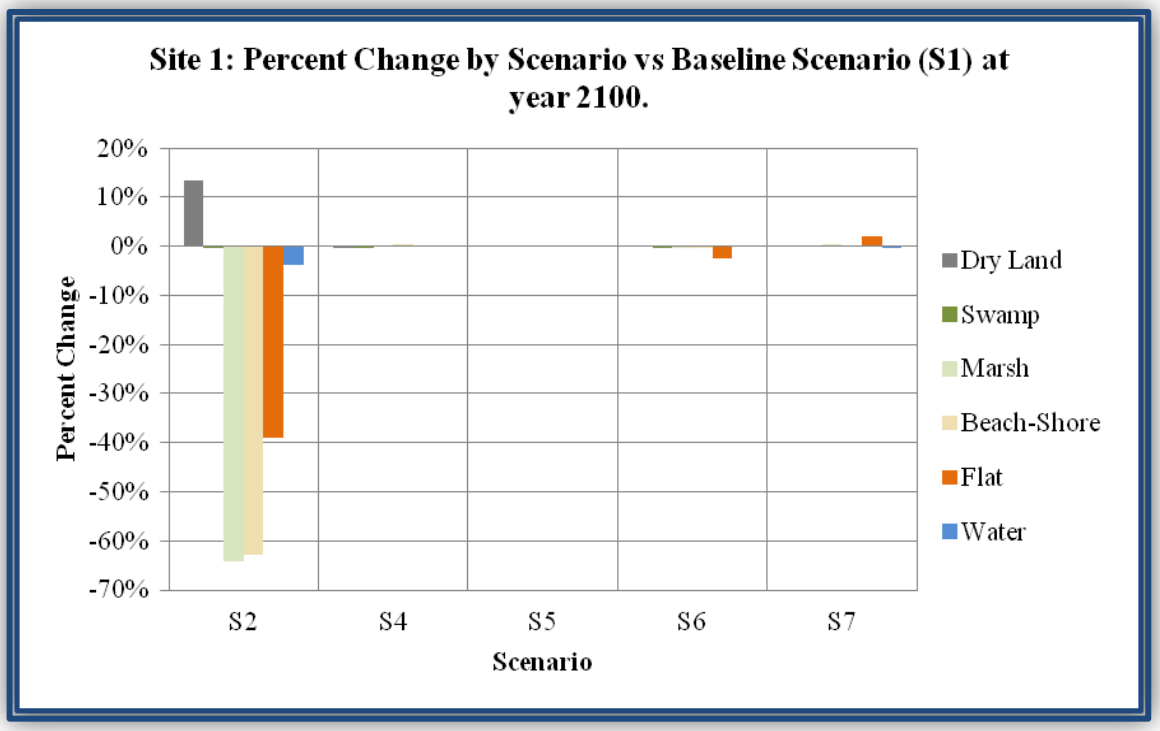

(a)

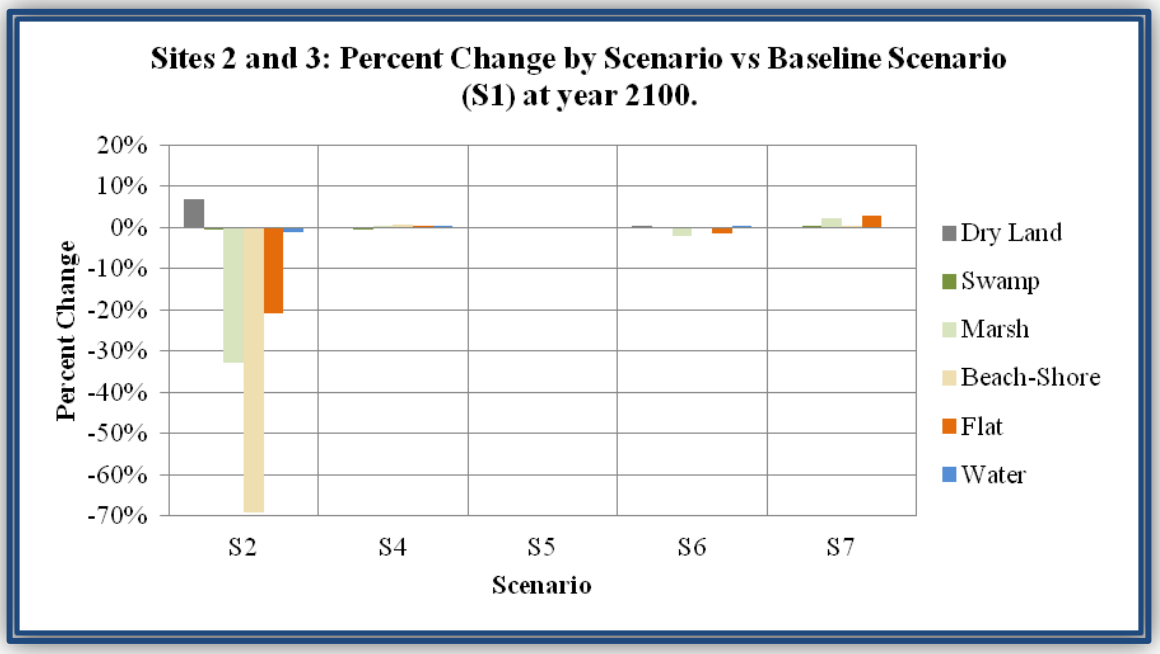

(b)

Figure 81. Model sensitivity to input scenarios. The figures present the change in SLAMM output for a given scenario relative to the baseline scenario (S1): (a) Site 1 and (b) Sites 2 and 3.

In comparison to other scenarios, *S2* showed significant changes relative to *S1*. *S2* assumed that all dry lands were protected. *S4* assumed the opposite condition - where no dry lands were

protected. Thus, we can conclude that the existing protection strategy (*S1*) was similar to the minimalistic protection strategy (*S4*). *Scenarios 5-7* addressed model sensitivity to input parameters (i.e., storm frequency, accretion, and erosion), and although we used extreme changes in these parameters, the model was somewhat insensitive (i.e., all changes were less than 5 percent). Accretion and erosion rates showed marginal sensitivity as shown by *S6* and *S7*. However, *S5* indicated no discernible sensitivity to the storm frequency parameters for either site location.

The model results were also used to address changes in the site associated with multiple values of SLR. The range in percent change for all land classification schemes, versus the initial condition, across all scenarios, was calculated and analyzed to determine SLAMM's sensitivity to SLR, as shown in Figure 82.

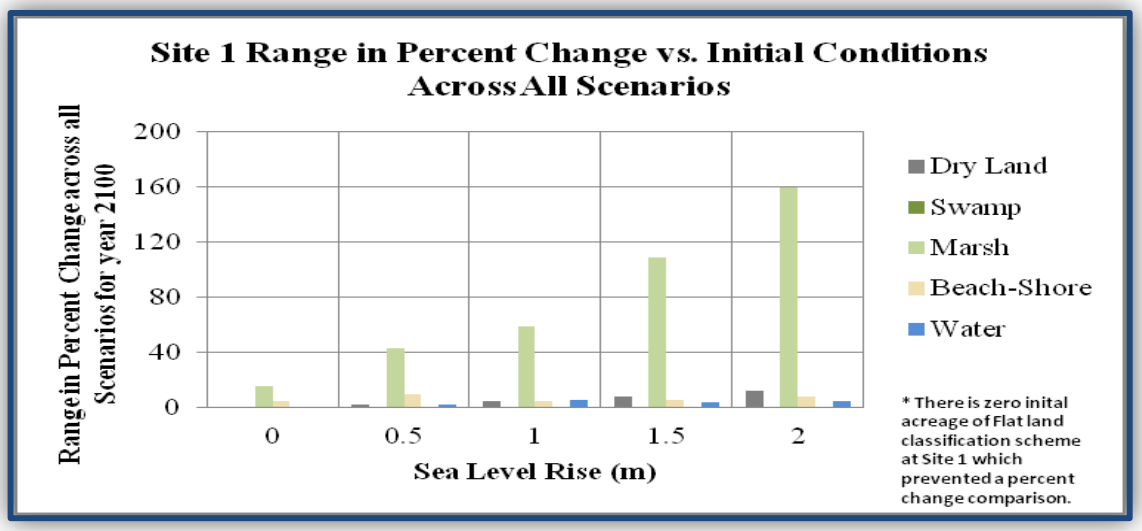

(a)

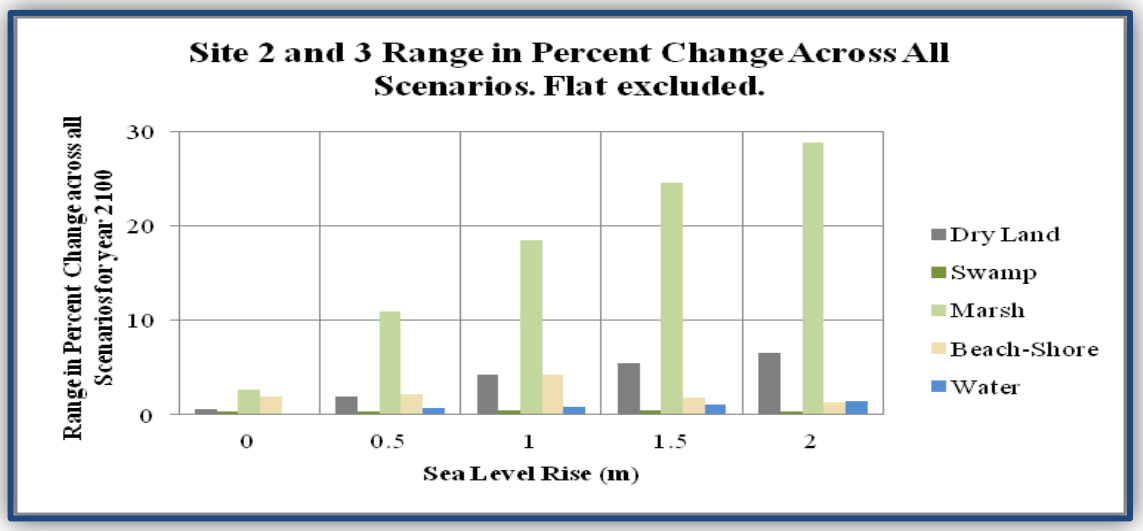

(b)

Figure 82. Changes in land area with SLR relative to the initial condition for: (a) Site 1 and (b) Sites 2 and 3. Note that for both sites, changes in marsh area were excluded because they were very large due to low initial coverage (i.e., greater than 100 percent).

4.2.2 Summary and Discussion

The objective of this effort was to forecast the evolution of coastal ecosystems under sea level rise as it pertained to land use and cover changes. As summarized in the results section above, coastal evolution processes in the study system are complex, but were generalized as: (1) reductions in dry lands, swamps, and beach/shore environments, (2) increases in open water and tidal flats, and (3) variable responses of marsh ecosystems. While some ecosystems were reduced, other systems gained. A potentially important (and somewhat counterintuitive) conclusion in the face of SLR was that a strategic retreat from the coast would provide room for

ecosystems to migrate inland, and SLR would, in fact, benefit coastal ecosystems that are currently constrained by developed lands.

The ecological consequences of these changes are likely significant due not only to direct loss of habitat (e.g., swamp), but also because of alteration of the relative distribution and spatial position of habitats. For instance, while only a minor component of the landscape (less than 0.1 percent of cover in 2000), tidal freshwater marshes play a disproportionately large role as breeding and foraging grounds for a variety of taxa such as colonial waterbirds and estuarine fishes and are a significant source of detritus for other coastal ecosystems. Future analyses should examine changes in the relative distribution and connectivity of habitat types in an effort to further articulate the ecological consequences of habitat switching and loss.

To assess these changes, we have applied SLAMM and conducted an analysis of the sensitivity of this model to six alternative input scenarios. This analysis indicated that SLAMM was highly sensitive to the protection strategy. Although this conclusion may seem obvious, this highlights the need for long term coastal planning in light of sea level rise. While SLAMM offers a strong heuristic tool to perform these simulations, the climate change projections under which it operates are oftentimes extremely uncertain, and regularly applied to highly sensitive management decisions - an extremely challenging environment in which to operate.

4.3. Regional Surge and Wave Assessment

4.3.1 Outputs and Technical Results

Prior to initiation of the storm surge and wave simulations, all storm wind fields were created by manual execution of the TC96 PBL wind model for each storm. These wind fields were used to drive coupled simulations of water levels and waves using ADCIRC and SWAN. Monitoring of each storm simulation was required to ascertain successful completion. Completion could be halted for several reasons but primarily were caused either by a High Performance Computing (HPC) system shut down or ADCIRC mesh instabilities. If the cause was HPC system related, the simulations was restarted at the point of halt using a “hot start” procedure. If the cause was mesh instability, the location was identified and the instability resolved by manual mesh edits. Each storm simulation produced numerous files of time series results, including surge water levels as well as wave heights and periods. Results were post processed to produce graphics of peak surge, wave height and wave period over the entire storm simulation. Time series files recorded model results over the entire ADCIRC mesh at one-hour time increments. Scripts were executed to extract pertinent surge and wave information for the study focus area surrounding NSN.

Once storm simulations were completed for each SLR scenario, analyses were performed using MATLAB scripts to compute SLR impacts to the 50- and 100-yr return interval storm surges and waves. Existing condition return periods were established from existing FEMA Digital Flood Insurance Rate Maps (DFIRMs) as well as analyses of storm simulations results at 0.0 m SLR. Return periods were computed at all ADCIRC nodes within the NSN study area. DFIRMs are created based on hundreds (or thousands) of storm simulations to statistically evaluate the 1 percent probability surges throughout a region. In this study, we selected storms that generated

approximately 1 percent surge levels at the site. Note that there were no DFIRM Base Flood Elevations (BFEs) available for NSN at the time of this study.

4.3.1.1 Wind Fields

The outputs from the TC96 PBL model were wind fields for the selected hurricanes listed in Table 9 above. Figure 83 shows an example plot of maximum 1-min average wind speeds for storm 449 along its entire track.

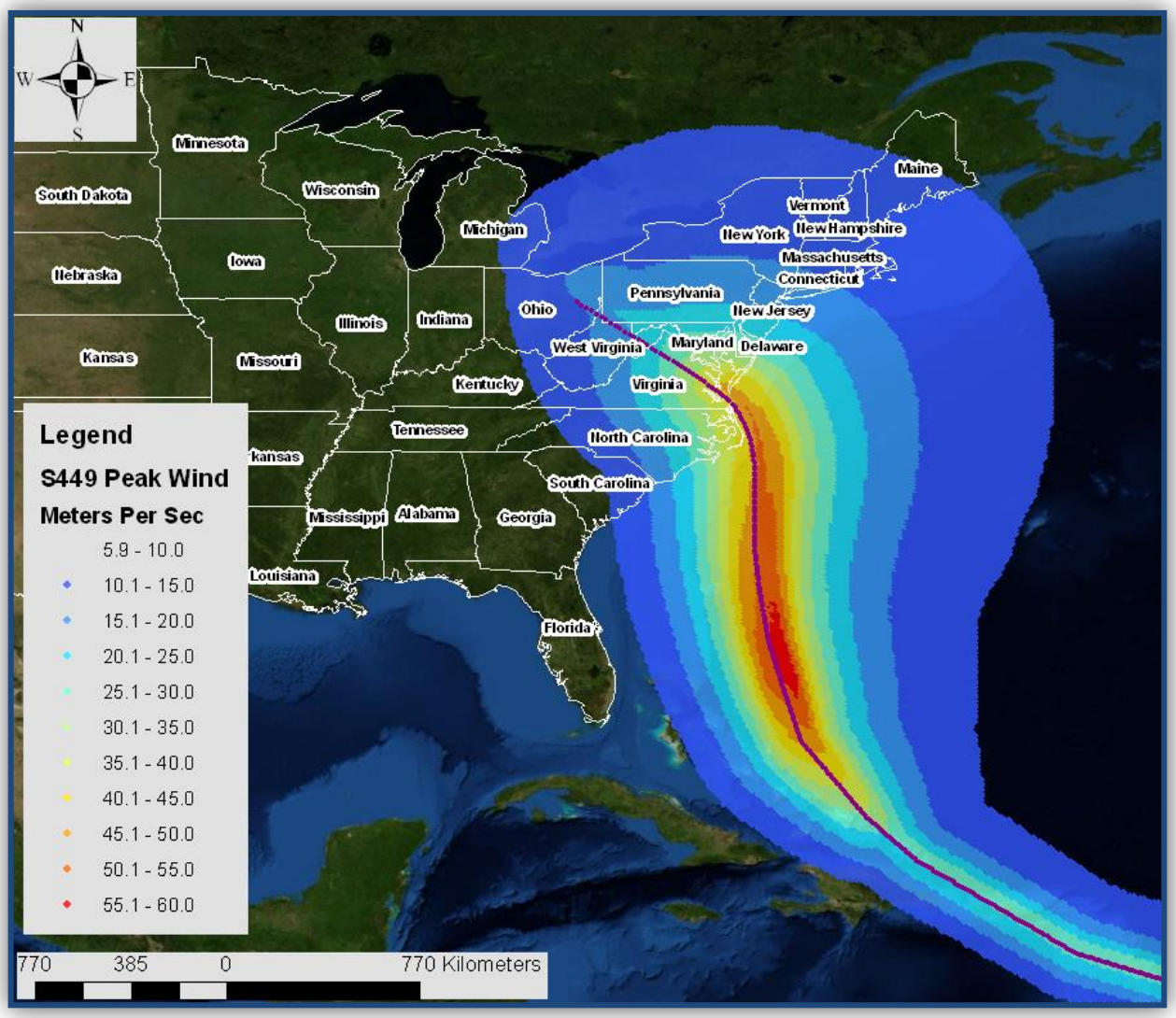

Figure 83. Maximum wind speed in m/s for Hurricane 449 (i.e., the 100-yr return interval storm assessed in the project).

This is not a snapshot of the wind speed but the envelope of the maximum wind speeds throughout the duration of the storm. Note that the maximum winds speeds occurred on the right-hand side of the track. In this storm, winds exceeded 60 m/s [approximately 130 miles per hour

(mph)] - the equivalent of a Category 4 storm on the Saffir-Simpson scale. Storm 449 produced approximately 100-yr return interval storm water levels at the NSN and will be used in the following sections to illustrate model results. Figure 84 shows a plot of the maximum 1-min average wind speeds for Storm 293 along its track.

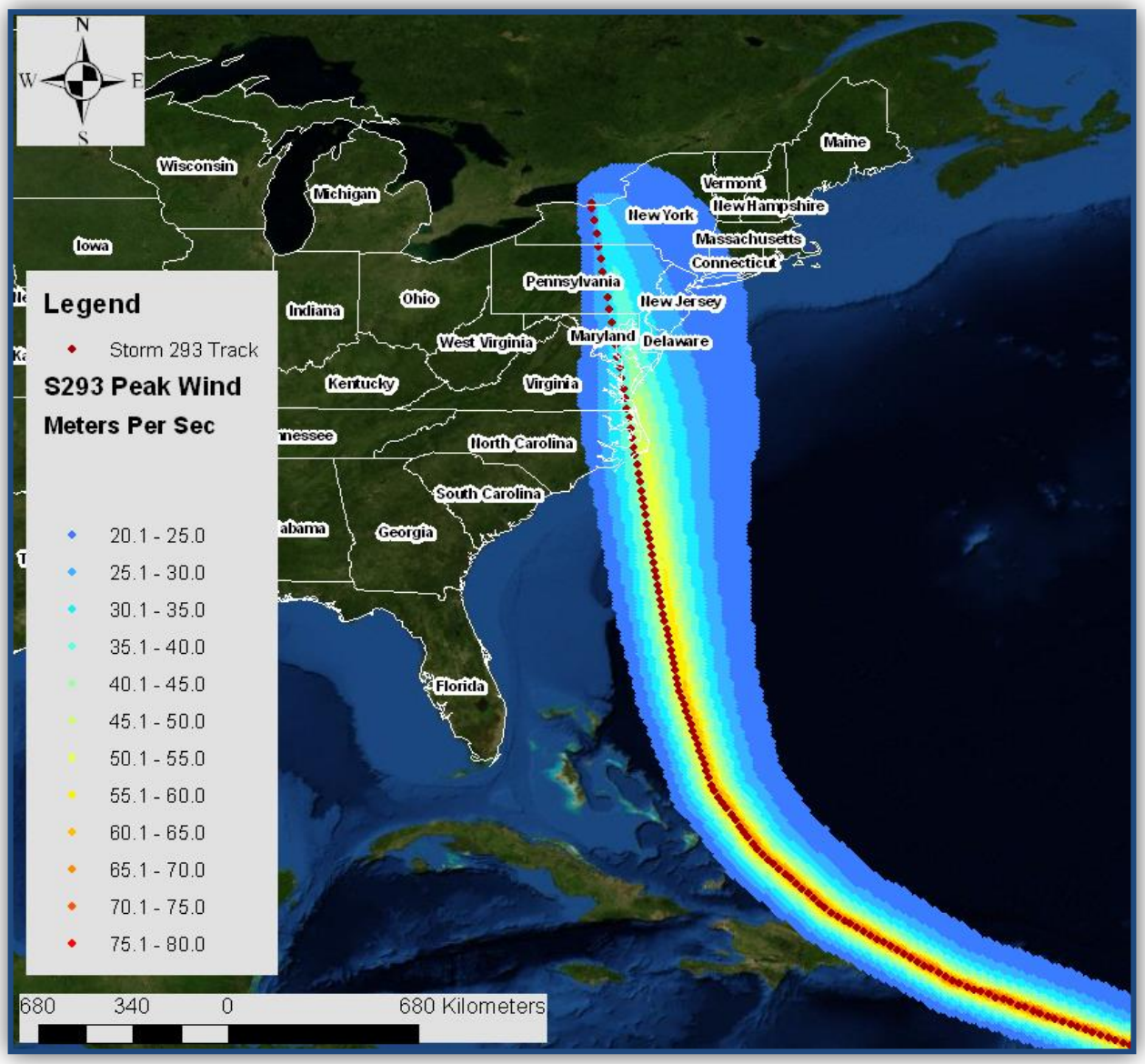

Figure 84. Maximum wind speed in m/s for Hurricane 293 (i.e., the 50-yr return interval storm assessed in the project).

Storm 293 produced approximately 50-yr water levels at NSN. Storm 293 peak wind speeds were slightly higher than Storm 449, but the higher wind speeds were far off the coast. Because storm 293 traversed a different track than storm 449, lower surges were produced at NSN.

The generated winds fields were the input to the circulation and wave models at both the regional and nearshore scales. The storms were not modified to reflect climate change, although there exists a potential for climate change to result in more intense and/or more frequent storms (IPCC 2007). The same wind fields were used to drive the circulation and wave models for all the prescribed SLR scenarios.

4.3.1.2 Regional Water Levels

Regional water levels were generated for each of the storms in Table 9 and Table 10 with ADCIRC simulations. ADCIRC was driven with the wind fields generated by the PBL model and wave stresses produced by the SWAN model. Bathymetry/topography and friction coefficients derived from the land cover and interpolated onto the model mesh were also incorporated into the ADCIRC analyses. Time histories of water surface elevations for every mesh node in the model domain were produced by the ADCIRC runs. Each storm was run with the prescribed SLR scenarios (i.e., 0.0, 0.5, 1.0, 1.5, and 2.0 m) applied uniformly over the mesh. All water levels were reported relative to the NAVD88 datum. The ADCIRC output was applied as a boundary condition for the follow-on nearshore modeling (refer to *Section 3.5*) and as input to the damage functions (refer to *Section 3.9*).

Figure 85 illustrates maximum water levels (surge) for Storm 449 at two resolutions around the NSN for the existing conditions (0.0 m SLR). The color contours show the upper envelope of maximum water level for each mesh node throughout the storm. The storm track is shown by the red dashed line. In Figure 85, the highest local surges were seen north of the base on the eastern shoreline of Hampton, VA, and southwest of the base in the Nansemond and Elizabeth Rivers. The highest surges (greater than four meters) were located outside of the region of interest on the ocean side of the Eastern Shore of Virginia Delmarva Peninsula.

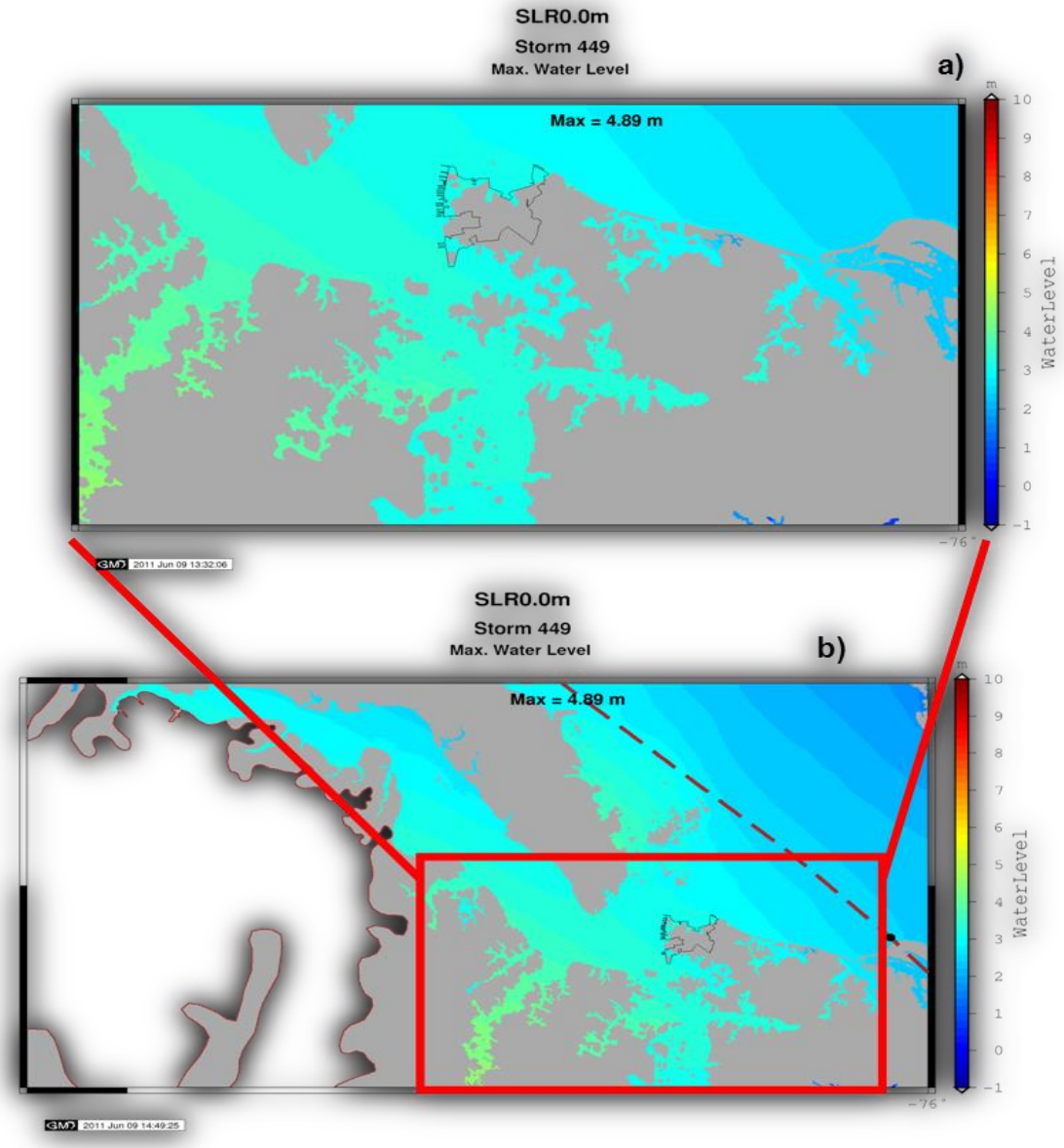

Figure 85. (a) Regional peak water levels for Storm 449 for 0.0 m SLR. (b) A zoomed in version of the same information (Storm 449, 0.0 m SLR) with the focus on the NSN specifically. Water levels (m) were relative to NAVD88.

Figure 86 illustrates maximum zero-moment wave height for Storm 449 at two resolutions around the NSN for the existing conditions (0.0 m SLR). The color contours show the upper envelope of maximum wave height for each mesh node throughout the storm. The storm track is shown by the red dashed line. In Figure 86, the highest wave heights near the base (approximately three meters) were seen in the lower bay. The west-facing orientation of the base piers sheltered them for the ocean-generated waves.

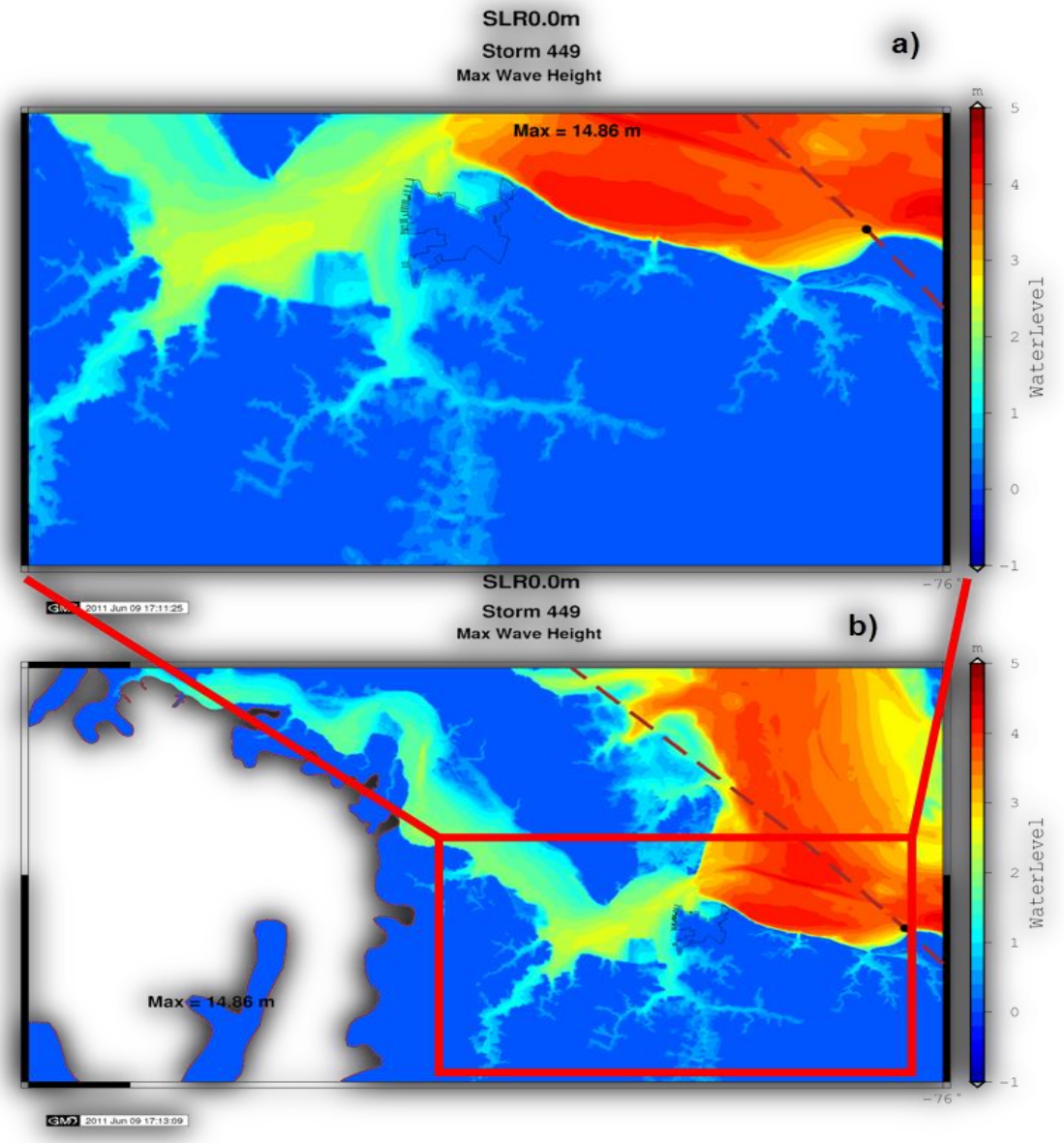

Figure 86. (a) Regional peak wave heights for Storm 449 for 0 m SLR. (b) A zoomed in version of the same information (Storm 449, 0m SLR) with the focus on the NSN specifically.

Figure 87 and Figure 88 compare SLR scenarios and their resultant maximum water levels and wave heights for Storm 449 from the same frame of reference (hovering over the NSN). Water levels at 0.5 m of SLR [Figure 87 (a)] were seen to inundate NSN. Inundation progressively increased with SLR increments [panels (b), (c), and (d) respectively] with all areas under water at 2.0 m of SLR. Wave heights followed a similar pattern [0.5 m SLR Figure 88, panel (a)] and showed progressive increases in wave heights with SLR increases [panels (b), (c), and (d) respectively]. The larger surges enabled larger waves to form and propagate over the base during the storm event.

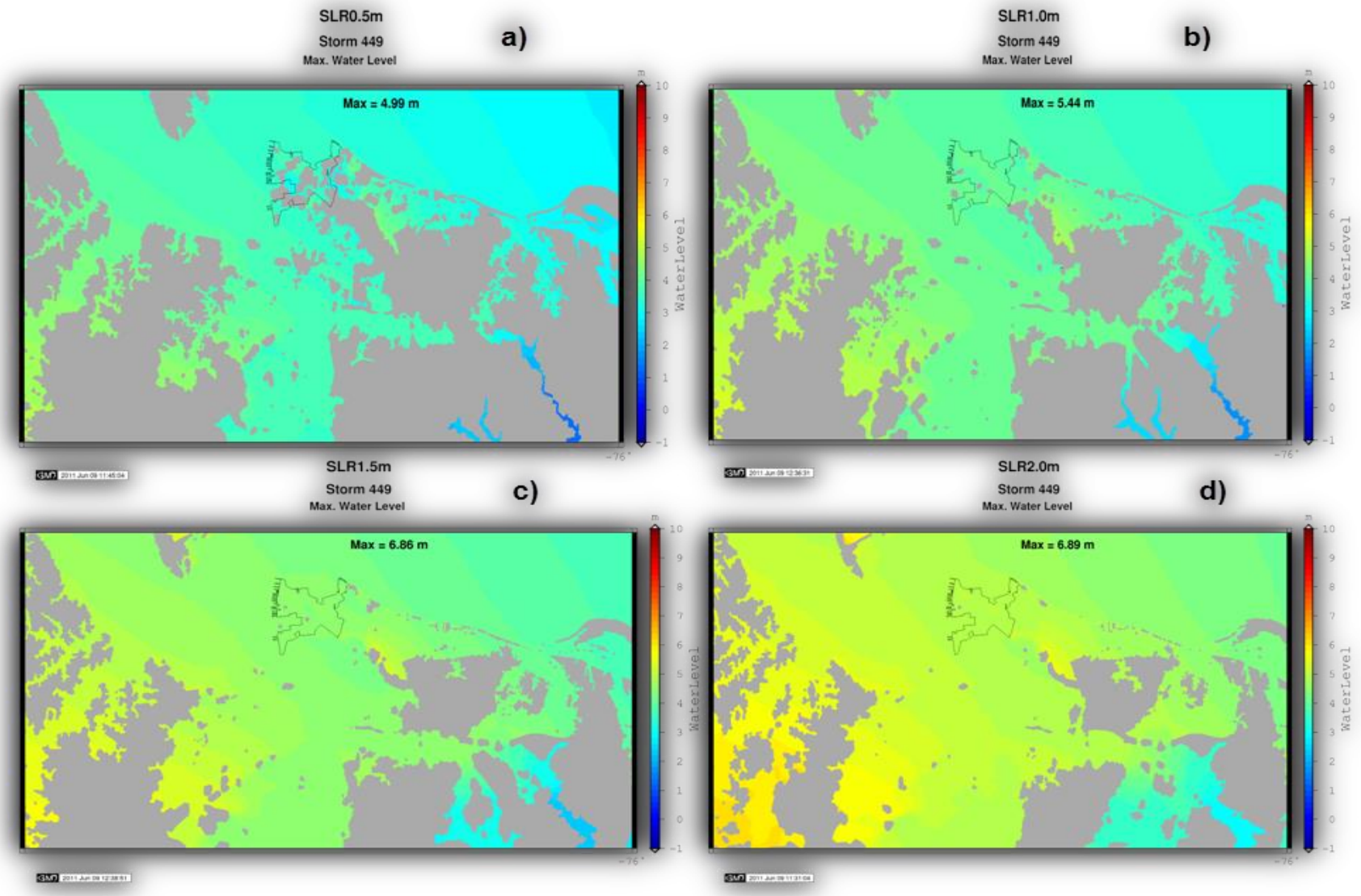

Figure 87. Regional peak surge heights under the Storm 449 (100-yr return interval storm) for the (a) 0.5 m, (b) 1.0 m, (c) 1.5 m, (d) 2.0 m SLR scenarios.

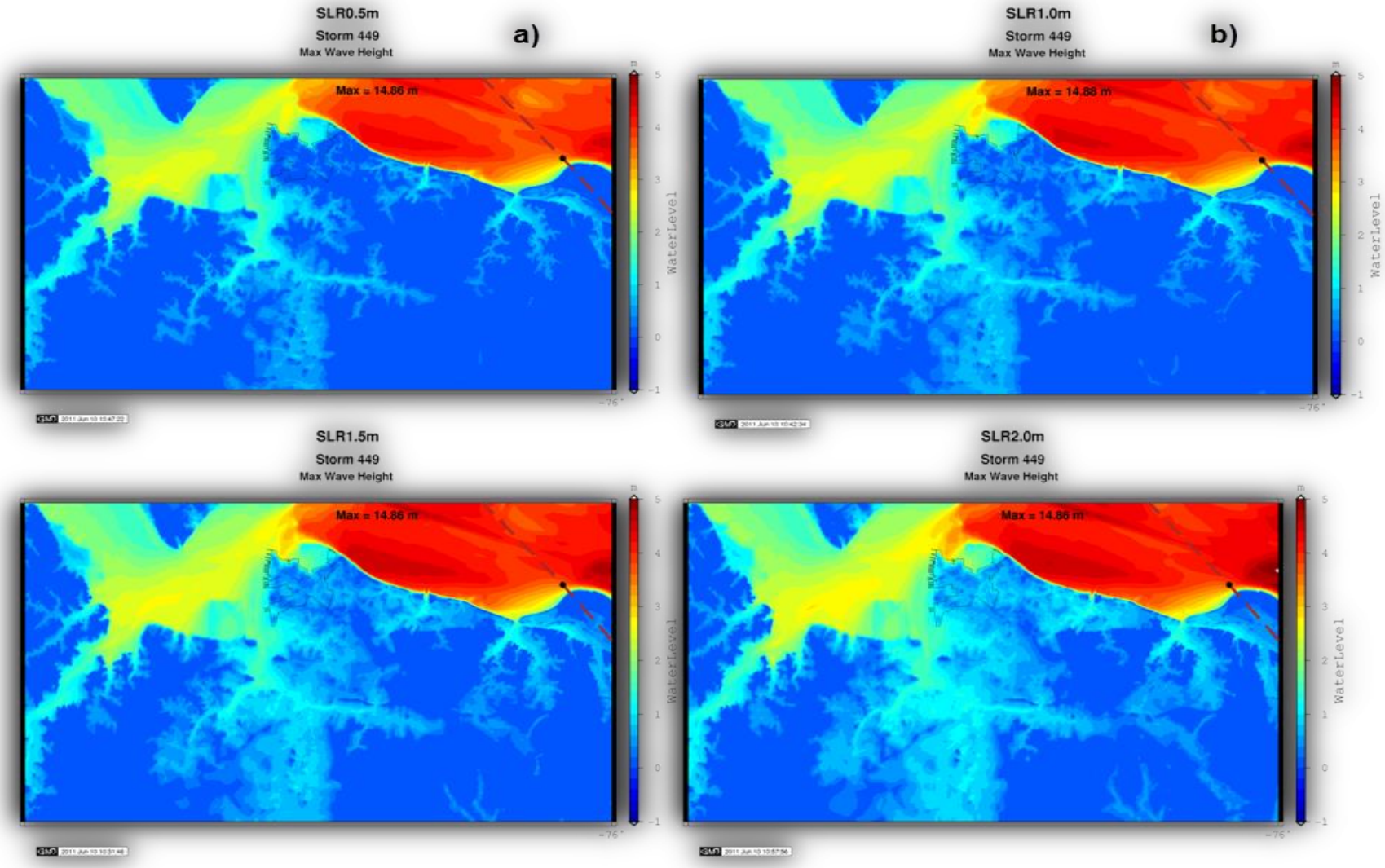

Figure 88. Regional wave heights (m) under the Storm 449 (100-yr return interval storm) for the (a) 0.5 m, (b) 1.0 m, (c) 1.5 m, (d) 2.0 m SLR scenarios.

4.3.1.3 Water Level and Wave Analyses

A full frequency analysis for still water levels at the NSN would have required literally hundreds of storm simulations for existing sea level conditions repeated for each of the prescribed SLR scenarios, resulting in massive computational resource requirements. Instead, we opted to employ "representative" storms (Table 9 and Table 10) selected from the large number of storms generated by FEMA to estimate and evaluate the impact of SLR on simulated peak water levels and waves and associated return periods.

For each SLR scenario and all simulated storms, the surges and wave heights within the study region were compared to the 0.0 m SLR simulations. The relative amplification of the surge (waves) was evaluated. Typically in shallow areas and wetlands, the amplification was significant. In relatively deep areas, the amplification was relatively small (response to SLR was linear) (Smith et al. 2010). Total differences were computed between peak surge levels for each SLR scenario increment (0.0 - 2.0 m). Normalized differences were computed by dividing each group by its respective SLR increment. For example, the total differences between present and peak storm surge levels, for each storm, produced for SLR increment 0.5 m, were divided by 0.5 m. Differences for 1.0 m, 1.5 m, and 2.0 m were divided by the increment value. Descriptive statistics for each group of normalized differences were computed for all mesh nodes which encompassed the Norfolk and Hampton Roads region. These statistics quantified the impacts of SLR at each node for the suite of storms rather than one specific event. Approximately 55,000 nodes of the ADCIRC mesh were used to compute the distribution of the means and variances of the normalized differences at point locations surrounding the study area. Figure 89 shows surge statistics for each scenario. The normalized differences had a larger spread of values and were highest at SLR 0.5 m. These values decreased for each increase in SLR. These analyses showed a higher degree of nonlinear response for the lower SLR increments (0.5 and 1.0 m) and gradual movement towards a linear response at the higher levels of 1.5 m and 2.0 m (see also Smith et al. 2010).

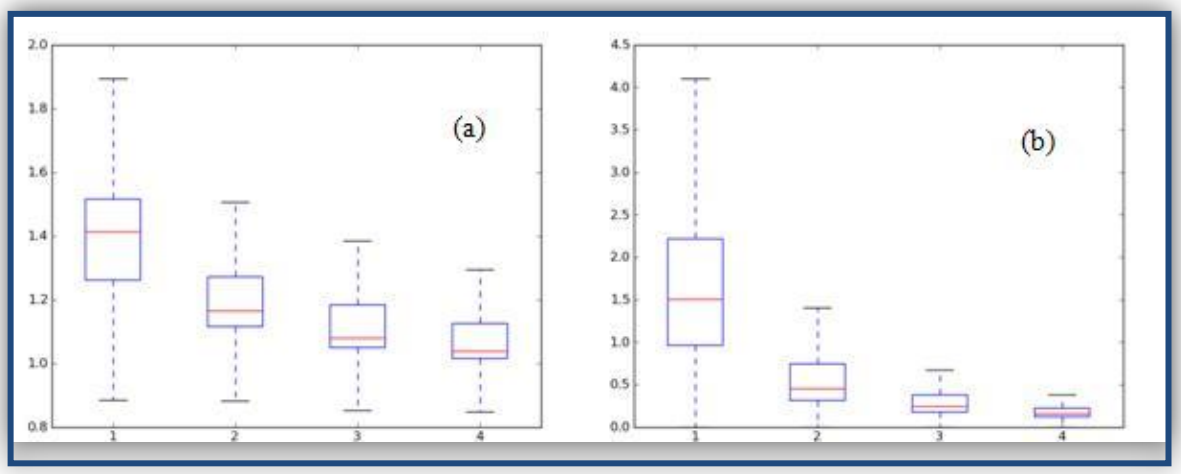

Figure 89. Means (a) and variances (b) of normalized differences for each SLR scenario increment where 1 = SLR 0.5 m, 2 = SLR 1.0 m, 3 = SLR 1.5 m, and 4 = SLR 2.0 m.

The nonlinear results were not surprising. Surge propagation, frictional dissipation, and wave breaking are nonlinear processes related to water depth, so as depth changed through SLR, the response themselves were expected to be nonlinear. Moreover, nonlinear amplifications are most prevalent in shallow areas (where the total water depth -- surge + bathymetry depth -- is small), thus nonlinear amplifications were anticipated for the smaller SLR increments. Finally, differences in surge were normalized by the SLR increment, so an increase in water level of 0.25 m above the SLR increment generated an amplification effect of 1.5 for 0.5 m SLR and 1.25 for 1.0 m SLR.

Computation of the descriptive statistics at each mesh node provided a geospatial view of overall impact. The variances of SLR increment 0.5 m and 1.0 m within a sub-area of the study were computed (refer to Figure 90 and Figure 91 respectively). Low variance indicated small variability in the peak water level response of all simulated storms at that location. Higher variance implied a more nonlinear response and large variability of responses among storms at that location for that SLR increment level. The high degree of geospatial variance occurred in marsh areas intermittently flooded by tides as well as areas protected by surrounding topography. Cross correlation was performed with the normalized variance of the 0.5 m SLR and the NLCD. The highest variances occurred in the wetlands and forested categories as well as crop lands. These results were consistent with the significant area of crop lands on the Delmarva Peninsula which experienced high surge variances due to low topographic elevations.

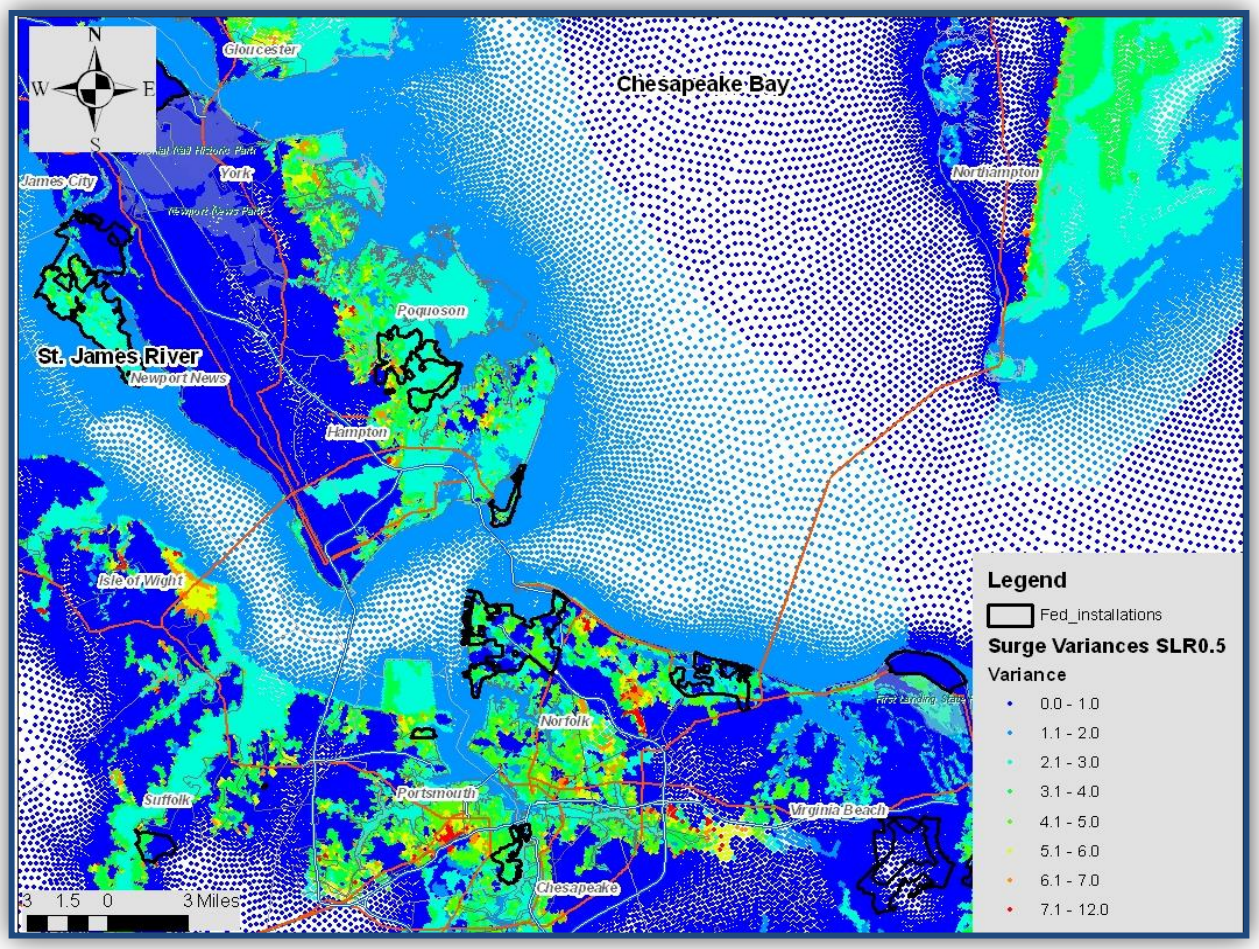

Figure 90. Variance of normalized surge differences for SLR scenario 0.5 m.

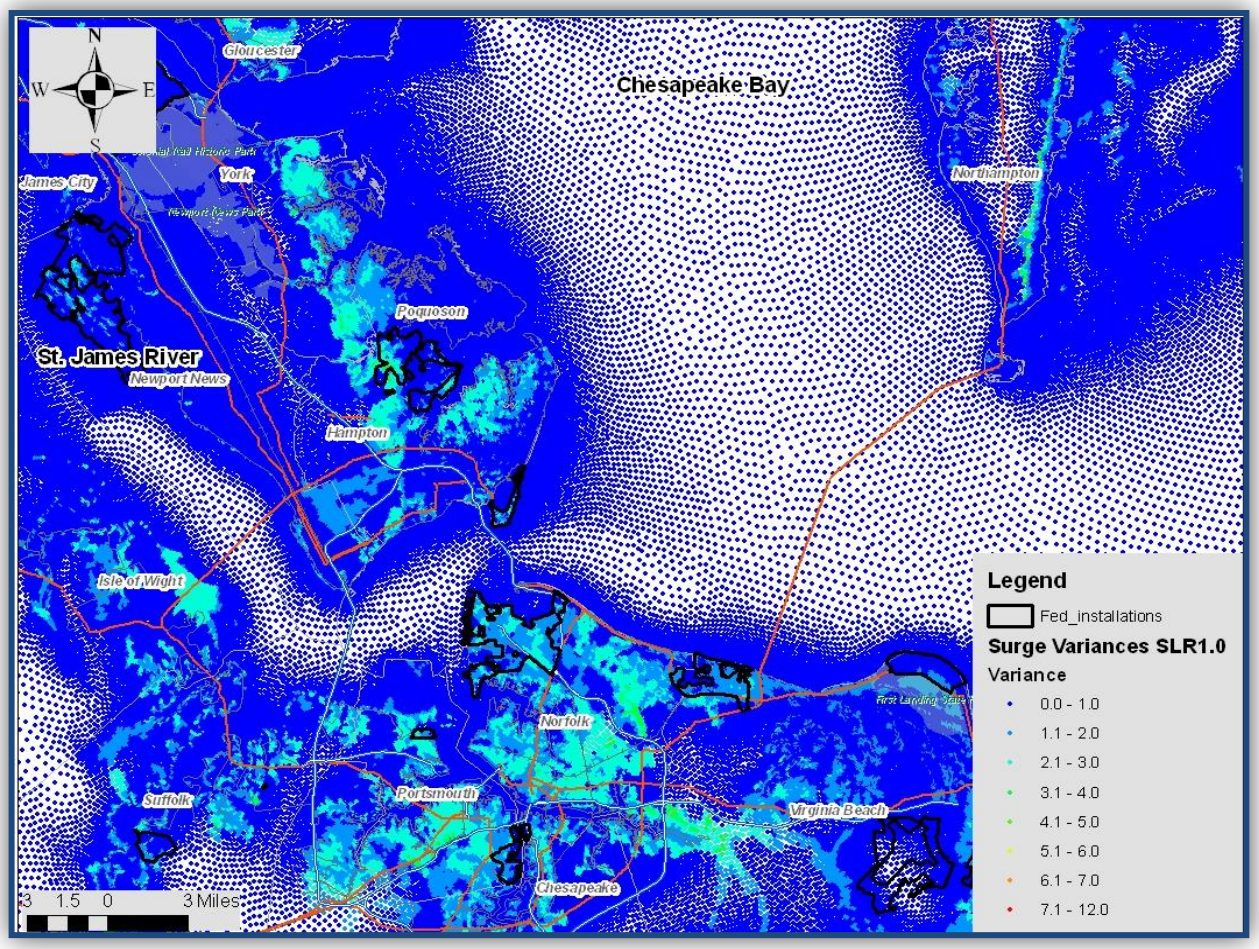

Figure 91. Variance of normalized surge differences for SLR scenario 1.0 m

The nonlinear impacts of SLR were also evident in the estimated return periods of surge and waves along the coast. The 50- and 100-yr return interval values were estimated from the subset of storm simulations following closely the JPM-OS methodology established post-Hurricane Katrina and implemented in the FEMA Region III effort. This methodology followed the Joint Probability Method which relied on creation of statistical distributions of individual hurricane parameters such as central pressure, radius to maximum winds, forward velocity, direction, etc. Sampling from these distributions was performed to create model hurricanes that could or could not have occurred. A suite of storms was created and associated with a probability based upon its specific characteristics.[1] A probability or weight for each synthetic storm was established by the FEMA team with the sum over all storms equal to unity. The probability that a hurricane induced water elevation was exceeded during time period *t* was,

$$\mathrm{Pt}(\eta > \eta 0) = 1 - \sum \mathrm{P}(\eta < \eta 0 \mid \mathrm{x})\ \mathrm{pt}(\mathrm{x}) \qquad \textbf{(15)}$$

[1] FEMA Region III Storm Surge Study, http://www.r3coastal.com/home/storm-surge-study (Accessed April 2014).

Where $P(\eta < \eta_0 \mid x)$ was the probability that the water elevation η was less than η_0 given that x storms occurred, and $p_t(x)$ was the probability of x storms occurring during time period t. From *Equation 15*, with $p_t(x)$ defined with a Poisson distribution and t as one year, the annual probability of exceeding a storm surge elevation is,

$$Pa(\eta > \eta 0) = 1 - exp[-\lambda P(\eta > \eta 0)] \quad \textbf{(16)}$$

Where λ was the average annual number of storms across the coastline segments and $P(\eta > \eta_0)$ was the probability that water elevation, η, was greater than η_0 given the occurrence of any one storm. The annual occurrence rate, λ, was 0.1561 for this region.

In order to apply *Equations 15* and *16*, all surge responses for 17 tropical storms for all ADCIRC points within and surrounding the study area were compiled for each SLR scenario. For each scenario and each point, the surges were rank ordered for each storm response. Surge response for storms not simulated were estimated by linear distance weighted interpolation along tracks critical to the study site or set with minimum response values for the remaining storms. The return periods for each point for each scenario were based on the scenario surge responses. Figure 92 and Figure 93 show the 100-yr return interval surge (still water level) values for each SLR scenario.

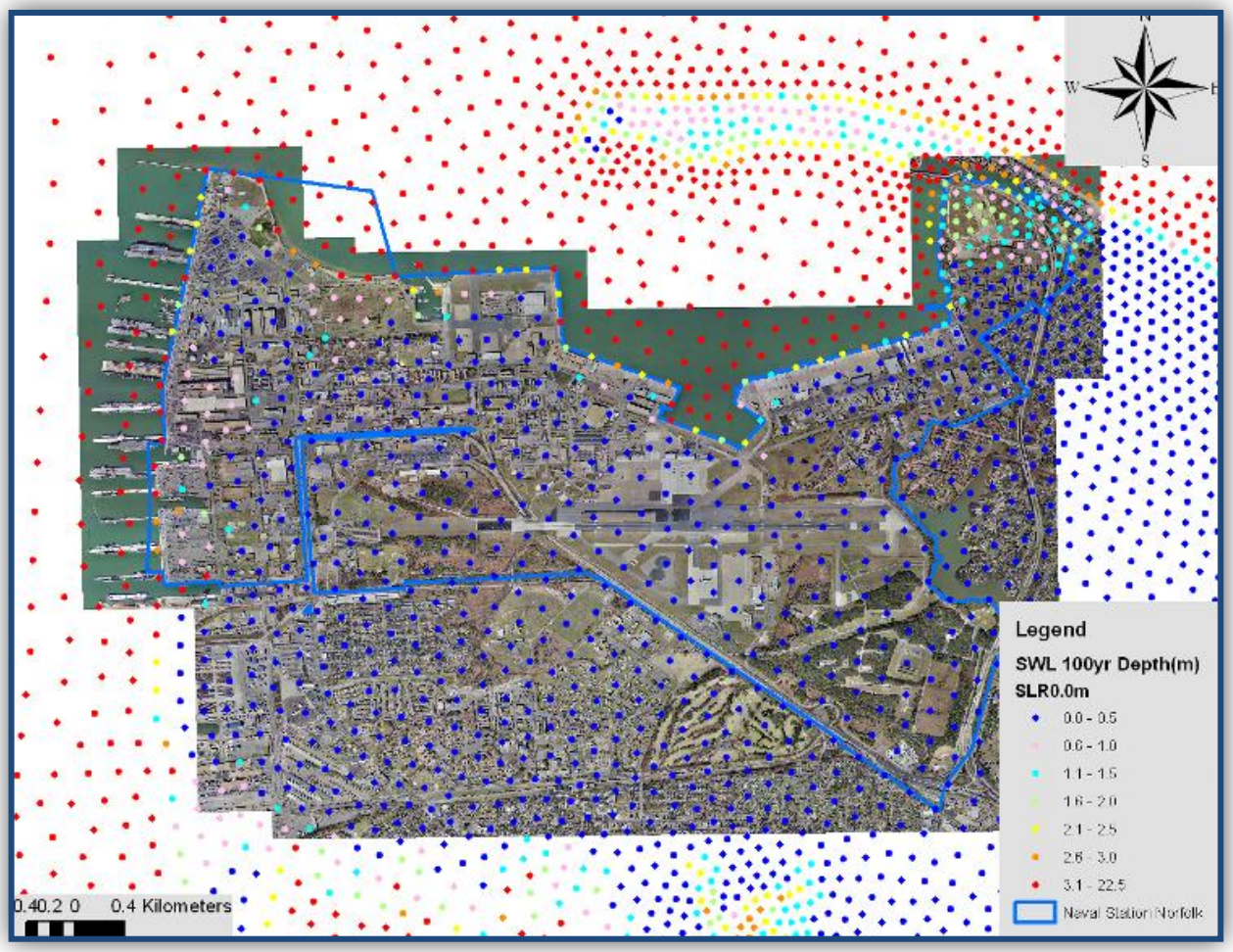

Figure 92. 100-yr return interval surge values (shown here as depth of water in meters) under the 0.0 m SLR scenario.[2]

[2] SWL refers to Still Water Level aka surge.

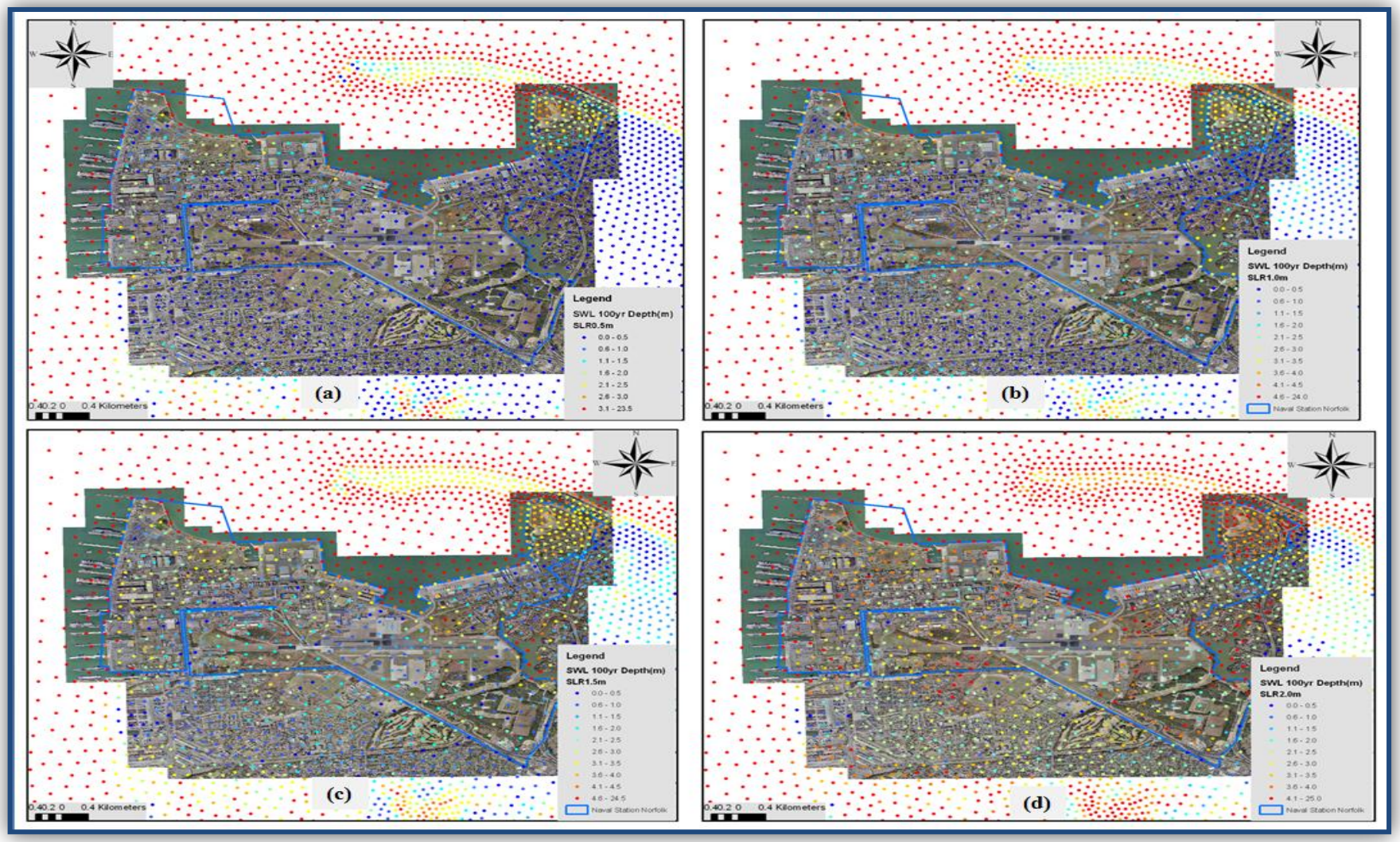

Figure 93. 100-yr return interval surge values (shown here as depth of water in meters) under the (a) 0.5 m, (b) 1.0 m, (c) 1.5 m, and (d) 2.0 m SLR scenarios.

It was evident that the return values were not strictly linearly increasing, and the topography elevations, proximity to the water, as well as surrounding features all impact the final results. In general, the higher the sea level increment, the further storms were able to penetrate inland and thus provide additional responses for return value computation and subsequently higher return elevations and water depths. To quantify the overall change and increase, Figure 94 shows the difference between the SLR 0.0 m and SLR 2.0 m 100-yr return interval values.

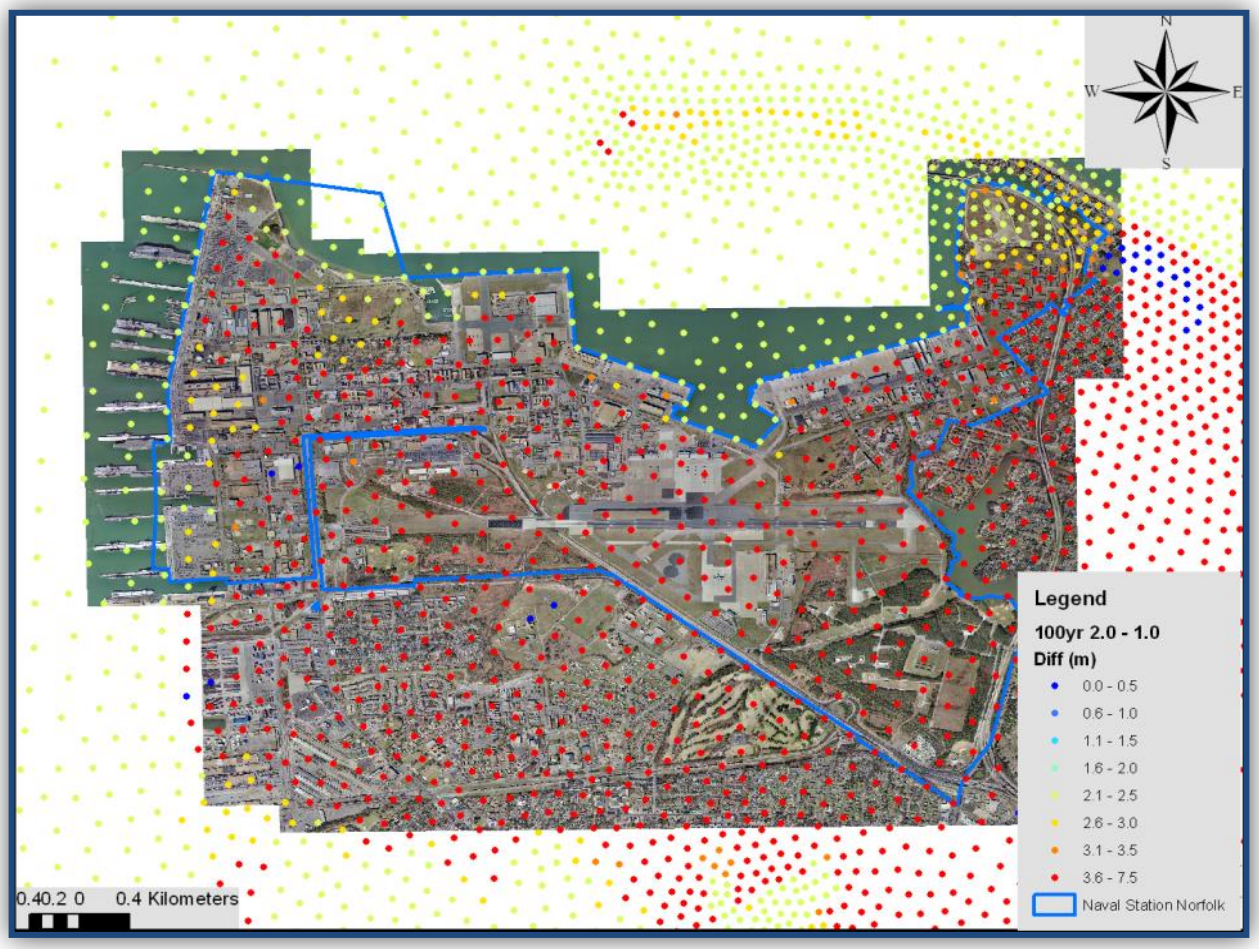

Figure 94. Difference between SLR 2.0 m minus SLR 1.0 m 100-yr return interval surge values (m).

Wave height impacts also demonstrated nonlinear characteristics and the methodology used to compute still water level (surge) returns was implemented to estimate wave heights for each SLR scenario. Again, surge propagation, frictional dissipation, and wave breaking as well as shallow water depths and normalization of the surge by SLR increments generated the amplifications shown in the figure. Figure 95 compares the estimated wave heights for the five prescribed SLR scenarios excluding SLR increment of 1.5 m.

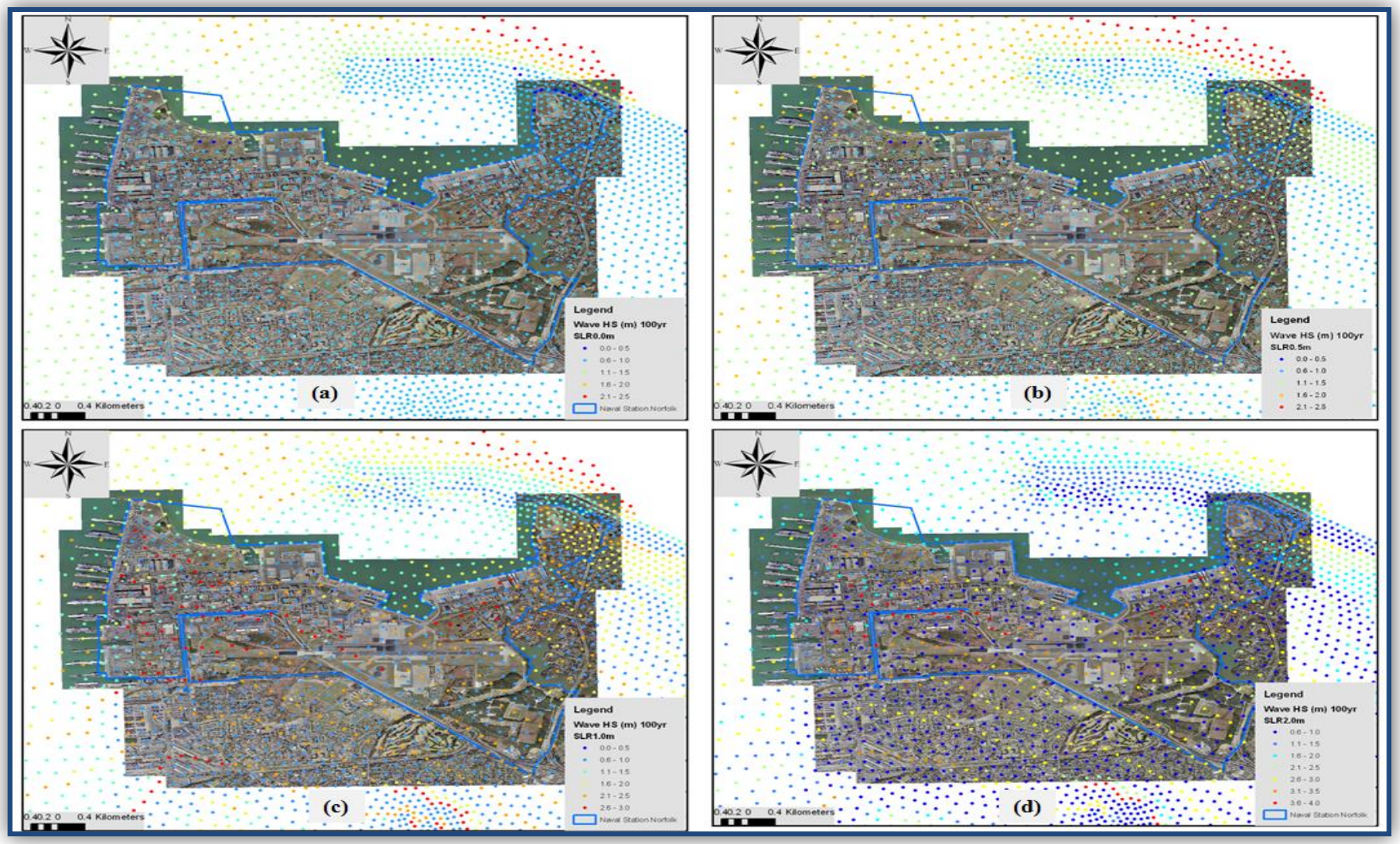

Figure 95. Estimated wave heights (m) for the 100-yr return interval storm under the (a) 0.0 m, (b) 0.5 m, (c) 1.0 m, and 2.0 m (d) SLR scenarios.

Both still water level (surge) and wave height return values were computed for the 50-yr and 100-yr return interval storms for each SLR increment and all nodes, as shown in the above figures. Surge and wave heights formed two components of the group of forcing parameters created for risk analyses. All forcing components provided for risk computations included:

a. Still Water (Surge) Elevation (m),
b. Still Water (Surge) Depth (m),
c. Still Water (Surge) Velocity (m/s),
d. Wave Height (m),
e. Wave Depth (m), and
f. Wave Speed (m/s).

The depth of surge, wave depth, surge current velocity, wave velocity, wave period, and wave length were computed for all nodes for each SLR increment. Analyses of wave periods for all storms were performed to determine a wave period (for the study area) representing the 50-yr and 100-yr return interval values. A 6-second wave period was estimated for the 50-yr value and a 10 second wave period was estimated for the 100-yr return interval value. Surge elevations, depths and velocities, along with wave heights and velocities, were computed following the frequency methodology previously described. Wave depths were computed as half of the wave heights (linear crest elevation about the still water level). Wave speeds were the maximum orbital velocities at the water surface. Linear wave theory equations were used to compute these velocities (Dean et al. 1991). *Equation 17* was used to estimate deepwater wave length (L_o), using the specific 50-yr and 100-yr return interval wave periods (T). *Equation 18* was then used to explicitly estimate the specific shallow-water wave length (L), at each node in the study area (Fenton and McKee 1989). The maximum orbital velocity was computed using *Equation 19* using the shallow-water wave length at each node.

$$L_o = \frac{gT^2}{2\pi} \tag{17}$$

$$L = L_o \left\{ \tanh\left[\left(\frac{2\pi}{T} \left(\frac{d}{g} \right)^{0.5} \right)^{1.5} \right] \right\}^{2/3} \tag{18}$$

$$u_{\max} = \frac{gHT}{2L} \tag{19}$$

Where g was gravity, H was wave height, T was peak period, L was wave length, and d was depth (with surge). These parameters formed forcing components for the risk assessment evaluation.

4.3.1.4 Wind Analyses

To compute wind loading factors at the study site, wind velocity return values were required. Due to the limited number of synthetic storms simulated and the small footprint of the study area, specific return values could not be estimated using only the synthetic storms. Existing wind speed data along the eastern U.S. coast were used for forcing levels for this project. With the recognition of global climate change there have been efforts to estimate both historic wind speeds and impacts of warming on future storms and wind speeds. The project did not consider future wind speed changes due to climate change, and focused instead on water level and wave responses related specifically to the prescribed SLR increments.

The wind speed return levels were computed for one-minute wind averages at 10 meter elevation (Table 29). These values were developed with a peak over threshold analysis of 26 years of data from National Data Buoy Center (NDBC) Station CHLV2 – Chesapeake Light, Virginia, using a threshold wind speed of 20 m/s. This wind station was located at 36.910 N, 75.710 W**.** The extremal analysis applied a Weibull Distribution with k = 1.00, resulting in a correlation coefficient of 0.98 and sum of squares residual of 0.07 m/s. These wind speeds were representative across the NSN.

Table 29. Wind speed return levels.

Return Intervals (yr)	Wind Speed (1-min average at 10 m elevation) (m/s)
1	24
10	34
50	40
100	43
Nor'easter	29

4.3.1.5 1 and 10-Yr Return Interval Wave Analyses

Similar to the wind analysis described in the previous section, the 1- and 10-yr return wave conditions were estimated from measurements. The data source was NDBC Station 44099, Cape Henry, Virginia, which was a Waverider buoy located at 36.901 N, 75.720 W. The return values were developed with a peak over threshold analysis of three years of data using a threshold wave height of 2.1 m. The extremal analysis applied a Weibull Distribution with k = 1.00, resulting in a correlation coefficient of 0.99 and sum of squares residual of 0.04 meter. The 1- and 10-yr significant wave heights at the buoy were 3.8 and 5.3 m, respectively (with peak periods of 10 and 12 seconds). These waves were transformed into lower Chesapeake Bay using the steady-state wave model STWAVE (Smith et al. 2001) to provide boundary conditions to the CMS-WAVE model of 1-yr wave height of 2.1 m and peak period of 10 seconds, and 10-yr wave height of 2.6 m and peak period of 12 seconds. The 1- and 10-yr return interval water levels were estimated from the Sewell's Point tide gauge (National Ocean Service Station 8638610) located at 36.947N, 76.330W. The return values were developed with a peak over threshold analysis of 21 years of data using a threshold wave height of 1.0 m. The extremal analysis applied a Weibull Distribution with k = 1.00, resulting in a correlation coefficient of 0.99 and sum of squares

residual of 0.09 m. The 1- and 10-yr return interval water levels were 1.2 and 1.7 m, respectively.

4.3.2 Summary and Discussion

Variability in the location and timing of storm genesis can influence storm character at land-fall, and even small changes can lead to large changes in land-fall location and impact (Burkett and Davidson 2012). Although no consensus exists regarding projections of climate-induce storm genesis, factors such as frequency, storm track, intensity, and storm size could certainly be affected (either positively or negatively) by climate change, and SLR is virtually certain to exacerbate storm related hazards. Table 30 and Figure 96 provide a glimpse of the forcings (maximum winds, surge, and wave velocities) generated by the regional surge and wave modeling. Nonlinearity in these figures can be explained by taking into account the nonlinear physical mechanics surrounding surge dynamics (i.e., surge propagation, frictional dissipation, and wave breaking). These values served as new input to the nearshore modeling follow-on analyses, that in turn directly fed the structural analyses and risk assessments of the prescribed SLR and coastal storm impacts for the study on NSN. In actuality, individual forcing values were generated across the model domain at the mesh element or cellular level (the triangular, unstructured mesh cell sizes ranged from 20 m up to several kilometers) for each scenario. But, it is useful to explore the maximum forcings generated over the installation to grasp the magnitude of change experienced across the range of scenarios. As expected, increasing levels of SLR generated ever-increasing levels of storm surge and wave forces threatening the integrity of built infrastructure on the installation.

Table 30. Final maximum storm forcings generated by the regional storm assessment for this study based on the 449 (100-yr) and 293 (50-yr) return interval storms under the five SLR scenarios. NE refers to the October 1982 Nor'easter.

Storm Return Interval (yr)	Regional Surge and Waves Assessment (ADCIRC, SWAN, and TC96)														
	Maximum Wind Speed (mph)					Maximum Surge (m)					Maximum Wave Velocity (mps)				
	SLR Scenario					SLR Scenario					SLR Scenario				
	0.0	0.5	1.0	1.5	2.0	0.0	0.5	1.0	1.5	2.0	0.0	0.5	1.0	1.5	2.0
1	53.7	53.7	53.7	53.7	53.7	--	--	--	--	--	--	--	--	--	--
10	76.1	76.1	76.1	76.1	76.1	--	--	--	--	--	--	--	--	--	--
50	89.5	89.5	89.5	89.5	89.5	1.6	2.5	3.2	3.8	4.3	1.0	1.5	1.7	1.7	1.7
100	96.1	96.1	96.1	96.1	96.1	3.0	3.5	4.5	5.2	5.8	1.5	1.8	1.9	2.0	2.0
NE	67.3	67.3	67.3	67.3	67.3	--	--	--	--	--	--	--	--	--	--

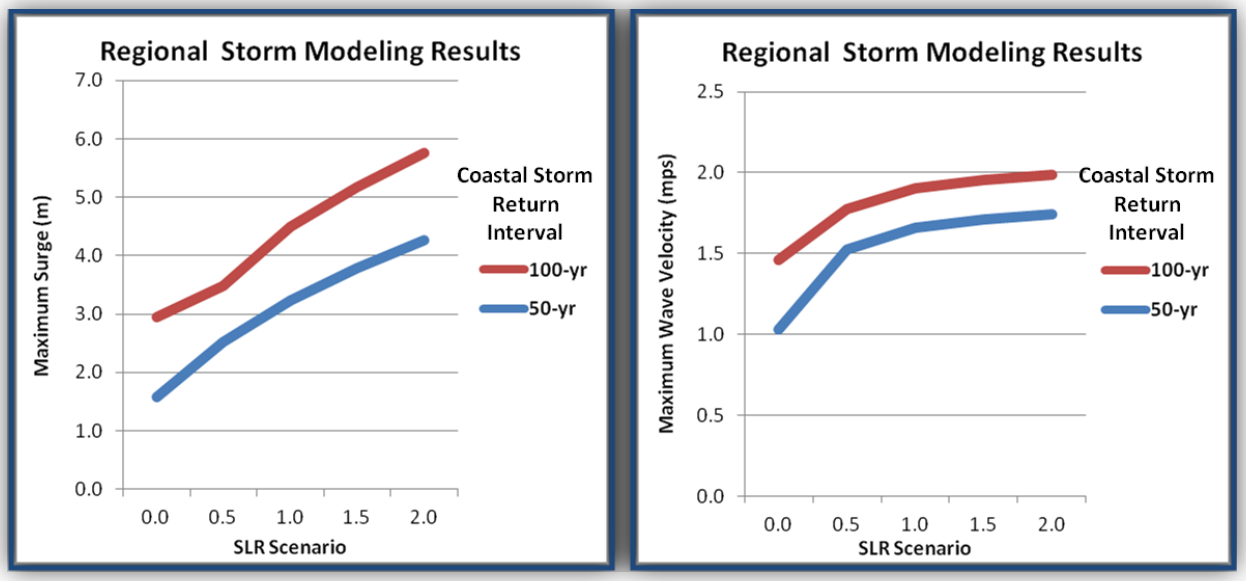

Figure 96. Final maximum storm forcing trends generated by the regional storm assessment for this study based on the 449 (100-yr) and 293 (50-yr) return interval storms under the five prescribed SLR scenarios.

4.4. Nearshore Wave Assessment

4.4.1 Outputs and Technical Results

4.4.1.1 Storm Surge

Figure 97 and Figure 98 show the CMS results (i.e., maximum water surface elevations) of the simulations of 100-yr return interval storm under the five prescribed SLR scenarios. Land areas (with exception of the rivers) were quite flat with elevations oftentimes less than 2 m above MSL. The highest elevations were found north of the city of Norfolk, VA. Even under the baseline (i.e., existing) conditions, most of the installation was under the maximum surge level post-storm. The higher areas east of the NSN stayed above the maximum surge level under the 2.0 m SLR scenario. Much of the Craney Island disposal site remained dry as well, where the 12-meter dikes built surrounding the disposal site offer protection from the most severe storms and the highest SLR scenarios.

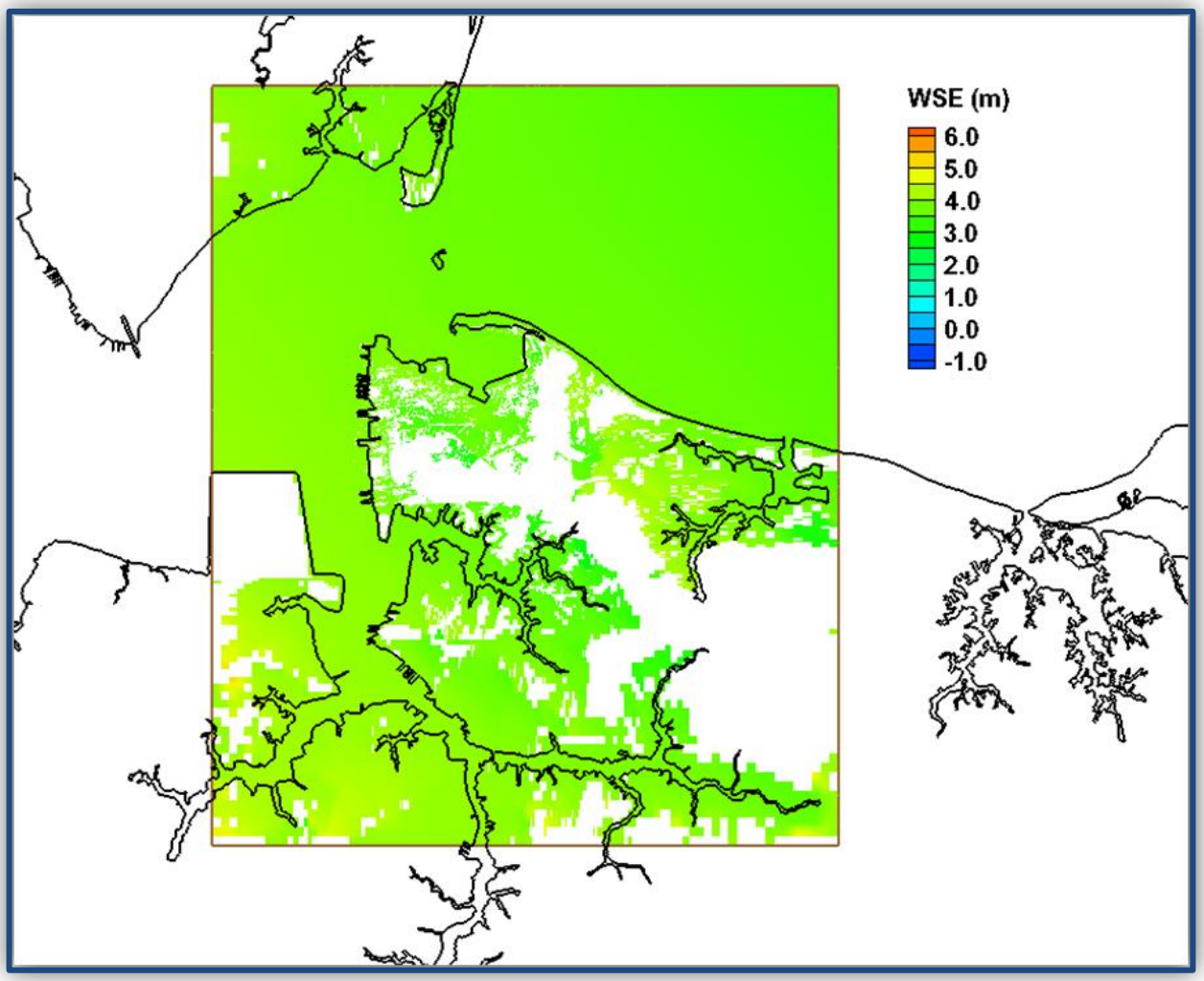

Figure 97. Maximum water surface elevation (WSE) attributed to the 100-yr return interval tropical storm under the existing condition.

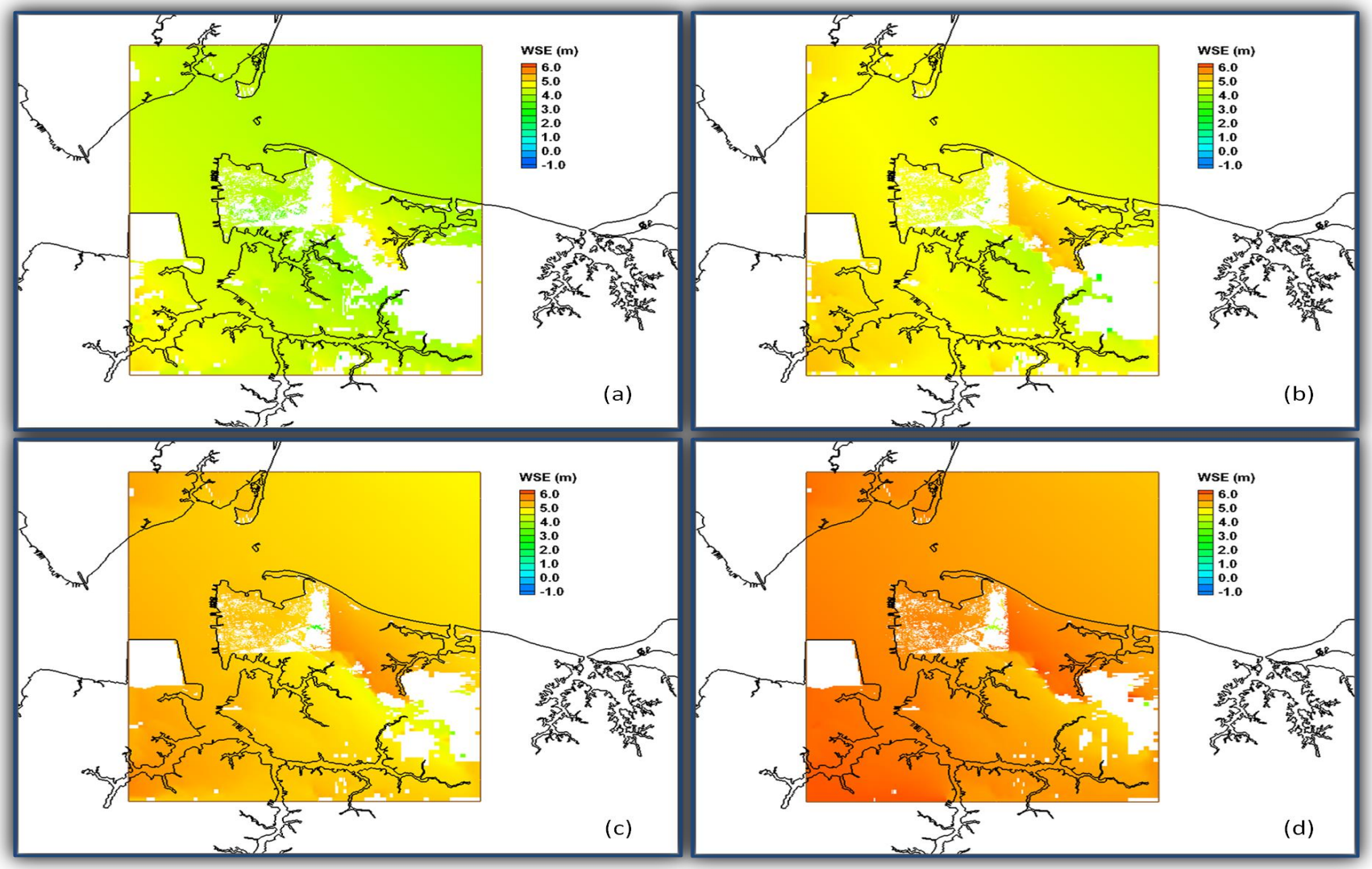

Figure 98. Maximum water surface elevation (WSE) attributed to the 100-yr return interval tropical storm under the (a) 0.5 m, (b) 1.0 m, (c) 1.5 m, and (d) 2.0 m SLR scenarios.

Figure 99 illustrates the calculated water surface elevations at the three locations for the existing condition and the five SLR scenarios under the influences of the 100-yr return interval storms.

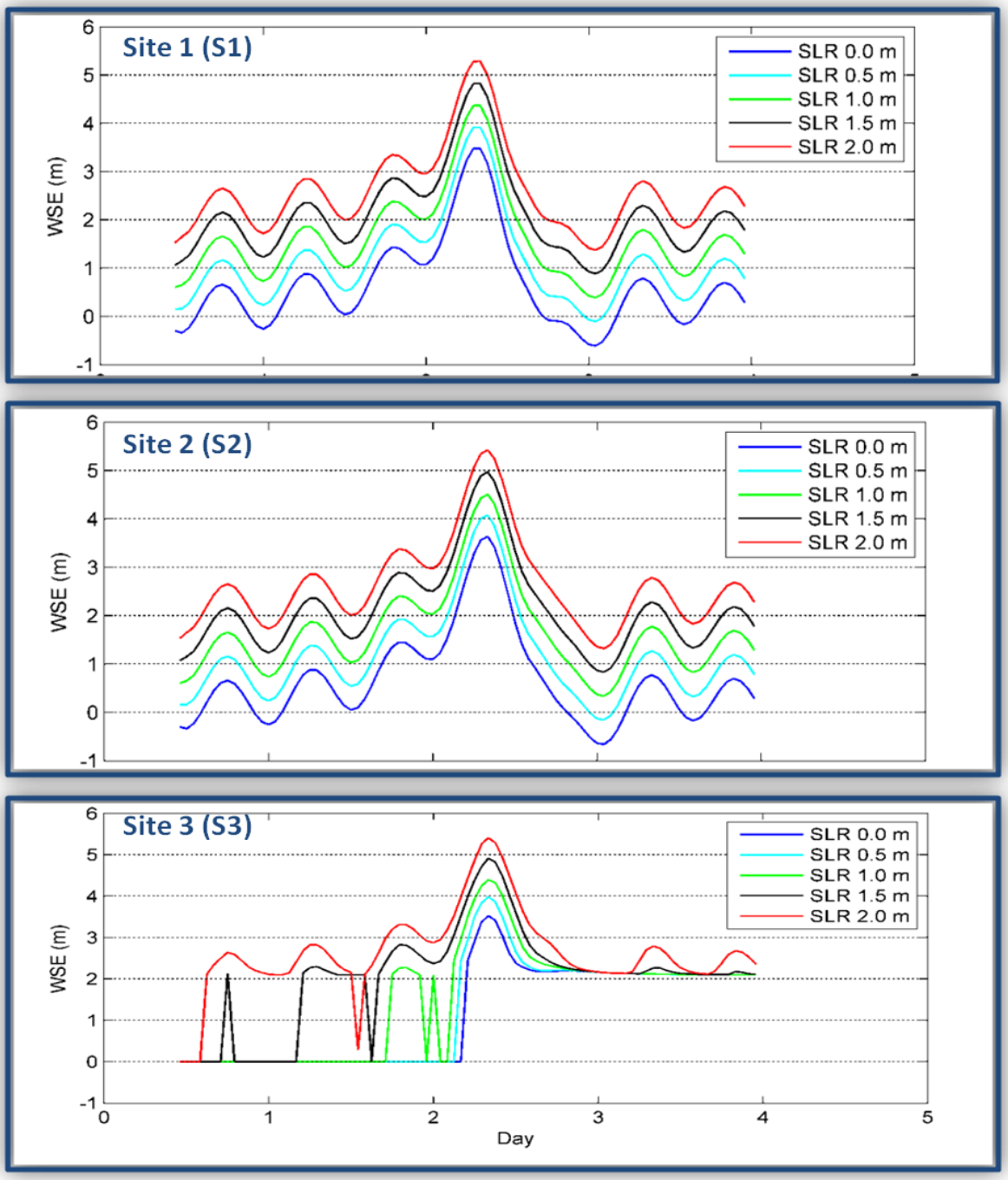

Figure 99. Water surface elevation (WSE) attributed to the 100-yr return interval tropical storm under the five SLR scenarios at *Sites 1*, *2*, and *3* (corresponding to locations identified as "S1," "S2," and "S3" in Figure 26 above).

Tidal and surge signals at *Sites 1* and *2* coincided with tidal forcing implemented at the model open boundaries. Water piled up nearshore as tidal waves propagates from open water to the harbor area. Figure 99 above shows that the surge level at *Site 2* was generally higher than *Site 1* and the difference was as large as 0.5 meter. A different inundation response was found at *Site 3*. The regular tidal condition did not flood the installation area for the existing condition, the 0.5 m, and 1.0 m SLR scenarios, but did for the 1.5 m and the 2.0 m SLR scenarios. The storm surge raised the peak water level to 3.6 m under the existing condition and to 5.4 m under the 2.0 m SLR scenario. The passage of the storm generated high surge levels and inundated the NSN under the various SLR scenarios.

Table 31 lists the areas inundated due to the 1-yr, 10-yr, 50-yr, 100-yr return interval, and the historical winter storms with different SLR scenarios for NSN.

Table 31. Percent inundation of the NSN under the prescribed SLR scenarios and storm event combinations based on the CMS analyses.

SLR (m)	Storm Return Interval				
	1-yr	10-yr	50-yr	Nor'easter	100-yr
0.0	1	2	8	12	63
0.5	3	7	19	27	71
1.0	8	15	34	51	74
1.5	17	33	57	68	76
2.0	36	55	69	73	78

We found that flooding increased exponentially with increase SLR and storm intensities. Surge generated by all five storms inundated approximately 50-80 percent of NSN under the 2.0 m SLR scenario (Figure 100).[3]

[3] Note that this analysis is only a first approximation of surface flooding – follow-on GSSHA modeling presented in the next section uses this information as boundary conditions and incorporates infiltration, topography, storm drainage networks (or the lack thereof), and precipitation.

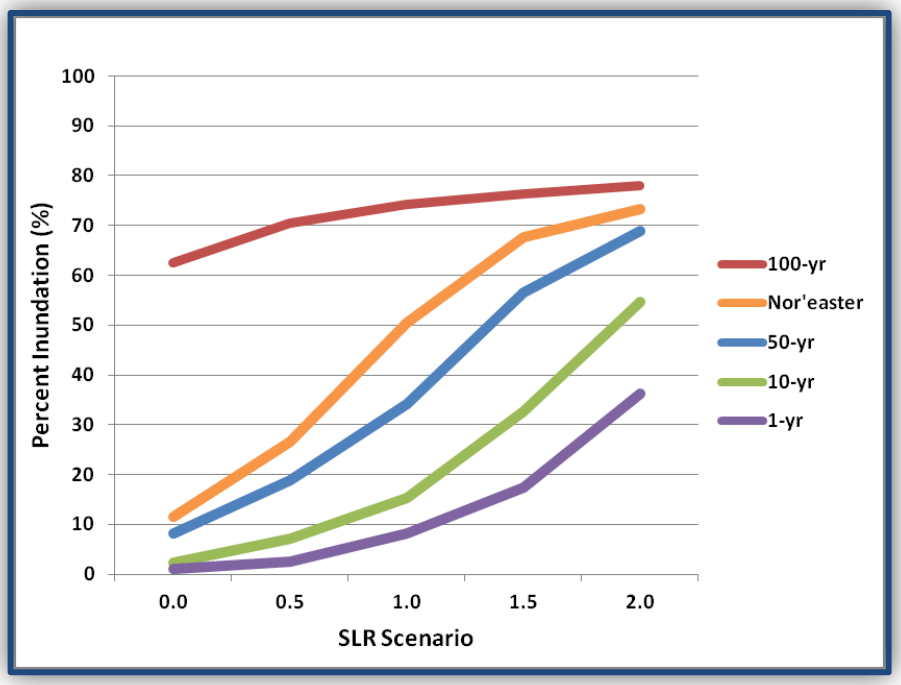

Figure 100. CMS projections of inundation on the NSN under the prescribed SLR scenarios for the assessed storms.

4.4.1.2 Waves

Figure 101 and Figure 102 show the maximum significant wave heights through the 100-yr return interval storm simulations corresponding to 0, 0.5, 1, 1.5, and 2 m SLR scenarios, respectively.

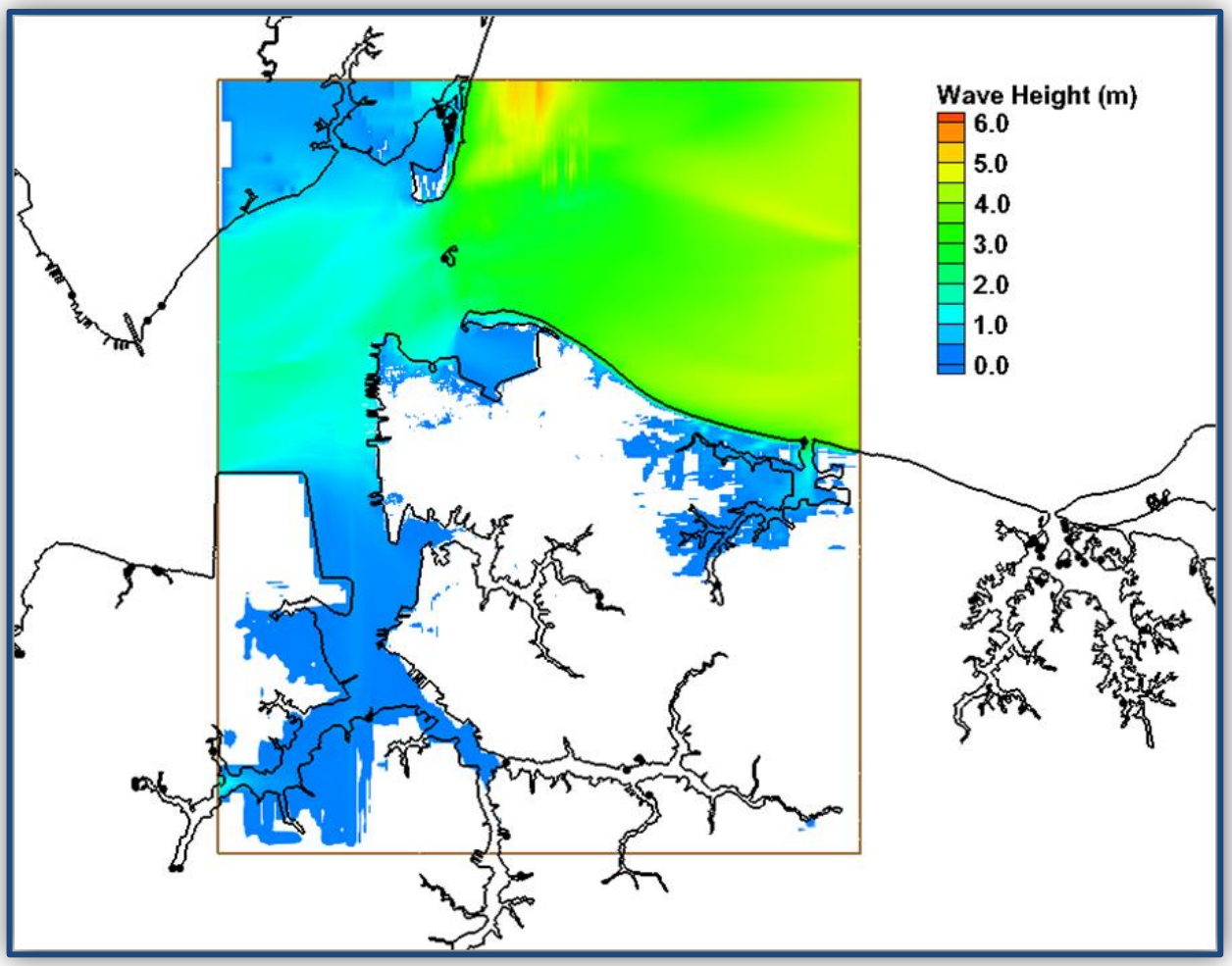

Figure 101. Maximum wave height (m) attributed to the 100-yr return interval tropical storm under the existing (0.0 m SLR) condition.

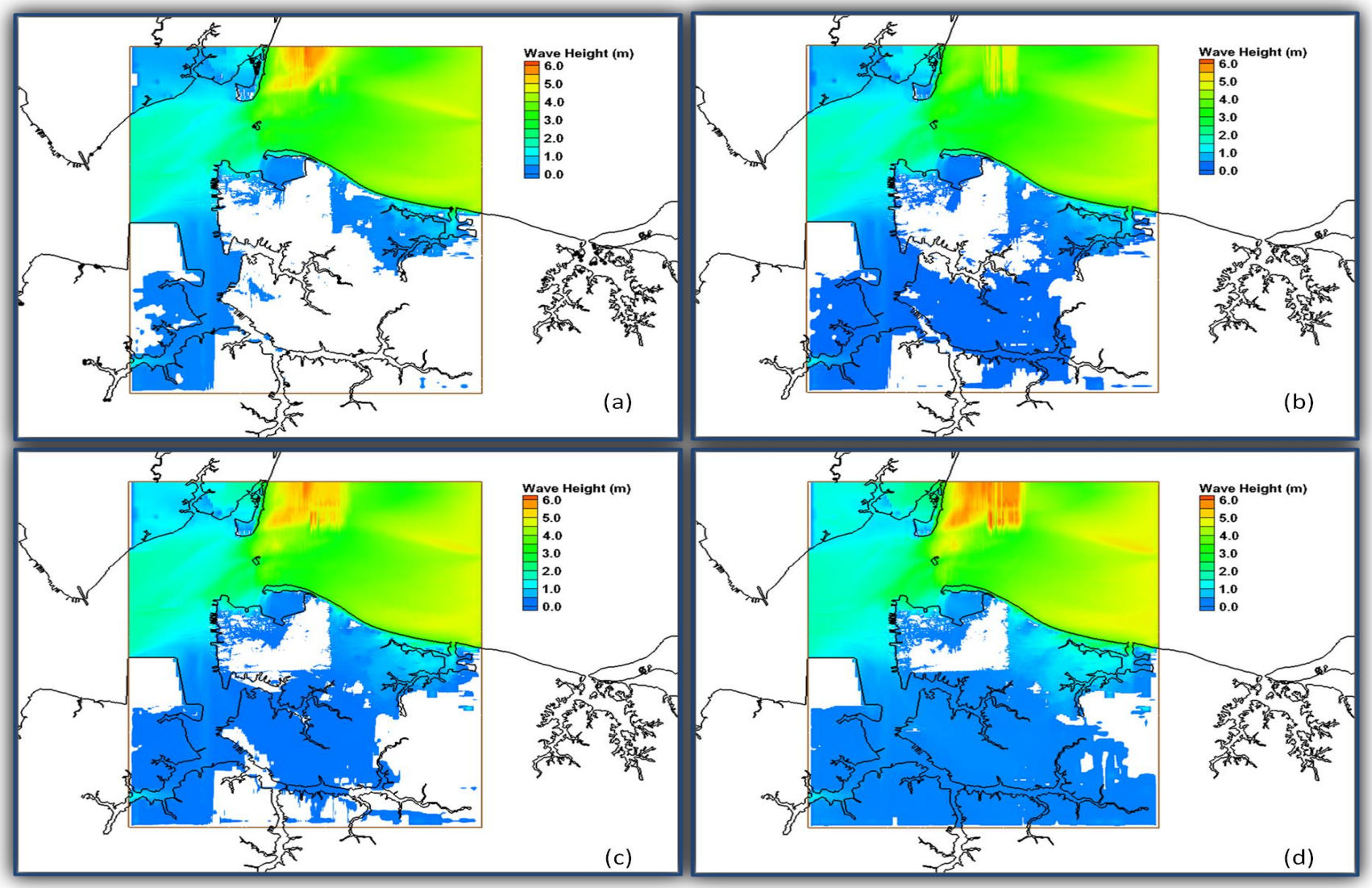

Figure 102. Maximum wave height (m) attributed to the 100-yr return interval tropical storm under the (a) 0.5 m, (b) 1.0 m, (c) 1.5 m, and (d) 2.0 m SLR scenarios.

Large significant wave heights near the open boundaries propagated into the model domain and both decreased and broke as waves approached nearshore (and harbor areas) or overtopped low-lying areas. Wave activity over the base had a consistent coverage pattern, yet wave heights driven by storm surge on the installation generally had amplitudes of only a few centimeters. Larger waves of more than one meter were identified (refer to Figure 101 and Figure 102 above), and were situated close to the oceanfront under the various SLR scenarios. North of the CMS domain, extreme wave heights went as high as six meters under the 1.5 m and 2.0 m prescribed SLR scenarios. The time series of forcing conditions and model outputs revealed that the waves propagating from the Chesapeake Bay side encountered strong opposite wind- and tide-induced currents along the navigation channels as the storm passed over the area. The energy received from the currents resulted in significantly increased wave heights.

Figure 103 shows the time series of significant wave height, wave period, and wave direction at *Sites S1*, *S2*, and *S3*, respectively. The wave direction followed meteorological convention where a wave direction of 0º indicated propagated from the north. Wave parameters displayed at *S1* were similar to waves specified at the open boundary (Figure 31 above). Waves evidently dissipated and diffracted when entering the Hampton Roads area and traveled near the coast.

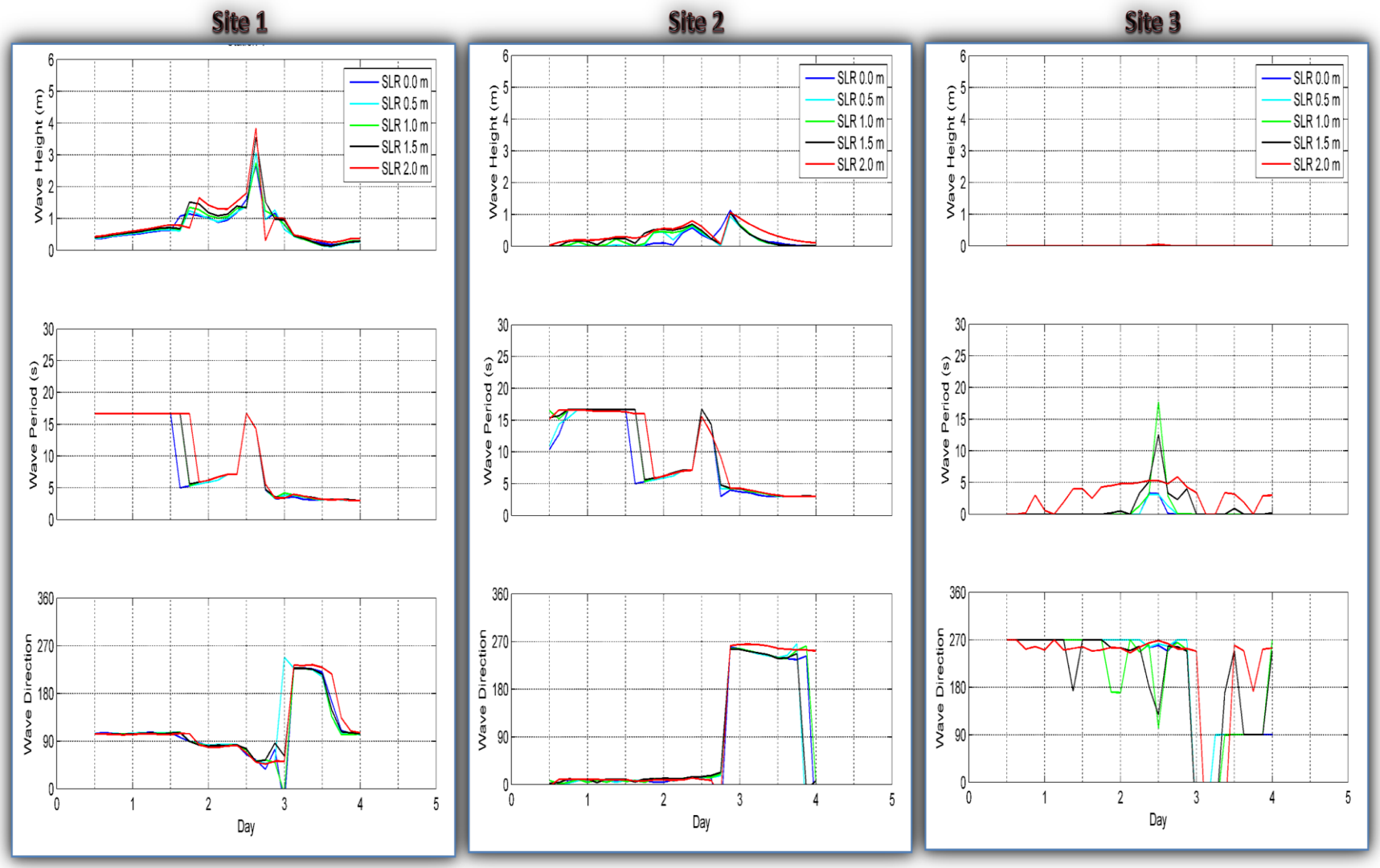

Figure 103. Wave parameters attributed to the 100-yr return interval tropical storm under the five SLR scenarios at *Sites 1*, *2*, and *3*.

The coastal effects on wave propagation were further demonstrated by wave parameters at *Site 2* (Figure 103 above). Small short-period wind waves predominantly propagated from the west under the 0.0 m and 0.5 m SLR scenarios. Long-period swells reached *Site 2* from the north under the 1.0, 1.5, and 2.0 m SLR scenarios. Wave activities on the flooded lands in *Site 3* were insignificant (refer to *Site 3* in Figure 103 above).

4.4.1.3 Sediment Transport

Sediment transport modeling focused both on NSN and the surrounding navigation channels in the Chesapeake Bay. Because a large area of the installation was covered by concrete and buildings, most of the base was represented as "hard bottom" (non-erodible) for the sediment transport calculations (Figure 28 above). In addition, the sandy bottoms in the estuarine system were assigned a median grain size of 0.2 mm in the CMS analyses.

Figure 104 and Figure 105 show the calculated morphology changes (sediment gain or loss) corresponding to the 100-yr return interval storm for 0.0 m, 0.5 m, 1.0 m, 1.5 m, and 2 m SLR scenarios, respectively. Most of the sediment activities occurred along the navigation channels, although the erosion and accretion patterns across the five SLR scenarios were virtually indistinguishable upon inspection. The maximum erosion and accretion values ranged between 3.0 to 3.5 m, with average morphological changes along the channels registered at values less than 1.0 meter. Figure 106 shows the time series of depth changes at *Sites 1*, *2*, and *3*.

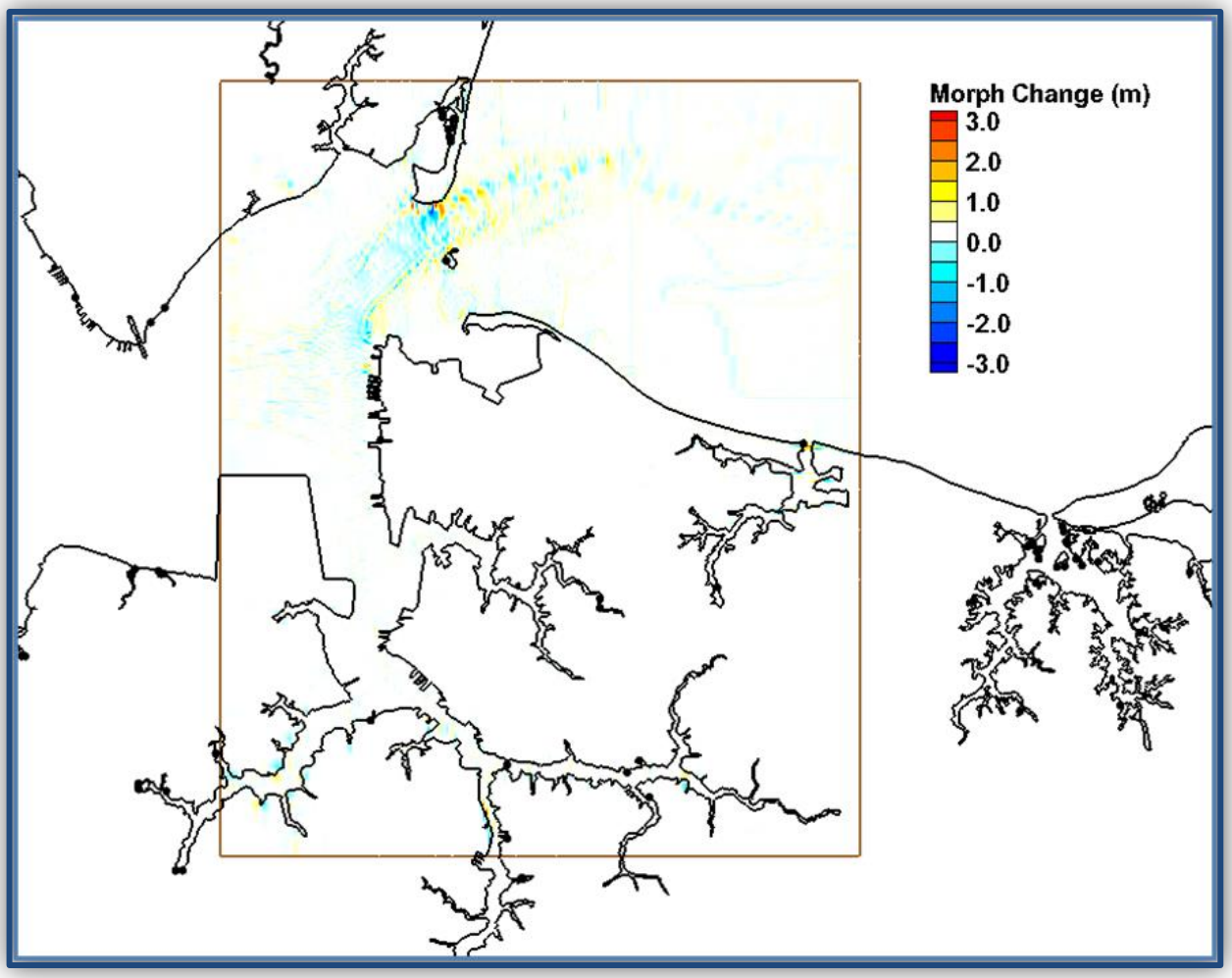

Figure 104. Morphological changes attributed to the 100-yr return interval tropical storm under the existing condition (0.0 m SLR).

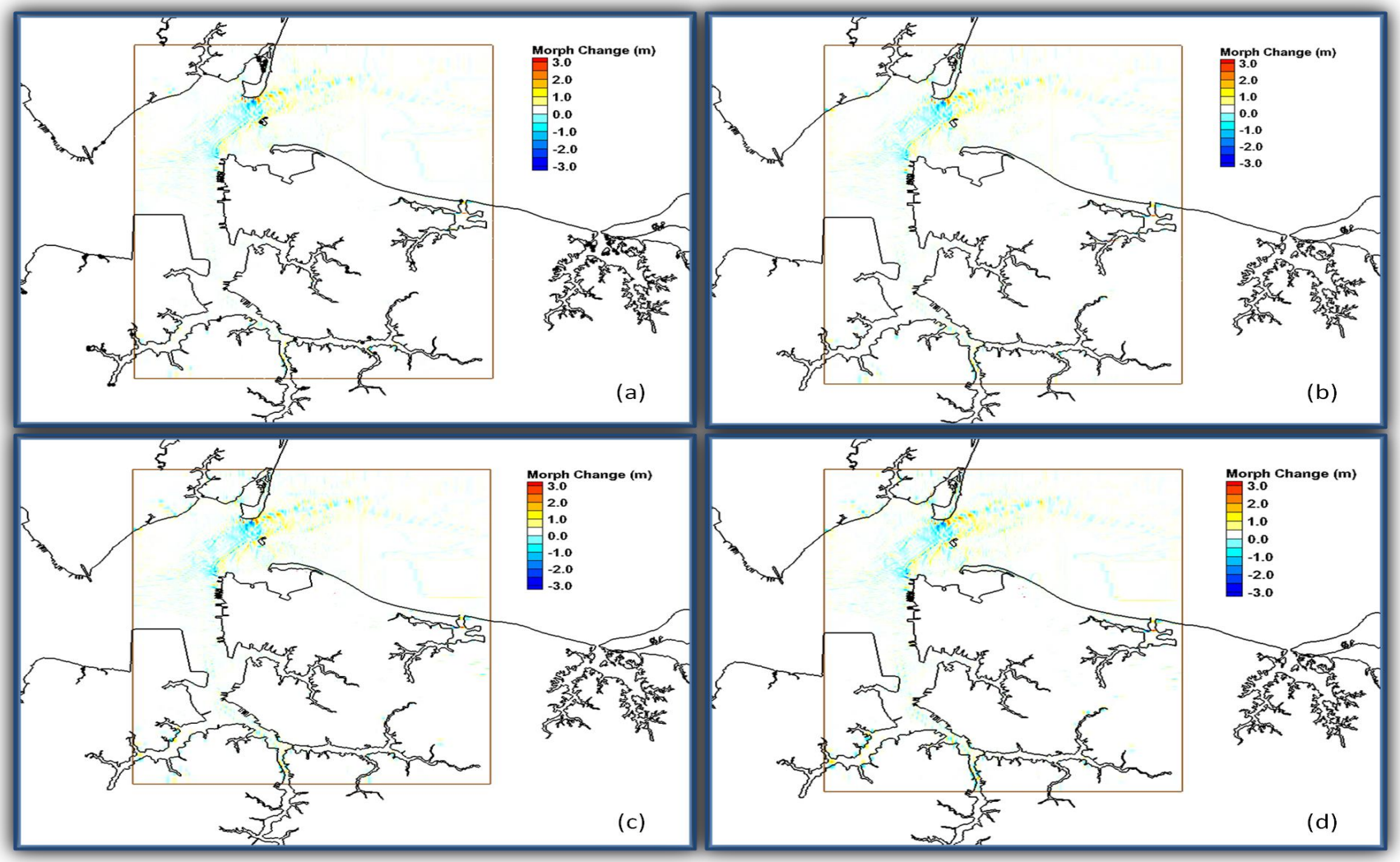

Figure 105. Morphological changes attributed to the 100-yr return interval tropical storm under the (a) 0.5 m, (b) 1.0 m, (c) 1.5 m, and (d) 2.0 m SLR scenarios. Most of the changes were confined to the estuary and channel.

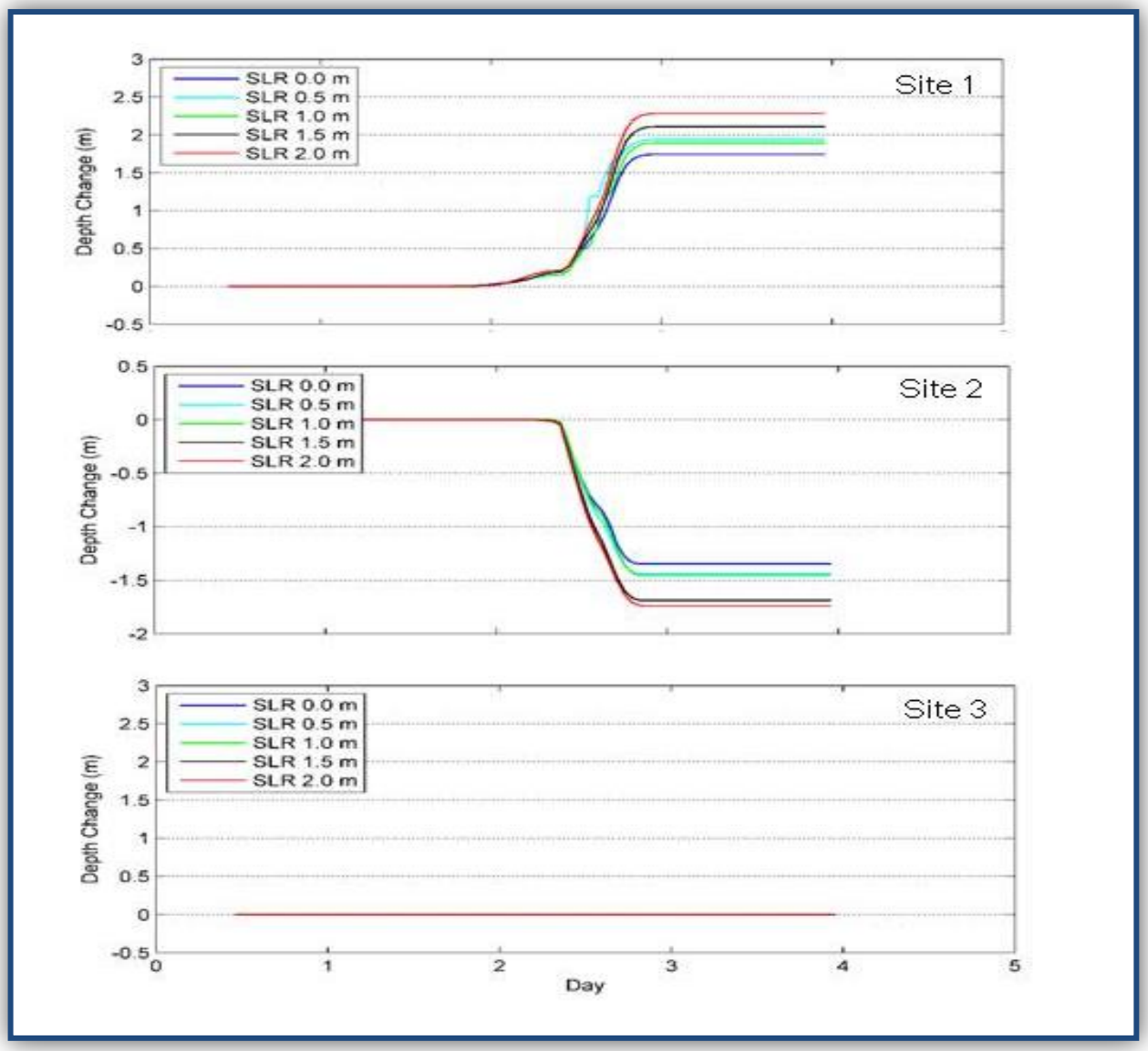

Figure 106. Depth change attributed to the 100-yr return interval tropical storm under five SLR scenarios at *Sites 1*, *2*, and *3*.

More sediment movement occurred in the main navigation channel as a result of the passage of the 100-yr return interval storm. Located on the northern flank of the Hampton Roads navigation channel, Site 1 was shown to be a net accretion site (i.e., in response to increasing SLR, higher deposition rates were experienced). The maximum accretion at Site 1 was approximately 2.3 m under the 2.0 m SLR scenario. Conversely, the 100-yr return interval storm generated a net volume loss at Site 2 (i.e., in response to increasing SLR, higher erosion rates were experienced), a location in the middle of the channel leading to a naval pier. The maximum erosion at Site 2 was approximately 1.7 m under the 2.0 m SLR scenario. Figure 106 above shows no significant sediment activities at the land location (i.e., *Site 3*).

Sediment transport in this system is controlled by currents and waves. Analyzing model output, it is found that the calculated current speeds (not shown here) and wave heights (Figure 67) at Sites 1, 2, and 3 increase with the increase of SLR values. The stronger currents and wave actions result in larger sediment erosion/deposition as shown in Figure 106 above.

To estimate total sediment volume changes in the main navigation channel, a polygon area was pre-delineated as shown in Figure 26. The morphology and bed volume changes within the channel were estimated at the end of the 4-day simulation. Table 32 shows the total sediment volume changes for five storms under the five SLR scenarios.

Table 32. Channel volume changes in Hampton Roads (10^5 m^3) for the five SLR scenarios. Positive values indicate accretion, while negative values indicate erosion.

SLR (m)	1-yr	10-yr	50-yr	100-yr	Nor'easter
0.0	0.155	0.481	-1.195	-2.616	-1.362
0.5	0.139	0.466	-1.354	-2.495	-1.467
1.0	0.050	0.429	-1.346	-3.364	-1.986
1.5	0.601	0.488	-1.686	-3.906	-2.238
2.0	0.700	0.560	-1.664	-4.745	-1.727

Related to currents and waves, erosion was shown to increase with increasing SLR and storm intensity, and a net volume loss (i.e., negative value) was realized with the more intense storms (50-yr+ return intervals).The volume loss for the 100-yr storm virtually tripled that of the 50-yr return interval storm. The 1-yr and 10-yr return interval storms generated small volume changes and a net accretion within the model domain. As the specifications of constant wave parameters for the storms inject some uncertainty into the analyses, the results in Table 32 above simply imply possible channel cleanup due to strong storms and short-term needs for post-storm channel dredging.

4.4.2 Summary and Discussion

SLR will profoundly affect shoreline character and nearshore process, altering coastal and channel morphologies, altering sediment transport, and contributing significantly to coastal inundation and surge. Table 33 and Figure 107 provides an indication of the forcings (maximum surge, accretion, and erosion) generated by the nearshore modeling efforts. These values served as inputs to the follow-on flood modeling analyses, and were in turn directly fed into the structural analyses and risk assessments of the prescribed SLR and coastal storm impacts for the study on NSN. In actuality, individual forcing values were generated across the model domain at the mesh element or cellular level (the non-uniform rectangular grids cells with 10+ m resolution) for each scenario. But, it is useful to explore the maximum forcings generated over the installation to grasp the magnitude of change experienced across the range of scenarios. As expected, increasing levels of SLR generated ever-increasing levels of storm surge and wave forces, while accretion and erosion rates varied with storm intensity and SLR depths threatening the integrity of built infrastructure on the installation.

Table 33. Final maximum storm forcings generated by the nearshore assessment for this study based on the five storms. NE refers to the 1982 Nor'easter. [4]

Storm Return Interval	Nearshore Assessment (CMS)														
	Surge + Tide Height (m)					Accretion in Channel (m)					Erosion in Channel (m)				
	SLR Scenario					SLR Scenario					SLR Scenario				
	0.0	**0.5**	**1.0**	**1.5**	**2.0**	**0.0**	**0.5**	**1.0**	**1.5**	**2.0**	**0.0**	**0.5**	**1.0**	**1.5**	**2.0**
1	1.2	1.7	2.1	2.6	3.0	1.0	1.4	1.7	1.9	1.7	1.0	1.3	1.5	1.6	1.4
10	1.7	2.1	2.6	3.1	3.6	2.0	2.0	2.4	2.6	3.2	2.0	1.9	2.3	2.6	2.4
50	2.2	2.8	3.2	3.7	4.1	3.5	3.6	3.6	3.6	3.5	3.0	3.2	3.2	3.2	3.2
100	3.6	4.1	4.5	5.0	5.4	4.0	3.6	3.5	3.6	3.7	3.5	3.4	3.3	3.5	3.7
NE	2.3	2.9	3.3	3.8	4.2	2.5	2.2	2.2	2.5	2.5	2.0	1.9	1.8	2.0	2.0

[4] Not surprisingly, the surge results generated by CMS for the 50- and 100-yr storms were similar to those produced by the ADCIRC/SWAN analyses - both models are based on the same governing equations.

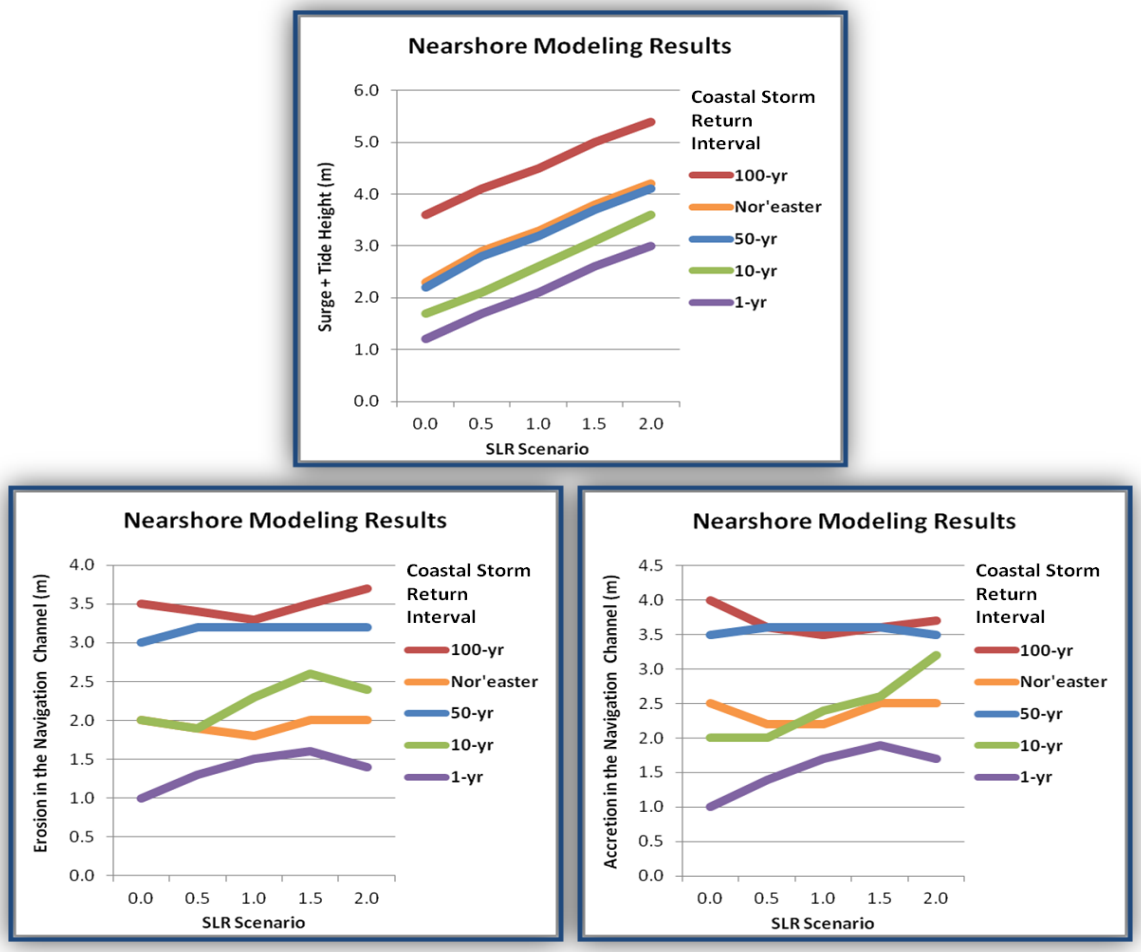

Figure 107. Final maximum storm forcing trends generated by the nearshore assessment for this study based on the five analyzed storms under the five prescribed SLR scenarios.

4.5. Surface Flood Routing Assessment

4.5.1 Outputs and Technical Results

The surface flood routing simulations generated temporal water depths at every grid cell of the study area for each design storm and SLR scenario.

4.5.1.1 Initial Flooding due to SLR Only

Prior to running the flood simulations, an analysis was completed to determine the flood extent due solely to rise in MSL. Figure 108 depicts the SLR-induced flooding at on the study site under the prescribed SLR scenarios.[5]

[5] Note that causality (rising sea levels due to glacial melt, currents, ocean expansion, subsidence, etc.) were ignored in these analyses. Refer to Boon et al. 2010 and Boon 2012 for detailed discussions on this subject.

Figure 108. Flood extent due to rise in sea level only.

4.5.1.2 Flooding Due to SLR, Sea Surge, and Precipitation

As previously mentioned, the GSSHA model simulated the effects of SLR, sea surge, and precipitation on the NSN. In total, five SLR scenarios (0.0 m – 2.0 m) and five storm events (viz. 1-yr, 10-yr, 50-yr, 100-yr return interval tropical storms, and the October 1982 Nor'easter) were simulated making a total of 25 runs (Figure 109 - Figure 113). The temporally- and spatially-varied results were post-processed to determine the maximum flood depth in each cell over the entire simulation.

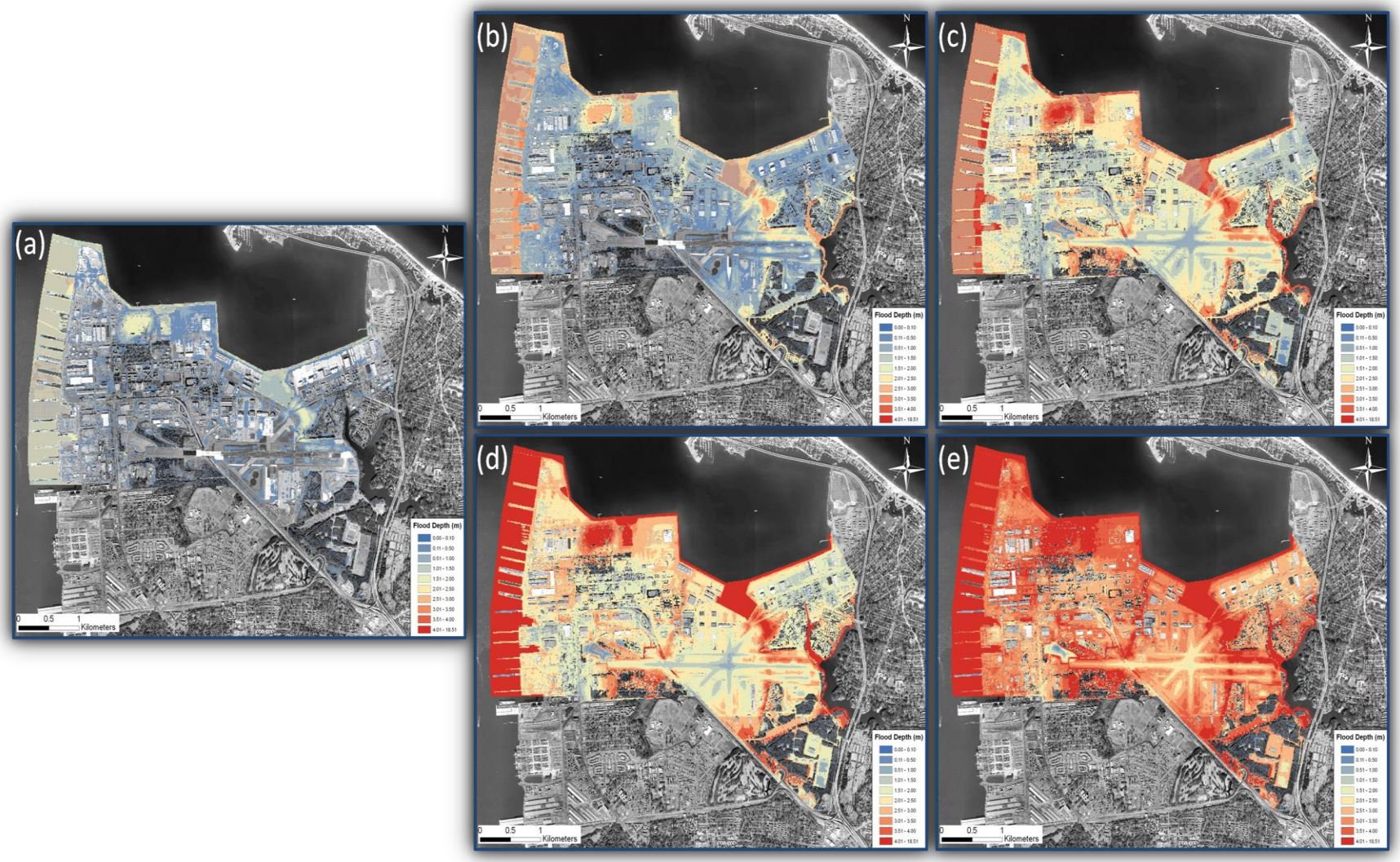

Figure 109. Flood routing and maximum depths (m) under the 1-yr return interval storm event for SLR 0.0 m (a), SLR 0.5 m (b), SLR 1.0 m (c), SLR 1.5 m (d), and SLR 2.0 m (e) scenarios.

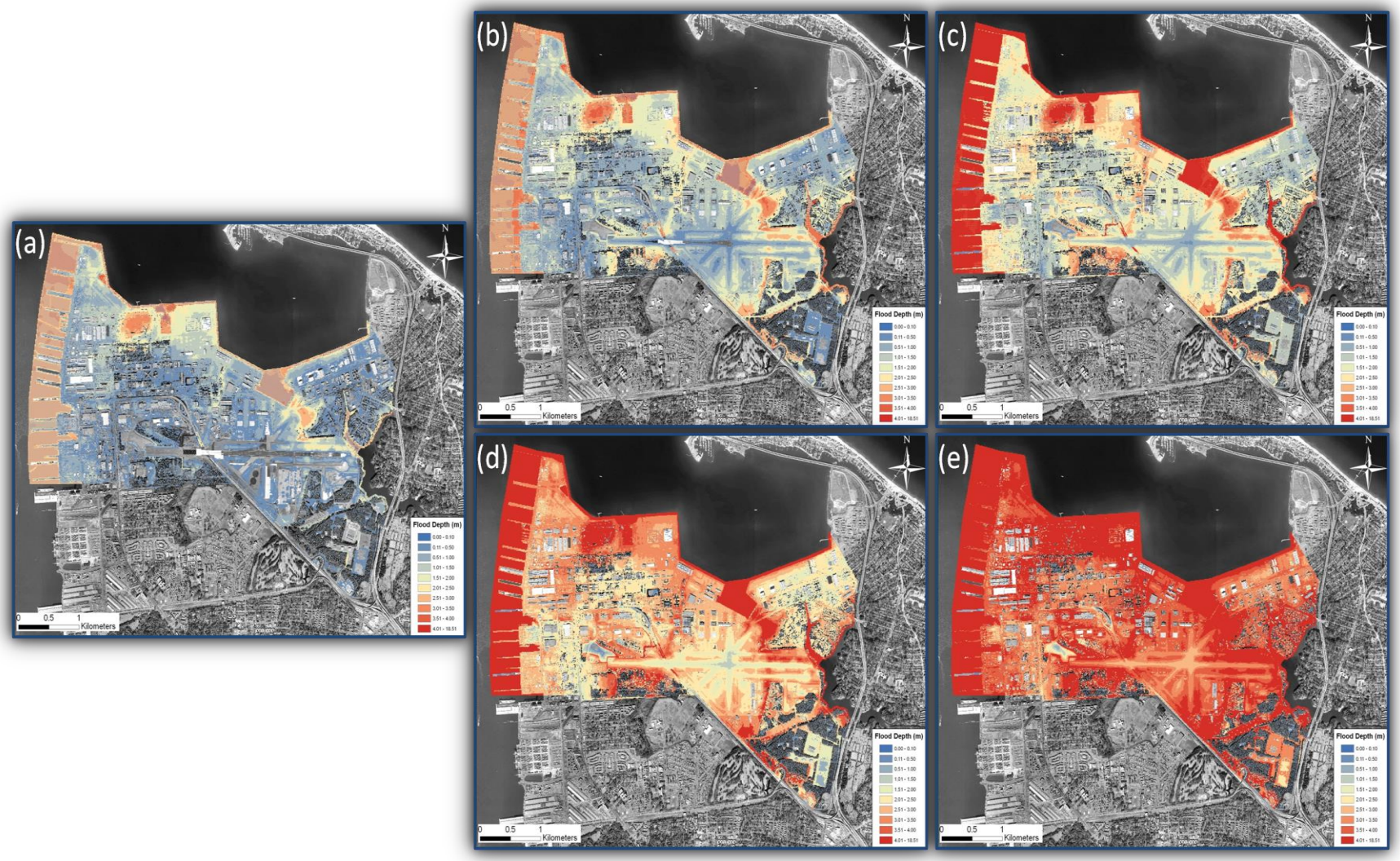

Figure 110. Flood routing and maximum depths (m) under the 10-yr return interval storm event for the (a) 0.0 m, (b) 0.5 m, (c) 1.0 m, (d) 1.5 m, and (e) 2.0 m SLR scenarios.

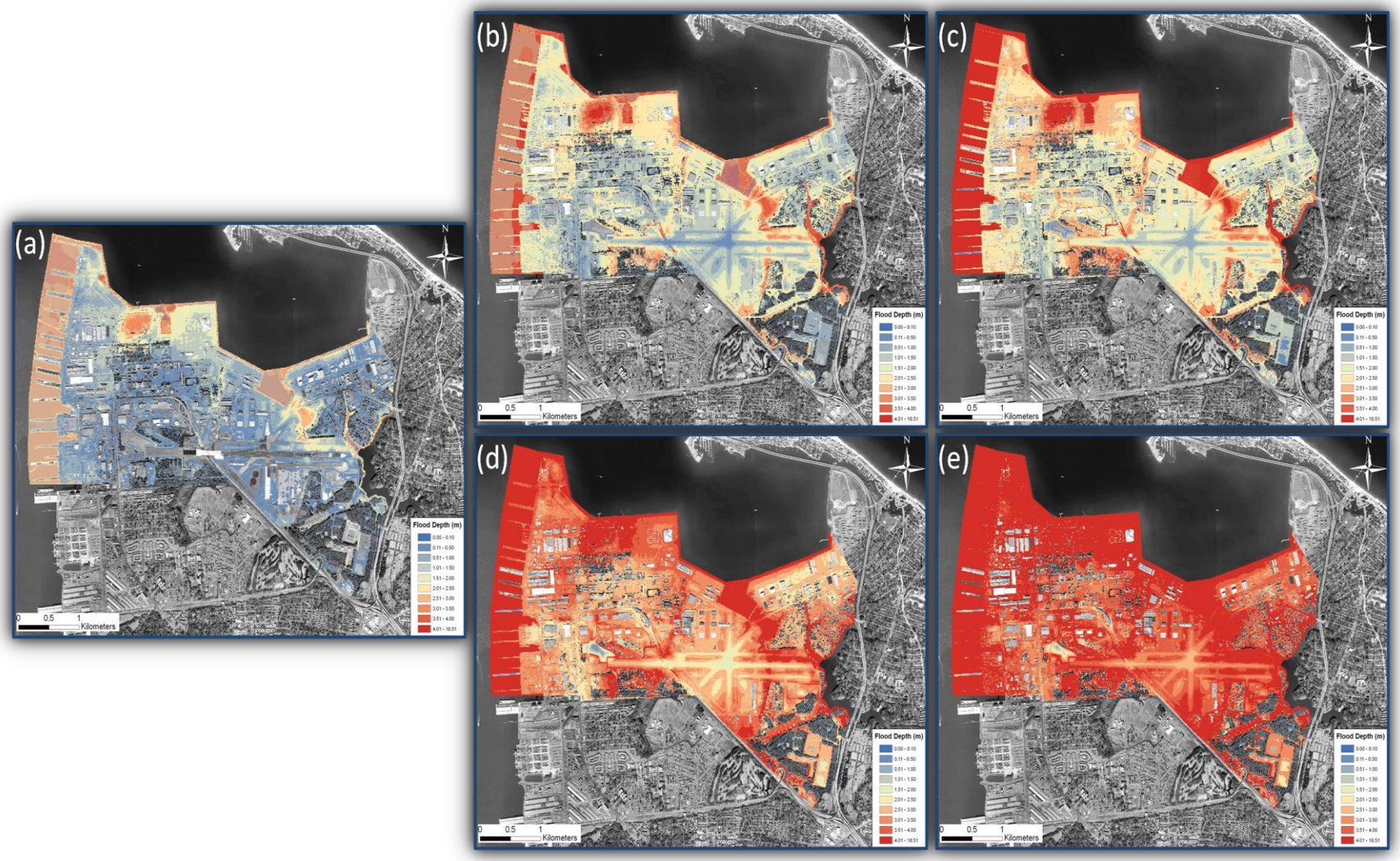

Figure 111. Flood routing and maximum depths (m) under the 50-yr return interval storm event for the (a) 0.0 m, (b) 0.5 m, (c) 1.0 m, (d) 1.5 m, and (e) 2.0 m SLR scenarios.

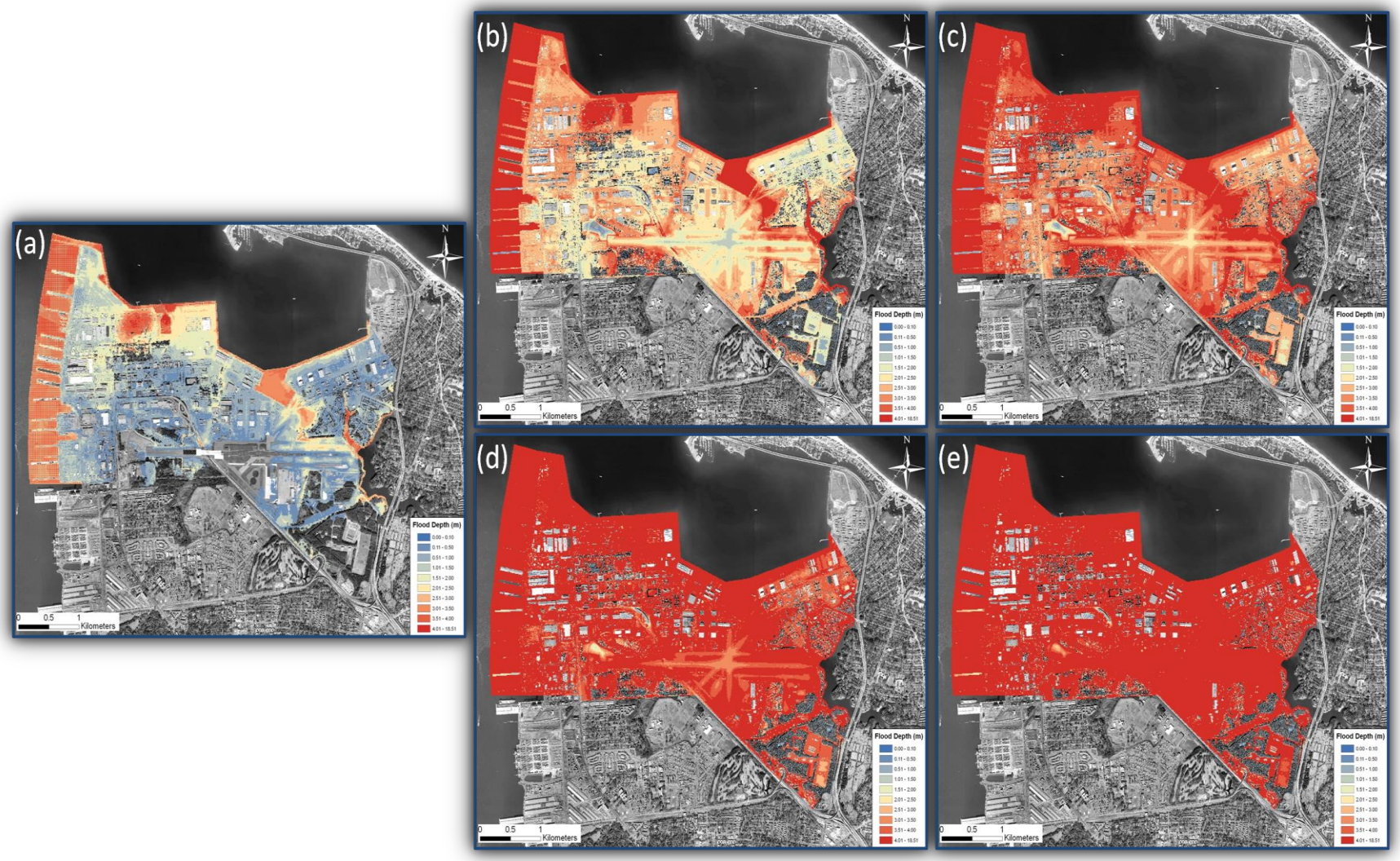

Figure 112. Flood routing and maximum depths (m) under the 100-yr return interval storm event for the (a) 0.0 m, (b) 0.5 m, (c) 1.0 m, (d) 1.5 m, and (e) 2.0 m SLR scenarios.

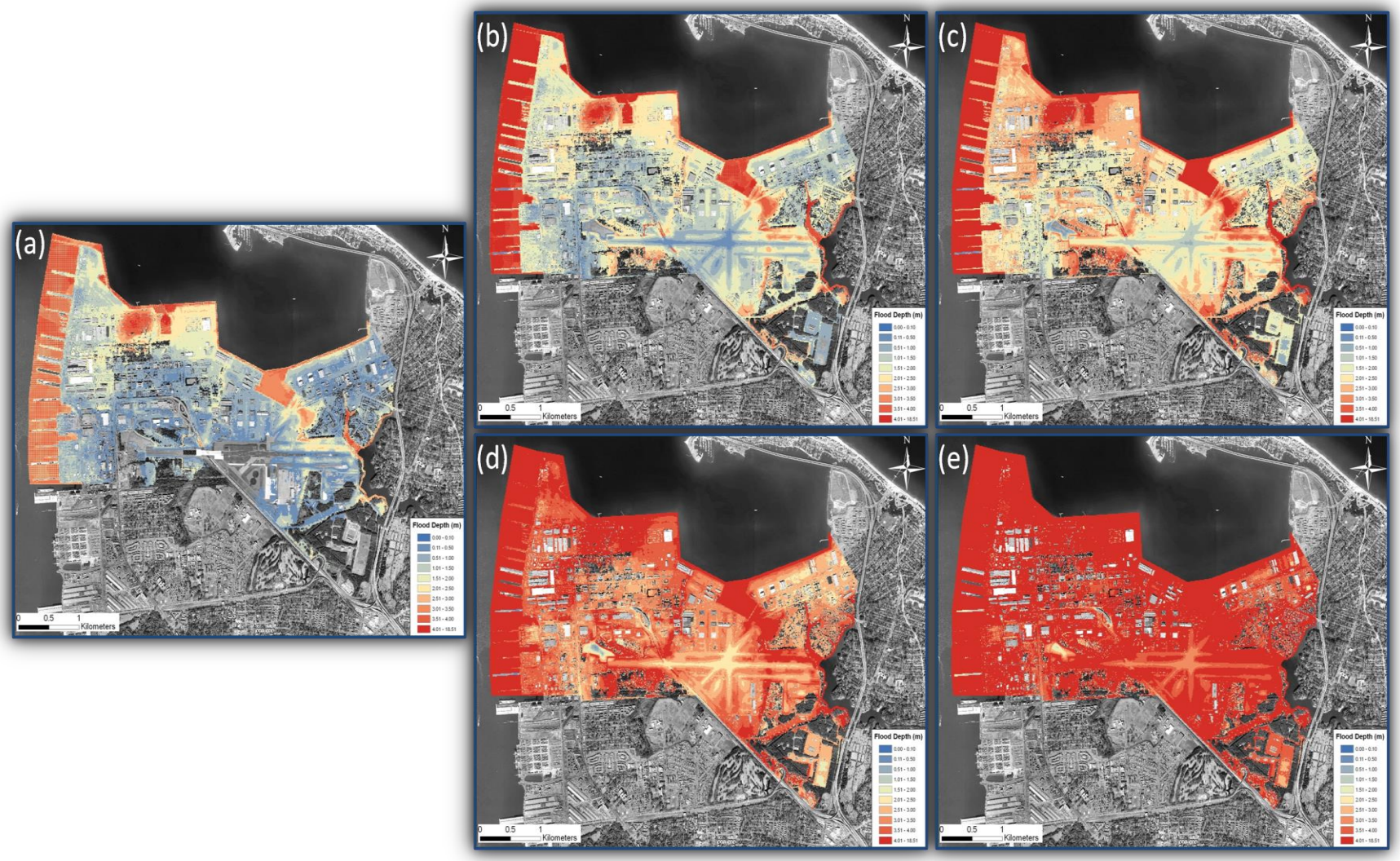

Figure 113. Flood routing and maximum depths (m) under the historical 1982 nor'easter event for the (a) 0.0 m, (b) 0.5 m, (c) 1.0 m, (d) 1.5 m, and (e) 2.0 m SLR scenarios.

No water depth measurement data were available within the study area with which to calibrate the model results for the 0.0 m SLR results. However, the 1-yr 0.0 m SLR scenario represented an average "worst storm of the year" condition. The model results depicted in Figure 109 (a) and anecdotal descriptions of conditions during heavy rainfall events at the installation can provide a qualitative comparison of model results to reality. In the early stages of the project, we held discussions with NSN public works personnel regarding the performance of the drainage network during heavy rain conditions at the site. They indicated that local street flooding up to depths of six inches or more is a common occurrence during heavy rains across the installation, particularly in low-lying areas. The results shown in Figure 109 (a) appear consistent with this description.

4.5.2 Summary and Discussion

When coastal storms make landfall on or near coastal installations, rising sea levels have significant potential to exacerbate the magnitude of inland flooding on a large scale. Increased precipitation patterns and aging infrastructure (particularly inadequate or ineffective storm drainage networks such as those seen on the study site) will only serve to heighten the potential risks and threaten the future sustainability of critical assets and mission capabilities. Table 33 and Figure 107 offer estimated characterizations of the forcings (maximum water depths) generated by the surface flood routing modeling efforts. These values were delivered to the structural analyses and risk assessments as response to the prescribed SLR and coastal storm impacts for the study on NSN. In actuality, individual forcing values were generated across the model domain at the mesh element or cellular level ($10m^2$ grid cells) for each scenario. But, it is useful to explore the maximum forcings generated over the installation to grasp the magnitude of change experienced across the range of scenarios. As expected, increasing levels of SLR generated ever-increasing depths of flooding with increasing with storm intensity and SLR depths thereby threatening the integrity of built infrastructure on the installation.

Table 34. Final maximum storm forcings generated by the surface flood routing assessment for this study based on the five analyzed storms.

Storm Return Interval	Surface Flood Routing Assessment (GSSHA)				
	Maximum Water Depths (m)				
	SLR Scenario				
	0.0	0.5	1.0	1.5	2.0
1	2.4	3.7	4.8	5.0	6.3
10	3.4	4.3	5.3	5.5	6.8
50	3.9	4.6	5.5	6.1	7.2
100	4.8	5.6	6.6	7.8	9.1
Nor'easter	4.2	4.4	5.6	6.5	7.8

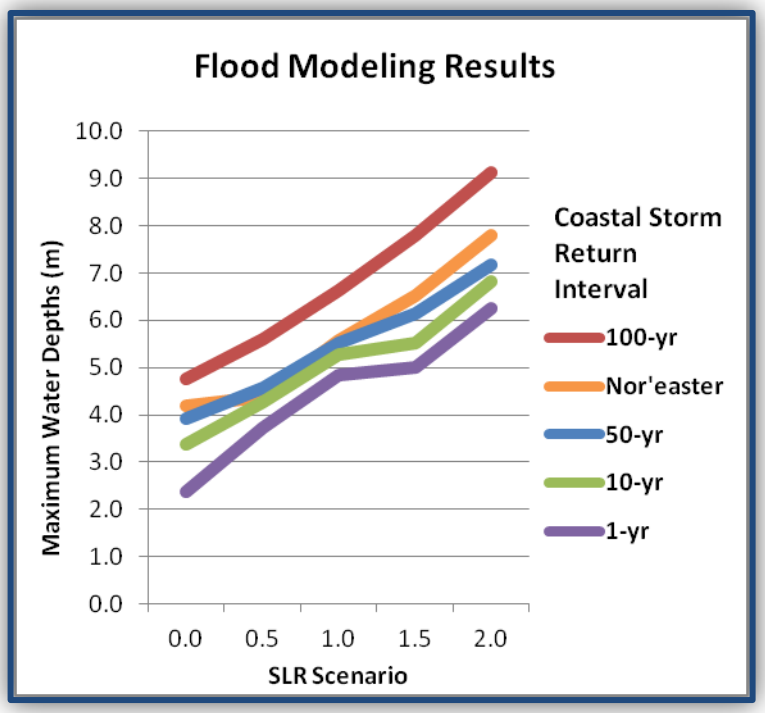

Figure 114. Final maximum water depth forcing trends generated by the surface flood routing assessment for this study based on the five analyzed storms under the five prescribed SLR scenarios.

4.6. Mission Decomposition and Asset Capability Network

This section contains descriptions of the analysis and decomposition for the NSN study. Because this section was intended for public release, the information below has been summarized, and does not provide details of specific assets or vulnerabilities. Specific information about assets is contained in FOUO supplemental materials.

4.6.1 Decomposition and Operationalization of the ACN

Decomposition of the mission and operationalization[6] of the ACN required the identification of individual capabilities supporting the missions on NSN as well as key or critical assets contributing to the capabilities on the site. For purposes of this study, seven individual capabilities were decomposed into their contributing assets on NSN including:

1) Providing physical access to the berths,
2) Providing the berthing spaces themselves,
3) Removal of wastewater,
4) Removal of oily waste,
5) Providing potable water,
6) Providing electric power, and
7) Providing steam.

Below the details of the decompositions are provided.

4.6.1.1 Provide Physical Access to Berths

For purposes of this study, the *Support Ship Harbor Movements* mission at NSN was dependent solely on the *Provide Physical Access to Berths* capability. In essence, this meant that the mission would only be fulfilled if ships could safely navigate from the open ocean to berthing spaces through channels of sufficient depth and width. In general, it was assumed that a rise in sea level would result in deeper channels, which was considered a positive benefit. However, it was conceivable that changes in geomorphology during storm events would have negative impacts to the mission – specifically increased sedimentation that would impede navigation of the harbor approaches. Figure 115 illustrates the dependency of the *Support Ship Port Harbor Movements* mission on the three navigation channels considered in this study.

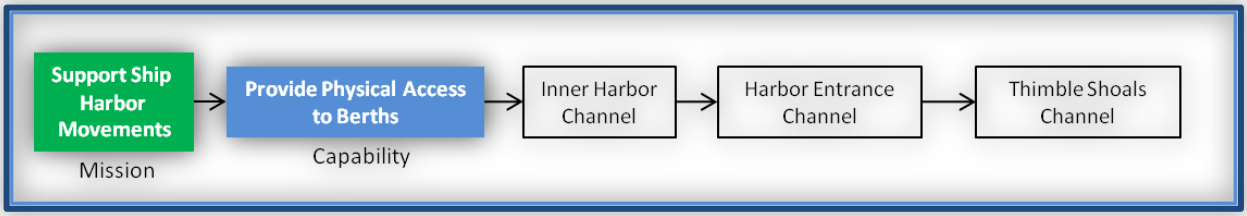

Figure 115. Asset decomposition and dependency flow diagram detailing the provision of physical access to berths at NSN.

4.6.1.2 Provide Berthing Space

For purposes of this study, the *Provide At-Berth Support* mission at NSN was dependent in part on the *Provide Physical Access to Berths* capability. Naval ships at NSN were moored in "berthing spaces" alongside piers that protruded perpendicularly from the shore out into the

[6] Defining the infrastructure network so that it can be measured or expressed quantitatively.

channel. These berthing spaces were designed to provide adequate depths to float the ships at low tide, and with sufficient freeboard (height from water's surface to the top of the pier) to allow fenders or camels to ride against their sides for the purpose of holding the ships away from the pier. For study purposes, we chose to focus on the NSN missions addressing aircraft carriers (CVNs), and focused solely on Piers 11, 12, or 14 which provided berth and support for these larger ships. The CVNs had a 41-ft maximum draft, and maintenance dredging was deployed to maintain a 51-ft maximum berthing depth. CVNs had cooling water intakes on the bottom of their hull that required adequate depths below their keels to avoid ingesting debris and bottom dwelling marine life. Note that the NSN had a particular problem with "hydroids," small animals that were plentiful on the harbor bottom, and posed a particular threat to these activities. Figure 116 shows the principal components analyzed, including Piers 11, 12, and 14, and their associated berthing spaces.

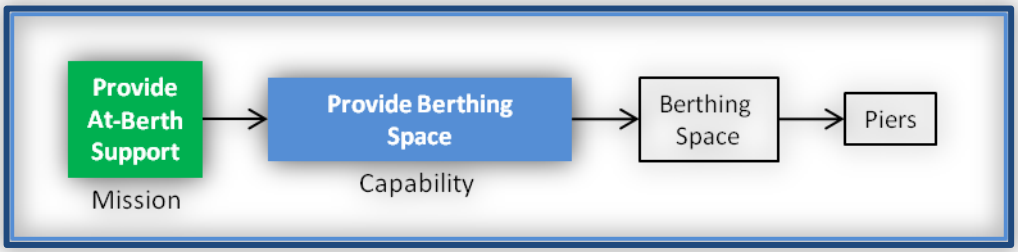

Figure 116. Asset decomposition and dependency flow diagram for the berthing spaces at NSN.

4.6.1.3 Remove Wastewater

For purposes of this study, the *Provide At-Berth Support* mission at NSN was also dependent in part on the *Remove Wastewater* capability. When CVNs were in port, they diverted wastewater from their onboard tanks and treatment plants to dedicated lines located on the piers. Wastewater was generated from food preparation, showers, laundry, ship cleaning, and bathroom facilities. The amount collected was dependent on the number of sailors on-board the ship and the type of ship. This wastewater was pumped off the ships through flexible hoses to pump houses near the piers. The wastewater system on NSN was a gravity system, i.e., the mixed liquids and solids flowed through sloped pipes by gravity to lift station wet sumps, where pumps raised the effluent to a secondary pipe network, where it again flowed by gravity to the main municipal lift station, and eventually flowed out to the civilian wastewater treatment plant. The pumps at the lift stations relied on electricity to operate. All lift stations included in the analysis were supported by individual backup generators to maintain operation in the event of power failure. The pump motors were located in underground dry sumps adjacent to the wet sumps. The principal components of the wastewater system analyzed in this study included gravity drains (i.e., specifically the sections on Piers 11,12, and 14), lift stations (pumps and structures), backup generators, and dedicated transformers (Figure 117).

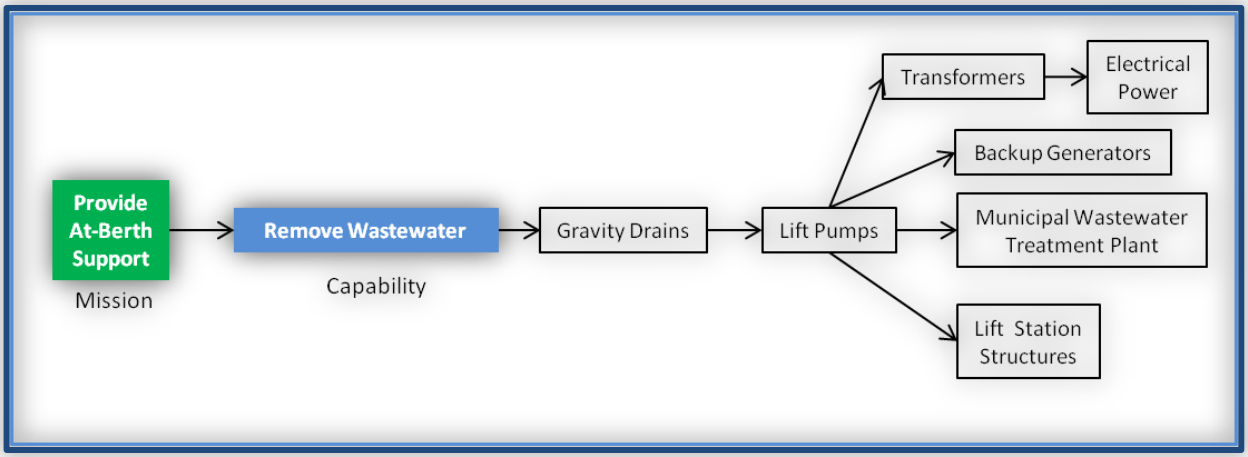

Figure 117. Asset decomposition and dependency flow diagram for the wastewater removal system on NSN.

4.6.1.4 Remove Oily Waste

For purposes of this study, the *Provide At-Berth Support* mission at NSN was also dependent in part on the *Remove Oily Waste* capability as well. Machinery in the CVNs required various forms of petroleum lubricants that had to be changed and that often leaked and collected in the bilges (bottom) or other spaces. Proper disposal of this oily waste was mandatory. The NSN Piers 11, 12, and 13 were equipped with a dedicated oily waste collection system similar to the wastewater system described above. Oily waste was pumped off the ships through flexible hoses that flowed by gravity drain to oily waste sumps adjacent to the waste water sumps, and then out to an oily waste storage tank. Periodically, the stored oily waste was pumped to nearby Craney Island via a buried line, where it was processed and returned to the station via barge to be burned at the boiler plant. The principal components of the oily waste system analyzed for this study included the oily waste gravity drains (the sections on piers 11, 12, and 14), the lift stations (pumps and structures), the backup generators (for Piers 12 and 14), and the dedicated transformers (Figure 118).

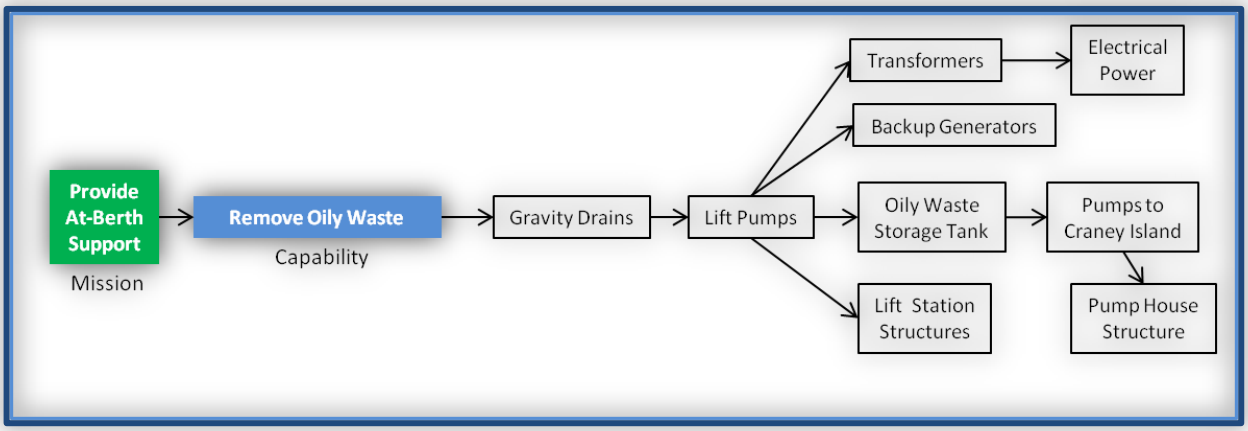

Figure 118. Asset decomposition and dependency flow diagram for the oily waste removal system on NSN.

4.6.1.5 Provide Potable Water

For purposes of this study, the *Provide At-Berth Support* mission at NSN was also dependent in part on the *Provide Potable Water* capability as well. CVNs at NSN required substantial amounts of potable water for drinking, food preparation, showers, and laundry with the amount required dependent on the number of sailors onboard each ship. The City of Norfolk provided water to NSN through multiple connection points. There were two potable water storage tanks in use on NSN. Booster pumps were used to provide additional pressure to the station distribution and firefighting systems. The key system components considered included the water tanks, the booster pumps, the backup systems, and the water distribution system. The distribution system was buried underground, so only the pipes that extended out onto Piers 11, 12, and 14 were considered. Figure 119 illustrates the dependency structure of the NSN potable water system.

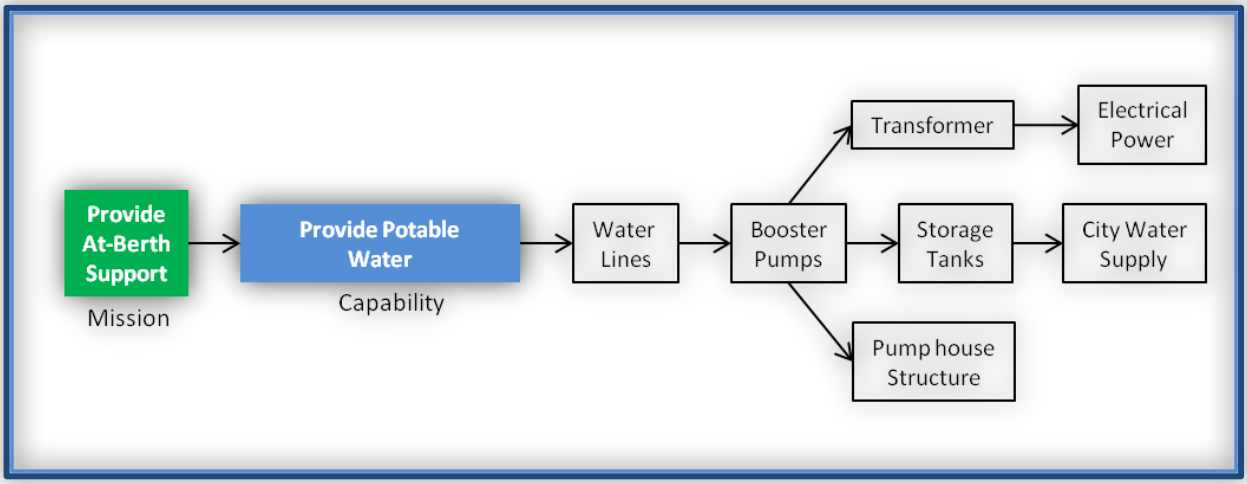

Figure 119. Asset decomposition and dependency flow diagram for the potable water distribution system on NSN.

Note that the booster pumps depended on electrical power (an engine-driven booster pump was available as well). Each of the pump houses had dedicated electrical transformers nearby. Note that the pumps were also dependent on the two pump house structures as well, with the assumption that the collapse of a pump house would cause the booster pumps (or their controls) to become inoperable.

4.6.1.6 Provide Electric Power

For purposes of this study, the *Provide At-Berth Support* mission at NSN was also dependent in part on the *Provide Electrical Power* capability as well. CVNs at NSN required electrical power while in port in order to remain operational. They generally extracted power from the piers where they were moored (i.e., *shore power*), even though they had the capability to generate power using onboard equipment. Generating power onboard, however, was less efficient, produced emissions, and required additional crew to be present to stand watch. In addition, onboard electrical power generation was not available if the equipment was being serviced while the ship was in port. Commercial power was delivered by Dominion Virginia Power through an

electrical power transmission system supplied by a large number of redundant generating stations, with the nearby Surry Nuclear power plant the closest large station. Power came onto the station from off base. The principal components analyzed for this study included various substations on NSN, the distribution lines, and several critical transformers (Figure 120).

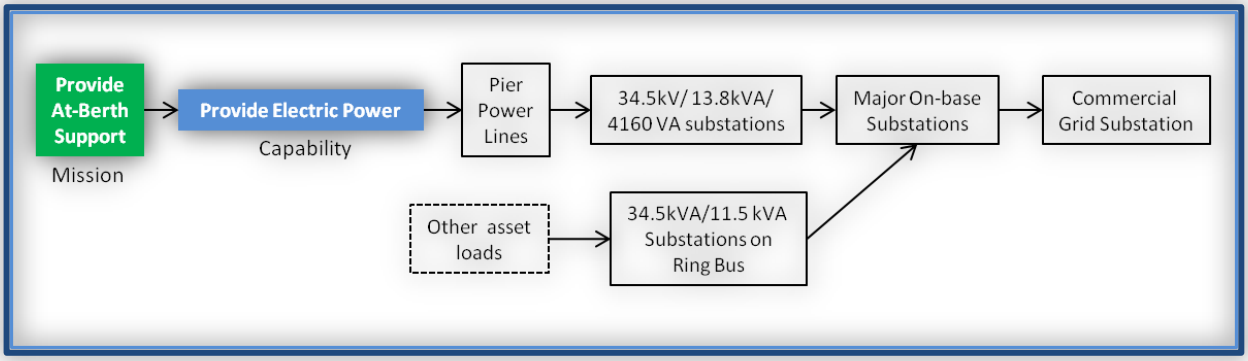

Figure 120. Asset decomposition and dependency flow diagram for the electrical power distribution system on NSN.

For purposes of this analysis, a substation was defined as a set of transformers, switch gears, and control equipment grouped together. Dependency was analyzed for shore power to the ships on Piers 11, 12, and 14, as well as to other assets that required electrical power. Power fed directly to the ships was provided at 480 Volts, 4160 volt amperes (VA), or 13.8 kVA (kilo volt amperes, thousand VA). For CVNs specifically, only 4160 VA or 13.8 kVA (i.e., *Ford Class*) was required. Although many of the piers had 480V distribution onboard, the 480V distribution subsystem was disregarded because it was not needed by the CVNs (i.e., the primary focus of this study). Other assets on the station were either fed from a 34.5 kVA distribution network or from an 11.5 kVA network. The electrical system on the station was robust and highly redundant, including a ring bus architecture on the 11.5 kVA network with the ability to feed substations through multiple paths. Power lines were buried and waterproofed on the station, so only lines leading onto the piers were considered at risk. The primary threat to the substations was assumed to be flooding induced by storm surge and SLR, so we focused exclusively on identifying the elevations at which transformers and switch gear were exposed to these hazards. In theory, electrical equipment (i.e., transformers) inundated with salt water could be rinsed with deionized water, dried, and restored to service, as long as they were not energized when flooded. In some cases, individual transformers were significant contributions to other asset loads, so they were incorporated into the analysis as well.

4.6.1.7 Provide Steam

For purposes of this study, the *Provide At-Berth Support* mission at NSN was also dependent in part on the *Provide Steam* capability as well. CVNs at NSN used steam for propulsion and auxiliary purposes such as cooking, heating, hot water, compressed air, and electrical power generation. In port, steam was provided at 150 pounds per square inch (psi) so that the onboard reactors could be shut down (i.e., *cold iron*). As with the electrical power generation, it was possible to run the reactors in port, but required engineering watches to maintain equipment.

CVNs required 5000-7000 pounds per hour of steam. Steam for the ships (and facility heating) was produced at two boiler plants located on the station. The boilers in the plants were normally fired by natural gas, with some dual fuel capabilities. Dual fired boilers primarily used natural gas but would also run on #5 Fuel oil. Fuel type use was determined by economics. Once the steam was produced, it was distributed to the ships through 250 psi steam pipelines that were elevated and mounted on reinforced concrete columns (pylons). Steam for the ships was reduced to 150 psi before going underground to the piers. Unlike the underground power lines, water lines and waste lines, the above-ground, exposed nature of the steam lines meant that they were critical to the vulnerability analysis. The principal components of the steam system analyzed in this study included the steam lines (on-pier, 150 psi, and 250 psi), the natural gas supply, the boilers, the fuel tanks, the fuel pumps, the backup generators, the substations, and the potable water system. As can be seen in Figure 121, the steam system was highly dependent on other infrastructure systems.

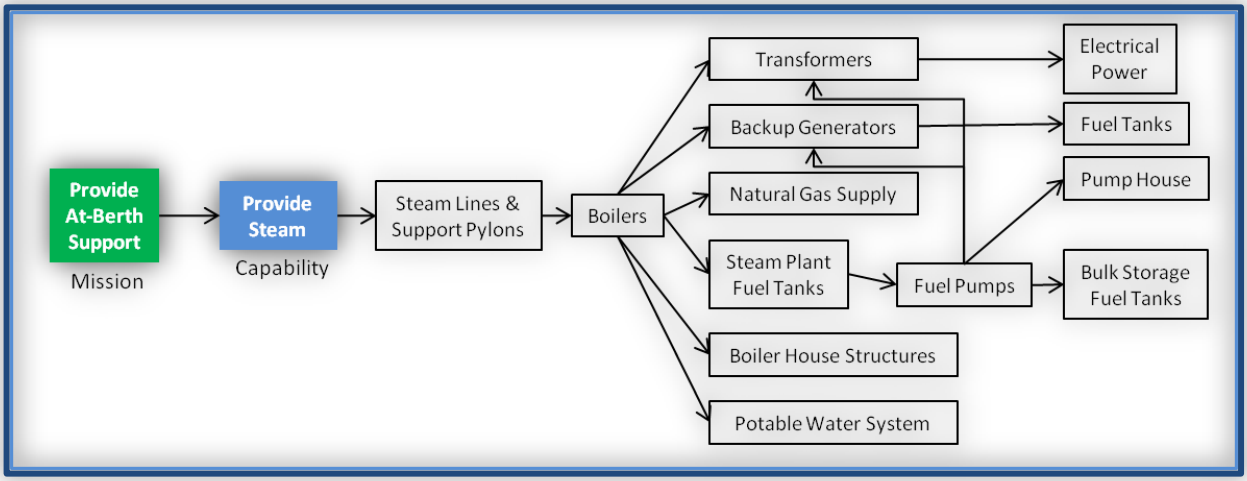

Figure 121. Asset decomposition and dependency flow diagram for the steam distribution system on NSN.

Note that natural gas was supplied by the Virginia Natural Gas Company. Other than buried natural gas lines and a connection point at each boiler plant, there was no relevant natural gas infrastructure on the station. There were two large diesel storage tanks at one of the plants. These storage tanks received # 5 fuel oil and reclaimed oil from three bulk storage tanks. At this same plant, diesel fuel for the backup generators was stored in the two day tanks.

4.6.2 Summary and Discussion

It was important to note that the results of this study, particularly the analysis of structural vulnerability of the NSN's assets, were considered *For Official Use Only (FOUO)*, and as such could not be released to the general public. Suffice it to say that the individual decomposed capabilities and their supporting systems were mapped and then assessed both individually (at the asset level) and systematically (at the system and capability levels) using a standard GIS network schema. Note that we used engineering judgment to determine the level of detail to use in the Geographic Information System (GIS) to quantify operability, damage, and remediation on

a case-by-case basis. Products such as that shown in Figure 122 have been developed for the installation to assist in the planning and assessment of asset vulnerability and risk in the face of coastal storms and SLR.

Figure 122. A hypothetical example of a mapping product that could be generated using the approach detailing an asset distribution system that provides resources (e.g., electricity, water, steam, etc.) to the piers on a naval installation.

The intent of study was to demonstrate a capability to characterize asset fragility and quantify the risk to mission impairment under the threat of SLR and coastal hazards at a meaningful, actionable scale using a systems approach. Although not apparent in Figure 122 above, each system was composed of numerous assets that were mapped on a 10-m grid scale (Figure 123), and a set of heuristics were developed to handle instances where assets spanned multiple grid cells or where multiple assets were dependent upon one another to produce a capability.

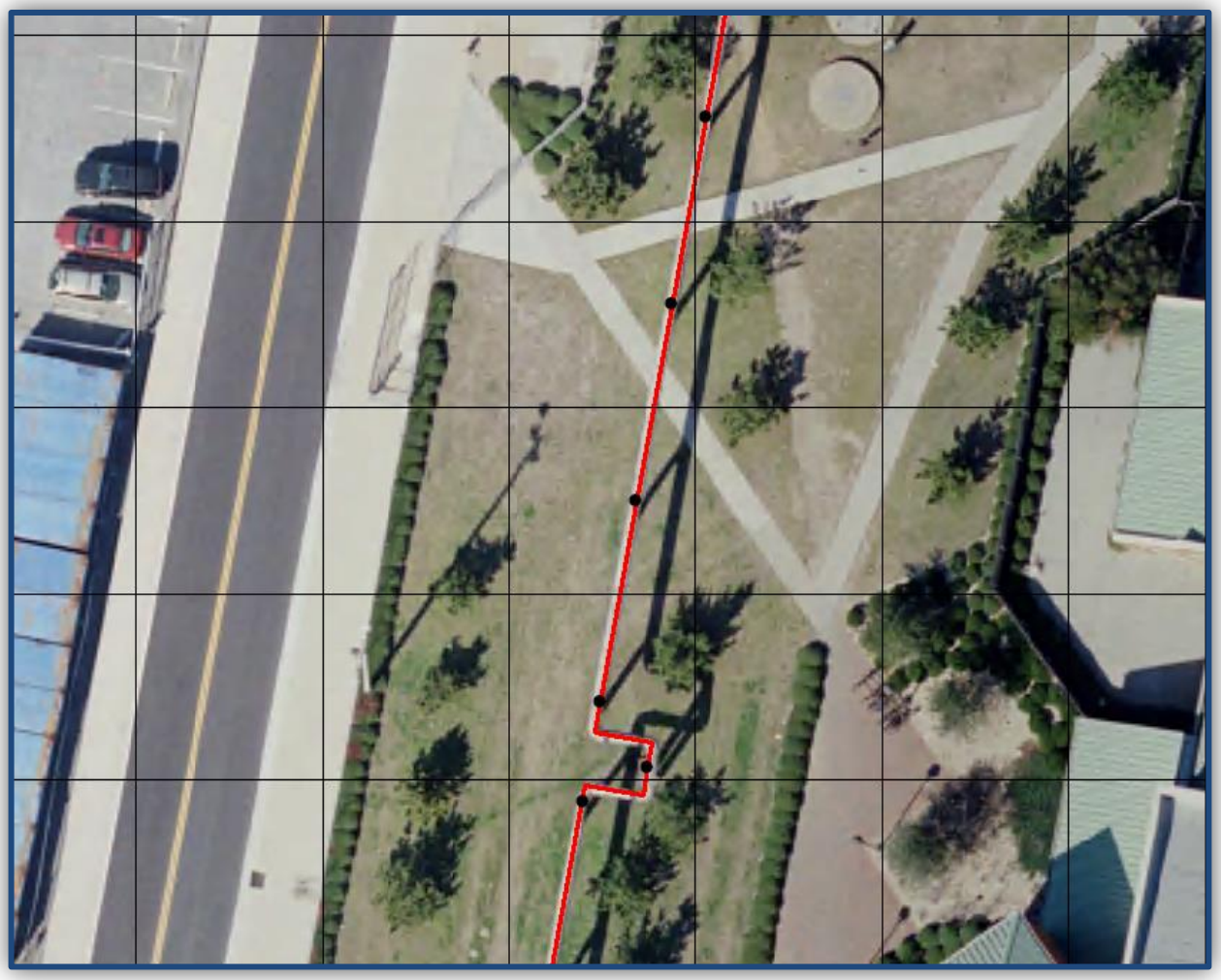

Figure 123. Example of the mapping products that have be generated by the study using the GIS-based ACN approach. Here, a small portion of the resource distribution system is represented in red, while supporting columns are represented as black dots.

For example, the distribution line shown in Figure 123 above (i.e., the red line) ran at an angle to the grid. Inspection showed that some grid cells had one column or support (i.e., represented by a black dot), one cell had two supports, and one cell had none. A heuristic was deployed assigning asset fragility to the column(s) in each cell. Probability of damage to the section of pipe in the cell was quantified based on the functional integrity not only of the supports within the cell, but also by those in adjacent cells as a true network schema. Damage to the assets, a segment of pipe or conduit spanning many cells, was based on the quantification of damage to its parts described as the number of fractures, while operability was determined based on a damage function and the operability of assets that each pipe or conduit was dependent upon. In the end, the asset composition and network schema were used to characterize structural fragility in the probabilistic assessment of mission impairment under the various SLR and storm scenarios.

4.7. Structural Assessment of Critical Infrastructure

A total of seven capabilities or systems and 22 assets were analyzed to generate results for the study. As was mentioned earlier, the technical results of the structural assessment were considered *FOUO*, but an example of one generic outcome has been offered here to demonstrate the approach and illustrate the effort expended to generate outputs for the risk analysis.

Pumps such as those shown below in Figure 124 were critical assets associated with both potable water supply systems and oily waste disposal systems on the study site.

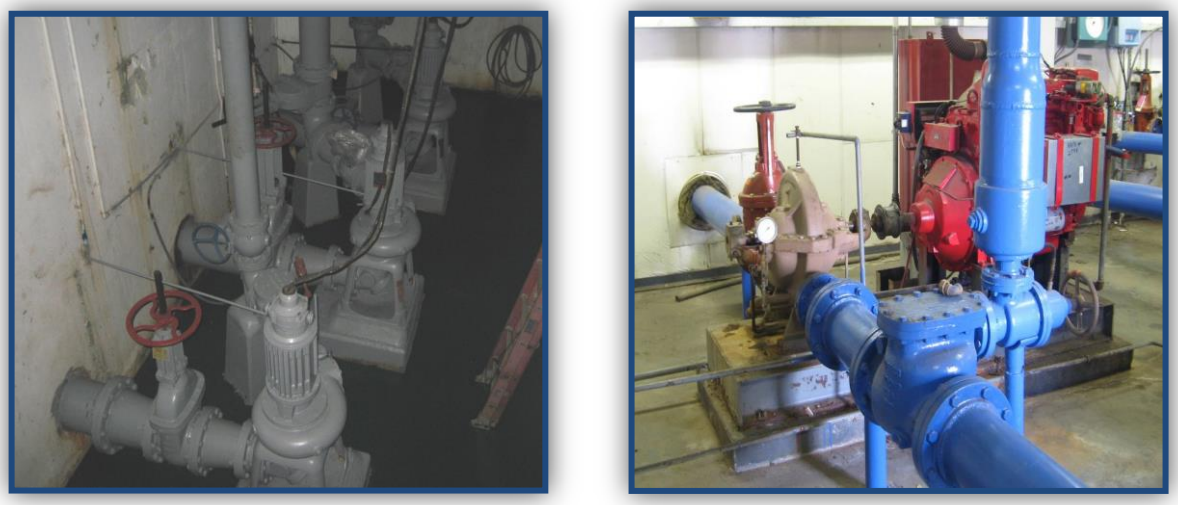

Figure 124. Examples of mechanical pumps associated with the oily waste and potable water systems on NSN.

For these assets, the damage anticipated in response to coastal storm impacts (exacerbated by SLR) was assumed to be primarily a function of electrical and mechanical fragility. Based on the information provided in Table 20 above, and structural composition of these types of assets, damage states were derived in Table 35 and fragility curves were devised to characterize the probability that the pumps failed as a function of the loadings generated under the prescribed SLR and return interval storm scenarios (Figure 125).

Table 35. Example damage state definitions for pump on the study site.

Baseline Condition	State Definition			
	None	Minor	Moderate	Severe
Asset is functional. No damage to pump station.	The asset is functional. Cleanup is required. 5% of the electromechanical equipment is damaged and must be repair or replace.	The asset is not functional. Cleanup is required. 30% of the electromechanical equipment is damaged and must be repair or replace.	The asset is not functional. Cleanup is required. 40% of the electromechanical equipment is damaged and must be repair or replace.	Asset is functional. No damage to pump station.

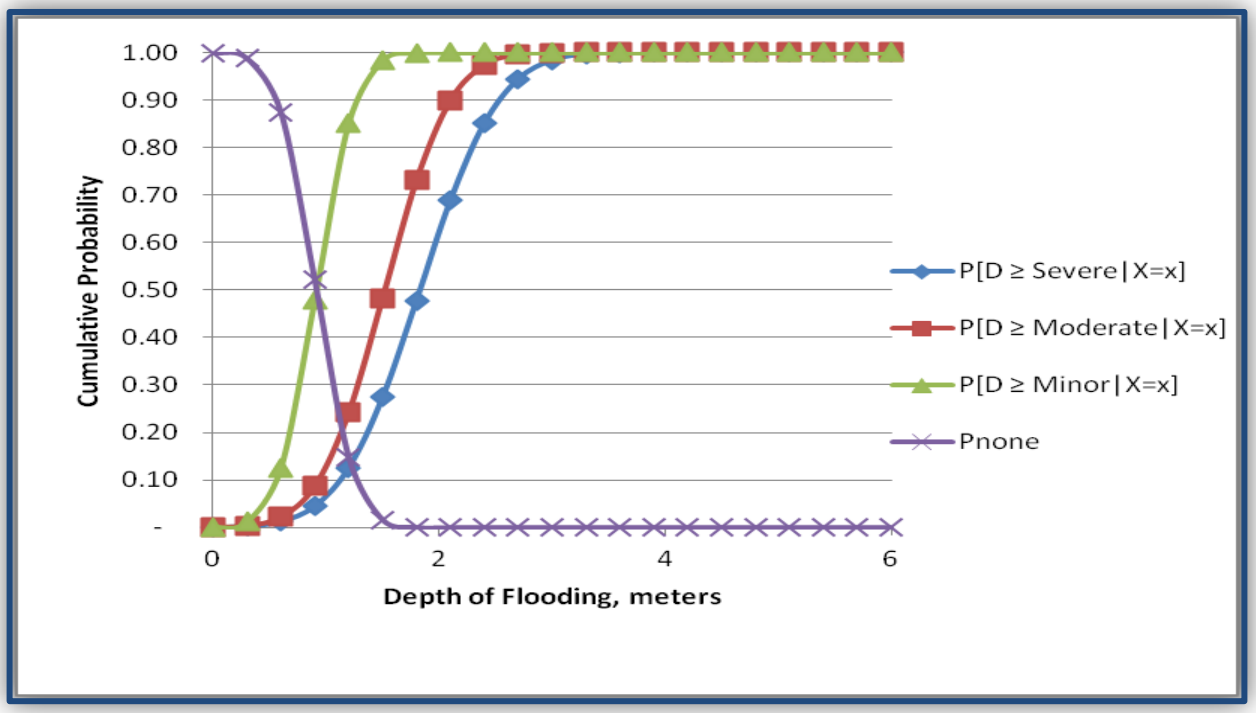

Figure 125. Example of the fragility curves for the assets analyzed under this study.

These products were then used in the study's scenario analysis.

4.8. Risk Assessment

For purposes of the case study, the NSN Risk Model was implemented by applying information to the model to assess the probabilities of random variable states for scenarios of interest, which focused on the five potential SLR states. The model calculated the posterior marginal probabilities of node states, which represented "beliefs" about the condition and functionality of the infrastructure system. When the *SEV* node was left un-instantiated, the posterior marginal probabilities were interpreted as the annual probability of asset damage states and functional impairments caused by coastal storms other than Nor'easters.[7] As the majority of the details of this analysis were considered FOUO in content, specific results of this risk assessment were relegated to FOUO supplemental materials. However snapshots of the risk assessment results have been included here to illustrate the methodology.

4.8.1 Effect of SLR and Storms on Assets

The risk assessment generated posterior marginal probabilities for asset damage states and function nodes under each of the five prescribed SLR scenarios in the form of tables which showed which assets had a high probability of being damaged by each of the coastal storms.

[7] Note that budgetary and time constraints limited this initial application to the four return-interval storms i.e., 1-yr, 10-yr, 50-yr, and 100-yr), excluding the assessment of the nor'easter.

These tables not only revealed the vulnerability of the various assets, but pinpointed the "tipping points" where changes in SLR resulted in significant increases in probabilities of damage and mission impairment. For example, Figure 126 shows a fragment of the NSN Risk Model showing four assets comprising the wastewater management infrastructure at Pier 14.

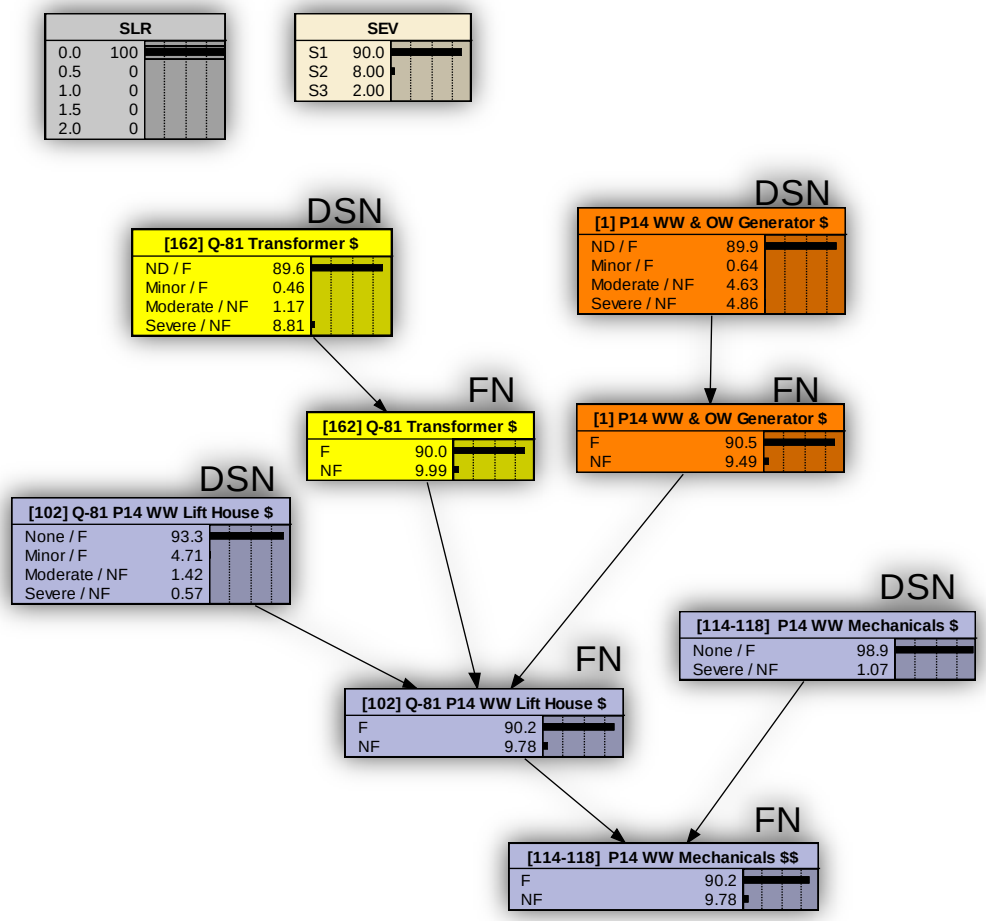

Figure 126. Fragment of the NSN Risk Model showing results for the Pier 14 wastewater management system infrastructure for the 0.0 m SLR scenario.

The two risk driver nodes (i.e., *SLR* and *SEV*) are also shown. Although the edges linking the ten pictured nodes to nodes representing the rest of the infrastructure network are not shown for clarity, these nodes are present and influence the results in this example. The *SLR* node has been instantiated to 0.0 m to reflect knowledge that sea level is at its present-day level and the *SEV* node is un-instantiated to compute the annual probabilities of asset damage and function states. Nodes marked *DSN* are Damage State Nodes that report the posterior marginal probabilities of each potential damage state for that asset. For example, the annual probability of the *Q-81 transformer* [*162*] being in the damage state *None* is 0.896. Nodes marked *FN* are asset Function Nodes that report the posterior marginal probabilities of each potential function state. For example, the annual probability of the *Q-81 transformer* being *Functional* is 0.900. These probabilities represent beliefs about the damage state and functionality of the system given

uncertain knowledge about coastal storm severity that is consistent with modeled storm return periods.

The NSN Risk Model was also implemented to explore how information about the damage or function state of some assets could be used to update the beliefs about the damage and function states at other assets. When the damage state or function state of one asset was observed, information was applied in one of two ways. If the information was hard, or certain, information was entered by instantiating the relevant node. For example, if the damage state of an asset was known with certainty to be *Moderate,* as that damage state was defined in the section on structural analysis (refer to *Section 3.9*), then the asset damage node for that asset was instantiated to *Moderate*. If the information was soft, or uncertain, then information was entered in the form of likelihoods or probability potentials. The likelihood was the probability of an asset's damage state given the evidence obtained by observation of the asset. A probability potential was simply another way of expressing that information. For example, inspection of an electrical transformer might have yielded evidence that made it difficult to determine its true damage state. In such cases, the likelihood of each potential damage state was evaluated given the available evidence. The problem of inferring asset damage states from evidence was beyond the scope of this project, but led to a very important discussion regarding how the NSN Risk Model should be interpreted.

It was already stated that posterior marginal probabilities represented the annual probability of asset damage and function states when the SLR node was instantiated and the SEV node was left un-instantiated. The implicit assumption was that a storm would certainly occur and the uncertainty was whether that storm would be an *S1*, *S2*, or *S3* storm. When the SEV node was instantiated, the posterior marginal probabilities represented the probability of asset damage and function state given knowledge of *SEV*. The posterior marginal probabilities no longer represented the annual probabilities of asset damage and function states because the probability distribution in the *SEV* node was updated and was no longer consistent with information about the frequency of storm events. Similarly, if the damage state of an asset was observed, and information about the assets damage state was entered into the NSN Risk Model, the implication was that a storm had occurred and caused damage to that particular asset. The NSN Risk Model updated the posterior marginal probabilities for other nodes to represent the damage and function state probabilities given that evidence. Updated probabilities represented beliefs about the state of other assets and factors influencing their damage state. For this reason, instantiation of asset damage and function nodes were not used to investigate how the disrepair or non-functionality of a particular asset would affect capabilities or mission performance. These types of studies would need to be undertaken using a different approach, described below.

Suppose that inspection of the Pier 14 wastewater lift station structure [*102*] revealed that its damage state was *Moderate* and the conditions of all other assets were unobserved. The asset damage node for [*102*] would be instantiated to update beliefs about the state of other assets in the system (Figure 127).

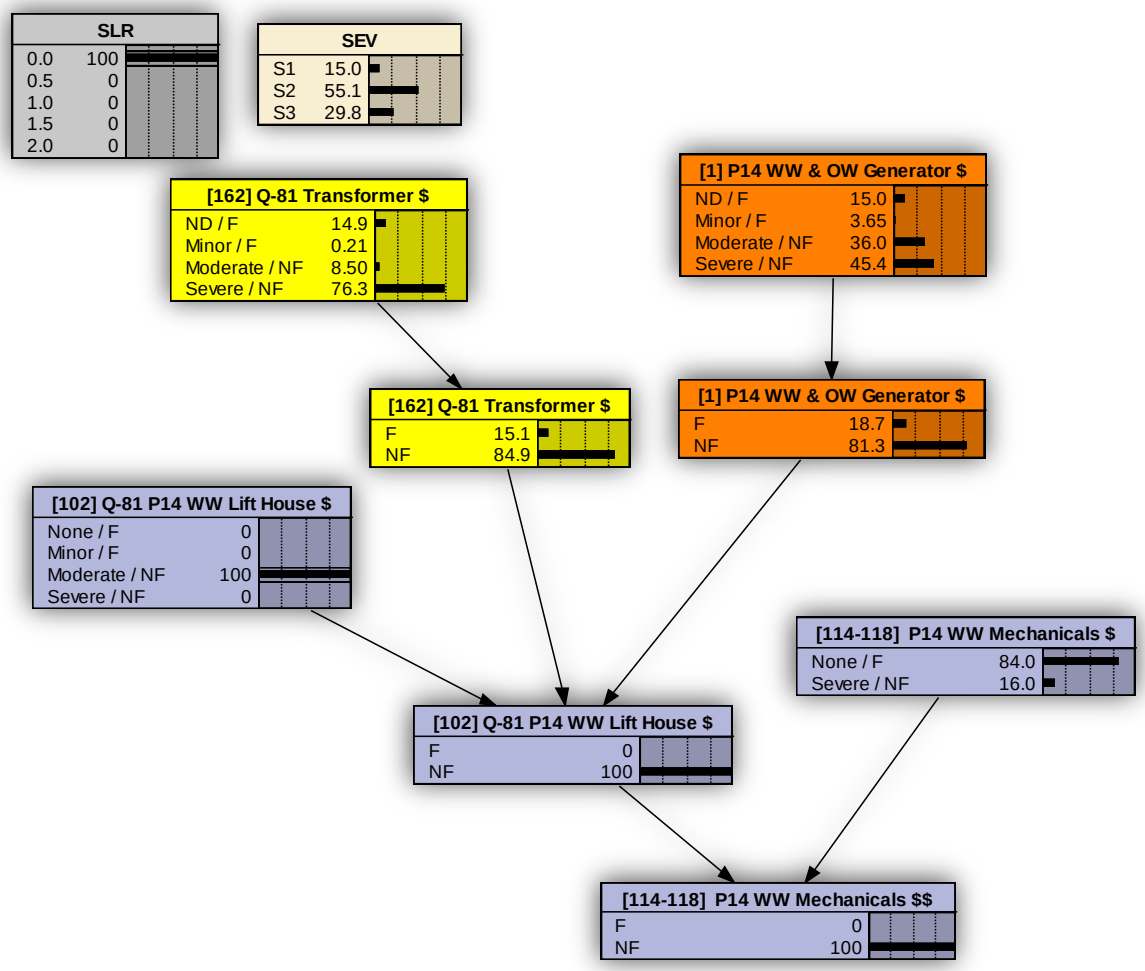

Figure 127. Fragment of the NSN Risk Model showing updated results for the Pier 14 wastewater management system infrastructure after observation of the Pier 14 wastewater lift house structure [102] revealed that the damages to the structure caused by a coastal storm were "Moderate."

The asset damage node for each unobserved DSN reveals the probability that the asset is in each of its potential damage states given knowledge of the state of [*102*]. For example, given the evidence at [*102*], the current belief about [*162*] is that the probability that it is in a *Severe* damage state is 0.763. Similarly, the probabilities of the asset function states are also reported. For example, given knowledge of the state of [*102*], the Pier 14 wastewater generator [*1*] has a probability of being *Non-Functional* equal to 0.813. The observation at [*102*] has permitted an inference about the severity of the storm causing the damages. This inference is reported in the SEV node, which reports the probability the damages have been caused by a storm of severity *S2* equals 0.551. The posterior marginal probabilities in the network no longer represent annual probabilities because the probability distribution in the SEV node has been updated based on observations of the damage state of [*102*].

To further illustrate how the Bayesian network can be interpreted, we can consider the following extension to the previous example. Suppose that, after the inspection of the wastewater lift house structure [*102*] reveals its damage state to be *Moderate*, additional observations of the electrical

generator [*1*] behind the wastewater lift station reveals that asset to be undamaged. This information can be entered into the Bayesian network by instantiation of the asset damage node for [*1*]. The network then updates the probabilities of asset damage and function state nodes (Figure 128).

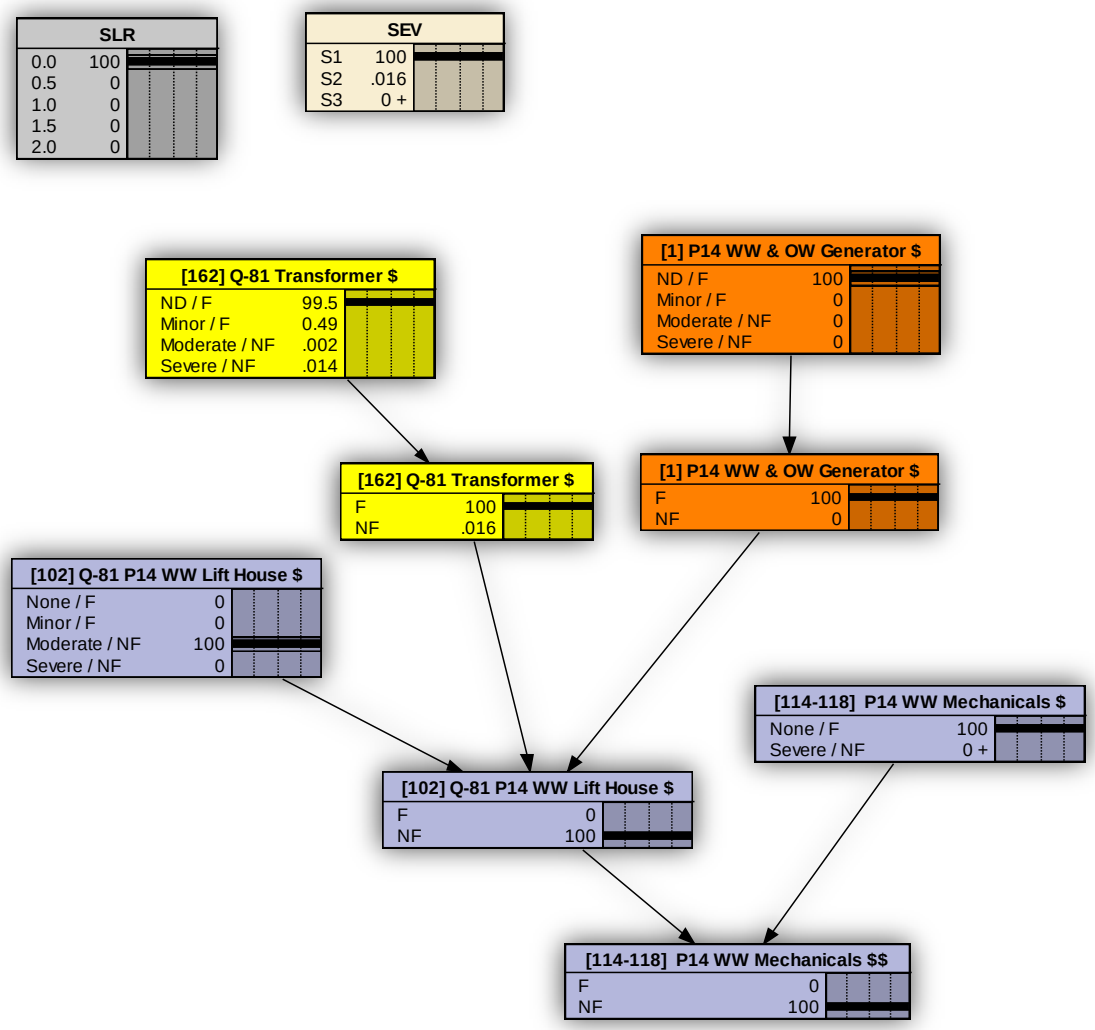

Figure 128. Fragment of the NSN Risk Model showing updated results for the Pier 14 wastewater management system infrastructure after observation of the Pier 14 wastewater generator [1]. The results revealed that the generator was undamaged and the asset damage node was instantiated.

This new evidence leads to a high degree of confidence in the damage state of unobserved assets. Evidence about the state of [*1*] leads to the belief that there is a high probability the *Q-81 electrical transformer* [*162*] and the Pier 14 wastewater pumps and mechanicals [*114-118*] are in an undamaged state. The probability that [*162*] is in a damage state of "*ND*" (synonymous with *None*) is 0.995 and the probability that [*114-118*] is undamaged is almost 1, even though these assets have not yet been inspected. In Figure 128 above, the *SEV* node reports an inference about the storm that has caused damage to [*102*]. In this case, there is a high degree of confidence that

damage to [*102*] is caused by an *S1* storm. The inference about storm severity is an example of diagnostic inference, or reasoning from effects to causes.

In Figure 128 above, the relationship between asset damage and function nodes deserves a discussion. The function state of Pier 14 wastewater pumps and mechanicals [*114-118*] is *Non-Functional* (*NF*) with a probability of 1 even though there is a very high probability that the pumps are undamaged. This functional state is attributed to damage to the *P14 wastewater lift house structure* [*102*]. The wastewater lift house structure serves to convey electricity from the *Q-81 transformer* [*162*] and the backup electrical generator [*1*] to the wastewater pumps [*114-118*]. There are four possible damage states for the wastewater lift house structure describing the degrees of penetration of the building envelope by flood waters. When damage states are developed, assumptions regarding the functionality of assets based on those damage states are also made. In this case, the assumption is that sufficient penetration of the building enveloped by flood waters consistent with a *Moderate* or *Severe* damage state will interfere with the conveyance of power to the pumps and equipment inside the structure. Thus, the functional state of the pumps is *NF* because the structure is in a *Moderate* damage state when the power supply is interrupted. In the Bayesian network, each asset damage node reports the assumed relationship between asset damage and asset function. This relationship is indicated following the damage state, with *F* to indicate the asset is functional given the damage state and *NF* to indicate the asset is non-functional given the damage state. In practice, there is uncertainty regarding the relationship between the asset damage state and the asset function state. At the time of this study, no information was available on which to base an uncertain relationship between asset damage and asset function, so this relationship has been modeled deterministically.

The preceding example demonstrates how asset damage state and function nodes have been interpreted and describes the implications of the implicit assumption that all damages to assets were caused by coastal storms. If an asset was observed to be damaged, then a storm must have occurred and caused those damages. If an asset was observed to be undamaged, then a storm must have occurred and the asset withstood the loads associated with that storm. If no evidence was available regarding the state or functionality of assets, the belief regarding the severity of the storm was consistent with the original return period curve for modeled storms. In this case, the posterior marginal probabilities in asset damage and function nodes were interpreted as annual probabilities of damage and function state.

The NSN Risk Model can be used to explore how topological variations in the infrastructure network might affect risks. For example, an asset can be removed from the network by removing the edges that linked the asset and function nodes to other parts of the network. The network will then describe how the system will perform without that asset. Similarly, new assets can be introduced and existing assets can be retrofitted to explore how these changes in the infrastructure network will affect performance. Proposals for new assets can be evaluated by introducing a new set of asset damage and function nodes for the proposed asset to test its effect on mission performance. Potential retrofits of assets can be evaluated by calculating new CPTs for the existing set of asset damage and function nodes representing that asset.

4.8.2 Effect of SLR and Storms on Capabilities

Inference is classified as predictive if the reasoning is from information about causes to assess potential effects and diagnostic if reasoning is from information about observed effects to potential causes. This section describes predictive inferences from the NSN Risk Model regarding the effects of sea-level rise on capability scores and the mission performance index. The section begins with a discussion of capability scores. These results of the NSN Risk Model are objective because they are insensitive to command priorities for providing those services. In contrast to capability scores, the mission performance index is a subjective assessment of performance based on capability scores. The subjectivity arises because the weights in the mission performance index reflect command-level priorities for at-berth support of CVNs.

Capability scores are reported for the three piers in Table 36.

Table 36. Capability scores and mission performance index for the five prescribed SLR scenarios in the NSN study.

Pier	SLR Scenario	Capability Scores								Mission Performance Index (MPI)[1]
		Provide Water	Provide Access	Provide Steam	Provide North Berth	Provide South Berth	Provide Oily Waste	Provide Electricity	Provide Wastewater	
11	0.0	0.9886	0.8643	0.9639	0.8356	-	0.9555	0.9807	0.9676	0.9551
	0.5	0.9271	0.8689	0.8517	0.9086	-	0.1370	0.8049	0.1717	0.6158
	1.0	0.4046	0.8753	0.0916	0.9545	-	0.0000	0.0040	0.0000	0.1885
	1.5	0.0018	0.9198	0.0000	0.9797	-	0.0000	0.0003	0.0000	0.1306
	2.0	0.0000	0.9225	0.0000	0.9919	-	0.0000	0.0000	0.0000	0.1312
12	0.0	0.9886	0.8643	0.9639	0.9721	0.9149	0.9572	0.9884	0.9710	0.9629
	0.5	0.9271	0.8689	0.8517	0.9974	0.9777	0.6999	0.9496	0.7660	0.8621
	1.0	0.4046	0.8753	0.0916	0.9999	0.9960	0.0028	0.3636	0.0040	0.3142
	1.5	0.0018	0.9198	0.0000	1.0000	0.9995	0.0000	0.0074	0.0000	0.1805
	2.0	0.0000	0.9225	0.0000	1.0000	1.0000	0.0000	0.0000	0.0000	0.1789
14	0.0	0.9886	0.8643	0.9639	0.9149	0.9852	0.9458	0.9879	0.9696	0.9620
	0.5	0.9271	0.8689	0.8517	0.9794	0.9994	0.6695	0.9469	0.7866	0.8629
	1.0	0.4046	0.8753	0.0916	0.9967	1.0000	0.0002	0.2978	0.0033	0.2995
	1.5	0.0018	0.9198	0.0000	0.9997	1.0000	0.0000	0.0068	0.0000	0.1803
	2.0	0.0000	0.9225	0.0000	0.9997	1.0000	0.0000	0.0000	0.0000	0.1789

[1]The mission performance index is described in Section 11.2.2.5 earlier in this report.

By definition, a capability score (ranging from 0 to 1), is considered an estimate of the annual probability that a capability is not disrupted at least once during the course of a year because of damage to physical assets caused by a coastal storm in the study. The probability of service interruption given an SLR scenario is the complement of the capability score for that SLR scenario. Figure 129 - Figure 131 plot the conditional probability of service interruption at Piers 11, 12, and 14 for the case study. These results revealed a sharp increase in the probability of service interruption between 0.5 and 1.5 m SLR.

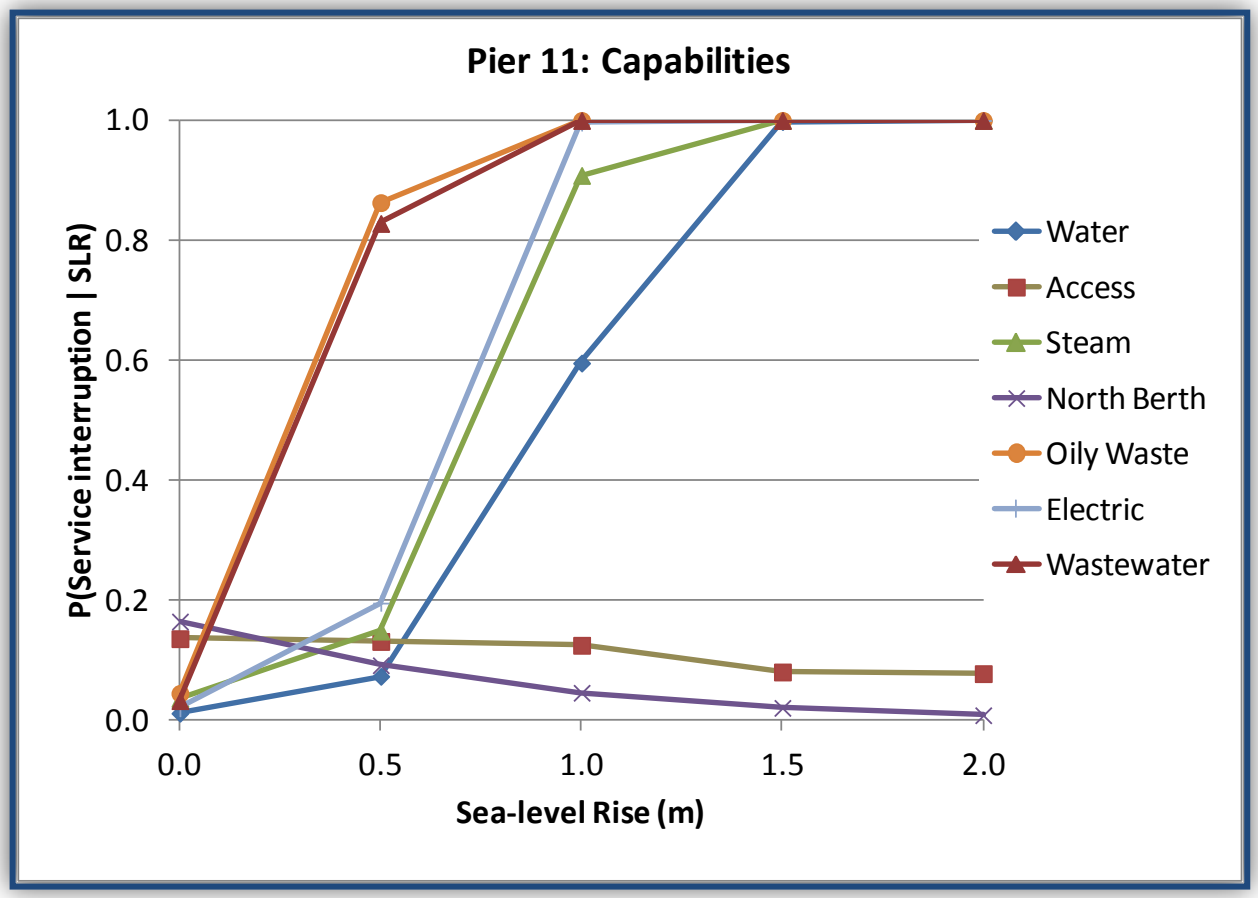

Figure 129. Conditional probabilities of service interruptions occurring at least once during the course of a year for the five prescribed SLR scenarios for Pier 11 in the study.

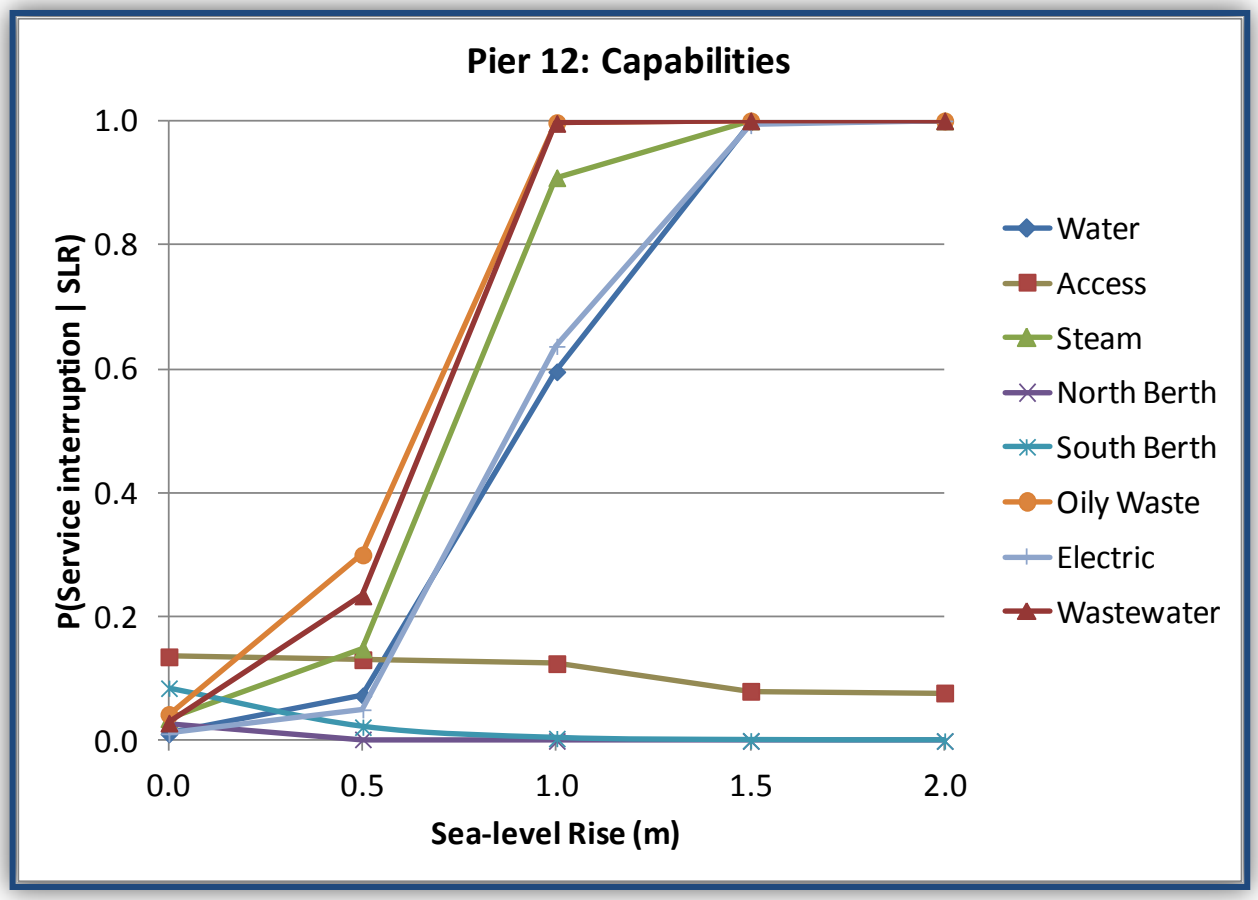

Figure 130. Conditional probabilities of service interruptions occurring at least once during the course of a year for the five prescribed SLR scenarios for Pier 12 in the study.

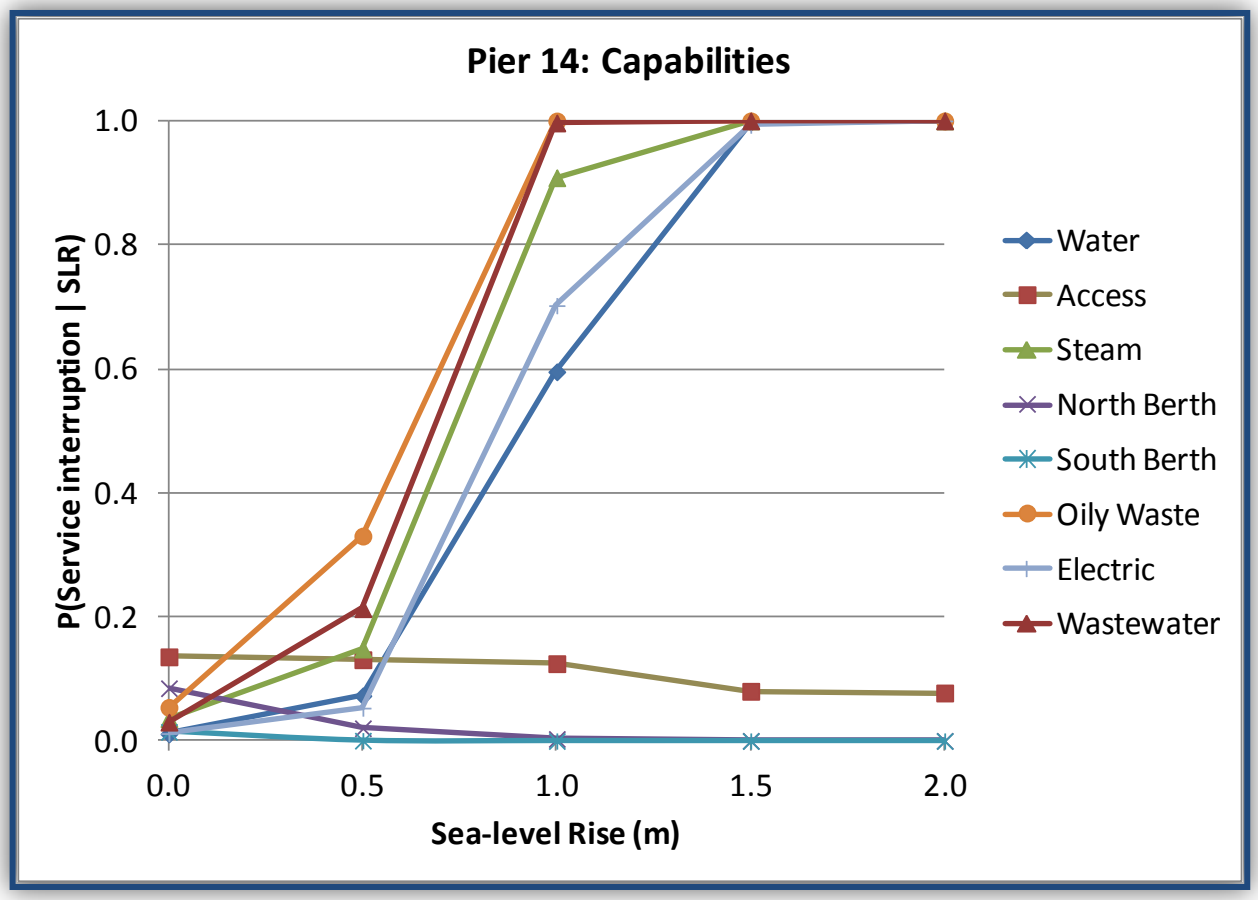

Figure 131. Conditional probabilities of service interruptions occurring at least once during the course of a year for the five prescribed SLR scenarios for Pier 14 in the study.

As the figures illustrate, three of the capabilities responded positively to SLR (i.e., *Provide Access*, *Provide North Berth*, and *Provide South Berth*). Increasing capability scores for access suggest that, if there was any corresponding increase in sedimentation in the Inner Harbor, Harbor Entrance, and Thimble Shoals Channels following a storm, the reductions in limiting depth would be more than compensated for by increased sea levels. The trend in the capability score for *Provide Access* can be seen in Table 36 above, which shows the capability score increasing from 0.864 to 0.923 as SLR increased from 0.0 to 2.0 m. The capability scores for *Provide North Berth* and *Provide South Berth* also increased as sea levels rose from 0.0 to 2.0 m. These capabilities describe the combined effects of sedimentation in berthing areas following a storm and loss of freeboard. We found that any increase in sedimentation in the berthing areas and/or navigation channels were more than compensated for by rising sea levels. This result was consistent with interviews on the installation, which indicated that, with regular maintenance dredging of berthing areas, no dredging was needed following named storms. At SLR = 2.0 m, there was still sufficient freeboard to dock CVNs at each pier. However, freeboard diminished as sea levels rose and, without sufficient freeboard, CVNs could not dock at the piers. At the 2.0 m SLR state, there would be approximately four meters of freeboard at Pier 11 and approximately 0.3 m of freeboard at Piers 12 and 14. Thus, while the capabilities to *Provide North Berth* and

Provide South Berth improved as sea levels rose, this positive effect of SLR on the capability score would not continue indefinitely. A 2.5 m increase in sea level will submerge the pier decks at Piers 12 and 14 and prevent CVNs from docking at those piers. As described previously, the potential for wave overtopping during non-storm periods as sea levels rose was not considered in this study.

Each of the remaining capability scores was negatively impacted by SLR. As shown in Table 36 above, capability scores for water, steam, oily waste, electricity, and wastewater were approximately 0.94 or higher at each pier under the baseline sea level scenario. All of these capabilities scores decreased to zero under the prescribed 2.0 m SLR scenario. The results suggest that two meters of SLR greatly increases the probability of service interruptions at the three piers that are capable of accommodating CVNs. Capability scores only provide information on the frequency of at least one interruption in a year and provide no information on the duration of the interruption, the severity of damage to infrastructure, or the cost to repair the infrastructure and restore the capability. Posterior marginal probabilities for asset damage nodes (contained in the FOUO supplemental materials) in the case study were developed to assess the severity of damage to infrastructure in terms of the definitions for damage states.

The effect of SLR on capabilities needed to *Provide At-Berth Support* for CVNs can be seen graphically in Figure 129 - Figure 131, which plots the conditional probability of service interruption over the five prescribed SLR scenarios. The probability of service interruption decreased for the *Provide Access*, *Provide North Berth*, and *Provide South Berth* capabilities. The probability of service interruption for utility services increased. The *Provide Wastewater* and *Provide Oily Waste* capabilities appeared to be the most vulnerable capabilities and the probabilities of service interruption responded similarly because these two capabilities depended upon a shared set of infrastructure located very near the waterfront. The *Provide Electricity* capability exhibited a somewhat different response to SLR at Pier 11 than at Piers 12 and 14. This was attributed to the location of the Pier 11 substation on the lower deck. At Piers 12 and 14, the substations are located on land within 1,000 ft of the waterfront. The capabilities *Provide Steam* and *Provide Water* responded similarly to SLR at each of the three piers.

Capability scores were plotted against SLR for each level of storm severity (SEV) (Figure 132 and Figure 133).

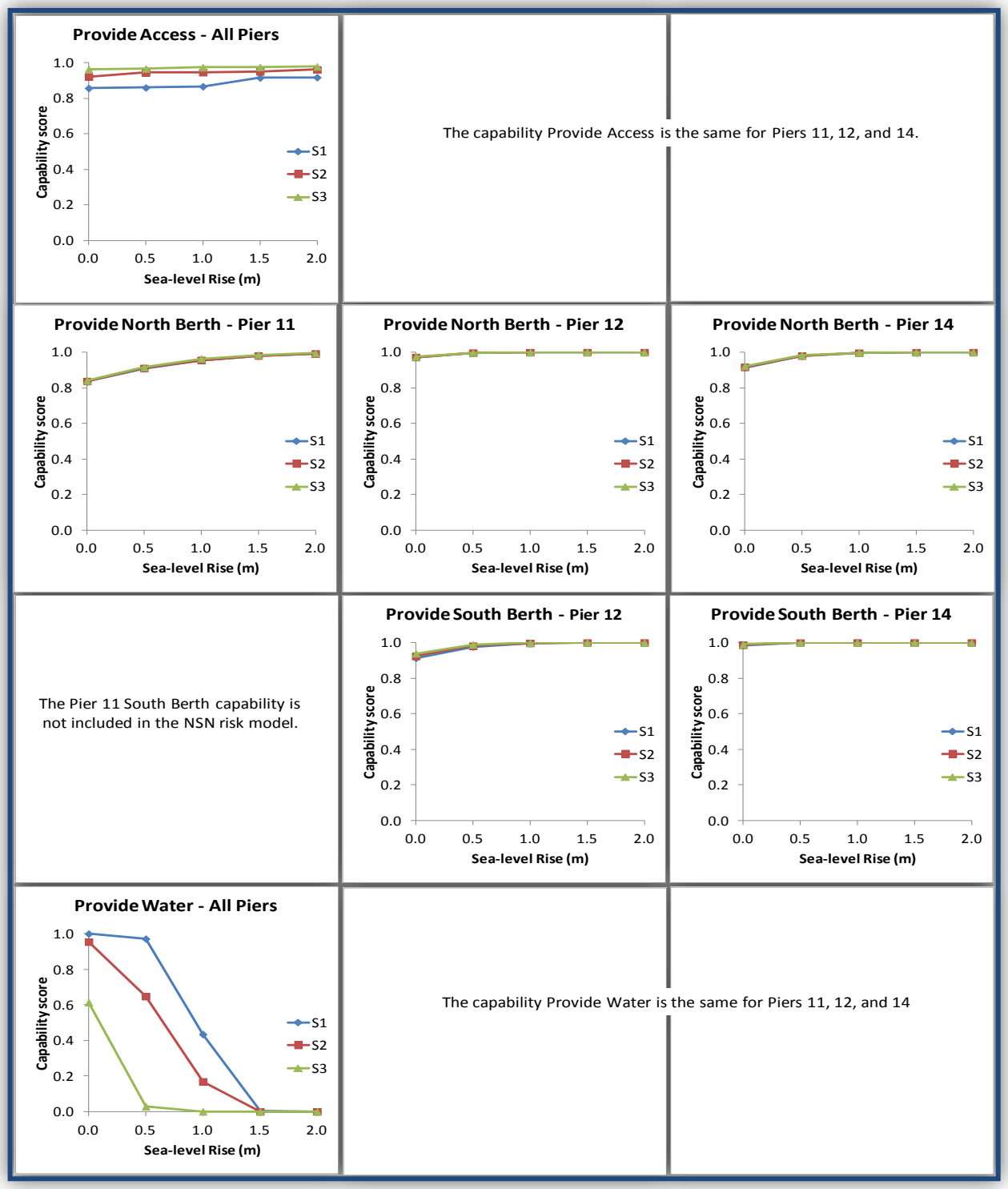

Figure 132. Capability scores by SLR and SEV scenario (*Potable Water Provisioning* and *Berthing* capabilities) for the study.

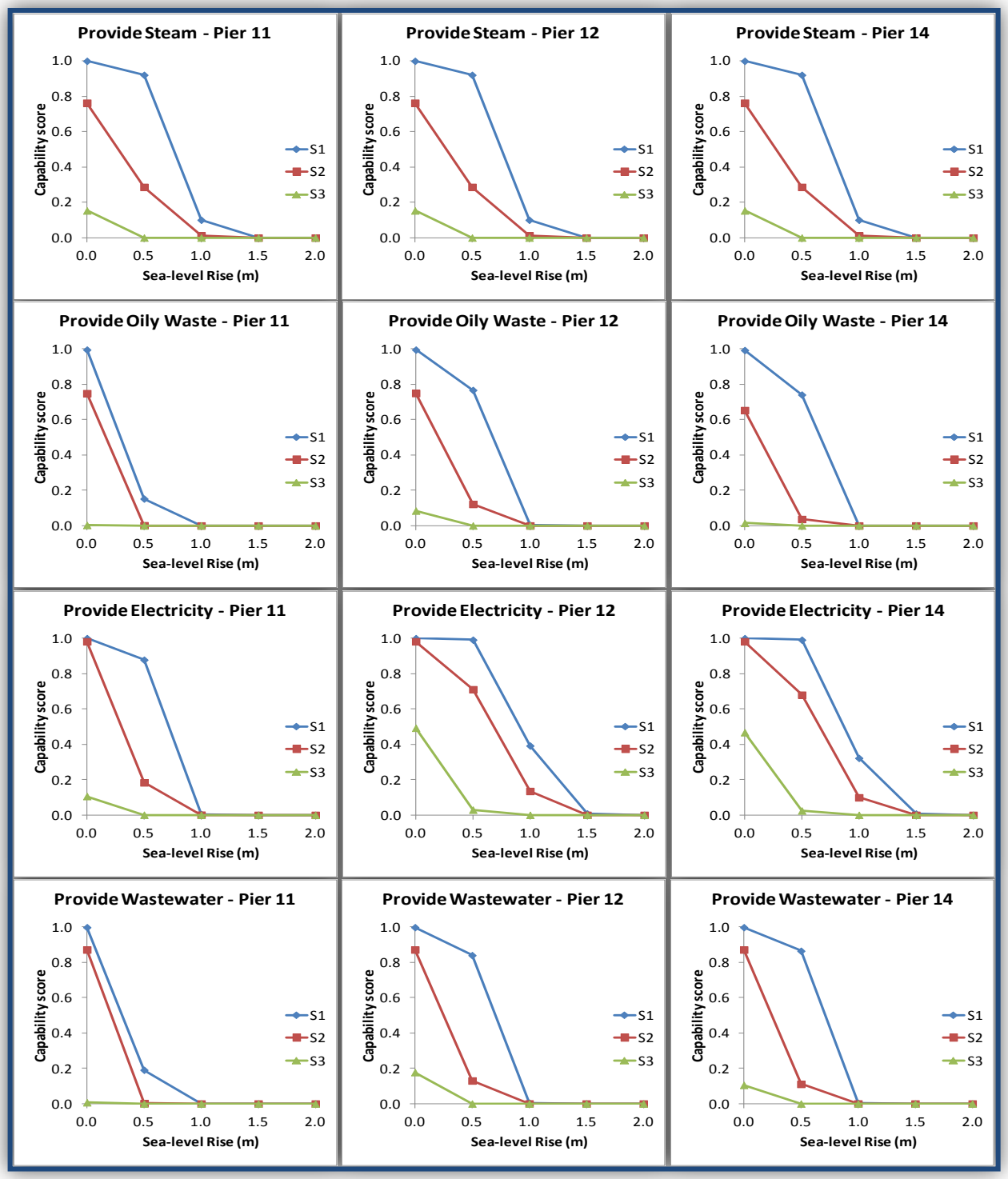

Figure 133. Capability scores by SLR and SEV scenario (*Steam*, *Oily Waste*, *Electricity*, and *Wastewater* capabilities) for the study.

Because these probabilities were conditioned on the storm severity, they can be interpreted as the probability that a storm of given severity (*S1*, *S2*, or *S3*) will not cause the interruption of a capability under the prescribed SLR scenario. In Figure 132 above, the plot for *Provide Access* shows that, as storm severity increased, there was a net increase in final controlling depth of navigation channels. This suggests that higher levels of storm severity cause net erosion in the channels. This result applies equally to all three piers. In contrast, coastal storm severity appears to have very little effect on the final controlling depths in berthing areas.

Capability scores for those capabilities dependent on infrastructure utilization exhibited a more pronounced response to increases in storm severity. For example, this can be seen for the *Provide Water* capability in Figure 132 above, and for the remaining capabilities in Figure 133 above. The *Provide Water* capability is represented by a single node in the Bayesian network, so only one plot that applies to all three piers, was shown in Figure 132 above. Under the baseline SLR scenario, the *Provide Water* capability appears to be fairly robust, with a high probability of no service interruption given an *S1* or an *S2* storm. This probability of no service interruption decreased to 0.614 in the event of an *S3* storm. As sea levels rose, the probability of no service interruption also increased, as indicated by the decreasing capability scores. Under the 1.5 and 2.0 m SLR scenario, the probability of experiencing at least one service interruption during the course of a year was 1. Other capabilities exhibited a similar pattern of response to increases in storm severity and sea level. The *Provide Oily Waste* and *Provide Wastewater* capabilities had a low probability of being interrupted by an *S1* storm, but a high probability of being interrupted by an *S2* or an *S3* storm. This was also true of the *Provide Electricity* capability at Pier 11.

4.8.3 Effect of SLR and Storms on Mission Performance

The MPI transformed information provided by the seven or eight capability scores into a single measure of performance. In short, the MPI described, on a scale of 0 to 1, how well the mission to *Provide At-Berth Support* for CVNs was performed with respect to the objective to minimize the probability that capabilities were interrupted by coastal storms. For this study, the MPI had a specific interpretation intended for assessing the effects of SLR on the capabilities at the installation. The MPI did not account for other attributes such as efficiency, safety, and cost that might also be considered in a more general assessment of performance. Methods used to calculate the MPI were described earlier in this report. Recall that the MPI is considered a value-laden measure of performance because it incorporates information about command priorities of capabilities. This contrasts with the results presented in *Section 4.8.2 above*, which are considered objective measures of performance expressed in terms of probabilities.

For purposes of this study, the MPI is a weighted value function that provides a one-dimensional measure with which to evaluate the effect of SLR on mission performance. Below, two realizations of the MPI have been presented. The first realization assumes that all potential improvements of capability scores from their minimum value to their maximum value are equally important to mission performance. This realization provides a benchmark for assessing what impact the NSN priorities actually had on the evaluation of mission performance. The second realization incorporates swing weights that were obtained from the NSN Ship Support Officer (LT Cory Maccumbee). Swing weights are summarized in Table 37.

Table 37. Swing weights obtained from the NSN Ship Support Officer for the study.

Capability	Pier	
	11	**12 and 14**
Provide Electric Power	0.230	0.217
Provide Wastewater	0.230	0.217
Provide Steam	0.172	0.163
Provide Potable Water	0.115	0.109
Provide Oily Waste	0.115	0.109
Provide Access	0.080	0.076
Provide North Berth	0.057	0.054
Provide South Berth	-	0.054

Although potential improvements in capability scores relative to the worst case scenario varied somewhat, these differences were minimal and a single set of weights were obtained for Pier 12 to apply to all of the piers. The *Provide Electricity* and *Provide Wastewater* capabilities were deemed most important, followed by the *Provide Steam*, *Provide Potable Water*, and *Provide Oily Waste* capabilities. The least important capabilities were identified as the *Provide Access*, *Provide North Berth*, and *Provide South Berth* options. The relatively low weights on navigation and berthing capabilities can be explained as follows. Under baseline conditions (0.0 m SLR), when navigation channel and berthing area drafts are at a minimum, there is sufficient limiting depth to support the movement and docking of CVNs following storm events. As sea level rises, the limiting depths in navigation channels and berthing areas increase. Therefore, the potential changes in the *Provide Access*, *Provide North Berth*, and *Provide South Berth* capabilities were perceived to be unimportant relative to potential changes in other capability scores.

The swing weight elicitation was followed up with a set of choice experiments for validation of the swing weights. In the choice experiment, the respondent (LT Cory Maccumbee, NSN Ship Support Officer) evaluated a pair of mission performance scenarios described in terms of randomly generated capability scores at a pier. He then chose the scenario that, in his view, represented the highest level of performance. Ten pairs of performance scenarios were randomly generated. Using the swing weights provided by the officer, the MPI accurately predicted the choices 60 percent of the time. Inaccurate predictions were clearly associated with harder choices. With one exception, the inaccurate predictions occurred when the difference in the MPI between the choices was less than about 0.05 (Figure 134).

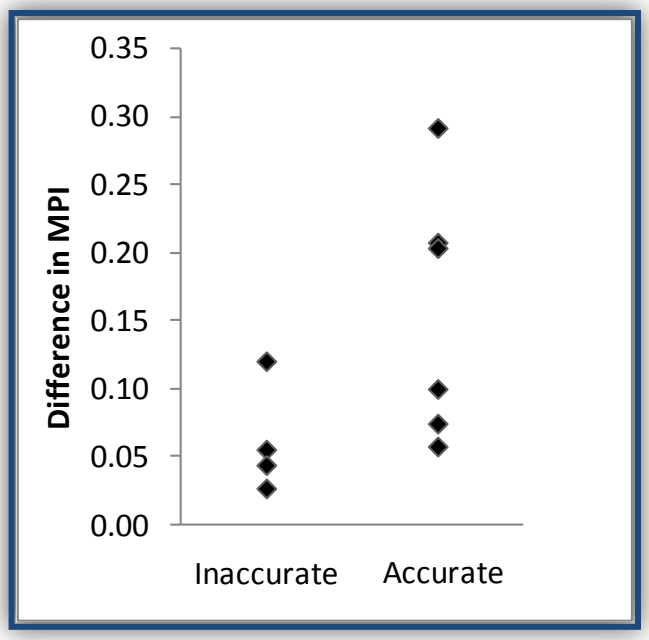

Figure 134. Difference in the MPI between choice scenarios, showing that MPI prediction errors occurred when the difference in the MPI between the scenarios was less than about 0.05.

Figure 135 (a) plots the expected MPI calculated using equal weights under the five prescribed SLR scenarios.

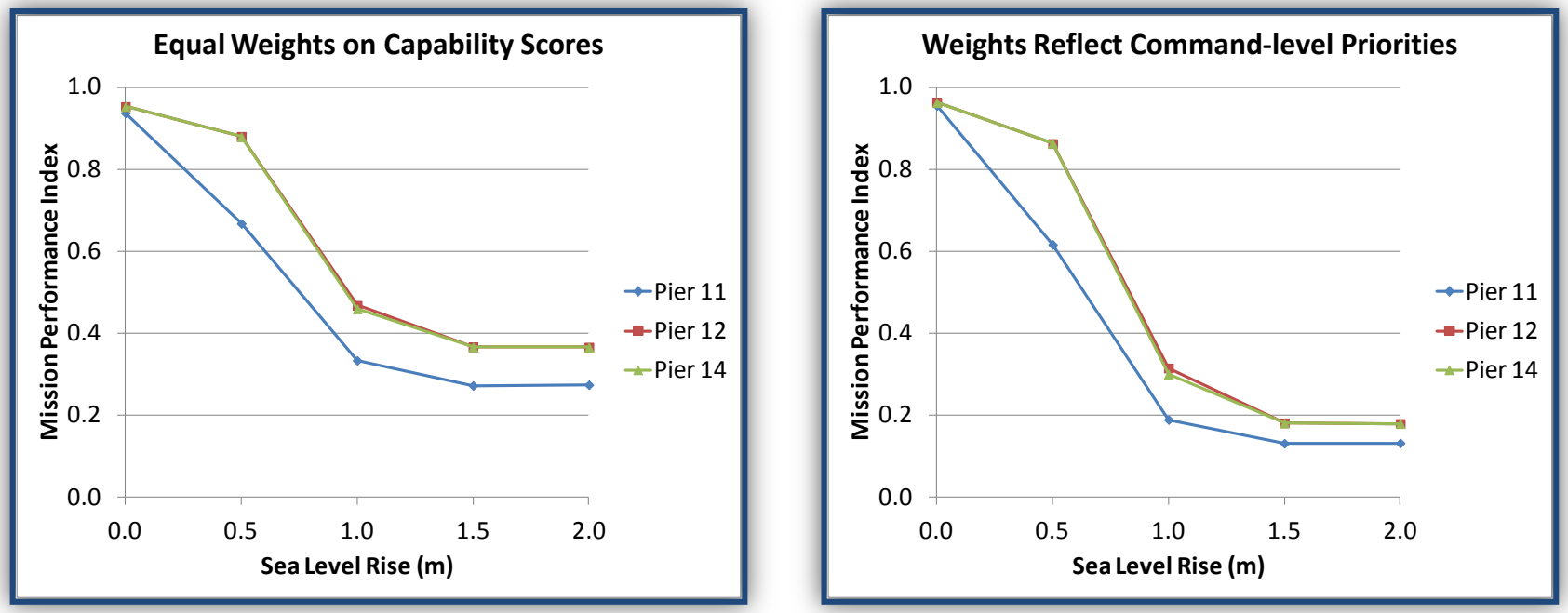

Figure 135. The expected MPI for Piers 11, 12, and 14. (a) MPI was calculated using equal weights on capability scores, and (b) weights reflecting command-level priorities.

Under baseline sea level conditions, Piers 12 and 14 had similar MPIs and Pier 11 had an MPI that was only slightly less than Piers 12 and 14. The strongest effect of SLR on mission performance was seen between the 0.5 and 1.0 m SLR scenarios. As sea levels rose, the MPIs at Piers 12 and 14 remained similar, while the effect on MPI at Pier 11 was more pronounced. This difference has been attributed to the increased levels of exposure and vulnerability of several assets that supported Pier 11 capabilities. As shown in Figure 135 (b) above, assets that supported the *Provide Oily Waste*, *Provide Wastewater*, and *Provide Electricity* capabilities were more likely to be interrupted by coastal storms.

The MPI decreased most rapidly between the 0.5 and 1.0 m SLR scenario, but continued to decline with the next SLR scenario increment (i.e., 1.5 m SLR). Above 1.5 m, expected MPIs reached a plateau, indicating that sea levels above 1.5 m would have little effect on mission performance. We believe this occurred for two reasons. First, when sea levels increased to 1.5 m, all utility services to the piers were interrupted by coastal storm damage to assets at least once a year. While it was expected that the frequency of these service interruptions would increase even as sea levels rose above 1.5 m, the MPI plateaued because it was not designed to register the effects of multiple interruptions during a year. Second, SLR had a positive effect on navigation and berthing capabilities, likely counteracting negative contributions to the MPI values. However, it should be noted that the positive effect on berthing area capabilities increased only up to the point that the piers were overtopped. For Piers 12 and 14, this occurred when sea level reached 2.3 m.

Figure 135 (b) above plots the expected MPI calculated using NSN swing weights. A comparison of this plot with Figure 135 (a) above reveals that SLR had a stronger effect on mission performance when NSN priorities were taken into account. The effect of SLR on expected MPI was much stronger between the 0.5 and 1.0 m SLR scenarios. Both plots showed that the effect of SLR on MPI diminished and later leveled-off as sea levels rose above 1.5 m. This plateau was lower when NSN priorities were taken into consideration when calculating the MPIs.

For purposes of this study, we used loss exceedance curves to describe the probability that potential losses would exceed some critical amount, and we expressed potential losses in terms of expected MPIs. In Figure 136 (a), MPIs were calculated assuming equal weights for all capabilities and in Figure 136 (b), MPIs were calculated using swing weights to incorporate NSN priorities for capabilities.

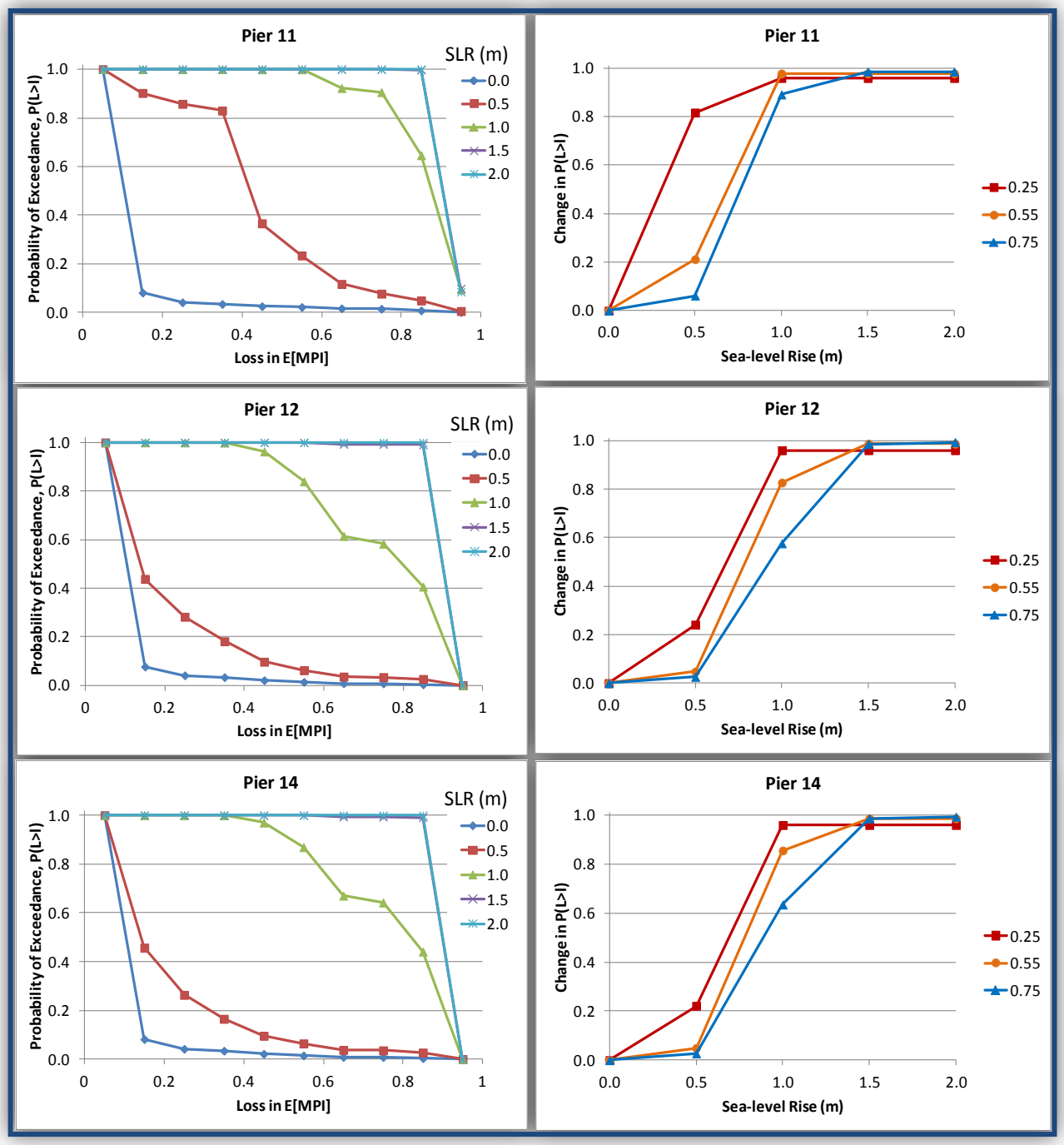

(a) **(b)**

Figure 136. (a) Loss exceedance curves for expected MPIs derived under the five prescribed SLR scenarios. (b) Change in the probability of realizing three potential levels of loss. Equal weights were used in calculating MPIs.

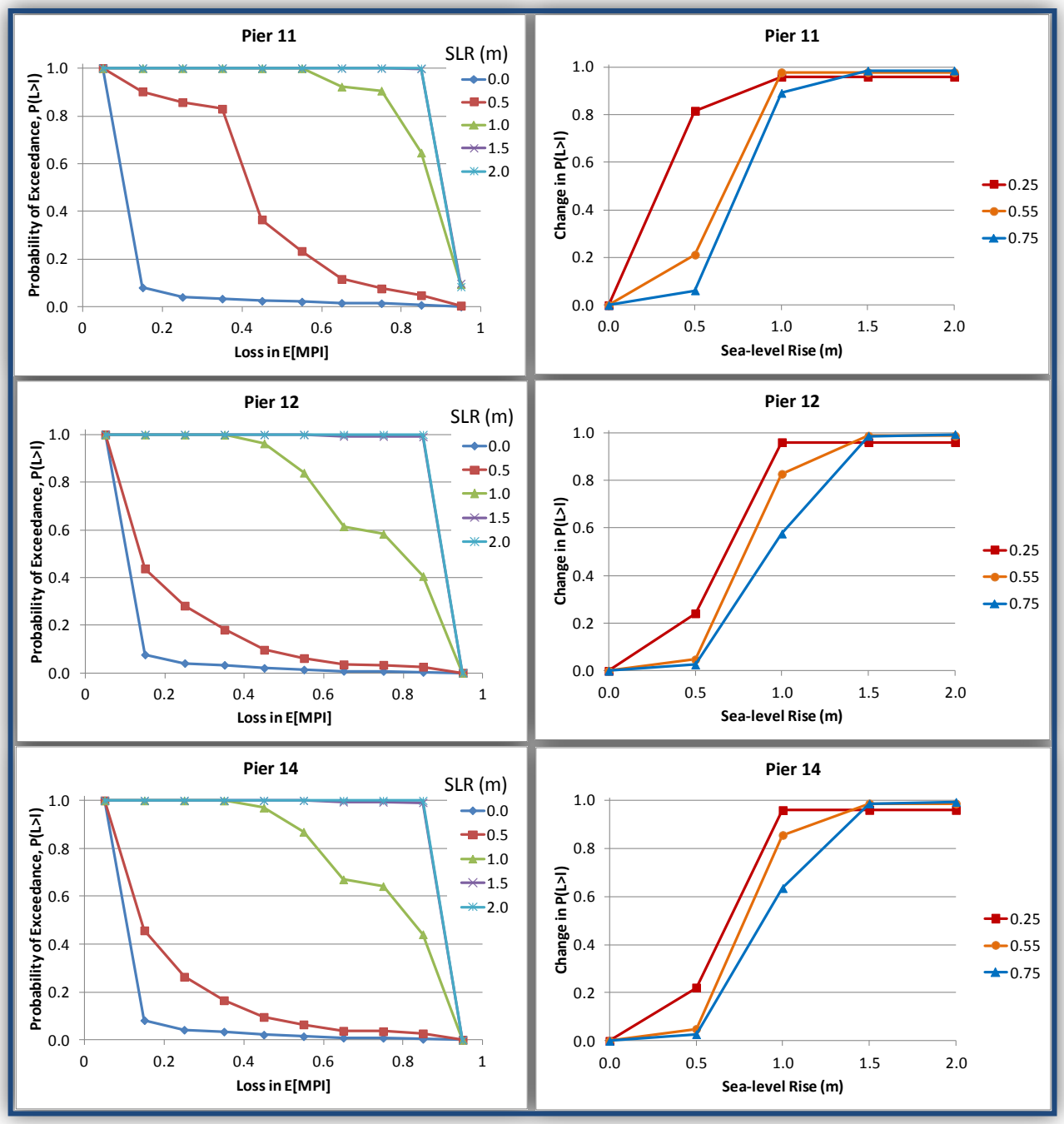

Figure 137. (a) Loss exceedance curves for expected MPIs derived under the five prescribed SLR scenarios. (b) Change in the probability of realizing three potential levels of loss. Weights used in calculating MPIs reflect command-level priorities for providing at-berth support to CVNs.

Each (a) panel in Figure 136 shows a loss exceedance curve for each SLR scenario on a pier-by-pier basis. The general pattern in these results was similar among the three piers. The curves

were concave for the 0.0 m and 0.5 m SLR scenarios. These curves transitioned to convex shapes for the 1.0 m, 1.5 m, and 2.0 m SLR scenarios. The increase in sea level at which these transitions presented themselves was regarded as the "tipping point," which occurred between the 0.5 m and 1.0 m SLR scenarios.

The (b) panels in Figure 136 and Figure 137 above show how sea level affected the probability of a fixed loss in MPI relative to MPI under baseline conditions. While this information has been essentially contained in the loss exceedance curves shown previously, it is easier for the end users to visualize the results in this manner. In Figure 136 (b) above, which assumed equal weights on capabilities, the effect of SLR on a 25 and 55 point loss in the MPIs were similar at each of the three piers. At Pier 11, increased sea levels raised the probability to a 0.75 point loss in MPI, although this effect was not observed at Piers 12 and 14. This difference has been attributed to an increase in exposure and vulnerability of the electric substation on the lower deck of Pier 11 and the oily waste and wastewater pumps thereon. Loss exceedance curves showed a similar pattern when NSN command priorities for the capabilities were factored into the MPI. However, there was a tendency for higher potential losses in expected MPI to have higher probabilities. This can be seen in Figure 137 (b) above, which shows that the probability of a 0.75 loss in expected MPI was as strongly influenced by SLR as 0.25 and 0.55 losses in expected MPI.

4.8.4 Implementation of the NSN Risk Model to Evaluate Potential Adaptations to SLR

The NSN Risk Model was also designed to explore adaptive management strategies via "what if" scenario analysis. Proposed changes in the ACN (i.e., insertions/deletions of assets or replacements/retrofits of assets) can be reflected in the model to actively manage system response and manage regrets. Here we explore several hypothetical modifications to the infrastructure network to demonstrate these capabilities. In general, these analyses require either a change in the structure of the model's DAG (representing an insertion or removal of an asset) or a change in one or more of the CPTs (representing the replacement or retrofit of an asset). The four hypothetical modifications considered for this study included:

1) the removal of the primary steam plant from the infrastructure network;
2) the removal of several backup electric power generators from the network;
3) the flood proofing of these same generators; and
4) the flood proofing of the wastewater lift pumps, transformers, and backup electrical generators at each waterfront lift station.

These scenarios are presented in greater detail in the next sections.

4.8.4.1 What-if Scenario #1: Removal of a Steam Plant from the Infrastructure Network

Two steam plants were included in the NSN Risk Model for purposes of illustration – a primary and a secondary plant (either of which were capable of satisfying all of the requirements for steam on the installation on their own). Note that steam is distributed to the piers from the steam plants through a common network of steam lines. The first "what if" scenario explored the removal of the primary steam plant from the infrastructure network for purposes of operational

efficiency improvements. The model then analyzed the effect of this decision in the revised capability scores. Functionally, this topological variation was implemented by modifying the CPT in the primary steam plant function node so that the probability that $p(Functionality = F)$ was set to zero under all combinations of asset damage node states.

The effect on the *Provide Steam* capability is summarized in Table 38.

Table 38. Capability scores for the *Provide Steam* capability showing the effect of removing the primary steam plant from the infrastructure network.

Pier	SLR	Capability Scores		Difference
		With 1° Steam Plant	Without 1° Steam Plant	
11	0.0	0.955	0.941	0.014
	0.5	0.616	0.614	0.002
	1.0	0.188	0.188	0.000
	1.5	0.131	0.131	0.000
	2.0	0.131	0.131	0.000
12	0.0	0.963	0.950	0.013
	0.5	0.862	0.860	0.002
	1.0	0.314	0.314	0.000
	1.5	0.180	0.180	0.000
	2.0	0.179	0.179	0.000
14	0.0	0.962	0.949	0.013
	0.5	0.863	0.861	0.002
	1.0	0.299	0.299	0.000
	1.5	0.180	0.180	0.000
	2.0	0.179	0.179	0.000

The *Provide Steam* capability was the only capability affected by the hypothetical change in the network. The effect was similar at all three piers - at baseline sea level, the capability scores were 0.955, 0.963, and 0.962, at Piers 11, 12, and 14, respectively. Removing the primary plant increased the annual probability of steam service interruption by 0.014 at Pier 11 and 0.013 at Piers 12 and 14. As shown in Table 38 above, this effect was largest under baseline sea level conditions and the effect decreased to zero under the 1.0 m SLR scenario. The diminishing effect of redundancy on capability scores as the sea levels rose has been attributed to the corresponding increase in the frequency of damage to other steam system assets. In other words, SLR eroded the benefits of redundancy in steam generation. This effect was also seen in subsequent analyses describing how changes in elements of the networked infrastructure affected capability scores.

In absolute terms, the effect of redundancy in steam generation on the reliability of the *Provide Steam* capability was small. However, the magnitude of the effect by itself was not sufficient to fully evaluate the benefits of redundancy in steam generation. A full evaluation of maintenance and operating costs would need to be factored into the evaluation to fully capture the value of redundancy. Note that a consideration of these costs was beyond the scope of this study. It should also be noted that steam plant redundancy could have mitigated risks associated with hazards other than coastal storms (i.e., failure of equipment inside the auxiliary steam plant). Risks associated with hazards other than coastal storms have not been considered in the NSN Risk Model, but the model could be adapted to address these risks.

4.8.4.2 What-if Scenario #2: & 3: Removal vs. Flood-proofing of the Backup Electric Generators

In the event that power supply to the installation is lost, several diesel generators are available to generate backup electrical power to the primary steam plant, which is then distributed via the ring bus to transformers on the installation. Two "what-if" scenarios were devised to consider the impairment to the *Provide At-Berth Support* mission. In the first scenario, the backup generators were removed from the network by modifying function nodes in the model so that they were considered *Non-Functional* under all asset damage states. In the second scenario, the backup generators were flood-proofed by modifying function nodes in the model so that these assets remained *Functional* under all asset damage states. Results of the scenario analyses are summarized in Table 39 and Table 40 below.

Table 39. Difference in the capability scores for utility services that were potentially affected by removal or flood-proofing of the backup electric power generators supporting the primary steam plant.

Pier	SLR	DIFFERENCE IN CAPABILITY SCORES					DIFFERENCE IN MISSION PERFORMANCE INDEX
		Water	Steam	Oily Waste	Electric	Wastewater	
11	0.0	0.00E+00	0.00E+00	0.00E+00	0.00E+00	0.00E+00	0.00E+00
	0.5	5.10E-04	2.00E-05	0.00E+00	0.00E+00	0.00E+00	6.21E-05
	1.0	9.67E-02	1.88E-02	9.73E-07	0.00E+00	1.18E-06	1.44E-02
	1.5	7.05E-03	2.49E-05	1.24E-10	0.00E+00	4.12E-10	8.15E-04
	2.0	1.14E-07	4.10E-14	1.01E-18	0.00E+00	4.54E-16	1.31E-08
12	0.0	0.00E+00	0.00E+00	0.00E+00	0.00E+00	0.00E+00	0.00E+00
	0.5	5.10E-04	2.00E-05	1.00E-05	0.00E+00	0.00E+00	5.98E-05
	1.0	9.67E-02	1.88E-02	6.57E-04	0.00E+00	1.70E-05	1.37E-02
	1.5	7.05E-03	0.00E+00	6.84E-07	0.00E+00	1.37E-08	7.67E-04
	2.0	1.14E-07	0.00E+00	4.01E-13	0.00E+00	1.90E-13	1.24E-08
14	0.0	0.00E+00	0.00E+00	0.00E+00	0.00E+00	0.00E+00	0.00E+00
	0.5	5.10E-04	2.00E-05	0.00E+00	0.00E+00	0.00E+00	5.87E-05
	1.0	9.67E-02	1.88E-02	3.58E-05	0.00E+00	5.57E-05	1.36E-02
	1.5	7.05E-03	0.00E+00	2.11E-10	0.00E+00	3.58E-08	7.67E-04
	2.0	1.14E-07	0.00E+00	1.52E-19	0.00E+00	2.05E-13	1.24E-08

Table 40. Capability scores for utility services that were potentially affected by flood-proofing or removal of the backup electric power generators supporting the primary steam plant.

Pier	SLR	FLOODPROOF GENERATORS					REMOVE GENERATORS				
		Water	Steam	Oily Waste	Electric	Waste-water	Water	Steam	Oily Waste	Electric	Waste-water
11	0.0	0.9886	0.9637	0.9555	0.9807	0.9676	0.9886	0.9637	0.9555	0.9807	0.9676
	0.5	0.9275	0.8515	0.1370	0.8049	0.1717	0.9270	0.8515	0.1370	0.8049	0.1717
	1.0	0.4780	0.1055	0.0000	0.0040	0.0000	0.3812	0.0866	0.0000	0.0040	0.0000
	1.5	0.0086	0.0000	0.0000	0.0003	0.0000	0.0015	0.0000	0.0000	0.0003	0.0000
	2.0	0.0000	0.0000	0.0000	0.0000	0.0000	0.0000	0.0000	0.0000	0.0000	0.0000
12	0.0	0.9886	0.9637	0.9572	0.9884	0.9710	0.9886	0.9637	0.9572	0.9884	0.9710
	0.5	0.9275	0.8515	0.6999	0.9496	0.7660	0.9270	0.8515	0.6999	0.9496	0.7660
	1.0	0.4780	0.1055	0.0033	0.3636	0.0040	0.3812	0.0866	0.0027	0.3636	0.0040
	1.5	0.0086	0.0000	0.0000	0.0074	0.0000	0.0015	0.0000	0.0000	0.0074	0.0000
	2.0	0.0000	0.0000	0.0000	0.0000	0.0000	0.0000	0.0000	0.0000	0.0000	0.0000
14	0.0	0.9886	0.9637	0.9458	0.9879	0.9696	0.9886	0.9637	0.9458	0.9879	0.9696
	0.5	0.9275	0.8515	0.6695	0.9469	0.7866	0.9270	0.8515	0.6695	0.9469	0.7866
	1.0	0.4780	0.1055	0.0002	0.2978	0.0033	0.3812	0.0866	0.0001	0.2978	0.0033
	1.5	0.0086	0.0000	0.0000	0.0068	0.0000	0.0015	0.0000	0.0000	0.0068	0.0000
	2.0	0.0000	0.0000	0.0000	0.0000	0.0000	0.0000	0.0000	0.0000	0.0000	0.0000

Under the 0.0 m SLR scenario, neither flood-proofing nor removing the backup generators from the infrastructure network had any effect on the capability scores. Yet, as the sea levels rose, some benefits were realized. For example, under the 1.0 m SLR scenario, flood-proofing of the generators increased the capability score to *Provide Water* at Pier 11 from 0.3812 to 0.4780. This represented a 25 percent increase in the reliability of the *Provide Water* capability at Pier 11. When sea levels rose above one meter however, the flood-proofing benefits diminished because there was a high probability that the transformers supported by the generators themselves would be flooded and rendered *Non-Functional.*

Several other capabilities (i.e., *Provide Steam*, *Provide Oily Waste*, and *Provide Wastewater*) were also affected by flood-proofing of the generators at higher SLR scenarios. In general, the effects on these other capabilities were relatively small. The *Provide Electricity* capability at each pier remained unaffected by either the removal or flood-proofing of the generators because the substations that supplied electric power to the ships were independent of these generators. For those capabilities that were affected by these generators, the lack of benefits under baseline sea level conditions has been explained by the low probability of flooding at these generators under these scenarios. The benefits increased as the probability of flooding at these generators increased with SLR. However, beyond a critical threshold (e.g., 1.0 m SLR), the probability that other assets supporting the capabilities were rendered *Non-Functional* by storm loads increased to a point that obviated any potential benefit of flood-proofing the generators. The difference in the magnitude of the effects on the *Provide Steam* and *Provide Wastewater* capabilities has been explained by the physical location of relevant assets on the installation. Assets supporting the *Provide Wastewater* capability are located on the waterfront where they are more exposed to storm loads. Assets supporting the *Provide Steam* capability are, in general, located further inland and were are protected from storm loads. Removal and flood-proofing the generators represent the extremes in the spectrum of potential changes that could be made to the existing system. Therefore, results in Table 40 above can be interpreted as lower and upper bounds on the capability scores for any potential changes in reliability of these generators. For example, the effect of any retrofits that might decrease the reliability of the existing generators short of total removal or increase the reliability of the existing generators short of flood-proofing are bracketed within these bounds. It was also conceivable that new assets could be introduced into the infrastructure network and these changes might also affect the capability scores. For example, the installation of a second bank of backup electric power generators in a more protected location on the installation would provide additional redundancy to increase the reliability of electric power service on the installation. While this type of change in the infrastructure network can also be explored using the NSN Risk Model, the effect of introducing new assets on capability scores would not necessarily be bracketed within the bounds described in Table 40 above.

The backup generators exist primarily as a contingency in the event of a loss of power from the civilian grid, which is an event that might be caused by any number of reasons unrelated to coastal storms. For example, a lightning strike at the Sewell's Point substation could cause a loss of power on the installation or a coastal storm could cause damage to electric utility infrastructure upstream of the Sewell's Point substation. For purposes of this study, we only considered a loss of power caused by coastal storm loads on those assets in the NSN Risk Model. In other words, the model does not include the benefits these generators might provide in terms of reducing the probability that electric power is lost for other reasons.

4.8.4.3 What-if Scenario #4: Flood-Proofing Wastewater Infrastructure along the Waterfront

Flood-proofing the wastewater infrastructure at each of the wastewater lift stations located along the waterfront was one way to increase expected mission performance on the installation. Under this final "what-if" scenario, modifications to electric transformers, backup electric power generators, connections between transformers and waste water pumps (including their controls), and the waste water pumps themselves were proposed to offer a degree of flood-proofing. Modifications to these assets were implemented within the NSN Risk Model by changing the CPTs in the relevant function nodes so that the transformers, generators, wastewater pumps, and lift station buildings were *Functional* under all asset damage states. Results have been summarized for the *Provide Wastewater* capability in Table 41 and have been graphically derived in Figure 138.

Table 41. Capability scores for *Provide Wastewater* capability at each pier showing the effects of flood-proofing wastewater infrastructure along the waterfront.

Pier	SLR	Capability Score		Difference
		Current	Flood-proofed	
11	0.0	0.9676	0.9922	0.0247
	0.5	0.1717	0.8352	0.6635
	1.0	0.0000	0.0640	0.0640
	1.5	0.0000	0.0049	0.0049
	2.0	0.0000	0.0001	0.0001
12	0.0	0.9710	0.9922	0.0212
	0.5	0.7660	0.8352	0.0692
	1.0	0.0040	0.0640	0.0600
	1.5	0.0000	0.0049	0.0049
	2.0	0.0000	0.0001	0.0001
14	0.0	0.9696	0.9922	0.0227
	0.5	0.7866	0.8352	0.0486
	1.0	0.0033	0.0640	0.0607
	1.5	0.0000	0.0049	0.0049
	2.0	0.0000	0.0001	0.0001

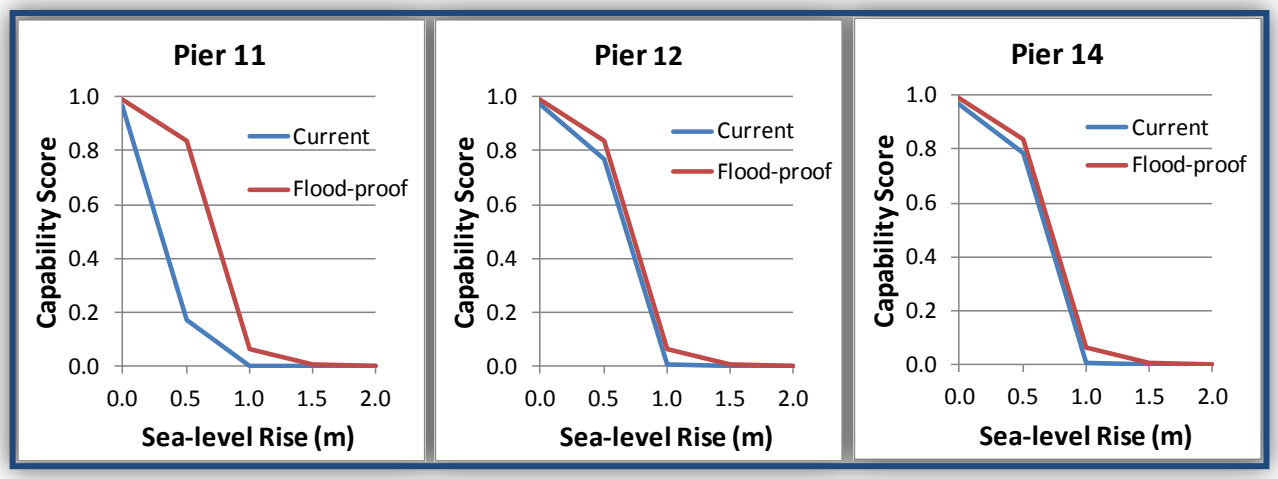

Figure 138. Effects of flood-proofing wastewater infrastructure on the waterfront in terms of capability scores for the *Provide Wastewater* capability.

Under the 0.0 m SLR scenario, the flood-proofing on Pier 11's support systems produced increased capability scores for the *Provide Wastewater* capability (the score increased by 0.0247 points from 0.9676 to 0.9922). The increased effects on the capability scores at Piers 12 and 14 were 0.0212 and 0.0227, respectively. Under the next SLR increment (i.e., 0.5 m), the potential benefits at Pier 11 increased by 0.6635. At Piers 12 and 14 the benefits increased by 0.0692 and 0.048 respectively. As sea level rose above 1.0 m, the benefits of flood-proofing wastewater infrastructure diminished. This effect has been attributed to coastal storms causing damage to other infrastructure elsewhere on the installation at higher sea level states, which undermine flood-proofing improvements to the infrastructure along the waterfront.

Results have also been summarized for the *Provide Oily Waste* capability in Table 42 and Figure 139.

Table 42. Capability scores for the *Provide Oily Waste* capability at each pier showing the effects of flood-proofing wastewater infrastructure along the waterfront.

Pier	SLR	Capability Score		Difference
		Current	Flood-proofed	
11	0.0	0.9555	0.9687	0.0132
	0.5	0.1370	0.5629	0.4259
	1.0	0.0000	0.0024	0.0024
	1.5	0.0000	0.0000	0.0000
	2.0	0.0000	0.0000	0.0000
12	0.0	0.9572	0.9693	0.0121
	0.5	0.6999	0.7033	0.0034
	1.0	0.0028	0.0037	0.0008
	1.5	0.0000	0.0000	0.0000
	2.0	0.0000	0.0000	0.0000
14	0.0	0.9458	0.9678	0.0220
	0.5	0.6695	0.6908	0.0213
	1.0	0.0002	0.0006	0.0005
	1.5	0.0000	0.0000	0.0000
	2.0	0.0000	0.0000	0.0000

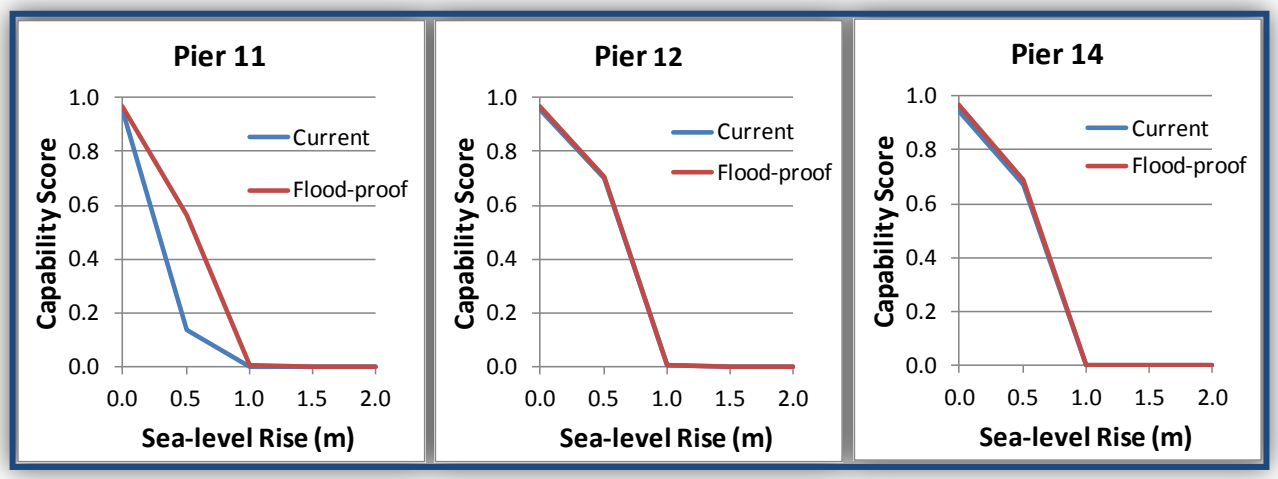

Figure 139. Effects of flood-proofing wastewater infrastructure along the waterfront in terms of capability scores for the *Provide Oily Waste* capability.

On NSN, the system used to remove oily wastewater from the ships is closely related to the wastewater system. Control systems for oily waste pumps are housed inside the wastewater lift house structures, and the oily wastewater pumps are located nearby. Therefore, flood-proofing of the wastewater infrastructure on the waterfront also led to improvements in the scores for the *Provide Oily Waste* capability. Table 42 above presents capability scores for the *Provide Oily Waste* capability under the what-if scenario. Under the 0.0 m SLR scenario, flood-proofing of the wastewater infrastructure along the waterfront increased the *Provide Oily Waste* capability scores at Pier 11 from 0.9555 to 0.9687. Similar improvements were realized at Piers 12 and 14. Under the 0.5 m SLR scenario, a dramatic improvement in the *Provide Oily Waste* capability

was realized at Pier 11, but this benefit diminished as SLR increased to one meter (refer to Figure 139 above).

The overall effects of flood-proofing the wastewater infrastructure on the waterfront were viewed in terms of the MPI as well. In Figure 140, the MPI has been plotted at each pier over the five prescribed SLR scenarios.

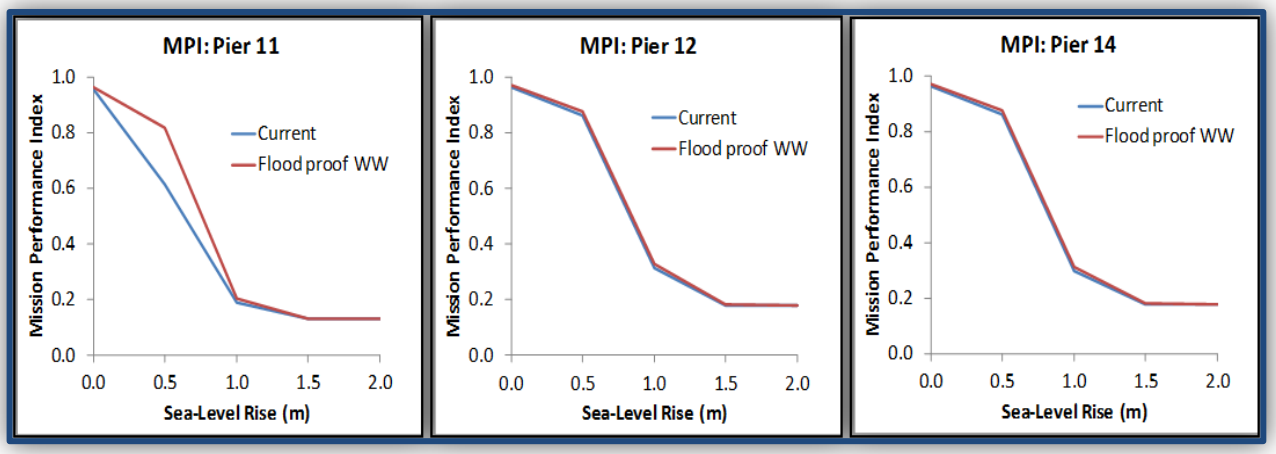

Figure 140. Effect of flood-proofing the wastewater infrastructure on the waterfront in terms of MPI.

The largest improvement in MPIs was seen at Pier 11 under the 0.5 m SLR scenario. Flood-proofing wastewater infrastructure increased the MPI from 0.6157 to 0.8172, which was almost a 33 percent increase. Improvements in MPIs at Piers 12 and 14 were notably smaller.

4.9. Results of the Geophysical Survey

4.9.1 Outputs and Technical Results

The electrical resistivity data have been presented as 2D filtered field data, and resistivity and conductivity inversion sections. The raw field data were filtered to remove erratic spikes and unstable readings caused by poor electrode contact and/or the presence of extremely resistive or conductive subsurface material. The data were processed and inverted using the software EarthImager2D (AGI, version 2.4.1). It is important to remember that the field data were plotted as apparent resistivity and pseudo-depth, and the inverted data represent the true resistivity (or conductivity) and depth. There can be significant differences between the apparent and true resistivity plots. The inversion of most data sets resulted in a depth of investigation of 15.8 m (51.8 ft). The color scale is logarithmic, with the dark colors (blues) representing low values and the reds representing high values. The EM-31 data have been presented as profile plots along the resistivity survey line. The well data have been presented as point data on an aerial map of the project area. A summary of the EM-31 conductivity profiles (Figure 141), resistivity data (measured and inverted resistivity and conductivity sections) (Figure 142), resistivity/conductivity saturation and saline boundaries, and their corresponding depths (Table 43), and TDS levels in measured monitoring wells (Figure 143) are provided for the nine

surveyed sites below. In addition, each of the nine sites has been profiled in the sections immediately thereafter.

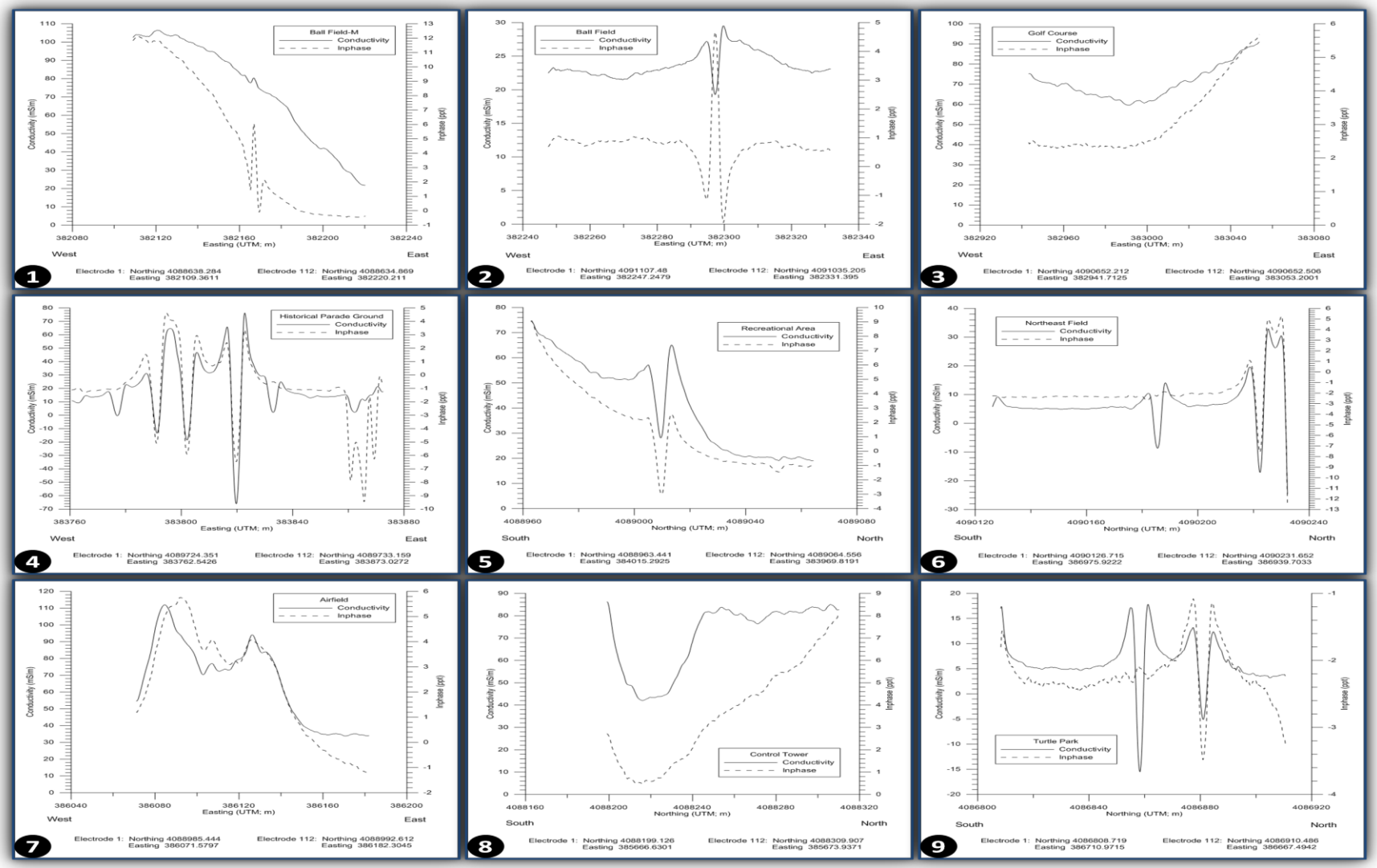

Figure 141. Results of the EM-31 terrain conductivity survey along the profile line at the nine sites.

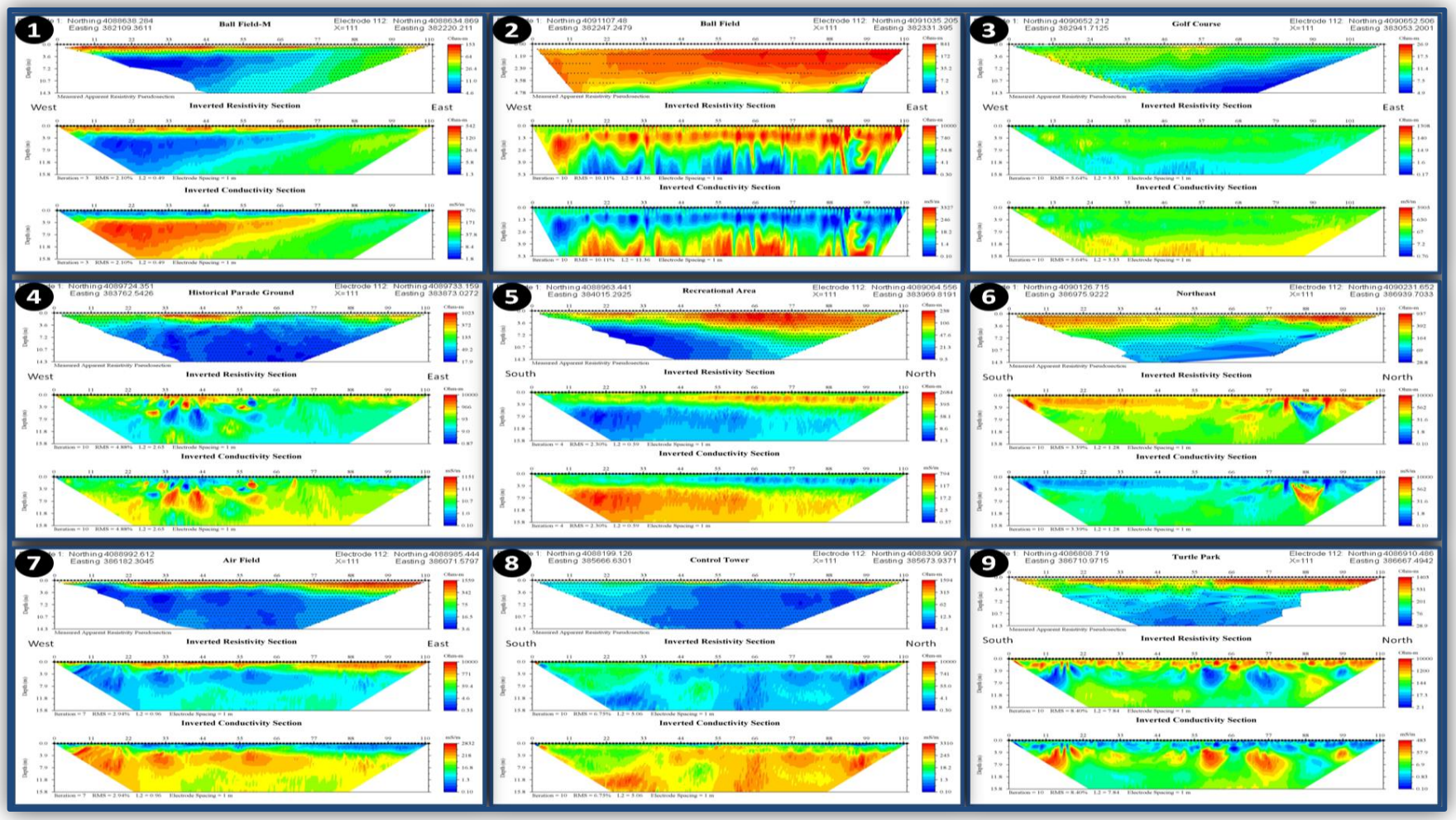

Figure 142. Resistivity inversion results for the nine sampling sites. The top plot was the measured apparent resistivity data; middle plot was the inverted resistivity section; bottom plot was the inverted conductivity section, which was the reciprocal of the resistivity.

Table 43. Summary of the resistivity/conductivity saturation and saline boundaries with their corresponding depths.

Site	Saturation Boundary Estimated Resistivity (<=) (Ω-m)	Saline Boundary Estimated Resistivity (<=) (Ω-m)	Saturation Boundary Estimated Conductivity (>) (mS/m)	Saline Boundary Estimated Conductivity(>) (mS/m)	Estimated Depth Saturation Boundary (m)	Estimated Depth Saline Boundary (m)
1−Ball Field-M	56	12	18	81	0.5 to 2	1 to 3
2−Ball Field	100	15	10	67	1.1 to 4.9	2.5 to 4.5
3−Golf Course	+	8.5	+	118	+	2.4 to 10.5
4−Historical Parade Ground	52 (?)	+	19 (?)	+	3 (?)	>15*
5−Recreational Area	94	14^	11	72^	2.5 to 5	4.5 to 7.5
6−Northeast Area	133	+	8	+	2 to 7	>15*
7−Airfield	214	+	5	+	0.5 to 3.3	>15*
8−Control Tower	100	+	10	+	>0.5*	>15*
9−Turtle Park	+	+	+	+	+	>15*

+ cannot be determined from the data
* can be any value greater than value specified
^ possible high clay content

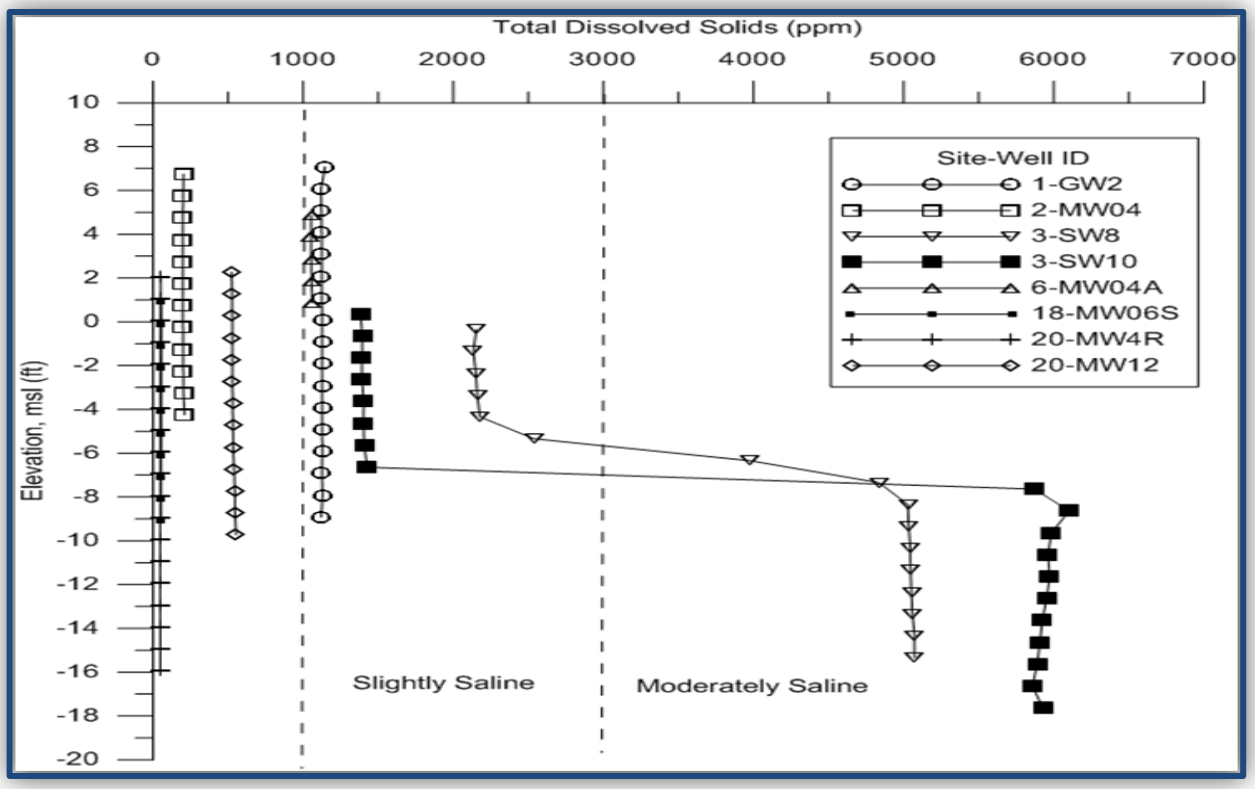

Figure 143. Total dissolved solids levels in measured monitoring wells.

4.9.1.1 Site 1−Ball Field-M

Site 1−Ball Field-M ("M" being adjacent to a McDonald's®) traverses a ball field and extends into an open field. It was located in the southwest section of the study area near the intersection of B Avenue and 2nd Street (Figure 59 above). The survey line basically ran west to east and extended 111 m (Figure 144). The gate in the outfield fence was positioned at 55.5 m along the line between electrodes 56 and 57.

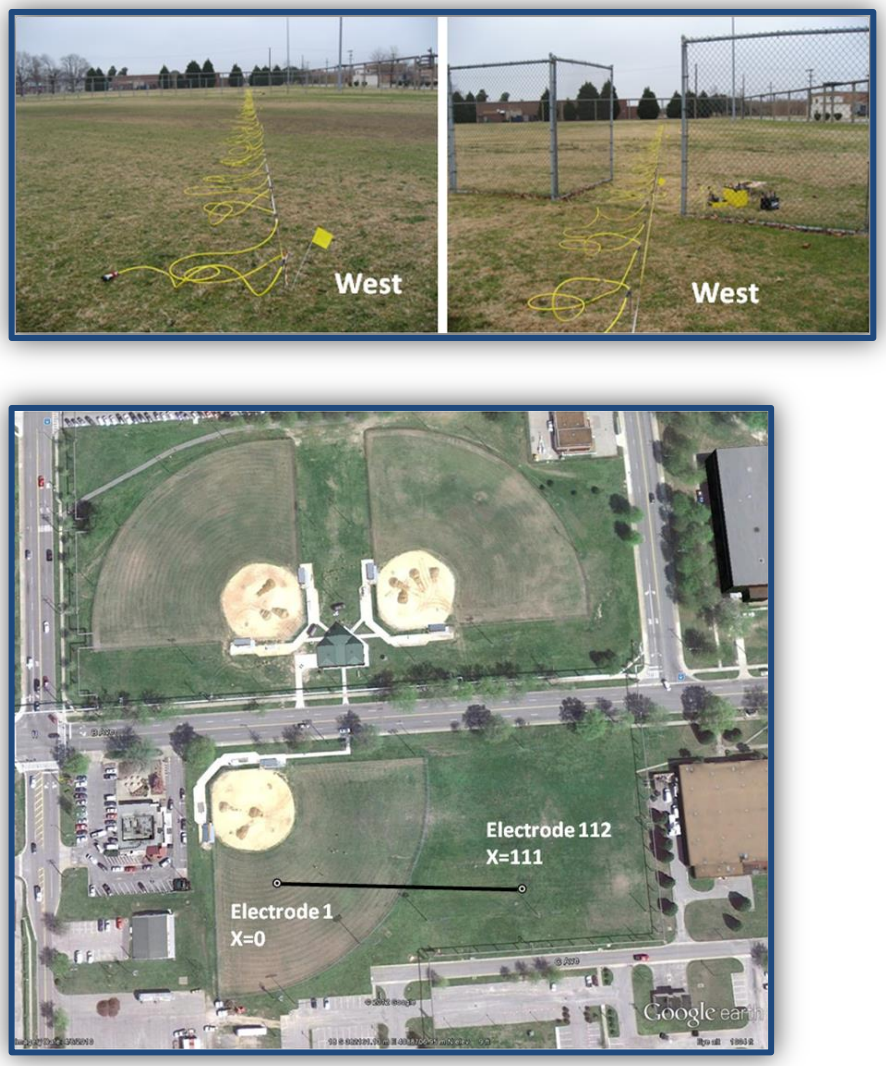

Figure 144. Photograph showing a view of the Ball Field-M site and the location of the fence gate along the survey line, and aerial view. The site was located near the intersection of B Avenue and 2nd Street.

The conductivity declined steadily from west (high conductivity, greater than 100 mS/m) to east (moderate conductivity, 20 mS/m). The distinct anomaly seen in the inphase curve (dashed line) was caused by the gate in the outfield chain-link fence. The dots on the measured apparent resistivity pseudo-section (top plot) indicate the pseudo-depth of a measurement, and represent which measurements were used in the inversion. The data suggest a thin, resistive (greater than 82 Ω-m) layer to a depth of two meters at the western edge that thins out at the eastern edge. This resistive layer overlies a moderately resistive (12-56 Ω-m) layer, which was interpreted as saturated soil. At a depth of about three meters resistivity was a low wedge (less than 12 Ω-m) that thinned from west to east, and pinched out at about 90 m east along the survey line. We believe this low resistivity wedge is a soil layer saturated by saltwater intrusion. The conductivity section is the reciprocal of the resistivity, thus showing a high conductivity wedge that corresponded to the saltwater intrusion. The resistivity data correlated well with the EM-31 conductivity profile, with both datasets indicating high (low) conductivity (resistivity) at the

western end of the survey line that transitioned to moderate conductivity (resistivity) at the eastern end (refer to *Graph 1* in Figure 141 and Figure 142 above). There were no monitoring wells measured near this site, although wells 3-SW8 and 3-SW10 (Figure 59 above) were located at approximately the same easting and were proximal to the bay and Ball Field-M. The depth of the water table below ground surface at these wells is 2.6 m (*3-SW8*) and 1.7 m (*3-SW10*), with average TDS levels of 3,908 ppm and 4,029 ppm (Figure 143 above), respectively. These data support an interpretation of saturated soils at a depth of two meters and the presence of saltwater intrusion at site Ball Field-M.

4.9.1.2 Site 2−Ball Field

Site 2−Ball Field crosses through two ball fields and is located in the northwest corner of the project area along Hughes Dr. (Figure 59 above). The survey line basically ran west to east and extended 111 m (Figure 145).

Figure 145. Photograph and aerial view of the Ball Field site located near the western end of Hughes Drive.

The terrain conductivity data, shown in *Graph 2* in Figure 141 above, indicates a near-surface conductivity of about 23 mS/m. Both the conductivity and inphase curves show an anomaly, which was likely caused by a buried utility line. Note that in the measured apparent resistivity pseudo-section (refer to *Graph 2's* top plot in Figure 142 above) that the section only extends to a depth of five meters (compared to 15.8 m at Ball Field-M), and that numerous dots, representing pseudo-depth measurement locations, are absent. The subsurface soils were quite conductive at this site, thus deep penetration of the current was not achieved (current followed the path of least resistance). The TDS levels in the two measured monitoring wells (*3-SW8* and *3-SW10*) near this site increased significantly at a depth that corresponded to a loss of electrical current penetration (Figure 143 above). The upper two to three meters were resistive (greater than 100 Ω-m), with this resistive layer extending to a depth of five meters at the western end. The red "spikes" presented in the eastern half of the section which extended deeper into the subsurface were likely an artifact of sparse data, and therefore do not represent a geologic feature. Below the resistive layer at a depth ranging from two to five meters was a moderately resistive layer (15 - 100 Ω-m); this layer likely consists of saturated soils. Saline intrusion

appeared to be present where the resistivity (conductivity) was less (greater) than 15 Ω-m (67 mS/m) at variable depths along the section, but no shallower than 2.5 m. The monitoring wells *3-SW8* and *3-SW10* (Figure 59 above) near this site corroborate an interpretation of saturated soil at a depth of two to five meters, and the presence of saltwater intrusion (greater than 2.5 m depth).

4.9.1.3 Site 3−Golf Course

Site 3−Golf Course is located in the northwest section of the project area on the north side of the golf course along Hughes Dr. (Figure 59 above). The survey line basically ran west to east and extended 111 m (Figure 146).

Figure 146. Photograph and aerial view of the Golf Course site located along Hughes Drive.

This area differs from the previous two sites, with no high resistivity layer present directly below the ground surface. The EM-31 terrain conductivity data (refer to *Graph 3* in Figure 141 above) showed a moderately high to high (60 - 90 Ω-m) conductivity layer, with the conductivity gradually decreasing from west to east toward the center of the profile line, and then increasing to the east. The resistivity data (refer to *Graph 3* in Figure 142 above) agreed with this trend, and also revealed a high conductivity (greater than 118 mS/m) layer at a depth from 2.4 to 10.5 m below ground surface, which likely represents saltwater intrusion. No definitive boundary was seen in the data that indicates a change from unsaturated to saturated material. The closest monitoring wells to this site were again *3-SW8* and *3-SW10* (Figure 59 above). Both wells have TDS levels indicating moderate saline conditions and support an interpretation of the presence of saltwater intrusion at this site.

4.9.1.4 Site 4−Historical Parade Ground

Site 4−Historical Parade Ground is located southeast of the golf course, at the intersection of Bainbridge Ave. and Franklin St. (Figure 59 above). The survey line basically ran west to east and extended 111 m (Figure 147).

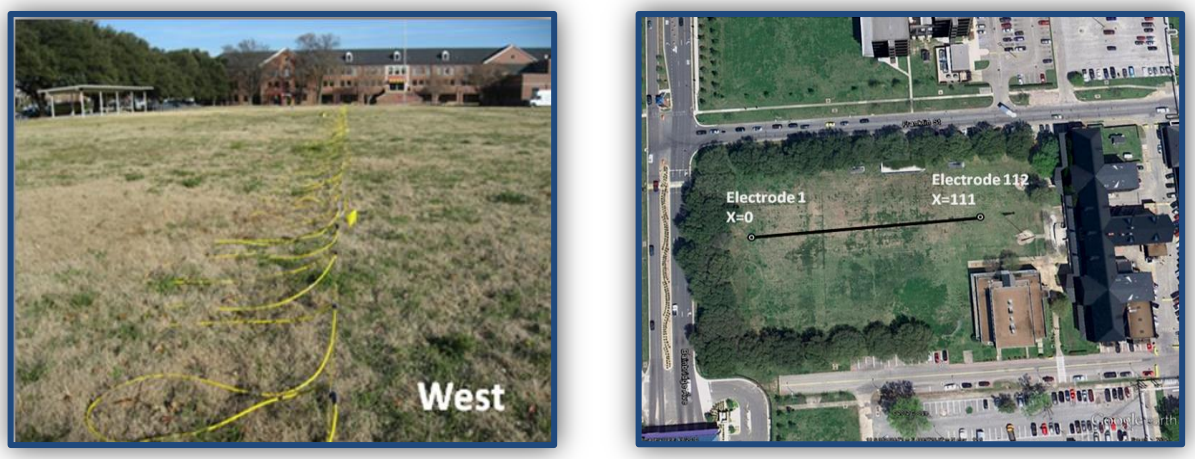

Figure 147. Photograph and aerial view of the Historical Parade Ground site located at the intersection of Bainbridge Avenue and Franklin Street.

There were multiple anomalies present in the terrain conductivity data (refer to *Graph 4* in Figure 141 above), which were likely associated with utilities crossing the profile line. The background conductivity appeared to be low, approximately 15 mS/m. The anomalous region in the shallow near-surface between x = 20 - 60 was probably caused by the presence of the numerous buried utilities (refer to *Graph 4* in Figure 142 above). There were two distinct conductivity regions identified (less than or greater than 35 mS/m),although we are unsure what geologic boundary generated this distinction. It is possible that the boundary (19 mS/m) is associated with the water table (depth about three meters). The saline boundary was not identifiable in this dataset. The closest monitoring wells to this site were *20-MW4R* and *20-MW12* (Figure 59 above), with measured water-table depths (below ground surface) of 2.2 m and 2.1 m, respectively. Based on these data, it is probable that the boundary identified at 3-meter depth does correspond to the water table. The average TDS levels (Figure 143 above) at these two wells were 49 (*20-MW4R*) and 535 (*20-MW12*), indicating fresh water to their respective well depths of 12 m and 6 m.

4.9.1.5 Site 5−Recreational Area

Site 5−Recreational Area is located in the central region of the project area proximal to building U-93 at the intersection of First Ave. and West C Street (Figure 59 above). The survey line basically ran south to north and extended 111 m (Figure 148).

Figure 148. Photograph of the Recreational Area site located near building U-93 at the intersection of First Avenue. and West C.

The EM-31 conductivity profile (refer to *Graph 5* in Figure 141 above) shows that a buried utility line is present near the center of the profile, and that the conductivity is moderately high (about 75 mS/m) at the south end and gradually decreases to a value of 20 mS/m at the north end. This same character was seen in the resistivity and conductivity sections (refer to *Graph 5* in Figure 142 above). A near-surface resistive (greater than 94 Ω-m) layer was intermittent in the southern portion of the section, which corresponds to a higher conductivity in the EM-31 data, and became continuous at x = 44 with a slight thickening to the north. Saturated soils appear to be present at a depth range 2.5 to 5 m, and were represented by a conductivity of more than 11 mS/m. Saltwater intrusion may be present at the southern portion of the survey line where conductivity values were more than 72 mS/m at a depth of 4.5 to 7.5 m (Table 43 above). There were no monitoring wells near the Recreational Area that were measured, but the site was situated about halfway between wells *6-MW04A* and *20-MW4R* (Figure 59 above). Well *6-MW04A* has an average TDS level of 1,055 ppm, which just exceeds the fresh water limit of 1,000 ppm, whereas well *20-MW4R* is well below this limit with a TDS level of 49 ppm (Figure 143 above). These data suggest that the possible saltwater intrusion boundary of conductivity values more than 72 mS/m mentioned above may actually represent a soil with a higher clay content.

4.9.1.6 Site 6−Northeast Area

Site 6−Northeast Area is located in a field in the northeast corner of the project area (Figure 59 above). It was near the intersection of Tenth Ave. and Warehouse St. The survey line basically ran south to north and extended 111 m (Figure 149).

Figure 149. Aerial view of the Northeast Area site located near the intersection of Tenth Avenue. and Warehouse Street.

The terrain conductivity data indicates a near-surface conductivity of about 7 mS/m (refer to *Graph 6* in Figure 141 above). There were four anomalies present in the data: one at the south end, one near the center of the profile line, and two within the northern 10 m of the profile. As at the previous sites, buried utility lines were suspected of being the source of these anomalies. Results of the electrical resistivity survey are given in *Graph 6* in Figure 142 above. The apparent resistivity pseudo-section (top plot of *Graph 6* in Figure 142 above) shows that the majority of data points collected in the northern portion of the section were of poor quality and not used in the inversion. Thus, the anomalous region beyond x = 80 was suspect. As indicated in the EM-31 data, there was a resistive (greater than 133 Ω-m; less than eight mS/m) near-surface layer that extends to a depth of two to seven meters (thickens toward the center of the section). Beneath this resistive layer was a moderately conductive (8 to 65 mS/m) layer that extends to the investigation depth (15.8 m) of the survey. It was possible that this layer may be saturated. Although the survey site was relatively close to Willoughby Bay, the depth of investigation of this survey was not sufficient to detect the saline boundary (Table 43 above). No monitoring wells exist in this region of the project area that could confirm the water-table depth or assist in determining the presence of saltwater intrusion.

4.9.1.7 Site 7−Airfield

Site 7−Airfield is located proximal to the airfield outside the northern boundary fence at the east end, off of Patrol Road (Figure 59 above). The survey line basically ran west to east and extended 111 m (Figure 150).

Figure 150. Photograph and aerial view of the Airfield site located outside of the airfield northern boundary fence off of Patrol Road.

The terrain conductivity data shows variations in the conductivity along the profile, which reflect changes in the conductivity of the saturated soils (refer to *Graph 7* in Figure 141 above). The conductivity section (refer to the bottom plot of *Graph 7* in Figure 142 above) agrees with the shallower EM-31 conductivity profile, with high conductivity at the west end at a shallow depth and the depth and conductivity of this layer increasing (depth) with decreasing (conductivity) to the east. There was a near-surface resistive (greater than 214 Ω-m) layer that thickens to the east, ranging in thickness from 0.5 to 3 m. Below the resistive layer was a moderately conductivity (5 to 61 mS/m) layer that was probably saturated soil. The higher conductivity (greater than 61 mS/m) soils were also saturated and likely contain a greater amount of clay. There were no monitoring wells present in this area. However, the wells that were measured on the eastern side of the project area all had TDS levels below 1,000 ppm (Figure 143 above), indicating no saltwater intrusion. Based on this information, it was assumed that the higher conductivity soils detected in this survey likely reflect high clay content soils.

4.9.1.8 Site 8−Control Tower

Site 8−Control Tower is located in the field east of the LP212 AMC control tower near Air Terminal Road (Figure 59 above). The survey line basically ran south to north and extended 111 m (Figure 151).

Figure 151. Photograph and aerial view of the Control Tower site located off of Air Terminal Road behind LP212 AMC Terminal Tower.

The conductivity of the shallower soils was moderately high (approximately 82 mS/m) along most of the profile line, except where it dropped dramatically to about 43 mS/m between x = 13 and x = 25 at the south end of the profile line (refer to *Graph 8* in Figure 141 above). This corresponds with the electrical conductivity section (refer to the bottom plot of *Graph 8* in Figure 142 above) which show that the section is dominated by soils having a conductivity greater than 67 mS/m, except in the near surface and in the region *x* less than 33, depth 0 - 10 m, where moderate conductivity values (10 - 67 mS/m) exist. Saturated soils were likely to be present at a depth greater than 0.5 m. Although the deeper soils displayed some very high conductivity values (greater than 1,000 mS/m), their distribution in the subsurface suggest these represent high clay content soils rather than the presence of saltwater intrusion. The Control Tower site is located on the east side of the project area where no monitoring wells exist, and measured TDS levels in the closest wells indicated fresh water (Figure 143 above). These data supported the electrical resistivity interpretation of saturated clayey soils rather than saltwater intrusion.

4.9.1.9 Site 9−Turtle Park

Site 9−Turtle Park is a ball field located in the southeast corner of the project area along Patrol Road (Figure 59 above). The survey line basically ran south to north and extended 111 m (Figure 152).

Figure 152. Photograph and aerial view of the Turtle Park ball field site located along Patrol Road.

The EM-31 conductivity data (refer to *Graph 9* in Figure 141 above) shows one utility crossing the profile line at northing 4086880 (near station x = 72). The strong conductivity response at northing 4086858 (near station x = 48) was caused by a non-metallic object. The high conductivity at the south end of the line was caused by the instrument being adjacent to the backstop fence. The background conductivity of the subsurface soils in the upper six meters was about 5 mS/m. The resistivity section (refer to the middle plot of *Graph 8* in Figure 142 above) shows a discontinuous resistive (greater than 416 Ω-m) layer with variable thickness in the upper four meters. There were five low resistivity zones within the section centered about x = 14, 20, 60, 76, and 99, at top depths of 1.7 - 2.5 m. The validity of these zones was suspect because they correspond with regions in the apparent resistivity pseudo-section (top plot) where there was poor data quality. The background conductivity (bottom plot) for soils below 4-m depth was 2.5 to 20 mS/m, which does not suggest the presence of saturated soil. Also, depth to the freshwater-saltwater interface was deeper than the investigation depth of this survey. This site was near two monitoring wells (*2-MW04* and *18-MW06S*) where groundwater depth and TDS levels were measured (Figure 143 above). At both wells the groundwater table was detected at less than one meter, and the highest average TDS level was 201 ppm (*2-MW04*) (Figure 143 above). Although the groundwater table could not be determined using electrical resistivity, based on the water table levels detected in the monitoring wells it was likely the depth to ground water was within two meters of the ground surface.

4.9.2 Summary and Discussion

Nine electrical resistivity surveys were conducted and eight monitoring wells were sampled to obtain an estimate of the depth to the water table and saltwater intrusion boundary within a designated project area on NSN. The electrical resistivity soundings had a maximum depth of investigation of 15.8 m. Based on conductivity values, the depth to saturated soils was identified at seven of the nine sites (refer to Table 43 above). These depths were agreeable with water-table depths measured in monitoring wells within the area. Using the electrical resistivity method, the presence of saltwater intrusion was identified at four of the five sites located in the western half of the project area (refer to Table 43 above). Measurements of TDS levels in monitoring wells

confirm this, with moderately saline water present in wells along the western project boundary proximal to the bay, and becoming fresher to the east. Sites where the presence of saltwater intrusion has not been identified do not mean that saltwater intrusion has not occurred, but rather indicate that, if present, the boundary is deeper than the 15.8 m investigation depth of the resistivity survey.

4.10. Surface Flood Routing Re-Assessment with Groundwater Modeling Inputs

Using the same 25 scenarios of coastal storm intensities and SLR levels as the original analysis, but incorporating the new groundwater simulations into the flood routing simulations, we generated new estimates of flooding and probabilities of mission impairment described below.

4.10.1 Outputs and Technical Results

Surface flood routing assessments for all key installation assets were computed by the same means described in detail in *Section 3.6* using the GSSHA numerical simulation tool, with some important differences – in the new analysis GSSHA's 1-dimensional vertical infiltration and 2D groundwater flow were employed using the results from the AdH-WASH groundwater simulations. Unlike the previous surface flood routing computations, the new GSSHA simulations included the impacts from groundwater through the use of the AdH-WASH water table elevation results and groundwater aquifer parameterization, generating temporal hydrographs of water depth at every grid cell of the study area for each design storm and SLR scenario. The GSSHA model simulated the combined effects of SLR, storm surge, groundwater, and precipitation on the study site. In total, five prescribed SLR scenarios (0.0 m – 2.0 m) and five analyzed storm events (i.e., the 1-yr, 10-yr, 50-yr, 100-yr return intervals, and the historical 1982 nor'easter) were simulated making a total of 25 runs. The temporally- and spatially-varied results were analyzed to determine the maximum flood depth in each cell over the entire simulation. Figure 153 - Figure 157 depict the new maximum flood depths due to the range of storm events and SLR scenarios.

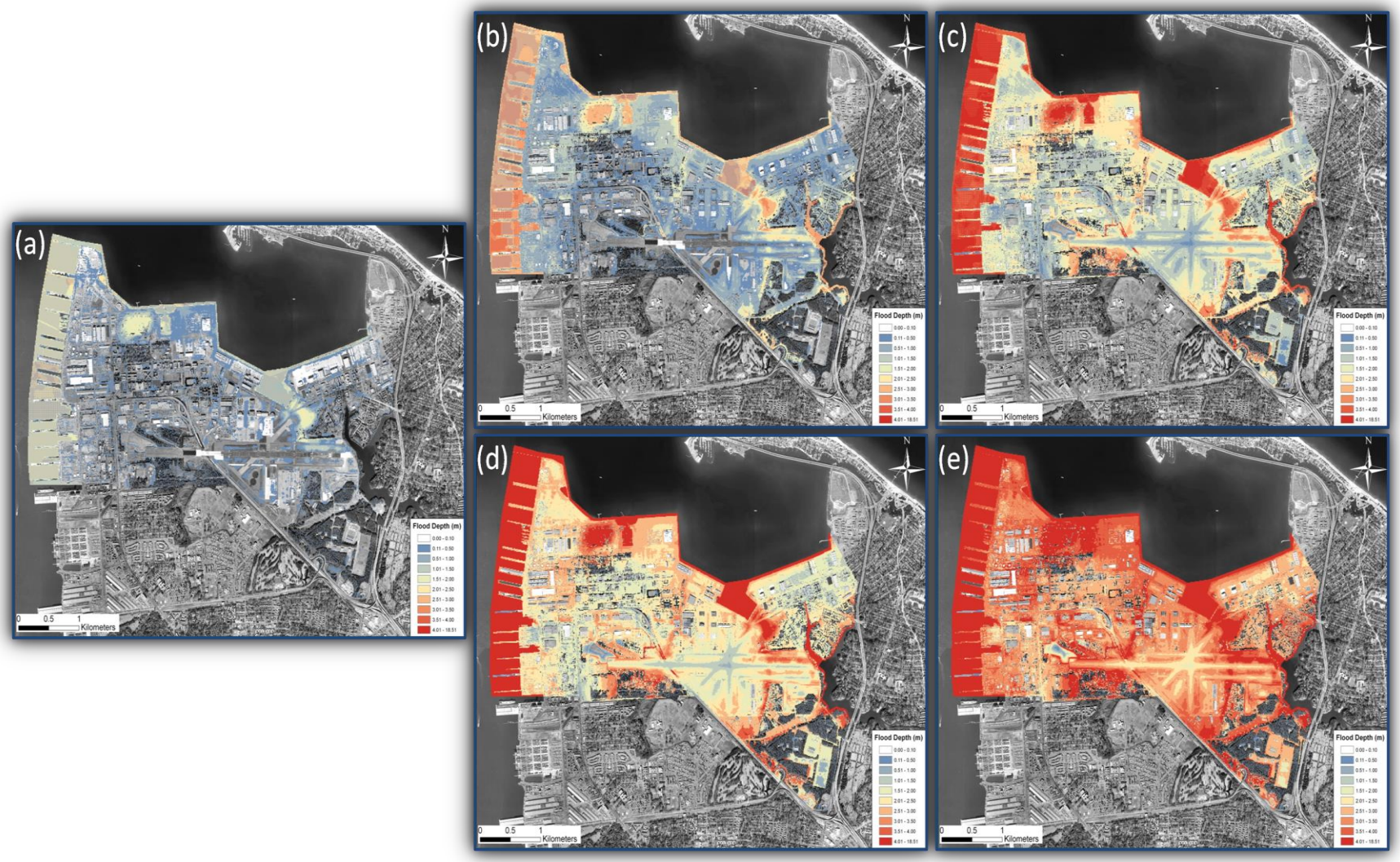

Figure 153. New flood routing and maximum depths (m) under the 1-yr return interval storm event for the (a) 0.0 m, (b) 0.5 m, (c) 1.0 m, (d) 1.5 m, and (e) 2.0 m SLR scenarios with groundwater modeling incorporated into GSSHA's analysis.

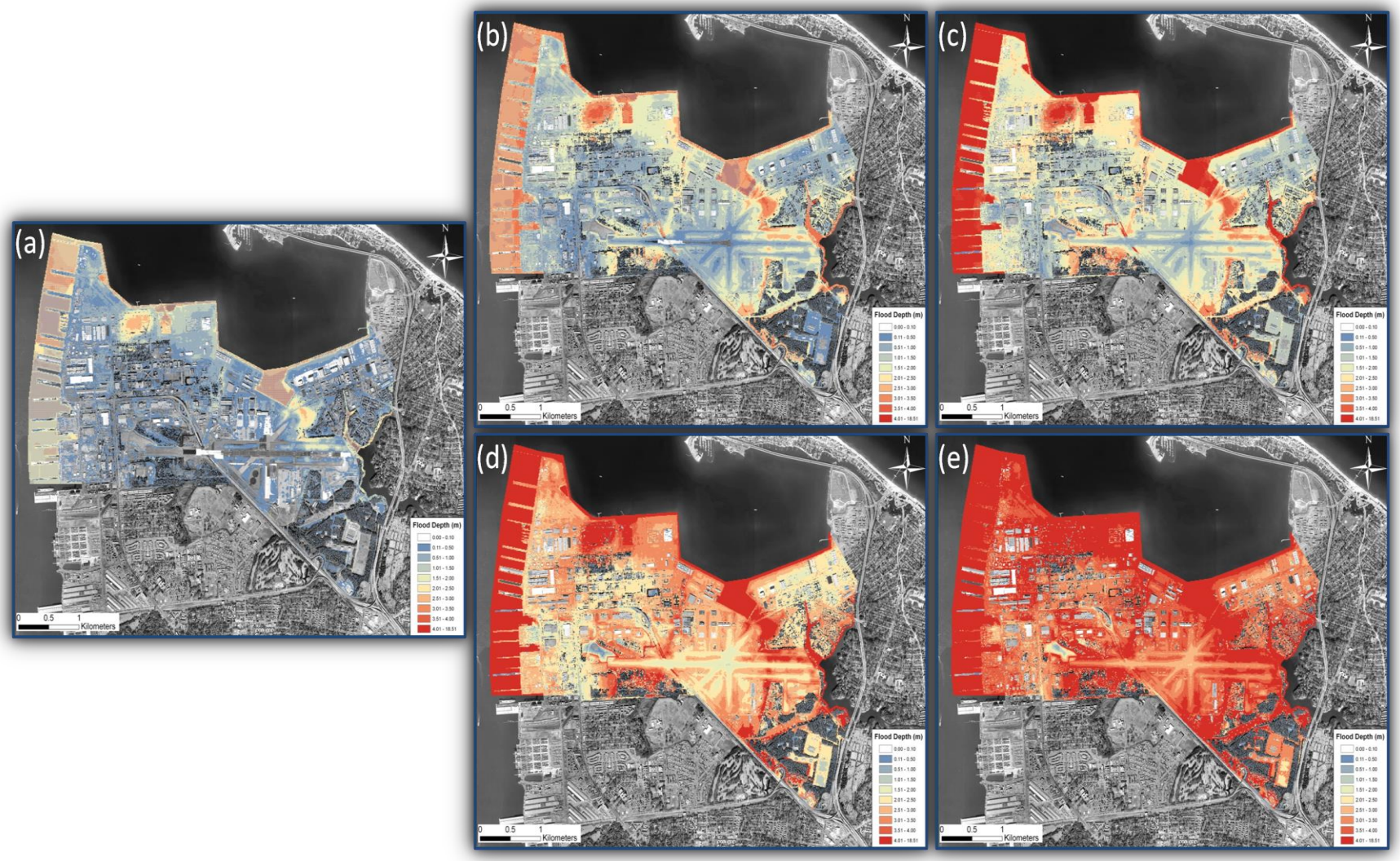

Figure 154. New flood routing and maximum depths (m) under the 10-yr return interval storm event for the (a) 0.0 m, (b) 0.5 m, (c) 1.0 m, (d) 1.5 m, and (e) 2.0 m SLR scenarios with groundwater modeling incorporated into GSSHA's analysis.

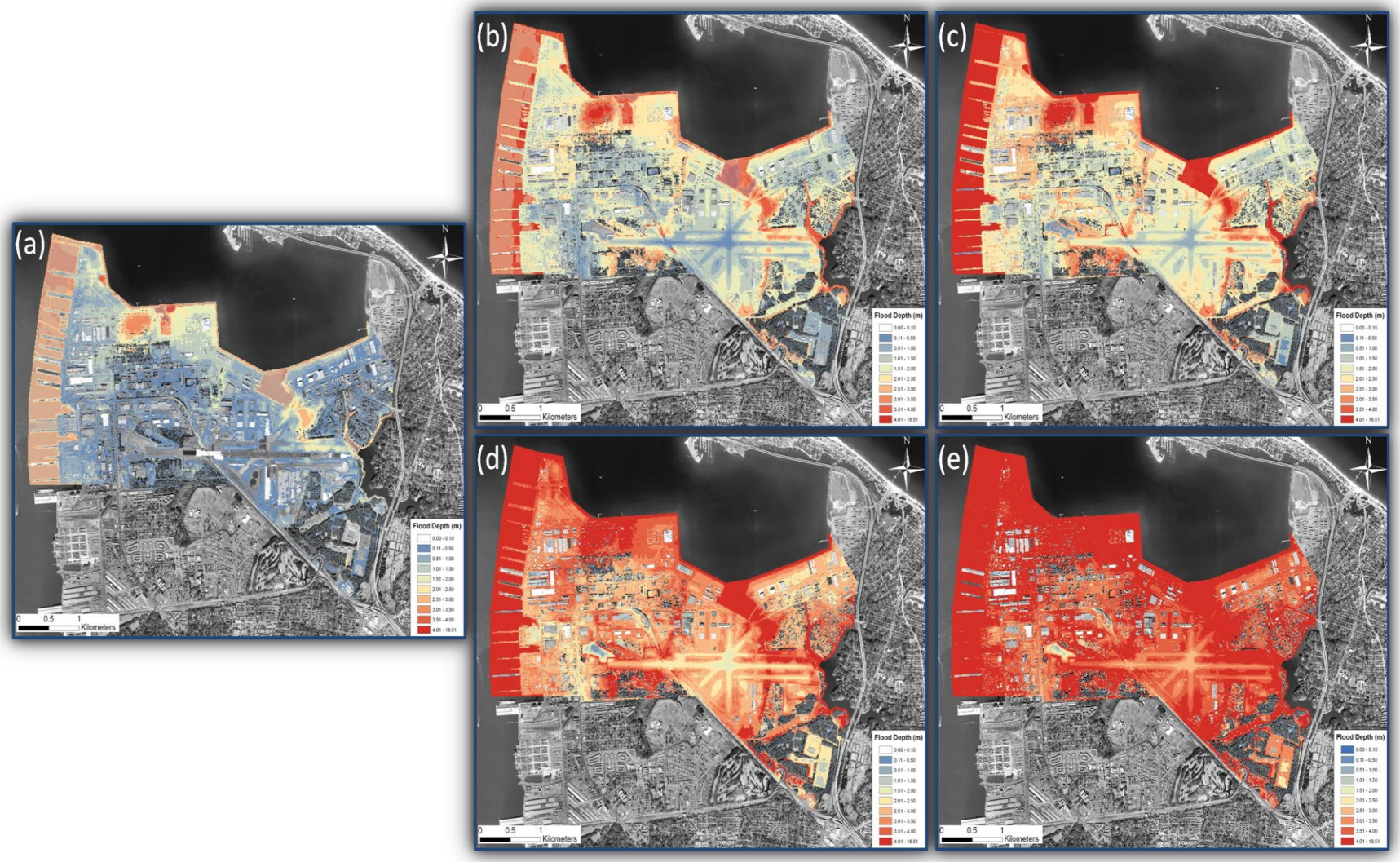

Figure 155. New flood routing and maximum depths (m) under the 50-yr return interval storm event for the (a) 0.0 m, (b) 0.5 m, (c) 1.0 m, (d) 1.5 m, and (e) 2.0 m SLR scenarios with groundwater modeling incorporated into GSSHA's analysis.

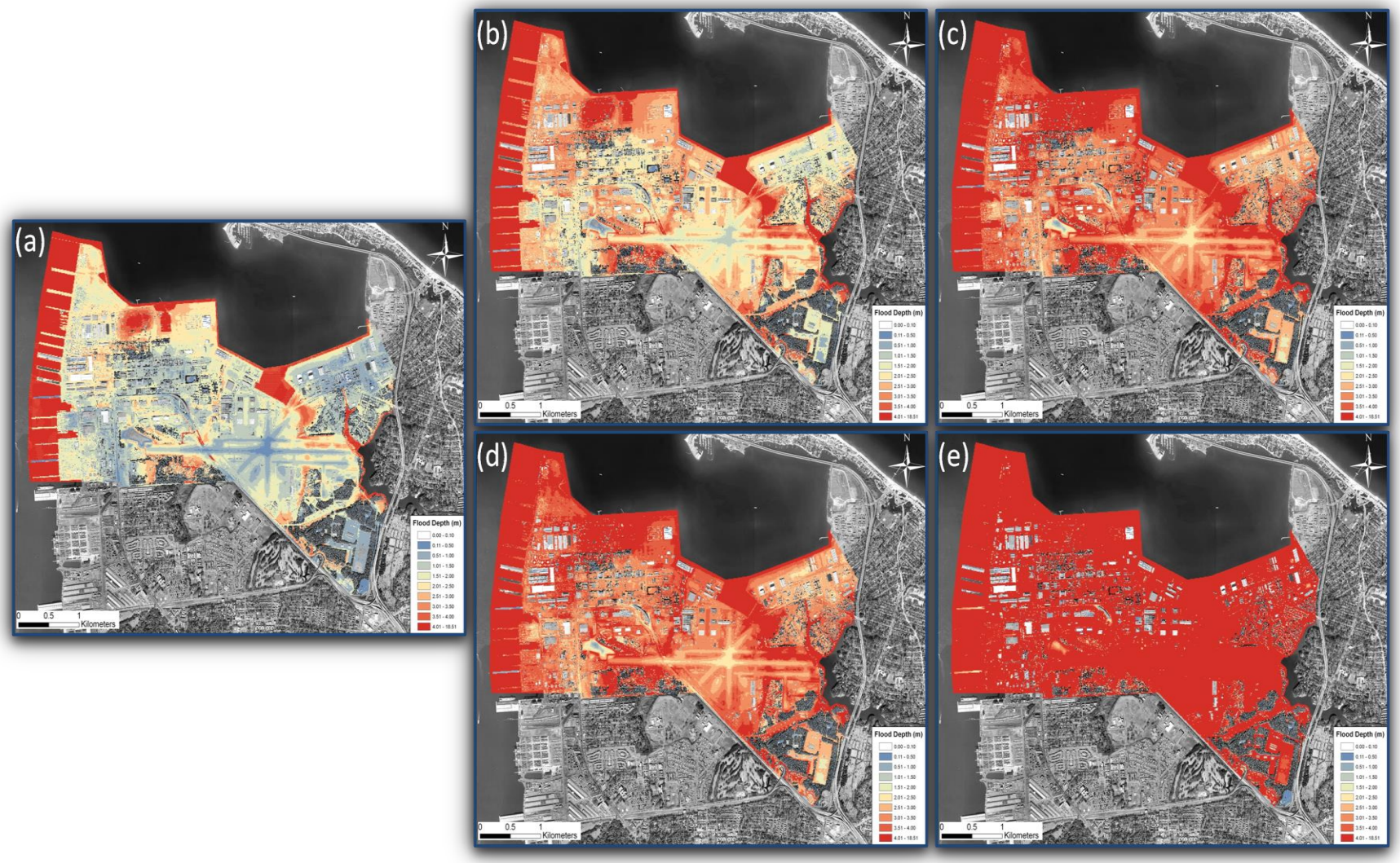

Figure 156. New flood routing and maximum depths (m) under the 100-yr return interval storm event for the (a) 0.0 m, (b) 0.5 m, (c) 1.0 m, (d) 1.5 m, and (e) 2.0 m SLR scenarios with groundwater modeling incorporated into GSSHA's analysis.

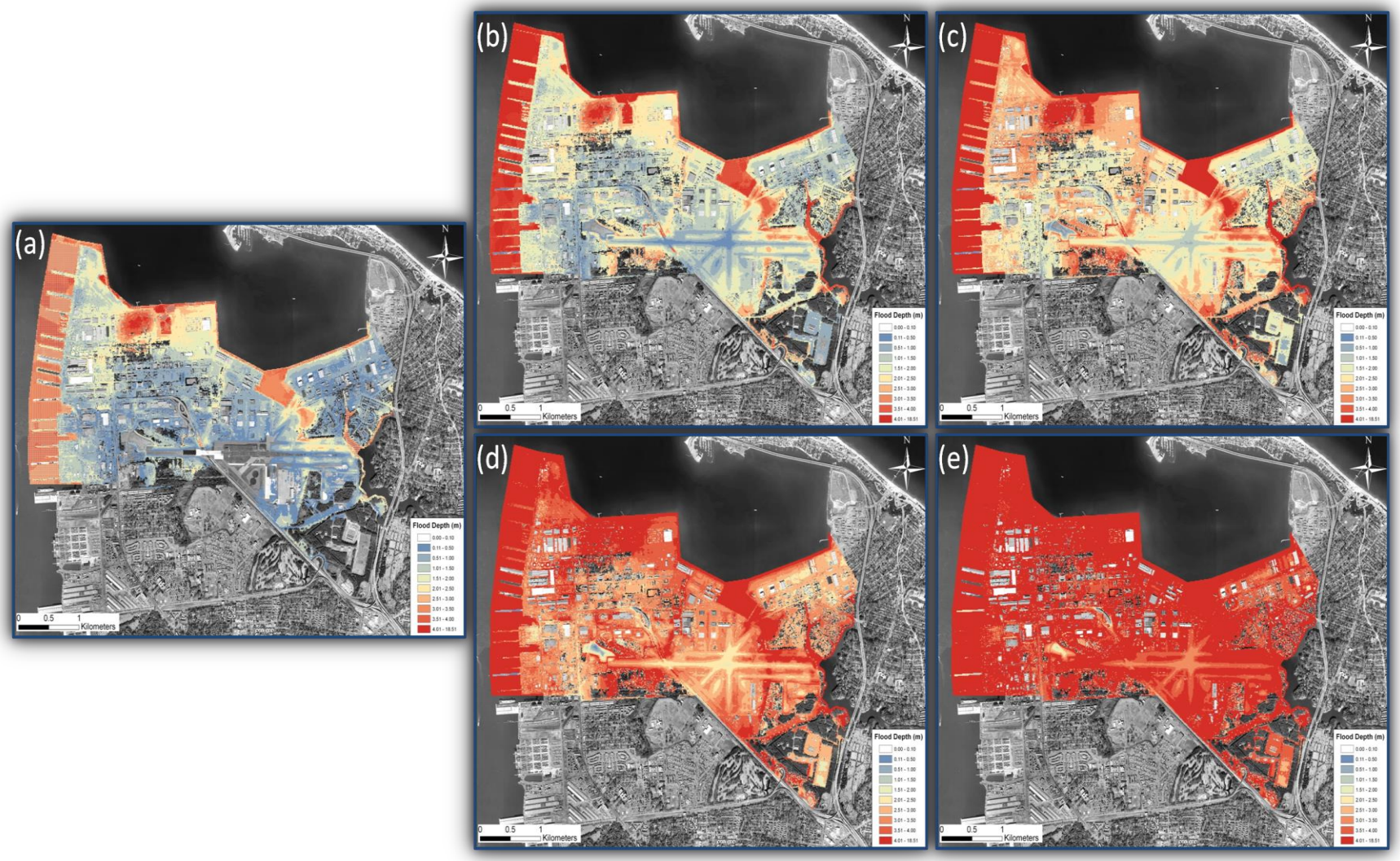

Figure 157. New flood routing and maximum depths (m) under the historical 1982 nor'easter event for the (a) 0.0 m, (b) 0.5 m, (c) 1.0 m, (d) 1.5 m, and (e) 2.0 m SLR scenarios with groundwater modeling incorporated into GSSHA's analysis.

Visual comparisons of the effects of including groundwater influences (reduced aquifer storage capacity and subsequent reductions in infiltration rates) on the surface flood routing simulations were created by subtracting the maximum flooding results presented in *Section 3.6* (refer to Figure 109 - Figure 113) that did not include groundwater influences from the new results that did include groundwater influences, as depicted in Figure 158. Results of these comparisons across all twenty-five scenarios are presented in Figure 159 through Figure 163.

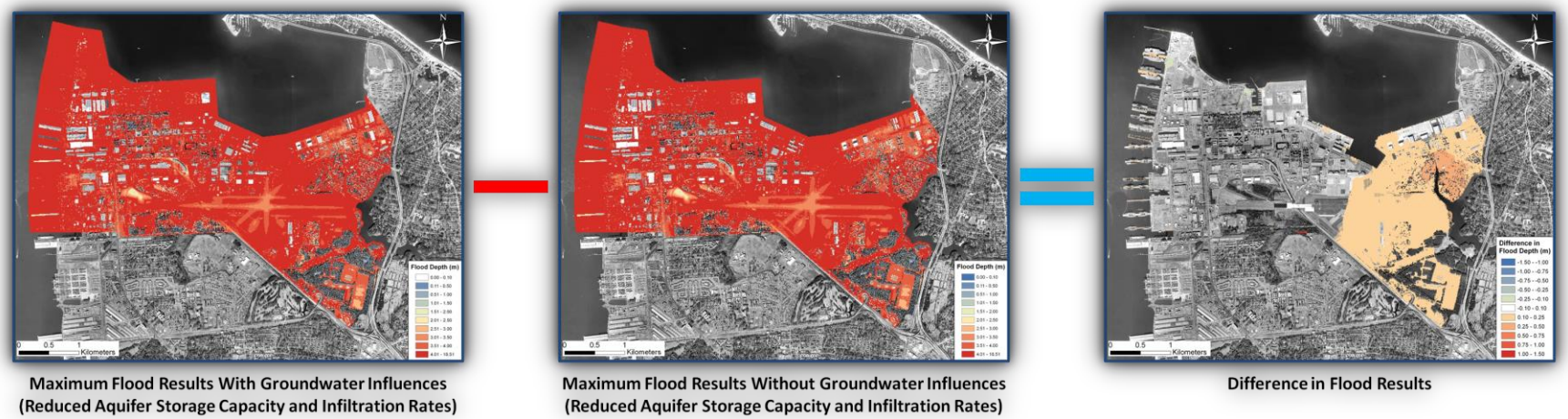

Figure 158. Spatial analysis used to generate difference maps for the flood results generated in the GSSHA analysis (groundwater-driven minus non-groundwater driver results). Note that blue colorations (far right-hand panel) indicate a decrease in projected flooding depths (0.1 − 1.0 meter less than original projections), while red colorations indicate an increase in projected maximum flooding depths (0.1 meter − 1.5 meter greater than original projections).

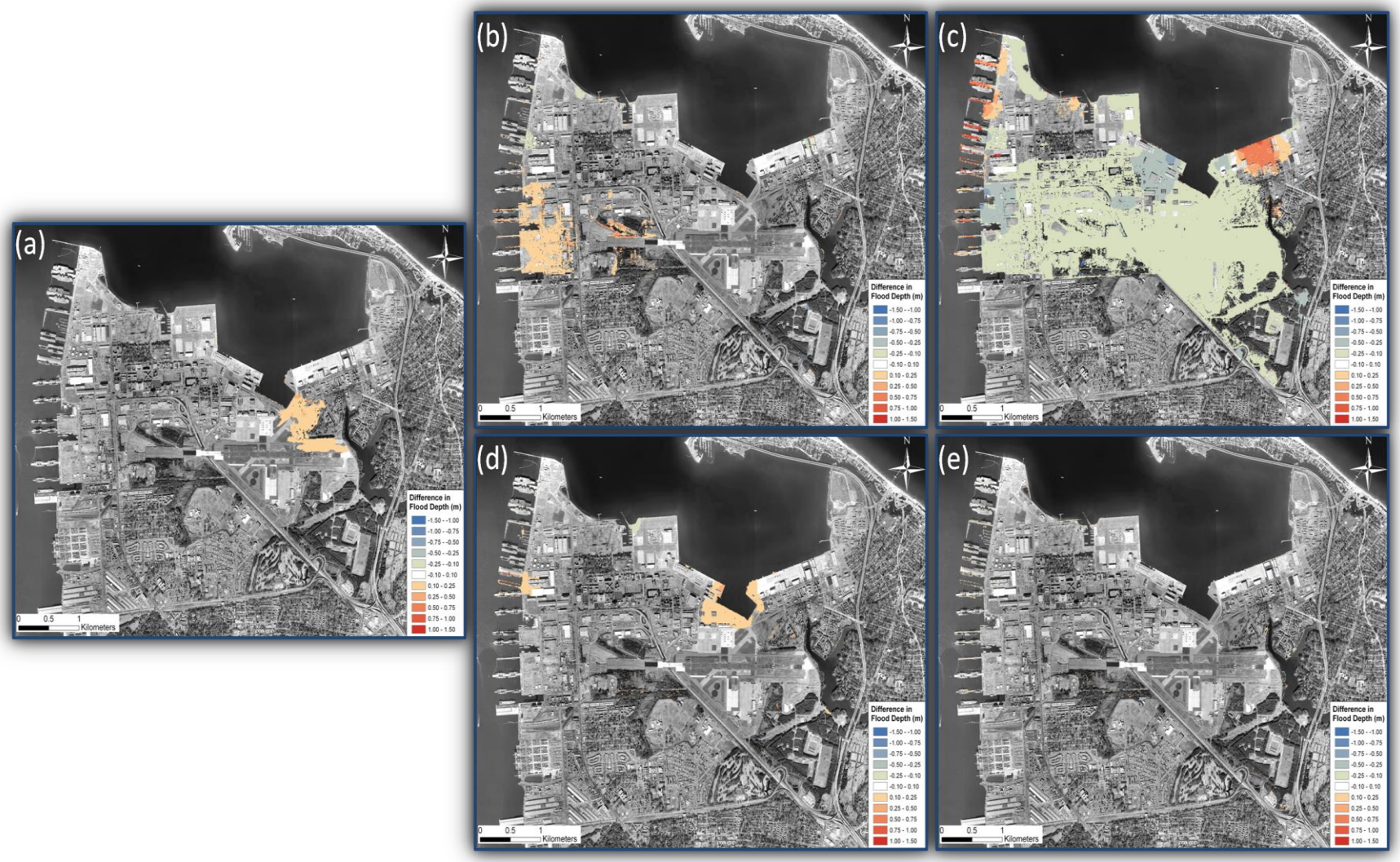

Figure 159. Difference in maximum flooding depths under the 1-yr return interval storm event for the (a) 0.0 m, (b) 0.5 m, (c) 1.0 m, (d) 1.5 m, and (e) 2.0 m SLR scenarios with groundwater modeling incorporated into GSSHA's analysis.

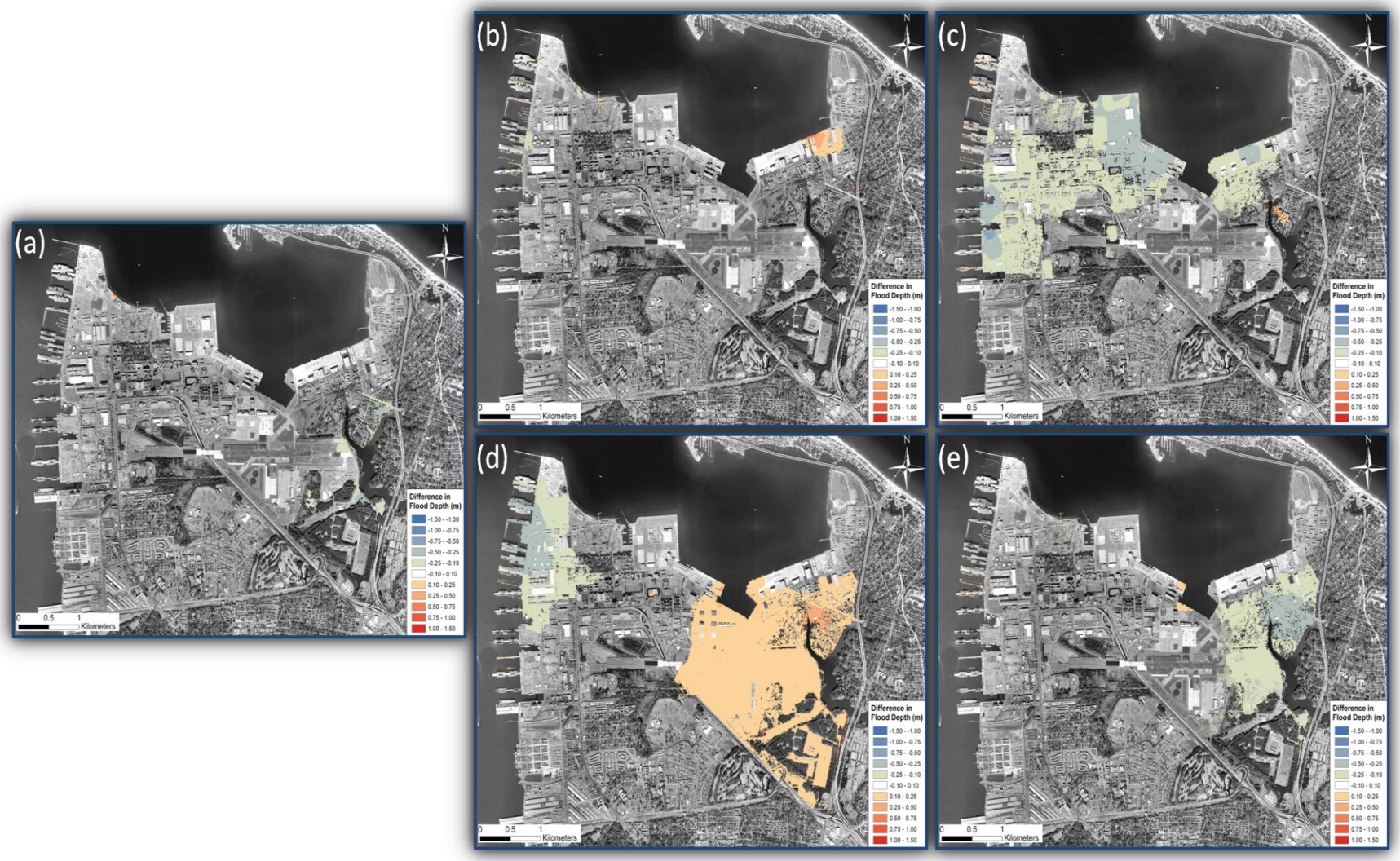

Figure 160. Difference in maximum flooding depths under the 10-yr return interval storm event for the (a) 0.0 m, (b) 0.5 m, (c) 1.0 m, (d) 1.5 m, and (e) 2.0 m SLR scenarios with groundwater modeling incorporated into GSSHA's analysis.

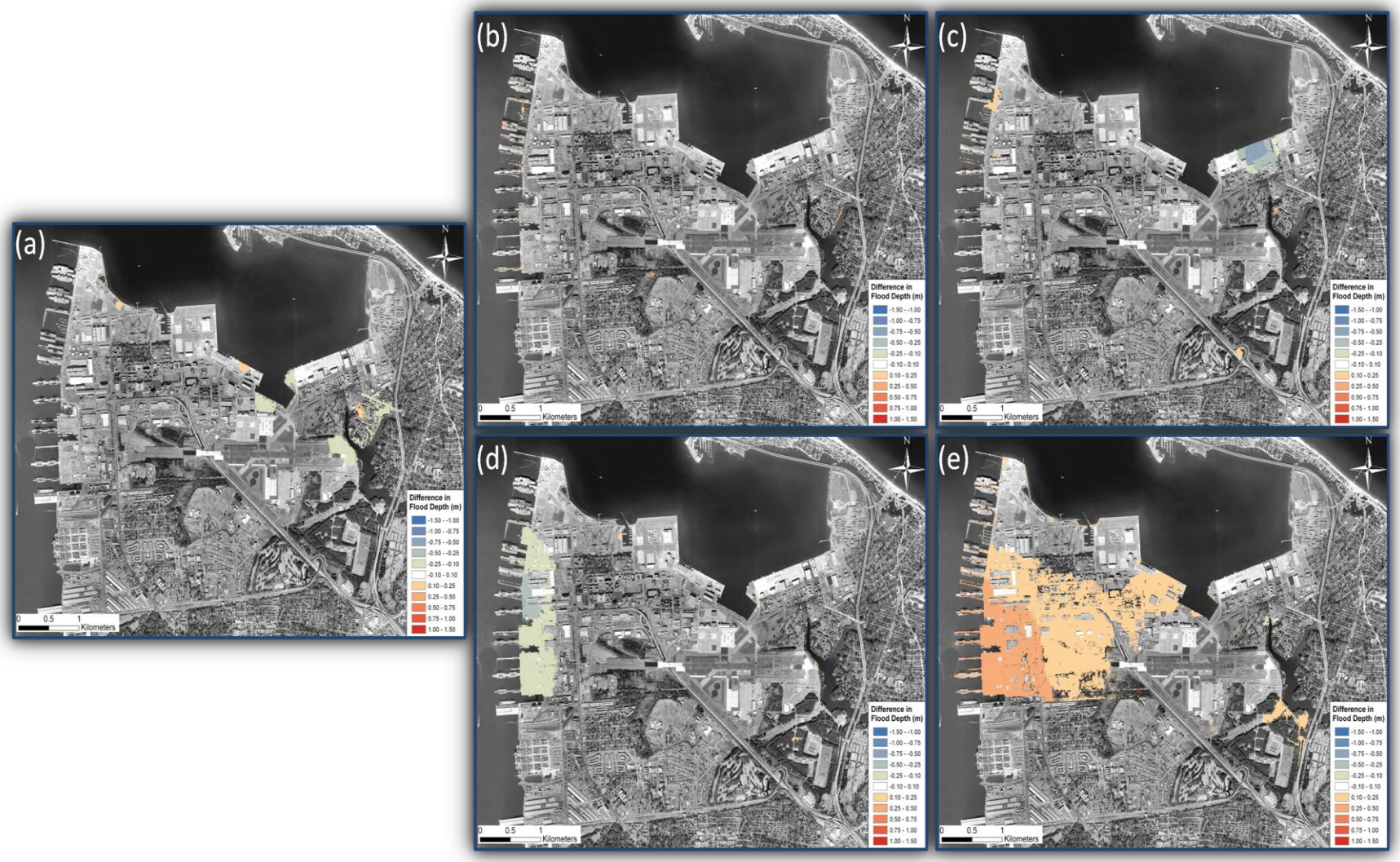

Figure 161. Difference in maximum flooding depths under the 50-yr return interval storm event for the (a) 0.0 m, (b) 0.5 m, (c) 1.0 m, (d) 1.5 m, and (e) 2.0 m SLR scenarios with groundwater modeling incorporated into GSSHA's analysis.

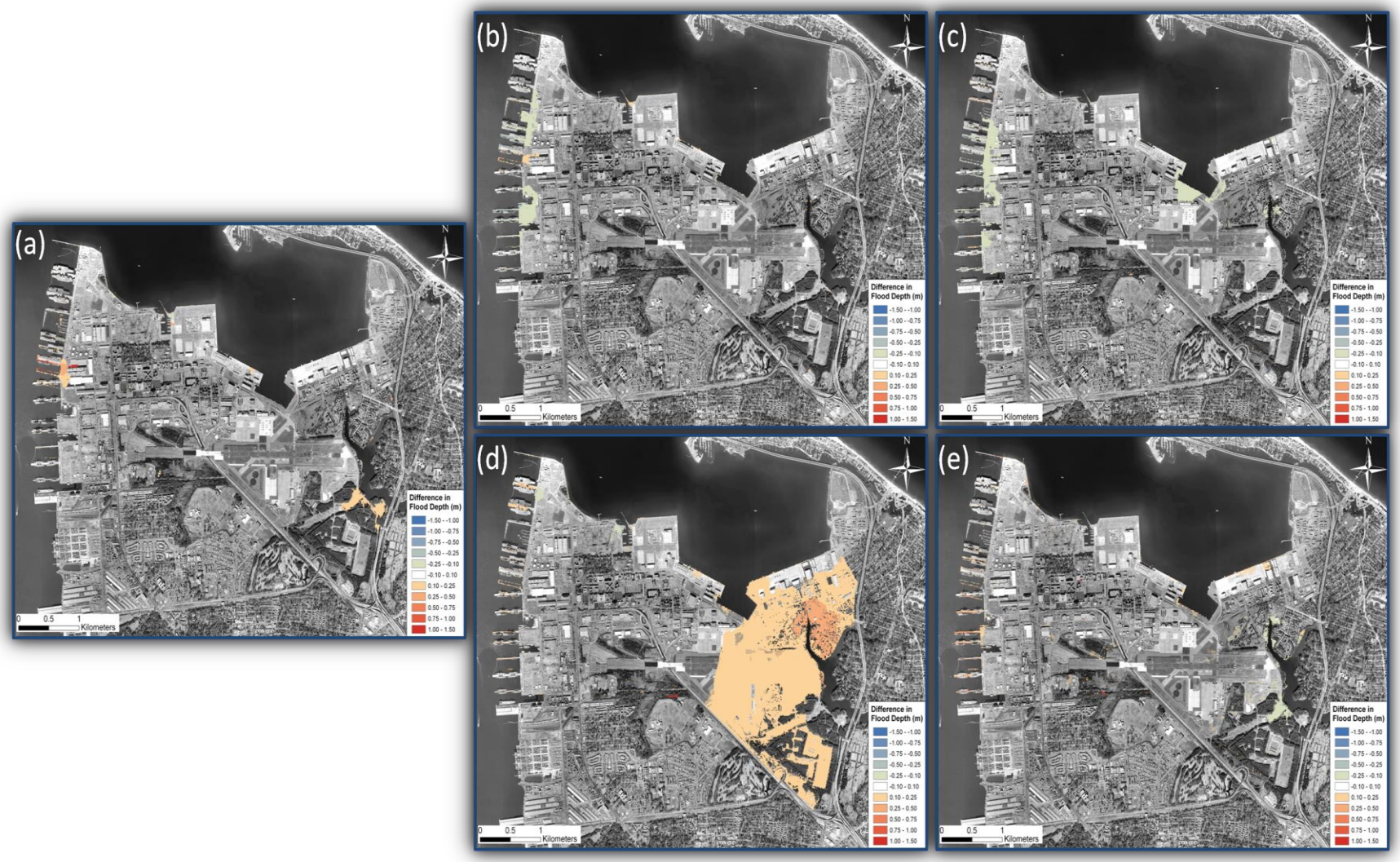

Figure 162. Difference in maximum flooding depths under the 100-yr return interval storm event for the (a) 0.0 m, (b) 0.5 m, (c) 1.0 m, (d) 1.5 m, and (e) 2.0 m SLR scenarios with groundwater modeling incorporated into GSSHA's analysis.

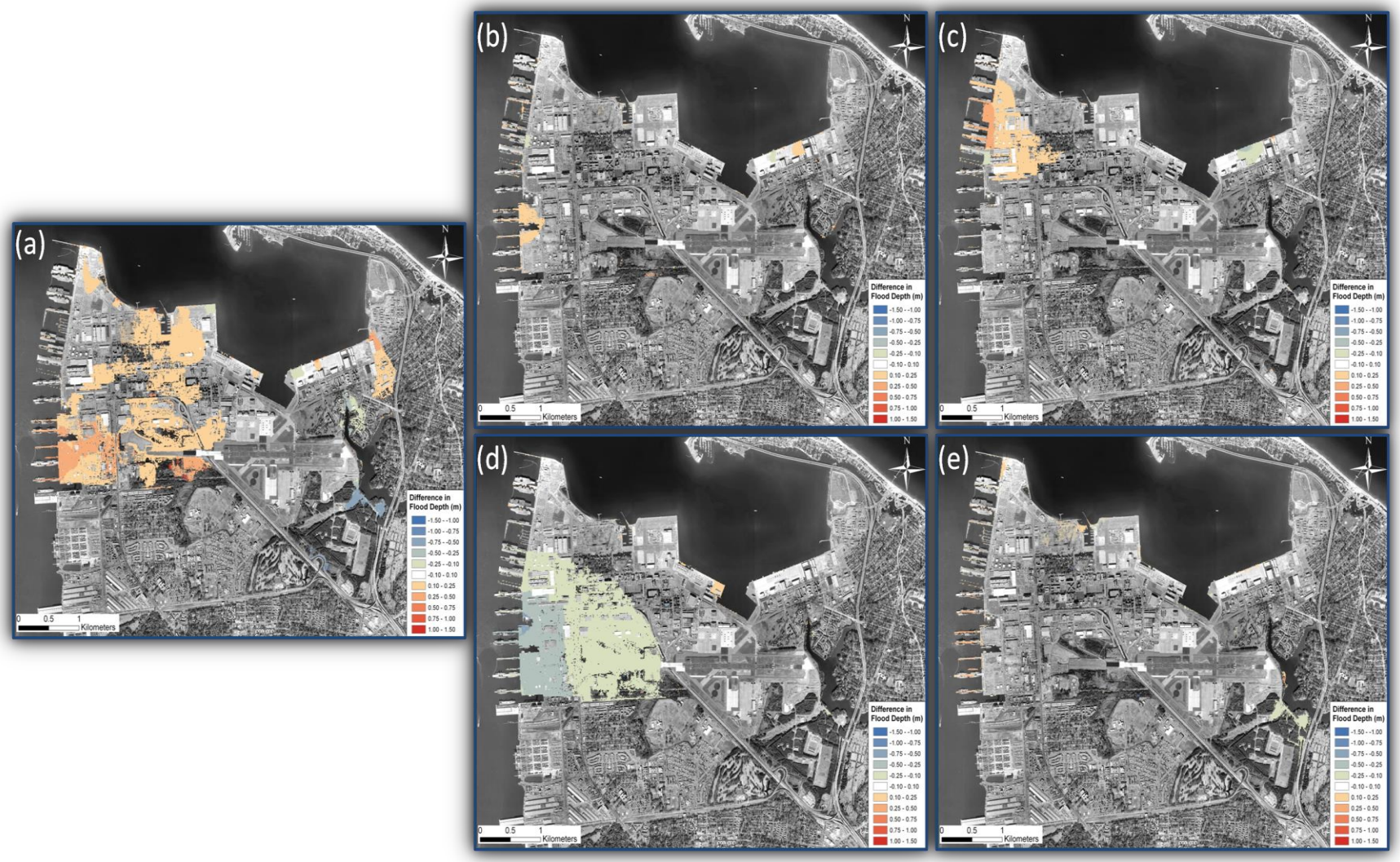

Figure 163. Difference in maximum flooding depths under the historical 1982 nor'easter storm event for the (a) 0.0 m, (b) 0.5 m, (c) 1.0 m, (d) 1.5 m, and (e) 2.0 m SLR scenarios with groundwater modeling incorporated into GSSHA's analysis.

4.10.2 Summary and Discussion

The results shown above definitively demonstrate the value of characterizing reductions in aquifer storage capacity and reduced infiltration rates (driven by saltwater intrusion into the aquifer with SLR) when modeling coastal flooding exacerbated by SLR. In every storm series of model runs (i.e., 1, 10, 50, 100 return interval and nor'easter storms) the difference maps indicate a change in flooding depths (either positively or negatively), aptly demonstrating the value of incorporating this level of detail into the critical analysis of flooding when assessing impacts caused by SLR and coastal storms. In other words, there was a measureable difference between the GSSHA results when constant rates of infiltration versus variable rates of infiltration (based on reduced aquifer storage capacity caused by saltwater intrusion driven by SLR) were used in the flood routing analysis. This finding would suggest that simplifying assumptions about groundwater impacts due to the combined effects of sea level rise, infiltration, soil moisture, and salt water-fresh water boundaries in the groundwater cannot be easily made in terms of magnitude or direction of impact. Overall the impacts shown in this re-analysis indicate that the magnitude was not often large (oftentimes less than a 0.5 meter difference), and that in most instances, these differences were localized (i.e., they did not cover large areas of the installation). Large changes were not expected in this revised assessment given the sandy soil and shallow depth to the water table across the installation. Given a different hydrogeologic setting, including groundwater effects could show a more significant impact to the study results. On the other hand, in every series, at least one anomalous or significant difference (in terms of magnitude and coverage) was observed [refer to panel *(c)* in Figure 159; panel *(d)* in Figure 160; panel *(e)* in Figure 161; panel *(d)* in Figure 162; and panel *(a)* in Figure 163]. We concluded that this re-analysis offered a meaningful and significant contribution to the overall assessment of flooding on the installation threatened by SLR and coastal storms.

Table 44 and Figure 164 offer a comparison of the forcings (maximum water depths from across the study area, not at any specific location) generated by the original analysis and this revised assessment. These values served as new responses to the prescribed SLR and coastal storm impacts for the study on NSN. As before, individual forcing values were generated across the model domain at the mesh element or cellular level (10-m^2 grid cells) for each scenario. Again, it is useful to explore the maximum forcings generated over the installation to grasp the magnitude of change experienced across the range of scenarios.

Table 44. Comparison of final maximum storm forcings generated by the two surface flood routing assessments (without and with groundwater forcings) for this study based on the five storms. Values in red indicate increases in maximum flooding depths, while values in green indicate decreases in maximum flooding depths. NE relates to the historical 1982 nor'easter.

Storm Return Interval	Surface Flood Routing Assessment (GSSHA + w/o Groundwater Influences)					Surface Flood Routing Assessment (GSSHA + with Groundwater Influences)				
	Maximum Water Depths (m)					Maximum Water Depths (m)				
	SLR Scenario					SLR Scenario				
	0.0	0.5	1.0	1.5	2.0	0.0	0.5	1.0	1.5	2.0
1	2.4	3.7	4.8	5.0	6.3	2.5	3.6	4.9	5.1	6.2
10	3.4	4.3	5.3	5.5	6.8	3.4	4.2	5.0	5.6	6.7
50	3.9	4.6	5.5	6.1	7.2	4.1	4.6	5.1	6.1	7.2
100	4.8	5.6	6.6	7.8	9.1	4.9	5.6	6.5	7.7	9.1
NE	4.2	4.4	5.6	6.5	7.8	4.6	4.7	5.3	6.5	7.7

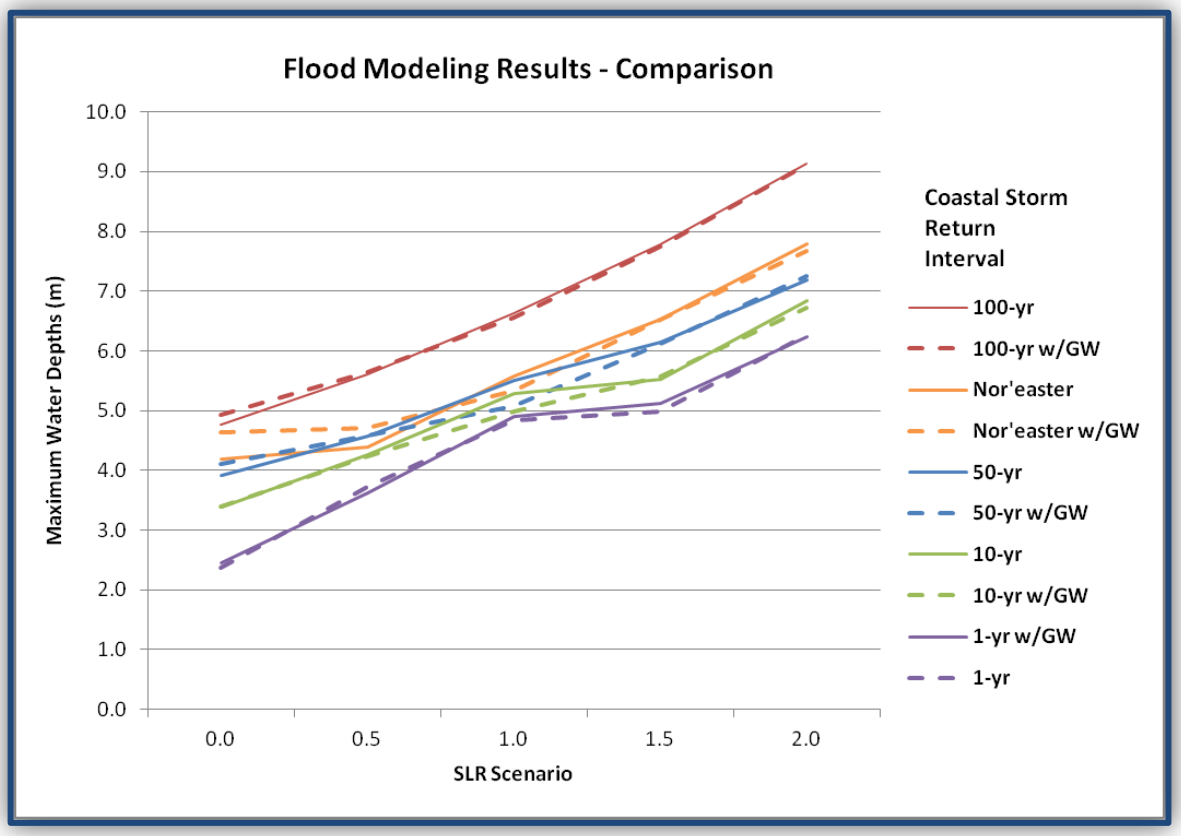

Figure 164. Comparison of final maximum water depth forcing trends generated by the two surface flood routing assessments (groundwater influences vs. original analysis) for this study based on the five analyzed storms under the five prescribed SLR scenarios.

4.11. Re-Assessment of Risks Incorporating Groundwater Analysis

4.11.1 Outputs and Technical Results

The NSN Risk Model application was revised using the re-assessment of GSSHA flood model outputs that accounted for the influence of SLR-driven saltwater intrusion into the groundwater aquifer that in turn altered infiltration rates and exacerbated surface flooding impacts. Conditional probability tables (CPTs) for all asset damage nodes were recalculated using the revised GSSHA model outputs. The assets affected by these new flood elevations included fuel tanks, generators, electrical substations, transformers, backup electrical generators, steam lines, and water, wastewater, and fuel pumps. There were no changes to the structure of the Bayesian network. In other words, the mission to *Provide At-Berth Support* for CVNs at each pier was still supported by several capabilities, including the *Provide Water*, *Provide Steam*, *Provide Electricity*, *Provide Wastewater*, *Provide Oily Waste*, *Provide Access*, *Provide North Berth*, and *Provide South Berth* capabilities. The NSN Risk Model once again estimated a capability score for each capability. The capability score was again assessed as the probability that each of these capabilities would not be interrupted at least once during the course of a year as a result of damage to assets that supported these capabilities. Capability scores were again aggregated using the same weighted value function to calculate an MPI for each pier. The weights in this multi-attribute value function continued to represent command-level priorities for providing services to CVNs at berth.

The capability scores from the revised NSN Risk Model are reported for each pier and each SLR scenario in Table 45 and plotted in Figure 165 - Figure 167.

Table 45. Revised capability scores and mission performance index for the five prescribed SLR scenarios from the revised NSN Risk Model.

Pier	SLR Scenario	Capability Scores								Mission Performance Index (MPI)[1]
		Provide Water	Provide Access	Provide Steam	Provide North Berth	Provide South Berth	Provide Oily Waste	Provide Electricity	Provide Wastewater	
11	0.0	0.9885	0.8643	0.9638	0.8356	-	0.9554	0.9817	0.9676	0.9553
	0.5	0.9268	0.8689	0.8468	0.9086	-	0.2515	0.8462	0.3350	0.6751
	1.0	0.7116	0.8753	0.3954	0.9545	-	0.0000	0.0099	0.0000	0.2775
	1.5	0.0023	0.9198	0.0000	0.9797	-	0.0000	0.0011	0.0000	0.1308
	2.0	0.0000	0.9225	0.0000	0.9919	-	0.0000	0.0000	0.0000	0.1312
12	0.0	0.9885	0.8643	0.9638	0.9721	0.9149	0.9569	0.9884	0.9704	0.9627
	0.5	0.9268	0.8689	0.8468	0.9974	0.9777	0.6414	0.9491	0.7527	0.8519
	1.0	0.7116	0.8753	0.3954	0.9999	0.9960	0.0034	0.4062	0.0032	0.4063
	1.5	0.0023	0.9198	0.0000	1.0000	0.9995	0.0000	0.0115	0.0000	0.1814
	2.0	0.0000	0.9225	0.0000	1.0000	1.0000	0.0000	0.0000	0.0000	0.1789
14	0.0	0.9885	0.8643	0.9638	0.9149	0.9852	0.9457	0.9878	0.9692	0.9619
	0.5	0.9268	0.8689	0.8468	0.9794	0.9994	0.6019	0.9456	0.7607	0.8488
	1.0	0.7116	0.8753	0.3954	0.9967	1.0000	0.0001	0.3162	0.0044	0.3867
	1.5	0.0023	0.9198	0.0000	0.9997	1.0000	0.0000	0.0089	0.0000	0.1809
	2.0	0.0000	0.9225	0.0000	0.9997	1.0000	0.0000	0.0000	0.0000	0.1789

[1]The mission performance index is described in *Section 3.9* of this report.

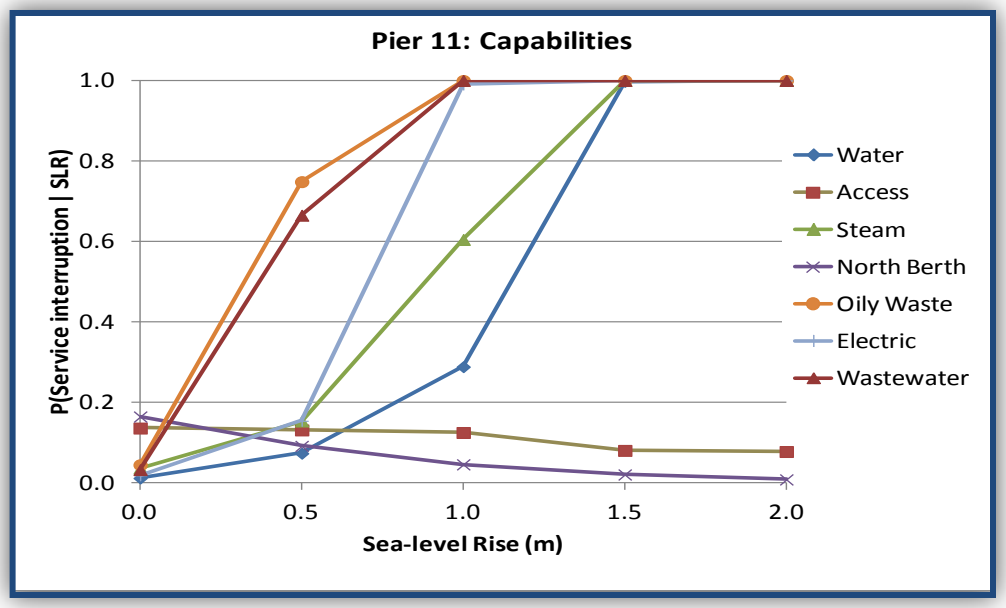

Figure 165. Revised conditional probabilities of service interruptions occurring at least once during the course of a year for the five prescribed SLR scenarios for Pier 11.

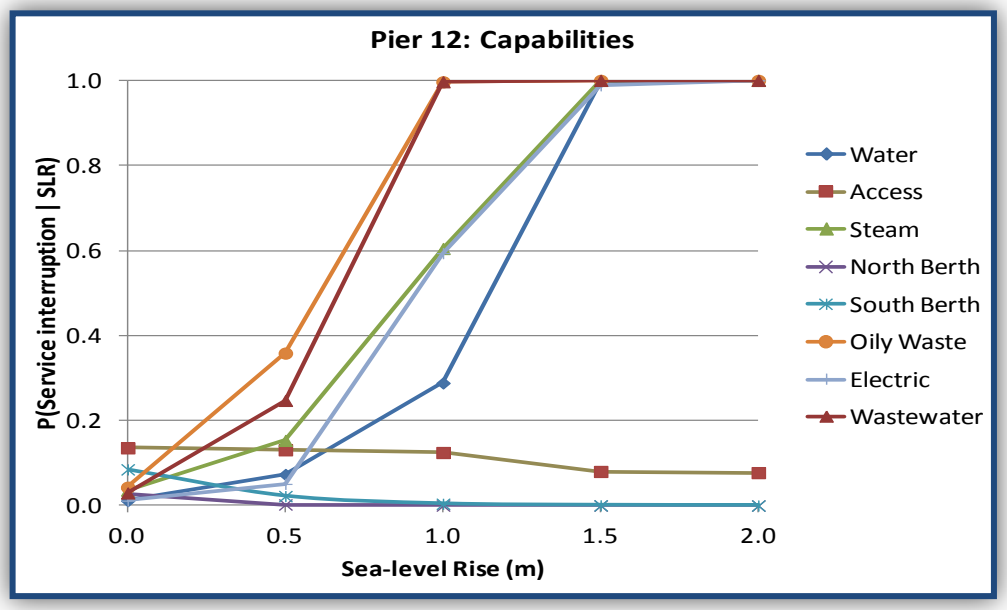

Figure 166. Revised conditional probabilities of service interruptions occurring at least once during the course of a year for the five prescribed SLR scenarios for Pier 12.

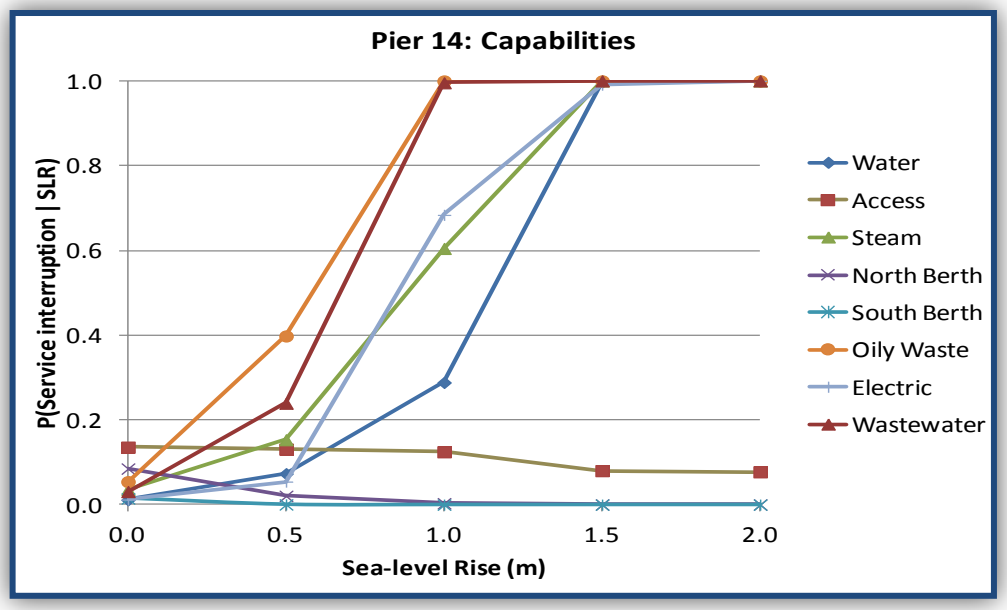

Figure 167. Revised conditional probabilities of service interruptions occurring at least once during the course of a year for the five prescribed SLR scenarios for Pier 14.

Recall that the probabilities of service interruptions are the complement of the capability scores. Under the revised assessment, the *Provide Oily Waste* and *Provide Wastewater* capabilities at Pier 11 were shown to be the most sensitive to SLR. In the case of the *Provide Oily Waste* capability at Pier 11, the probability of service interruption increased from 0.0446 to 0.7458 between SLR states 0.0 m and 0.5 m. In the case of the *Provide Wastewater* capability, the probability of service interruption increased from 0.0324 to 0.6650 between the 0.0 m and 0.5m SLR states.

The *Provide Electricity* capability showed greater sensitivity to SLR at Pier 11 than at Piers 12 and 14. At Pier 11, the probability of service interruption increased to 0.9901 under the 1.0 m SLR scenario. At Piers 12 and 14, the probability of service interruptions under the 1.0 m SLR scenario was 0.5938 and 0.6838, respectively. This difference in the probability of service interruption was again attributed to the location of the Pier 11 substation on the lower deck of Pier 11. At Piers 12 and 14, the substations were located on land within 1,000 ft of the waterfront. Other capabilities such as *Provide Steam* and *Provide Water* responded similarly to SLR at each of the three piers. Capabilities related to navigation and berthing (i.e., *Provide Access*, *Provide North Berth*, and *Provide South Berth*) improved at higher SLR states since rising sea levels had a tendency to increase limiting depths.

Figure 168 and Figure 169 plot the capability scores for each SLR and return interval storm severity scenario under the new assessment.

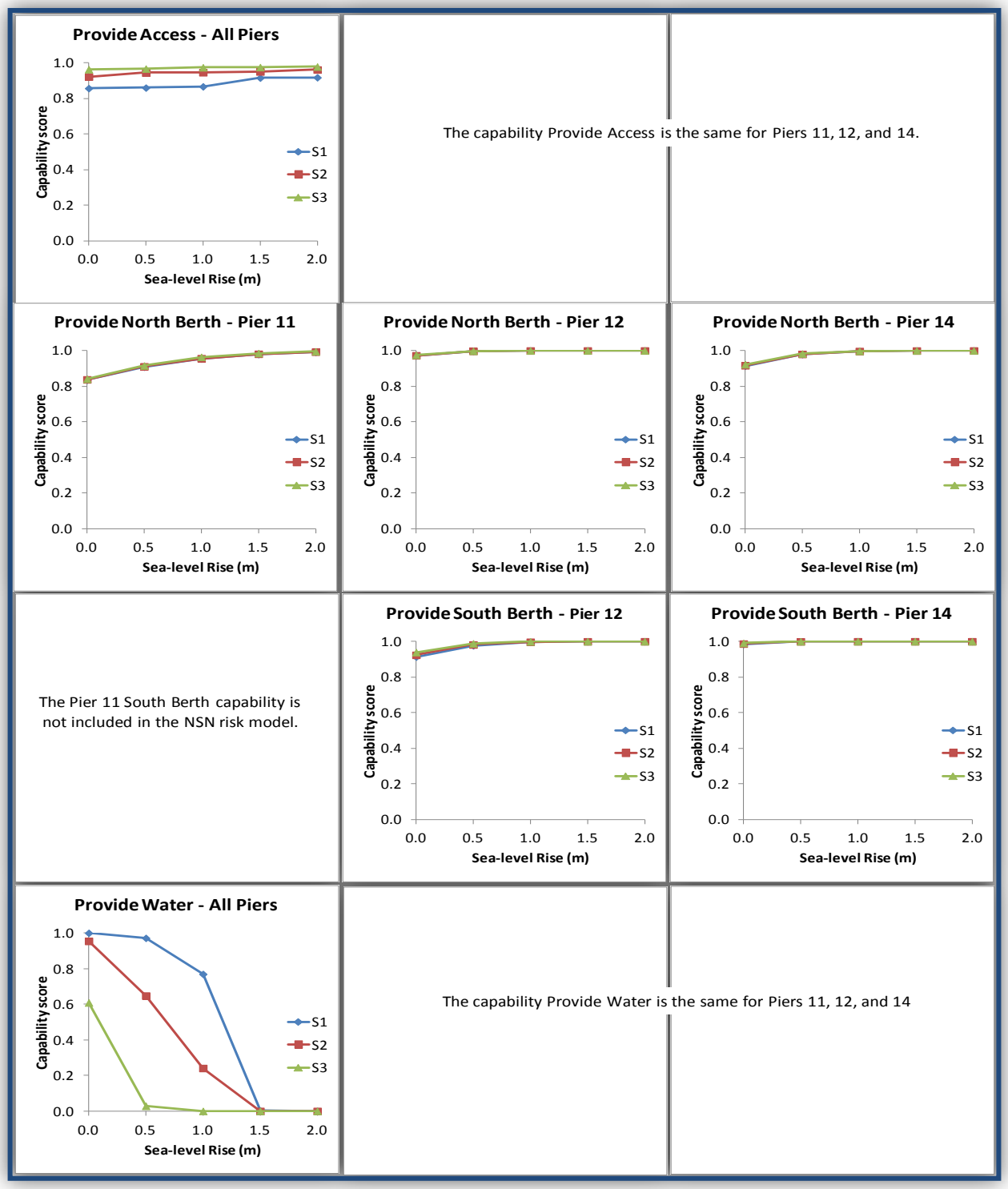

Figure 168. Revised capability scores by SLR and SEV for the NSN Risk Model incorporating the influences of reduced aquifer storage capacity and variable infiltration rates into the flooding assessment (*Potable Water Provisioning*, and *Berthing* capabilities).

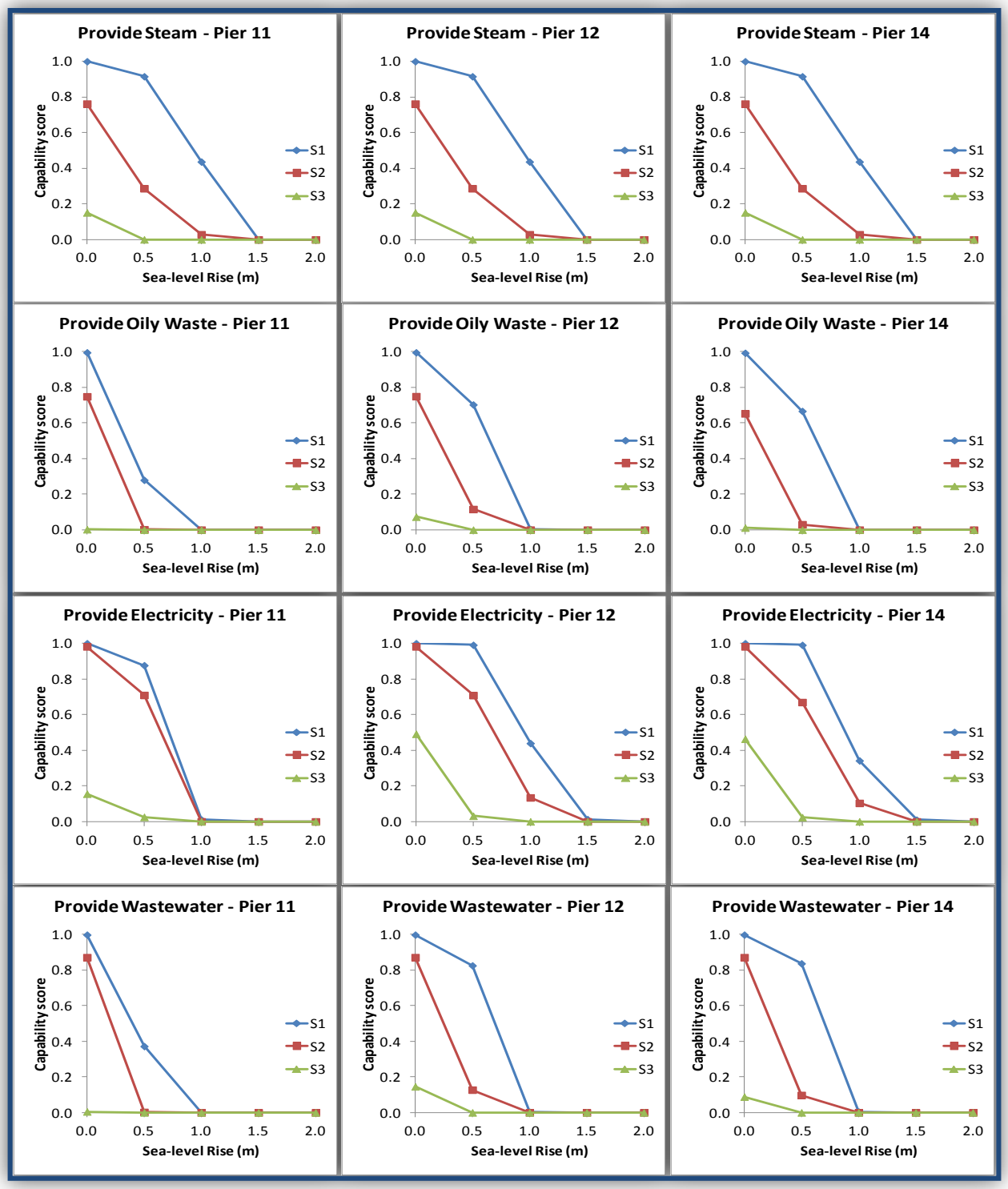

Figure 169. Revised capability scores by SLR and SEV for the NSN Risk Model incorporating the influences of reduced aquifer storage capacity and variable infiltration rates into the flooding assessment (*Steam*, *Oily Waste*, *Electricity*, and *Wastewater* capabilities).

Since these probabilities are conditioned on return interval storm severities, they can be interpreted as the probability that a storm of given severity (SEV = *S1*, *S2*, or *S3*) will cause the interruption of a capability under the stated SLR scenario. In Figure 168 above, the plot for the *Provide Access* capability shows that, as storm severity increased, there was a net increase in final controlling depth of navigation channels. This suggested that higher levels of SEV caused net erosion in the channels, and this result applied equally to all three piers. In contrast, SEV appeared to have very little effect on the final controlling depths in berthing areas. Capability scores for those capabilities that depended upon utility infrastructure exhibited a more pronounced response to increased SEV. For example, this can be seen for the *Provide Water* capability in Figure 168 above, and for the remaining capabilities in Figure 169 above. The *Provide Water* capability is represented by a single node in the Bayesian network, so only one plot is applicable to all three piers (Figure 168 above). Under the baseline SLR scenario, the *Provide Water* capability was fairly robust, with a high probability of no service interruption given an *S1* or an *S2* storm. This probability of no service interruption decreased to 0.609 in the event of an *S3* storm. At higher sea level states, the probability of service interruption also increased, as indicated by the decreasing capability scores. Under the 1.5 m and 2.0 m SLR scenarios, the probability of experiencing at least one service interruption during the course of a year was 0.9977 and 1.0, respectively. Other capabilities exhibited a similar pattern of response to increased SEV and SLR. For example, the *Provide Oily Waste* and *Provide Wastewater* capabilities had a relatively low probability of being interrupted by an *S2* storm at the 0.0 m SLR state, but when the SLR increased to 0.5 m, there was a very high probability of experiencing at least one service interruption during the course of a year.

Again, the MPIs were re-calculated using the weights that reflected command-level priorities for providing at-berth support for CVNs (Figure 170).

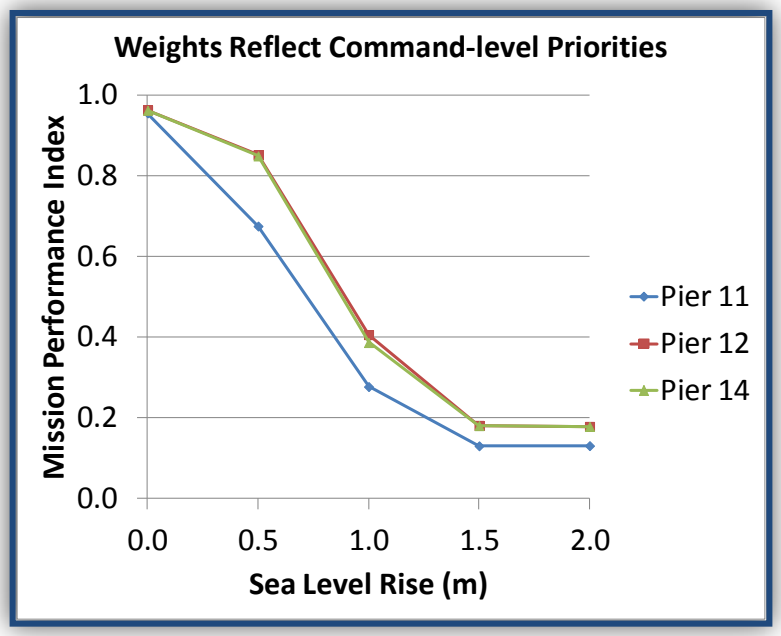

Figure 170. Revised effects of SLR on the MPIs calculated using weights that reflected command-level priorities for *Providing At-berth Support* for CVNs under the new risk assessment.

Under the 0.0 m SLR scenario, the MPIs were approximately equal at each of the three piers. At higher SLR states, the MPI at Pier 11 decreased more rapidly than at Piers 12 and 14. At higher SLR states, the MPIs stopped decreasing in response to SLR because all of the capability scores related to utility services were at (or near) zero. The MPI did not reach zero because the capability scores related to navigation and berthing remained high. As explained in the *Section 3.9*, capability scores for berthing were expected to decrease precipitously at SLR states greater than 2.0 m as the piers were overtopped and the ability to moor ships to each of the piers was lost.

Figure 171 (a) plots the loss-exceedance curves for the MPI at each pier.

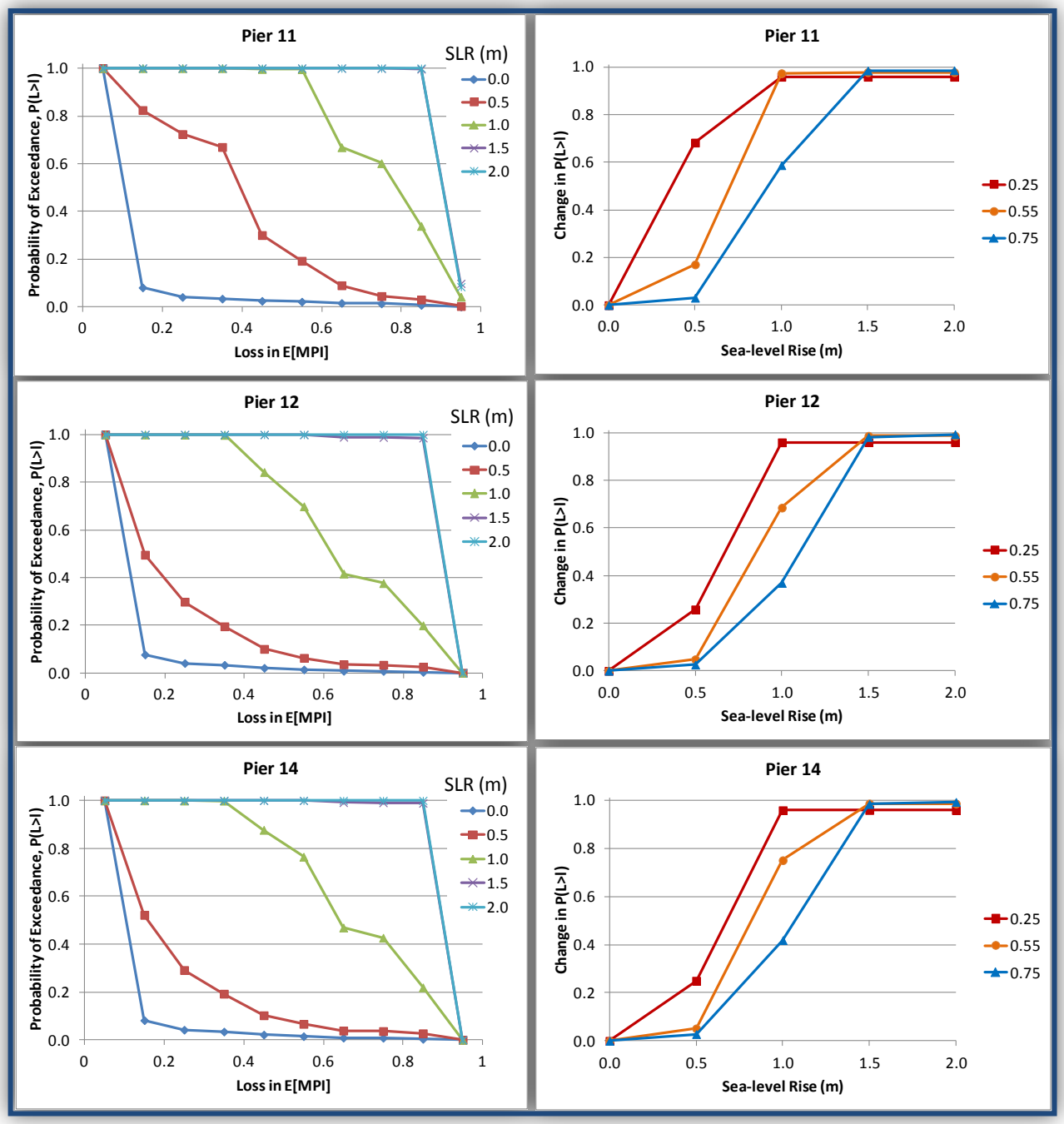

Figure 171. (a) New loss-exceedance curves for expected MPI. (b) Change in the probability of realizing three potential levels of loss. Weights used in calculating MPI reflect command level priorities for providing at-berth support to CVNs.

Figure 171 (a) above shows that, under the 0.0 m SLR scenario, the probability of exceeding a 0.15 loss in MPI was 0.0816. This result was similar at Piers 12 and 14. The probability of

exceeding a 0.15 loss in MPI was 0.0765 at Pier 12 and 0.0819 at Pier 14. These probabilities increased at higher SLR states. The greatest increase occurred at Pier 11. The probability of exceeding a 0.15 loss in MPI increased to 0.8244 at Pier 11, 0.4593 at Pier 12, and 0.5218 at Pier 14. The higher probabilities of exceedance at Pier 11 were attributed to the relatively high probabilities of service interruption for the *Provide Wastewater*, *Provide Oily Waste*, and *Provide Electricity* capabilities. Figure 171 (b) above plots the corresponding change in the probability of realizing three potential levels of loss (25, 55, and 75 percent) relative to the probability of realizing that level of loss under the 0.0 m SLR scenario. As discussed in *Section 4.8*, the SLR "tipping point" for the installation was once again located between the 0.5 m and 1.0 m SLR scenarios.

4.11.2 Summary and Discussion

This discussion below focuses on how the results of the NSN risk model changed when aquifer storage capacity and variable infiltration rates were incorporated into the GSSHA flood simulation. Specifically, the effects on damage states, function states, capability scores, and mission performance indices have been considered.

4.11.2.1 Effect of New Groundwater Modeling on Asset Damage Nodes

The effect of incorporating groundwater influences on flooding can be summarized in terms of differences in the probability of an asset damage state random variable *D* being in state *i* for a given SLR scenario. The difference, Δp, is the difference in the damage state probability that is calculated when groundwater influences are ignored, $p(D_i \mid SLR)_{NO\_GW}$, and the damage state probability that is calculated when groundwater influences are considered, $p(D_i \mid SLR)_{NO\_GW}$:

$$\Delta p = p(D_i \mid SLR)_{NO\_GW} - p(D_i \mid SLR)_{GW}. \quad \textbf{(33)}$$

When Δp is negative, the probability of the damage state is greater when the influences of reduced aquifer storage capacity and variable infiltration rates are considered. Conversely, when Δp is positive, the probability of the damage state is less. The sum of these differences in probabilities over damage states *Minor*, *Moderate*, and *Severe* is the difference in the probability of being in a damage state other than *None*. Table 46 reports the change in the probability of being in a damage state other than *None*. Differences in probability have been rounded to the fourth decimal place, so the table does not report effects that were less than $0.5E^{-4}$.

Table 46. Difference in the probability of the asset being in a *Minor*, *Moderate*, or *Severe* damage state when the influences of groundwater influences were considered in the GSSHA model runs. Negative values (shown in red) indicate that the probability of being *Non-Functional* was greater when these influences were considered. Positive values (shown in green) indicate the probability of being *Non-Functional* was lower when these influences were considered.

NODE	DESCRIPTION	SLR Scenario				
		0.0 m	0.5 m	1.0 m	1.5 m	2.0 m
133	P11 Draft North	0.0000	0.0000	0.0000	0.0000	0.0000
132	P12 South Draft	0.0000	0.0000	0.0000	0.0000	0.0000
131	P12 North Draft	0.0000	0.0000	0.0000	0.0000	0.0000
130	P14 South Draft	0.0000	0.0000	0.0000	0.0000	0.0000
129	P14 North Draft	0.0000	0.0000	0.0000	0.0000	0.0000
1	Generator	-0.0016	-0.0287	-0.0004	0.0000	0.0000
174	Generator	-0.0008	-0.0324	0.0509	0.0001	0.0000
2	Generator	0.0006	0.0001	0.0000	0.0000	0.0000
3 - 6	Generators	-0.0001	0.0056	0.0020	0.0000	0.0000
164	Generator	-0.0009	-0.0050	-0.0221	0.0011	0.0000
148	Substation	0.0000	-0.0002	0.2215	0.0014	0.0001
8	Substation	-0.0004	-0.0116	0.0218	0.0019	0.0000
154	Substation	-0.0026	-0.0003	0.0254	-0.0003	0.0000
153	Substation	0.0000	0.0000	0.0587	-0.0024	0.0000
152	Substation	-0.0001	-0.0140	0.1450	0.0050	0.0002
150	Substation	0.0000	-0.0002	0.1738	0.0027	0.0002
11	Substation	-0.0004	0.0016	-0.0541	**0.0142**	0.0000
9	Substation	0.0001	-0.0042	0.0081	0.0003	0.0000
157	Substation	0.0003	0.0758	0.0002	0.0004	0.0000
10	Substation	-0.0005	-0.0108	-0.0450	0.0038	0.0000
168	Transformer	-0.0015	0.0013	0.0586	0.0000	0.0000
163	Transformer	-0.0018	-0.0044	0.0000	0.0000	0.0000
162	Transformer	-0.0014	-0.0064	0.0000	0.0000	0.0000
169	Transformer	-0.0002	-0.0005	0.0000	0.0000	0.0000
171	Transformer	-0.0003	-0.0004	0.1778	0.0000	0.0000
161	Transformer	-0.0008	-0.0730	0.0155	0.0000	0.0000
167	Transformer	-0.0001	-0.0004	0.0000	0.0000	0.0000
165	Transformer	0.0004	0.0035	0.0000	0.0000	0.0000
159-160	Transformer	-0.0002	0.0035	0.0098	0.0000	0.0000
138	P11 North Freeboard	0.0000	0.0000	0.0000	0.0000	0.0000
136	P12 North Freeboard	0.0000	0.0000	0.0000	0.0000	0.0000
137	P12 South Freeboard	0.0000	0.0000	0.0000	0.0000	0.0000
134	P14 South Freeboard	0.0000	0.0000	0.0000	0.0000	0.0000
135	P14 North Freeboard	0.0000	0.0000	0.0000	0.0000	0.0000
121	Thimble Shoals Channel	0.0000	0.0000	0.0000	0.0000	0.0000
122	Harbor Entrance Channel	0.0000	0.0000	0.0000	0.0000	0.0000
123	Inner Harbor Channel	0.0000	0.0000	0.0000	0.0000	0.0000
37	Pump House	0.0000	0.0000	0.0000	0.0000	0.0000
44	Pump	-0.0001	-0.0533	0.0016	0.0000	0.0000
144	Fuel Pump House	0.0000	0.0000	0.0000	0.0000	0.0000
158	Fuel Pumps	-0.0002	-0.1441	0.0067	0.0000	0.0000
45	Fuel Storage Tanks	0.0000	0.0000	0.0000	0.0000	0.0000
65	Steam Line (250 psi, Tall Pylons)	0.0000	0.0000	0.0000	0.0000	0.0000
66	Steam Line (250 psi, Tall Pylons)	0.0000	0.0000	0.0000	0.0000	0.0000
76D	Steam Line (250 psi, Tall Pylons)	0.0000	0.0000	0.0000	0.0000	0.0000
76F	Steam Line (250 psi, Tall Pylons)	0.0000	0.0000	0.0000	0.0000	0.0000
55A	Steam Line (250 psi, Short Pylons)	0.0000	0.0000	0.0000	0.0000	0.0000

(Continued)

NODE	DESCRIPTION	SLR Scenario				
		0.0 m	0.5 m	1.0 m	1.5 m	2.0 m
74A	Steam Line (250 psi, Short Pylons)	0.0000	0.0000	0.0000	0.0000	0.0000
55B	Steam Line (250 psi, Short Pylons)	0.0000	0.0000	0.0000	0.0000	0.0000
74C	Steam Line (250 psi, Short Pylons)	0.0000	0.0000	0.0000	0.0000	0.0000
74D	Steam Line (250 psi, Short Pylons)	0.0000	0.0000	0.0000	0.0000	0.0000
69	Steam Line (250 psi, Short Pylons)	0.0000	0.0000	0.0000	0.0000	0.0000
54A	Steam Line (250 psi, Tall Pylons)	0.0000	0.0000	0.0000	0.0001	0.0000
63	Steam Line (250 psi, Tall Pylons)	0.0000	0.0000	0.0000	0.0000	0.0000
76A	Steam Line (250 psi, Tall Pylons)	0.0000	0.0000	0.0000	0.0000	0.0000
79A	Steam Line (250 psi, Tall Pylons)	0.0000	0.0000	0.0000	0.0000	0.0000
80	Steam Line (250 psi, Tall Pylons)	0.0000	0.0000	0.0000	0.0000	0.0000
81	Steam Line (250 psi, Tall Pylons)	0.0000	0.0000	0.0000	0.0000	0.0000
54B	Steam Line (250 psi, Tall Pylons)	0.0000	0.0000	0.0000	0.0000	0.0000
64	Steam Line (250 psi, Tall Pylons)	0.0000	0.0000	0.0000	0.0000	0.0000
74B	Steam Line (250 psi, Tall Pylons)	0.0000	0.0000	0.0000	0.0000	0.0000
76B	Steam Line (250 psi, Tall Pylons)	0.0000	0.0000	0.0000	0.0000	0.0000
79B	Steam Line (250 psi, Tall Pylons)	0.0000	0.0000	0.0000	0.0000	0.0000
54C	Steam Line (250 psi, Tall Pylons)	0.0000	0.0000	0.0000	0.0000	0.0000
76C	Steam Line (250 psi, Tall Pylons)	0.0000	0.0000	0.0000	0.0000	0.0000
79C	Steam Line (250 psi, Tall Pylons)	0.0000	0.0000	0.0000	0.0000	0.0000
54D	Steam Line (250 psi, Tall Pylons)	0.0000	0.0000	0.0000	0.0001	0.0000
74D	Steam Line (250 psi, Tall Pylons)	0.0000	0.0000	0.0000	0.0000	0.0000
76E	Steam Line (250 psi, Tall Pylons)	0.0000	0.0000	0.0000	0.0000	0.0000
76G	Steam Line (250 psi, Tall Pylons)	0.0000	0.0000	0.0000	0.0000	0.0000
59	Steam Line (250 psi, Tall Pylons)	0.0000	0.0000	0.0000	0.0000	0.0000
60	Steam Line (250 psi, Tall Pylons)	0.0000	0.0000	0.0000	0.0000	0.0000
67	Steam Line (250 psi, Tall Pylons)	0.0000	0.0000	0.0000	0.0000	0.0000
72	Steam Line (250 psi, Tall Pylons)	0.0000	0.0000	0.0000	0.0000	0.0001
82	Steam Line (250 psi, Tall Pylons)	0.0000	0.0000	0.0000	0.0000	0.0000
83	Steam Line (250 psi, Tall Pylons)	0.0000	0.0000	0.0000	0.0000	0.0000
84	Steam Line (250 psi, Tall Pylons)	0.0000	0.0000	0.0000	0.0000	0.0000
85	Steam Line (250 psi, Tall Pylons)	0.0000	0.0000	0.0000	0.0000	0.0000
87	Steam Line (250 psi, Tall Pylons)	0.0000	0.0000	0.0000	0.0000	0.0000
88	Primary Steam Plant Building	0.0000	0.0000	0.0000	0.0000	0.0000
143	Auxiliary Steam Plant Building	0.0000	0.0000	0.0000	0.0000	0.0000
175	Steam Plant Mechanicals	-0.0001	0.0003	0.2766	0.0134	0.0000
89	Steam Plant Mechanicals	0.0000	0.0000	0.0733	-0.0051	0.0000
95-98	Water Pumps	0.0000	0.0000	0.0014	0.0322	0.0002
94	Pump House	0.0000	0.0000	0.0000	0.0000	0.0000
172	Pump House	0.0000	0.0000	0.0000	0.0000	0.0000
173	Water Pumps	-0.0002	-0.0109	-0.0006	-0.0003	0.0000
100	Water Treatment Plant	0.0000	0.0000	0.0000	0.0000	0.0000
101	Wastewater Lift House	0.0000	0.0000	0.0000	0.0000	0.0000
102	Wastewater Lift House	0.0000	0.0000	0.0000	0.0000	0.0000
103	Wastewater Lift House	0.0000	0.0000	0.0000	0.0000	0.0000
110	HRSD Lift Station	0.0000	0.0000	0.0000	0.0000	0.0000
111-113	Wastewater Mechanicals	-0.0010	-0.0036	-0.0380	-0.0380	-0.0380
114-118	Wastewater Mechanicals	-0.0005	-0.0109	-0.0282	-0.0282	-0.0282
117-119	Wastewater Mechanicals	-0.0004	0.1178	0.0266	0.0266	0.0266

The results presented in Table 46 above reveal three interesting patterns in the differences in damage state probabilities at assets. First, the effect of groundwater influences on the probability of damage to assets tended to increase as the SLR state was increased from 0.0 m to 1.0 m and then tended to decrease as the SLR state was increased from 1.0 m to 2.0 m. Second, the sign of

the effect of groundwater influences on the probability of damage to assets was non-uniform across assets at any given SLR state. Groundwater influences may cause the probability of damage to be reduced at one asset while caused the probability of damage to be greater at another asset. Thirdly, at any one asset, accounting for groundwater influences on flooding depths caused the probability of damage to increase at one SLR state, but caused the probability of damage of that same asset to decrease at another SLR state.

The absence of a uniform negative or positive trend in probabilities across the entire suite of assets and SLR scenarios suggest that: 1) groundwater influences varied across the installation, and 2) these variations had different effects on flooding at different SLR states. The GSSHA model inputs to the revised risk assessment were reviewed at selected assets across the study site to confirm that these effects were genuine and could be attributed to the differences in flood depths across the SLR states.

4.11.2.2 Effect of New Groundwater Modeling on Function Nodes

A change in the probability of damage to assets has a corresponding effect on the probability of that asset being in a *Non-Functional* state. Small changes in the probability of an asset being non-functional can ripple throughout the network in unexpected ways and cause correspondingly large changes in the probability of other assets becoming *Non-Functional*. The effects associated with incorporating aquifer storage capacity on flooding are summarized in Table 47, which reports the change in the probability of each asset being in a *Non-Functional* state at each SLR state.

Table 47. Difference in the probability of an asset being Non-Functional when the influence of groundwater was considered in the GSSHA model re-runs. Negative values (shown in red) indicate that the probability of being *Non-Functional* was greater when these influences were considered. Positive values (shown in green) indicate the probability of being *Non-Functional* was lower when these influences were considered.

NODE	DESCRIPTION	SLR Scenario				
		0.0 m	0.5 m	1.0 m	1.5 m	2.0 m
133	P11 Draft North	0.0000	0.0000	0.0000	0.0000	0.0000
132	P12 South Draft	0.0000	0.0000	0.0000	0.0000	0.0000
131	P12 North Draft	0.0000	0.0000	0.0000	0.0000	0.0000
130	P14 South Draft	0.0000	0.0000	0.0000	0.0000	0.0000
129	P14 North Draft	0.0000	0.0000	0.0000	0.0000	0.0000
1	Generator	-0.0004	-0.0178	-0.0300	0.0080	0.0000
174	Generator	0.0000	0.0002	0.2396	0.0255	0.0004
2	Generator	0.0001	0.0457	0.0002	0.0000	0.0000
3 - 6	Generators	-0.0002	0.0003	0.1120	-0.0011	0.0000
164	Generator	-0.0002	0.0004	-0.1063	0.0769	0.0006
148	Substation	0.0000	-0.0001	0.0682	0.0054	0.0032
8	Substation	-0.0001	-0.0011	0.0516	0.0016	0.0000
154	Substation	-0.0003	-0.0006	0.0871	0.0001	0.0000
153	Substation	0.0000	-0.0001	0.1451	-0.0048	0.0000
152	Substation	0.0000	-0.0003	0.2073	0.0070	0.0001
150	Substation	0.0000	-0.0001	0.0906	0.0054	0.0005
11	Substation	0.0000	-0.0005	0.0426	0.0042	0.0000
9	Substation	0.0000	-0.0006	0.0551	0.0046	0.0000
157	Substation	0.0010	0.0413	0.0060	0.0008	0.0000
10	Substation	-0.0001	-0.0013	0.0184	0.0021	0.0000

NODE	DESCRIPTION	SLR Scenario				
		0.0 m	0.5 m	1.0 m	1.5 m	2.0 m
168	Transformer	0.0000	0.0000	0.3196	0.0009	0.0000
163	Transformer	-0.0009	-0.0042	-0.0226	0.0004	0.0000
162	Transformer	-0.0007	-0.0452	-0.0023	0.0001	0.0000
169	Transformer	-0.0002	-0.0715	0.0008	0.0000	0.0000
171	Transformer	0.0000	-0.0002	0.2979	0.0010	0.0000
161	Transformer	-0.0001	-0.0002	0.2860	0.0035	0.0000
167	Transformer	-0.0001	-0.0150	0.0033	-0.0001	0.0000
165	Transformer	-0.0001	0.1589	0.0016	0.0000	0.0000
159 - 160	Transformer	-0.0001	0.0001	0.1712	-0.0002	0.0000
138	P11 North Freeboard	0.0000	0.0000	0.0000	0.0000	0.0000
136	P12 North Freeboard	0.0000	0.0000	0.0000	0.0000	0.0000
137	P12 South Freeboard	0.0000	0.0000	0.0000	0.0000	0.0000
134	P14 South Freeboard	0.0000	0.0000	0.0000	0.0000	0.0000
135	P14 North Freeboard	0.0000	0.0000	0.0000	0.0000	0.0000
121	Thimble Shoals Channel	0.0000	0.0000	0.0000	0.0000	0.0000
122	Harbor Entrance Channel	0.0000	0.0000	0.0000	0.0000	0.0000
123	Inner Harbor Channel	0.0000	0.0000	0.0000	0.0000	0.0000
37	Pump House	0.0000	-0.0001	0.2954	0.0010	0.0000
44	Pump	-0.0002	-0.0602	0.0754	0.0000	0.0000
144	Fuel Pump House	-0.0002	-0.0713	0.0007	0.0000	0.0000
158	Fuel Pumps	-0.0002	-0.0731	0.0002	0.0000	0.0000
45	Fuel Storage Tanks	0.0000	0.0000	0.0000	-0.0020	0.0015
65	Steam Line (250 psi, Tall Pylons)	-0.0001	-0.0711	0.0001	0.0000	0.0000
66	Steam Line (250 psi, Tall Pylons)	-0.0001	-0.0711	0.0001	0.0000	0.0000
76D	Steam Line (250 psi, Tall Pylons)	-0.0001	-0.0049	0.3038	0.0000	0.0000
76F	Steam Line (250 psi, Tall Pylons)	-0.0001	-0.0049	0.3038	0.0000	0.0000
55A	Steam Line (250 psi, Short Pylons)	-0.0001	-0.0711	0.0001	0.0000	0.0000
74A	Steam Line (250 psi, Short Pylons)	-0.0001	-0.0711	0.0001	0.0000	0.0000
55B	Steam Line (250 psi, Short Pylons)	-0.0001	-0.0711	0.0001	0.0000	0.0000
74C	Steam Line (250 psi, Short Pylons)	-0.0001	-0.0711	0.0001	0.0000	0.0000
74D	Steam Line (250 psi, Short Pylons)	-0.0001	-0.0711	0.0001	0.0000	0.0000
69	Steam Line (250 psi, Short Pylons)	-0.0001	-0.0711	0.0001	0.0000	0.0000
54A	Steam Line (250 psi, Tall Pylons)	-0.0001	-0.0049	0.3038	0.0000	0.0000
63	Steam Line (250 psi, Tall Pylons)	-0.0001	-0.0711	0.0001	0.0000	0.0000
76A	Steam Line (250 psi, Tall Pylons)	-0.0001	-0.0049	0.3038	0.0000	0.0000
79A	Steam Line (250 psi, Tall Pylons)	-0.0001	-0.0711	0.0001	0.0000	0.0000
80	Steam Line (250 psi, Tall Pylons)	-0.0001	-0.0711	0.0001	0.0000	0.0000
81	Steam Line (250 psi, Tall Pylons)	-0.0001	-0.0711	0.0001	0.0000	0.0000
54B	Steam Line (250 psi, Tall Pylons)	-0.0001	-0.0049	0.3038	0.0000	0.0000
64	Steam Line (250 psi, Tall Pylons)	-0.0001	-0.0711	0.0001	0.0000	0.0000
74B	Steam Line (250 psi, Tall Pylons)	-0.0001	-0.0711	0.0001	0.0000	0.0000
76B	Steam Line (250 psi, Tall Pylons)	-0.0001	-0.0049	0.3038	0.0000	0.0000
79B	Steam Line (250 psi, Tall Pylons)	-0.0001	-0.0711	0.0001	0.0000	0.0000
54C	Steam Line (250 psi, Tall Pylons)	-0.0001	-0.0049	0.3038	0.0000	0.0000
76C	Steam Line (250 psi, Tall Pylons)	-0.0001	-0.0049	0.3038	0.0000	0.0000
79C	Steam Line (250 psi, Tall Pylons)	-0.0001	-0.0711	0.0001	0.0000	0.0000
54D	Steam Line (250 psi, Tall Pylons)	-0.0001	-0.0049	0.3038	0.0000	0.0000
74D	Steam Line (250 psi, Tall Pylons)	-0.0001	-0.0711	0.0001	0.0000	0.0000
76E	Steam Line (250 psi, Tall Pylons)	-0.0001	-0.0049	0.3038	0.0000	0.0000
76G	Steam Line (250 psi, Tall Pylons)	-0.0001	-0.0049	0.3038	0.0000	0.0000
59	Steam Line (250 psi, Tall Pylons)	-0.0001	-0.0711	0.0001	0.0000	0.0000
60	Steam Line (250 psi, Tall Pylons)	-0.0001	-0.0711	0.0001	0.0000	0.0000
67	Steam Line (250 psi, Tall Pylons)	-0.0001	-0.0711	0.0001	0.0000	0.0000
72	Steam Line (250 psi, Tall Pylons)	-0.0001	-0.0711	0.0001	0.0000	0.0000

NODE	DESCRIPTION	SLR Scenario				
		0.0 m	0.5 m	1.0 m	1.5 m	2.0 m
82	Steam Line (250 psi, Tall Pylons)	-0.0001	-0.0711	0.0001	0.0000	0.0000
83	Steam Line (250 psi, Tall Pylons)	0.0000	-0.0002	0.3037	0.0000	0.0000
84	Steam Line (250 psi, Tall Pylons)	-0.0001	-0.0049	0.3038	0.0000	0.0000
85	Steam Line (250 psi, Tall Pylons)	-0.0001	-0.0711	0.0001	0.0000	0.0000
87	Steam Line (250 psi, Tall Pylons)	-0.0001	-0.0711	0.0001	0.0000	0.0000
88	P-1 Primary Steam Plant Building	0.0000	0.0001	0.1699	-0.0002	0.0000
143	Auxiliary Steam Plant Building	0.0000	0.0000	0.2065	0.0258	0.0004
175	Steam Plant Mechanicals	0.0000	-0.0002	0.3037	0.0000	0.0000
89	Steam Plant Mechanicals	-0.0001	-0.0711	0.0001	0.0000	0.0000
95 - 98	Water Pumps	0.0000	0.0000	0.3073	0.0005	0.0000
94	Pump House	0.0000	0.0000	0.3069	0.0009	0.0000
172	Pump House	-0.0001	-0.0148	0.0033	-0.0001	0.0000
173	Water Pumps	-0.0002	-0.0072	0.0000	0.0000	0.0000
100	Water Treatment Plant	0.0000	0.0000	0.0000	0.0000	0.0000
101	Wastewater Lift House	-0.0001	0.0002	-0.1073	0.0765	0.0006
102	Wastewater Lift House	-0.0003	-0.0109	-0.0306	0.0080	0.0000
103	Wastewater Lift House	-0.0001	0.1773	0.0017	0.0000	0.0000
110	HRSD Lift Station	-0.0009	-0.0111	0.0517	0.0004	0.0000
111 - 113	Wastewater Mechanicals	-0.0001	-0.0711	0.0001	0.0000	0.0000
114 - 118	Wastewater Mechanicals	-0.0001	-0.0711	0.0001	0.0000	0.0000
117 - 119	Wastewater Mechanicals	0.0000	-0.0002	0.3037	0.0000	0.0000

The effect is in essence the difference between the probability of an asset being in a non-functional state when the influences of groundwater are ignored, $p(F_i \mid SLR)_{NO\_GW}$, and the probability of an asset being in a non-functional state when the influences of groundwater are modeled, $p(F_i \mid SLR)_{GW}$:

$$\Delta p = p(F_i \mid SLR)_{NO\_GW} - p(F_i \mid SLR)_{GW} \quad \textbf{(34)}$$

The patterns in Table 47 above are similar to the patterns observed in Table 46 above. First, the effect on the probability of each asset being non-functional tended to increase as the SLR state was increased from 0.0 m to 1.0 m, and then tended to decrease as the SLR state was increased from 1.0 m to 2.0 m. Second, the sign of the effect was non-uniform across assets at any given SLR state. Changes in flooding depths (driven by reduced aquifer storage capacity and variations in infiltration rates) caused the probability of being non-functional to be reduced at one asset while it caused the probability of being non-functional to be greater at another asset. Thirdly, at any one asset, accounting for these groundwater influences on flooding depths caused the probability of being non-functional to increase at one SLR state, but caused the probability of being non-functional at that asset to decrease at another SLR state. All of these effects can be explained by corresponding changes in asset damage state probabilities.

Some of the largest impacts on functionality were observed in the steam system under the 1.0 m SLR scenario. The probability that steam lines were *Non-Functional* was reduced to 0.3037 when groundwater influences were accounted for in the flood modeling, and were attributed to

the lower damage state probabilities at supporting assets. In other words, the decrease in probability of being *Non-Functional* at these assets reduced the probability of steam lines being *Non-Functional*. Note that in Table 46 above, the effect of accounting for the groundwater influence's on flooding on the probability of steam lines being in a damage state other than *None* is less than 0.0005.

4.11.2.3 Effect of New Groundwater Modeling on Capability Scores and Mission Performance

Figure 172 and Table 48 compare the capability scores from the original risk assessment with the capability scores from the revised risk assessment, which incorporated the influence of groundwater. Note that the *Provide Access*, *Provide North Berth*, and *Provide South Berth* capabilities have not been plotted here because they were unaffected by these groundwater influences.

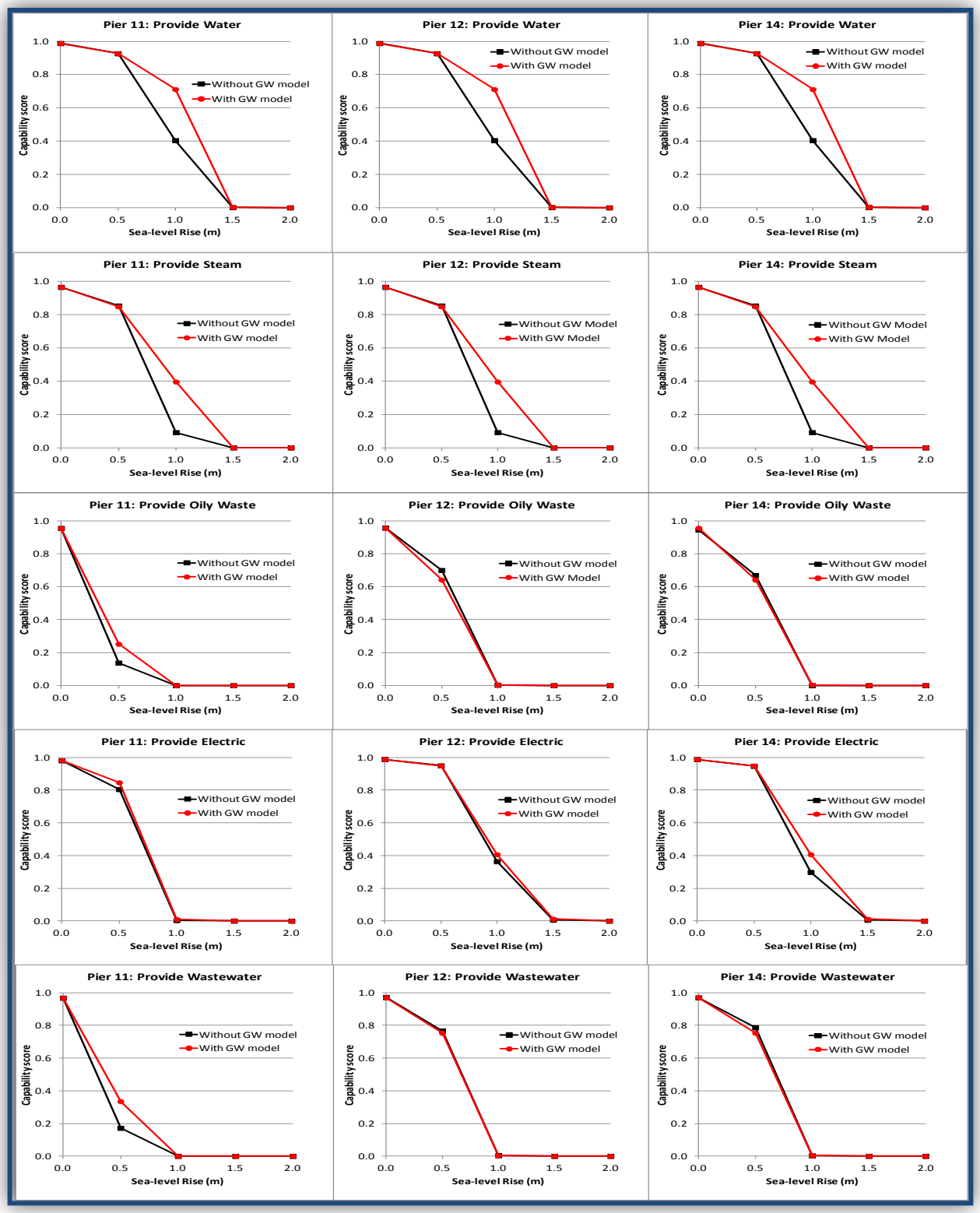

Figure 172. Effects of new groundwater (GW) modeling results on the revised capability scores.

Table 48. Differences in capability scores and mission performance index. Negative values (shown in red) indicate that capability scores and mission performance indices were greater when groundwater influences on flooding are accounted for in the new GSSHA model analyses.

Pier	SLR Scenario	Capability Scores								Mission Performance Index (MPI)[1]
		Provide Water	Provide Access	Provide Steam	Provide North Berth	Provide South Berth	Provide Oily Waste	Provide Electricity	Provide Wastewater	
11	0.0	0.0001	0.0000	0.0001	0.0000	0.0000	0.0000	-0.0010	0.0000	**-0.0002**
	0.5	0.0002	0.0000	0.0049	0.0000	0.0000	-0.1145	-0.0413	-0.1633	**-0.0593**
	1.0	-0.3070	0.0000	-0.3038	0.0000	0.0000	0.0000	-0.0060	0.0000	**-0.0890**
	1.5	-0.0005	0.0000	0.0000	0.0000	0.0000	0.0000	-0.0008	0.0000	**-0.0002**
	2.0	0.0000	0.0000	0.0000	0.0000	0.0000	0.0000	0.0000	0.0000	**0.0000**
12	0.0	0.0001	0.0000	0.0001	0.0000	0.0000	0.0002	0.0000	0.0006	**0.0002**
	0.5	0.0002	0.0000	0.0049	0.0000	0.0000	0.0585	0.0005	0.0133	**0.0102**
	1.0	-0.3070	0.0000	-0.3038	0.0000	0.0000	-0.0006	-0.0426	0.0008	**-0.0921**
	1.5	-0.0005	0.0000	0.0000	0.0000	0.0000	0.0000	-0.0042	0.0000	**-0.0010**
	2.0	0.0000	0.0000	0.0000	0.0000	0.0000	0.0000	0.0000	0.0000	**0.0000**
14	0.0	0.0001	0.0000	0.0001	0.0000	0.0000	0.0001	0.0001	0.0003	**0.0001**
	0.5	0.0002	0.0000	0.0049	0.0000	0.0000	0.0676	0.0013	0.0259	**0.0141**
	1.0	-0.3070	0.0000	-0.3038	0.0000	0.0000	0.0000	-0.0184	-0.0011	**-0.0871**
	1.5	-0.0005	0.0000	0.0000	0.0000	0.0000	0.0000	-0.0021	0.0000	**-0.0005**
	2.0	0.0000	0.0000	0.0000	0.0000	0.0000	0.0000	0.0000	0.0000	**0.0000**

Figure 172 shows that, in most cases, the capability scores changed very little. However, relatively large effects were seen for the *Provide Water* and *Provide Steam* capabilities under the 1.0 m SLR scenario. For the *Provide Water* capability, the score was 0.3070 higher when the groundwater influences were considered in the revised GSSHA model analyses. This appeared to reflect a lower probability of the *Asset #168* (a transformer) changed from a *Moderate* to a *Severe* damage state. For the *Provide Steam* capability, the score was higher because the probabilities of the *Asset #161* (another transformer), *Asset #174* (a generator), and *Asset #175* (the steam plant mechanicals) switched from *Moderate* to *Severe* damage states when groundwater influences were considered in the re-analysis of flooding. Differences in capability scores were also seen in the cases of the *Provide Wastewater* and *Provide Oily Waste* capabilities at Piers 12 and 14. These capability scores were slightly lower when the groundwater influences on flooding were considered in the re-analysis. Overall, the original conclusions drawn in the initial analysis still hold true - capability scores at NSN decreased rapidly between the 0.5 m and 1.5 m SLR scenarios.

Recall that the MPIs at each pier are calculated as the weighted sums of the capability scores for each pier (Table 48 above). The weights in this function describe the relative importance of each capability as described previously and reflect command level priorities to provide services to CVNs at berth. Figure 173 plots the MPIs for each pier and Table 48 above summarizes the differences between the original and revised assessments. The largest differences occurred under the 1.0 m SLR scenario, where the MPI was 0.0890 higher at Pier 11 when groundwater influences were accounted for in the new GSSHA model runs. Similarly, the MPI was 0.0921 higher at Pier 12 and 0.0871 higher at Pier 14 in the revised assessment. As with the original risk assessment, the revised NSN Risk Model showed that a major degradation in the ability to perform the mission at NSN occurred between SLR state 0.5 m and SLR state 1.0 m (i.e., the "tipping point" was still readily apparent).

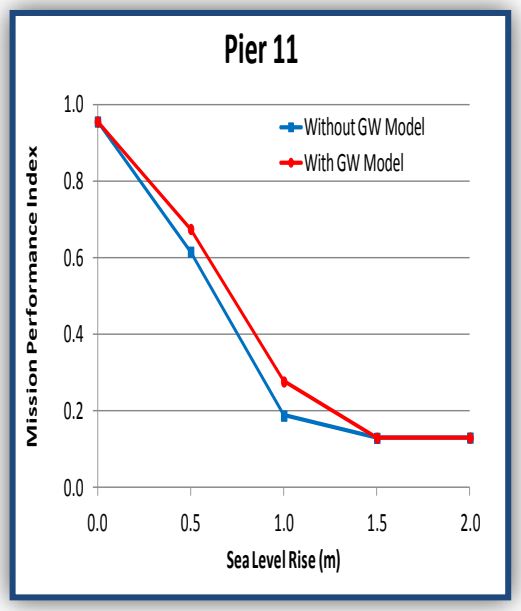

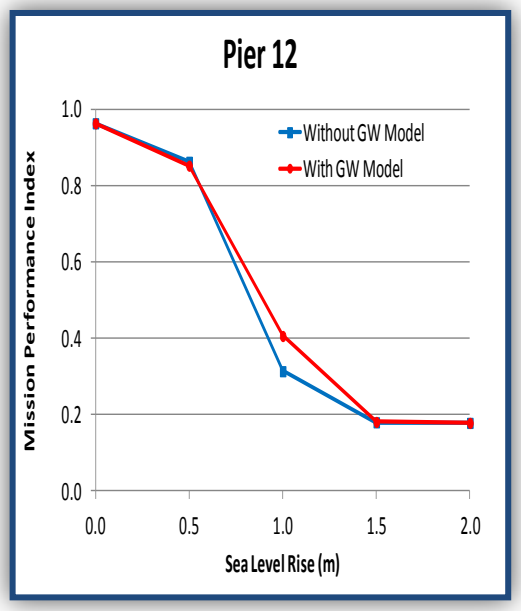

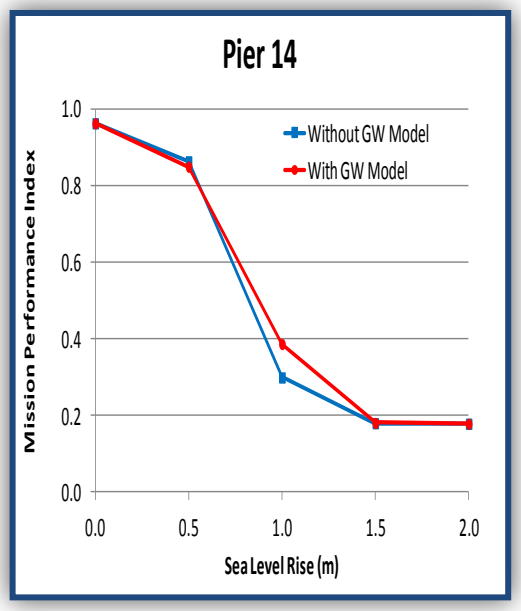

Figure 173. Effects of groundwater (GW) influences on the flood modeling results and the subsequent changes to MPI scores.

5. Conclusions and Implications for Future Research and Implementation

5.1. Overall Study Synthesis

In this study, we set out to develop and demonstrate a robust, scientifically defensible approach to quantify risks to mission performance and transparently communicate these to the end user, providing policymakers with relevant information to develop guidance that promotes sustainable operations, and empowers on-the-ground military planners with the actionable information to make risk-informed decisions regarding threats to existing and future infrastructure development, considering climate change and SLR. By systematically characterizing the existing environment, predicting changes to the coastline, simulating coastal storms moving across the region, quantifying the resultant "forcings" (i.e., floodwaters, waves, winds), and constructing a dependency-based network model of the installation's assets and capabilities, we have laid the foundation to assess damages caused by coastal storms under a range of SLR scenarios. Under this new paradigm, the latest innovations in storm probability analytics and high fidelity coastal wave/storm surge inundation models provide robust scientific input to an innovative Bayesian network designed to quantify risks to mission in a real-time, decision-relevant manner. Underpinning the models, we have developed a geomorphically-driven, ecologically-based land conversion simulation projecting inundation and habitat switching driven by SLR to capture a range of potential future long-term conditions.

These tasks have been independently productive (several conference papers and proceedings have been produced) and have proven to be mutually supportive. More importantly, the models performed as expected and no technical difficulties of their applications in the test case were experienced. The individual efforts have generated significant results and offer important scientific conclusions. The following sections offer more details of each step in the framework on a component-by-component basis.

5.1.1 Geomorphological and Ecological Modeling to Characterize Changes to the Coastal Shoreline

Baseline characterization of existing coastal geomorphology and ecology make it possible to predict changes in coastal shorelines threatened by rising sea levels and hurricanes. Of particular importance are the effects arising from changes in erosion/accretion rates, subsidence, and wetland conversions, which ultimately result in increases in open water areas. In these instances, increases in open water fetch can contribute to hazardous conditions at docks, reduce berthing times, damage infrastructure, and contribute to more flooding of low areas. Our work has led to a better understanding of the methods, models, and tools that can be used to assess coastal geomorphology and ecological response to changing sea levels. Both the straight-line (i.e., bathtub) and SLAMM models, methodologies, and results developed in this study can be applied to other locations in the Hampton Roads area (with only minor adjustments). However, shifting the models outside the study domain (refer to *Sites 1*, *2*, and *3* in Figure 8 of *Chapter 3: Materials and Methods*) will necessitate the collection of new baseline data to calibrate the model.

As a proof of concept, we developed a geomorphological classification system for the Hampton Roads area (VA), and derived subsidence rates that were fed directly into an analysis of ecosystem response in three areas located at the mouth of the Chesapeake Bay. We developed both a straight-line model and employed the SLAMM to simulate SLR under the five prescribed scenarios, and generated a series of GIS-based shapefiles and exposure maps visualizing the response of the system to SLR over a 100-year time period (2000-2100). Overall, our simulations predict: 1) reductions in dry lands, swamps, and beach/shore environments; 2) significant increases in open water and tidal flats; and 3) variable responses in fresh and tidal marshes. The ecological consequences of these changes could be significant - not only will there be a direct loss of habitat (e.g., swamp), but the relative distribution and connectivity of habitats will be dramatically altered. Tidal and freshwater marshes, for example, play a disproportionately large role as breeding and foraging grounds for a variety of taxa (e.g., colonial waterbirds and estuarine fishes) and are a significant source of detritus for other coastal ecosystems, yet their spatial extent is less than 0.1 percent across the entire study area. Losses of these areas could have cascading effects impacting the production of ecosystem goods and services across the system. As with any study, models are only as good as their assumptions and data inputs. For example, SLAMM simulations are oftentimes constrained by the accuracy of the elevation and land use classification data. In our case, we attempted to overcome these limitations by acquiring high resolution elevation mapping (10 m scale) and the most recent land vegetation cover available from the 2001/2002 NLCD. We also performed a sensitivity of the SLAMM, altering inputs (levels of protection, erosion/accretion rates, and storm frequencies) and comparing the results across scenarios. We found that SLAMM is extremely sensitive to protection strategies, and future applications of this tool must take this sensitivity into account.

5.1.2 Hurricane Simulations and Forcing Generation

Although coastal storms occur intermittently, they can have long-term impacts on the military's infrastructure and mission performance. Coupled with a rise in sea level, these impacts can be more extensive in the future due to changes in storm intensity, frequency and track. In addition to higher sea levels, increased surge can raise the potential for more intensive inland flooding. A rise in relative sea level could potentially shift the maximum water levels and wave heights produced by these storms in a nonlinear fashion (Smith et al. 2010). Moreover, the complex interactions between nearshore elements (i.e., barrier islands, dunes, estuaries, wetlands, beaches, etc.) complicate the situation. Rising sea levels will have profound effects on nearshore conditions (increasing flooding frequency and inundating low-lying coastal areas), while other driving processes (e.g., erosion/accretion) will compound the effects of coastal nearshore and shoreline evolution. Significant increases in rainfall accompanying these storms, compounded by aging infrastructure (particularly inadequate or ineffective storm drainage networks), and the loss of groundwater aquifer storage capacity (due to rising groundwater levels and saltwater intrusion) will only serve to heighten installation exposure and threaten the future sustainability of coastal installations. Our work has led to a better understanding of the methods, models, and tools that can be used to quantify the resultant forcings arising from coastal storms and changing sea levels that threaten critical infrastructure in the coastal zone. The regionally-scaled models, methodologies, and results can be applied to other locations in the Hampton Roads area (with only minor adjustments). The nearshore and inland models and methodologies can also be applied to other locations in the area, but their application would require new site-specific data to

recalibrate their baseline conditions. Moreover, both the regional and local models can be used in other locations outside the Hampton Roads area, but these shifts in domain would likely require new baseline data to calibrate the systems.

As a proof of concept, we used a combination of regional, nearshore, surface/subsurface flood routing, and groundwater models to simulate a series of storms under a range of SLR scenarios and generated resultant forcings (i.e., winds, waves, surge, sediment transport, flooding depths, etc.) threatening the NSN case study site and its surrounding environs. We used three high fidelity numerical models (TC96, ADCIRC, and SWAN) to simulate tropical/extra-tropical storms to provide information on storm development and progression at the regional scale. A high-resolution integrated surge, wave, and sediment transport model (CMS) was then used to assess escalating surge, waves, sediment accretion and erosion in the nearshore setting to resolve nearshore coastal and land coverage features at the local scale. Coupling the regional and local models, we were able to calculate the changes in water surface elevation, storm surge, and storm waves, as well as sediment transport and morphological changes in the nearshore and low-lying coastal settings surrounding the study site. Inland flooding was modeled using a spatially distributed physically-based hydrologic simulation model (GSSHA), which was informed by a hybridized groundwater model (Adh-WASH) that captured changes in aquifer storage capacity with SLR-driven salt water intrusion into the groundwater aquifer.

With the incremental inclusion of each hydrodynamic model to the analysis in a stepwise fashion, we were able to significantly refine the level of detail considered in quantifying the area's exposure, and adjust our estimates of surge levels, wave heights, and flooding depths. Each model application generated a series of GIS-based shapefiles and exposure maps visualizing the response of the system under the 25 separate SLR-storm scenarios. Overall, our simulations predict:

1) Maximum winds ranging from 24 m/s (for the 1-yr return interval storms) to 43 m/s (for the 100-yr return interval storms),
2) Maximum surge ranging from 1.2 m (under the 0.0 SLR + 1-yr return interval storm) to 5.4 m (under the 2.0 m SLR + 100-yr return interval storm), and
3) Maximum flooding depths ranging from 2.5 m (under the 0.0 SLR + 1-yr return interval storm) to 9.1 m (under the 2.0 m SLR + 100-yr return interval storm).[1]

The analysis of groundwater contributions to the flooding situation was particularly informative. Our groundwater model predicted 23 percent decrease in infiltration under the 0.5 m SLR and an 80 percent decrease in infiltration under the 2.0 m SLR scenario, indicating a significant decrease in groundwater storage capacity. In every scenario run with GSSHA coupled to the groundwater results, the difference maps indicated a change in flooding depths (either positively or negatively), aptly demonstrating the value of incorporating this level of detail into the critical analysis of flooding when assessing impacts caused by SLR and coastal storms. In other words, there was a measureable difference between the GSSHA results when constant rates of infiltration versus variable rates of infiltration (based on reduced aquifer storage capacity caused

[1] Storm forcings/loadings varied spatially across the modeling domains – only the maximums have been reported here.

by saltwater intrusion driven by SLR) were used in the flood routing analysis. This finding would suggest that simplifying assumptions about groundwater impacts due to the combined effects of sea level rise, infiltration, soil moisture, and salt water-fresh water boundaries in the groundwater cannot be easily made in terms of magnitude or direction of impact. At NSN, groundwater is not used as a potable water supply. However, at other sites, groundwater impacts could be a significant factor to be considered where characterizing impacts to water supply.

5.1.3 Asset Capability Network (ACN) Development

Once an installation's exposure to storm forcings has been characterized, the sensitivity and adaptive capacity of the installation's critical infrastructure must be explored to meaningfully quantify risks to mission performance. Experience has taught us that the dynamics, complexity, and risks germane to military operations on coastal installations cannot be adequately assessed by characterizing risks to individual infrastructure assets independently. The best way to fully capture the threats of SLR and coastal storms on these sites is to take a holistic, network-based approach that systematically captures the intricate, highly interdependent relationships among infrastructure assets, system capabilities, and missions. A holistic systems approach shifts the decision-making focus from individual, isolated assets to an interdependent system of assets that acting together offer specific capabilities and provide key services. Moreover, the systems approach shifts the focus from individual and immediate concerns to regional and long-term solutions. The systems approach incorporates anticipatory and adaptive management to effectively manage a site's aging infrastructure in a sustainable manner with explicit regret management. The essential function of a network-based systems approach is to provide an organized framework that supports a balanced evaluation of all relevant issues (e.g., storm forcings and asset fragilities) at appropriate scales of space and time. Management of a system to reduce the risk of coastal storm damage and increase resiliency includes actively monitoring the system and providing readily-accessible, actionable information to the installation managers in a timely manner. By providing information that accurately represents the present state of the system, decisions can be made as to where investments are needed. "Weak links" in the system can be proactively protected (i.e., flood-proofed), or, if these portions of the system fail, contingency plans can be established in advance. Our work has led to a better understanding of the methods, models, and tools that can be used to model a coastal installation's critical assets from a systems perspective. Our Asset Capability Network (ACN) approach decomposes the key missions into critical capabilities, services and contributing assets in a spatially-explicit manner, capturing the interdependencies of these components, and reaching beyond the installation's fence line to capture dependencies on municipal utilities. This approach could be easily applied to other locations both in the Hampton Roads area, as well as other locals worldwide.

As a proof of concept, we developed an ACN for a case study on NSN, focused on two missions (i.e., *At-Berth Support* and *Support of Ship Harbor Movement*), seven capabilities (i.e., *Provide Berthing Space*, *Provide Portable Water*, *Provide Electric Power*, *Remove Wastewater*, *Remove Oily Waste*, *Provide Steam*, and *Provide Physical Access to Berths*), and 16 groups of assets ranging from individual structures (i.e., buildings, piers, boilers, transformers, pumps etc.) to distribution systems (i.e., natural gas, steam, and fuel/oil pipelines), to the various channels out in the Chesapeake Bay offering access to the installation. These assets were mapped in a GIS at a

10-m scale, and the database itself has been offered to the NSN for future master planning and assessment purposes.

5.1.4 Structural Fragility Analysis

Once an installation's critical infrastructure assets have been identified and mapped within an ACN, the fragility of these assets must be quantified probabilistically in terms of damage state based on structural loadings at each level of storm severity under the various SLR scenarios. Oftentimes, fragility curves are used to describe the conditional probability of an asset's failure over the full range of loads to which that asset might be exposed. The shape of a fragility curve describes uncertainty in the capacity of the asset to withstand a load or, alternatively, uncertainty in what load will cause the asset to fail. Fragility curve development methodologies span the gamut of judgmental, empirical and analytical techniques. Each approach has its strengths and weaknesses. Oftentimes, the solution is to take a hybridized approach driven by the availability of data, the reliability of the expertise of subject matter experts, and the availability and capabilities of analytic tools to generate the curves. Our work has led to a better understanding of these methods, models, and tools. Our straightforward five-step approach begins with a determination of which loadings (winds, waves, flooding depths, etc.) threaten each asset category. We then identify the most likely failure load (i.e., bending, shearing, etc), and calculate both the capacity of the asset to resist that failure and the load acting (i.e., the demand) that produces the mode of failure. As a last step, we generate the probability of damage (i.e., the fragility curve) based on the capacity and demand. This 5-step approach could be easily applied to other locations both in the Hampton Roads area, as well as other locals worldwide.

As a proof of concept, we developed a catalogue of fragility curves for 22 separate types of assets on the NSN under the prescribed storm and SLR scenarios. The capacity of each asset to resist failure, and the measure of loads acting on these assets that generate these modes of failure, was captured in damage state tables. In general, these damage states corresponded to those described in HAZUS-MH MR-4. Two to four damage states were defined for the assessment ranging from *None* to *Severe*. Where possible, parametric analysis (supplemented by empirical data and professional judgment) were used to develop the individual damage functions in fragility curves. Predicted wind speeds, water depths and wave velocities generated by the storm analyses (described in the previous sections) were fed into the HAZUS curves, and damages were then generated for the varying water heights under the five prescribed SLR scenarios. Predictions of the extent of structural damages to buildings were then estimated. SAP2000 was used to estimate the response of the piers under a combination of the various SLR scenarios. We included frame models for low resolution structures where little information was available and developed detailed finite element models for structures when the information was available. Parameter studies were performed with the models to develop damage envelopes, and actual predicted wind and flood scenarios were used to develop damage estimates. These fragility curves have been offered to the NSN for future master planning and assessment purposes.

5.1.5 Risk Modeling

Rising sea levels threaten to increase risks to coastal military installations. A risk is a potential loss of uncertain severity. The task of risk assessment is to quantify the probability of potential

losses. Risks to mission performance are assessed using a Bayesian network approach. The Bayesian network is a model of the joint probability distribution of a set of random variables that determine mission performance. The functional interdependence among infrastructure assets is represented in the network diagram (Figure 53 in *Section 3.9.1.1* of *Chapter 3*), which describes the dependence and conditional independence relationships within the infrastructure system. The random variables in the network characterize storm loads, levels of damage to assets (damage states), levels of functional performance, mission capabilities, and an index characterizing overall performance with respect to the mission of interest. The probabilities of potential losses in mission performance are estimated for a set of coastal storms in combination with a variety of SLR scenarios. Our efforts have led to advancements in the application of inference-based probabilistic models to characterize the uncertainty of the systems threatened by SLR and coastal storm hazards. Our approach can be used to conduct both diagnostic and predictive inference of the infrastructure damage resulting from storm forcings, allowing managers and planners to incorporate proactive risk-reducing strategies into their long-term adaptive management strategies, addressing residual risks, and managing regrets. This approach could be easily applied to other locations both in the Hampton Roads area, as well as other locals worldwide.

As a proof of concept, we developed a Bayesian network model for the NSN case study. Our model was comprised of five types of nodes, including two risk drivers, 95 asset damage nodes, 97 asset function nodes, 19 capability nodes, and three mission performance nodes. The NSN Risk Model now holds more than 13,000 conditional probabilities characterizing the fragility of the assets with regards to their location, condition, and structural composition, and the relational network quantifies impacts to capabilities and the risks to mission performance due to exposure to storm hazards and SLR. In deploying the model, we clearly demonstrated that SLR is a significant and pervasive threat multiplier to mission sustainability, significantly increasing loadings on built infrastructure, and dramatically increasing risks to system capabilities and service provisioning. In particular, we found that the *Oily Waste* and *Waste Water Removal* systems were acutely vulnerable and likely to be incapacitated once sea levels rose above 1.0 meter. The analysis also showed that Pier 11 was more vulnerable than Piers 12 and 14 due to the positioning of critical assets on its lower deck. Furthermore, the results showed that the probabilities of damage to infrastructure and losses in mission performance began to increase dramatically between 0.5 m and 1.0 m of sea level rise indicating a threshold or "tipping point." Armed with this information, installation planners can now justify the formulation of new designs or the retrofit of existing assets to meet these loadings thresholds ensuring mission sustainability in the face of climate change and rising sea levels. In other words, the analytical framework communicated an actionable construct that suggested that operations and policymakers should consider altering the status quo to incorporate proactive design and management strategies to prevent or anticipate impairments based on the risks. The case study application also demonstrated how the benefits of potential modifications in the reliability of physical assets and network topology could be investigated. Several hypothetical modifications to physical assets and changes in network topology were explored including: 1) the benefit of redundancy in steam generation; 2) the benefit of having system-wide backup electric power generation capacity; 3) the potential benefit of flood-proofing system-wide backup electric power generation capacity; and 4) the potential benefit of flood-proofing wastewater infrastructure on the waterfront. We also compared the inclusion of groundwater modeling into

the risk assessment, and determined that the probability of damage to assets tended to increase as the SLR state was increased from 0.0 m to 1.0 m and then tended to decrease as the SLR state was increased from 1.0 m to 2.0 m. Varying groundwater levels across the installation, and varying flood responses under the different SLR states installation-wide, yielded non-uniform responses across the various assets, and the effects to mission performance (MPI scores) was negligible.

5.2. Our Risk-Based Approach: Strengths and Limitations

Vulnerability and risk assessments can be conducted with varying degrees of rigor and complexity. The choice of what kind of assessment to conduct is dependent on the goals and objectives of the study and the study's problem context. Of particular concern is the desired granularity of the answers, the quality of the data available for assessment purposes, and the amount of resources available to fund the assessment at one or more installations. The risk-based framework presented here is a relatively detailed evaluation of vulnerabilities and risks, developed with the intent of characterizing these threats and risks at a high resolution to ensure the answers will be delivered at an actionable scale (at the asset level). It is important to note that this approach can be ported to other sites or communities. Moreover, the models utilized herein are modular, and can be modified or tailored to meet the needs of the decision-makers at various scales and/or granularities. That said, the approach has both strengths and limitations (Table 49). The key to successfully utilizing the risk-based approach is to establish clear goals and objectives early-on, strategically deploy the various models, and modify the structure of the risk assessment to meet the needs of the decision makers.

Table 49. Comparison of the study framework's strengths and limitations.

Strengths	Limitations
• Can be scaled in approach to document and inform decision makers and stakeholders on risks and residual risks of loss to objectives, and especially during facilitation to show which objectives compete and those that don't during tradeoff and scenario-based parametric sensitivity analyses. • Can be used to inform objective-based tradeoffs for aptly understanding and managing potentially deep regrets, especially those considered irreversible from the spatiotemporal, unique and scarce resource and imperative-objective (i.e., failure equals fatal outcome) perspectives. • Can be used strategically to identify knowledge/information gaps and both inform and justify sequential resource investment decisions for focused/applicable scientific and technical discovery that enrich phases of analysis as they progress. • Can be used to inform lifecycle decisions for adaptation in sustaining objectives toward responsible management of investments made. • Lends itself well to effective/impactful visualization at all levels of required resolution in communications and understanding. • Can be expanded to describe systems performance on second and third-order effects of interest, thereby enhancing the potential to cultivate multi- organization partnership investment portfolios, in which synergies derived have economies-of-scale effects/efficiencies for those investing in and benefiting from its use.	• Requires significant knowledge, expertise, information, tools, time, and finances to perform, however, that can improve with continual application and learning. • Requires an engaged relatively educated decision maker and stakeholders, but in this context, can serve as a mechanism to stimulate engagement, educate, and transform culture/societal behaviors about relevant issues and concerns. • There is the potential for the framework to be misapplied and/or biased if not properly quality controlled, as well as if there are attempts by participants during elicitation to "game" the system toward swaying the outcomes of analysis.

5.3. Knowledge Gaps and Remaining Research Questions

As we have shown herein, the assessment of vulnerabilities and risks to mission performance in the face of climate change and SLR can be complex, and the application of the these techniques presents its own unique challenges. Much work remains on how to improve upon our approach, how to capture the system's response to these threats, and how best to manage and adapt to these threats. We have identified here a few key knowledge gaps encountered in the study:

- High resolution topographic-bathymetric data are limiting in many locations. Moreover, the accuracy, timing of data collection, and ownership of these data sets are often in question;
- Installation data, specifically location and design/specifications of critical infrastructure assets and systems, have not been standardized across installations, and are in some cases limited in content, outdated, and/or distributed across numerous databases that limits the data's utility;
- Groundwater well data are limiting, and oftentimes held by offsite contractors;
- Uncertainty has not been adequately quantified with respect to coupled modeling results, and could significantly affect the quantification of risks;
- Observed data (particularly gauge data) are limited and restricts the degree to which the surface hydrodynamic models can be verified and validated; and
- More advanced sediment modeling is needed to better capture erosion and accretion both onsite and in the channels surrounding installations.

Several significant research questions still remain. Below we offer a few avenues of study that could be pursued to move the state of the science and state of the practice forward.

5.3.1 Improving Ecological Modeling

Notably, the majority of the NSN case study site is characterized as "built" infrastructure, and less than five percent remains in marsh or inland open water at the time of this study. As such, the risk of SLR impacting these habitats had virtually no bearing on mission sustainability and the application of the risk assessment illustrated as much. However, should this risk-based analytical approach be ported to other installations (e.g., Langley Air Force Base, Dam Neck Naval Combat Training Center, Naval Amphibious Base Little Creek, and numerous others in the Hampton Roads area and beyond), particularly those whose natural resources (air, water, and land) are considered assets that must be managed and sustained in order for the military to achieve a particular mission (e.g., training), it will become imperative that these natural infrastructure impacts be characterized and their response to climate change be quantified to support risk-informed decision making. We foresee a future need to capture changes to vegetative community structure and function driven by changing climate and rising sea levels through the development and application of spatially-explicit ecosystem-scale community models. Through the combination of abiotic components (e.g., magnitude, frequency, and timing of precipitation, storm and runoff events, the amount of SLR, the location and placement of accreting or subsiding sediments, etc.) generated by the framework's climatic, geomorphic, and hydrologic (including sediment transport) models and the biotic components (e.g., diversity, structure, composition, distribution, patch dynamics, etc.) of the system's setting, the risk assessment can be better attuned to these situations. The intent would be to develop tools that could predict ecosystem response to climate change, and test their efficacy by assessing a series of climate change/anthropogenic stressor scenarios allowing the military to characterize exposure, sensitivity and adaptive capacity of the natural infrastructure on (and around) the installations. These vulnerabilities and the inherent threats to the ecosystem services they provide sustaining military activities on the installation would then be incorporated into the risk analysis to quantify the holistic probability of mission failure. The results in turn could then be used to

establish the foundations for monitoring and adaptive management (i.e., pinpointing "tipping points" and/or thresholds).

5.3.2 Enhancing Coastal Storm Modeling

In *Section 3.1.1* of this report, we discussed the operational constraints under which we developed and demonstrated the risk-based analytical framework. As the study progressed, we compiled a series of "lessons learned" and future research initiatives that could be implemented to enhance the framework's analytic capabilities. For example, the coastal storm modeling in this study was limited by both resources and time constraints. As such, we limited their analysis to only a handful of storms, and specifically focused on two "representative" storms to quantify potential coastal forcings. In future applications, a more robust storm dataset could provide more insight into probabilistic forcing conditions. Furthermore, for purposes of simplification and clarity we held storm frequencies constant, and did not inject climate change drivers into the parameterization of storms. In future analyses, a sensitivity analysis could be conducted that incorporated changes in storm parameters (central pressure, radius of maximum winds, tracks/heading, forward speed, landfall decay, etc.) driven by increases in sea surface temperatures and alterations in ocean currents arising from global climate change to re-asses storm forcings and frequencies. Along those same lines, changes in winds due to changes in sea surface temperatures, ocean currents, salinity, etc. could be incorporated into a reassessment of forcings under the SLR scenarios.

5.3.3 Refining the Risk Model's Architecture

There are many opportunities to refine the architecture and formulation of the Bayesian model constructed for the NSN study. In the current construct, the relationships between asset damage states and function states are deterministic. However, in general, the damage state definitions used in this study were not specific enough to make any more than probabilistic conclusions about functionality given information about the damage state. More elaborate studies of changes in infrastructure network topology and asset reliability are certainly possible. For example, these studies might include modifications to the configuration of assets, the relocation of assets on the installation, and imperfect retrofits of physical assets to improve their reliability. The approach could be improved by developing a method to assess the uncertainty in function states given information about the damage states. In this first version, capability scores were defined as the probability that a service was not interrupted at least once a year because of damages to physical assets caused by coastal storms. The capability score relayed no information about the duration of service interruptions and gave equal weight to service interruptions that required hours, days, weeks, or months to restore. Service interruptions lasting weeks or months should be distinguished from service interruptions lasting hours or days in future potential applications. If it were possible to obtain information about the cost and duration of repairs needed to restore an asset given its damage state, capability nodes could be re-formulated to incorporate this information. Finally, there are potential improvements in the MPI used in this study. The MPI was calculated from a set of capability scores and reached a minimum when the probability of each capability being interrupted at least once during the course of a year was equal to one. However, as sea-level rises, the frequencies of service interruption are likely to increase above

once per year. The MPI could be re-formulated to account for higher frequencies of service interruption.

5.3.4 Additional Risk Analyses to Consider

Aside from issues related to the architecture of the NSN Risk Model, there are a number of practical issues that might be addressed to refine the model's risk assessment. An obvious potential for improvement would be to include nor'easters among the coastal storms that are considered in the risk model. Another potential improvement would be to refine the fragility curves used to predict the probability of asset damage states. With several notable exceptions, fragility curves used in this study were based on information from FEMA's HAZUS model. Although site-specific information was used in selecting fragility curves for this analysis, these curves might be further refined by considering even more specific information about the assets. The NSN Risk Model can be easily updated to incorporate refined fragility curves, although this will require a re-calculation of CPTs. Another potential improvement to the NSN Risk Model might be to increase the resolution of the assets. The NSN Risk Model presently includes information about 95 physical assets, including several that were either lumped into a single node for the purpose of analysis or disregarded because fragility analysis suggested that the risks of physical damage to that asset from a 100-year return interval storm were minimal. Rather than representing a single physical asset with one node, each asset might be represented by multiple nodes, each representing a component of that physical asset. This increase in resolution comes at a cost, and those costs as well as the need for additional resolution, should be evaluated before pursuing this potential improvement.

5.3.5 Expanding the Risk Model's Domain

The assessment of risks to mission impairment in the case study focused almost exclusively on the state of assets inside the installation's fence line. Should a coastal storm impact the area, with or without rising sea levels to multiply the threat, there is significant potential for the surrounding municipalities to be similarly affected by the storm's hazards. Moreover, the installation itself does not normally operate without electric power supplied from the grid and water piped in from the upstream reservoir. Finally, the vast majority of the installation's civilian workforce resides in the surrounding municipality and will be required to use the region's transportation network to commute in and off the post in the storm's aftermath. For these reasons, an obvious enhancement to the Bayesian model's construct would include an expansion of the system accountings to include these more regional influences.

5.4. Potential for Direct Implementation by DoD and Others

There is potential for our framework to be utilized by DoD in general, by city and district managers outside the DoD, by base managers and planners on NSN, and by local and regional decision makers across the Hampton Roads area. These entities could use the framework to assess critical vulnerabilities and characterize risks to system performance arising from sea level rise and coastal storm hazards. Master planners could use the approach to assess future response and mitigation strategies. Moreover, the framework could be used to assess adaptive management solutions informing future investment opportunities.

Although the risk assessment framework was not specifically designed to support asset management, there are several instances where the risk-based network could be used to: 1) assess minimum levels of operational service requirements, 2) identify increases in fragility as infrastructure ages, 3) monitor critical infrastructure performance and help determine maintenance priorities, 4) expose maintenance backlogs, and 5) inform decisions regarding periodic major rehabilitation/replacement/re-capitalization. The conditional analysis performed by the Bayesian network could be used to identify these concerns and assess proposed solutions, placing emphasis on prioritizing and managing assets under expected and extreme plausible scenario-based stressors to service production from a systems perspective. In effect, the capabilities developed under the project now afford installations the opportunity to re-evaluate relative performance of existing conditions, future no-action conditions, as well as structural and non-structural risk mitigating alternatives to sustain military installation assets and mission capabilities at multiple scales. This final product provides a robust, scientifically defensible approach that transparently communicates risks to the end-user and can help policymakers develop guidance to promote sustainability in the face of climate change and SLR.

6. Literature Cited

Almond, R. G. 1992. *An Extended Example for Testing Graphical Belief*, Technical Report 6, Statistical Sciences Inc., Seattle WA.

Alvarez-Rogel, J. A., J. J. Martinez-Sanchez, L. C. Blazquez, and C. M. M. Semitiel. 2006. A conceptual model of salt marsh plant distribution in coastal dunes of southeastern Spain. *Wetlands* 26:703-717.

Anderson, K. E., D. R. Cahoon, S. K. Gill, B. T. Gutierrez, E. R. Thieler, J. G. Titus, and S. J. Williams. 2009. Preface: Report Motivation and Guidance for Using this Synthesis/Assessment Report. In: *Coastal Sensitivity to sea level Rise: A Focus on the Mid-Atlantic Region.* A report by the U. S. Climate Change Science Program and the Subcommittee on Global Change Research. [J. G. Titus (coordinating lead author), K. E. Anderson, D. R. Cahoon, D. B. Gesch, S. K. Gill, B. T. Gutierrez, E. R. Thieler, and S. J. Williams (lead authors)]. U. S. Environmental Protection Agency, Washington DC, pp. xiii-viv.

Attoh-Okine, N. O., A. T. Cooper, and S. A. Mensah. 2009. Formulation of resilience index of urban infrastructure using belief functions. *IEEE Systems Journal* 3(2):147-153.

Barabási, A. 2004. Linked: How Everything Is Connected to Everything Else and What It Means, Penguin Group, New York, New York, 297 pp.

Barlow, P. M., and E. G. Reichard. 2010. Saltwater intrusion in coastal regions of North America. *Hydrogeology Journal* 18:247-260. doi:10. 1007/s10040-009-0514-3.

Barton, D. N., T. Saloranta, S. J. Moe, H. O. Eggestad, and S. Kuikka. 2008. Bayesian belief networks as a meta-modeling tool in integrated river basin management – Pros and cons in evaluating nutrient abatement decisions under uncertainty in a Norwegian river basin. *Ecological Economics* 66:91-104.

Bayes, T. 1763. An essay towards solving a problem in the doctrine of changes. *Philosophical Transactions of the Royal Society* 53: 370-418.

Bensi, M., A. der Kiureghian, and D. Straub. 2009. *Modeling infrastructure system performance using BN*. In Proc. of the 10th International Conference on Structural Safety and Reliability. Osaka, Japan, September 13-17, 2009.

Blanton, B., L. Stillwell, H. Roberts, J. Atkinson, S. Zou, M. Forte, J. Hanson and R. Luettich. 2011. Coastal Storm Surge Analysis: Computational System; Report 2: Intermediate Submission No. 1.2. Technical Report ERDC/CHL TR-11-1, Report 2, Engineer Research and Development Center (ERDC), Vicksburg, MS, 39p. Available online at: http://chl.erdc.usace.army.mil/chl.aspx?p=s&a=PUBLICATIONS;694 (Accessed 23 Feb 2012).

Bonnin, G. M., et al. 2006. Precipitation-Frequency Atlas of the United States. N. W. S. NOAA. Silver Spring, Maryland.

Booij, N, R.C., Ris, and L.H. Holthuijsen. 1999. A third-generation wave model for coastal regions, Part I, Model description and validation. *J. Geoph. Research* 104:7649-7666.

Boon, J. D. 2012. Evidence of sea level acceleration at U.S. and Canadian tide stations, Atlantic Coast, North America, *Journal of Coastal Research* 28(6):1437-1445.

Boon, J. D., J. M. Brubaker, and D. R. Forrest. 2010. *Chesapeake Bay Land Subsidence and Sea Level Change: An Evaluation of past and present trends and Future Outlook*. Special Report No. 425 in Applied Marine Science and Ocean Engineering, developed for the USACE Norfolk District by the Virginia Institute of Marine Science, 41 p.

Brekke, L. D., J. E. Kiang, J. R. Olsen, R. S. Pulwarty, D. A. Raff, D. P. Turnipseed, R. Webb, and K. D. White. 2009. *Climate change and water resources management—A federal perspective.* U.S. Geological Survey Circular 1331, 65 p. Available online at: http://pubs.usgs.gov/circ/1331/ (Accessed December 2010).

Bricker-Urso S., S. W. Nixon, J. K. Cochran, D. J. Hirschberg, and C. Hunt. 1989. Accretion rates and sediment accumulation in Rhode Island salt marshes. *Estuaries* 12(4):300-317.

Bunya, S., J. C. Dietrich, J. J. Westerink, B. A. Ebersole, J. M. Smith, J. H. Atkinson, R. Jensen, D. T. Resio, R. A. Luettich, C. Dawson, V. J. Cardone, A. T. Cox, M. D. Powell, H. J. Westerink, H. J. Roberts. 2010. A High-Resolution Coupled Riverine Flow, Tide, Wind, Wind Wave and Storm Surge Model for Southern Louisiana and Mississippi: Part I - Model Development and Validation. *Monthly Weather Review* 138(2):345-377.

Burkett, V.R. and M. A. Davidson. 2012. *Coastal Impacts, Adaptation and Vulnerability: A Technical Input to the 2012 National Climate Assessment*. Cooperative Report to the 2013 National Climate Assessment, pp. 150.

Buttolph, A. M., C. W. Reed, N. C. Kraus, N. Ono, M. Larson, B. Camenen, H. Hanson, T. Wamsley, and A. K. Zundel. 2006. *Two-dimensional depth-averaged circulation model CMS-M2D: Version 3.0, Report 2, sediment transport and morphology change*. Coastal and Hydraulics Laboratory Technical Report ERDC/CHL-TR-06-7. Vicksburg, MS: U.S. Army Engineer Research and Development Center.

Cahoon, D. R., P. F. Hensel, T. Spencer, D. J. Reed, K. L. McKee, and N. Saintilan. 2006. Coastal wetland vulnerability to relative sea level rise: wetland elevation trends and process controls in *Ecological Studies*, Vol. 190, J. T. A. Verhoeven, B. Beltman, R. Bobbink, and D. F. Whigham, Editors, Springer-Verlag, Berlin. pp. 271-292.

CH2MHILL. 2000. *Final Soil Background Investigation Report, Naval Station Norfolk, Norfolk, Virginia*, Prepared for the Department of the Navy, Atlantic Division, Naval Facilities Engineering Command, Norfolk, Virginia (Contract N62470-95-D-6007; CTO Task Order 01 17). Available online at:

https://niris.navfac.navy.mil/Document_Management%2FMID_ATLANTIC%2FNORFOLK_NB%2FBASEWIDE%2FADMIN%20RECORD%2F/N61463_001756.pdf (Accessed November 2012).

_____. 2011. *Draft Site Management Plan Fiscal Year 2012, Naval Station Norfolk, Norfolk, Virginia* Prepared for the Department of the Navy's Mid Atlantic Naval Facilities Engineering Command (NAVFAC) under Contract Task Order WE21, NAVFAC CLEAN 1000 Program, Contract N62470-08-D-1000.

Church, J. A., T. Aarup, P. L. Woodworth, W. S. Wilson, R. J. Nicholls, R. Rayner, K. Lambeck, G. T. Mitchum, K. Steffen, A. Cazenave, G. Blewitt, J. X. Mitrovica, and J. A. Lowe. 2010. Sea level rise variability - synthesis and outlook for the future (Chapter 13). In, *Understanding Sea Level Rise and Variability* by Church, J. A., P. L. Woodworth, T. Aarup, and W. S. Wilson (eds.), Wiley-Blackwell.

Clough J. S. and E. C. Larson. 2010. SLAMM 6 beta, Users manual. January 2010. Warren Pinnacle Consulting, Inc.

Clough J. S., Park R. A., and Fuller R.. 2010. SLAMM 6 beta Technical documentation. January 2010. Warren Pinnacle Consulting, Inc.

Committee on Mitigating Shore Erosion along Sheltered Coasts. 2007. Mitigating shore erosion along sheltered coasts. Ocean Studies Board, National Research Council, National Academies Press, Washington, D. C.

Cowell P. J., B. G. Thom, R. A. Jones, C. H. Everts, and D. Simanovic. 2006. Management of uncertainty in predicting climate-change impacts on beaches. *Journal of Coastal Research* 22(1):232-245.

Cowell P.J. and T. Q. Zeng. 2003. Integrating uncertainty theories with GIS for modeling coastal hazards of climate change. *Marine Geodesy*, 26 (1):5-18.

Cox, A. T., J. A. Greenwood. V. J. Cardone, and V. R. Swail. 1995. An interactive objective kinematic analysis system. Proceedings 4th International Workshop on Wave Hindcasting and Forecasting. October 16-20. 1995. Banff, Alberta. p. 109-118.

Craft C., J. Clough, J. Ehman, S. Joye, R. Park, S. Pennings, H. Guo, and M. Machmuller. 2009a. Forecasting the effects of accelerated SLR on tidal marsh ecosystem services. *Frontiers in Ecology and the Environment* 7(2):73-78.

Craft C., S. Pennings, J. Clough, R. Park, and J. Ehman. 2009b. sea level rise and ecosystem services: A response to Kirwan and Guntenspergen. *Frontiers in Ecology and the Environment* 7(3):127-128.

Cunningham P., J. Morris, M. Fonseca, C. Currin, and C. Tobias. 2008. Defense coastal estuarine research program: Coastal Wetlands Module. SI-1413. Strategic Environmental Research and Development Program (SERDP).

Davis, S. M., E. E. Gaiser, W. F. Loftus, and A. E. Huffman. 2005. Southern marl prairies conceptual ecological model. *Wetlands* 25:821-831.

Dean R., Dalrymple, R., 1991, Water Wave Mechanics for Engineers and Scientists Vol. 2, World Scientific Publishing Co. Inc.

Department of Defense (DoD). 2010a. Quadrennial defense review report: February 2010. Department of Defense. Available online at: http://www.defense.gov/QDR/images/QDR_as_of_12Feb10_1000.pdf (Accessed January 2011).

_____. 2010b. DoD Policy and Responsibilities for Critical Infrastructure (DoD Directive 3020. 40). Available online at: www. fas. org/irp/doddir/dod/d3020_40. pdf (Accessed December 2010).

_____. 2008. Department of Defense Manual (DODM 3020. 45), Defense critical infrastructure program (DCIP): DCIP Remediation Planning. Volume 2. October, 2008.

Donoghue, J. D., at.al. 2010. Modeling the risk to military infrastructure from future coastal sea level change (SERDP RC-1700). SERDP-ESTCP Technical Symposium and Workshop, Dec. 1, 2010. Available online at: http://symposium2010.serdp-estcp.org/Technical-Sessions/2A (Accessed 26 January 2012).

Downer, C. W. and F. L. Ogden, 2004. GSSHA: A model for simulating diverse streamflow generating processes. *Journal of Hydrologic Engineering* 9(3):161-174.

Downer, C. W., F. L. Ogden, J. M. Niedzialek, and S. Liu, 2006. Gridded Surface/Subsurface Hydrologic Analysis (GSSHA) Model: A model for simulating diverse streamflow producing processes, p. 131-159, in *Watershed Models*, V. P. Singh, and D. Frevert, eds., Taylor and Francis Group, CRC Press, 637 pp.

Dudenjoeffer, D. D., Permann, M. R., and Mianic, M. 2006. CIMS: A Framework for Infrastructure Interdependency Modeling, Proc. 2006 Winter Simulation Conference. IEEE, pp 478-485. Available online at: http://www.inl.gov/technicalpublications/Documents/3578215.pdf (Accessed December 2010).

Ehman J. 2008. Data report on SLAMM model results for ten National Wildlife Refuges in South Carolina and Georgia: Wolf Island NWR, Georgia. Report prepared for U. S. Fish and Wildlife Service. (Available online at: http://www.fws.gov/southeast/climate/action/Wolf%20Island%20SLAMM%20Report.pdf (Accessed 22 Feb. 2012).

Engelhart, S. E., B. P. Horton, b. c. Douglas, W. R. Peltier, and T. E. Törnqvist. 2010. Spatial variability of late Holocene and 20th century sea level rise along the Atlantic coast of the United States. *Geology* 37(12):1115-1118.

Erwin R. M., D. R. Cahoon, D. J. Prosser, G. M. Sanders, and P. Hensel. 2006. Surface elevation dynamics in vegetated *Spartina* marshes versus unvegetated tidal ponds along the Mid-Atlantic Coast, USA, with implication to waterbirds. *Estuaries and Coasts* 29(1):96-106.

Ezer, T., L. P. Atkinson, W. B. Corlett and J. L. Blanco. 2013. Gulf Stream's induced sea level rise and variability along the U.S. mid-Atlantic coast. *Journal of Geophysical Research* 118(2):685-697, available online at: http://onlinelibrary.wiley.com/doi/10.1002/jgrc.20091/full (Accessed 6 June 2014).

Ezer, T. and W. B. Corlett. 2012a. Analysis of relative sea level variations and trends in the Chesapeake Bay: Is there evidence for acceleration in sea level rise? MTS/IEE Oceans '12 Conference, IEE Xplore Papers #2478367, available online at: http://www.ccpo.odu.edu/~tezer/PAPERS/2012_MTS-IEEE_SLR.pdf (Accessed 19 Dec. 2012).

Ezer, T. and W. B. Corlett. 2012b. Is sea level rise accelerating in the Chesapeake Bay? A demonstration of a novel new approach for analyzing sea level data. *Geophysical Research Letters* 39, L19605, doi:10.1029/2012GL053435, available online at: http://www.agu.org/pubs/crossref/2012/2012GL053435.shtml (Accessed 19 Dec. 2012).

Fenton, N., and M. Neil. 2001. Making decisions: Using Bayesian nets and MCDA. *Knowledge-based systems* 14:307-325.

Fischenich, J. C. 2008. The application of conceptual models to ecosystem restoration. EMRRP Technical Notes Collection. ERDC TN-EMRRP-EBA-01. Vicksburg, MS: U. S. Army Engineer Research and Development Center (ERDC).

Galbraith H., R. Jones, R. Park, J. Clough, S. Herrod-Julius, B. Harrington, and G. Page. 2002. Global climate change and sea level rise: Potential losses of intertidal habitat for shorebirds. *Waterbirds* 25(2):173-183.

Galbraith H., R. Jones, R. Park, J. Clough, S. Herrod-Julius, B. Harrington, and G. Page. 2005. Global climate change and sea level rise: Potential losses of intertidal habitat for shorebirds. USDA Forest Service General Technical Report. PSW-GTR-191.

Gemitzi, A., V. A. Tsihrintzis, O. Christou, and C. Petalas. 2007. Use of GIS in siting stabilization pond facilities for domestic wastewater treatment. *Journal of Environmental Management* 82:155-166.

Gesch, D. B., B. T. Gutierrez, and S. K. Gill. 2009. Coastal elevations. In: *Coastal Sensitivity to sea level Rise: A Focus on the Mid-Atlantic Region.* A report by the U. S. Climate Change Science Program and the Subcommittee on Global Change Research. [J. G. Titus (coordinating lead author), K. E. Anderson, D. R. Cahoon, D. B. Gesch, S. K. Gill, B. T. Gutierrez, E. R. Thieler, and S. J. Williams (lead authors)]. U. S. Environmental Protection Agency, Washington DC, pp. 25-42.

Gill, S. K., R. Wright, J. G. Titus, R. Kafalenos, and K. Wright. 2009. Population, land use, and infrastructure. In: *Coastal Sensitivity to sea level Rise: A Focus on the Mid-Atlantic Region*. A report by the U. S. Climate Change Science Program and the Subcommittee on Global Change Research. [J. G. Titus (coordinating lead author), K. E. Anderson, D. R. Cahoon, D. B. Gesch, S. K. Gill, B. T. Gutierrez, E. R. Thieler, and S. J. Williams (lead authors)]. U. S. Environmental Protection Agency, Washington DC, pp. 105-116.

Glick, P., J. Clough, and B. Nunley. 2007. SLR and coastal habitat in the Pacific northwest: an analysis for Puget Sound, southwestern Washington, and northwestern Oregon. National Wildlife Federation. 94 p. Available online at: http://www.nwf.org/~/media/PDFs/Water/200707_PacificNWSeaLevelRise_Report.ashx (Accessed 22 Feb. 2012).

Glick, P., Clough, J., and B. Nunley. 2008. SLR and Coastal Habitats in the Chesapeake Bay Region, Technical Report, May 2008. National Wildlife Federation, Reston, VA, 121 p. Available online at: http://www. nwf. org/Global-Warming/Effects-on-Wildlife-and-Habitat/Estuaries-and-Coastal-Wetlands/Chesapeake-Bay. aspx (Accessed January 2011).

Grinsted, A., J. C. Moore, and S. Jevrejeva. 2010. Reconstructing sea level from paleo and projected temperatures 200 to 2100 AD. *Climate Dynamics*, 34:461-472.

Groves, C., Valutis, L. Vosick, D., Neely, B., Wheaton, K., Touval, J., and Runnels, B. 2000. *Designing a Geography of Hope: A Practitioner's Handbook to Ecoregional* Conservation Planning, Volumes 1 and 2, 2nd Edition. Available online at: http://conserveonline. org/docs/2000/11/GOH2-v1. pdf and http://conserveonline. org/docs/2000/11/GOH2-v2. pdf (Accessed January 2011).

Groves, C. R. 2003. Drafting a conservation blueprint: a practitioner's guide to planning for biodiversity. Island Press, Washington, D. C.

Groves, C. R., D. B. Jensen, L. L. Valutis, K. H. Redford, M. L. Shaffer, J. M. Scott, J. F. Baumgartner, J. V. Higgins, M. W. Beck, and M. G. Anderson. 2002. Planning for biodiversity conservation: putting conservation science into practice. *BioScience* 52:499-512.

Gutierrez, B. T., S. J. Williams, and E. R. Theiler. 2009a. Ocean coasts. Chapter 3 in Coastal Sensitivity to Sea Level Rise: A focus on the Mid-Atlantic Region (Eds. Titus et al.). Synthesis and Assessment Product 4. 1. U. S. Climate Change Science Program.

Hamby D. M. 1995. A comparison of sensitivity analysis techniques. *Health Physics* 68(2):195-204.

Harwell, M. A., V. Myers, T. Younb, A. Bartuska, N. Gassman, J. H. Gentile, C. C. Harwell, S. Appelbaum, J. Barko, B. Causey, C. Johnson, A. McLean, R. Smola, P. Templet, and S. Tosini. 1999. A framework for an ecosystem integrity report card. *BioScience* 49:543-556.

Harwell, M. A., V. Myers, T. Younb, A. Bartuska, N. Gassman, J. H. Gentile, C. C. Harwell, S. Appelbaum, J. Barko, B. Causey, C. Johnson, A. McLean, R. Smola, P. Templet, and S. Tosini. 1999. A framework for an ecosystem integrity report card. *BioScience* 49:543-556.

Henderson, J. E., and L. J. O'Neil. 2004. Conceptual models to support environmental planning and operations. SMART Technical Notes Collection. ERDC/TN SMART-04-9. Vicksburg, MS: U. S. Army Engineer Research and Development Center (ERDC).

Henderson, J. E., and L. J. O'Neil. 2007. Template for conceptual model construction: model components and application of the template. SWWRP Technical Notes Collection, ERDC TN-SWWRP-07-7. Vicksburg, MS: U. S. Army Engineer Research and Development Center (ERDC). Available online at: https://swwrp. usace. army. mil/ (Accessed December 2010).

Higgs, G. 2007. Integrating multi-criteria techniques with geographical information systems in waste facility location to enhance public participation. *Waste Management Research* 24:105-117.

Hilton, T. W., R. G. Najjar, L. Zhong and M. Li. 2008. Is there a signal of sea level rise in Chesapeake Bay salinity? *J. Geophys. Res.*, 113, C09002, doi:10. 1029/2007JC004247.

Horton, R., C. Herweijer, C. Rosenzweig, J. Liu, V. Gornitz, and A. C. Ruane. 2008. Sea level rise projections for current generation CGCMs based on the semi-empirical method. *Geophysical Research Letters* 35:1-5.

Intergovernmental Panel on Climate Change (IPCC). 2007. Fourth assessment report. Available online at: http://www.ipcc.ch/ (Accessed 26 January 2012).

Intergovernmental Panel on Climate Change (IPCC). 2014. Fifth assessment report. Available online at: http://www.ipcc.ch/ (Accessed 10 March 2014).

Jarvis J. C. 2010. Vertical accretion rates in coastal Louisiana: A review of the scientific literature. *ERDC/EL TN-10-5*. U. S. Army Engineer Research and Development Center (ERDC). Vicksburg, Mississippi.

Jevrejeva, S., A. Grinsted, J. C. Moore, and S. Holgate. 2006. Nonlinear trends and multiyear cycles in sea level records. *Journal of Geophysical Research* 111:1-11.

Jevrejeva, S., J. C. Moore, and A. Grinsted. 2010. How will sea level respond to changes in natural and anthropogenic forcings by 2100? *Geophysical Research Letters* 37:1-5.

Johannes, R. E.. 1980. The ecological significance of the submarine discharge of groundwater. *Marine Ecology Progress Series 3*, 365-373.

Karl, T. R., J. M. Melillo, and T. C Peterson (eds.). 2009. *Global Climate Change Impacts in the United States*. Cambridge University Press, Cambridge, MA, p.188.

Keeney, R. L, and H. Raiffa. 1993. *Decisions with Multiple Objectives: Preferences and Value Tradeoffs*, Cambridge University Press, Cambridge, MA, p. 569.

Kentula, M. E. 1997. A comparison of approaches to prioritizing sites for riparian restoration. *Restoration Ecology* 5(4S):69-74.

Kerr, P.C., Donahue, A. S., Weterink, J. J., Leuttich, Jr., R. A., Zheng, L. Y., Weisberg, R. H., Huang, Y., Wang, H. V., Teng, Y., Forrest, D. R., Roland, A.,. Haase, A. T., Kramer, A. W., Taylor, A. A., Rhome, J. R., Semeraro, L. N., Westerink, H. J., Kennedy, A. B., Smith, J. M., Powell, M. D., Cardone, V. J.., and Cox, A. T. 2013. U.S. IOOS coastal and ocean modeling testbed: Inter-model evaluation of tides, waves, and hurricane surge in the Gulf of Mexico. *Journal of Geophysical Research: Oceans,* Vol. 118, 5129-5172, doi: 10.1002/jgrc.20376.

Kirwan M.L. and Murray A.B. 2008. Ecological and morphological response of brackish tidal marshland to the next century of sea level rise: Westham Island, British Columbia. *Global and Planetary Change*. Elsevier, Vol. 60, pp. 471-486.

Kleinosky, L.R., Yarnal, B., and Fisher, A. 2006. Vulnerability of Hampton Roads, Virginia to storm-surge flooding and sea level rise. Natural Hazards, 40(1). Available online at: http://www.cara.psu.edu/about/publications/2006-Kleinosky%20et%20al.pdf (Accessed 21 February 2012).

Knutson, P. L., Ford, J. C., and Inskeep, M. R. 1981. National survey of planted salt marshes (vegetative stabilization and wave stress). *Wetlands* 1(1):129-157.

Koch, J.V. 2010. Costs of defending against rising sea levels and flooding in Mid-Atlantic Metropolitan Coastal Areas: The Basic Issues. *Journal of Regional Analysis and Policy*, 40(1):53-60. Available online at: http://www.jamesvkoch.com/uploads/Cost_of_Defending_Against_Rising_Sea_Levels_and_Flooding.pdf (Accessed 21 February, 2012).

Koller, D. and N. Friedman. 2009. *Probabilistic Graphical Models: Principles and Techniques*, MIT Press, Boston p. 1231.

Koller, D., N. Friedman, L. Getoor, and B. Taskar. 2007. Graphical models in a nutshell (Chapter 2) in Getoor, L. and B. Taskar (Eds), *Introduction to Statistical Relational Learning*, MIT Press, Cambridge, Massachusetts.

Kraft J. S., H. I. Yi, and M. D. Khalequzzaman. 1992. Geologic and human factors in the decline of the tidal salt marsh lithosome: The Delaware Estuary and Atlantic Coastal Zone. *Sedimentary Geology* 80:233-246.

Kuikka, S., M. Hilden, H. Gislason, S. Hansson, H. Sparholt, and O. Varis. 1999. Modeling environmentally driven uncertainties in Baltic cod (*Gadus morhua*) management by Bayesian influence diagrams. *Canadian Journal of Fisheries and Aquatic Science,* 56:629-641.

Lambeck, K., and J. Chappell. 2001. Sea Level Change through the Last Glacial Cycle. *Science* 292:679-686.

Langseth, H. 2008. Bayesian networks in reliability: The good, the bad, and the ugly, Pages 1-8 in Bedford, T., Quigley, J., Walls, L., Alkali, B., Daneshkhah, A., and Hardman, G., (Eds.) *Advances in Mathematical Modeling for Reliability: Proceedings of the 5th International Conference on Mathematical Methods in Reliability*, July 1-5, 2007, Glasgow, Scotland.

Langseth, H., and L. Portinale. 2005. Bayesian networks in reliability. *Reliability Engineering and System Safety* 92:92-108.

Lee J. K., Park R. A., and Mausel P. W. 1992. Application of geoprocessing and simulation modeling to estimate impacts of sea level rise on the northwest coast of Florida. *Photogrammetric Engineering and Remote Sensing* 58:1579-1586.

Lewis, Ted G. 2008 Critical Infrastructure Protection in Homeland Security: Defending a Networked Nation. Wiley, New Jersey, ISBN: 978-0-471-78628-32006.

Lin, L., Demirbilek, Z., Mase, H., Zheng, J., and Yamada, F., 2008. CMS-Wave: a nearshore spectral wave processes model for coastal inlets and navigation projects. Coastal and Hydraulics Laboratory Technical Report ERDC/CHL TR-08-13. Vicksburg, MS: U.S. Army Engineer Research and Development Center (ERDC).

Lin, N., Emanuel, K. A., Smith, J. A., and Vanmarcke, E. 2010. Risk assessment of hurricane storm surge for New York City. *Journal of Geophysical Research* vol. 115, D18121, doi 10.1029/2009JD013630.

Luettich, R.A., Westerink, J.J. 2004. Formulation and Numerical Implementation of the 2D/3D ADCIRC Finite Element Model Version 44. Adcirc.org. Available online at: http://adcirc. org/adcirc_theory_2004_12_08. pdf (Accessed 23 Feb. 2012).

Lynn, N., N. Singpurwalla, and A. Smith. 1998. Bayesian assessment of network reliability. *SIAM Review*, 40(2):202-227.

Marcot, B. 2006. Characterizing species at risk 1: Modeling rare species under the Northwest Forest Plan, Ecology and Society 11(2):10. Available online at: http://www.ecologyandsociety.org/vol11/iss2/art10/ (Accessed January 2011).

Mase, H. 2001. Multidirectional random wave transformation model based on energy balance equation. *Coastal Engineering Journal* 43(4):317–337.

Masterson, J. P. and S. P. Garabedian. 2007. Effects of sea level rise on ground water flow in a coastal aquifer system, *Ground Water*, 45(2):209-217.

McGranahan, G., D. Balk, and B. Anderson. 2007. The rising tide: assessing the risks of climate change and human settlements in low elevation coastal zones. *Environment & Urbanization* 19(1):17-37.

McLean, R. F., A. Tsyban, A. Burkett, J. O. Codignotto, D. L. Forbes, N. Mimura, R. J. Beamish, and V. Ittekkot. 2001. Coastal zones and marine ecosystems. *In:* Mccarthy, J. J., O. F. Canziani, N. A. Leary, D. J. Dokken, and K. S. White, (eds.), *Climate Change 2001: Impacts, Adaptation and Vulnerability.* Cambridge: Cambridge University Press: 343–380.

Melby, J. A., E. F. Thompson, M. A. Cialone, J. M. Smith, L. E. Borgman, Z. Demirbilek, J. L. Hanson, and L. Lin. 2005. Life-cycle analysis of mid-bay and Poplar Island projects, Chesapeake Bay, Maryland. Coastal and Hydraulics Laboratory Technical Report ERDC/CHL-TR-05-12. Vicksburg, Mississippi: U.S. Army Engineer Research and Development Center (ERDC).

Mickler R. 2008. Sea level rise risk assessment for the DoD coastal installations. Project 08-410. Legacy Program. Department of Defense. (Available online at: http://www.dodworkshops.org/files/ClimateChange/Fact_Sheet_Sea_Level_Rise_Risk_Assessment_for_DoD_Coastal_Installations.pdf (Accessed 22 Feb. 2012)

Mickler R. and D. Welch. 2009. Sea level rise risk assessment for the Dare County peninsula. Proceedings of the 2009 Atlantic White-Cedar Symposium. June 2009. Greenville, North Carolina.

Modarres, M., M. Kaminskiy, and V. Krivtsov. 2010. *Reliability Engineering and Risk Analysis: A Practical Guide*, CRC Press, Boca Raton pp. 454.

Moore, J. C., S. Jevrejeva, and A. Grinsted. 2010. Efficacy of geoengineering to limit 21st century sea level rise. *Proceedings of the National Academy of Sciences* 107(36):15699-15703.

Morris J. T., P. V. Sundareshwar, C. T. Nietch, B. Kjerfve, and D. R. Cahoon. 2002. Responses of coastal wetlands to rising sea level. *Ecology* 83(10):2869-2877.

National Oceanic and Atmospheric Administration (NOAA). 2010. November 11-13th 2009 nor'easter. National Weather Service. Available online at: http://www.erh.noaa.gov/er/akq/wx_events/other/November%2011-13th%20Noreaster.pdf (Accessed January 2011).

National Intelligence Council (NIC). 2008. National Security Implications of Global Climate Change Through 2030. 58 pp.

National Research Council (NRC). 1987. *Responding to Changes in Sea Level: Engineering Implications.* Committee on Engineering Implications of Changes in Relative Mean Sea Level, Marine Board, National Research Council: National Academy Press: Washington, D. C., 160 p.

_____. 2007. *Mitigating Shore Erosion Along Sheltered Coasts.* National Academies Press, Washington, D.C. 174 pp.

_____. 2008. *Urban Stormwater Management in the United States.* National Academies Press, Washington, DC.

_____. 2010. *Adapting to the Impacts of Climate Change, America's Climate Choices: Panel on Adapting to the Impacts of Climate Change*. National Academies Press, Washington, DC.

National Oceanic and Atmospheric Administration (NOAA). 2012. Mean Sea Level Trend 8638610 Sewells Point, Virginia. Available online from NOAA Tides and Currents: http://tidesandcurrents.noaa.gov/sltrends/sltrends_station.shtml?stnid=8638610 (Accessed 5 November 2012).

Natural Resources Conservation Service (NRCS), United States Department of Agriculture. 2010. Soil Survey Geographic (SSURGO) Database for Tidewater Cities Area, Virginia. Available online at http://soildatamart.nrcs.usda.gov , (Accessed 5/11/2011).

Naval Facilities Engineering Command (NAVFAC). 1998. "*ITG – Facilities Homeporting Criteria for Nimitz Class CVNs*," Memo from Commander, NAVFAC Criteria Office, November 3.

_____. No Date. "Tide Level Steam Isolation Table: PWBL.OOX Rev A"

Nelson, E. J. (2001). Watershed Modeling system (WMS). Ver. 6.1 HTML Help Document. Environmental Modeling Research Laboratory, Brigham Young University, Provo, UT.

Nicholson, A. E., C. R. Twardy, K. B. Korb, and L. R. Hope. 2008. Decision support for clinical cardiovascular risk assessment, pages 33-52 in Pourret, O., Naim, P., and Marcot, B. [Eds.] *Bayesian Networks: A Practical Guide to Applications*, John Wiley and Sons, Ltd., Chichester, pp. 428.

Noss, R. F., and A. Cooperrider. 1994. *Saving Nature's Legacy: Protecting and Restoring Biodiversity.* Defenders of Wildlife and Island Press, Washington, D. C.

Nuttle, W. K., and J. W. Portnoy. 1992. Effect of rising sea level on runoff and groundwater discharge to coastal ecosystems, *Estuarine, Coastal and Shelf Science,* 34:203-212.

Office of the Secretary of Defense (OSD). 2011. Report of the Defense Science Board Task Force on Trends and Implications of Climate Change on National and International Security. Available online at: http://www.acq.osd.mil/dsb/reports/ADA552760.pdf (Accessed 7 November 2012).

Ogden, J. C., S. M. Davis, T. K. Barnes, K. J. Jacobs, and J. H. Gentile. 2005. Total system conceptual ecological model. *Wetlands* 25:955-979.

Ogden, F. L. and B. Saghafian. 1997. Green and ampt infiltration with redistribution. *Journal of Irrigation and Drainage Engineering* 123(5): 386-393.

Onisko, A. 2008. Medical diagnosis, pp. 17-32 in Pourret, O., Naim, P., and Marcot, B. [Eds.] *Bayesian Networks: A Practical Guide to Applications*, John Wiley and Sons, Ltd., Chichester, pp. 428.

PAM 525-66. 2005. Army Force Operating Capabilities, TRADOC, Fort Monroe, VA. Available online at: http://www.tradoc.army.mil/tpubs/pams/p525-66.pdf (Accessed January 2011).

Park R.A. 1991. Global climate change and greenhouse emissions. pp. 171-182. Subcommittee on Health and Environment, U.S. House of Representatives, Washington.

Park R. A., Armentano, T. V. and Cloonan C. L. 1986. Predicting the effects of sea level rise on coastal wetlands. In Effects of Changes in Stratospheric Ozone and Global Climate. Vol. 4: Sea Level Rise (Ed. J. G. Titus). U. S. Environmental Protection Agency, Washington, D. C.

Park R. A., M. S. Trehan, P. W. Mausel, and R. C. Howe. 1989a. The effects of sea level rise on U. S. coastal wetlands. In *The Potential Effects of Global Climate Change on the United States* (Eds. Smith J. B. and Tirpak D. A.), Appendix B - Sea Level Rise. U. S. Environmental Protection Agency, Washington, D. C.

Park R. A., M. S. Trehan, P. W. Mausel, and R. C. Howe. 1989b. The effects of sea level rise on U. S. coastal wetlands and lowlands. Holcomb Research Institute. Butler University. Indianapolis, Indiana.

Park R. A., J. K. Lee, and D. Canning. 1993. Potential effects of sea level rise on Puget Sound wetlands. *Geocarto International* 8:99-110.

Park R. A., J. S. Clough, R. Jones, and H. Galbraith. 2003. Modeling the impacts of sea level rise. Proceedings of the 13th Biennial Coastal Zone Conference. Baltimore, MD, July 13-17, 2003. Available online at: http://www.csc.noaa.gov/cz2003/proceedings/pdf_files/park.pdf (Accessed 22 Feb. 2012).

Parris, A., P. Bromirski, V. Burkett, D. Cayan, M. Culver, J. Hall, R. Horton, K. Knuuti, R. Moss, J. Obeysekera, A. Sallenger, and J. Weiss. 2012. *Global Sea Level Rise Scenarios for the U.S. National Climate Assessment*. NOAA Tech Memo OAR CPO-1. 37 pp.

Pasternack G. B., W. B. Hilgartner, and G. S. Brush. 2000. Biogeomorphology of an upper Chesapeake Bay river-mouth tidal freshwater marsh. *Wetlands* 20(3):520-537.

Pearl, J. 1988. Probabilistic Reasoning in Intelligent Systems: Networks of Plausible Inference, Morgan Kauffman Publishers, Inc., San Francisco p. 552.

Pfeffer, W. T., J. T. Harper, and S. O'Neel. 2008. Kinematic constraints on glacier contributions to 21st-century sea level rise. *Science* 321:1340-1343.

Pilkey O. H. and J. A. G. Cooper. 2004. Society and sea level rise. *Science* 303:1781-1782.

Poag, C.W. 1998. The Chesapeake Bay Bolide Impact: A New View of Coastal Plain Evolution, U.S. Geological Survey Fact Sheet 049-98. Available online at: http://marine.usgs.gov/fact-sheets/fs49-98/ (Accessed 9 November 2011).

Poiani, K. A., B. D. Richter, M. G. Anderson, and H. E. Richter. 2000. Biodiversity conservation at multiple scales: functional sites, landscapes, and networks. *BioScience* 50:133-146.

Pollino, C. A., A. K. White, B. T. Hart. 2007a. Examination of conflicts and improved strategies for the management of an endangered Eucalypt species using Bayesian networks. *Ecological Modelling* 201:37-59.

Pollino, C. A., O. Woodberry, A. Nicholson, K. Korb, K., and B. T. Hart. 2007b. Parameterization and evaluation of a Bayesian network for use in an ecological risk assessment. *Environmental Modelling and Software* 22:1140-1152.

Pourret O. 2008. Introduction to Bayesian networks, pages 1-13 in Pourret, O., Naim, P., and Marcot, B. [Eds.] *Bayesian Networks: A Practical Guide to Applications*, John Wiley and Sons, Ltd., Chichester, pp. 428.

Powers, D.S., and T. S. Bruce. 1999. The Effects of the Chesapeake Bay Impact Crater on the Geological Framework and Correlation of Hydrogeologic Units of the Lower York-James Peninsula, Virginia. U.S. Geological Survey Professional Paper 1612, U.S. Geological Survey, Department of the Interior. U.S. Government Printing Office, Washington, 82p. Available online at http://pubs.usgs.gov/pp/p1612/. (Accessed 21 February 2011).

Rahmstorf, S. 2007. A semi-empirical approach to projecting future sea level rise. *Science* 315:368-370.

Rawls, W. J. 1983. Estimating soil bulk density from particle size analyses and organic matter content. *Soil Science* 135: 123-125.

Rawls, W. J. and D. L. Brakensiek. 1985. Prediction of soil water properties for hydrologic modeling. *Watershed Management in the Eighties*, Denver, CO, Irrigation and Drainage Div., ASCE.

Rawls, W. J., et al. 1983. Green-ampt infiltration parameters from soils data. *Journal of Hydraulic Engineering* 109(1): 62-70.

Rawls, W. J., et al. 1982. Estimating soil water properties. *Transactions of the ASAE* 25(5): 1316-1328.

Reed D. J., D. A. Bishara, D. R. Cahoon, J. Donnelly, M. Kearney, A. S. Kolker, L. L. Leonard, R. A. Orson, and J. C. Stevenson. 2008. Site-specific scenarios for wetlands accretion as sea level rises in the Mid-Atlantic Region. Section 2. 1 in: Background Documents Supporting Climate Change Science Program Synthesis and Assessment Product 4. 1, Titus and Strange (Eds.). EPA 430R07004. U. S. Environmental Protection Agency. Washington, DC.

Reed, D. A., K. C. Kapur, and R. D. Christie. 2009. Methodology of assessing the resilience of networked infrastructure. *IEEE Systems Journal*, 3(2):174-180.

Redford, K. H., Coppolillo, P., Sanderson, E. W., Da Fonseca, G. A. B., Dinerstein, E., Groves, C., Mace, G., Maginnis, S., Mittermeier, R. A., Noss, R., Olson, D., Robinson, J. G., Vedder, A., and Wright, M. 2003. Mapping the conservation landscape. *Conservation Biology* 17(1):116-131.

Rinaldi, S., J. Peerenboom, and T. Kelly. 2001. Identifying, Understanding, and Analyzing Critical Infrastructure Interdependencies. *IEEE Control Systems Magazine* 6:11-25.

Ris, R. C., N. Booij and L. H. Holthuijsen. 1999. A third-generation wave model for coastal regions, Part II, Verification, *J. Geophys. Res*. C4, 104:7667-7681.

Rodin, A. S., and E. Boerwinkle. 2005. Mining genetic epidemiology data with Bayesian networks 1: Bayesian networks and example application (plasma apoE levels), *Bioinformatics* 21(15):3273-3278.

Russell, G. D., Hawkins, C. P., O'Neill, M. P. 1997. The role of GIS in selecting sites for riparian restoration based on hydrology and land use. *Restoration Ecology* 5(4S):56-68.

Russo, E. J., and Hall, J. 2012. Implications for coastal military installations and readiness, pages 95-100 In: Burkett, V.R. and M. A. Davidson, (Eds.) *Coastal Impacts, Adaptation and Vulnerability: A Technical Input to the 2012 National Climate Assessment*. Cooperative Report to the 2013 National Climate Assessment, pp. 150.

Russo, E. J., Jr., B. McBride, E. Bennett, H. Bjornsson, M. Brklacich, G. Bromberg, g. Butte, K. Geiss, K. Lewis, M. Merad , R. Nyer, and A. Tkachuk. 2011. National security perspectives on addressing instabilities arising from climate change impacts on the environment, pages 259-270 In: Linkov, I., and T. S. Bridges (eds). Climate Change: Global Change and Local Adaptation, NATO Science for Peace and Security Series C: Environmental Security, doi 10.1007/978-94-007-1770-1_1, Springer Sciences+Busincess Media B. V.

Sahagian, D. L., and Holland, S. M. 1991. Eustatic sea level curve based on a stable frame of reference: preliminary results. *Geology 19:*1208-1212.

Sallenger, A. H., Jr., K. S. Doran, and P. A. Howard. 2012. Hotspot of accelerated SLR on the Atlantic coast of North America. *Nature Climate Change*, doi:10.1038/NCILMATE1597 (24 June, 2012).

Scheraga, J. D. 2008. Opportunities to Anticipate and Adapt to the Effects of Climate Change on Water Quality in *Coping with Climate Change: National Summit Proceedings*, Rosina M. Bierbaum, Daniel G. Brown, and Jan L. McAlpine, editors, University of Michigan School of Natural Resources and Environment, pp. 62-74.

Schultz, M. T., B. P. Gouldby, J. D. Simm, and J. L. Wibowo. 2010. Beyond the factor of safety: developing fragility curves to characterize system reliability. ERDC SR-10-1. Engineer Research and Development Center (ERDC), Vicksburg, MS, 39p. Available online at: http://www.google.com/url?sa=t&rct=j&q=&esrc=s&frm=1&source=web&cd=1&cad=rja&uact=8&ved=0CCIQFjAA&url=http%3A%2F%2Fwww.dtic.mil%2Fget-tr-doc%2Fpdf%3FAD%3DADA525580&ei=OwaOU-e_JYifyATSrYLgCA&usg=AFQjCNGIkzvGa16te2E1ZgiL6xQzrN1q3g&bvm=bv.68191837,d.aWw (Accessed 3 Jun 2014).

Strategic Environmental Research and Development Program (SERDP). 2011. The Department of Defense and Climate Change: Initiating a Dialogue, Workshop Proceedings, Aurora, CO. Available online at: http://www.serdp.org/content/download/14842/171263/file/DoD%20Climate%20Change%20Workshop% (Accessed 7 November 2012).

_____ 2013. Assessing Impacts of Climate Change on Coastal Military Installations: Policy Implications. US Department of Defense.

Smith, J. M., Sherlock, A. R., and Resio, D. T. 2001. "STWAVE: Steady-State Spectral Wave Model, User's Guide for STWAVE Version 3.0," ERDC/CHL SR-01-01, U.S. Army Engineer Research and Development Center, Vicksburg, MS, 80 pp.

Smith, J. M., M. A. Cialone, T. V. Wamsley, and T. O. McAlpin. 2010. Potential impact of sea level rise on coastal surges in southeast Louisiana. *Ocean Engineering* 37:37-47, doi: 10. 1016/joceaneg. 2009. 07. 008.

Stolper D., J. H. List, and E. R. Thieler. 2005. Simulating the evolution of coastal morphology and stratigraphy with a new morphological-behavior model (GEOMBEST). *Marine Geology* 218(1-4):17-36.

Taylor, L. A., B. W. Eakins, K. S. Carignan, R. R. Warnken, T. Sazonova, D. C. Schoolcraft, and G. F. Sharman. 2008. *Digital Elevation Model of Virginia Beach, Virginia: procedures, data sources and analysis.* NOAA Technical Memorandum NESDIS NGDC-7. National Geophysical Data Geophysics Division, Boulder, Colorado.

Thompson, E. F., and V. J. Cardone. 1996. Practical modeling of hurricane surface wind fields. *Journal of Waterway, Port, Coastal, and Ocean Engineering* 122(4):195-205.

Titus, J.G., Craghan, M. Gill, S.K. and Williams, S.J. 2009. Shore protection and retreat. In: *Coastal Sensitivity to sea level Rise: A Focus on the Mid-Atlantic Region.* A report by the U.S. Climate Change Science Program and the Subcommittee on Global Change Research. [J.G. Titus (coordinating lead author), K.E. Anderson, D.R. Cahoon, D.B.

Gesch, S.K. Gill, B.T. Gutierrez, E.R. Thieler, and S.J. Williams (lead authors)]. U.S. Environmental Protection Agency, Washington DC, pp. 87-104.

Titus J.G. and M. Craghan. 2009. Shore protection and retreat. In: *Coastal Sensitivity to sea level Rise: A Focus on the Mid-Atlantic Region.* A report by the U. S. Climate Change Science Program and the Subcommittee on Global Change Research. [J. G. Titus (coordinating lead author), K. E. Anderson, D. R. Cahoon, D. B. Gesch, S. K. Gill, B. T. Gutierrez, E. R. Thieler, and S. J. Williams (lead authors)]. U. S. Environmental Protection Agency, Washington DC, 87-104.

Titus, J. G. 2009. *Coastal Sensitivity to sea level Rise: A Focus on the Mid-Atlantic Region.* A report by the U. S. Climate Change Science Program and the Subcommittee on Global Change Research. [J. G. Titus (coordinating lead author), K. E. Anderson, D. R. Cahoon, D. B. Gesch, S. K. Gill, B. T. Gutierrez, E. R. Thieler, and S. J. Williams (lead authors)]. U. S. Environmental Protection Agency, Washington DC, pp. 117-122.

Titus J.G., Park R.A., Leatherman S.P., Weggel J.R., Greene M.S., Mausel P.W., Trehan M.S., Brown S., Grant C., Yohe G.W. 1991. Greenhouse effect and sea level rise: Loss of land and the cost of holding back the sea. *Coastal Management* 19:171-204.

Turner R. E., B. L. Howes, J. M. Teal, C. S. Milan, E. M. Swenson, and D. D. Goehringer-Toner. 2009. Salt marshes and eutrophication: An unsustainable outcome. *Limnology and Oceanography* 54(5):1634-1642.

U. S. Army Corps of Engineers (USACE). 1994. Facility and Component Explosive Damage Assessment Program (FACEDAP) Theory Manual, Version 1.2. Technical Report 92-2, Omaha, NE. Available online at: https://pdc.usace.army.mil/software/facedap/help/pdc-tr-92-2-theory-man.pdf (Accessed January 2011.

_____. 2005. Coastal Engineering Manual, Appendix A, Glossary of Coastal Terminology. Available online at: http://140. 194. 76. 129/publications/eng-manuals/em1110-2-1100/AppA/a-a. pdf (Accessed December 2010).

_____. 2011. Sea level Change Considerations in Civil Works Programs, CECW-CE Circular No. 1165-2-212. Available online at http://planning.usace.army.mil/toolbox/library/ECs/EC11652212Nov2011.pdf (Accessed 7 November 2012).

_____. 2013. Incorporating Sea Level Change in Civil Works Programs, CECW-CE Regulation No. 1100-2-8162. Available online at: http://www.publications.usace.army.mil/Portals/76/Publications/EngineerRegulations/ER_1100-2-8162.pdf (Accessed 10 April 2014).

_____. 2014. Procedures to Evaluate Sea Level Change: Impacts, Responses, and Adaptation, CECW-CE Technical Letter No. 1100-2-1 (Draft). Soon to be available online at: http://www.corpsclimate.us/etl.cfm (Accessed 10 April 2014).

U. S. Army Corps of Engineers (USACE) and Federal Emergency Management Agency (FEMA). 2005. Hurricane Isabel assessment, review of hurricane evacuation study products and other aspects of the National Hurricane Mitigation and Preparedness Program (NHMPP) in the context of the Hurricane Isabel response. Report prepared by Post, Buckley, Schuh and Jernigan, Tallahassee, FL, 301 pp. Available online at: http://www.csc.noaa.gov/hes/docs/postStorm/Isabel_PostStorm_Summary. pdf (Accessed December 2010.

U.S. Navy. 2010. U.S. Navy Climate Change Roadmap. Task Force Climate Change / Oceanographer of the Navy. Available online at: http://www.navy.mil/navydata/documents/CCR.pdf (Accessed 23 January 2012).

Uusitalo, L. 2007. Advantages and challenges of Bayesian networks in environmental modeling. *Ecological Modeling* 203(2007):312-318.

Vermeer, M. and S. Rahmstorf. 2009. Global sea level linked to global temperature. *Proceedings of the National Academy of Sciences* 106(51):21527-21532.

von Winterfeldt, D. and W. Edwards. 1986. *Decision Analysis and Behavioral Research*, Cambridge University Press, New York, NY, 624 pg.

Watzin, M. C., R. L. Smyth, E. A. Cassell, W. C. Hession, R. E. Manning, and D. W. Rubenstein. 2005. Ecosystem indicators and an environmental score card for the Lake Champlain Basin Program. Technical Report No. 46, Rubenstein School of Environment and Natural Resources, University of Vermont, Burlington, Vermont.

Westerink, J.J., Luettich, R.A,, Feyen, J.C., Atkinson, J.H., Dawson, C., Roberts, H.J., *et al*. 2008. A Basin to Channel Scale Unstructured Grid Hurricane Storm Surge Model Applied to Southern Louisiana. *Monthly Weather Review* 136(3):833-864.

Williams, S. J., B. T. Gutierrez, J. G. Titus, S. K. Gill, D. R. Cahoon, E. R. Thieler, K. E. Anderson, D. FitzGerald, V. Burkett, and J. Samenow. 2009. SLR and its effects on the coast. In: *Coastal Sensitivity to sea level Rise: A Focus on the Mid-Atlantic Region*. A report by the U.S. Climate Change Science Program and the Subcommittee on Global Change Research. [J.G. Titus (coordinating lead author), K.E. Anderson, D.R. Cahoon, D.B. Gesch, S.K. Gill, B.T. Gutierrez, E.R. Thieler, and S.J. Williams (lead authors)]. U.S. Environmental Protection Agency, Washington DC, pp. 11-24.

Wilson, A. G., and A. V. Huzurbazar. 2007. *Bayesian networks for multilevel system reliability*. Reliability Engineering and System Safety, 92:1413-1420.

Wilson, A. G., L. A. McNamara, and G. D. Wilson. 2007. Information integration for complex systems. *Reliability Engineering and System Safety* 92:121-130.

Wu, S. -Y., R. Najjar, and J. Siewert. 2009. Potential impacts of sea level rise on the Mid- and Upper-Atlantic Region of the United States, *Climatic Change*, 95:121-138, doi:10. 1007/s10584-008-9522-x.

Yeh, G. T., H. P. Cheng, J. R. Cheng, and H. C. Lin. 1998. A numerical model to simulate water flow and contaminant and sediment transport in WAterSHed systems of 1-D stream-river network, 2D overland regime, and 3D subsurface media (WASH123D: Version 2.0), CHL -98-19, Waterway Experimental Station, U. S. Army Corps of Engineers.

Yu, D. C., T. C. Nguyen, and P. Haddawy. 1999. Bayesian network model for reliability assessment of power systems. *IEEE Transactions on Power Systems* 14(2):426-432.

Zervas, C. 2009. Sea Level Variations of the United States 1854-2006. NOAA Tech. Rpt. NOS CO-OPS 053, NOAA National Ocean Service, Silver Spring, MD, 78p. and appendices (available online, http://tidesandcurrents.noaa.gov/publications/Tech_rpt_53.pdf (Accessed 21 February 2012).

Zijlema, M. 2010. Computation of wind-wave spectra in coastal waters with SWAN on unstructured grids. *Coastal Engineering* 57:267-277.

Zundel, A. K., 2006. Surface-water modeling system reference manual – Version 9. 2. Provo, UT: Brigham Young University Environmental Modeling Research Laboratory.

7. Glossary

ACCRETION	The accumulation of a sedimentary deposit that increases the size of a land area; this increase may be either lateral or vertical (Titus 2009). Net change in the relative elevation of the marsh surface in the tidal frame. Individual studies have distinguished between specific measures of elevation change (documented against a fixed datum) or surface accretion where methods focus on accumulation of material on or near the marsh surface (Reed et al. 2008).
ADVECTION–DIFFUSION METHOD	Advection-diffusion method solves the advection–diffusion equation of material transport in a fluid due to two processes: advection and diffusion.
AGGREGATION	Process in which the structural system is reduce to individual units of analysis.
AREA ASSET	An abstract node plus an area represented by an ordered set of points forming a polygon.
ASSET	A distinguishable entity that provides a service or capability. Assets are people, physical entities, or information located either within or outside the United States and employed, owned, or operated by domestic, foreign, public, or private sector organizations (DoD 2010b).
ASSET CAPABILITY NETWORK (ACN)	A network made up of missions, supporting capabilities, and the infrastructure assets that support them.
ASSET DECOMPOSITION	The process of identifying critical infrastructure (both built and natural) assets on an installation which (together) generate capabilities contributing to mission performance. Mapping the relationships between assets in an asset capability network (ACN) offers an opportunity to consider individual assets with respect to the entire system, exposing dependencies that could be significant in altering mission performance.
ASSET NODES	Considered to be concrete (as opposed to abstract) entities that support.

BANK	The rising ground bordering a lake, river, or sea; or of a river or channel, for which it is designated as right or left as the observer is facing downstream (USACE 2005).
BATHYMETRY	Measured water depths in an ocean or bay referenced to vertical and horizontal datums.
BAYESIAN NETWORK (Bn)	A probabilistic graphical model (i.e., a type of statistical model) that represents a set of random variables and their conditional dependencies via a Directed Acyclic Graph (DAG). In other words, a Bayesian network consists of two parts: 1) a DAG that depicts dependence and conditional independence among *nodes* representing elements of a system, and 2) a set of conditional probability tables that quantify the relationships among elements of that system *Nodes* represent random variables in the Bayesian sense - they may be observable quantities, latent variables, unknown parameters or hypotheses. *Edges* represent conditional dependencies; nodes which are not connected represent variables which are conditionally independent of each other. Each node is associated with a probability function that takes as input a particular set of values for the node's parent variables and gives the probability of the variable represented by the node (http://en.wikipedia.org/wiki/Bayesian_Network). Bayesian networks provide a means of parsimoniously expressing joint probability distributions over many interrelated hypotheses. A Bayesian network consists of a DAG and a set of local distributions. Each node in the graph represents a random variable. A random variable denotes an attribute, feature, or hypothesis about which we may be uncertain. Each random variable has a set of mutually exclusive and collectively exhaustive possible values. That is, exactly one of the possible values is or will be the actual value, and we are uncertain about which one it is. The graph represents direct qualitative dependence relationships; the local distributions represent quantitative information about the strength of those dependencies. The graph and the local distributions together represent a joint distribution over the random variables denoted by the nodes of the graph (http://www.pr-owl.org/basics/bn.php).

BEACH	The zone of unconsolidated material that extends landward from the low water line to the place where there is marked change in material or physiographic form, or to the line of permanent vegetation (usually the effective limit of storm waves). The seaward limit of a beach--unless otherwise specified--is the mean low water line. A beach includes foreshore and backshore (USACE 2005).
BEACH FILL	Material placed on a beach to renourish eroding shores, usually pumped by dredge but sometimes delivered by trucks (USACE 2005).
BLUFF	A high, steep bank or cliff (USACE 2005).
CAPABILITIES	(aka abstract nodes) - They support Missions.
CASCADE EFFECTS	A phenomenon in which failure in one asset sweeps through a network to cause failure of other parts of a network (Lewis 2008).
CHILD NODE	A node in a Bayesian network may contain a value or condition. Each node in a network has zero or more **child nodes**, which are below it in the diagram (by convention, these diagrams are drawn growing downwards). A node that has a child is called the child's parent node (or ancestor node, or superior). A node has at most one parent.
CLIMATE CHANGE	A change in the state of the climate that can be identified (e.g., by using statistical tests) by changes in the mean and/or the variability of its properties, and that persists for an extended period, typically decades or longer. Climate change may be due to natural internal processes or external forcings, or to persistent anthropogenic changes in the composition of the atmosphere or in land use (IPCC 2007 Glossary). A change of climate which is attributed directly or indirectly to human activity that alters the composition of the global atmosphere and which is in addition to natural climate variability observed over comparable time periods [United Nations Framework Convention on Climate Change (UNFCCC)].
COASTAL PLAIN	Any lowland area bordering a sea or ocean, extending inland to the nearest elevated land, and sloping very gently seaward (Titus 2009).

COASTAL ZONE	The area extending from the ocean inland across the region directly influenced by marine processes (Titus 2009).
COASTLINE	The line that forms the boundary between the coast and the shore or the line that forms the boundary between the land and the water (Titus 2009).
COLLECTIVELY EXHAUSTIVE	The set of potential states for a random variable represents the universe of potential states for that random variable.
CONDITIONAL PROBABILITY TABLE (CPT)	For nodes in the Bayesian network that had at least one parent, the CPT gave the probability of each node state conditional on the state(s) of the parent node(s).
CONCEPUTUAL MODELS	Conceptual models are descriptions of the general functional relationships among essential components of an ecosystem. They tell the story of "how the system works" and, in the case of ecosystem restoration, how restoration actions aim to alter those processes or attributes for the betterment of the system (Fischenich et al. 2008).
CONDITIONAL INDEPENDENCE	A term that describes the independence of two events given knowledge of a third event. In probabilistic graphical models, the lack of an arc connecting nodes that represent random variables represents a conditional independence assumption (conditional independence).
CROSS SECTION	Intersection of a body in 3Dimensional space with a plane (cross section).
DAMAGE CRITERIA	In a 0% damage there is no appreciable damage; the component is reusable without repair. In a 30% damage there is a moderate damage; the component is probably repairable. In a 60% damage there is severe damage; the component is not worth repairing, but it has not failed. In a 100% of damage the component is definitely beyond repair, but it has not necessarily collapsed.
DAMAGE FUNCTION	Prediction function based on a statistical fit of the damage results from a parameter study.
DAMAGE STATES	Levels of classification for a qualitative and quantitative description of damage.

DATUM	A datum is a reference point or surface against which position measurements are made, and an associated model of the shape of the earth for computing positions [*see North American Datum of 1983 (NAD83) and North American Vertical Datum of 1988 (NAVD88)*].
DEFENSE CRITICAL INFRASTRUCTURE (DCI)	The composite of DoD and non-DoD assets essential to project, support, and sustain military forces and operations worldwide. (DoD 2010b).
DEFENSE CRITICAL INFRASTRUCTURE PROGRAM (DCIP)	A DoD risk management program that seeks to ensure the availability of DCI (DoD 2010b).
DEPTH-INTEGRATED CONTINUITY EQUATION	Three-dimensional variables in the equation are depth-averaged by vertical integration and the equation becomes two-dimensional.
DIGITAL ELEVATION MODEL (DEM)	The digital representation of the ground surface or terrain using a set of elevation data (Titus 2009).
DIRECTED ACYCLIC GRAPH	A directed graph with no directed cycles (i.e., feedback loops). A graph (object-based flow diagram) formed by a collection of vertices (i.e., nodes) and directed edges, each edge connecting one node to another, such that there is no way to start at some vertex *v* and follow a sequence of edges that eventually loops back to *v* again
DIRECTED EDGE	In a Bayesian network, a set of ordered pairs of nodes are connected by arrows or directed edges, and their presence indicates dependence between the connected nodes. An edge $a = (x, y)$ is considered to be directed from x to y; y is called the head and x is called the tail of the arc; y is said to be a direct successor of x, and x is said to be a direct predecessor of y.

DISCRETE RANDOM VARIABLE	A random variable that may take on only a countable number of distinct values such as 0,1,2,3,4, etc. Discrete random variables are usually (but not necessarily) counts. If a random variable can take only a finite number of distinct values, then it must be discrete. Examples of discrete random variables include the number of children in a family, the Friday night attendance at a cinema, the number of patients in a doctor's surgery, the number of defective light bulbs in a box of ten. The probability distribution of a discrete random variable is a list of probabilities associated with each of its possible values. It is also sometimes called the probability function or the probability mass function
DISCRETIZATION	The process of converting continuous features or variables to discretized or nominal features.
DRIVERS	Changes in natural systems are the result of forces on a system's structure and function - these forces are called drivers (Henderson and O'Neil 2004, 2007). Drivers are the natural and anthropogenic structures, processes, or regimes that control or cause ('force') changes in environmental conditions, i.e., drivers identify the source or cause of the stressors in conceptual models (Henderson and O'Neil 2007). Drivers are an organizational device to allow a team to start a model with the "big picture" in mind. Sources of drivers may be natural or anthropogenic. The identification of drivers entails a comprehensive description of the system, identifying the structures, processes, and regimes that define the system and cause changes in system conditions.
DYNAMIC COUPLING	A dynamic coupling is a mechanism for connecting two numerical models that feed the updated results between the models as a model computation is conducted.
EDGES	Lines or arrows in a Bayesian network connecting nodes that signify causal influences between linked variables.
EFFECTS	A direct change, result or consequence caused by an action or phenomenon.

EQUILIBRIUM AND NON-EQUILIBRIUM SEDIMENT TRANSPORT	Equilibrium sediment transport is reached when there are no bed changes (erosion and deposition rates are balanced) in a system. The opposite of an equilibrium system is a non-equilibrium system in which erosion and deposition rates are instantaneously off balance.
EROSION	The wearing away of land by the action of natural forces. On a beach, the carrying away of beach material by wave action, tidal currents, littoral currents, or by deflation (USACE 2005). The mechanical removal of sedimentary material by gravity, running water, moving ice, or wind; in the context of coastal settings erosion refers to the landward retreat of a shoreline indicator such as the water line, the berm crest, or the vegetation line; the loss occurs when sediments are entrained into the water column and transported from the source (Titus 2009).
ESSENTIAL SYSTEM COMPONENTS	An organizing device in conceptual modeling, showing the major components acted on or through which the stressors act to cause or result in endpoints in the system (Henderson and O'Neil 2004, 2007). The organizing categories reflect or respond to the model domain, the process being used for development or construction of the model, and the resources of interest. Some examples include: individuals, populations, communities, ecosystems, processes (physical, chemical, and biological), and/or landscape patterns.
ESTUARY	(1) The part of a river that is affected by tides. (2) The region near a river mouth in which the fresh water of the river mixes with the salt water of the sea and which received both fluvial and littoral sediment influx (USACE 2005).
EXTRA-TROPICAL STORM (i.e., nor'easters occurring in the Mid-Atlantic U.S.)	A cyclonic weather system, occurring in the middle or high latitudes (e.g., poleward of the tropics) that is generated by colliding airmasses; such weather systems often spawn large storms that occur between late fall and early spring (Titus 2009).
FACTORIZATION	The decomposition of an object into a product or other objects, or factors, which when multiplied back together yields the original value.

FETCH	The area in which seas are generated by a wind having a fairly constant direction and speed. Sometimes used synonymously with fetch length (USACE 2005). (Titus 2009).
FINITE-VOLUME MODEL	The governing equations are solved over discrete control volumes. Finite volume methods recast the governing partial differential equations (typically the Navier-Stokes equations) in a conservative form, and then discretize the new equation. This guarantees the conservation of fluxes through a particular control volume (sediment transport).
FLOODING	The temporary submergence of land that is normally dry, often due to periodic events such as storms (Titus 2009).
FORCINGS	Structural loadings applied to a component of a structure or to the structure as a unit (forcings). Factors that alter a particular physical, chemical, or biological system (Titus 2009).
FRAGILITY CURVE	A curve that describes the probability that a system will fail as a function of the load on that system.
FREEBOARD	The distance between the water surface and the top of the pier deck.
FULL-PLANE WAVE MODEL	The numerical program to calculate the wave propagation in any direction at sea.
GEOGRAPHICAL INFORMATION SYSTEM (GIS)	Database of information which is geographically referenced, usually with an associated visualization system (USACE 2005).
GEOLOGIC FRAMEWORK	The underlying geological setting, structure, and lithology (rock/sediment type) in a given area (Titus 2009).

GEOMORPHOLOGY	That branch of physical geography which deals with the form of the Earth, the general configuration of its surface, the distribution of the land, water, etc. The investigation of the history of geologic changes through the interpretation of topographic forms (USACE 2005). The external structure, form, and arrangement of rocks or sediments in relation to the development of the surface of the Earth (Titus 2009).
GLOBAL SEA LEVEL RISE (EUSTATIC)	The average increase in the level of the world's oceans that occurs due to a variety of factors, the most significant being thermal expansion of the oceans and the addition of water by melting land-based ice sheets, ice caps, and glaciers (Anderson et al. 2009). A change in sea level caused by change in the relative volumes of the world's ocean basins and the total amount of ocean water (Sahagian and Holland 1991). The worldwide average rise in mean sea level; may be due to a number of different causes, such as the thermal expansion of sea water and the addition of water to the oceans from the melting of glaciers, ice caps, and ice sheets; contrast with relative SLR (Titus 2009).
GRAPH	A representation of a set of objects where some pairs of the objects are connected by links. The interconnected objects are represented by mathematical abstractions called *nodes*, and the links that connect some pairs of nodes are called *edges*. Typically, a graph in a Bayesian Network is depicted in diagrammatic form as a set of boxes for the *nodes*, joined by lines or curves for the *edges*.
GRID NESTING	The numerical model technique to interlock several grids of different resolution and size for the wave propagation from coarser to finer grids.
HABITAT SWITCHING	Shifts in vegetative community type given long-term shifts in salinity, freshwater input, sea level, or other drivers (habitat switching).
HALF-PLANE WAVE MODEL	The numerical program to calculate the wave propagation only from the sea towards shore in a 180-deg sector.

HAZARD	A situation that poses a level of threat to life, health, property, or environment. Most hazards are dormant or potential, with only a theoretical risk of harm; however, once a hazard becomes "active", it can create an emergency situation. A hazard does not exist when it is happening. A hazardous situation that has come to pass is called an incident. Hazard and vulnerability interact together to create risk (hazard).
HIGH WATER MARK (i.e., ordinary water mark or mean high water mark)	A demarcation between the publicly owned land along the water and privately owned land which has legal implications regarding public access to the shore; generally based on mean high water, the definition varies by state; along beaches with significant waves, it may be based on the line of vegetation, the water mark caused by wave runup, surveys of the elevation of mean high water, or other procedures (Titus 2009).
HORIZONTAL DATUM	Horizontal datums are used for describing a point on the earth's surface, in latitude and longitude or another coordinate system [*see North American Datum of 1983 (NAD83) and North American Vertical Datum of 1988 (NAVD88)*].
HYDRODYNAMIC MODEL	A suite of mathematical models that solve continuity and momentum equations to study fluid mechanics.
INFRASTRUCTURE	The framework of interdependent physical and cyber-based systems comprising identifiable industries, institutions (including people and procedures), and distribution capabilities that provide a reliable flow of products and services essential to the defense and economic security of the United States, to the smooth functioning of government at all levels, and to society as a whole (DoD 2010b).
INSTANTIATE	In computer programming, an individual object of a certain class is defined as a “type” while an actual usage of a class is called an "instance". Each instance of a class can have different values for its instance variables (i.e., its “state”). For the Bayesian network application presented herein, instantiation referred to the application of hard evidence to indicate that a discrete random variable was in one of its potential states.
INTER-DEPENDENCY	Relationships or connections between entities of different DoD Components and defense infrastructure sectors (DoD 2010b).

INTRA-DEPENDENCY	Relationships or connections between entities of a DoD Component and a defense infrastructure sector (DoD 2010b).
JOINT PROBABILITY DISTRIBUTION	In the study of probability (i.e., the study of the measure of the expectation that an event will occur or a statement is true), given two random variables *X* and *Y* that are defined on the same probability space, the joint distribution for *X* and *Y*, defines the probability of events defined in terms of both *X* and *Y*.
INUNDATION	The submergence of land by water, particularly in a coastal setting (Titus 2009).
LIGHT DETECTION AND RANGING (LiDAR)	a remote sensing instrument that uses laser light pulses to measure the elevation of the land surface with a high degree of accuracy and precision (Titus 2009).
LINEAR ASSET	An abstract node plus a linear feature represented by an ordered set of points. For example, a steam line would be represented by a Linear Asset.
LOADING ENVIRONMENT	Time and space variation of the loadings.
LOADINGS	Forces applied to a component of a structure or to the structure as a unit (structural loading).
MARGINAL PROBABILITY DISTRIBUTIONS	The marginal distribution of a subset of a collection of random variables is the probability distribution of the variables contained in the subset. The term “marginal variable” is used to refer to those variables in the subset of variables being retained. These terms are dubbed "marginal" because they used to be found by summing values in a table along rows or columns, and writing the sum in the margins of the table. The distribution of the marginal variables (the marginal distribution) is obtained by marginalizing over the distribution of the variables being discarded, and the discarded variables are said to have been marginalized out.
MARGINAL PROBABILITY TABLE (MPT)	For nodes in the Bayesian network that lacked parents, the MPT contains the unconditional probability of each potential node state.

MATERIAL PROPERTIES	Quantitative property of a material, usually with a unit that may be used as a metric of value to compare the benefits of one material versus another. Material properties include Yield Stress, Ultimate Stress and Young Modulus of Elasticity (material properties).
MEAN HIGH WATER	a tidal datum; the average height of high water levels observed over a 19-year period (Titus 2009).
MEAN HIGHER HIGH WATER	The average of the higher high water height of each tidal day observed over the national tidal datum epoch (Titus 2009).
MEAN SEA LEVEL (MSL)	The "still water level" (i.e., the level of the sea with high frequency motions such as wind waves averaged out); averaged over a period of time such as a month or a year, such that periodic changes in sea level (e.g., due to the tides) are also averaged out; the values of MSL are measured with respect to the level of marks on land (called benchmarks) (Titus 2009).
MISSION ASSURANCE	A process to ensure that assigned tasks or duties can be performed in accordance with the intended purpose or plan. It is a summation of the activities and measures taken to ensure that required capabilities and all supporting infrastructures are available to the Department of Defense to carry out the National Military Strategy. It links numerous risk management program activities and security-related functions, such as force protection; antiterrorism; critical infrastructure protection; IA; continuity of operations; chemical, biological, radiological, nuclear, and high explosive defense; readiness; and installation preparedness to create the synergy required for the Department of Defense to mobilize, deploy, support, and sustain military operations throughout the continuum of operations (DoD 2010b).
MISSION NODE	A type of abstract node the represents the mission being supported. It is intended to support a concept, rather than a physical entity. Mission nodes are normally instantiated at the root of an ACN tree.
MITIGATION	Actions taken in response to a warning or after an incident occurs that are intended to lessen the potentially adverse effects on a given military operation or infrastructure (DoD 2010b).
MUTUALLY EXCLUSIVE	If the state of a random variable is observed in nature, it can be associated with exactly one of the potential states in the model.

NATIONAL TIDAL DATUM EPOCH (NTDE)	The latest 19-year time period over which NOAA has computed and published official tidal datums and local mean sea level elevations from tide station records; currently, the latest NTDE is 1983-2001 (Titus 2009).
NEARSHORE	The zone extending from the shoreline seaward to a short, but indefinite distance offshore (Titus 2009). For this study, we assumed nearshore modeling would be employed within 5-10 miles of the coastline.
NETWORK	A group or system of interconnected or cooperating entities, normally characterized as being nodes (assets), and the connections that link them (DoD 2010b).
NODE	A point in a network topology where lines intersect. In Bayesian network DAGs, *nodes* represent random variables (i.e., observable quantities, latent variables, unknown parameters or hypotheses).
NODE STATE	One of the potential values of a random variable (i.e., node) in a Bayesian network (i.e., *Functional* (*F*) or *Nonfunctional* (*NF*). For purposes of this study, nodes with parents are defined by conditional probability tables that give, for every possible state of the variable, a probability of being in that state given the state of all parent node variables. Nodes without any parents are called roots and are defined by marginal probability distributions.
NON-UNIFORM CARTESIAN GRID	A rectangular numerical model grid consisting of variable cell sizes.
NOR'EASTER (i.e., extra-tropical storms occurring in the Mid-Atlantic U.S.)	The name given to the strong northeasterly winds associated with extra-tropical cyclones that occur along the East Coast of the United States and Canada; these storms often cause beach erosion and structural damage; wind gusts associated with these storms can approach and sometimes exceed hurricane force in intensity (Titus 2009) (nor'easter).
NORTH AMERICAN DATUM OF 1983 (NAD83)	The official horizontal datum used for the primary geodetic network in North America (*see Datum and Horizontal Datum)*.

NORTH AMERICAN VERTICAL DATUM OF 1988 (NAVD88)	A fixed reference for elevations determined by geodetic leveling, derived from a general adjustment of the first-order terrestrial leveling networks of the United States, Canada, and Mexico (*see Datum and Vertical Datum).*
OPEN BOUNDARY	The water boundary of a numerical model computational domain.
OPERATIONALIZE	To define a concept or variable so that it can be measured or expressed quantitatively.
OVERWASH	The sediment that is transported from the beach across a barrier and is deposited in an apron-like accumulation along the backside of the barrier; overwash usually occurs during storms when waves break through the frontal dune ridge and flow landward toward the marsh or lagoon (Titus 2009).
PARENT NODE	A node in a Bayesian network may contain a value or condition. Each node in a network has zero or more child nodes, which are below it in the diagram (by convention, these diagrams are drawn growing downwards). A node that has a child is called the child's **parent node** (or ancestor node, or superior). A node has at most one parent. In a Bayesian network, nodes with parents are defined by conditional probability tables that give, for every possible state of the variable, a probability of being in that state given the state of all parent node variables
POINT ASSET	An Asset plus a 3D georeferenced location (latitude, longitude, elevation. Global Coordinate System (GCS) WGS 1984). For example, an electrical substation would most likely be represented as a point node.
POSTERIOR PROBABILITIES	The posterior probability of *Y* given the state of one or more random variables, *X*, is simply the probability that *Y* is in a particular state given the observations or evidence about other nodes, *X*.
PRIOR PROBABILITY	As represented in the Bayes' theorem, $P(Y_{j=i})$ is called the *prior probability* - the probability that *Y* is in the i^{th} state before the evidence becomes available.

PROBABILITY	A number expressing the frequency of the occurrence of an event or the degree of belief that an event will occur. Probabilities are given a value between 0 (will not occur) and 1 (will occur). The higher the probability of an event, the more certain we are that the event will occur.
RELATIVE SEA LEVEL	Sea level measured by a tide gauge with respect to the land upon which it is situated. Mean sea level is normally defined as the average relative sea level over a period, such as a month or a year, long enough to average out transients such as waves and tides (IPCC 2007 Glossary).
RELATIVE SEA LEVEL RISE	The change in sea level relative to the elevation of the adjacent land, which can also subside or rise due to natural and human-induced factors. Relative sea level chances include both global SLR and changes in the vertical elevation of the land surface (Anderson et al. 2009). A change in the elevation of the sea surface compared with some local land surface (Sahagian and Holland 1991). The rise in sea level measured with respect to a specified vertical datum relative to the land, which may also be changing elevation over time; typically measured using a tide gauge; compare with global SLR (Titus 2009).
REMEDIATION	Actions taken to correct known deficiencies and weaknesses once a vulnerability has been identified.
RISK	Combination of the magnitude of the potential consequence(s) of climate change impact(s) and the likelihood that the consequence(s) will occur (NRC 2010). Probability and severity of loss linked to threats or hazards and vulnerabilities (DoD 2010b).
ROOTS	Nodes without parents. In a Bayesian network, roots are defined by marginal probability distributions.
SCALE FREE NETWORK	A network that shows degree distribution (i.e., the distribution of number of edges connected to nodes) that follows a power law (Barabási 2004).

SEDIMENT	Solid materials or fragments that originate from the breakup of rock and are transported by air, water or ice, or that accumulate by other natural agents such as chemical precipitation or biological secretions; solid materials that have settled from being suspended, as in moving water or air (Titus 2009).
SEDIMENT MASS BALANCE	The overall balance between sediment in transport and sediment being deposited on the bed (sediment).
SEDIMENT TRANSPORT	Sediment transport is the movement of solid particles (sediment), typically due to a combination of the force of gravity acting on the sediment, and/or the movement of the fluid in which the sediment is entrained (sediment transport).
SENSITIVITY	The change in an output value given the unit change in an input value.
SHORE	The narrow strip of land in immediate contact with the sea, including the zone between high and low water lines. A shore of unconsolidated material is usually called a beach. Also used in a general sense to mean the coastal area (e.g., to live at the shore). Also sometimes known as the littoral (USACE 2005).
SHORELINE	The intersection of a specified plane of water with the shore or beach (e.g., the high water shoreline would be the intersection of the plane of mean high water with the shore or beach). The line delineating the shoreline on National Ocean Service nautical charts and surveys approximates the mean high water line (USACE 2005).
SHORELINE ARMORING	A method of shore protection that prevents shore erosion through the use of hardened structures such as seawalls, bulkheads, and revetments (Titus 2009).
SIGNIFICANT WAVE HEIGHTS	The average of the highest one-third wave heights in a random wave field, where the wave height of an individual wave is the vertical distance from the wave crest to the wave trough.
SPECTRAL WAVE TRANSFORMATION MODEL	The numerical program computes spatial and temporal changes of wave energy in the ocean.

STATIONARITY	The concept that while climate may exhibit variability, the underlying statistics that describe the climate (such as its mean and variance) do not change over time. Rather, these characteristics are stationary. This leads to an assumption that the past represents a reasonable proxy for the future ().
STEERING MODULE	The operation of running two numerical models alternately and feeding updated model results to each others.
STORM SURGE	A rise above normal water level on the open coast due to the action of wind stress on the water surface. Storm surge resulting from a hurricane also includes the rise in level due to atmospheric pressure reduction as well as that due to wind stress.
STRESSORS	Stressors are the physical, chemical, biological, and human-influenced changes that result from the drivers. These changes can be natural and modest in effect (e.g., plant production), or anthropogenic and severe (e.g., induced erosion, water quality changes, and habitat loss (Henderson and O'Neil 2007). A change may not be a stressor until a threshold is met, causing a substantive transformation or effect on a significant resource or category of resources. The term stressor is used to describe these changes because the stressor changes (i.e., stresses, configures, or transforms) the system. Stressor is presented as a neutral term because some changes are intended to be positive, e.g., increase in dissolved oxygen, and some are negative, e.g., an increase in invasive species.
STRUCTURAL ANALYSIS	Comprises the set of physical laws and mathematics required to study and predict the behavior of structures. The primary objective is the computation of deformations, internal forces, and stresses (structural analysis).
STRUCTURE SOIL INTERACTION	The process in which the response of the soil influences the motion of the structure and the motion of the structure influences the response of the soil (structural soil interaction).
SUBSIDENCE	The downward settling of the Earth's crust relative to its surroundings (Titus 2009).

SURGE	(1) The name applied to wave motion with a period intermediate between that of the ordinary wind wave and that of the tide, say from ½ to 60 min. It is low height, usually less than 0.9 m (3 ft). See also SEICHE. (2) In fluid flow, long interval variations in velocity and pressure, not necessarily periodic, perhaps even transient in nature (USACE 2005).
SYSTEMS APPROACH	A systems approach is a set practices within a framework that are based on the belief that the component parts of a system can best be understood in the context of relationships with each other and with other systems, rather than in isolation.
SYSTEM ASSET	A special class of Asset that contains other assets and "rolls up" their behavior. For instance, a Steam System would contain the boiler building, boilers, and different types of steam lines.
THERMAL EXPANSION	In connection with sea level, this refers to the increase in volume (and decrease in density) that results from warming water. A warming of the ocean leads to an expansion of the ocean volume and hence an increase in sea level (IPCC 2007 Glossary).
TIDAL DATUM	A baseline elevation used as a vertical point of reference from which heights or depths can be reckoned; called a tidal datum when defined in terms of a certain phase of the tide (Titus 2009).
TIPPING POINT	A critical point in the evolution of a system that leads to new and potentially irreversible effects at a rate that can either be much faster or much slower than forcing (Titus 2009). In terms of infrastructure operation and maintenance, this is considered the point in which a minor annoyance becomes a catastrophic impairment affecting mission performance.
TOPOGRAPHY	Measured land elevation referenced to vertical and horizontal datums.

TROPICAL CYCLONE	A storm system characterized by a large low-pressure center and numerous thunderstorms that produce strong winds and heavy rain. Tropical cyclones strengthen when water evaporated from the ocean is released as the saturated air rises, resulting in condensation of water vapor contained in the moist air. The term "tropical" refers both to the geographical origin of these systems, which usually form in tropical regions of the globe, and to their formation in maritime tropical air masses. The term "cyclone" refers to such storms' cyclonic nature, with counterclockwise wind flow in the Northern Hemisphere and clockwise wind flow in the Southern Hemisphere. The opposite direction of the wind flow is a result of the Coriolis force. Depending on its location and strength, a tropical cyclone is referred to by names such as hurricane, typhoon, tropical storm, cyclonic storm, tropical depression, and simply cyclone.
UNCERTAINTY	Lack of knowledge about the value of a quantity.
UNSTRUCTURED MESH (or GRID)	An unstructured (or irregular) grid is a tessellation of a part of the Euclidean plane or Euclidean space by simple shapes, such as triangles or tetrahedra, in an irregular pattern. Grids of this type may be used in finite element analysis when the input to be analyzed has an irregular shape (unstructured grid).
VERTICAL DATUM	Vertical datums are used to measure elevations or underwater depths [see North American Datum of 1983 (NAD83) and North American Vertical Datum of 1988 (NAVD88)].
VULNERABLE STRUCTURAL COMPONENTS	Components in a structural system which are likely to have a permanent damage after the loads are removed. A susceptibility to loss.
WAVE DIFFRACTION AND REFLECTION	The change in wave propagation into the shadow and along the face of obstacles.
WAVE PERIOD	The time between the passage of two successive wave crests pass a fixed point. The peak period is the period associated with the most energetic waves in a random wave field.
WAVE RADIATION STRESS	The flux of momentum carried by the water surface gravity waves.
WAVE REFRACTION	The change in wave propagation as affected by the presence of bathymetry.

WAVE RUN-UP	The maximum elevation the gravity waves reach on the beach relative to the still water level.
WAVE SETUP	Superevelvation of the water surface elevation due to the onshore momentum flux of breaking waves.
WAVE-ACTION BALANCE AND DIFFRACTION EQUATION	The mathematical description of the total wave energy and momentum changes as the net of energy gain and loss in addition to the wave diffraction mechanism.
WETLAND CONVERSION	See habitat switching.
WETLANDS	Lands whose saturation with water is the dominant factor determining the nature of soil development and the types of plant and animal communities that live in the soil and on its surface (e.g. Mangrove forests) (USACE 2005).
WHARF	A structure built on the shore of a harbor, river, or canal, so that vessels may lie alongside to receive and discharge cargo and passengers (USACE 2005).

Appendix A: GIS Data Management

GIS Database Design

The ERDC Geospatial Data Analysis Facility was responsible for providing and managing geospatial data associated with the SERDP 1701 project. A standard GIS data design was needed in order to take full advantage of the available geospatial data and new data being generated. GIS database design was a "living" activity, which involves continual effort during the scientific discovery, information building, and intellectual product formation processes of the research. To accomplish these tasks the Spatial Data Standards for Facilities, Infrastructure and Environment (SDSFIE) was selected as the data schema. The SDSFIE was recognized as the geospatial enterprise standard across the entire DoD business mission area. The purpose of this standard was to establish the content requirements for the collection and interchange of features and to facilitate the maintenance and use of that information by all users of GIS.

NSN had developed a comprehensive geospatial database of utilities and environmental features. The data was converted to the SDSFIE standard. Figure A-1 shows a portion of the Norfolk geodatabase.

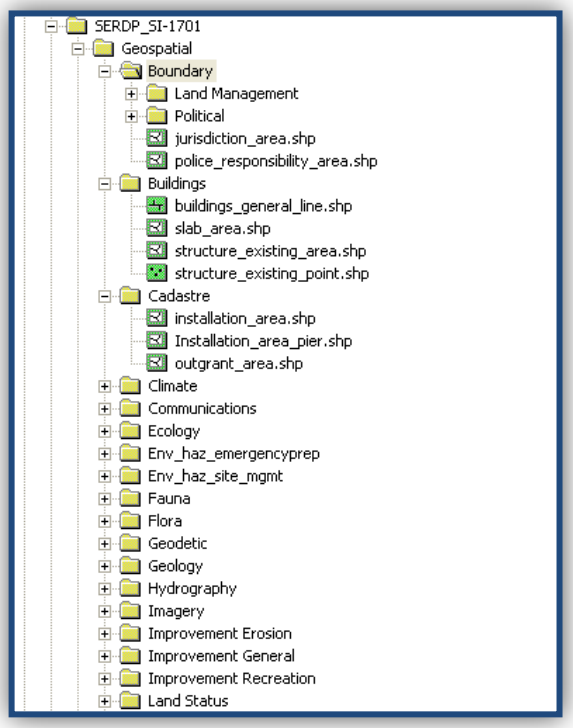

Figure A-1. Norfolk geodatabase architecture.

Additional data (*i.e.*, Atlantic storm parameters, regional storm surge/wave modeling, groundwater characterization effects, and regional geomorphic evolution), were incorporated into the geospatial database as they were derived. The study initially used ArcGIS 9.3, and upgraded to ArcGIS 10 later in the study.

In addition, we developed a data portal, which is a website that acted as a gateway providing a single access point to multiple data sources. The web environment allowed the community of information users and providers to share project content. The web portal consisted of five main sections: *Home*, *Geospatial Layers*, *Maps and Videos*, *Interactive Map*, and *Databases and Software* (Figure A-2).

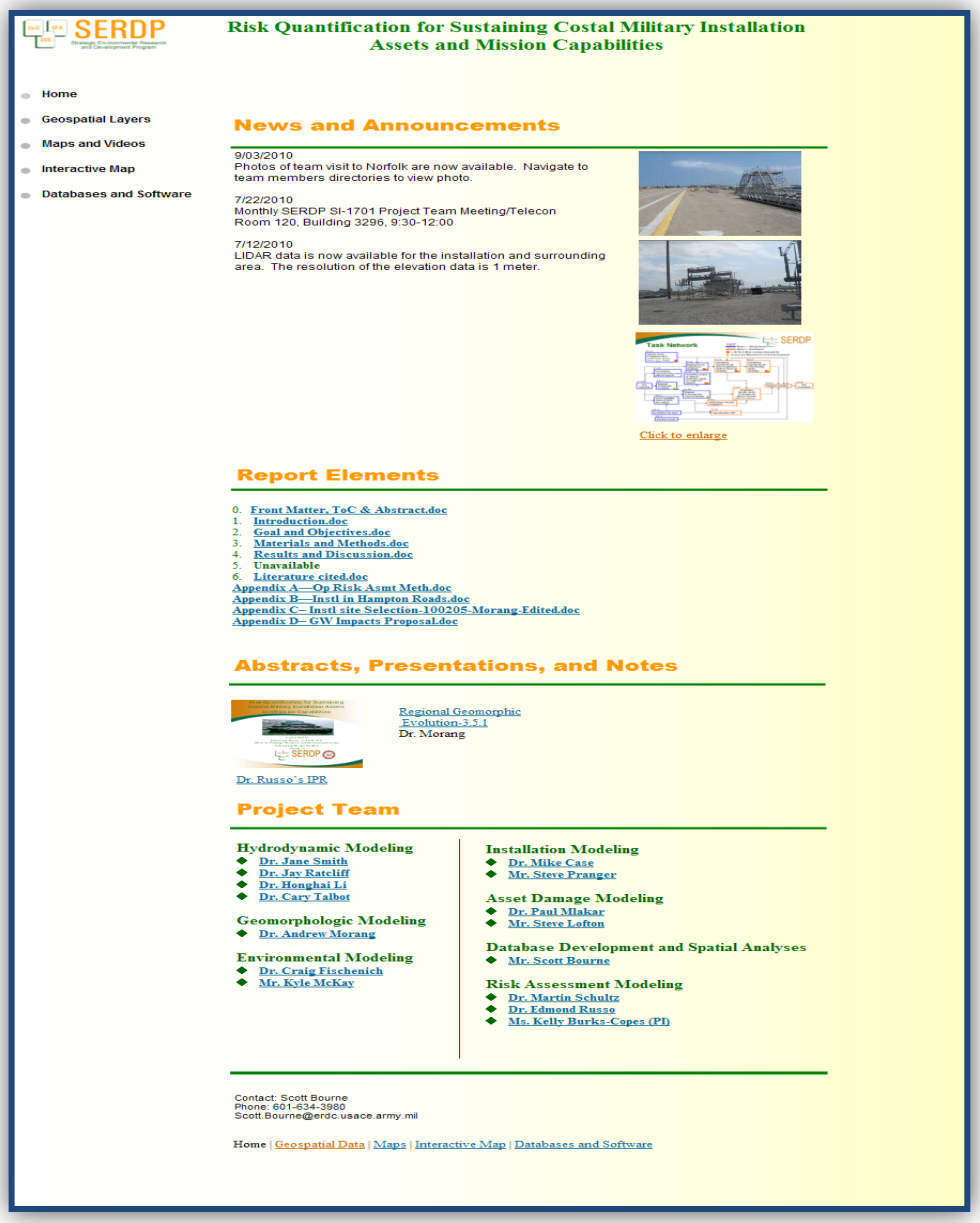

Figure A-2. Team network portal.

We accessed these sections via the *Home Page* shown here. The Geospatial Layers page provided all the data that was acquired from NSN. Each geospatial feature class was downloaded as a shapefile. The data was organized to conform to the SDSFIE standard. The Maps and

Videos page provided a location where maps and videos of model output were posted for viewing and downloading.

The Interactive Map was an ArcGIS Server web application. ArcGIS Server provided the ability to publish GIS web services. It was a platform for building enterprise GIS applications that were centrally managed, support multiple users, and included advanced GIS functionality. Developing this web GIS environment greatly expanded the use of location based data and allowed researchers to distribute their data to the other researchers. At the time of this study, the ArcGIS Server technology provided organizations with the ability to manage and deploy web services for mapping, data management, and geospatial analytics, organizations can more easily leverage their internal GIS resources, as well as services hosted on other GIS servers, and put them to work. The SERDP web application is shown in Figure A-3.

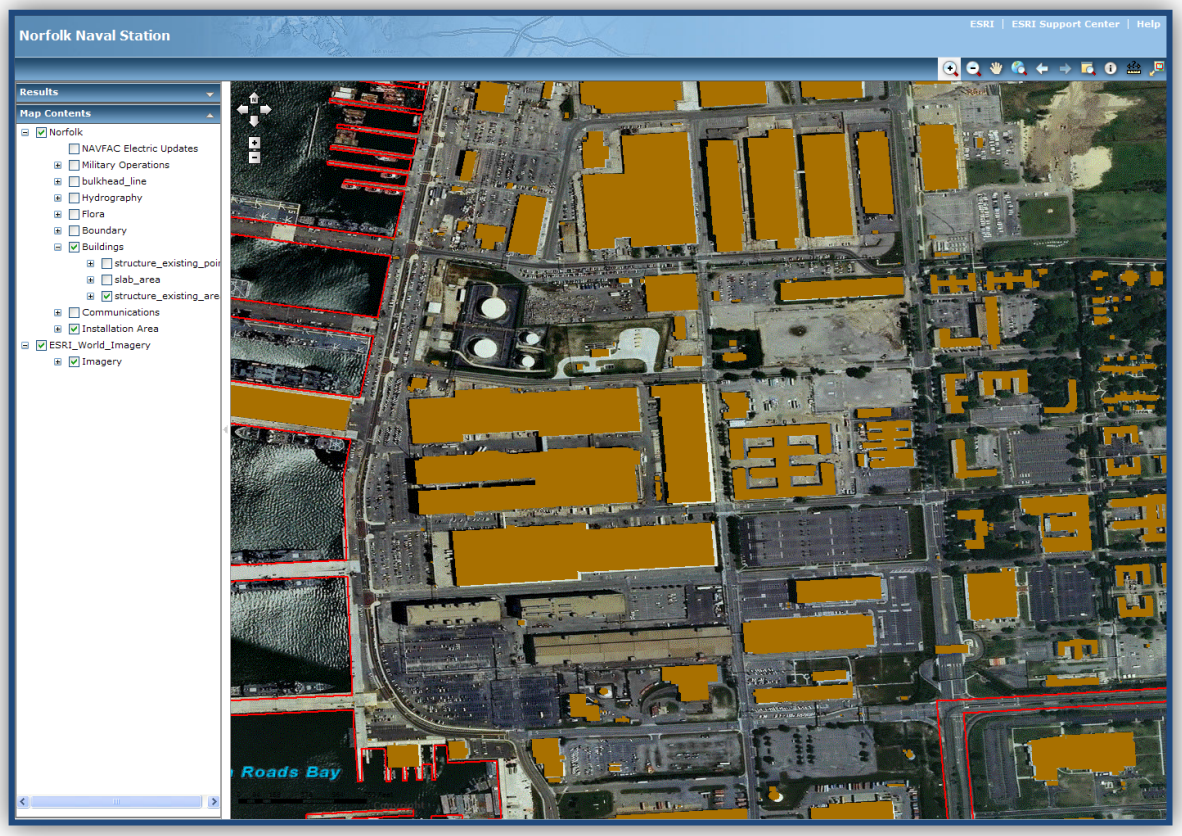

Figure A-3. Interactive map of the study site.

The database and software pages offered a location where all database information could be accessed. Also on the page was a link to ArcGIS Explorer. ArcGIS Explorer was a free, downloadable GIS viewer that offered the users a more powerful tool than the ArcGIS web application to explore and visualize geospatial data.

GIS Database Assembly

At the beginning of the project, we decided that geospatial data were needed for the installation. These data included Digital Elevation Models (DEM), utilities data (ex. electrical, steam, storm water, water, and transportation), and imagery (satellite and aerial). Assembling these data was a highly interactive exercise that required several geoprocessing steps, including mosaicking, clipping, re-projectioning, and format conversions. These data combined with data from the hydrodynamic modeling and the operationalization of the ACN contributed directly to the population of the project's geodatabase.

Using a GIS for data assembly expedited the procedure of combining output and data from these tasks. To assemble all the data types we decided to build an environmental loading 10-m^2 grid that covered the entire installation and navigation channel. Figure A-4 shows part of the installation and the 10-m^2 grid.

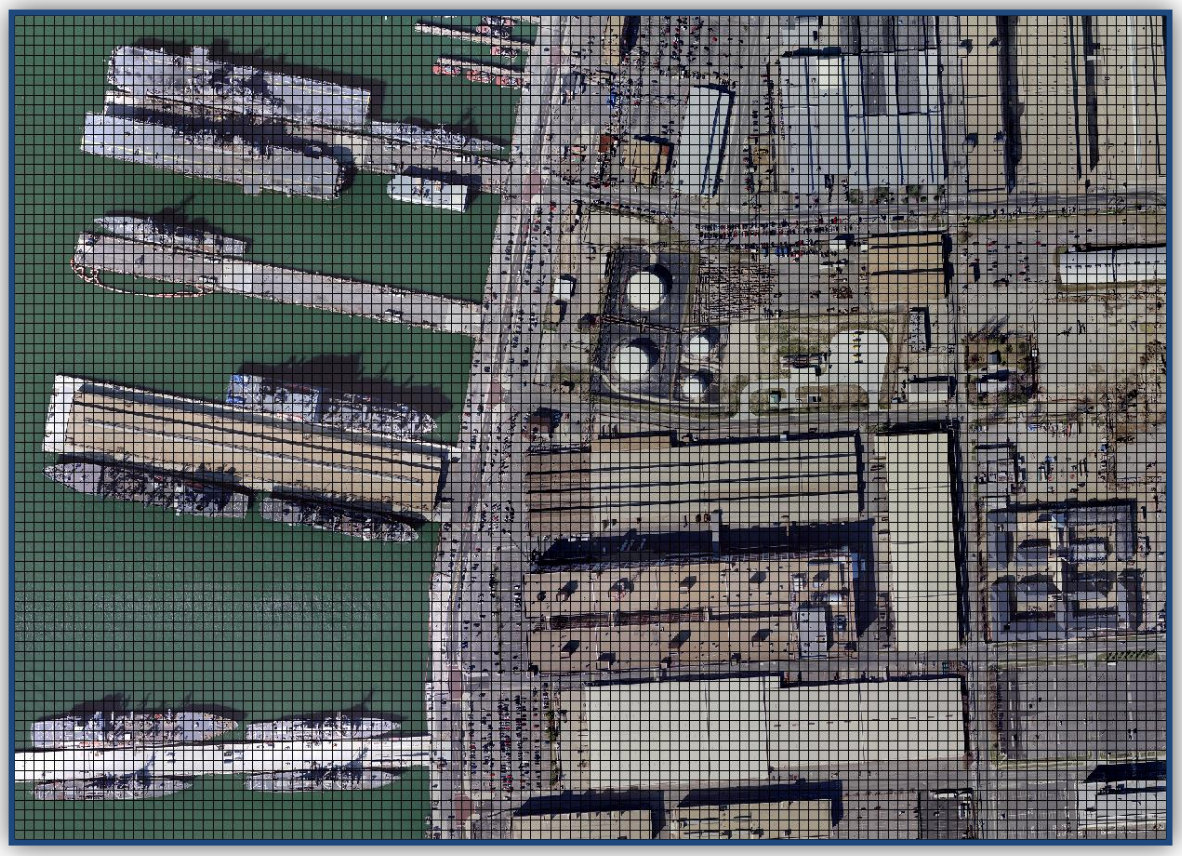

Figure A-4. The project's 10m^2 environmental loading grid.

The 10-meter environmental loading grid was a polygon layer and each grid cell had a unique ID. The unique cell IDs were assigned to the geospatial assets used in the ACN. We used an identity analysis geoprocessing step to assign unique cell IDs to each asset. The process computed a geometric intersection of the assets and grid layer. The assets or portions thereof that

overlapped the grid layer were assigned the Cell ID of those grid features. Figure A-5 shows a section of the primary underground conductor asset that fell within one of the cells.

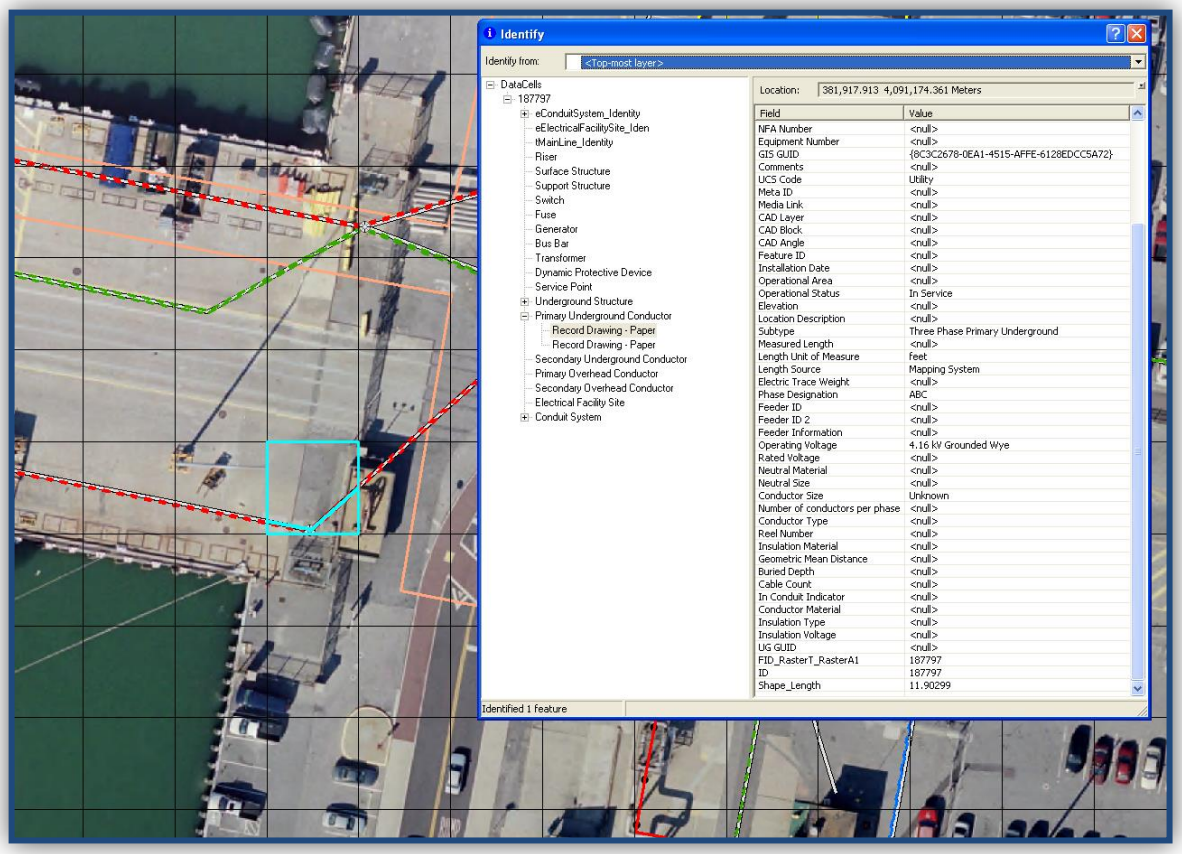

Figure A-5. Electrical asset located in a single cell.

Extraction of the environmental loading data and assigning it to the cell required a series of geoprocessing steps. First raster layers of the environmental loadings were generated. Next the cell midpoints were used to extract the environmental loading information. *Extract Values to Points* was the command to accomplish this step. This command extracted the cell values of the environmental loading data based on the set of midpoints. These midpoints also had the same cell IDs as the 10-m^2 grid layer. The midpoints and the 10-m^2 grid layer were spatially joined based on the unique ID value, thus, assigning the loading data to the 10-m^2 grid layer. Figure A-6 shows an example of the information for a single cell.

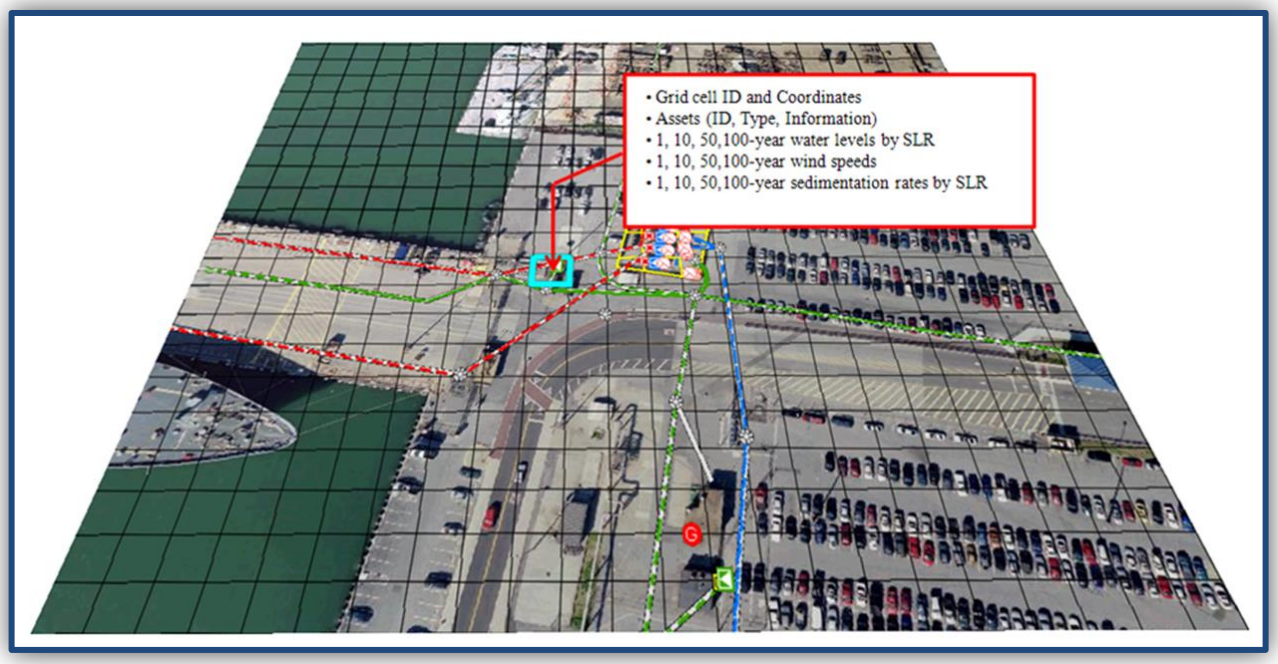

Figure A-6. Assets and environmental loadings of a single cell for the project.

Appendix B: List of Scientific/Technical Publications

Honghai Li, Lihwa Lin, and Kelly A. Burks-Copes (2013) Modeling of Coastal Inundation, Storm Surge, and Relative SLR at Naval Station Norfolk, Norfolk, Virginia, U.S.A.. Journal of Coastal Research 29(1):18-30. (Available online at: http://dx.doi.org/10.2112/JCOASTRES-D-12-00056.1, Accessed May 2014).

Appendix C: Other Supporting Materials

In 2011, we received one of the highest awards in the ERDC – the *ERDC Research and Development Award* for leveraging its prior experiences, world-class interdisciplinary technical expertise, body of knowledge, and computing bases, to innovate at the frontier of research to deliver advanced science and technology to the field by demonstrating an integrated our coastal hazard risk assessment framework that was designed to manage sea level rise uncertainties and communicate the risks of mission impairment to end-users and policymakers in a meaningful manner thereby supporting mission sustainability into the long-term.

In addition, we regularly coordinated and conducted onsite briefings to NAVFAC and the Navy's Task Force Climate Change providing regular status updates on details regarding the study's ongoing context and vision in order to garner insight into the inner-workings of the NSN. In particular, the following personnel were considered critical collaborators and provided key input into the analyses presented here:

- CAPT Tim Galluadet and Ms. Courtney St. John (Navy's Task Force Climate Change)
- CAPT Mark R. Libonate, Commanding Officer Naval Facilities Engineering Command (NAVFAC) Mid-Atlantic, Civil Engineer Corps, United States Navy
- CDR Frederick A. Hintermister, Office of the Deputy Assistant Secretary of the Navy, Infrastructure Strategy and Analysis, Critical Infrastructure Protection (ODASN IS& A CIP)
- Mr. Anthony L. Farmer, Structural Engineering TDC Capital Improvements Business Line, NAVFAC Mid-Atlantic
- Mr. Robert Baldwin, Regional Community Plans and Liaison Officer, Asset Management Branch, NAVFAC Mid Atlantic
- Dr. Richard A. Gardner, Environmental Department Head, Engineering Services Center (ESC), NAVFAC
- Dr. Shun Ling, Environmental Office Head, ESC, NAVFAC
- Mr. Timothy J. McHale, ESC, NAVFAC
- Ms. Jennie Dummer ESC, NAVFAC
- Mr. Robert L. Butters, P.E., Facilities Planner, NAVFAC
- Mr. John H. Salley, R.A., Deputy Public Works Officer, NAVFAC.

We will continue to collaborate with these partners into the future.

DEPARTMENT OF THE NAVY
NAVAL FACILITIES ENGINEERING SERVICE CENTER
1100 23RD AVE
PORT HUENEME, CA 93043-4370

IN REPLY REFER TO
5090
4 Jan 2011

From: Commanding Officer, Naval Facilities Engineering Service Center, Port Hueneme, CA
To: Commander, Engineer Research and Development Center, U.S. Army Corps of Engineers, Vicksburg, MS

Subj: LETTER OF SUPPORT, SERDP PROJECT 1701

Ref: (a) SERDP Project 1701, Risk Quantification for Sustaining Coastal Military Installation Assets and Mission Capabilities

1. I am sending this letter to express support for your work on Project 1701 (reference (a)), being performed under the sponsorship of the Strategic Environmental Research and Development Program (SERDP). Your team at the Engineer Research and Development Center (ERDC), under the leadership of Dr. Edmund Russo and Ms. Kelly Burks-Copes, is developing a methodology to assess risks to military coastal infrastructure caused by future storm events exacerbated by projected sea level rise. To aid in development of this methodology, the ERDC project team has reviewed candidate sites in the Hampton Roads area and has selected Naval Base Norfolk as the subject for the study.

2. This project is of special interest to the Naval Facilities Engineering Service Center (NAVFAC ESC) since we are tasked with providing specialty engineering services to the Naval shore community including the risks associated with climate change such as sea level rise. We too view Naval Base Norfolk as the single best site for this project because it is the Navy's largest shore installation and because it is in a vulnerable location from the perspective of sea level rise and storm events.

3. The ERDC project team has established technical goals and objectives that are appropriate to this work including the development of robust and scientifically defensible methods, tools, and technologies that can be transferred to the military community of practice. We are closely following the team's progress in the development of multiple scientific and engineering models that can be integrated into a climate change risk assessment, eventually leading to effective ways to manage the risk. We hope to employ the products of this work at more than 70 Navy installations world-wide that may be imperiled by sea level rise.

4. I wish to express my personal gratitude to Ms. Burks-Copes for her hospitality in hosting four representatives of NAVFAC ESC at your facility in September. Ms. Burks-Copes assembled the ERDC project team from multiple laboratories for an enlightening series of presentations and discussions. In November, we participated in the ERDC briefing to representatives of Naval Facilities Engineering Command, Mid Atlantic (NAVFAC MIDLANT) at Naval Base

Norfolk. In December, we witnessed the importance accorded your work by the SERDP Program Manager, Dr. John Hall, during a dedicated sea level rise meeting at the SERDP conference in Washington D.C.

5. We at NAVFAC ESC regard your work on this project as world-class, being performed by a team of multi-disciplined experts carefully selected from throughout the ERDC laboratories. We eagerly anticipate the products of your work so that we can begin applying them to our global shore infrastructure.

RICHARD A. GARDNER
By direction